

UNIVERSITY OF SOUTHAMPTON

FACULTY OF SCIENCE

School of Physics & Astronomy

**The Manifestly Gauge Invariant  
Exact Renormalisation Group**

Volume I of II

by

**Oliver Jacob Rosten**

Thesis for the degree of Doctor of Philosophy

March 2005

UNIVERSITY OF SOUTHAMPTON

ABSTRACT

FACULTY OF SCIENCE

SCHOOL OF PHYSICS & ASTRONOMY

Doctor of Philosophy

THE MANIFESTLY GAUGE INVARIANT EXACT RENORMALISATION  
GROUP

by Oliver Jacob Rosten

We construct a manifestly gauge invariant Exact Renormalisation Group (ERG) whose form is suitable for computation in  $SU(N)$  Yang-Mills theory, beyond one-loop. An effective cutoff is implemented by embedding the physical  $SU(N)$  theory in a spontaneously broken  $SU(N|N)$  Yang-Mills theory.

To facilitate computations within this scheme, which proceed at every step without fixing the gauge, we develop a set of diagrammatic techniques. As an initial test of the formalism, the one-loop  $SU(N)$  Yang-Mills  $\beta$ -function,  $\beta_1$ , is computed, and the standard, universal answer is reproduced.

It is recognised that the computational technique can be greatly simplified. Using these simplifications, a partial proof is given that, to all orders in perturbation theory, the explicit dependence of perturbative  $\beta$ -function coefficients,  $\beta_n$ , on certain non-universal elements of the manifestly gauge invariant ERG cancels out. This partial proof yields an extremely compact, diagrammatic form for the surviving contributions to arbitrary  $\beta_n$ , up to a set of terms which are yet to be dealt with. The validity of the compact expression is reliant on an unproven assertion at the third loop order and above.

Starting from the compact expression for  $\beta_n$ , we specialise to  $\beta_2$  and explicitly construct the set of terms yet to be dealt with. From the resulting diagrammatic expression for  $\beta_2$ , we extract a numerical coefficient which, in the limit that the coupling of one of the unphysical regulator fields is tuned to zero, yields the standard, universal answer. Thus, we have performed the very first two-loop, continuum calculation in Yang-Mills theory, without fixing the gauge.

# Contents

<b>Acknowledgements</b>	<b>xxv</b>
<b>Motivation</b>	<b>xxvii</b>
<b>Structure of Thesis</b>	<b>xxx</b>
<b>I Setup</b>	<b>1</b>
<b>1 Introduction</b>	<b>2</b>
1.1 An ERG for Scalar Field Theory . . . . .	2
1.1.1 The Polchinski Equation . . . . .	2
1.1.2 Properties of the Polchinski Equation . . . . .	4
1.2 The Manifestly Gauge Invariant Exact Renormalisation Group	8
1.2.1 Regularisation . . . . .	8
1.2.2 The Flow Equation . . . . .	20
1.2.3 Diagrammatics . . . . .	23
1.2.4 The Broken Phase . . . . .	34
1.2.5 The Weak Coupling Expansion . . . . .	39
<b>2 The New Flow Equation</b>	<b>41</b>
2.1 The Need for a New Flow Equation . . . . .	41
2.2 Modifying the Flow Equation . . . . .	43
2.3 The New Diagrammatics-I . . . . .	45
2.3.1 The Symmetric Phase . . . . .	45
2.3.2 The Broken Phase . . . . .	47
2.4 The New Diagrammatics-II . . . . .	60

2.4.1	Construction . . . . .	60
2.4.2	Identical Fields . . . . .	63
2.4.3	Additional Notation . . . . .	65
2.4.4	Constraints in the $C$ -sector . . . . .	66
2.5	The Weak Coupling Expansion . . . . .	67
2.5.1	The flow Equation . . . . .	67
2.5.2	The Two-Point, Tree Level Vertices . . . . .	70
2.5.3	The Zero-Point Kernels and Effective Propagators . . . . .	76
2.5.4	Diagrammatic Identities . . . . .	79
2.5.5	Universality . . . . .	84
2.5.6	Constraints in the $C$ -sector . . . . .	87
<b>II</b>	<b>Techniques</b>	<b>89</b>
<b>3</b>	<b>Further Diagrammatic Techniques</b>	<b>90</b>
3.1	Gauge Remainders . . . . .	91
3.1.1	Vertices . . . . .	91
3.1.2	Wines . . . . .	98
3.1.3	Gauge Invariance . . . . .	100
3.1.4	Cancellations Between Pushes forward / Pulls back . . . . .	105
3.1.5	Charge Conjugation . . . . .	106
3.1.6	Complete Diagrams . . . . .	107
3.1.7	Socket Notation . . . . .	115
3.1.8	Nested Contributions . . . . .	117
3.1.9	Double Gauge Remainders . . . . .	119
3.2	Momentum Expansions . . . . .	122
3.2.1	Basics . . . . .	122
3.2.2	Wines . . . . .	125
3.2.3	Algebraic Expansions . . . . .	126
3.2.4	Complete Diagrams . . . . .	126
3.3	More Diagrammatic Identities . . . . .	132

<b>4</b>	<b>One Loop Diagrammatics</b>	<b>136</b>
4.1	A Diagrammatic Expression for $\beta_1$ . . . . .	137
4.1.1	The Starting Point . . . . .	137
4.1.2	Diagrammatic Manipulations . . . . .	139
4.1.3	The $B'(0)$ Terms . . . . .	153
4.2	Conclusions . . . . .	155
<b>5</b>	<b><math>\Lambda</math>-Derivative Terms</b>	<b>158</b>
5.1	Introduction . . . . .	158
5.2	1-loop Integrals . . . . .	160
5.2.1	Vanishing Diagrams . . . . .	160
5.2.2	IR Regularisation Provided by $p$ . . . . .	162
5.2.3	Loop Integrals Independent of $p$ . . . . .	167
5.3	2-loop Integrals . . . . .	168
5.3.1	The Factorisable Case . . . . .	169
5.3.2	The Non-Factorisable Case . . . . .	169
5.3.3	Considerations for $\beta_2$ . . . . .	170
5.4	Subtraction Techniques . . . . .	171
5.4.1	Basics . . . . .	171
5.4.2	Generalisation to the Gauge Case . . . . .	173
5.4.3	Application to Terms Manipulable at $\mathcal{O}(p^2)$ . . . . .	175
5.5	Ensuring Universality . . . . .	178
<b>III</b>	<b><math>\beta_{n+}</math> Diagrammatics</b>	<b>184</b>
<b>6</b>	<b>Introduction</b>	<b>185</b>
<b>7</b>	<b>Initial Recasting</b>	<b>188</b>
7.1	Level-Zero Manipulations . . . . .	188
7.2	Level-One Manipulations . . . . .	191
7.2.1	Diagram 7.1 . . . . .	191
7.2.2	Diagram 7.2 . . . . .	197
7.3	Level-Two Manipulations . . . . .	203
7.3.1	Diagram 7.8 . . . . .	204

7.3.2	Diagram 7.7 . . . . .	214
7.3.3	Diagram 7.20 . . . . .	222
7.4	Level-Three Manipulations . . . . .	236
7.4.1	Diagram 7.31 . . . . .	237
7.5	The Critical Level . . . . .	249
<b>8</b>	<b>Gauge Remainders</b>	<b>252</b>
8.1	Type-Ia Gauge Remainders . . . . .	253
8.2	Type-Ib Gauge Remainders . . . . .	271
8.3	Type-II Gauge Remainders . . . . .	288
8.4	Type-III Gauge Remainders . . . . .	306
<b>9</b>	<b>Further Diagrammatic Identities</b>	<b>309</b>
9.1	The New Identities . . . . .	309
9.2	Application . . . . .	324
<b>10</b>	<b>Iterating the Diagrammatic Procedure</b>	<b>332</b>
<b>11</b>	<b>Terms with an <math>\mathcal{O}(p^2)</math> Stub</b>	<b>367</b>
11.1	$\mathcal{O}(p^2)$ Terms of Type Ia . . . . .	367
11.2	$\mathcal{O}(p^2)$ Terms of Types Ib and II . . . . .	368
<b>IV</b>	<b>Computation of <math>\beta_2</math> and Conclusions</b>	<b>374</b>
<b>12</b>	<b>Two Loop Diagrammatics</b>	<b>375</b>
12.1	Specialising Equation (10.1) . . . . .	376
12.1.1	Diagrams which can be Discarded . . . . .	376
12.1.2	Cancellations Between Diagrams . . . . .	377
12.1.3	Compact Notation . . . . .	378
12.1.4	Generation of Terms . . . . .	379
12.2	Terms with an $\mathcal{O}(p^2)$ Stub . . . . .	382
12.3	$\beta$ -Terms . . . . .	389
12.4	$\alpha$ -Terms . . . . .	391
12.5	Simplifications . . . . .	394

<b>13 Numerical Evaluation of <math>\beta_2</math></b>	<b>399</b>
13.1 Vanishing Diagrams . . . . .	400
13.1.1 Diagrams which Vanish Individually . . . . .	401
13.1.2 Diagrams which Vanish as a Set . . . . .	401
13.1.3 Diagrams which Possess Vanishing Components . . . . .	402
13.2 Finite Diagrams . . . . .	403
13.2.1 Universal Diagrams . . . . .	404
13.2.2 Non-Universal Diagrams . . . . .	407
13.3 The Standard Set as a Sub-Diagram . . . . .	410
13.3.1 Mirroring the Cancellations of Section 13.2.2 . . . . .	411
13.3.2 Generating the Constructed Diagrams . . . . .	414
13.4 Further Subtractions . . . . .	432
13.4.1 Subtractions for Terms Generated in Chapter 12 . . . . .	432
13.4.2 Subtractions for Terms Generated in Section 13.3 . . . . .	436
13.5 Further Manipulations . . . . .	439
13.5.1 Removal of Non-Computable Contributions to the Stan- dard Set . . . . .	444
13.5.2 Removal of Non-Computable Contributions to the Little Set . . . . .	449
13.5.3 Final Remainders . . . . .	453
13.6 The $\alpha$ -terms . . . . .	454
13.6.1 The Problem . . . . .	454
13.6.2 Behaviour of $h(\alpha)$ . . . . .	457
13.6.3 Behaviour of $\tilde{H}(\alpha)$ . . . . .	460
13.7 Computation of $\beta_2$ . . . . .	463
13.8 Conclusions . . . . .	465
<b>14 Conclusion</b>	<b>468</b>
14.1 Summary . . . . .	468
14.2 Discussion . . . . .	473
14.3 Future Work . . . . .	476
14.4 Outlook . . . . .	478

<b>A Ingredients of the Weak Coupling Flow Equations</b>	<b>479</b>
A.1 Two-Point, Tree Level Vertices . . . . .	479
A.2 The Zero-Point Kernels and Effective Propagators . . . . .	480
A.3 The Gauge Remainders . . . . .	481
<b>B Diagrammatic Identities</b>	<b>482</b>
<b>C Examples of Classical Flows</b>	<b>490</b>
<b>D Simplified Expression for <math>\beta_2</math></b>	<b>493</b>
<b>Bibliography</b>	<b>498</b>

# List of Figures

1.1	Diagrammatic representation of the action. . . . .	24
1.2	Expansion of a single supertrace in powers of $\mathcal{A}$ and $\mathcal{C}$ . . . . .	24
1.3	Diagrammatic representation of the wines. . . . .	25
1.4	True diagrammatic representation of equation (1.27). . . . .	26
1.5	Diagrammatic representation of the flow equation, assuming that all fields are $\mathcal{C}$ s. . . . .	27
1.6	Example of the classical part of the flow. . . . .	28
1.7	Reinterpretation of figure 1.6, where now the diagrammatic el- ements comprise just the vertex coefficient functions and the wine vertex coefficient functions. . . . .	29
1.8	A term which survives, despite naïvely vanishing by group the- ory considerations. . . . .	33
1.9	Diagrammatic representation of equation (1.25). . . . .	34
1.10	Diagrammatic representation of differentiation with respect to a partial supermatrix, $Y$ . . . . .	36
1.11	Diagrammatic representation of equation (1.58), where diagrams in which the wine bites its own tail have been discarded. . . . .	40
2.1	Diagrammatics for the classical part of the new flow equation. . .	46
2.2	Interpretation of the double circle notation. . . . .	47
2.3	Diagrammatics for the quantum part of the new flow equation. . .	47
2.4	Classical part of the flow of a vertex decorated by two $A^1$ s. . .	49
2.5	Attachment of a wine via $\delta/\delta A^1$ . . . . .	52
2.6	A re-expression of figure 2.5. . . . .	53
2.7	Classical part of the flow of a two-point vertex decorated by the fields $A^1$ , $A^2$ , $C^1$ , $C^2$ , $F$ and $\bar{F}$ . . . . .	54

2.8	The attachment corrections for $\dot{\Delta}^{A^1 A^1}$ . . . . .	54
2.9	The attachment corrections for $\dot{\Delta}^{A^1 A^1}$ and $\dot{\Delta}^{A^2 A^2}$ . . . . .	55
2.10	Example of how the broken phase form of (1.41) mixes different wines. . . . .	57
2.11	Unpacking a wine, ‘decorated’ by a $C^1$ and a $\sigma$ . . . . .	58
2.12	The diagrammatic form of the flow equation, when we treat single and multiple supertrace terms together. . . . .	61
2.13	A new style vertex decorated by two $A^1$ s and a $C^1$ . . . . .	61
2.14	A new style (dummy) wine decorated by a single $A^1$ . . . . .	62
2.15	The flow of a vertex decorated by two $A^1$ s (or $A^2$ s), using the new diagrammatics. . . . .	64
2.16	An example of the meaning of FAS. . . . .	65
2.17	Forcing a vertex on an implicitly decorated diagram to have precisely two decorations. . . . .	66
2.18	The constraint arising from ensuring that the position of the minimum of the Higgs potential is unaffected by quantum corrections. . . . .	66
2.19	The new diagrammatic form for the weak coupling flow equation. . . . .	69
2.20	Flow of all possible two-point, tree level vertices. . . . .	71
2.21	The flow of $S_0^{C^1,2,C^1,2}(p)$ . . . . .	75
2.22	The effective propagator relation. . . . .	80
2.23	Showing how $1/N$ corrections to the effective propagator relation vanish. . . . .	81
2.24	The weak coupling regime constraint to ensure that the minimum of the superhiggs potential is not shifted by quantum corrections. . . . .	88
3.1	Diagrammatics for the Ward Identities. . . . .	91
3.2	Diagrammatic form of the first order no- $\mathcal{A}^0$ relations. . . . .	96
3.3	Prescription adopted for internal fermionic fields decorating a vertex struck by a gauge remainder. . . . .	97
3.4	A gauge remainder strikes a vertex in which a component of $\mathcal{A}$ has been replaced by a component of $\mathcal{C}$ . . . . .	97

3.5	Contraction of an arbitrary wine with one of its momenta. . . .	99
3.6	Flow of a vertex decorated by the fields $f_1 \cdots f_n$ . . . . .	101
3.7	The push forward and / or pull back round the vertex cancels the pull back and / or push forward down the wine. . . . .	102
3.8	The push forward round the vertex does not quite cancel the pull back down the wine. . . . .	103
3.9	Two diagrams which, after the gauge remainders strike the ex- plicitly drawn fields, cancel by the coincident line identities. . .	104
3.10	An example of applying CC to lone vertices struck by a gauge remainder. . . . .	108
3.11	Example of a gauge remainders in a complete diagram. . . . .	109
3.12	Two components of diagram 3.10 which are not equal, due to their differing supertrace structure. . . . .	109
3.13	Example of a gauge remainder on a wine, in a full diagram. . .	111
3.14	Two sub-diagrams between which, after the action of the gauge remainders, certain contributions are guaranteed to cancel. . .	112
3.15	A diagram for which corrections to supersplitting / supersowing are restricted. . . . .	114
3.16	Gauge remainder which produces a diagram in which the effec- tive propagator relation can be applied. . . . .	115
3.17	Basic idea of socket notation. . . . .	116
3.18	Partner diagrams to diagrams 3.21 and 3.23. . . . .	117
3.19	Result of processing diagram 3.19. . . . .	117
3.20	An arbitrarily nested gauge remainder bites a socket on a vertex.	118
3.21	An arbitrarily nested version of the hook. . . . .	119
3.22	An example of a double gauge remainder diagram. . . . .	120
3.23	Result of allowing one gauge remainder in diagram 3.30 to act.	120
3.24	A trivial redrawing of diagram 3.33. . . . .	121
3.25	Two of the terms produced by processing diagrams 3.31 and 3.34.	121
3.26	A trivial redrawing of diagram 3.36. . . . .	122
3.27	Diagrammatics expression for a vertex decorated by an $A$ -field carrying zero momentum. . . . .	123

3.28	Re-expressing a three-point vertex with zero momentum entering along an $A$ -field. . . . .	124
3.29	Re-expressing a four-point vertex with zero momentum entering along an $A$ -field. . . . .	125
3.30	A field ordered one-point wine with zero momentum entering along a decorative $A$ -field can be expressed as the momentum derivative of a zero-point wine. . . . .	126
3.31	Manipulation of a diagram at $\mathcal{O}(p^2)$ . Discontinuities in momentum flow are indicated by a bar. . . . .	127
3.32	Example of a two-loop diagram in which we choose to Taylor expand in momenta, rather than this choice being forced upon us.	128
3.33	A set of diagrams which naturally combine. . . . .	131
3.34	Completely diagrammatic representation of diagrams 3.45 and 3.46.	132
3.35	The first step in redrawing a diagram to yield a diagrammatic identity. . . . .	134
3.36	A diagrammatic identity. . . . .	135
3.37	Diagrammatic identity 9. . . . .	135
4.1	A diagrammatic representation of the equation for $\beta_1$ . . . . .	138
4.2	The manipulation of diagram 4.1. . . . .	140
4.3	The re-expression of diagram 4.9, using the tree-level flow equation. . . . .	141
4.4	Manipulation of diagrams 4.10–4.12, 4.15 and 4.16. . . . .	142
4.5	Manipulation of diagram 4.19 using the tree level flow equations.	144
4.6	Manipulation of diagram 4.13 using the tree level flow equation.	145
4.7	Terms arising from processing the gauge remainders of the diagrams in figures 4.5 and 4.6. . . . .	147
4.8	Diagrams arising from processing the nested gauge remainders of figure 4.7. . . . .	148
4.9	Re-drawing of diagrams 4.51 and 4.62 using diagrammatic identity 8 and their subsequent conversion into $\Lambda$ -derivative terms.	149
4.10	Manipulations at $\mathcal{O}(p^2)$ , followed by a re-expression of the resulting diagrams. . . . .	150

4.11	The final conversion into $\Lambda$ -derivative terms. . . . .	151
4.12	The set of $B'(0)$ terms (which do not manifestly vanish at $\mathcal{O}(p^2)$ ). . . . .	152
4.13	Diagrammatic, gauge invariant expression for $\beta_1$ , phrased entirely in terms of $\Lambda$ -derivatives. . . . .	152
4.14	The result of contracting the standard set with its external momentum. The first three diagrams on the r.h.s. cancel and the fourth vanishes by Lorentz invariance. . . . .	154
5.1	Two diagrams which give a vanishing contribution to $\beta_1$ in $D = 4$ . . . . .	160
5.2	The standard set struck by $\Lambda\partial_\Lambda _\alpha$ . . . . .	162
5.3	The little set struck by $\Lambda\partial_\Lambda _\alpha$ . . . . .	168
5.4	Reproduction of diagram 4.54, with explicit momentum routing. . . . .	176
5.5	A two-loop diagram with an $\mathcal{O}(p^2)$ stub, which cannot be Taylor expanded in $p$ , and its subtraction. . . . .	176
5.6	The contribution to diagram 5.9 not removed by its subtraction. . . . .	177
5.7	The flow of a vertex decorated by an arbitrary number of $C$ s. . . . .	179
5.8	The flow of a vertex decorated by a single $A$ and an arbitrary number of $C$ s. . . . .	180
7.1	A diagrammatic representation of the equation for $\beta_{n+}$ . Vertices are tagged alphabetically. . . . .	189
7.2	Isolation of the manipulable component of diagram 7.1. . . . .	191
7.3	The result of processing diagram 7.3. . . . .	192
7.4	Splitting off the tree level two-point, tree level vertices from diagram 7.6. . . . .	195
7.5	Partial decoration of diagram 7.9 with either an external field or an effective propagator. . . . .	196
7.6	Result of tying up the loose end in diagram 7.10, followed by subsequent application of the effective propagator relation. . . . .	196
7.7	Isolation of those components of diagram 7.2 which can be usefully processed. . . . .	198
7.8	Result of processing diagram 7.12 by converting it into a $\Lambda$ -derivative term, plus corrections. . . . .	199
7.9	A re-expression of diagram 7.16. . . . .	200

7.10 Isolation of the components of diagram 7.15 containing a two-point, tree level vertex. . . . .	201
7.11 Decoration of the two-point, tree level vertices of diagrams 7.18 and 7.21 and application of the effective propagator relation. . . . .	203
7.12 Isolation of the manipulable component of diagram 7.8. . . . .	205
7.13 Attachment of the effective propagator to diagram 7.24. . . . .	205
7.14 The canonical form of the $\Lambda$ -derivative term for diagrams I.1 and I.2. . . . .	206
7.15 Manipulation of diagram 7.24. . . . .	208
7.16 Attachment of $J_A$ effective propagators, the loose ends of which all attach to the bottom vertex. . . . .	209
7.17 Isolation of those components of diagram 7.27 containing a two-point, tree level vertex. . . . .	211
7.18 Tying up the loose ends of diagram 7.30, together with application of the effective propagator relation. . . . .	212
7.19 Partial decoration of diagram 7.32. . . . .	213
7.20 Result of processing the manipulable component of diagram 7.7. . . . .	215
7.21 Result of splitting off two-point, tree level vertices from diagram 7.37. . . . .	216
7.22 Isolation of the manipulable component of a level- $J$ diagram, formed by the repeated action of $a_1$ . . . . .	217
7.23 The result of processing diagram G.2. . . . .	218
7.24 Isolation of the two-point, tree level vertices of diagram G.5 and etc. . . . .	218
7.25 Manipulation of diagram G.7. . . . .	220
7.26 Isolation of selected components of diagram G.9. . . . .	220
7.27 Attaching the effective propagator to the component of diagram 7.20 with an undecorated wine. . . . .	223
7.28 Specialisation of diagram I.4 to two specific realisations of $\{r, t\}$ , which we assume to be different. . . . .	224
7.29 Conversion of diagrams I.5 and I.6 into a $\Lambda$ -derivative term. . . . .	224
7.30 A trial form for the $\Lambda$ -derivative term arising from diagram 7.20. . . . .	225
7.31 The result of processing the manipulable part of diagram 7.20. . . . .	227

7.32 Isolation of the two-point, tree level vertices in diagram 7.42 and etc. . . . .	228
7.33 Processing a level- $J$ diagram formed by the repeated action of $a_0$ .	230
7.34 The result of processing diagram G.17. . . . .	232
7.35 Isolation of two-point, tree level vertices in diagram G.20, and the results of their subsequent decoration. . . . .	233
7.36 Final result of the exhaustive manipulation of diagram 7.2. . .	236
7.37 A trial form for the $\Lambda$ -derivative term arising from diagram 7.31.	238
7.38 The result of processing diagram 7.31. . . . .	239
7.39 Isolation of two-point, tree level vertices in diagram 7.47 and etc.	240
7.40 Showing how diagrams 7.52, 7.29, 7.34 and 7.35 combine to cancel diagram 7.17. . . . .	242
7.41 Isolation of the manipulable part of a level- $J$ diagram. . . . .	244
7.42 Selected terms arising from the manipulation of diagram G.25.	245
7.43 Diagrammatic expression for $\beta_{n_+}$ arising from the exhaustive manipulation of diagrams 7.2 and 7.1. . . . .	250
8.1 Type-Ia gauge remainders. . . . .	254
8.2 Re-expression of diagrams G.41 and G.42. . . . .	256
8.3 Result of processing diagrams G.43 and G.44. . . . .	257
8.4 Result of processing diagram G.38. . . . .	257
8.5 Partial decoration of diagram G.53, in which all loose ends have been tied up and the effective propagator relation has been applied.	258
8.6 Result of processing diagrams G.39 and G.40. . . . .	259
8.7 Separating off the two-point, tree level vertices from diagrams G.35– G.37, after the action of the gauge remainder. . . . .	261
8.8 Partial decoration of diagram G.71. . . . .	262
8.9 The result of processing diagram G.68. . . . .	264
8.10 An example of diagram $X$ . . . . .	265
8.11 An example of diagram $Y$ . . . . .	266
8.12 Result of processing diagram G.76. . . . .	268
8.13 An example of the new types of diagram arising from processing nested gauge remainders. . . . .	269

8.14	Type-Ib gauge remainders. . . . .	272
8.15	Diagrams arising from processing diagrams G.96 and G.97 that are not cancelled when diagram G.93 is processed. . . . .	273
8.16	Diagrams arising from processing diagrams G.93–G.95 that are not cancelled by other diagrams arising from figure 8.14. . . . .	274
8.17	The result of combining diagrams G.103 and G.104 with dia- grams G.59 and G.60. . . . .	276
8.18	Nested gauge remainder contributions arising from the manip- ulation of diagrams G.90–G.92. . . . .	278
8.19	Result of combining (the surviving contributions to) diagrams G.90– G.92 with diagrams G.69, G.70, G.72, G.73, G.105 and G.106. . . . .	279
8.20	Analogues of the diagrams of figure 8.13 generated by type-Ib gauge remainders. . . . .	281
8.21	The simplest versions of diagrams in which a two-point, tree level vertex is attached to a bitten gauge remainder. . . . .	284
8.22	An arbitrarily nested version of diagram G.99 and a nested ver- sion of the combination of diagrams G.60 and G.104. . . . .	285
8.23	Combining diagrams I.9 and I.10 into a $\Lambda$ -derivative term. . . . .	286
8.24	Type-II gauge remainders. . . . .	289
8.25	Some of the terms generated by processing diagram G.145. . . . .	291
8.26	Result of processing diagrams G.148, G.149 and G.151, up to terms which are guaranteed to cancel, via cancellation mecha- nisms 11 and 12. . . . .	293
8.27	Nested gauge remainder terms generated from diagrams G.144– G.146 and G.150. . . . .	294
8.28	The minimal set of terms arising from processing diagrams G.156, G.157, G.170 and G.171 and their analogues with additional ver- tices, up to terms with an $\mathcal{O}(p^2)$ stub. . . . .	296
8.29	Surviving contributions from diagrams G.155 and G.169, mod- ulo terms with an $\mathcal{O}(p^2)$ stub. . . . .	297
8.30	Surviving terms from diagrams G.154, G.166–G.168 and the nested version of diagram G.144, up to additionally nested dia- grams and terms with an $\mathcal{O}(p^2)$ stub. . . . .	300

8.31	Additional diagrams comprising a two-point, tree level vertex joined to a bitten gauge remainder. They are spawned by diagrams G.192 and G.193. . . . .	302
8.32	Additional diagrams comprising a two-point, tree level vertex joined to a bitten gauge remainder, whose lineage can be traced back to diagram G.166. . . . .	302
8.33	Collecting together diagrams G.158, G.159, G.196 and G.197, which have been combined in pairs, and diagrams G.180–G.183, and G.218–G.221. . . . .	304
8.34	Resulting of promoting the effective propagator of diagrams G.230 and G.231 to a decoration and detaching the wine from the vertex. . . . .	305
8.35	Type-III gauge remainders. . . . .	307
8.36	The minimal set of terms produced by applying the diagrammatic procedure, until exhaustion, to diagrams G.240–G.246. . . . .	308
9.1	An example of the type of $\Lambda$ -derivative term we expect to arise from the gauge remainder sector of the calculation. . . . .	310
9.2	Examples of some of the new types of term we expect to generate when we process diagrams like I.16. . . . .	310
9.3	A two-point, tree level vertex, generated by the action of a gauge remainder and decorated by $\curvearrowright$ . . . . .	311
9.4	Further decoration of the previous diagram. . . . .	311
9.5	A possible pair of field ordered diagrams formed from a term in which the structure $\curvearrowright$ is attached to a two-point, tree level vertex which has been formed by the action of a gauge remainder. . . . .	312
9.6	Diagrammatic identity 10. . . . .	313
9.7	Two diagrams which are special cases of diagram I.18. . . . .	313
9.8	The first two sub-diagrams show the algebraic part of diagram G.89, where we have used the effective propagator relation. The final sub-diagram shows the algebraic part of diagram I.22. . . . .	314
9.9	Sub-diagram 9.9 with specific field content. . . . .	315
9.10	Partner diagrams to those of figure 9.8, in which the nested gauge remainder has changed character. . . . .	316

9.11	Diagrammatic identity 11. . . . .	317
9.12	The nested versions of diagrams G.88 and G.89. . . . .	318
9.13	Particular type-Ia gauge remainders arising from the conversion of diagrams possessing a nested version of $\curvearrowright$ into a $\Lambda$ -derivative term. . . . .	318
9.14	A set of diagrams, possessing three performed gauge remainders, which sum to zero. . . . .	319
9.15	The three partner diagrams to diagram I.39. . . . .	320
9.16	A trivial redrawing of sub-diagram I.42. . . . .	321
9.17	The two partners of sub-diagrams I.40 and I.41. Any other combination of external fields will cause the diagrams to vanish. . . . .	322
9.18	Diagrammatic identity 12. . . . .	323
9.19	Four diagrams which sum to zero when all fields are in the $A$ -sector. . . . .	324
9.20	A re-expression of a series of diagrams, using diagrammatic identities 11–13. . . . .	326
9.21	Combining diagrams G.198, G.199, G.230 and G.231 with diagrams G.130 and G.131. . . . .	328
9.22	Result of combining the nested versions of diagrams G.158 and G.159 with the nested versions of diagrams G.196 and G.197. . . . .	328
9.23	Result of applying diagrammatic identities 11 and 12, as appropriate, to diagrams G.255–G.262 and G.232–G.239. . . . .	329
9.24	Result of combining diagrams G.263–G.274, nested versions of diagrams G.198 and G.199, diagrams G.132–G.139 and the nested version of diagrams G.130 and G.131. . . . .	331
10.1	Combination of diagrams G.99, G.113 and G.123–G.126. . . . .	333
10.2	Converting diagram G.303 into a $\Lambda$ -derivative term. . . . .	334
10.3	Re-expression of the diagrams of figure 10.2. . . . .	335
10.4	Isolation of the two-point, tree level vertices of diagram G.313. . . . .	336
10.5	The result of processing diagrams G.315 and G.316. . . . .	337
10.6	New types of diagram arising from iterating the diagrammatic procedure. . . . .	339

10.7	Result of combining diagrams G.324 and G.328 with diagrams G.152 and G.153. . . . .	340
10.8	The minimal set of new types of diagram arising from processing the gauge remainders spawned by terms with $>$ among the decorations. . . . .	341
10.9	The minimal set of terms spawned by diagrams G.334–G.336, up to nested versions of the parent diagrams and diagrams with an $\mathcal{O}(p^2)$ stub. . . . .	342
10.10	An example of a candidate for conversion into a $\Lambda$ -derivative term, possessing the structure $\text{---}\curvearrowright$ both as a decoration and as the component of the diagram hit by $-\Lambda\partial_\Lambda$ . . . . .	342
10.11	A $\Lambda$ -derivative term for a diagram decorated by two gauge remainders. . . . .	343
10.12	Further diagrams which should be amongst those represented by diagram G.345. . . . .	344
10.13	The candidate for a $\Lambda$ -derivative term with $m$ decorative gauge remainders. . . . .	345
10.14	A term generated by the corrections to diagram I.58 for $m = m' < m_{\max}$ . . . . .	346
10.15	A generic form of diagram I.58, in which the decorative $>$ s have been explicitly arranged. . . . .	347
10.16	The diagrams which spawned the $i$ th cluster of diagram I.60 with $q_i = q'_i - 1$ . . . . .	348
10.17	New types of diagram arising from the decoration of version of diagram G.315. . . . .	350
10.18	New types of diagram arising from the decoration of version of diagram G.316. . . . .	352
10.19	New types of gauge remainder diagrams arising from iterating the diagrammatic procedure. . . . .	355
10.20	The result of combining diagrams G.355–G.358 and G.369–G.372 with diagrams G.202–G.205, G.200, G.201, G.216 and G.217. . . . .	356

10.21	Example of a new type of diagram formed when a type-Ia gauge remainder generates a two-point, tree level vertex, to which a nested gauge remainder is attached, via an effective propagator.	357
10.22	The minimal set of diagrams surviving diagrams arising from diagrams G.379–G.382.	359
10.23	Combination of diagrams G.391–G.394 and G.339–G.344.	360
10.24	The minimal set of diagrams surviving diagrams arising from diagrams G.373–G.378, which cannot be written as nestings of terms generated earlier in this section, up to diagrams with an $\mathcal{O}(p^2)$ stub.	363
10.25	Diagrammatic expression for $\beta_{n+}$ including gauge remainder terms.	365
11.1	An example of a diagram which, whilst possessing an $\mathcal{O}(p^2)$ stub has $\mathcal{O}(p^0)$ components.	369
11.2	Example of three two-loop diagrams, components of which can be combined into total momentum derivatives, at $\mathcal{O}(p^2)$ .	370
11.3	Result of processing diagram I.70, using diagrammatic identity 5.	371
11.4	Combination of a diagram derived from I.72 and two $\mathcal{O}(p^2)$ diagrams of type-II.	372
11.5	Rewriting diagrams I.74–I.76 as a $\Lambda$ -derivative term.	373
12.1	Four diagrams, two of which cancel and two of which do not.	377
12.2	Shorthand for two diagrams always guaranteed to occur together.	379
12.3	The set of diagrams possessing one-loop vertices, the elements of which are not individually transverse in $p$ .	379
12.4	Diagrams for which both one-loop sub-diagrams are found in the diagrammatic expression for $\beta_1$ .	381
12.5	Diagrams with an $A_\mu^1 A_\nu^1 C$ vertex.	383
12.6	The final set of $\Lambda$ -derivatives which can be obtained directly from equation (10.1): part I.	384
12.7	The final set of $\Lambda$ -derivatives which can be obtained directly from equation (10.1): part II.	385
12.8	The first set of $\Lambda$ -derivative terms with an $\mathcal{O}(p^2)$ stub.	386

12.9	The second set of $\Lambda$ -derivative terms with an $\mathcal{O}(p^2)$ stub. . . .	388
12.10	The third set of $\Lambda$ -derivative terms with an $\mathcal{O}(p^2)$ stub. . . . .	390
12.11	Terms with an $\mathcal{O}(p^2)$ stub which are not Taylor expandable to the desired order in $p$ . . . . .	390
12.12	All $\beta$ -terms. . . . .	391
12.13	$\alpha$ -terms of the first type. . . . .	392
12.14	$\alpha$ -terms of the second type. . . . .	392
12.15	All remaining $\alpha$ -terms. . . . .	394
12.16	Result of combining the diagrams of figure 12.4, diagrams 12.58– 12.61 and 12.77–12.80. . . . .	395
12.17	Result of combining diagrams . . . . .	397
12.18	Result of combining diagrams 12.112 and 12.113 with 12.75– 12.76 and then combining the result with diagrams 12.114–12.116.398	398
13.1	Three diagrams which do not separately vanish as $\epsilon \rightarrow 0$ , but vanish when combined into a set related by gauge invariance. . .	402
13.2	Two components of a diagram, one of which can and one of which cannot be discarded. . . . .	402
13.3	Reproduction of diagram 12.41. . . . .	404
13.4	Extracting the dependence of a transverse one-loop diagram on its external momentum. . . . .	407
13.5	The complete set of diagrams which contain the one-loop dia- gram shown in figure 13.4. . . . .	408
13.6	Taylor expanding the four-point vertex of diagram 13.6. . . . .	409
13.7	Terms we construct to allow us to mirror the cancellations of the previous section. . . . .	413
13.8	The terms surviving from the analogue of figure 13.5, in which the common one-loop sub-diagram is the standard set. . . . .	415
13.9	Manipulation of diagram 12.42 under $\Lambda\partial_\Lambda _\alpha$ . . . . .	417
13.10	Diagram 12.43 and its subtractions. . . . .	419
13.11	The cancellation of non-computable contributions between dia- gram 13.49 and its subtractions. . . . .	420
13.12	Diagram 12.45 and its subtractions. . . . .	422

13.13	The cancellation of non-computable contributions between diagram 13.63 and its subtractions. . . . .	423
13.14	Diagram 12.46 and its subtractions. . . . .	423
13.15	The cancellation of non-computable contributions between diagram 13.73 and its subtractions. . . . .	423
13.16	Diagram 12.47 and its subtractions. . . . .	424
13.17	The terms remaining after cancellation of non-computable contributions to diagrams 13.81 and diagram 13.88 by their subtractions. . . . .	425
13.18	The first two diagrams are a re-expression of diagrams 13.44, 13.46, 13.51 and 13.53 and the final two are a re-expression of diagrams 13.55, 13.57, 13.67 and 13.69. . . . .	426
13.19	The result of the diagrammatic manipulation of diagrams 13.48, 13.65, 13.75 and 13.77—part I. . . . .	427
13.20	The result of the diagrammatic manipulation of diagrams 13.48, 13.65, 13.75 and 13.77—part II. . . . .	428
13.21	The result of processing diagrams 13.61, 13.62, 13.71, 13.72, 13.80, 13.97 and 13.101. . . . .	431
13.22	Diagrams 12.65, 12.64, 12.67 and 12.66 and their subtractions. . . . .	433
13.23	The cancellation of contributions between the diagrams of figure 13.22. . . . .	434
13.24	The LHS of the figure shows diagrams 12.49, 12.50 and their subtractions. The parent diagrams have been combined into a single term, with an additional factor of two. The right hand side shows the cancellation of contributions between the three diagrams of the RHS. . . . .	435
13.25	The top row of the figure shows diagram 12.51 and its subtraction. The bottom shows the cancellation of contributions between all three diagrams of the top row. . . . .	436
13.26	Subtractions (and additions) for diagrams 12.68–12.72. . . . .	437
13.27	Result of combining diagrams 12.68–12.72 with both their subtractions and additions. . . . .	438
13.28	Subtractions for diagrams 13.87 and 13.94. . . . .	439

13.29	The result of combining diagrams 13.87 and 13.94 with their subtractions. . . . .	439
13.30	Subtractions for diagrams 13.123–13.133. . . . .	440
13.31	Result of the cancellation of components between diagrams 13.123–13.133 and both the subtractions and additions of figure 13.30—part I. . . . .	441
13.32	Result of the cancellation of components between diagrams 13.123–13.133 and both the subtractions and additions of figure 13.30—part II. . . . .	442
13.33	Result of isolating computable and non-computable contributions to diagrams 13.134–13.137, achieved via an implicit intermediate step involving the construction of subtractions. . . . .	443
13.34	The result of manipulating diagrams 13.225–13.228. . . . .	446
13.35	The rearrangement of diagrams 13.161, 13.113 and 13.114; the cancellation of components between 13.111, 13.112 and 13.245, 13.246; the manipulation of diagrams 13.189 and 13.191. . . . .	447
13.36	Showing how we can redraw diagram 13.163. . . . .	448
13.37	A redrawing of the first two columns of figure 13.35 (up to $\mathcal{O}(\epsilon)$ corrections). . . . .	449
13.38	Result of combining diagrams 13.138–13.140 with diagrams 13.31–13.33. . . . .	450
13.39	The result of combining diagrams 13.268–13.270 with diagrams 13.34–13.36. . . . .	451
13.40	The result of combining diagrams 13.179–13.182 with diagrams 13.240–13.243. . . . .	452
13.41	Result of manipulating diagram 13.277. . . . .	453
13.42	Result of redrawing diagrams 13.249, 13.250, 13.253 and 13.254. . . . .	454
13.43	Combining the remaining terms which possess an element of the little set explicitly under the influence of NC. . . . .	455
13.44	Cancellation of non-computable contributions between diagrams 13.289–13.292 and 12.117–12.119. . . . .	455
13.45	Showing diagrams 13.266 and 13.267 combine with diagrams 13.141 and 13.142. . . . .	455

13.46	Flow of a three-point, tree level vertex viewed as part of a whole diagram. . . . .	462
B.1	The effective propagator relation. . . . .	482
B.2	The first step in re-drawing a diagram to yield a diagrammatic identity. . . . .	485
B.3	A diagrammatic identity. . . . .	485
B.4	Diagrammatic identity 9. . . . .	486
B.5	Diagrammatic identity 10. . . . .	486
B.6	Diagrammatic identity 11. . . . .	487
B.7	Diagrammatic identity 12 . . . . .	487
B.8	Four diagrams for which it has been demonstrated that they sum to zero when all fields are in the $A$ -sector. . . . .	487
C.1	The flow of a three-point, tree level vertex decorated by three wildcard fields. . . . .	490
C.2	Flow of a three-point, tree level vertex decorated by $A_\mu^1(p)$ , $A_\nu^1(-p)$ and a dummy field. . . . .	491
C.3	Flow of a four-point, tree level vertex decorated by $A_\mu^1(p)$ , $A_\nu^1(-p)$ and two dummy fields. . . . .	492

# List of Tables

2.1	Prescription for unifying the relationships (2.64), (2.65), (2.66) and (2.68). . . . .	79
3.1	The flavour changing effect of pushing forward and / or pulling back the momentum of a fermionic field on to some other field.	93
3.2	The flavour changing effect of pushing forward and / or pulling back the momentum of a fermionic field on to the end of a wine.	100
3.3	Algebraic realisation of the derivative striking the four-point vertices of diagrams 3.43 and 3.44, for different momentum routing.	129
7.1	The history of the four diagrams which are candidates for level-two manipulations. . . . .	203
9.1	Possible flavours of the fields of the diagrams of figure 9.8. . . .	314
13.1	Contributions to $\beta_2$ . . . . .	465
A.1	Summary of the gauge remainders in each sector . . . . .	481

## DECLARATION OF AUTHORSHIP

I, Oliver Jacob Rosten declare that the thesis entitled

The Manifestly Gauge Invariant Exact Renormalisation Group

and the work presented in it are my own. I confirm that:

- this work was done mainly while in candidature for a research degree at this University;
- no part of this thesis has previously been submitted for a degree or any other qualification at this University or any other institution;
- where I have consulted the published work of others, this is always clearly attributed;
- where I have quoted from the work of others, the source is always given. With the exception of such quotations, this thesis is entirely my own work;
- I have acknowledged all main sources of help;
- where the thesis is based on work done by myself jointly with others, I have made clear exactly what was done by others and what I have contributed myself;
- none of this work has been published before submission.

Signed: .....

Date: .....

# Acknowledgements

I would like to thank my supervisor, Tim Morris, for friendship, help and for setting me on the right path. I acknowledge the Southampton University Development Trust without the kind support of which, this work would never have happened.

Thanks to Stefano, for helping me when I first started learning about the ERG and for bearing the brunt of my enthusiasm. Thanks to Daniel for much appreciated help with the bibliography.

I would like to thank the SHEP group for far too many things to list but, most importantly, for teaching me the value of intellectual integrity.

In helping to relieve the immense stress of academic work, I express my debt to the great composers but, most especially, to J. S. Bach, Beethoven and the incomparable Schubert.

My deepest thanks I save for last. First, to my family, Esther, Edward and Judith whom I love and appreciate, very much.

Finally, I would like to thank Claire for her endless love and support. Without her, and what she has brought to my life, this piece of work (much like myself) would be a pale imitation of what it is now.

To Harvey

# Motivation

The original motivation for this work was the development of a tool, formulated in the continuum, for the non-perturbative study of gauge theories and, in particular, Quantum Chromodynamics (QCD).

The idea of using the Exact Renormalisation Group (ERG) in this context is not a new one [63]–[82]. Compared to these methods, the formalism that we present in this thesis is in its formative stages; indeed we are yet to even attempt a non-perturbative calculation.

Nevertheless, we believe that our formalism—the Manifestly Gauge Invariant ERG (MGI-ERG) [51]–[60]—has great potential. The fundamental reason for this confidence is that the MGI-ERG combines two of the most powerful ideas in quantum field theory (QFT), those of Wilsonian Renormalisation [1] and gauge invariance, treating them on an equal footing. A novel consequence of this is that, within our framework, gauge invariance is *manifest*. That there is no need to fix the gauge is, in itself, encouraging for non-perturbative applications, since Gribov copies [104], and all associated problems, are entirely avoided.

The formalism that this thesis builds upon (discussed in section 1.2.1) has already been used to compute the perturbative one-loop Yang-Mills  $\beta$ -function [52, 53, 57] (henceforth referred to as  $\beta_1$ )—which, up until the work presented here, was the only analytical calculation performed in continuum gauge theory without fixing the gauge.

Though an interesting result in its own right, the primary goal of computing  $\beta_1$  was to test the formalism. Given the successful outcome, it is an obvious question to ask why the formalism was not immediately applied to non-perturbative problems. The point is that whilst the calculation of  $\beta_1$  was

crucial in establishing the consistency of the formalism, there were many aspects of the formalism which remained un-tested, in this comparatively simple piece of work.

The initial aim of this thesis was to compute the perturbative two-loop Yang-Mills  $\beta$ -function (henceforth referred to as  $\beta_2$ ), thereby providing a far more stringent test our approach.<sup>1</sup> With this achieved, the hope was that the stage would be set for application to the non-perturbative domain.<sup>2</sup>

Whilst we are now at this stage, the successful calculation of  $\beta_2$  has also opened up entirely unforeseen avenues of research. In its initial incarnation, the computation of  $\beta_2$  was almost prohibitively long; though demonstrating the consistency of the MGI-ERG beyond reasonable doubt, the difficulty associated with this was ominous. However, since completing the calculation of  $\beta_2$ , a deep structure to the calculation has been revealed.

At a stroke, this has removed almost all the difficulty associated with computing  $\beta_2$  in the MGI-ERG. Moreover, there are encouraging indications that the extraction of numerical values for  $\beta_n$  may be easier than for competitive techniques.<sup>3</sup> (Currently,  $\beta_4$  is the highest loop  $\beta$ -function coefficient to be computed using traditional techniques; to appreciate the complexity of this calculation see [108, 109].) Further investigation of the structure of  $\beta$ -function coefficients is a piece of research which follows directly. More interesting, however, is to see whether the kind of simplifications we see here are also manifest themselves in the computation of perturbative amplitudes.

Thus, whilst the original motivation for this thesis was simply to provide the groundwork for a formalism with a view to applying it to the non-perturbative study of QCD, this emphasis has changed somewhat. In retrospect, what this work has achieved is not only to demonstrate the consistency of the MGI-ERG, but also to go some way towards illuminating its perturbative structure.

---

<sup>1</sup>Within a class of massless renormalisation schemes, both  $\beta_1$  and  $\beta_2$  are universal, allowing meaningful comparison between our result and others.

<sup>2</sup>Though we should note that the generalisation to QCD, by the inclusion of quarks, is not necessarily trivial—see section 14.3.

<sup>3</sup>Of course, this is of real use only if either the MGI-ERG can be used to compute amplitudes, or a map is made between our scheme and (say)  $\overline{MS}$ . We note that such a map has been constructed for a different gauge invariant ERG [83].

This latter point has proven interesting in its own right, thereby extending the usefulness of this work and going beyond its original aims.

# Structure of Thesis

This thesis is arranged into four parts. The first part details the setup and breaks down into two chapters. Chapter 1 introduces the work on which this thesis is based. In particular, the Exact Renormalisation Group Equation (ERGE) of [57] is introduced, and its diagrammatic interpretation described. In chapter 2 we modify the flow equation for subsequent applications detailed in this thesis and introduce new diagrammatics.

The second part details techniques developed for the new flow equation. In chapter 3 we describe a new set of diagrammatic techniques. Their application is illustrated in chapter 4 by applying them to the computation of  $\beta_1$ . This allows us to reduce  $\beta_1$  to a set of terms differentiated with respect to the ERG scale,  $\Lambda$ .

In chapter 5 we show how to evaluate these terms, developing the formalism to the level suitable for extraction of  $\beta_2$ .

In the third part we investigate how the reduction of  $\beta_1$  to a set of  $\Lambda$ -derivative terms can be greatly simplified. We introduce and develop the methodology in chapter 7. This guides us to a formula which automatically generates (essentially) the  $\Lambda$ -derivative terms for a  $\beta$ -function coefficient of arbitrary order, up to two types of unprocessed terms. First, there are the ‘gauge remainders’ which we treat in chapters 8–10. Secondly, there are the ‘ $\mathcal{O}(p^2)$ ’ terms. A full treatment of these is beyond the scope of this thesis, but we comment on them in chapter 11.

The fourth and final part is devoted to the computation of  $\beta_2$  and our conclusions. In chapter 12, we use the results of chapter 10 to help us write down an expression for  $\beta_2$  in which all terms are differentiated with respect to  $\Lambda$  (there is an additional set of terms, the ‘ $\alpha$ -terms’, which vanish in a certain

limit). In chapter 13 we numerically evaluate this expression, using the results of chapter 5. Finally, in chapter 14, we conclude.

During a first reading of this thesis, it is recommended that the third part is omitted. As far as the rest of the thesis is concerned, the main result of this part is to allow us to jump straight to an expression for  $\beta_2$  in terms of (essentially)  $\Lambda$ -derivative diagrams. It should be noted that this expression can, in principle, be obtained with the methodology of part II and the diagrammatic identities introduced in part III, alone.

The work of chapter 1 is based on existing, published work. The modification of the flow equation of [57], done in chapter 2, is based on unpublished work by my collaborators, Tim Morris and Stefano Arnone. The remaining work of chapter 2 is a mixture of unpublished work by myself and Tim Morris. All the remaining work is my own, with the exception of that in section 13.6, which is based on unpublished work by Tim Morris.

**Part I**

**Setup**

# Chapter 1

## Introduction

The history of the Exact Renormalisation Group dates back to the seminal paper of Wilson and Kogut [1] and to the contemporary work of Wegner and Houghton [2]. Since then, it has gained a reputation as a powerful and flexible technique for addressing a wealth of problems in quantum field theory (QFT) (see e.g. [1]–[91]).

In this thesis, we will be dealing with a particular adaptation of the ERG for gauge theory [51]–[60]. Our starting point, however, is the simpler scalar field case [1, 2, 3], [7]–[25] which, in section 1.1, we use to illustrate some general features of ERGs. This then allows a transparent generalisation to the gauge theory case, done in section 1.2.

### 1.1 An ERG for Scalar Field Theory

Though the original work on the ERG [1, 2] was done in scalar field theory, we will utilise the equivalent but simpler analysis due to Polchinski [3]. In all that follows, we work in  $D$  dimensional Euclidean space.

#### 1.1.1 The Polchinski Equation

Given a scalar field theory, parametrised by  $\phi$ , we introduce two scales, by hand. The first is the bare cutoff,  $\Lambda_0$ ; physically, this can be taken to represent the scale at which our QFT ceases to be a good description of the phenomena we are trying to describe. Secondly, we introduce a much lower scale,  $\Lambda$ , henceforth referred to as the effective cutoff.

In scalar field theory, this procedure is essentially trivial, since there is no symmetry forbidding the naïve implementation of a cutoff. Much of the subtlety in the gauge theory case is due to the fact that precisely the opposite of this is true (see section 1.2.1).

The next step is to integrate out degrees of freedom between  $\Lambda_0$  and  $\Lambda$ . The effect of this procedure is to encode the information carried by the high energy modes into the effective action,  $S_\Lambda \equiv S$  [1, 2, 3], [16]–[20]. Rather than supposing that the remaining modes are sharply cutoff at  $\Lambda$ , a general cutoff function  $c_p \equiv c(p^2/\Lambda^2)$  is introduced, where  $p$  denotes the momentum of some mode. Of  $c_p$ , we demand the following:

1. that it dies off quickly enough as its argument tends to infinity; this ensures that our theory is properly regulated;
2. that  $c(0) = 1$ , ensuring that the IR behaviour of our theory is unaffected by the precise details of the UV cutoff.

The central ingredient for all that now follows is the Exact Renormalisation Group Equation (ERGE), or flow equation, which describes how the effective action varies with  $\Lambda$ . To enable us to write this down we introduce the ‘seed action’,  $\hat{S}$ , which we take to be equal to the regularised kinetic term [24],

$$\hat{S} = \frac{1}{2} \partial_\mu \phi \cdot c^{-1} \cdot \partial_\mu \phi,$$

where, for the functions  $f(x)$  and  $g(y)$  and a momentum space kernel  $W(p^2/\Lambda^2)$ ,

$$f \cdot W \cdot g = \iint d^D x d^D y f(x) W_{xy} g(y), \quad (1.1)$$

with

$$W_{xy} \equiv \int \frac{d^D p}{(2\pi)^D} W(p^2/\Lambda^2) e^{ip \cdot (x-y)}. \quad (1.2)$$

Defining  $\Sigma = S - 2\hat{S}$ , the Polchinski equation is, up to a discarded vacuum energy [3, 19, 20, 24],

$$\Lambda \partial_\Lambda S = -\frac{1}{\Lambda^2} \frac{\delta S}{\delta \phi} \cdot c' \cdot \frac{\delta \Sigma}{\delta \phi} + \frac{1}{\Lambda^2} \frac{\delta}{\delta \phi} \cdot c' \cdot \frac{\delta \Sigma}{\delta \phi}, \quad (1.3)$$

where a primed function is differentiated with respect to its argument. For what follows, it is useful to recast this equation. First, we define

$$\dot{X} = -\Lambda \partial_\Lambda X. \quad (1.4)$$

Secondly, we introduce a new function,

$$\Delta_p \equiv \frac{c_p}{p^2}, \quad (1.5)$$

and now rewrite equation (1.3) as follows:

$$\dot{S} = \frac{1}{2} \frac{\delta S}{\delta \phi} \cdot \dot{\Delta} \cdot \frac{\delta \Sigma}{\delta \phi} - \frac{1}{2} \frac{\delta}{\delta \phi} \cdot \dot{\Delta} \cdot \frac{\delta \Sigma}{\delta \phi}. \quad (1.6)$$

This recasting is done in anticipation of the crucial role to be played by  $\Delta_p$ . We notice from equation (1.5) that this object is, in our scalar example at any rate, just the regularised propagator [19, 24, 25]. That the regularised propagator appears in the flow equation is not an automatic (or necessary) feature of an ERGE; in scalar field theory, it generically<sup>1</sup> occurs as a consequence of a choice we are free to make for the solutions of the flow equation [24, 25]. In Yang-Mills theory, things are more subtle. When we adapt our framework to deal with Yang-Mills theory (see section 1.2.2) we find that we need never fix the gauge [52, 53] and so cannot even define a propagator. Nonetheless, in this case, we will find that there is an object which looks similar to and plays a role close to that of a regularised propagator, which does appear in the flow equation. Thus, we refer to  $\Delta_p$  as an effective propagator, mindful that we must not take its relationship to a *bona fide* propagator for granted.

### 1.1.2 Properties of the Polchinski Equation

There are four vital properties of the Polchinski equation, which play a central role in extending the formalism to encompass Yang-Mills theory:

1. All ingredients of the flow equation are infinitely differentiable in momenta. This property, referred to as quasilocality [21], guarantees that each RG step  $\Lambda \mapsto \Lambda - \delta\Lambda$  does not generate IR singularities [1].
2. The flow corresponds to integrating out degrees of freedom; this simply follows from the derivation of the Polchinski equation given in [20].
3. The partition function is left invariant under the flow, since  $e^{-S}$  transforms into a total derivative:

$$\Lambda \partial_\Lambda e^{-S} = \frac{1}{2} \frac{\delta}{\delta \phi} \cdot \dot{\Delta} \cdot \left( \frac{\delta \Sigma}{\delta \phi} e^{-S} \right). \quad (1.7)$$

---

<sup>1</sup>As opposed to in the special case of the Polchinski equation.

This ensures that, starting with some QFT at a high scale, our effective action is guaranteed to still be describing the same physics at a very much lower scale (implicitly assuming the first point, above).

4. The flow is self-similar [92]. This demands that the effective action depends only on the scale  $\Lambda$  (this can be straightforwardly extended to massive theories [21]), and thus is a ‘perfect action’ [93]. By definition, such actions lie on a renormalised trajectory guaranteeing, amongst other things, the existence of a continuum limit [20].

An important consequence of these points is that locality, a property which is generally not manifest in the Wilsonian effective action at some finite value of  $\Lambda$ , is guaranteed [57]. Due to invariance of the partition function under the flow (and the fact that the flow is free of IR divergences), we know that, if we are dealing with a local action at some scale, then we must have been dealing with a local action at all higher scales and are guaranteed to be dealing with a local action at all lower scales. Now, we know that the flow lies on a renormalised trajectory and that this trajectory is controlled by the free-field (a.k.a. Gaussian) fixed point. To obtain a continuum limit, the flow is tuned such that it passes arbitrarily close to the free-field fixed point. At this point, the action—being that of a non-interacting field theory—is local. Hence, locality is guaranteed at all other points along the flow.

It is worth commenting on the end of the renormalised trajectory, where  $\Lambda \rightarrow \infty$ . The action here is just the bare action, whose form is determined by the flow equation, but whose precise details amount to choices we are free to make. As is generally our philosophy, we leave these choices either unmade or at least implicit (see particularly section 13.6).

The crucial point recognised in [52] is that the Polchinski equation is just a special case of an equation with the above features; we now take these features to *define* what we mean by an ERGE. This idea is more rigorously explored in [61, 62], where it was realised that these generalised ERGs can be parametrised by a functional,  $\Psi$ , which induces a field redefinition along the flow.

With this in mind, we now make a non-trivial modification to the Polchinski equation: we desist from restricting the seed action to being just the kinetic term and allow it to become general, insisting only on the following requirements: first, that the vertices of  $\hat{S}$  be infinitely differentiable and secondly that  $\hat{S}$  leads to convergent momentum integrals [24, 25, 57]. These properties which, generally speaking, we assume to be implicitly fulfilled, are necessary for the consistency of the quantum theory (*ibid.*).

Having made this modification, we must now check that our new flow equation satisfies the requisite requirements.

From equation (1.7) it is clear that the partition function will still be left invariant under the flow. That the flow equation corresponds to integrating out can be argued as follows [52]:

1. we can ensure that the flow equation is regularised, so all momentum integrals are bounded;
2.  $\Lambda$  is the UV cutoff: momenta larger than some scale  $q$  must vanish in the limit  $q/\Lambda \rightarrow \infty$ ;
3. as  $\Lambda \rightarrow 0$  all remaining contributions from any non-vanishing momentum scale disappear;
4. *but* the physics is invariant under the flow.
5. Contributions from a given momentum scale must, therefore, be encoded in the effective action: we have integrated out!

The self similarity of the flow is unchanged: the flow equation is written only in terms of renormalised quantities, at the scale  $\Lambda$ . Thus, as our new flow equation satisfies the requisite requirements, it is perfectly valid [24, 25, 52, 57].

It is, of course, an obvious question as to what we have gained from this. Primarily, this generalisation is necessary if we wish to be able to treat Yang-Mills theory, as we will see in section 1.2.2. However, the generalisation is also of importance in its own right, as we now discuss.

The basic idea is that we do not expect the generalisation of the seed action to change the result of a computation of some universal quantity. Whilst this

follows from the validity of the new flow equation, there is also a useful physical interpretation: the freedom of  $\hat{S}$  represents the continuum version of the choice of blocking transformations in the application of Wilsonian RG techniques to latticised problems [1, 24].

That a calculation must yield a result independent of the precise details of many of the ingredients (we leave the cutoff functions general, too) leads to a highly constrained calculational procedure. Generally speaking, the only way to remove dependence on an instance of an unspecified (non-universal) component of  $\hat{S}$  is for there to be a second instance, of opposite sign. Indeed, this is so constraining that calculations can be performed almost entirely diagrammatically; in this way, the (universal) scalar one-loop and two-loop  $\beta$ -functions have been correctly evaluated [24, 25], as has the one-loop Yang-Mills  $\beta$ -function [57]. One of the major results of this thesis is a computation of the two-loop Yang-Mills  $\beta$ -function.

Now, whilst the freedom to leave the seed action largely unspecified has guided us to an efficient calculational procedure we have, in some sense, complicated the issue. Certainly, in scalar field theory where a general seed action is not required, we have made life harder for ourselves by leaving it as general as possible. The most obvious resolution to this is to simply regard the freedom of the seed action as scaffolding: it has guided us to an efficient calculational procedure, but now we can dispense with it, keeping the procedure but choosing the simplest form for the seed action, consistent with our approach.

However, a consequence of one of the other major results of this thesis is that this point seems to be moot. Certainly, for the calculation of  $\beta$ -function coefficients—to any order in perturbation theory—it is possible to show that explicit dependence on  $\hat{S}$  is guaranteed to cancel out; indeed we give a compact expression for the diagrammatic form of  $\beta$ -function coefficients, after the cancellations have occurred (see part III).<sup>2</sup> Thus, at least up until this stage of a calculation, where any remaining seed action dependence is now implicit, it makes no difference how complicated a seed action has been chosen; we can simply bypass the entire procedure of cancelling explicit instances of seed

---

<sup>2</sup>Strictly, what we present is an incomplete expression for Yang-Mills theory. However, the scalar case is effectively contained within this partial analysis.

action components. Moreover, there are intriguing indications that, at any loop order, even the implicit seed action dependence cancels out, though the investigation of this will be saved for the future [60].

## 1.2 The Manifestly Gauge Invariant Exact Renormalisation Group

With the review of ERGs for scalar field theory behind us, we are now in a position to generalise the formalism for the application to Yang-Mills theory. The central issue is how to reconcile non-Abelian gauge theory with the notion of a momentum cutoff, since a straightforward implementation of the latter breaks the former. One approach is to work in a gauge fixed formalism and to allow this breaking to occur. The effects of the breaking can be kept track of with the ‘modified Ward Identities’ and it is hoped that they vanishes in the limit where the momentum cutoff is removed [8], [26]–[48].

The approach upon which this thesis is based is one in which a regulator for Yang-Mills is built that respects gauge invariance [6]; we review this in section 1.2.1.<sup>3</sup> Then, in section 1.2.2 we detail the construction of a regulated, (manifestly) gauge invariant flow equation. Some important properties of the flow equation are discussed in sections 1.2.3–1.2.5. Much of the material in [57] is repeated in this part of the thesis, as it forms the basis for everything that follows. However, for the diagrammatic techniques in particular, we try to simplify and clarify the exposition, wherever possible.

### 1.2.1 Regularisation

In this section, we review the regularisation of Yang-Mills theory<sup>4</sup> introduced by Arnone *et al.* [6]. This is a three-step procedure. First, we introduce the notion of a gauge invariant cutoff function [52]. However, just as with

---

<sup>3</sup>For an alternative approach, based on the Vilkovisky-DeWitt [94, 95] formalism, see [49, 50].

<sup>4</sup>Strictly speaking, this regularisation is valid for  $SU(N)$  Yang-Mills theory. Generalisation to other gauge groups should be straightforward, though we make no such attempt to do so here.

gauge invariant higher derivative regularisation [96, 97, 98] (to which our approach is closely related), this proves insufficient to completely regulate the theory [6, 107]: certain one-loop divergences survive. To cure these divergences, we introduce a set of gauge invariant Pauli-Villars (PV) fields. Whereas these were originally put in by hand [51, 52, 53], it was later recognised that they arise in a natural way [4, 5, 6]. Specifically, we embed our Yang-Mills theory in a certain graded Lie group which, when broken in a particular manner, yields a set of heavy fields which provide the necessary PV regularisation. Finally, a pre-regulator is required to consistently define the regularisation scheme [6].

Rather than following the historical approach of first introducing the covariantized cutoff functions and then implementing the PV regularisation, we will follow the approach of [6], where the embedding of  $SU(N)$  gauge theory into the graded lie algebra,  $SU(N|N)$ , is performed first. It is logical to proceed in this manner, not least because the covariantised cutoff regularisation applies to the entire  $SU(N|N)$  gauge theory, and not just the physical  $SU(N)$  part. Indeed, this makes it particularly clear that the problem of overlapping divergences, commonly associated with PV regularisation, is avoided in this set-up: because the covariantised cutoff regularisation applies to all fields, it applies to diagrams with external PV fields, obviating the problem.

### $SU(N|N)$ Regularisation

A detailed discussion of the  $SU(N|N)$  Lie superalgebra can be found in [99]. However, we follow [6], which focuses on the elements necessary for our purposes.

We begin by looking at the graded Lie supergroup,  $SU(N|M)$ . The defining representation is furnished by Hermitian  $(N + M) \times (N + M)$  matrices,

$$\mathcal{H} = \begin{pmatrix} H_N & \theta \\ \theta^\dagger & H_M \end{pmatrix},$$

where  $H_N(H_M)$  is an  $N \times N(M \times M)$  Hermitian matrix with complex bosonic elements and  $\theta$  is an  $N \times M$  matrix whose elements are complex Grassmann numbers.

The supertrace—which replaces the trace as the natural cyclic invariant—is

defined by

$$\text{str } \mathcal{H} \equiv \text{tr } \sigma \mathcal{H},$$

where

$$\sigma \equiv \sigma_3 = \begin{pmatrix} \mathbb{1}_N & 0 \\ 0 & -\mathbb{1}_N \end{pmatrix}.$$

When expressing an element of the group in terms of the generators and corresponding superangles, we use the convention that only the superangles carry Grassmann character. Hence, the generators are taken to be Hermitian, complex valued matrices; the superalgebra is thus constructed via both commutators and anticommutators. The matrices that form the superalgebra of  $SU(N|M)$  must be supertraceless.

For what follows, it will be instructive to focus on the bosonic part of the superalgebra. The traceless parts of  $H_N$  and  $H_M$  furnish the defining representation of the  $SU(N)$  and  $SU(M)$  groups, respectively. The orthogonal, traceful part of  $\mathcal{H}$  yields a  $U(1)$ . Thus, the bosonic part of the  $SU(N|M)$  superalgebra forms an  $SU(N) \times SU(M) \times U(1)$  subalgebra.

When we specialise  $M = N$ —as we now do—the  $U(1)$  subalgebra is generated by the identity,  $\mathbb{1}_{2N}$ . Note, though, that  $SU(N|N)$  cannot be decomposed into the product of smaller algebras, since the identity is generated by fermionic elements of the algebra. For example,

$$\{\sigma_1, \sigma_1\} = 2\mathbb{1}_{2N},$$

where

$$\sigma_1 = \begin{pmatrix} 0 & \mathbb{1}_N \\ \mathbb{1}_N & 0 \end{pmatrix}.$$

We define the generators to be  $S_\alpha \equiv \{\mathbb{1}, T_A\}$ , where the rank of  $\mathbb{1}$  is to be henceforth determined by the context. The generator  $\mathbb{1}$  has been separated out, in recognition of the special role it will play. The remaining generators are given by  $T_A$ , where  $A$  runs over the  $2(N^2 - 1)$  bosonic generators and the  $2N^2$  fermionic generators.

An element of the  $SU(N|N)$  superalgebra can thus be written

$$\begin{aligned} \mathcal{H} &= \mathcal{H}^\alpha S_\alpha = \mathcal{H}^0 \mathbb{1} + \mathcal{H}^A T_A, \\ (\mathcal{H})^i_j &= \mathcal{H}^0 \delta^i_j + \mathcal{H}^A (T_A)^i_j. \end{aligned}$$

The Killing supermetric is defined to be

$$h_{\alpha\beta} = 2\text{str} (S_\alpha S_\beta),$$

where the generators are normalised such that

$$h_{\alpha\beta} = \left( \begin{array}{c|c|c|c} 0 & & & \\ \hline & 1 & & \\ & & 1 & \\ & & & \ddots \\ \hline & & -1 & \\ & & & -1 \\ & & & \ddots \\ \hline & & & \begin{array}{cc} 0 & i \\ -i & 0 \\ & 0 & i \\ & -i & 0 \\ & & & \ddots \end{array} \end{array} \right). \quad (1.8)$$

$\underbrace{\hspace{1.5cm}}_{U(1)} \quad \underbrace{\hspace{2.5cm}}_{SU_1(N)} \quad \underbrace{\hspace{2.5cm}}_{SU_2(N)} \quad \underbrace{\hspace{2.5cm}}_{\text{Fermionic}}$

The supermetric is not invertible, on account of the  $U(1)$  generator commuting with everything. However, we can usefully define the restriction of  $h_{\alpha\beta}$  to the  $T_A$  space:

$$g_{AB} = 2\text{str} (T_A T_B) = h_{AB},$$

which does have an inverse:

$$g_{AB} g^{BC} = g^{CB} g_{BA} = \delta_A^C.$$

This metric can be used to raise and lower indices:

$$X_A \equiv g_{AB} X^B \Rightarrow X^A = X_B g^{AB} \neq X_B g^{BA},$$

the inequality following from (1.8). The requirement that  $X^A T_A = X_A T^A$  guides us to the dual relations for raising and lowering indices on the generators:

$$T^A \equiv T_B g^{BA}.$$

The completeness relation for the  $T^A$  is

$$(T^A)^i_j (T_A)^k_l = \frac{1}{2} \delta_l^i (\sigma_3)^k_j - \frac{1}{4N} \left[ \delta_j^i (\sigma_3)^k_l + (\sigma_3)^i_j \delta_l^k \right]. \quad (1.9)$$

Having introduced the  $SU(N|N)$  algebra, we now demonstrate how we can utilise it to construct a set of regulating fields for our physical  $SU(N)$  gauge theory. The physical gauge theory has connection  $A_\mu^1(x) \equiv A_{a\mu}^1 \tau_1^a$ , where  $\tau_1^a$  are the generators of  $SU(N)$ , normalised to  $\text{tr}(\tau_1^a \tau_1^b) = \delta^{ab}/2$ .

We now embed  $A_\mu^1$  into the superfield  $\mathcal{A}_\mu \equiv \mathcal{A}_\mu^\alpha S_\alpha$ :

$$\mathcal{A}_\mu = \begin{pmatrix} A_\mu^1 & B_\mu \\ \bar{B}_\mu & A_\mu^2 \end{pmatrix} + \mathcal{A}_\mu^0 \mathbb{1}.$$

$A^2$  is an unphysical copy of our original  $SU(N)$  gauge theory.  $B$  and  $\bar{B}$  are unphysical, wrong statistics (i.e. fermionic) gauge fields; it is these that will acquire mass and provide PV regularisation. Lastly, there is a central term, corresponding to the field  $\mathcal{A}_\mu^0$ . In chapters 2 and 3 we will, for the first time, arrive at a full understanding of the role that this field plays, within the MGI-ERG.

For much of this chapter, it will prove useful to treat the block diagonal and block off-diagonal components of  $\mathcal{A}$  together, which we represent by  $A$  and  $B$ , respectively. Whether  $B$  refers to both block-off diagonal components of just to the top-most one depends on the context; we hope this is not confusing.

Construction of an  $SU(N|N)$  gauge theory proceeds in the usual manner. First, we define the covariant derivative

$$\nabla_\mu = \partial_\mu - i\mathcal{A}_\mu \tag{1.10}$$

where, for future convenience, we have scaled out the coupling  $g$ . The superfield strength is now just  $\mathcal{F}_{\mu\nu} = i[\nabla_\mu, \nabla_\nu]$ . In anticipation of the covariantised cutoff regularisation, the kinetic term will be of the form

$$\text{str} \mathcal{F}_{\mu\nu} \left( \frac{\nabla}{\Lambda} \right)^n \cdot \mathcal{F}_{\mu\nu} \tag{1.11}$$

where the dot, in this context, tells us that  $\nabla$  acts via commutation.

There are a number of important things to note about the kinetic term. The first is that, since it is built out of commutators, it does not have an  $\mathcal{A}^0$  component. Thus, if  $\mathcal{A}^0$ , were to appear anywhere else in the action, it would act as a Lagrange multiplier. To avoid the unwanted constraints that this would

entail, we demand that the action is independent of  $\mathcal{A}^0$ .<sup>5</sup> Hence, in addition to being invariant under supergauge transformations, parameterised by  $\Omega$ , the action is also invariant under ‘no- $\mathcal{A}^0$ ’ symmetry [6, 57, 55]:  $\delta\mathcal{A}_\mu^0(x) = \lambda_\mu(x)$ . Hence, the action is invariant under the shift

$$\delta\mathcal{A}_\mu = \nabla_\mu \cdot \Omega + \lambda_\mu \mathbb{1}. \quad (1.12)$$

The second point about the kinetic term (1.11) is that the supertrace structure causes  $A^2$  to come with the wrong sign action, leading to a violation of unitarity [6]. We will return to this issue after a discussion of the breaking of  $SU(N|N)$ , to which we now turn.

To break  $SU(N|N)$  down to its bosonic subgroup  $SU(N) \times SU(N) \times U(1)$ , we introduce the superscalar field  $\mathcal{C}$  which transforms under the adjoint representation of  $U(N|N)$  [6]:

$$\mathcal{C} = \begin{pmatrix} C^1 & D \\ \bar{D} & C^2 \end{pmatrix}. \quad (1.13)$$

Note that we have not factored out  $\mathcal{C}^0$ :  $C^1$ , unlike  $A^1$ , is not identified with a physical field and so it is not an inconvenience to allow it to contain a  $\mathcal{C}^0$  component. Under supergauge transformations,

$$\delta\mathcal{C} = -i[\mathcal{C}, \Omega].$$

The idea now is to allow  $\mathcal{C}$  to develop a vacuum expectation value along the  $\sigma$  direction, thereby spontaneously breaking the  $SU(N|N)$  invariance, via the Higgs mechanism. The fermionic fields,  $B$  and  $D$ , acquire masses of order  $\Lambda$ . If we were to work in the unitarity gauge, then  $B$  eats the Goldstone fermion,  $D$ . However, we do not fix the gauge and so these two fields mix, under gauge transformations. This observation underpins the diagrammatic techniques of [57] and, as a consequence, is of vital importance to much of the work that follows.

One of the necessary properties that our regularisation scheme must obey is that any unphysical regulating fields decouple, in the limit that the symmetry

---

<sup>5</sup>We cannot, however, simply get rid of  $\mathcal{A}^0$ , since it is generated by (fermionic) gauge transformations [6]. It is possible to modify the representation of the Lie bracket [99, 6] to remove  $\mathcal{A}^0$ , but we do not pursue this any further as it seems to complicate matters.

breaking scale tends to infinity. The fermionic fields and the bosonic components of the superhiggs field can be given an arbitrarily high mass, decoupling as required. The field  $A^2$ , on the other hand, remains massless. However, it only communicates with the physical  $A^1$  field via the heavy fermionic fields; the lowest dimension effective interaction,

$$\frac{1}{\Lambda^4} \text{tr} \left( F_{\mu\nu}^1 \right)^2 \text{tr} \left( F_{\mu\nu}^2 \right)^2,$$

is irrelevant guaranteeing that, if our theory is renormalisable, then  $A^2$  will decouple, courtesy of the Appelquist-Carazzone theorem [100]. Once our covariant cutoff regularisation is in place, our theory will indeed be renormalisable, so long as  $D \leq 4$ . Thus, in the limit that  $\Lambda \rightarrow \infty$ , we recover our physical, unitary,  $SU(N)$  gauge theory.

We conclude this section by describing how to perform functional derivatives with respect to  $\mathcal{A}$  and  $\mathcal{C}$ . This is straightforward in the latter case:  $\mathcal{C}$  is an unconstrained superfield ( $\mathcal{A}$ , on the other hand, must be supertraceless which leads to complications) and so [53, 57, 6]:

$$\frac{\delta}{\delta \mathcal{C}} \equiv \begin{pmatrix} \frac{\delta}{\delta C^1} & -\frac{\delta}{\delta \bar{D}} \\ \frac{\delta}{\delta D} & -\frac{\delta}{\delta C^2} \end{pmatrix}.$$

Following [53, 57] we introduce the constant supermatrices  $X$  and  $Y$  and, neglecting the irrelevant spatial dependence, schematically represent first supersowing, whereby two supertraces are sown together:

$$\frac{\partial}{\partial \mathcal{C}} \text{str} \mathcal{C} Y = Y \implies \text{str} X \frac{\partial}{\partial \mathcal{C}} \text{str} \mathcal{C} Y = \text{str} X Y, \quad (1.14)$$

and secondly supersplitting, whereby a single supertrace is split into two supertraces:

$$\text{str} \frac{\partial}{\partial \mathcal{C}} X \mathcal{C} Y = \text{str} X \text{str} Y. \quad (1.15)$$

For  $\mathcal{A}$ , however, we define [6]

$$\frac{\delta}{\delta \mathcal{A}_\mu} \equiv 2T_A \frac{\delta}{\delta A_{A\mu}} + \frac{\sigma}{2N} \frac{\delta}{\delta \mathcal{A}_\mu^0}, \quad (1.16)$$

where  $T_A$ , as before, are the traceless generators of  $SU(N|N)$  i.e.

$$\mathcal{A}_\mu = \mathcal{A}_\mu^0 \mathbb{1} + \mathcal{A}_\mu^A T_A.$$

It is not surprising that, in this context, we do not have exact supersowing and supersplitting as we had above; rather, there will be corrections,

$$\text{str } X \frac{\partial}{\partial \mathcal{A}} \text{str } \mathcal{A} Y = \text{str } X Y - \frac{1}{2N} \text{str } X \text{tr } Y \quad (1.17)$$

$$\text{str } \frac{\partial}{\partial \mathcal{A}} X \mathcal{A} Y = \text{str } X \text{str } Y - \frac{1}{2N} \text{tr } X Y, \quad (1.18)$$

which follow from the completeness relation (1.9).

Under supergauge transformations, the functional derivatives transform as follows [57]:

$$\delta \left( \frac{\delta}{\delta \mathcal{C}} \right) = -i \left[ \frac{\delta}{\delta \mathcal{C}}, \Omega \right] \quad (1.19)$$

$$\delta \left( \frac{\delta}{\delta \mathcal{A}_\mu} \right) = -i \left[ \frac{\delta}{\delta \mathcal{A}_\mu}, \Omega \right] + i \frac{1}{2N} \text{tr} \left[ \frac{\delta}{\delta \mathcal{A}_\mu}, \Omega \right]. \quad (1.20)$$

Notice that  $\delta/\delta \mathcal{A}$  does not transform homogeneously: there is a correction term which ensures that  $\delta/\delta \mathcal{A}$  remains traceless. This proves important when we come to construct our flow equation: the structure of the flow equation must be such that the correction term vanishes.

### Covariant Cutoff Regularisation

The key to incorporating a covariantised cutoff is the appropriate generalisation of equations (1.1) and (1.2). Thus, we consider replacing  $f$  and  $g$  with two supermatrix representations,  $u$  and  $v$ . Knowing that our aim is to create a supergauge invariant, we use this to define what we mean by the covariantisation of the kernel,  $W$  [52, 57]:

$$u \{W\}_{\mathcal{A}} v = \sum_{n=0}^{\infty} \int d^D x d^D y d^D x_1 \cdots d^D x_n \overline{W}_{\mu_1 \cdots \mu_n}(x_1, \dots, x_n; x, y) \text{str} [u(x) \mathcal{A}_{\mu_1}(x_1) \cdots \mathcal{A}_{\mu_n}(x_n) \cdot v(y)] \quad (1.21)$$

where, without loss of generality, we can demand that  $u \{W\}_{\mathcal{A}} v = v \{W\}_{\mathcal{A}} u$ . The subscript  $\mathcal{A}$  tells us that the covariantisation involves only the supergauge field,  $\mathcal{A}$ ; we will involve the superscalar  $\mathcal{C}$ , shortly. The  $\overline{W}_{\mu_1 \cdots \mu_n}(x_1, \dots, x_n; x, y)$  are called the vertices of the ‘wine’  $\{W\}_{\mathcal{A}}$ . Each of the  $\mathcal{A}$ s in (1.21) acts via commutation on the expression to its right, as indicated by the dot between

$\mathcal{A}_{\mu_n}$  and  $v(y)$ .<sup>6</sup>

By demanding this commutator structure, we ensure that the wines respect no- $\mathcal{A}^0$  symmetry. Moreover, since  $\mathbb{1}$  commutes with everything, if  $v = \mathbb{1}g(y)$  for all  $y$ , only the term corresponding to the zero-point wine survives:

$$u \{W\}_{\mathcal{A}} \mathbb{1}g(y) = (\text{str } u) \cdot W \cdot g. \quad (1.22)$$

This identity is of particular importance. Indeed, in section 1.2.2, following [57], we will show that it is actually required if our flow equation is to be supergauge invariant. The relationships between the wine vertices arising from supergauge invariance are discussed in sections 1.2.4 and 3.1.2.

Rather than working with the wine vertices,  $\overline{W}$ , of (1.21), it is more convenient to expand out the commutators. Doing so, we relabel the supergauge fields that appear on the r.h.s. of  $v(y)$  in terms of  $\mathcal{A}_{\nu_i}(y_i)$  [53]:

$$\begin{aligned} u \{W\}_{\mathcal{A}} v &= \sum_{m,n=0}^{\infty} \int d^D x d^D y d^D x_1 \cdots d^D x_n d^D y_1 \cdots d^D y_m \\ &W_{\mu_1 \cdots \mu_n, \nu_1 \cdots \nu_m}(x_1, \dots, x_n; y_1, \dots, y_m; x, y) \\ &\text{str} [u(x) \mathcal{A}_{\mu_1}(x_1) \cdots \mathcal{A}_{\mu_n}(x_n) v(y) \mathcal{A}_{\nu_1}(y_1) \cdots \mathcal{A}_{\nu_m}(y_m)]. \end{aligned} \quad (1.23)$$

In the case where both  $m, n = 0$ , we drop the arguments  $x_1 \cdots x_n$  and  $y_1 \cdots y_m$ . The resulting vertex, which we denote simply by  $W_{xy}$ , will commonly be referred to as a ‘zero-point’ wine. A wine vertex with an additional argument is a ‘one-point’ wine, and so forth.

The new wine vertices,  $W_{\mu_1 \cdots \mu_n, \nu_1 \cdots \nu_m}(x_1, \dots, x_n; y_1, \dots, y_m; x, y)$ , are related to the  $\overline{W}$ ; from these relationships there follows a set of identities between the various new vertices—the ‘coincident line identities’ of [52] and [53]. We give these in momentum space:

$$\begin{aligned} &W_{\mu_1 \cdots \mu_n, \nu_1 \cdots \nu_m}(p_1, \dots, p_n; q_1, \dots, q_m; r, s) \\ &= (-)^m \sum_{\text{interleaves}} W_{\lambda_1 \cdots \lambda_{m+n}}(k_1, \dots, k_{m+n}; r, s), \end{aligned} \quad (1.24)$$

where the sum runs over all interleaves of the sequences  $p_1^{\mu_1}, \dots, p_n^{\mu_n}$  and  $q_m^{\nu_m}, \dots, q_1^{\nu_1}$ . In other words, the ordered sequence  $k_1^{\lambda_1}, \dots, k_{m+n}^{\lambda_{m+n}}$  comprises

---

<sup>6</sup>In determining what, precisely, each  $\mathcal{A}$  acts on, we arrange for the argument of the (cyclically invariant) supertrace to be of the form indicated in (1.21) i.e. if the fields have been cycled around, we bring them back to the form of (1.21).

all arrangements of  $p^\mu$ s and  $q^\nu$ s such that the  $p^\mu$ s are ordered with respect to each other and the  $q^\nu$ s are in reverse order.

For our purposes, we will require not (1.24), but a relationship which follows:<sup>7</sup>

$$W_{\lambda_1 \dots \lambda_n}(k_1, \dots, k_n; r, s) + W_{;\lambda_1 \dots \lambda_n}(; k_1, \dots, k_n; r, s) + \sum_{m=1}^{n-1} W_{\lambda_1 \dots \lambda_m, \lambda_{m+1} \dots \lambda_n}(k_1, \dots, k_m; k_{m+1}, \dots, k_n; r, s) = 0. \quad (1.25)$$

To introduce  $\mathcal{C}$ s is straightforward and can be done in the most convenient manner. In [57] the strategy used was to restrict instances of  $\mathcal{C}$ s to both ends of a wine, and demand that they act via commutation. Thus, the ‘full wine’,  $\{W\}$  was defined

$$u\{W\}v = u\{W\}_{\mathcal{A}}v - \frac{1}{4}\mathcal{C} \cdot u\{W_m\}_{\mathcal{A}}\mathcal{C} \cdot v, \quad (1.26)$$

where  $W_m(p, \Lambda)$  is just some new kernel.

We will essentially use equation (1.26) but choose to lift the restriction that instances of  $\mathcal{C}$  occur only at the ends of the wine. We do this because, as we will see in section 2.4, it is natural in the diagrammatic framework we develop. Moreover, it will not increase the amount of work we have to do in an actual calculation. Nonetheless, we demand that these additional instances of  $\mathcal{C}$  also act via commutation, meaning that (1.22) is preserved for the full wine and that (1.24) is appropriately generalised to include fields which are Lorentz scalars.

We should note that, in chapter 2, the flow equation is modified such that there are terms which generate instances of  $\mathcal{C}$  to which wines attach. Though these  $\mathcal{C}$ s are not decorations of the wine in the sense we have just discussed, it is often useful to treat them as such. However, these  $\mathcal{C}$ s act via anticommutation, rather than commutation. When treating them as part of a wine, they can always be ‘unpacked’, so that all remaining decorative  $\mathcal{C}$ s do, indeed, act via commutation.

When viewed as part of the wine, these new instances of  $\mathcal{C}$  give rise to multi-supertrace components of the wine which, in our current set up do not

---

<sup>7</sup>This relationship is most easily understood diagrammatically—see figure 1.9.

exist. Again, there is nothing to stop us from introducing such terms in complete generality since, in the diagrammatic framework of section 2.4, they are incorporated naturally.

In addition to modifying (1.23) to include  $\mathcal{C}$ s, we will anticipate the form of the flow equation by supposing that  $u$  and  $v$  involve functional derivatives. If these derivatives are with respect to the superfields  $Z_1$  and  $Z_2$ , then the structure of the flow equations turns out to be such that we can label the different wines by these fields. Hence, we have [57]:

$$\begin{aligned} \frac{\delta}{\delta Z_1^c} \left\{ W^{Z_1 Z_2} \right\} \frac{\delta}{\delta Z_2^c} &= \sum_{m,n=0}^{\infty} \int d^D x d^D y d^D x_1 \cdots d^D x_n d^D y_1 \cdots d^D y_m \\ &W_{a_1 \cdots a_n, b_1 \cdots b_m}^{X_1 \cdots X_n, Y_1 \cdots Y_m, Z_1 Z_2}(x_1, \dots, x_n; y_1, \dots, y_m; x, y) \\ &\text{str} \left[ \frac{\delta}{\delta Z_1^c(x)} X_1^{a_1}(x_1) \cdots X_n^{a_n}(x_n) \frac{\delta}{\delta Z_2^c(y)} Y_1^{b_1}(y_1) \cdots Y_m^{b_m}(y_m) \right], \end{aligned} \quad (1.27)$$

where the superfields  $X_i$ ,  $Y_i$  and  $Z_i$  are either  $\mathcal{A}$ s or  $\mathcal{C}$ s. The indices  $a_i$ ,  $b_i$  and  $c$  are, respectively, equal to  $\mu_i$ ,  $\nu_i$  and  $\rho$  in the case that the field which they label is a  $\mathcal{A}$  and are null when they label a  $\mathcal{C}$ . The wine vertices of (1.27) satisfy coincident line identities (1.22) and (1.24); the commutators arising from the action of the superfields have been expanded out.

We now have all the ingredients we need to regularise  $SU(N)$  gauge theory, via a (covariantised) cutoff [6]. Having embedded our gauge theory in the supergauge field,  $\mathcal{A}$ , we apply higher derivative regularisation to the  $\mathcal{A}$  kinetic term, via the cutoff function  $c$ :

$$\frac{1}{2} \mathcal{F}_{\mu\nu} \left\{ c^{-1} \right\} \mathcal{F}_{\mu\nu}.$$

Similarly, we can use the cutoff function  $\tilde{c}$  to sufficiently improve the UV behaviour of the superscalar kinetic term. In [6], it was assumed that the asymptotic behaviour of the cutoff functions is governed by a power law<sup>8</sup>:

$$c_p \sim \left( \frac{p^2}{\Lambda^2} \right)^{-r}, \quad \tilde{c}_p \sim \left( \frac{p^2}{\Lambda^2} \right)^{-\tilde{r}}.$$

It was then proven that, provided the following constraints are satisfied

$$r - \tilde{r} > 1, \quad \tilde{r} > 1, \quad (1.28)$$

---

<sup>8</sup>There is no reason to suspect that regularisation cannot be achieved with different cutoff profiles.

the physical  $SU(N)$  gauge theory is, indeed, properly regulated in  $D \leq 4$ .

It should be noted that to unambiguously define contributions which are finite only by virtue of the PV regularisation, a pre-regulator [97, 98, 106, 51] must be used, in  $D = 4$ . To understand this, consider some PV regulated loop integral. Gauge invariance demands that such an integral be invariant under shifting the loop momenta. However, such a shift can generate a non-vanishing surface term. The effect of our pre-regulator is to discard such terms; for the purposes of this thesis—where we can perform calculations in  $D = 4 - 2\epsilon$ —we use dimensional regularisation to automatically remove such contributions. We emphasise that, assuming we are investigating phenomena that can be studied in an intermediate dimension, there is no barrier to utilising dimensional regularisation as a pre-regulator, even non-perturbatively [6]. Interestingly, as we will discuss in the conclusion, it seems that there may be a diagrammatic recipe for implementing pre-regularisation, which one might hope would be applicable to phenomena for which one must strictly work in  $D = 4$ .

Finally, it has been traditional to impose the following constraints [51, 53, 57]:

$$\frac{\delta}{\delta \mathcal{A}_\mu} \{W\} = 0, \quad \frac{\delta}{\delta \mathcal{C}} \{W\} = 0. \quad (1.29)$$

As we will see, when we introduce the diagrammatics for our flow equation, this restriction forbids certain types of diagram—the diagrams in which ‘a wine bites its own tail’ [51, 52]. The problem with these diagrams is that they are not properly UV regularised; though our gauge theory *is* properly regularised, this does not necessarily imply that the flow equation is properly regularised. This is a deep issue: the constraint (1.29) can be implemented by an implicit choice of covariantisation but, strictly, this requires that we temporarily *break* gauge invariance, restoring it only after an appropriate limit is taken (*ibid.*). For much of this thesis, we will use this prescription, and thus simply never draw the diagrams in which the wine bites its own tail. However, the work of part III implies a more satisfactory resolution to this problem, which is discussed in the conclusion.

## 1.2.2 The Flow Equation

Having introduced both the ERG and a regularisation scheme for  $SU(N)$  Yang-Mills theory, based on a cutoff, we can now combine the two. The regularised,<sup>9</sup> manifestly supergauge invariant flow equation of [57] is:

$$\Lambda \partial_\Lambda S = -a_0[S, \Sigma_g] + a_1[\Sigma_g], \quad (1.30)$$

where

$$a_0[S, \Sigma_g] = \frac{1}{2} \frac{\delta S}{\delta \mathcal{A}_\mu} \{ \dot{\Delta}^{\mathcal{A}\mathcal{A}} \} \frac{\delta \Sigma_g}{\delta \mathcal{A}_\mu} + \frac{1}{2} \frac{\delta S}{\delta \mathcal{C}} \{ \dot{\Delta}^{\mathcal{C}\mathcal{C}} \} \frac{\delta \Sigma_g}{\delta \mathcal{C}} \quad (1.31)$$

and

$$a_1[\Sigma_g] = \frac{1}{2} \frac{\delta}{\delta \mathcal{A}_\mu} \{ \dot{\Delta}^{\mathcal{A}\mathcal{A}} \} \frac{\delta \Sigma_g}{\delta \mathcal{A}_\mu} + \frac{1}{2} \frac{\delta}{\delta \mathcal{C}} \{ \dot{\Delta}^{\mathcal{C}\mathcal{C}} \} \frac{\delta \Sigma_g}{\delta \mathcal{C}}. \quad (1.32)$$

We immediately note the similarity of the above to the scalar equation (1.6). Superficially, the only differences are as follows. First, we have the two fields,  $\mathcal{A}$  and  $\mathcal{C}$ , introduced in a symmetric fashion, rather than the single field,  $\phi$ . Secondly, we have implemented the covariantisation of the cutoff functions. However, there is a more subtle difference. Recall that the scalar equation involves the functional  $\Sigma = S - 2\hat{S}$ . The above equations, though, involve a slightly different quantity,

$$\Sigma_g = g^2 S - 2\hat{S}.$$

Let us examine where this difference comes from. Consider performing a straightforward generalisation of the scalar equation to a form suitable for Yang-Mills theory. This is most easily done by using Abelian gauge theory, as an intermediate step [52]. In this case, there is no need to covariantise the cutoff and so we simply let  $\phi \rightarrow A_\mu$  in our scalar flow equation, where the covariant derivative is defined to be  $D_\mu = \partial_\mu - igA_\mu$ .

However, when we generalise to non-Abelian gauge theory, it is desirable to scale  $g$  out of the covariant derivative viz equation (1.10). The exact preservation of relationship (1.12) now implies that, given the form of the covariant derivative (1.10),  $\mathcal{A}$  cannot renormalise: it is only  $g$  that runs (*ibid.*).

Let us consider making the change  $A_\mu \rightarrow A_\mu/g$  in our ERG for Abelian gauge theory; we choose also to let  $\hat{S} \rightarrow \hat{S}/g^2$ . The flow equation is

$$\Lambda \partial_\Lambda S + \frac{\beta}{g} \int d^D x A_\mu(x) \frac{\delta S}{\delta A_\mu(x)} = -\frac{1}{2} \frac{\delta S}{\delta A_\mu} \cdot \dot{\Delta} \cdot \frac{\delta \Sigma_g}{\delta A_\mu} + \frac{1}{2} \frac{\delta}{\delta A_\mu} \cdot \dot{\Delta} \cdot \frac{\delta \Sigma_g}{\delta A_\mu},$$

---

<sup>9</sup>Up to the subtlety of wines biting their tails.

where  $\beta \equiv \Lambda \partial_\Lambda g$ . The presence of the second term on the left is undesirable, since it destroys manifest gauge invariance: gauge transformations generate a term containing  $\partial_\mu(\delta S/\delta A_\mu)$ . We can demonstrate that this term vanishes, using gauge invariance, but that it does so is not manifestly the case.

The solution is simply to drop the  $\beta$ -term (*ibid.*). Thus, equations (1.30)–(1.32) do not represent a trivial generalisation of the scalar flow equation. However, our non-Abelian flow equation satisfies the necessary requirements and so is perfectly valid.

At this point it is worth pausing to repeat the argument of [57] that our non-Abelian flow equation is actually gauge invariant. Invariance of the  $\delta/\delta\mathcal{C}$  terms follows directly from the homogeneous transformation of  $\delta/\delta\mathcal{C}$  (equation (1.19)), enforcing constraints on the wine vertices. These constraints will be discussed in sections 1.2.4 and 3.1.2.

In the  $A$ -sector, however, matters are complicated by the inhomogeneous transformation of  $\delta/\delta\mathcal{A}$ , given by equation (1.20). Under a supergauge transformation, we can use equations (1.20) and (1.22) to give:

$$\delta \left( \frac{\delta S}{\delta \mathcal{A}_\mu} \{ \dot{\Delta}^{\mathcal{A}\mathcal{A}} \} \frac{\delta \Sigma_g}{\delta \mathcal{A}_\mu} \right) = \frac{i}{2N} \text{tr} \left[ \frac{\delta S}{\delta \mathcal{A}_\mu}, \Omega \right] \cdot \dot{\Delta}^{\mathcal{A}\mathcal{A}} \cdot \text{str} \frac{\delta \Sigma_g}{\delta \mathcal{A}_\mu} + (S \leftrightarrow \Sigma_g).$$

By equation (1.16) and no- $\mathcal{A}^0$  symmetry,

$$\text{str} \frac{\delta \Sigma_g}{\delta \mathcal{A}_\mu} = \frac{\delta \Sigma_g}{\delta \mathcal{A}_\mu^0} = 0$$

and likewise for the term with  $S \leftrightarrow \Sigma_g$ . Gauge invariance of the quantum term follows, similarly.

We emphasise that the demonstration of gauge invariance depends, crucially, on two ingredients: equation (1.22) and no- $\mathcal{A}^0$  symmetry. We recall that equation (1.22) is intimately connected with the coincident line identities; we will need to use this later, when examining gauge invariance in the broken phase.

That our flow equation satisfies the requisite requirements ensures that two possible sources for concern are alleviated. On the one hand, we have discussed already that locality is guaranteed. On the other hand, we might wonder whether it is *really*  $SU(N)$  Yang-Mills theory that we are describing at low energies; after all, we expect a hugely complicated action depending

on all the component fields of  $\mathcal{A}$  and  $\mathcal{C}$ . However, we know that the partition function, and hence the physics we are describing, is invariant under the flow. Since, in  $D \leq 4$ , the regulator fields decouple—as they must—as  $\Lambda \rightarrow \infty$ , we are describing  $SU(N)$  Yang-Mills theory at the top end of the renormalised trajectory, and thus everywhere else along it.<sup>10</sup>

The next point to make about the flow equation is the novel mass dimension of  $\mathcal{C}$ : whereas we might expect  $\mathcal{C}$  to come with mass dimension one, we choose instead for it to have mass dimension zero [57]. The reason relates to properly implementing the regularisation into the ERG. From [6], the higher derivative regularisation scale and the effective spontaneous symmetry breaking scale must be tied together, both flowing with  $\Lambda$ . In general, this is not guaranteed within the ERG, but occurs only if the seed action is suitably constrained; these constraints are particularly simple if  $\mathcal{C}$  is dimensionless.

Let us define  $V(\mathcal{C})$  to be the effective superhiggs potential in  $S$ , minimised when  $\mathcal{C}$  acquires its effective vacuum expectation value  $\bar{\mathcal{C}}$ . We also introduce a separate—and generally different—potential,  $\hat{V}(\mathcal{C})$ , for  $\hat{S}$ . Now, the nice thing about  $\mathcal{C}$  being dimensionless is that, classically, we can insist that the minima of both  $V$  and  $\hat{V}$  lie at  $\mathcal{C} = \sigma$  [57]. This immediately implies that neither action, at the classical level, has a one-point  $\mathcal{C}$  vertex in the broken phase.

Protecting  $\bar{\mathcal{C}} = \sigma$  from loop corrections can be done by tuning  $\hat{S}$ . In section 2.4.4 we will see explicitly how this is done.

The set-up of the flow equation is completed by defining  $g$  through a renormalisation condition. As in [52, 57],  $g$  is the coupling of the physical  $SU(N)$  field,  $A^1$ , and so:

$$S[\mathcal{A} = A^1, \mathcal{C} = \bar{\mathcal{C}}] = \frac{1}{2g^2} \text{tr} \int d^D x \left( F_{\mu\nu}^1 \right)^2 + \dots, \quad (1.33)$$

where the ellipsis denotes higher dimension operators and ignored vacuum energy.

---

<sup>10</sup>As pointed out in [57], asymptotic freedom ensures that strong corrections do not affect the conclusions we draw as  $\Lambda \rightarrow \infty$ .

### 1.2.3 Diagrammatics

#### Diagrammatics for the Action

The flow equations have a particularly simple diagrammatic interpretation, as a consequence of the supersowing and supersplitting relations (1.14), (1.15), (1.17) and (1.18). To describe these diagrammatics, we must first give a superfield expansion for the action. This is simple: supergauge invariance demands that this expansion be in terms of supertraces and products of supertraces [57]:

$$\begin{aligned}
S &= \sum_{n=1}^{\infty} \frac{1}{s_n} \int d^D x_1 \cdots d^D x_n S_{a_1 \cdots a_n}^{X_1 \cdots X_n}(x_1, \cdots, x_n) \text{str} X_1^{a_1}(x_1) \cdots X_n^{a_n}(x_n) \\
&+ \frac{1}{2!} \sum_{m,n=0}^{\infty} \frac{1}{s_n s_m} \int d^D x_1 \cdots d^D x_n d^D y_1 \cdots d^D y_m \\
&\quad S_{a_1 \cdots a_n, b_1 \cdots b_m}^{X_1 \cdots X_n, Y_1 \cdots Y_m}(x_1, \cdots, x_n; y_1 \cdots y_m) \\
&\quad \text{str} X_1^{a_1}(x_1) \cdots X_n^{a_n}(x_n) \text{str} Y_1^{b_1}(y_1) \cdots Y_m^{b_m}(y_m) \\
&+ \dots
\end{aligned} \tag{1.34}$$

where, in the symmetric phase, the  $X^{a_i}$  are  $\mathcal{A}_{\mu_i}$  or  $\mathcal{C}$  and the  $Y_j^{b_j}$  are  $\mathcal{A}_{\nu_i}$  or  $\mathcal{C}$  and the vacuum energy is ignored. Due to the invariance of the supertrace under cyclic permutations of its arguments, we take only one cyclic ordering for the lists  $X_1 \cdots X_n$ ,  $Y_1 \cdots Y_m$  in the sums over  $n, m$ .

Given that the arguments of each element of the lists  $X_1 \cdots X_n$ ,  $Y_1 \cdots Y_m$  are dummy arguments, we now want to check if any terms in our sums are invariant under non-trivial cyclic permutations of the fields. The coefficients  $s_n$  ( $s_m$ ) represent the order of any such cyclic subgroup. Thus, for the single supertrace term

$$\frac{1}{s_n} S^{\mathcal{A}\mathcal{C}\mathcal{A}\mathcal{C}} \text{str} \mathcal{A}\mathcal{C}\mathcal{A}\mathcal{C},$$

in which we have suppressed position arguments and Lorentz indices, we take  $s_n = 2$ .

We write the momentum space vertices as

$$\begin{aligned}
&S_{a_1 \cdots a_n}^{X_1 \cdots X_n}(p_1, \cdots, p_n) (2\pi)^D \delta \left( \sum_{i=1}^n p_i \right) \\
&= \int d^D x_1 \cdots d^D x_n e^{-i \sum_i x_i \cdot p_i} S_{a_1 \cdots a_n}^{X_1 \cdots X_n}(x_1, \cdots, x_n),
\end{aligned}$$

where all momenta are taken to point into the vertex. We will employ the

shorthand

$$S_{a_1 a_2}^{X_1 X_2}(p) \equiv S_{a_1 a_2}^{X_1 X_2}(p, -p).$$

The diagrammatic representation of the action is given in figure 1.1.

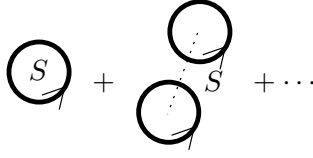


Figure 1.1: Diagrammatic representation of the action.

Each circle stands for a single supertrace containing any number of fields. The  $S$  is to remind us that this is an expansion of the action, since the seed action  $\hat{S}$  has a similar expansion. The dotted line reminds us that the two supertraces in the double supertrace term are part of the same vertex. The arrows indicate the cyclic sense in which fields should be read off; henceforth, this will always be done in the counterclockwise sense and so these arrows will generally be dropped.<sup>11</sup> In turn, each of these supertraces can now be expanded in terms of a sum over all explicit, cyclically independent combinations of fields, as in figure 1.2, where closed circles represent  $\mathcal{A}$ s and open circles represent  $\mathcal{C}$ s.

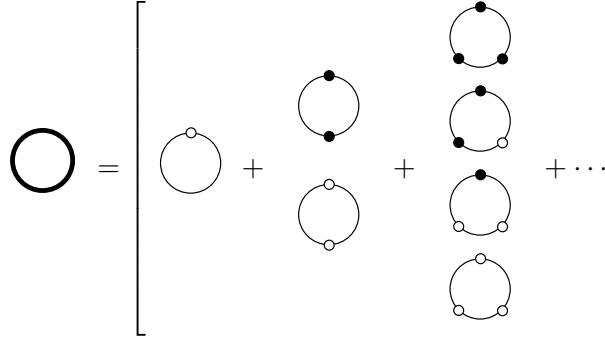


Figure 1.2: Expansion of a single supertrace in powers of  $\mathcal{A}$  and  $\mathcal{C}$ .

<sup>11</sup>Arrows can always be dropped in complete diagrams formed by the flow equation. However, if we look at the diagrammatic representation of a wine, in isolation, then it will be necessary to keep these arrows.

In this case, we have chosen not to indicate whether the supertraces we are considering come from the Wilsonian effective action, the seed action, or some linear combination of the two.

Explicit instances of fields are referred to as decorations. Note that there are no supertraces containing a single  $\mathcal{A}$ , since  $\text{str } \mathcal{A} = 0$ . The  $\text{str } \mathcal{AC}$  vertex vanishes by charge conjugation invariance, under which  $\mathcal{A} \rightarrow -\mathcal{A}^T$  and  $\mathcal{C} \rightarrow \mathcal{C}^T$  [57]; the transpose of a supermatrix being defined as in [53]:

$$\text{for } X = \begin{pmatrix} X^{11} & X^{12} \\ X^{21} & X^{22} \end{pmatrix}, \quad X^T \equiv \begin{pmatrix} X^{11T} & -X^{21T} \\ X^{12T} & X^{22T} \end{pmatrix}.$$

The extra sign in the top right element ensures that we can rewrite

$$\text{str } X^T Y^T \cdots Z^T = \text{str } Z \cdots Y X, \quad (1.35)$$

since this sign compensates for the sign picked up upon the anticommutation of fermionic fields in the above re-ordering.<sup>12</sup>

As it stands, figures 1.1 and 1.2 provide representations of the action (1.34). However, as we will see shortly, it is often useful to interpret the explicitly decorated terms as just the vertex coefficient functions  $S_{a_1 \dots a_n}^{X_1 \dots X_n}(p_1, \dots, p_n)$  etc., the accompanying supertrace(s) and cyclic symmetry factors having been stripped off.

### Diagrammatics for the Wines

The wines have a very similar diagrammatic expansion [53, 57] to the action, as indicated in figure 1.3.

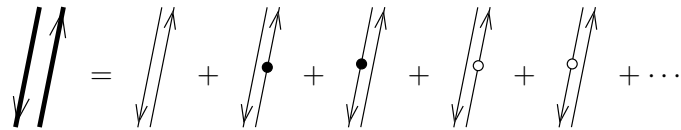


Figure 1.3: Diagrammatic representation of the wines.

---

<sup>12</sup>The definition of the transpose, though it ensures (1.35), is not unique [53].

The ellipsis represents terms with any number of fields distributed in all possible ways between the two sides of the wine. We should note that figure 1.3 is not strictly a representation of equation (1.27). Equation (1.27) involves not only the wine vertices and the associated decorative fields, but also two functional derivatives which sit at the ends of the wine. For the purposes of this chapter, we can just directly include these functional derivatives in our diagrammatics; they would act as unambiguous labels for the different wines in the flow equation, as shown in figure 1.4.



Figure 1.4: True diagrammatic representation of equation (1.27).

The grey circles can be either both  $\mathcal{A}$ s or both  $\mathcal{C}$ s; since they sit at the end of the wine they represent functional derivatives and label the wine.

We are almost ready to give a diagrammatic representation of the flow equation, in the symmetric phase. Indeed, if we were to allow only decorations by  $\mathcal{C}$ , we could do this immediately, by virtue of the exact supersowing relation (1.14) and exact supersplitting relation (1.15).

### Diagrammatic Flow Equation in the $\mathcal{C}$ -sector

For that which follows in this section, we assume all fields, including those that have been differentiated, to be in the  $\mathcal{C}$ -sector. In this case, we note that the exact supersowing relation applies to the classical part of the flow equation (1.31). This is easy to see from equation (1.23) (with the restriction to decoration by  $\mathcal{A}$  removed) if we take  $u = \delta S / \delta \mathcal{C}$  and  $v = \delta \Sigma_g / \delta \mathcal{C}$ . From the l.h.s. of equation (1.14), both of these derivatives produce just a string of superfields; everything is tied back into a supertrace by the covariantisation.

Similarly, the supersplitting relation applies to the quantum part of the flow equation (1.32). Thus, in this scenario, we can represent the flow equation as

shown in figure 1.5 [57]; the ellipses represent terms with additional supertraces.

$$\left[ \begin{array}{c} \text{circle } S \\ + \\ \text{two circles } S \\ + \dots \end{array} \right] \bullet = \frac{1}{2} \left[ \begin{array}{c} \text{dumbbell } S, \Sigma_g \\ - \\ \text{figure-eight } \Sigma_g \\ - \\ \text{figure-eight } \Sigma_g \end{array} \right] + \dots$$

Figure 1.5: Diagrammatic representation of the flow equation, assuming that all fields are  $\mathcal{C}$ s.

There are a number of important points to make about this figure. The first is that the final diagram is the term for which the wine bites its own tail. As discussed already, we will henceforth discard such terms.

Let us now focus on the dumbbell-like structure, which represents the classical term. The lobe at the top of the diagram (which encloses  $S$ ) was spawned by  $\delta S/\delta \mathcal{C}$ . This derivative breaks  $S$  open, by knocking out a  $\mathcal{C}$ , represented by the open circle sitting at the bottom of the lobe. The interpretation of the bottom lobe is much the same, though this time it is  $\Sigma_g$  that has been differentiated. The two broken supertraces are now joined back together by the wine. Note that we need not put arrows on the wine: the counterclockwise sense in which we read off fields is determined by the lobes.

At the moment, we are taking the l.h.s. of the equation to directly represent the action—symmetry factors and all—and so we must be quite careful to interpret figure 1.5 in a way that is consistent with both figure 1.1 and equation (1.34). (This is not entirely clear in either [52] or [57].) We will shortly see that there is a prescription which enables us to remove all symmetry factors, as we would hope.

To be specific, suppose that the vertex whose flow we are computing has  $m$  supertraces, the first of which is decorated by  $s_1$   $\mathcal{C}$ s and the last of which is decorated by  $s_m$   $\mathcal{C}$ s. Hence, the overall symmetry factor is

$$\frac{1}{m! \prod_{i=1}^m s_i}. \tag{1.36}$$

Whereas the vertex whose flow we are computing comes with this overall factor, the diagrams on the r.h.s. of figure 1.5 come with additional factors, due to the derivatives breaking open  $S$  and  $\Sigma_g$ .

Let us illustrate this with an example. We consider the classical part of the flow of all double supertrace terms with one  $\mathcal{C}$  on one supertrace and two  $\mathcal{C}$ s on the other. Thus we combine  $S^{\mathcal{C}\mathcal{C},\mathcal{C}}\text{str}\mathcal{C}\text{str}\mathcal{C}$  with  $S^{\mathcal{C},\mathcal{C}\mathcal{C}}\text{str}\mathcal{C}\text{str}\mathcal{C}$ . This has the effect of killing the  $1/m!$  in equation (1.36).

Figure 1.6 depicts the flow, where the ellipsis denotes un-drawn terms in which  $\mathcal{C}$ s decorate the wine and the missing quantum term.

$$\left[ \begin{array}{c} \text{---} \\ \circ \\ \text{---} \\ S \\ \text{---} \\ \circ \\ \text{---} \end{array} \right] \bullet = \frac{1}{2} \left[ \begin{array}{c} 4 \begin{array}{c} \text{---} \\ \circ \\ \text{---} \\ S \\ \text{---} \\ \circ \\ \text{---} \\ \Sigma_g \end{array} + 4 \begin{array}{c} \text{---} \\ \circ \\ \text{---} \\ \Sigma_g \\ \text{---} \\ \circ \\ \text{---} \\ S \end{array} \\ + 2 \begin{array}{c} \text{---} \\ \circ \\ \text{---} \\ S \\ \text{---} \\ \circ \\ \text{---} \\ \Sigma_g \end{array} + 2 \begin{array}{c} \text{---} \\ \circ \\ \text{---} \\ \Sigma_g \\ \text{---} \\ \circ \\ \text{---} \\ S \end{array} \\ + 2 \begin{array}{c} \text{---} \\ \circ \\ \text{---} \\ S \\ \text{---} \\ \circ \\ \text{---} \\ \Sigma_g \end{array} + \dots \end{array} \right]$$

Figure 1.6: Example of the classical part of the flow.

Notice that on the r.h.s., as with the l.h.s., each  $S^{\mathcal{C},\mathcal{C}\mathcal{C}}$  vertex is counted twice, since we do not care which of the supertraces comes ‘first’. Again, this has the effect of killing the  $1/m!$  coming from equation (1.36).

A factor of two arises each time we differentiate a supertrace containing two  $\mathcal{C}$ s. The final diagram has a factor of two due to the symmetry of the double supertrace vertex: either of the  $\text{str}\mathcal{C}$ s could be differentiated, with the same result.

Let us now consider changing the interpretation of the diagrammatics: we will strip off the common supertrace structure and extract the symmetry factors  $1/s_i$  and  $1/m!$  from the vertices. Note that only the final diagram has a



This recipe clearly works in our example: the diagrams with a relative factor of two are precisely those for which we can cyclically permute the fields on the dumbbell structure. In a very real sense, we can think of stripping off the supertraces as promoting the dummy arguments carried by the fields to actual arguments. In this sense, the fields each effectively carry a label. Thus, when we draw all dumbbell structures, we count differently the various cyclic permutations of the fields.

Returning now to figure 1.5, we look at the quantum term, which we note looks somewhat like a padlock. The treatment of this term is much the same as with the classical term, in that we can remove all symmetry factors by computing the flow of vertex coefficient functions. However, things are complicated by the fact that, unlike the dumbbell term, the quantum term has a minimum of two supertraces (the inner circuit is not connected to the outer circuit). If either of these supertraces is empty, the diagram will vanish since  $\text{str } \mathbb{1} = 0$ . Consequently, the quantum part of the flow relates  $m$  supertrace vertices to  $m - 1$  supertrace vertices (this receives corrections in the broken phase). To compute the flow of a vertex coefficient function, we can use the following mnemonic, for the quantum term:

1. take an overall factor of  $1/2$ , corresponding to the  $1/2$  associated with  $a_1$  (see equation (1.32));
2. draw all quantum terms with the same implied supertrace structure as the vertex whose flow has been computed, where we sum over all cyclic permutations of the fields on both the inner and outer circuits of the padlock structure. Note also that we independently count the case where a given set of fields are on the inner / outer circuit.

### The Full Diagrammatic Flow Equation

Having described the diagrammatics of the flow equation with all fields in  $\mathcal{C}$ -sector, we now generalise to include  $\mathcal{A}$ s. The subtlety occurs due to the corrections to both supersowing (1.17) and supersplitting (1.18), when the differentiated fields are  $\mathcal{A}$ s.

Since we will be applying an extension of such considerations in chap-

ter 2, we review the methodology for computing the corrections given in [57]. Moreover, the intuition we will gain about the source of corrections to the diagrammatic flow equation will prove invaluable.

The idea is a simple one: if the superfield  $\mathcal{A}$  were unconstrained, rather than restricted to being supertraceless, then supersplitting and supersowing would be exact, just as in the  $\mathcal{C}$  sector. Thus we imagine promoting  $\mathcal{A}$  to a full superfield,  $\mathcal{A}^e$  via the map:

$$\mathcal{A}_\mu \mapsto \mathcal{A}_\mu^e \equiv \mathcal{A}_\mu + \sigma \mathcal{A}_\mu^\sigma.$$

We choose to take  $\mathcal{A}_\mu^\sigma$  arbitrary, so the map is not unique; similarly, with the extension of all functionals:

$$S^e[\mathcal{A}^e, \mathcal{C}] \equiv S[\mathcal{A} \mapsto \mathcal{A}^e, \mathcal{C}] \text{ etc.}$$

On the other hand, the reverse procedure, in which we project back to the supertraceless space is unique:

$$\pi \mathcal{A}_\mu^e = \mathcal{A}_\mu, \quad \pi S^e = S \text{ etc.}$$

Functional derivatives with respect to  $\mathcal{A}^e$  can be written [57]

$$\frac{\delta}{\delta \mathcal{A}_\mu^e} = \frac{\delta}{\delta \mathcal{A}_\mu} + \frac{\mathbb{1}}{2N} \frac{\delta}{\delta \mathcal{A}_\mu^\sigma}, \quad (1.37)$$

or, equivalently (*ibid.*)

$$\frac{\delta}{\delta \mathcal{A}_\mu} = \frac{\delta}{\delta \mathcal{A}_\mu^e} - \frac{\mathbb{1}}{2N} \text{tr} \frac{\delta}{\delta \mathcal{A}_\mu^e}. \quad (1.38)$$

Noting that  $\pi$  and  $\delta/\delta \mathcal{A}^\sigma$  do not commute, our strategy is as follows. We trivially rewrite both terms in the flow equation (equations (1.31) and (1.32)) by extending all functionals and then projecting out. Under the projection, we cannot simply exchange derivatives with respect to  $\mathcal{A}$  with derivatives with respect to  $\mathcal{A}^e$  but we can substitute for the former, in terms of the latter, using equation (1.37) or (1.38). Then we collect together terms into those for which supersowing / supersplitting is exact and those which are corrections.

Let us see how this works for the quantum term (1.32).

$$\frac{\delta}{\delta \mathcal{A}_\mu} \{ \dot{\Delta}^{\mathcal{A}\mathcal{A}} \} \frac{\delta \Sigma_g}{\delta \mathcal{A}_\mu} = \pi \left\{ \frac{\delta}{\delta \mathcal{A}_\mu} \{ \dot{\Delta}^{\mathcal{A}\mathcal{A}} \}^e \frac{\delta \Sigma_g^e}{\delta \mathcal{A}_\mu} \right\}. \quad (1.39)$$

Focusing on the term on which the projection operator acts, we substitute for unconstrained derivatives, using equation (1.37):

$$\begin{aligned} & \frac{\delta}{\delta \mathcal{A}_\mu^e} \{ \dot{\Delta}^{\mathcal{A}\mathcal{A}} \}^e \frac{\delta \Sigma_g^e}{\delta \mathcal{A}_\mu^e} - \frac{\mathbb{1}}{2N} \frac{\delta}{\delta \mathcal{A}_\mu^\sigma} \{ \dot{\Delta}^{\mathcal{A}\mathcal{A}} \}^e \frac{\delta \Sigma_g^e}{\delta \mathcal{A}_\mu^e} \\ & - \frac{\delta}{\delta \mathcal{A}_\mu^e} \{ \dot{\Delta}^{\mathcal{A}\mathcal{A}} \}^e \frac{\mathbb{1}}{2N} \frac{\delta \Sigma_g^e}{\delta \mathcal{A}_\mu^\sigma} + \frac{\mathbb{1}}{2N} \frac{\delta}{\delta \mathcal{A}_\mu^\sigma} \{ \dot{\Delta}^{\mathcal{A}\mathcal{A}} \}^e \frac{\mathbb{1}}{2N} \frac{\delta \Sigma_g^e}{\delta \mathcal{A}_\mu^\sigma}. \end{aligned}$$

The next step is to use equation (1.22). Immediately, this tells us that the final term vanishes. The second and third terms will involve

$$\text{str} \frac{\delta}{\delta \mathcal{A}_\mu^e} = \frac{\delta}{\delta \mathcal{A}_\mu^0},$$

by equations (1.37) and (1.16). Thus, equation (1.39) becomes:

$$\frac{\delta}{\delta \mathcal{A}_\mu} \{ \dot{\Delta}^{\mathcal{A}\mathcal{A}} \} \frac{\delta \Sigma_g}{\delta \mathcal{A}_\mu} = \pi \left\{ \frac{\delta}{\delta \mathcal{A}_\mu^e} \{ \dot{\Delta}^{\mathcal{A}\mathcal{A}} \}^e \frac{\delta \Sigma_g^e}{\delta \mathcal{A}_\mu^e} \right\} - \frac{1}{N} \pi \left\{ \frac{\delta}{\delta \mathcal{A}_\mu^\sigma} \cdot \dot{\Delta}^{\mathcal{A}\mathcal{A}} \cdot \frac{\delta \Sigma_g^e}{\delta \mathcal{A}_\mu^0} \right\}, \quad (1.40)$$

as in [57].

The first term represents exact supersplitting; the second term is the correction. The crucial point, emphasised by the presence of  $\delta/\delta \mathcal{A}_\mu^0$ , is that the correction term is tied up with no- $\mathcal{A}^0$  symmetry. Indeed, if the  $\Sigma_g^e$  of the last term were not extended, then the correction would just vanish, precisely by no- $\mathcal{A}^0$  symmetry.

The question is, does the extension of  $\Sigma_g$  lead to any surviving terms? Consider an unextended vertex containing an arbitrary number of supertraces, and suppose that one of these supertraces is just  $\text{str} \mathcal{A}\mathcal{A}$ . This part of the vertex is automatically no- $\mathcal{A}^0$  symmetric, which follows by recognising that the lowest order constraints implied by no- $\mathcal{A}^0$  symmetry can be deduced by making the transformation  $\delta \mathcal{A}_\mu = \lambda_\mu \mathbb{1}$  in equation (1.34) [57, 55].

However, it is only  $\text{str} \mathcal{A}\mathcal{A}$  terms that vanish when we make this transformation. For the action as a whole to be no- $\mathcal{A}^0$  symmetric, the survival of terms from this transformation implies relationships between the vertex coefficient functions. Now, these constraints are there, irrespective of whether or not we extend the action (and seed action).

Thus, when we do extend the actions,  $\delta \Sigma_g^e / \delta \mathcal{A}^0$  will vanish unless  $\delta \mathcal{A}^0$  strikes a  $\text{str} \mathcal{A}^e \mathcal{A}^e$ . In this extended case, such a contribution now survives since  $\text{str} \mathcal{A}^e \neq 0$ . Returning to equation (1.40), the  $\delta/\delta \mathcal{A}^\sigma$  must strike the

$\text{str } \mathcal{A}^e$ , since otherwise this contribution will vanish, upon projection to the restricted space. This yields a (super)group theory factor of  $-\frac{1}{N}\text{str } \sigma = -2$ .

Given that similar arguments tell us that the classical part of the flow equation (1.31) does not, in fact, receive any corrections to supersowing [57], we are ready to write down the full diagrammatic flow equation. We simply reproduce figure 1.5 (discarding the final diagram), where the differentiated fields (along with all decorations) can now be either both  $\mathcal{C}$ s or both  $\mathcal{A}$ s (the mixed case does not exist, since there is no  $\dot{\Delta}^{\mathcal{C}\mathcal{A}}$ ), so long as we use the following prescription: *if, in the quantum term, an undecorated wire attaches at both ends to a  $\text{str } \mathcal{A}\mathcal{A}$  term, then we supplement the usual group theory factor with an additional  $-2$ .*

In the unbroken phase, this actually causes a class of diagram which would naïvely vanish, to survive. These diagrams can possess any number of supertraces; the double supertrace case is shown in figure 1.8.

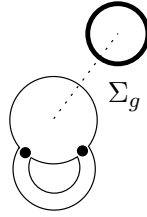


Figure 1.8: A term which survives, despite naïvely vanishing by group theory considerations.

Now, the expected group theory factor associated with this diagram arises from the two empty circuits in the padlock structure. These yield  $(\text{str } \mathbb{1})^2 = 0$ . However, according to our prescription, the group theory factor of this diagram is supplemented by  $-2$ , causing it to survive.

### The Coincident Line Identities

We can cast equation (1.25)—which we recall follows from the coincident line identities (1.24)—in a particularly simple diagrammatic form. This is shown in figure 1.9.

$$\begin{array}{c} \downarrow \\ \bullet d \\ \bullet c \\ \vdots \\ \bullet b \\ \bullet a \\ \downarrow \end{array} + \begin{array}{c} \downarrow \\ d \bullet \\ \bullet c \\ \vdots \\ \bullet b \\ \bullet a \\ \downarrow \end{array} + \dots + \begin{array}{c} \downarrow \\ \bullet b \\ \bullet c \\ \vdots \\ \bullet d \\ \bullet a \\ \downarrow \end{array} + \begin{array}{c} \downarrow \\ \bullet a \\ \bullet b \\ \vdots \\ \bullet c \\ \bullet d \\ \downarrow \end{array} = 0 \quad (1.41)$$

Figure 1.9: Diagrammatic representation of equation (1.25).

Notice that equation (1.41) implies equation (1.22), as it should. If the top (bottom) end of the wine is plugged by  $\mathbb{1}$ , rather than a functional derivative, then no matter what the bottom (top) end attaches to, we can cycle the decorations of the wine around, without changing the supertrace structure of the diagram as a whole. Hence, the only class of diagram to survive, in this case, is that for which the wine is undecorated.

#### 1.2.4 The Broken Phase

##### Using Partial Supermatrices

To work in the broken phase, in which we recall that  $\mathcal{C}$  fluctuates around  $\sigma$ , is easy. We decompose:

$$\mathcal{A}_\mu = A_\mu + B_\mu; \quad \mathcal{C} = C + D + \sigma. \quad (1.42)$$

Now, instead of decorating vertices with  $\mathcal{A}$ s and  $\mathcal{C}$ s, we decorate instead with the fields  $A, B, C, D$  and  $\sigma$ . We can simplify appearances of  $\sigma$  by noting that it (anti)commutes with  $(B, D)$   $A, C$ . Thus, we can take the convention [57] that all instances of  $\sigma$  are consecutive, upon which we use  $\sigma^2 = \mathbb{1}$  to remove all pairs. Consequently, vertices have at most one instance of  $\sigma$ , which we note does not come with a position label and can be ignored when determining symmetry factors [57]. Vertices must contain an even number of fermionic fields, else they can be cast as the supertrace of a block off-diagonal matrix, which vanishes.

To deal with the broken sector wines, let us return to equation (1.27). The fields  $X$  and  $Y$  can be any of  $A$ – $D$  and  $\sigma$ , whereas  $Z$  is restricted to

just the dynamical fields. Wines (assuming the diagrammatic interpretation of figure 1.4, as opposed to figure 1.3), like vertices, must be net bosonic, but we note that the functional derivatives can be with respect to opposite statistics partners (this then implies that there must be an odd number of fermionic decorations). Once again, we can simplify instances of  $\sigma$  by noting that it (anti)commutes with not only the decorations, but also the functional derivatives.

It is instructive to compare the zero-point wines in the symmetric phase to those in the broken phase. Let us start in the symmetric phase. From equation (1.26), we see that the second term does not contribute to  $\dot{\Delta}^{AA}$ , since it has at least two decorative  $\mathcal{C}$ s and so cannot contribute to a zero-point wine.

In the broken phase, we note that  $\sigma$  commutes with  $\delta/\delta A$ , and so the second term does not contribute to  $\dot{\Delta}^{AA}$ . Therefore,

$$\dot{\Delta}^{AA} = \dot{\Delta}^{\mathcal{A}\mathcal{A}}.$$

However,  $\sigma$  anticommutes with  $\delta/\delta B$  and so, in this case, there is an additional contribution:

$$\dot{\Delta}^{BB} = \dot{\Delta}^{\mathcal{A}\mathcal{A}} + \dot{\Delta}_m^{\mathcal{A}\mathcal{A}}.$$

Similarly,

$$\begin{aligned}\dot{\Delta}^{CC} &= \dot{\Delta}^{\mathcal{C}\mathcal{C}}, \\ \dot{\Delta}^{DD} &= \dot{\Delta}^{\mathcal{C}\mathcal{C}} + \dot{\Delta}_m^{\mathcal{C}\mathcal{C}}.\end{aligned}$$

Still following [57], we can reduce the number of fields we have to deal with in the broken sector by defining<sup>13</sup> the Euclidean five vector

$$F_M = (B_\mu, \sigma D). \tag{1.43}$$

Putting  $B$  and  $D$  on the same footing makes perfect sense since, as we have already noted, these fields gauge transform into each other, in the broken phase.

As one might hope, the  $B$  and  $D$  sector wines can be collected together into a composite  $F$  wine. For the zero-point kernel, we expect to find an object like

---

<sup>13</sup>Actually, this definition differs from that in [57] in which  $F = (B_\mu, D\sigma)$ ; the new definition will remove some annoying signs, later.

$\dot{\Delta}^{\sigma D \sigma D}$ . However, we can simplify this. Anticommuting one of the  $\sigma$ s through the functional derivative, we can combine it with the other, at the expense of a minus sign. Therefore, the zero-point  $F$ -wine looks like [57]

$$\dot{\Delta}_{MN}^{FF}(p) = \begin{pmatrix} \dot{\Delta}_p^{BB} \delta_{\mu\nu} & 0 \\ 0 & -\dot{\Delta}_p^{DD} \end{pmatrix}. \quad (1.44)$$

We note that there is no such object as a mixed  $BD$  wine, since this would require the existence of an  $\mathcal{AC}$  wine in the unbroken phase.

The diagrammatic flow equation receives correction, since we are no longer differentiating with respect to  $\mathcal{A}$  and  $\mathcal{C}$ , but only with respect to either their block diagonal or block off-diagonal components. The corrections are easy to deduce by introducing the projectors  $d_{\pm}$  on to the block (off) diagonal components [53]:

$$d_{\pm} X = \frac{1}{2} (X \pm \sigma X \sigma). \quad (1.45)$$

Hence, differentiating with respect to partial superfields yields insertions of  $\sigma$ . Representing these insertions by  $*$ , we see the diagrammatic interpretation in figure 1.10, where we differentiate with respect to the partial supermatrix,  $Y$ .

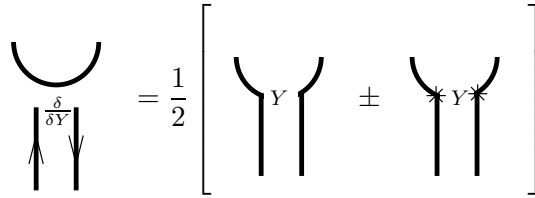


Figure 1.10: Diagrammatic representation of differentiation with respect to a partial supermatrix,  $Y$ .

Clearly, instances of  $\sigma$ , whether they come from vertices containing a  $\mathcal{C}$  in the unbroken phase or from differentiation with respect to partial supermatrices, affect the group theory structure of diagrams. For circuits containing fields, we may expect to find (implied) supertrace structures like  $\text{str } XY \cdots \sigma$ . For empty circuits, the effect is more profound. In the unbroken phase, if a

circuit is devoid of dynamical fields, then it must yield  $\text{str } \mathbb{1} = 0$ . However, in the broken phase we can have a circuit devoid of dynamical fields but which contains an insertion of  $\sigma$ . Such a circuit now yields  $\text{str } \sigma = 2N$ .

## Symmetries

We have already discussed no- $\mathcal{A}^0$  symmetry to the desired depth, for this section of the thesis. We will return to it, however, in chapters 2 and 3. The other symmetries we will make use of are the residual  $SU(N|N)$  symmetries left over, after symmetry breaking, and charge conjugation (CC) invariance, which we have already mentioned in the symmetric phase.<sup>14</sup>

The residual  $SU(N|N)$  symmetries follow from decomposing  $\Omega$  into bosonic and fermionic parts, which we denote by  $\omega = d_+\Omega$  and  $\tau = d_-\Omega$ , respectively. Defining  $D_\mu = \partial_\mu - iA_\mu$ , the unbroken bosonic gauge transformations give us [57]

$$\begin{aligned}
\delta A_\mu &= D_\mu \cdot \omega \\
\delta B_\mu &= -iB_\mu \cdot \omega \\
\delta C &= -iC \cdot \omega \\
\delta D &= -iD \cdot \omega,
\end{aligned}
\tag{1.46}$$

whereas the broken fermionic gauge transformations yield

$$\begin{aligned}
\delta B_\mu &= D_\mu \cdot \tau \\
\delta A_\mu &= -iB_\mu \cdot \tau \\
\delta D &= -iC \cdot \tau + 2i\tau\sigma \\
\delta C &= -iD \cdot \tau.
\end{aligned}
\tag{1.47}$$

Likewise, we can deduce the gauge transformation of functional derivatives with respect to the broken sector fields by decomposing equations (1.19) and (1.20). Doing so, it is apparent that  $\delta/\delta A$  does not transform homogeneously; gauge invariance of our broken phase flow equation is guaranteed by the coincident line identities.

---

<sup>14</sup>In [57], where both actions were restricted to single supertrace terms, use was made of the symmetry under  $C, D, \sigma \leftrightarrow -C, -D, -\sigma$ . In the current treatment, with this restriction lifted, the symmetry is of no use, since terms which appear to violate this symmetry e.g.  $S^{AAC}$  in fact do not. This is because we can always arrange for there to be an implicit  $\sigma$  hiding on a second supertrace, devoid of any dynamical fields e.g.  $S^{AAC, \sigma}$ .

Two Ward identities now follow from applying (1.46), (1.47) and the broken phase form of (1.19) and (1.20) to the field expansions (1.27) and (1.34). The (unbroken) bosonic gauge transformations [52, 57] yield

$$q_\nu U_{\dots a \nu b \dots}^{\dots XAY \dots}(\dots, p, q, r, \dots) = U_{\dots a b \dots}^{\dots XY \dots}(\dots, p, q+r, \dots) - U_{\dots a b \dots}^{\dots XY \dots}(\dots, p+q, r, \dots), \quad (1.48)$$

where  $U$  can be a vertex from either action or any wine and  $X, Y$  can be any of  $A, C, F$ . There is an appealing geometrical picture of this [51, 52, 57]: we can view the momentum of the field  $A_\nu$  as being pushed forward (diagrammatically, this is in the counterclockwise sense) on to the next obstruction with a plus and pulled back on to the previous obstruction with a minus. An obstruction is any dynamical field ( $\sigma$  commutes with  $\omega$ , and so is blind to this process), or a derivative with respect to any of the (dynamical) fields. Thus, in the case that the momentum of  $A_\nu$  hits the end of a wine, we take either  $X$  or  $Y$  above to be  $Z_1$  or  $Z_2$  in (1.27), as appropriate.

The second Ward identity follows from the (broken) fermionic gauge transformations and is most neatly written in terms of the composite field  $F$ , rather than its components  $B$  and  $\sigma D$ . To this end, we define a Euclidean five momentum [57]<sup>15</sup>

$$q_M = (q_\mu, 2). \quad (1.49)$$

The Ward identities corresponding to the broken, fermionic gauge transformations can now be written in the following compact form:

$$q_N U_{\dots a N b \dots}^{\dots XFY \dots}(\dots, p, q, r, \dots) = U_{\dots a b \dots}^{\dots \vec{XY} \dots}(\dots, p, q+r, \dots) - U_{\dots a b \dots}^{\dots \overleftarrow{XY} \dots}(\dots, p+q, r, \dots), \quad (1.50)$$

where  $X$  and  $Y$  are as before.<sup>16</sup> For  $X = A, C$ ,  $\vec{X} = \overleftarrow{X}$  is the corresponding opposite statistics partner.  $\vec{F}_M = (A_\mu, -C\sigma)$  and  $\overleftarrow{F}_M = (A_\mu, C\sigma)$ .<sup>17</sup>

The final symmetry we look at is charge conjugation (CC) invariance, which will play a central role in the techniques developed in chapter 3. Our  $SU(N|N)$  gauge theory in the broken phase is invariant under [57]:

$$A_\mu \rightarrow -A^T, \quad (1.51)$$

<sup>15</sup>Again, this definition is different from [57], where the two comes with a minus sign.

<sup>16</sup> $\sigma$  anticommutes with  $\tau$  and so if the momentum of a fermionic field is pushed through a  $\sigma$ , we pick up a minus sign.

<sup>17</sup>The signs of the  $C$ -components are opposite to [57].

$$C \rightarrow C^T, \quad (1.52)$$

$$F_M \rightarrow -F_M^T. \quad (1.53)$$

In chapter 3 we will see that both the Ward identities and CC have an intuitive and appealing diagrammatic interpretation.

### 1.2.5 The Weak Coupling Expansion

All calculations performed in this thesis are done in the perturbative regime, and so we now examine the form that the flow equations take, in this limit.

Following [52, 57], the action has the weak coupling expansion

$$S = \sum_{i=0}^{\infty} (g^2)^{i-1} S_i = \frac{1}{g^2} S_0 + S_1 + \dots, \quad (1.54)$$

where  $S_0$  is the classical effective action and the  $S_{i>0}$  the  $i$ th-loop corrections.

The seed action has a similar expansion:

$$\hat{S} = \sum_{i=0}^{\infty} g^{2i} \hat{S}_i. \quad (1.55)$$

Note that these definitions are consistent with  $\Sigma_g = g^2 S - 2\hat{S}$ ; identifying powers of  $g$  in the flow equation, it is clear that  $S_i$  and  $\hat{S}_i$  will always appear together. With this in mind, we now define

$$\Sigma_i = S_i - 2\hat{S}_i. \quad (1.56)$$

The  $\beta$ -function takes the usual form:

$$\beta \equiv \Lambda \partial_{\Lambda} g = \sum_{i=1}^{\infty} g^{2i+1} \beta_i. \quad (1.57)$$

We now substitute expansions (1.54), (1.55) and (1.57) into equation (1.30) and, using equation (1.56), obtain the weak coupling expansion of the flow equation:

$$\Lambda \partial_{\Lambda} S_n = -2 \sum_{r=1}^n (n-r-1) \beta_r S_{n-r} - \sum_{r=0}^n a_0 [S_{n-r}, \Sigma_r] + a_1 [\Sigma_{n-1}]. \quad (1.58)$$

To simplify the diagrammatics, in particular, we introduce the following shorthands:

$$n_r \equiv n - r, \quad n_+ \equiv n + 1, \quad n_- \equiv n - 1. \quad (1.59)$$

Furthermore, for a Wilsonian effective action vertex of loop order  $m$ , we will often refer to the vertex just as  $m$ , rather than  $S_m$ . Similarly, we will use  $\hat{m}$  to refer to  $\hat{S}_m$ . For tree level seed action vertices, we may abbreviate  $\hat{0}$  to just  $\hat{\cdot}$ .

In figure 1.11 we give a diagrammatic representation of equation (1.58) where, for the fields which have been differentiated, we sum over all dynamical, broken phase fields, discarding any combinations which correspond to wines that do not exist (e.g.  $AC$ ). For all other fields, we also allow instances of  $\sigma$ .

$$\left[ \textcircled{n} \right]^{\bullet} = 2 \sum_{r=1}^n (n-r-1) \beta_r \textcircled{n_r} + \frac{1}{2} \sum_{r=0}^n \textcircled{\begin{array}{c} n_r \\ \text{---} \\ \Sigma_r \end{array}} - \frac{1}{2} \textcircled{\begin{array}{c} \Sigma_{n-} \\ \text{---} \\ \text{---} \end{array}}$$

Figure 1.11: Diagrammatic representation of equation (1.58), where diagrams in which the wine bites its own tail have been discarded.

# Chapter 2

## The New Flow Equation

### 2.1 The Need for a New Flow Equation

Given the successful computation of  $\beta_1$  [57] using the flow equation of the previous chapter, (equations (1.30)–(1.32)), one may very well ask why it is necessary for the flow equation to be modified. The key point is that we expect the (unphysical) field  $A^2$  to come with its own coupling,  $g_2$ , which is distinct from  $g$  in the broken phase. In our computation of  $\beta_1$ , this consideration plays no role but, for higher loop calculations, it is of crucial importance.

To understand this, we recall the standard argument as to why the coefficients  $\beta_1$  and  $\beta_2$  are guaranteed to agree, between certain renormalisation schemes [103, 57]. Let us consider relating our coupling,  $g(\Lambda)$ , to some coupling  $\tilde{g}(\mu \mapsto \Lambda)$  which corresponds to a different renormalisation scheme.

Given the dimensionless one-loop matching coefficient,  $\eta$ , we can perturbatively match the two couplings:

$$\frac{1}{\tilde{g}^2} = \frac{1}{g^2} + \eta + \mathcal{O}(g^2).$$

Using the definition of the  $\beta$ -function (equation (1.57)) and its analogue for  $\tilde{g}$ , we obtain:

$$\tilde{\beta}_1 + g^2 \tilde{\beta}_2 = \beta_1 + g^2 \beta_2 + \Lambda \partial_\Lambda \eta + \mathcal{O}(g^4). \quad (2.1)$$

Thus, if  $\Lambda \partial_\Lambda \eta = 0$  (or, at any rate, does not contribute until  $\mathcal{O}(g^4)$ ), we will obtain  $\tilde{\beta}_1 = \beta_1$  and  $\tilde{\beta}_2 = \beta_2$ .

We must now examine under what conditions  $\Lambda \partial_\Lambda \eta$  vanishes. Clearly, if there is some finite physical scale other than  $\Lambda$ , then we will be able to construct

an  $\eta$  whose flow does not vanish. Similarly, this can be achieved by the presence of dimensionless running couplings, other than  $g$ .<sup>1</sup>

Within the MGI-ERG, there are two potential ways in which a running  $\eta$  can arise. The first is through a generic choice of  $\hat{S}$ , which can lead to even tree level running of  $\eta$ , destroying the agreement between the one-loop  $\beta$ -functions. In [57], it was demonstrated that such running can be removed by a suitable choice of  $\hat{S}$ . In section 5.5 we extend this argument to show that such running can in fact be removed to all orders.

However, this still leaves us with the dimensionless coupling  $g_2$  which, like  $g$ , we know to run at one-loop. There is no reason not to expect this to spoil agreement between our value of  $\beta_2$  and the standard one.

At this juncture, it is worth emphasising that a disagreement between our first two  $\beta$ -function coefficients and the standard values is not necessarily a signature of a sick formalism. Although often referred to as universal,  $\beta_1$  and  $\beta_2$  are not universal in the sense that a physically observable scattering amplitude is. They are better described as being pseudo-universal, since it can be *arranged* for them to depend only on universal details. Hence, there is nothing fundamentally wrong with the matching coefficient  $\eta$  running, even at tree level.

However, the whole point of computing  $\beta_2$  within the MGI-ERG is to provide a stringent test of the formalism. This is most easily done by arranging things so our value should coincide with the standard value and so we will loosely refer to our  $\beta$ -function coefficients as universal.

Let us return to equation (2.1) and consider  $\eta = \eta(g_2)$ . Now,

$$\Lambda \partial_\Lambda \eta = \Lambda \partial_\Lambda g_2 \frac{\partial \eta}{\partial g_2}.$$

Perturbatively, we know that  $\Lambda \partial_\Lambda g_2 \sim g_2^3$  and thus, if  $g_2$  were to vanish, then so does its flow. Hence, our strategy is to tune  $g_2 \rightarrow 0$ , at the end of our calculation. So long as  $\partial \eta / \partial g_2$  does not diverge in this limit, then we can hope to recover the usual  $\beta_2$ .

This is all very well and good, but we have still not said why we need to

---

<sup>1</sup>As noted in [57] this second point is equivalent to the first since dimensional transmutation leads to the introduction of some finite physical scale, other than  $\Lambda$ .

modify the flow equation. The trouble is that, in its current form, the flow equation cannot conveniently distinguish between the fields  $A^1$  and  $A^2$ . In order for us to isolate the effects of  $g_2$ , supplementary terms must be added, so that the necessary distinction can be made.

For convenience, we now define a new variable,

$$\alpha \equiv \frac{g_2^2}{g^2}. \quad (2.2)$$

We also now change notation slightly such that

$$\dot{X} \equiv -\Lambda \partial_\Lambda |_\alpha X; \quad (2.3)$$

this replacing our old definition (1.4).

## 2.2 Modifying the Flow Equation

Our aim is to modify the flow equation, so that it treats  $A^1$  and  $A^2$  differently. It is not hard to guess how to go about doing this. Currently, the flow equation involves objects like  $\delta\Sigma_g/\delta\mathcal{A}_\mu$ . In addition to terms such as this, we now want to try and include terms containing things like  $\sigma\delta\Sigma_g/\delta\mathcal{A}_\mu$ ; the presence of the  $\sigma$  will ensure that, in our new terms,  $A^2$  fields pick up a sign, relative to  $A^1$  fields. Consequently,  $A^1$  and  $A^2$  will be treated differently by the flow equation. The difficulty is ensuring that any terms we add to the flow equation respect no- $\mathcal{A}^0$  symmetry.

To this end, we introduce an operator,  $\mathcal{P}$ , which, when acting on the superfield  $X$ , removes the  $X^0$  component:

$$\mathcal{P}(X) = X - \frac{\mathbb{1}}{2N} \text{str}(\sigma X). \quad (2.4)$$

This then naturally leads us to the symmetric phase version of this operator,  $\mathcal{P}_\mathcal{C}$ , where

$$\mathcal{P}_\mathcal{C}(X) = X - \mathbb{1} \frac{\text{str}(\mathcal{C}X)}{\text{str}\mathcal{C}}. \quad (2.5)$$

We note that  $\mathcal{P}_\mathcal{C}$  is a projector, since it satisfies  $\mathcal{P}_\mathcal{C}^2 = \mathcal{P}_\mathcal{C}$ .

Now, we can use our projector to implement  $\sigma\delta\Sigma_g/\delta\mathcal{A}_\mu$  terms in our flow equation. In the broken phase, rather than multiplying  $\sigma$  by  $\delta\Sigma_g/\delta\mathcal{A}_\mu$ , we want

to first project out the  $\mathcal{A}^0$  part. Then, in the symmetric phase, we replace all  $\sigma$ s by  $\mathcal{C}$ s. Thus, the building blocks for our new terms look like

$$\mathcal{C}\mathcal{P}_{\mathcal{C}}\left(\frac{\delta\Sigma_g}{\delta\mathcal{A}_\mu}\right). \quad (2.6)$$

However, this is not quite what we want. If we are to introduce terms like

$$\mathcal{C}\frac{\delta\Sigma_g}{\delta\mathcal{A}_\mu},$$

then, to preserve CC invariance, we must also introduce terms like

$$\frac{\delta\Sigma_g}{\delta\mathcal{A}_\mu}\mathcal{C}.$$

To do this, we simply let the first  $\mathcal{C}$  of equation (2.6) act via anti-commutation.

The final change we must make to the building block (2.6), so that it is suitable for use in the flow equation, is to multiply though by  $\text{str}\mathcal{C}$ . If we were not to do this, then our flow equation would contain terms with an overall factor of  $1/\text{str}\mathcal{C}$ .

With these points in mind, we introduce a new wine,  $\{\dot{\Delta}_\sigma^{\mathcal{A}\mathcal{A}}\}$  and write down a new flow equation, which can distinguish between  $A^1$  and  $A^2$ , whilst respecting no- $\mathcal{A}^0$  symmetry.

$$-\Lambda\partial_\Lambda S = a_0[S, \Sigma_g] - a_1[\Sigma_g], \quad (2.7)$$

where

$$\begin{aligned} a_0[S, \Sigma_g] &= \frac{1}{2}\frac{\delta S}{\delta\mathcal{A}_\mu}\{\dot{\Delta}^{\mathcal{A}\mathcal{A}}\}\frac{\delta\Sigma_g}{\delta\mathcal{A}_\mu} + \frac{1}{2}\frac{\delta S}{\delta\mathcal{C}}\{\dot{\Delta}^{\mathcal{C}\mathcal{C}}\}\frac{\delta\Sigma_g}{\delta\mathcal{C}} \\ &+ \frac{1}{16N}\frac{\delta S}{\delta\mathcal{A}_\mu}\{\dot{\Delta}_\sigma^{\mathcal{A}\mathcal{A}}\}\left\{\mathcal{C}\text{str}\mathcal{C}, \mathcal{P}_{\mathcal{C}}\left(\frac{\delta\Sigma_g}{\delta\mathcal{A}_\mu}\right)\right\} \\ &+ \frac{1}{16N}\left\{\mathcal{C}\text{str}\mathcal{C}, \mathcal{P}_{\mathcal{C}}\left(\frac{\delta S}{\delta\mathcal{A}_\mu}\right)\right\}\{\dot{\Delta}_\sigma^{\mathcal{A}\mathcal{A}}\}\frac{\delta\Sigma_g}{\delta\mathcal{A}_\mu} \end{aligned} \quad (2.8)$$

and

$$\begin{aligned} a_1[\Sigma_g] &= \frac{1}{2}\frac{\delta}{\delta\mathcal{A}_\mu}\{\dot{\Delta}^{\mathcal{A}\mathcal{A}}\}\frac{\delta\Sigma_g}{\delta\mathcal{A}_\mu} + \frac{1}{2}\frac{\delta}{\delta\mathcal{C}}\{\dot{\Delta}^{\mathcal{C}\mathcal{C}}\}\frac{\delta\Sigma_g}{\delta\mathcal{C}} \\ &+ \frac{1}{16N}\frac{\delta}{\delta\mathcal{A}_\mu}\{\dot{\Delta}_\sigma^{\mathcal{A}\mathcal{A}}\}\left\{\mathcal{C}\text{str}\mathcal{C}, \mathcal{P}_{\mathcal{C}}\left(\frac{\delta\Sigma_g}{\delta\mathcal{A}_\mu}\right)\right\} \\ &+ \frac{1}{16N}\left\{\mathcal{C}\text{str}\mathcal{C}, \mathcal{P}_{\mathcal{C}}\left(\frac{\delta}{\delta\mathcal{A}_\mu}\right)\right\}\{\dot{\Delta}_\sigma^{\mathcal{A}\mathcal{A}}\}\frac{\delta\Sigma_g}{\delta\mathcal{A}_\mu}. \end{aligned} \quad (2.9)$$

There are several things to note about the new flow equation. First, it is indeed gauge invariant: it is straightforward to demonstrate that, for the new terms, the inhomogeneous part of  $\delta(\delta/\delta\mathcal{A})$  (see equation (1.20)) cancels out. Secondly, we note that the new terms come with an overall factor of  $1/16N$ . This is just a convenient normalisation factor, as we will see shortly. Thirdly, we have been completely diplomatic in the way the new terms have been introduced which is why, in addition to the anti-commutator structure,  $a_0$  (and  $a_1$ ) has two new parts, rather than one. This diplomacy is down to choice. We do this to maintain the simple diagrammatic rule that we decorate all structures in all possible ways.

Needless to say, our new flow equation satisfies the usual requirements we demand of a flow equation and so is perfectly valid. However, we do emphasise that our flow equation is by no means unique: there are an infinite class of good flow equations which distinguish between  $A^1$  and  $A^2$  whilst respecting no- $\mathcal{A}^0$  symmetry. We will return to this point in the conclusion.

## 2.3 The New Diagrammatics-I

### 2.3.1 The Symmetric Phase

By supplementing the flow equation with new terms, it is inevitable that our diagrammatics must change. The obvious expectation is that it must become more complicated, which is borne out in this section. However, this complication turns out to be a temporary evil, as we will be guided to diagrammatics which are actually simpler than those of the previous chapter!

The first thing to note in deriving diagrammatic rules for the new terms in the flow equation is that, for these new terms, supersowing and supersplitting are exact (this is straightforward to check, using the techniques of section 1.2.3).

Let us examine the new classical terms. Expanding out the projector, we have things like

$$\left[ \left\{ \mathcal{C}, \frac{\delta\Sigma_g}{\delta\mathcal{A}_\mu} \right\} \text{str} \mathcal{C} - 2\mathcal{C} \text{str} \left( \mathcal{C} \frac{\delta\Sigma_g}{\delta\mathcal{A}_\mu} \right) \right].$$

In the first term, we will be tying either  $\mathcal{C} \delta\Sigma/\delta\mathcal{A}_\mu$  or  $\delta\Sigma/\delta\mathcal{A}_\mu \mathcal{C}$  back into a supertrace. In the second term above, the  $\delta\Sigma/\delta\mathcal{A}_\mu$  is already part of a supertrace; it is the  $\mathcal{C}$  sitting outside the supertrace that must be tied up.

Now, either way, there is an instance of  $\mathcal{C}$  that is tied up by the covariantisation. Referring to the superfield expansion of the wine (1.23), it is clear that this  $\mathcal{C}$  sits just past the end of one side of the wine. Thus, as an intermediate step, we can represent the classical part of the flow equation as in figure 2.1. The double circle notation will be interpreted shortly, but we note that the double circles attach only to  $\dot{\Delta}_\sigma^{\mathcal{A}\mathcal{A}}$  wines (a corollary of which is that all functional derivatives are with respect to  $\mathcal{A}$ , in the new terms) and that their position arguments are the same as those of the functional derivatives they sit next to.

$$a_0[\Sigma_g] = \frac{1}{2} \left[ \begin{array}{c} \textcircled{S} \\ | \\ \textcircled{\Sigma_g} \end{array} \right] + \frac{1}{16N} \left[ \begin{array}{c} \textcircled{S} \\ | \\ \textcircled{\Sigma_g} \end{array} \right] + \left[ \begin{array}{c} \textcircled{S} \\ | \\ \textcircled{\Sigma_g} \end{array} \right] + \left[ \begin{array}{c} \textcircled{S} \\ | \\ \textcircled{\Sigma_g} \end{array} \right] + \left[ \begin{array}{c} \textcircled{S} \\ | \\ \textcircled{\Sigma_g} \end{array} \right]$$

Figure 2.1: Diagrammatics for the classical part of the new flow equation.

The interpretation of the double circles is simple. For the component which looks like

$$\mathcal{C} \frac{\delta \Sigma_g}{\delta \mathcal{A}_\mu} \text{str } \mathcal{C},$$

we have a dumbbell structure as usual but with

1. an extra  $\mathcal{C}$  sitting between one end of the wine and one of the lobes,
2. an accompanying  $\text{str } \mathcal{C}$ .

For the component looking like

$$\mathcal{C} \text{str} \left( \mathcal{C} \frac{\delta \Sigma_g}{\delta \mathcal{A}_\mu} \right),$$

the dumbbell structure now terminates in a  $\mathcal{C}$ , rather than the usual lobe. However, there is an accompanying supertrace, in which we can think of one of the  $\mathcal{A}$ s of  $\Sigma_g$  having been replaced by a  $\mathcal{C}$ . The diagrammatic interpretation is shown in figure 2.2.

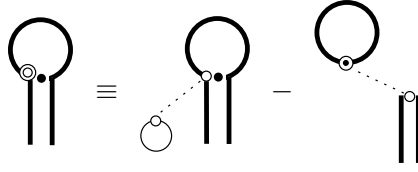


Figure 2.2: Interpretation of the double circle notation.

In both diagrams, the dotted line is a ‘false’ kernel which, if joining two fields with position arguments  $x$  and  $y$ , is taken as  $\delta(x - y)$ . The interpretation of the first diagram is straightforward. In the second diagram, the  $\odot$  tells us to replace an  $\mathcal{A}$  with a  $\mathcal{C}$ . As for the wine, it is ‘plugged’ by a  $\mathcal{C}$ , rather than ending in a functional derivative; the functional derivative being linked to this  $\mathcal{C}$  via a false kernel. In both diagrams of figure 2.2, the wine is of type  $\dot{\Delta}_\sigma^{\mathcal{A}\mathcal{A}}$ . Note that one the  $\mathcal{A}$ s which labels such wines may now be linked to the end of the wine by a false kernel.

The diagrammatics for the quantum term, shown in figure 2.3, is obvious (we ignore diagrams in which the wine bites its own tail).

$$a_0[\Sigma_g] = \frac{1}{2} \left( \text{Diagram 1} \right) + \frac{1}{16N} \left[ \text{Diagram 2} + \text{Diagram 3} + \text{Diagram 4} + \text{Diagram 5} \right]$$

Figure 2.3: Diagrammatics for the quantum part of the new flow equation.

### 2.3.2 The Broken Phase

Adapting the symmetric phase diagrammatics to the broken phase is harder than it was for the old flow equation.

With the old flow equation, we started off with fields  $\mathcal{A}$  and  $\mathcal{C}$  and broke the supersymmetry to give the dynamical fields  $A, C, F$  and insertions of  $\sigma$ . The flow equation was then written naturally in terms of vertices and wines decorated by these fields.

Now, however, whilst the symmetry breaking is still the same, the flow equation allows us to sensibly ‘look inside’  $A$  and compute the flow of (say) just  $A^1$ . The difficulty comes because  $A$  decomposes into not just  $A^1$  and  $A^2$ , but also  $\mathcal{A}^0$ ; the presence of this latter field is awkward. Nonetheless, we will find that there is a prescription we can use to automatically remove  $\mathcal{A}^0$  from the diagrammatics, so long as we accept some further corrections to supersowing and supersplitting.

Before doing this, let us look at the diagrammatics as would naturally follow from the previous chapter. As an illustration, we will consider the flow of a vertex decorated by two  $A^1$ s. In figure 2.4 we focus on the classical part of the flow equation. Filled circles represent  $A$ s and, if they are tagged with a ‘1’, then they are restricted to the  $A^1$  sector. We have suppressed the Lorentz indices of the decorative fields. Note also that we have attached our false kernel to instances of  $\sigma$ , which do not carry a position argument. If the  $\sigma$  has replaced an  $A$ , then the position argument of the  $A$  is the information carried by the appropriate end of the false kernel. However, the other end may attach to a  $\sigma$  with no associated field to provide a position argument. In this case, the false kernel does not carry a position space  $\delta$ -function, but just serves to remind us how the diagrams of which they comprise a part were formed. The ellipsis represents the un-drawn diagrams spawned by the quantum term.

There are a number of important points to make about the diagrams of figure 2.4.

Diagram 2.1 is the only diagram produced by a term from the original flow equation. The factor of  $1/2$  associated with the original  $a_0$  terms has been killed by the factor of two coming from summing over the two possible locations of the fields which decorate the dumbbell. Notice that the differentiated fields are in the  $A$ -sector only. Generically, the differentiated fields can also be  $F$ s and  $C$ s. However, both of these are forbidden in this case by our choice of external fields: in the former case because  $S^{AF}$  vertices do not exist and, in the latter case, because the  $S^{AC}$  vertex vanishes by CC.

Now, given that the external fields are both  $A^1$ s, it would perhaps be expected that the differentiated fields are  $A^1$ s, also. To investigate this, it is

$$\begin{aligned}
& -\Lambda \partial_\Lambda \left[ \begin{array}{c} 1 \\ \bullet \\ \text{S} \\ \bullet \\ 1 \end{array} \right] = \begin{array}{c} 2.1 \\ \bullet \\ \text{S} \\ \bullet \\ \text{\Sigma}_g \\ \bullet \\ 1 \end{array} \\
& + \frac{1}{16N} \left[ \begin{array}{c} 2.2 \\ \bullet \\ \text{S} \\ \bullet \\ \text{\Sigma}_g \\ \bullet \\ 1 \end{array} \right] 8 \quad -4 \quad \begin{array}{c} 2.3 \\ \bullet \\ \text{S} \\ \bullet \\ \text{\Sigma}_g \\ \bullet \\ 1 \end{array} \quad -4 \quad \begin{array}{c} 2.4 \\ \bullet \\ \text{\Sigma}_g \\ \bullet \\ \text{S} \\ \bullet \\ 1 \end{array} \quad + \dots
\end{aligned}$$

Figure 2.4: Classical part of the flow of a vertex decorated by two  $A^1$ s.

useful to construct the projectors

$$\sigma_+ \equiv \begin{pmatrix} \mathbb{1} & 0 \\ 0 & 0 \end{pmatrix}, \quad \sigma_- \equiv \begin{pmatrix} 0 & 0 \\ 0 & \mathbb{1} \end{pmatrix}. \quad (2.10)$$

As we would expect from a pair of projectors,  $\sigma_+^2 = \sigma_+$ ,  $\sigma_-^2 = \sigma_-$  and  $\sigma_+ \sigma_- = \sigma_- \sigma_+ = 0$ .

We cannot take the differentiated field to be just an  $A^1$ , since this would throw away the effects of  $\mathcal{A}^0$  which, for the time being, we must explicitly keep. In other words, we can think of the differentiated field as being  $\sigma_+ \mathcal{A} \sigma_+$ , but note that this has an  $\mathcal{A}^0$  component. The corrections to supersowing and splitting arising from differentiating the partial supermatrix  $\sigma_+ \mathcal{A} \sigma_+$  are just insertions of  $\sigma_+$  which, for classical terms at any rate, can just be ignored, since they do not change the supertrace structure.

Let us now focus on the wine in this diagram. Coming from one of the original terms in the flow equation, the wine must be just  $\dot{\Delta}^{AA}$ . The labels of the wine imply that it attaches at each end to  $\delta/\delta A$ . There is no problem with this as we can take the functional derivative to act with respect to a full  $A$ , the unwanted components being killed by the  $\sigma_+$ s. Finally, we note that there

cannot be any instances of  $\sigma$  on the wine: since such  $\sigma$ s act by commutation, the wine dies by virtue of the fact that  $[\sigma, \delta/\delta A] = 0$ .

Let us now turn to diagram 2.2. This is a combination of four diagrams produced by the additions to the flow equation, corresponding to the four ends of the wine on which the  $\sigma$  can sit. Since these diagrams are equivalent, we can add them. Summing over the two locations of the decorative fields gives an overall relative factor of eight, as shown. The wine is  $\dot{\Delta}_\sigma^{AA}$ . That it must be this, and not  $\dot{\Delta}^{AA}$ , can be deduced by the presence of the  $\sigma$  at one of its ends. The final point to note about this diagram is the extra supertrace, which is just  $\text{str } \sigma = 2N$ . Thus we see that this diagram has the same overall factor as the first diagram.

Diagram 2.3 necessitates some new notation. The vertex with argument  $S$  has a feature looking like  $\bullet$ . This tells us that an  $A$  has been differentiated and replaced with a  $\sigma$ . However, the vertex on which this feature is present already has a  $\sigma$  and so we combine them, to leave  $\text{str } \mathbb{1} = 0$ . In fact, we need never have drawn this diagram. The  $S$  vertex coefficient function is  $S^{A\sigma}$ ; single  $A$  vertices vanish by both CC and Lorentz invariance. In anticipation of what is to come, though, we note that multiple supertrace terms can have separate  $\text{str } A\sigma$  factors. This will play a key role in what follows, since  $\text{str } A\sigma$  is none other than  $2N\mathcal{A}^0$ .

Diagram 2.4 also vanishes for the reasons just discussed.

Thus, to recap, only the first two diagrams survive. They come with the same relative factor, have exactly the same vertices and so can be combined. The result will be that the two vertices are now joined by the sum of  $\dot{\Delta}^{AA}$  and  $\dot{\Delta}_\sigma^{AA}$ . It seems natural to define

$$\dot{\Delta}^{A^1A^1} \equiv \dot{\Delta}^{11} \equiv \dot{\Delta}^{AA} + \dot{\Delta}_\sigma^{AA}. \quad (2.11)$$

We can do an analogous analysis in the  $A^2$  sector. The key difference here is that the embedded  $\sigma$  of the analogue of diagram 2.2 gives rise to a minus sign since, whilst  $\text{str } A^1A^1\sigma = \text{str } A^1A^1$ ,  $\text{str } A^2A^2\sigma = -\text{str } A^2A^2$ . In this case, we are led to the definition

$$\dot{\Delta}^{A^2A^2} \equiv \dot{\Delta}^{22} \equiv \dot{\Delta}^{AA} - \dot{\Delta}_\sigma^{AA}. \quad (2.12)$$

However, neither (2.11) or (2.12) work quite as we would like: the wines  $\dot{\Delta}^{AA}$  and  $\dot{\Delta}_{\sigma}^{AA}$  do not attach to just  $A^1$  or  $A^2$ , as the labels of  $\dot{\Delta}^{11}$  and  $\dot{\Delta}^{22}$  seem to imply; we know that there is also attachment to  $\mathcal{A}^0$ .

Nonetheless, both the physics of the situation and the diagrammatics seem to be guiding us to a formalism where we work with  $A^1$ s and  $A^2$ s. It turns out that the most efficient way to proceed is to follow this lead. Recalling that

$$\frac{\delta}{\delta \mathcal{A}_{\mu}} = 2T_A \frac{\delta}{\delta \mathcal{A}_{A\mu}} + \frac{\sigma}{2N} \frac{\delta}{\delta \mathcal{A}_{\mu}^0}$$

we now split up the first term into derivatives with respect to  $A^1$  and  $A^2$ :

$$\frac{\delta}{\delta \mathcal{A}_{\mu}} = 2\sigma_+ \tau_1^a \frac{\delta}{\delta A_{\mu a}^1} - 2\sigma_- \tau_2^a \frac{\delta}{\delta A_{\mu a}^2} + \frac{\sigma}{2N} \frac{\delta}{\delta \mathcal{A}_{\mu}^0}, \quad (2.13)$$

where  $\tau_i^a$  are the generators of the  $SU(N)$  gauge theories carried by  $A^i$ , for  $i = 1, 2$ , normalised to  $\text{tr } \tau_i^a \tau_j^b = 1/2 \delta^{ab} \delta_{ij}$ . We now exploit no- $\mathcal{A}^0$  symmetry and so use the prescription that, since all *complete* functionals (as opposed to individual contributions—see below) are independent of  $\mathcal{A}^0$ , we can take  $\delta/\delta \mathcal{A}^0$  not to act.

At this point it is worth pausing to consider this in more detail. Let us return to figure 2.4. We noted in the first diagram that, tempting as it was to take both vertices to be  $S^{A^1 A^1}$ , we should instead take them to be  $S^{A^1 A}$  vertices. The thing stopping us from working with just  $A^1$ s is the differentiated field: we are of course at liberty to specialise the decorative fields to be whatever we want. Now, however, we are supposing the  $\delta/\delta \mathcal{A}^0$  does not act; in this case, we really can take the vertices to be  $S^{A^1 A^1}$ .

In this picture, diagrams 2.1 and 2.2 still combine but now, with all fields in the  $A^1$  sector, it is natural to talk of the vertices being joined by  $\dot{\Delta}^{11}$ .

What of the final two diagrams? We have already noted that they vanish anyway, but this is only an accidental feature of the particular vertex whose flow we chose to compute. The real point is that they both contain a  $\text{str } \sigma A = \text{str } \mathcal{A}^0$ , which is attached to a wine. In our new picture, we simply never draw such diagrams: we are not interested in external  $\mathcal{A}^0$ s and need not consider internal ones because we do not allow  $\delta/\delta \mathcal{A}^0$  to act.

It is important to realise, though, that this does not mean that the action does not contain  $\text{str } \sigma A$  components; indeed, precisely the opposite is necessary

for no- $\mathcal{A}^0$  symmetry to be preserved. To see this, consider part of the action:

$$\dots + \frac{1}{2} S^{AA\sigma} \text{str} AA\sigma + \frac{1}{2!} S^{A\sigma, A\sigma} \text{str} A\sigma \text{str} A\sigma + \dots$$

No- $\mathcal{A}^0$  symmetry, whose lowest order effects can be deduced by letting  $\delta A_\mu = \lambda \mathbb{1}$  [57, 55] tells us that

$$S^{AA\sigma} \text{str} A\sigma + S^{A\sigma, A\sigma} \text{str} \sigma \text{str} A\sigma = 0, \quad (2.14)$$

i.e. that  $S^{AA\sigma} = -2N S^{A\sigma, A\sigma}$ .

Thus, the presence of the  $S^{A\sigma, A\sigma}$  vertex in the action is necessary to ensure no- $\mathcal{A}^0$  symmetry; the point is that, when using the flow equations, we can choose never to attach to such objects.

Moreover, there is an additional simplification we find when working with  $A^1$ s and  $A^2$ s: all diagrams involving  $\bullet$  vanish. This is because the differentiated field is now restricted to being an  $A^1$  or  $A^2$ . However,

$$\text{str} \sigma \frac{\delta}{\delta A} = \text{tr} \sigma_+ \frac{\delta}{\delta A^1} - \text{tr} \sigma_- \frac{\delta}{\delta A^2} \equiv 0.$$

Had we still been using exact supersowing and supersplitting,  $\text{str} \sigma \delta / \delta A$  terms can survive, via the extension of  $\mathcal{A}$  to  $\mathcal{A}^e$  (cf. equation (1.37)).

There is, though, a price to pay for all this: supersowing and supersplitting both receive new corrections, which we henceforth refer to as attachment corrections. To compute these corrections, consider attachment of a wine via  $\delta / \delta A^1$ , as shown in figure 2.5.

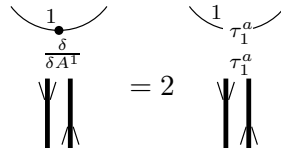


Figure 2.5: Attachment of a wine via  $\delta / \delta A^1$ .

Note that, in the second diagram, we have retained the ‘1’ which previously labelled the  $A^1$ , to remind us that the flavours of any fields which followed or preceded the  $A^1$  are restricted.

Next, we use the completeness relation for  $SU(N)$ ,

$$2(\tau_1^a)^i{}_j(\tau_1^a)^k{}_l = \delta^i{}_l\delta^k{}_j - \frac{1}{N}\delta^i{}_j\delta^k{}_l, \quad (2.15)$$

to obtain figure 2.6, where attachments like those in the first column of diagram on the r.h.s. will be henceforth referred to as direct.

Figure 2.6: A re-expression of figure 2.5.

There is a very similar expression for the  $A^2$  sector. Now, however,  $\sigma_+$ s are replaced with  $\sigma_-$ s and the sign of the  $1/N$  contribution flips, which can be traced back to (1.8). We can also understand the sign flip heuristically because we are tying everything back into supertraces and not traces; we recall that the supertrace yields the trace of the bottom block-diagonal of a supermatrix but picks up a minus sign (see e.g. equation (2.13)).

In the  $B, D$  and  $C$  sectors we do not get any  $1/N$  attachment corrections. Derivatives with respect to the fields  $B$  and  $\bar{B}$ , can simply be written

$$\frac{\delta}{\delta B} = \sigma_- \frac{\delta}{\delta \mathcal{A}} \sigma_+, \quad (2.16)$$

$$\frac{\delta}{\delta \bar{B}} = \sigma_+ \frac{\delta}{\delta \mathcal{A}} \sigma_-, \quad (2.17)$$

and so derivatives with respect to these partial superfields just yield insertions of  $\sigma_{\pm}$ .

In the  $C$ -sector,  $\mathcal{C}^0$  does not play a privileged role and so has not been factored out of the definition of  $C^1$  and  $C^2$  (see equation (1.13)). Hence, derivatives with respect to the components of  $\mathcal{C}$  simply yield insertions of  $\sigma_{\pm}$ .



The expression in figure 2.8 now simplifies. The loop in the middle of the final diagram is decorated only by  $\sigma_+^2$  and so yields  $\text{str } \sigma_+ = N$ . This diagram then cancels either of those with factor  $-1/N$ . We now redraw the remaining diagram with factor  $-1/N$ , as shown in figure 2.9, together with a similar expression in the  $A^2$  sector.

$$\begin{array}{c} \text{Diagram with loop 1, } \frac{\delta}{\delta A^1} \text{, loop 1, } \frac{\delta}{\delta A^1} \\ \text{---} \\ \text{Diagram with loop 1, } \frac{\delta}{\delta A^1} \text{, loop 1, } \frac{\delta}{\delta A^1} \end{array} = \begin{array}{c} \text{Diagram with loop 1, } \frac{\delta}{\delta A^1} \text{, loop 1, } \frac{\delta}{\delta A^1} \\ \text{---} \\ \text{Diagram with loop 1, } \frac{\delta}{\delta A^1} \text{, loop 1, } \frac{\delta}{\delta A^1} \end{array} - \frac{1}{N} \begin{array}{c} \text{Diagram with loop 1, } \frac{\delta}{\delta A^1} \text{, loop 1, } \frac{\delta}{\delta A^1} \\ \text{---} \\ \text{Diagram with loop 1, } \frac{\delta}{\delta A^1} \text{, loop 1, } \frac{\delta}{\delta A^1} \end{array} \quad (2.18)$$

$$\begin{array}{c} \text{Diagram with loop 2, } \frac{\delta}{\delta A^2} \text{, loop 2, } \frac{\delta}{\delta A^2} \\ \text{---} \\ \text{Diagram with loop 2, } \frac{\delta}{\delta A^2} \text{, loop 2, } \frac{\delta}{\delta A^2} \end{array} = \begin{array}{c} \text{Diagram with loop 2, } \frac{\delta}{\delta A^2} \text{, loop 2, } \frac{\delta}{\delta A^2} \\ \text{---} \\ \text{Diagram with loop 2, } \frac{\delta}{\delta A^2} \text{, loop 2, } \frac{\delta}{\delta A^2} \end{array} + \frac{1}{N} \begin{array}{c} \text{Diagram with loop 2, } \frac{\delta}{\delta A^2} \text{, loop 2, } \frac{\delta}{\delta A^2} \\ \text{---} \\ \text{Diagram with loop 2, } \frac{\delta}{\delta A^2} \text{, loop 2, } \frac{\delta}{\delta A^2} \end{array} \quad (2.19)$$

Figure 2.9: The attachment corrections for  $\dot{\Delta}^{A^1 A^1}$  and  $\dot{\Delta}^{A^2 A^2}$ .

Then meaning of the double dotted lines and the associated field hiding behind the line of the supertrace should be clear: the double dotted lines stand for  $\dot{\Delta}^{A^i A^i}$ , and the sub-sector of the associated fields tells us whether  $i = 1$  or  $2$ . (We will use the term sub-sector whenever we want to specify that some unlabelled field is a component of the one of the fields  $A$ ,  $C$  or  $F$ .)

Returning now to diagram 2.5 (figure 2.7) we should interpret the wine when the dummy fields are in the  $A^1$  or  $A^2$  sectors according to (2.18) and (2.19).

In our analysis of the terms spawned by the classical part of the flow equation, we have so far restricted ourselves to diagrams in which the wine is undecorated and for which there are no insertions of the dynamical components of  $\mathcal{C}$  (recall that such insertions occur as in figure 2.2).

Let us first relax just the former restriction and analyse the mapping into the  $A^1$ ,  $A^2$  basis. The simplest case to deal with is where the decorations of

the wines  $\{\dot{\Delta}^{AA}\}$  and  $\{\dot{\Delta}_{\sigma}^{AA}\}$  are, on each side *independently*, net bosonic. In this scenario, we are just mapped into the  $A^1, A^2$  basis, as before.

The next case to examine is where the decorations on one side of the wine are net bosonic but those on the other side are net (anti) fermionic. This immediately tells us that one of the functional derivatives sitting at the end of the wine must be (anti) fermionic. Now, as before, we would like to pair up diagrams with a  $\{\dot{\Delta}^{AA}\}$  wine with those with a  $\{\dot{\Delta}_{\sigma}^{AA}\}$  wine. However, there is a subtlety:  $\sigma$  anticommutes with net fermionic structures. Thus, of the four terms generated with a  $\sigma$  at the end of one side of the wine attached to a separate  $\text{str } \sigma$ , two cancel. Hence, the vertex from  $\{\dot{\Delta}_{\sigma}^{AA}\}$  has a factor of half relative to the vertex from  $\{\dot{\Delta}^{AA}\}$ .

We can still choose a prescription to map us into the  $A^1, A^2$  basis by absorbing this factor into our definition of e.g.  $\dot{\Delta}^{1B, F, \dots, \dots}$ , where both ellipses denote net bosonic decorations.<sup>3</sup>

The final case to examine is where the decorations on one side of the wine are net fermionic whilst those on the other side are net anti-fermionic.<sup>4</sup> The functional derivatives must both be bosonic and in separate sub-sectors.<sup>5</sup> There are no surviving contributions involving  $\{\dot{\Delta}_{\sigma}^{AA}\}$  vertices. Nonetheless, we can still define an object  $\{\dot{\Delta}^{A^1 A^2}\}$  though we note that it must have net fermionic decorations on both sides.

It is important to realise that the broken phase form of equation (1.41) (which we recall follows from the coincident line identities) for wines possessing fermionic decorations mixes contributions from different wines. This is because moving a fermionic decoration from one side of the wine, through a bosonic functional derivative, to the other side changes the sub-sector of the functional derivative. This is illustrated in figure 2.10, where we explicitly indicate which portions of the wine are unchanged by insertions of  $\sigma_{\pm}$ . Fermionic fields are denoted by diamonds.

---

<sup>3</sup>Note that the  $B$  denotes a functional derivative with respect to  $B$ ; since this removes a fermion, the wine decorations must be net fermionic.

<sup>4</sup>If the decorations on both sides are (anti) fermionic, then the vertex belongs to  $\{\dot{\Delta}^{F\bar{F}}\}$ .

<sup>5</sup>It is straightforward to check that one cannot construct a legal wine of this type for which the functional derivatives are fermionic and anti-fermionic.

Figure 2.10: Example of how the broken phase form of (1.41) mixes different wines.

We might worry that this picture is incompatible with gauge invariance:  $\delta/\delta A^1$  and  $\delta/\delta A^2$  necessarily strike different vertices and so it is perhaps not immediately obvious why the inhomogeneous part of  $\delta(\delta/\delta A)$  will cancel.

However, under gauge transformations, we recall that the inhomogeneous part of  $\delta(\delta/\delta A) \sim \mathbb{1} \text{tr} \left[ \frac{\delta}{\delta \mathcal{A}}, \Omega \right]$ . In both diagrams of figure 2.10, the  $\mathbb{1}$  plugs the top of the wine (it does not matter that the  $\mathbb{1}$  reduces to  $\sigma_+$  in one case and  $\sigma_-$  in the other, since there are other fields on the same portion of supertrace). The associated functional derivative is inside a separate trace, and so can strike the same thing in both diagrams. Thus, under gauge transformations of  $\delta/\delta A^1$  and  $\delta/\delta A^2$ , the non-homogeneous parts still vanish for the usual reasons, but we must be careful to recognise that the broken phase form of (1.41) involves vertices from different wines.

Let us now relax the second restriction above and so allow insertions of the dynamical components of  $\mathcal{C}$ . We have seen how diagrams with insertions of  $\sigma$ —linked with a separate  $\text{str} \sigma$ —arising from the new terms in the flow equation, can be combined with diagrams spawned by the original terms in the flow equation, in certain cases. However, diagrams with insertions of the dynamical components of  $\mathcal{C}$  can never be similarly combined. Hence, such diagrams occur only with  $\dot{\Delta}_\sigma^{A^A}$  wines and, moreover, there is no natural way of mapping such terms into the  $A^1, A^2$  basis. There is, of course, nothing to stop us performing functional derivatives with respect to  $A^1$  and  $A^2$  only—indeed, this is what we will do. However, the differentiated fields do not now label the wines in a natural way.

In fact, as we will see, considerations such as this ultimately do not bother us: we will find that, in our calculation of  $\beta$ -function coefficients, all these

awkward terms cancel, between themselves. Hence, our strategy is to lump all the unpleasant terms into our diagrammatic rules, so that they essentially become hidden. We can, at any stage, unpack them if necessary but, generally speaking, we will find that we do not need to do so.

To this end, we note that insertions of  $\mathcal{C}$  always occur at the ends of wines, and so include them in our diagrammatic rules for the wines. The actual interpretation is easy, but must be done with care. As a first example, consider unpacking a wine with two dummy fields at the end, ‘decorated’ by a  $C^1$  and a  $\sigma$ . This is shown in figure 2.11, where the ellipsis denotes wines arising from the new terms in the flow equation whose associated functional derivatives are fermionic.

Figure 2.11: Unpacking a wine, ‘decorated’ by a  $C^1$  and a  $\sigma$ .

It is thus apparent that the decoration of the parent wine by  $C^1$  and  $\sigma$  is not a decoration of a wine in the usual sense. Whilst the parent has components in which  $C^1$  and  $\sigma$  decorate the wine in the manner we are used to (the first three diagrams on the r.h.s.), it is also clear that it has components in which

either the  $C^1$  or  $\sigma$  is embedded at the end of the wine. However, it makes sense to recognise these embedded fields as decorations. By doing this, we are essentially generalising the notion of a wine to include multiple supertraces. Nonetheless, we are mindful that these new decorations behave differently from the ones we have encountered so far. In particular, since embedded components of  $\mathcal{C}$  do not act via commutation, wine vertices involving these embedded fields do not participate in relations such as (1.41).

The factor of  $1/32N$  deserves comment, since one would expect it to be a factor of two larger, from the new flow equation. However, the terms with the  $\dot{\Delta}_\sigma^{AA}$  wine can also be generated from a parent diagram in which the decorative  $C^1$  and  $\sigma$  are in a different order. Hence, we define the diagrammatic rules to compensate for this.

It may seem like we have missed two diagrams, in which  $C^1$  plugs one end of the wine. However, this leaves us with a  $\sigma\delta/\delta A$  which vanishes, in our picture, as we have already discussed.

Whilst our example involves  $C^1$  and  $\sigma$ , it is clear that we could instead have taken any pair of fields belonging to  $\mathcal{C}$ , though we must be very careful taking two instances of  $\sigma$ . If one of them is embedded at the end of the wine and the other is on a lone supertrace, then the corresponding diagram has been used, already, to map us into the  $A^1$ - $A^2$  basis. However, if one of the instances is a ‘normal’ decoration, then such diagrams should be counted. If there are two instances of  $\sigma$  on a wine, it would be natural to eliminate them via  $\sigma^2 = \mathbb{1}$ . Now, however, it is not necessarily correct to do this, as one could be on a different supertrace.

The interpretation of additional decorations of the parent is straightforward. Any instances of the components of  $\mathcal{A}$  are just treated like normal decorations of the wine. However, instances of the components of  $\mathcal{C}$  can act as either normal wine decorations or can be embedded at the ends. In the latter case, they must be accompanied by an additional component of  $\mathcal{C}$ , to create a valid diagram.

This completes the analysis of the diagrammatics we have performed for the new flow equation. We have not explicitly looked at the quantum term, but there are no new considerations in this case. Thus, we can summarise the

prescription that we use in the broken phase.

1. All decorative fields are instances of  $A^1$ ,  $A^2$ ,  $F$ ,  $\bar{F}$ ,  $C^1$ ,  $C^2$  and  $\sigma$ ;  $\mathcal{A}^0$  is excluded.
2. Differentiation is with respect to all dynamical fields, above, where:
  - (a) differentiation with respect to  $A^1$  or  $A^2$  leads to attachment corrections of the type shown in figure 2.6;
  - (b) differentiation with respect to all other fields just involves insertions of  $\sigma_{\pm}$ ;
  - (c) diagrams involving  $\text{str } \sigma \delta / \delta A^{1,2}$  vanish, identically.
3. Full diagrams without any insertions of the components of  $\mathcal{C}$  at the ends of the wine are naturally written in terms of the above fields and their corresponding kernels i.e.  $A^1$ s attach to a (decorated)  $\dot{\Delta}^{11}$  etc.
4. Full diagrams with insertions of the components of  $\mathcal{C}$  are restricted to those for which at least one insertion is not a  $\sigma$ . These diagrams involve the wine  $\dot{\Delta}_{\sigma}^{AA}$  but, for convenience, are packaged together with the decorated wines of the previous item.

## 2.4 The New Diagrammatics-II

### 2.4.1 Construction

The work of the previous section now guides us to a more compact and intuitive diagrammatics, which is considerably easier to deal with. By packaging up the remaining  $\dot{\Delta}_{\sigma}^{AA}$  wines with decorated instances of the other wines, we have taken a step in the right direction. In anticipation that these compact, packaged objects cancel in their entirety when we perform actual calculations, it clearly makes sense to bundle together wines of a different flavour. However, we have really done more than that, as we now point out.

Considering a full diagram with genuine decorations on one side of its wine, we know that these decorations are all on the same supertrace. However, fields embedded at the ends of a wine attach, via a false kernel, to fields which can be

on an entirely different supertrace. Thus, by packaging together terms as we did in the previous section, we have started to combine diagrams with differing supertrace structures. In this section, we extend this to its natural conclusion.

The basic idea is that, rather than considering diagrams with a specific supertrace structure, we instead sum over all legal supertrace structures, consistent with the decorative fields. Thus, let us suppose that we wish to compute the flow of all vertices which can be decorated by the set of fields  $\{f\}$ . The new flow equation takes a very simple, intuitive form, as shown in figure 2.12.

$$-\Lambda\partial_\Lambda \left[ \textcircled{S} \right]^{\{f\}} = \frac{1}{2} \left[ \begin{array}{c} \textcircled{\Sigma_g} \\ \bullet \\ \textcircled{S} \end{array} - \textcircled{\Sigma_g} \right]^{\{f\}}$$

Figure 2.12: The diagrammatic form of the flow equation, when we treat single and multiple supertrace terms together.

Let us now analyse each of the elements of figure 2.12 in turn. On the l.h.s., we have the set of vertices whose flow we are computing. This set comprises all cyclically independent arrangements of the fields  $\{f\}$ , over all possible (legal) supertrace structures. When we specify the fields  $\{f\}$ , we use a different notation from before. As an example, consider  $\{f\} = \{A_\mu^1, A_\nu^1, C^1\}$ , shown in figure 2.13. Note that we have not drawn any vertices comprising a supertrace decorated only by an  $A^1$ , since these vanish.

$$\left[ \textcircled{S} \right]^{A_\mu^1 A_\nu^1 C^1} \equiv \begin{array}{c} \overset{1}{\text{---}} \\ | \\ \textcircled{S} \\ | \\ \overset{1}{\text{---}} \\ \mu \quad \nu \end{array} = \begin{array}{c} \overset{1}{\text{---}} \\ | \\ \textcircled{S} \\ | \\ \overset{1}{\text{---}} \\ \mu \quad \nu \end{array} + \begin{array}{c} \overset{1}{\text{---}} \\ | \\ \textcircled{S} \\ | \\ \overset{1}{\text{---}} \\ \nu \quad \mu \end{array} + \begin{array}{c} \overset{1}{\text{---}} \\ | \\ \textcircled{S} \\ | \\ \overset{1}{\text{---}} \\ \nu \quad \mu \end{array}$$

Figure 2.13: A new style vertex decorated by two  $A^1$ s and a  $C^1$ .

It is apparent that we denote  $A$ s by wiggly lines and  $C$ s by dashed lines. A wildcard field will be denoted by a solid line.

Notice how, in the new style diagram, we explicitly indicate the sub-sector of all the fields. This is because there is no need for them to be on the same supertrace and so, for example, there is nothing to prevent an  $A^1 A^1 C^2$  vertex. In the old notation, however, all fields on the same circle are on the same supertrace and so, once we know the sub-sector of one field, the sub-sectors of the remaining fields on the same circle follow, uniquely.

To symbolically represent the new vertices, we will somewhat loosely write e.g.  $S_{\mu\nu}^{11C^1}$ . If we need to emphasise that we are using the new style diagrammatics, as opposed to the old style diagrammatics, then we will write  $S_{\mu\nu}^{\{11C^1\}}$ , reminding us that the fields are arranged in all cyclically independent ways over all possible (legal) supertrace structures.

With these points in mind, let us return to figure 2.12. The diagrams on the r.h.s. both involve the structure  $\text{---}\bullet\text{---}$ . This is a dummy kernel which attaches, at either end, to dummy fields. The fields at the ends can be any of  $A^1, A^2, C^1, C^2, \bar{F}$  or  $F$ , so long as the corresponding diagram actually exists. The dummy kernel can be decorated by any subset of the fields  $\{f\}$  where, if a pair of decorative fields are both components of  $\mathcal{C}$  (and one of them is dynamical), then we include the possibility that the kernel can be of the type  $\dot{\Delta}_\sigma^{AA}$ . In this case, we note that there are implicit factors of  $1/16N$ .

The relationship between the new diagrammatics for the wines and the old diagrammatics is straightforward, and is illustrated in figure 2.14 for the case of a new-style wine decorated by a single  $A^1$ .

$$\left[ \begin{array}{c} \bullet \\ | \end{array} \right]^{A^1} \equiv \bullet \text{---} \text{wavy} \text{---} \bullet = \begin{array}{c} \bullet \\ \uparrow \\ | \\ \bullet \\ \downarrow \\ \bullet \end{array} + \begin{array}{c} \bullet \\ \downarrow \\ | \\ \bullet \\ \uparrow \\ \bullet \end{array}$$

Figure 2.14: A new style (dummy) wine decorated by a single  $A^1$ .

Having described the new diagrammatics for vertices and kernels, we are nearly ready to complete our interpretation of figure 2.12. Before we do so, however, we use our new notation to hide one further detail: instances of  $\sigma$ .

When using the old flow equation, instances of  $\sigma$  mixed fields from different

sub-sectors e.g.  $\sigma C = C^1\sigma_+ - C^2\sigma_-$ . Now, however, instances of  $\sigma$  yield a constant factor of either  $\pm 1$  or  $2N$ . Thus, instances of  $\sigma$  can be replaced by numerical factors accompanying wines / vertices. We need only remember that the multiple supertrace decorations of wines arising from the new terms in the flow equation exist. Such terms require two instances of  $\mathcal{C}$  (at least one of which we take to be dynamical). In the case that one of these fields is a  $\sigma$ , we must remember that it is now hidden.

With these implicit instance of  $\sigma$  in mind, the interpretation of the r.h.s. of figure 2.12 is simple: the decorative fields  $\{f\}$  are distributed around the two diagrams in all possible, independent ways.

### 2.4.2 Identical Fields

Let us reconsider the flow of a vertex in our new diagrammatic approach by looking again at figure 2.12. Suppose that we wish to explicitly decorate with the set of fields  $\{f\}$ . In the case that some of these fields are identical—we will be more precise about the meaning of this shortly—the set of fully decorated diagrams on the r.h.s. can be simplified.

When explicitly decorating a diagram, we sum over all independent permutations of the fields. The individual components of each diagram—vertices and wines—automatically include all permutations of any decorations. So, the rule is that we must divide the fields  $\{f\}$  in all possible ways between the number of structures. Suppose we have two identical fields,  $X$  and  $Y$ , and suppose further that we have drawn the diagram in which  $X$  decorates structure  $U$  and  $Y$  decorates structure  $V$ . Rather than also counting the diagram in which  $X$  decorates  $V$  and  $Y$  decorates  $U$ , we can take just the first case and multiply by two.

As an example, we will compute the flow of a vertex decorated by  $A_\mu^1(p)$  and  $A_\nu^1(-p)$ . These fields are counted as identical: by Bose symmetry, the diagrams which they decorate are invariant under  $p_\mu \leftrightarrow -p_\nu$ . Thus, we obtain the diagrams of figure 2.15, where we have suppressed both Lorentz indices and sub-sector labels.

$$\begin{aligned}
-\Lambda\partial_\Lambda \text{ (diagram with } S \text{)} &= - \text{ (diagram with } \hat{S} \text{ and } S \text{)} - 2 \text{ (diagram with } \hat{S} \text{ and } S \text{)} + \text{ (diagram with } \Sigma_g \text{ and } S \text{)} \\
&= -\frac{1}{2} \left[ \text{ (diagram with } \Sigma_g \text{)} - 2 \text{ (diagram with } \Sigma_g \text{)} - \text{ (diagram with } \Sigma_g \text{)} \right]
\end{aligned}$$

Figure 2.15: The flow of a vertex decorated by two  $A^1$ s (or  $A^2$ s), using the new diagrammatics.

Since the fields  $A_\mu^1(p)$  and  $A_\nu^1(-p)$  are never differentiated, we call them external fields—as opposed to the internal fields sitting at the ends of the wines.

Let us start by looking at the dumbbell terms. The first diagram contains a one-point vertex. One-point vertices do not exist in the  $A$  or  $F$ -sectors, and we demand that Wilsonian effective action one-point vertices vanish, in order that the superhiggs potential is not shifted by quantum corrections [57]. Hence, the one-point vertex must be a seed action vertex in either of the  $C$  sub-sectors. Therefore, the external fields must decorate the  $S$ -lobe, rather than the  $\Sigma_g$  lobe. Since both of these fields are on the same vertex, there is no factor of two. However, by taking only the seed action part of the  $\Sigma_g$  vertex, we get a factor of  $-2$ . (Recall  $\Sigma_g = g^2 S - 2\hat{S}$ .)

The next dumbbell term comes with an additional factor of two, compared to the first, since the two external fields are now on different structures. We note that this diagram in fact vanishes, since if the wine is in the  $C$ -sector (as in the first diagram) then the bottom vertex is an  $AC$  vertex, which does not exist. The final dumbbell contains a ‘full’  $\Sigma_g$ . This diagram picks up a factor of two in recognition of the indistinguishability of the  $A_\mu^1(p)$  and  $A_\nu^1(-p)$ .

The first and third quantum terms do not pick up a factor of two, since the external fields decorate the same structure. The middle quantum term, on the other hand, comes with a relative factor of two.

When we come to use the MGI-ERG for computation, we will compute the

flow of vertices that are part of some complete diagram. Such vertices will generically contain fields which are external with respect to the diagram as a whole and some which are internal to the diagram as a whole (these latter fields can, of course, be external with respect to some sub-diagram). Whether or not internal fields—whose flavour, we recall, is summed over—can be treated as identical depends on the topology of the diagram in question. This will become clear when we start to manipulate complete diagrams in chapter 4.

### 2.4.3 Additional Notation

Whilst we will generally use the new diagrammatics thus described, from now on, it is occasionally useful to flip back to the old style mentality of specifying the supertrace structure. It turns out that, in this thesis, we only ever have recourse to do this for single supertrace terms and so introduce the notation ‘Fields as Shown’ or FAS. An example of this is illustrated in figure 2.16.

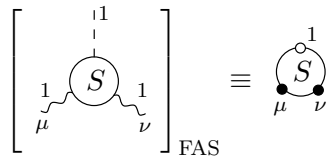


Figure 2.16: An example of the meaning of FAS.

The second new piece of notation allows us to perform an intermediate step between going from figure 2.12—where all the decorations are implicit—to a set of explicitly decorated diagrams.

Suppose that we have a diagram for which we want to focus on the components possessing a two-point vertex. So long as there is still at least one field sitting as an implicit decoration, we must specify that our vertex has precisely two decorations. We use a superscript on the vertex argument to denote this. Two examples are shown in figure 2.17.

In the first diagram, we see that we must use one and only one element of the set  $\{f\}$  to decorate the bottom vertex. In the second diagram, the elements

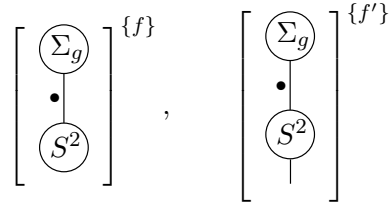


Figure 2.17: Forcing a vertex on an implicitly decorated diagram to have precisely two decorations.

of  $\{f'\}$  must all decorate some structure other than the bottom vertex.

#### 2.4.4 Constraints in the $C$ -sector

Recall from section 1.2.2 that, in order to ensure quantum corrections do not shift the minimum of the Higgs potential from the classical choice,  $\sigma$ ,  $\hat{S}$  is constrained. Assuming that these quantum corrections vanish means that all Wilsonian effective action one-point  $C$  vertices vanish. By computing the flow of an object we know to vanish, we arrive at the desired constraint equation, as shown in figure 2.18. Note that the external fields can be in either the 1 or 2 sub-sector.

$$\begin{aligned}
 -\Lambda \partial_\Lambda \begin{array}{c} \textcircled{S} \\ \vdots \end{array} = 0 &= \frac{1}{2} \left[ \begin{array}{c} \textcircled{\Sigma_g} \\ \bullet \\ \textcircled{S} \\ \vdots \end{array} + \begin{array}{c} \textcircled{S} \\ \bullet \\ \textcircled{\Sigma_g} \\ \vdots \end{array} - \begin{array}{c} \textcircled{\Sigma_g} \\ \bullet \\ \textcircled{\Sigma_g} \\ \vdots \end{array} - \begin{array}{c} \textcircled{\Sigma_g} \\ \bullet \\ \textcircled{\Sigma_g} \\ \vdots \end{array} \right] \\
 \Rightarrow -2 \begin{array}{c} \textcircled{\hat{S}} \\ \bullet \\ \textcircled{S} \\ \vdots \end{array} &= \begin{array}{c} \textcircled{\Sigma_g} \\ \bullet \\ \textcircled{\Sigma_g} \\ \vdots \end{array} + \begin{array}{c} \textcircled{\Sigma_g} \\ \bullet \\ \textcircled{\Sigma_g} \\ \vdots \end{array} \quad (2.20)
 \end{aligned}$$

Figure 2.18: The constraint arising from ensuring that the position of the minimum of the Higgs potential is unaffected by quantum corrections.

To go from the first line to the second line, we have used  $\Sigma_g = g^2 S - 2\hat{S}$  and have discarded all one-point, Wilsonian effective action vertices. To satisfy equation (2.20), we tune the one-point, seed action vertex in the first diagram, which is something we are free to do.

## 2.5 The Weak Coupling Expansion

### 2.5.1 The flow Equation

By isolating the effects of  $g_2$  (equivalently,  $\alpha$ ), the weak coupling expansion of the flow equation, (1.58), changes since we now write<sup>6</sup>

$$\Lambda \partial_\Lambda S = \Lambda \partial_\Lambda|_\alpha S + \Lambda \partial_\Lambda \alpha \frac{\partial S}{\partial \alpha}.$$

To obtain our new weak coupling expansion of the flow equation, it is necessary that we understand  $\Lambda \partial_\Lambda \alpha$ , in the perturbative domain. The first thing we note is that we have  $\beta$ -functions for both  $g$  and  $g_2$ , where the coefficients generically depend on  $\alpha$ :

$$\Lambda \partial_\Lambda \frac{1}{g^2} = -2 \sum_{i=1}^{\infty} \beta_i(\alpha) g^{2(i-1)} \quad (2.21)$$

$$\Lambda \partial_\Lambda \frac{1}{g_2^2} = -2 \sum_{i=1}^{\infty} \tilde{\beta}_i(1/\alpha) g_2^{2(i-1)}. \quad (2.22)$$

Now, we know already the value of  $\beta_1$  and, moreover, that it is independent of  $\alpha$  [57]. The coefficient  $\beta_2(\alpha)$  is what we will compute in this thesis. For generic  $\alpha$ , we expect it to disagree with the standard value but, as discussed earlier, hope that agreement is reached for  $\beta_2(0)$ .

What of the coefficients  $\tilde{\beta}_i(1/\alpha)$ ? These are determined through the renormalisation condition

$$S[\mathcal{A} = A^2, \mathcal{C} = \bar{\mathcal{C}}] = -\frac{1}{2\alpha g^2} \text{tr} \int d^D x \left( F_{\mu\nu}^2 \right)^2 + \dots, \quad (2.23)$$

where the ellipsis denotes higher dimension operators and ignored vacuum energy. The minus sign arises because the  $SU(N)$  Yang-Mills theory carried by  $A^2$  comes with the wrong sign kinetic term; if we were to absorb this sign

---

<sup>6</sup>We avoid writing  $\partial/\partial\alpha$  as  $\partial_\alpha$  to avoid confusion later, when we will have momentum derivatives which are written e.g.  $\partial_\alpha^k$ .

into the coupling,  $g_2^2$ , then we could think of our unphysical Yang-Mills theory as having imaginary coupling. Hence,  $\tilde{\beta}_1 = -\beta_1$  and  $\tilde{\beta}_2(0) = \beta_2(0)$ .<sup>7</sup>

Utilising equations (2.21) and (2.22) and rewriting  $g_2^2$  in terms of  $\alpha g_1^2$ , it is apparent that  $\Lambda \partial_\Lambda \alpha$  has the following weak coupling expansion:

$$\Lambda \partial_\Lambda \alpha = \sum_{i=1}^{\infty} \gamma_i g^{2i}, \quad (2.24)$$

where

$$\gamma_i = -2\alpha \left( \beta_i(\alpha) - \alpha^i \tilde{\beta}_i(1/\alpha) \right).$$

Knowing that  $\tilde{\beta}_1 = -\beta_1$ , we have

$$\gamma_1 = -2\beta_1 \alpha (1 + \alpha), \quad (2.25)$$

which it turns out we will need, for our computation of  $\beta_2$ .

Now, the weak coupling expansion reads:

$$\dot{S}_n = \sum_{r=1}^n \left[ 2(n-r-1)\beta_r S_{n-r} + \gamma_r \frac{\partial S_{n-r}}{\partial \alpha} \right] + \sum_{r=0}^n a_0 [S_{n-r}, \Sigma_r] - a_1 [\Sigma_{n-1}], \quad (2.26)$$

where we recall that  $\dot{S}$  has been redefined (equation (2.3)) to mean  $\Lambda \partial_\Lambda |_\alpha S$ . Incidentally, we note that the kernels  $\dot{\Delta}^{ff}$  appearing in the flow equation are defined according to the new definition of  $\dot{X}$  i.e. they are differentiated at constant  $\alpha$ . This is a choice we are free to make about the flow equation and do so, since it makes life easier.

The diagrammatics for the new weak coupling flow equation follow, directly. However, we note that the classical term can be brought into a more symmetrical form. This follows from the invariance of  $a_0[S_{n-r}, \Sigma_r] + a_0[S_r, \Sigma_{n-r}]$  under  $r \rightarrow n-r$ . We exploit this by recasting the classical term as follows:

$$\begin{aligned} a_0[\bar{S}_{n-r}, \bar{S}_r] &\equiv a_0[S_{n-r}, S_r] - a_0[S_{n-r}, \hat{S}_r] - a_0[\hat{S}_{n-r}, S_r]. \\ &= \begin{cases} \frac{1}{2} (a_0[S_{n-r}, \Sigma_r] + a_0[S_r, \Sigma_{n-r}]) & n-r \neq r \\ a_0[S_r, \Sigma_r] & n-r = r. \end{cases} \end{aligned} \quad (2.27)$$

Hence, we can rewrite the flow equation in the following form:

$$\dot{S}_n = \sum_{r=1}^n \left[ 2(n-r-1)\beta_r S_{n-r} + \gamma_r \frac{\partial S_{n-r}}{\partial \alpha} \right] + \sum_{r=0}^n a_0 [\bar{S}_{n-r}, \bar{S}_r] - a_1 [\Sigma_{n-1}]. \quad (2.28)$$

---

<sup>7</sup>We note that there is no reason to expect  $\tilde{\beta}_2(1/\alpha) = \beta_2(\alpha)$  since  $g$  and  $g_2$  are not treated symmetrically in the flow equation.

The diagrammatic version is shown in figure 2.19, where we have used the various shorthands described in section 1.2.5.

$$\left[ \begin{array}{c} \bullet \\ \circlearrowleft n \end{array} \right] \{f\} = \left[ 2 \sum_{r=1}^n \left[ (n_r - 1) \beta_r + \gamma_r \frac{\partial}{\partial \alpha} \right] \begin{array}{c} \bullet \\ \circlearrowleft n_r \end{array} + \frac{1}{2} \sum_{r=0}^n \begin{array}{c} \bullet \\ \circlearrowleft \bar{n}_r \\ \bullet \\ \circlearrowleft \bar{r} \end{array} - \frac{1}{2} \begin{array}{c} \bullet \\ \circlearrowleft \Sigma_{n-} \end{array} \right] \{f\}$$

Figure 2.19: The new diagrammatic form for the weak coupling flow equation.

Terms like the one on the l.h.s., in which the entire diagram is struck by  $\Lambda \partial_\Lambda |_\alpha$ , are referred to as  $\Lambda$ -derivative terms. On the r.h.s., in addition to the usual classical and quantum terms, we have the so called  $\beta$  and  $\alpha$  terms.

It is worth remarking that the diagrammatics of figure 2.19 can be applied to the old flow equation as well: we simply take the fields  $\{f\}$  to be  $As$ ,  $Cs$  and  $Fs$  and interpret the wines accordingly. Notice, indeed, that the old flow equation actually provides a very strong clue as to the (algebraic) form the new flow equation must take. Consider taking  $\{f\} = AA$  (i.e. we are using the old flow equation) and, as in [57], working only with single supertrace terms.<sup>8</sup>

Now, something odd is going on with the quantum term. Naïvely, this goes as  $\text{str } AA \text{str } \mathbb{1} = 0$ . However, we know from section 1.2.4 that, since we are differentiating with respect to only partial supermatrices, we must perform the  $\sigma$  algebra, as in figure 1.10. Thus, the quantum term survives, going as  $\text{str } AA \sigma \text{str } \sigma$ , which introduces a relative minus sign in the  $A^2$ -sector. In the computation of  $\beta_1$  in [57], this minus sign is telling us that  $\tilde{\beta}_1 = -\beta_1$ .

Thus, the flow equation is guiding us to the sort of new terms we need in order to properly distinguish  $A^1$  and  $A^2$ : namely terms possessing a wine which can be decorated by a single  $\sigma$ . Returning to our example of the flow of  $AA$ , we will have a new quantum term which, after performing the  $\sigma$  algebra, will go as  $\text{str } AA \text{str } \sigma$ , where the  $\sigma$  from the wine has combined with a  $\sigma$

<sup>8</sup>This prevents vertices containing  $\sigma$  and an even number of the dynamical components of  $\mathcal{C}$ , since such terms are not invariant under  $\mathcal{C} \rightarrow -\mathcal{C}$ . This restriction simplifies the following analysis which, anyway, is intended for illustrative purposes only.

from the  $\sigma$  algebra. Moreover, the existence of a wine decorated by a single  $\sigma$  necessitates that the restriction to single supertrace terms is lifted (we can now hide instances of  $\sigma$  on otherwise empty supertraces, allowing us to preserve  $\mathcal{C} \rightarrow -\mathcal{C}$  symmetry). This ineluctably guides us to the current formalism.

### 2.5.2 The Two-Point, Tree Level Vertices

In preparation for the calculation of  $\beta$ -function coefficients, we now determine the two-point, tree level vertices. Of the two-point, tree level vertices, we demand that:

1. they are consistent with the renormalisation conditions (1.33) and (2.23);
2. full  $SU(N|N)$  invariance is recovered in the  $\mathcal{A}$  sector and full  $U(N|N)$  invariance is recovered in the  $C$ -sector, for sufficiently high energies;
3. the high energy behaviour is consistent with the constraints (1.28) (or their appropriate generalisation), to ensure that the regularisation does its job.

These three points are not sufficient to uniquely determine the two-point, tree level vertices and, indeed, it is not strictly necessary to do so. Nonetheless, we have found it useful to have concrete algebraic expressions. We save for the future a more general treatment which, with the understanding of the MGI-ERG we now have, should be straightforward [60].

To determine the two-point, tree level vertices, our starting point is the tree level, classical flow equation, obtained by specialising equation (2.26) or (2.28) to  $n = 0$ :

$$\dot{S}_0 = a_0[S_0, \Sigma_0]. \quad (2.29)$$

We now further specialise, to consider the flow of all two-point vertices, as shown in figure 2.20. Recall that the solid lines represent dummy fields, which we choose to be instances of  $A^1$ ,  $A^2$ ,  $C^1$ ,  $C^2$ ,  $\bar{F}$  and  $F$ .

There are a number of things to note. First, the overall half associated with  $a_0$  terms has been killed by the two ways in which the dumbbell structure

$$\text{Diagram: } \begin{array}{c} | \\ \circ 0 \\ | \end{array} \bullet = \begin{array}{c} | \\ \circ \Sigma_0 \\ | \bullet \\ | \\ \circ 0 \\ | \end{array} \quad (2.30)$$

Figure 2.20: Flow of all possible two-point, tree level vertices.

can be decorated by the two wildcard fields. Secondly, there is no possibility of embedding components of  $\mathcal{C}$  at the ends of the wines and so the  $\hat{\Delta}_\sigma^{AA}$  kernel does not appear.<sup>9</sup> Lastly, diagrams containing one-point, tree level vertices have not been drawn, since these vertices do not exist in any sector, for either action.<sup>10</sup>

We can now solve equation (2.30) (with appropriate boundary conditions—see section 2.5.5), giving an expression for the Wilsonian effective action, two-point, tree level vertices in terms of the seed action two-point, tree level vertices and the zero-point kernels.

The next step to make is to follow [51, 52, 53, 57] and utilise the freedom inherent in  $\hat{S}$  by choosing the two-point, tree level (single supertrace) components of  $\hat{S}$  to be equal to the two-point, tree level (single supertrace) components of  $S$  i.e.

$$\hat{S}_{0RS}^{ff}(k) = S_{0RS}^{ff}(k).$$

We emphasise that this is simply a choice we make, since it turns out to be helpful to do so.

We now choose a form for the two-point, tree level  $\hat{S}$  vertices, based on the general properties they must possess. In [57], this has been done already for the special case of  $\alpha = 1$  and we summarise the results below:

$$\hat{S}_{0\mu\nu}^{AA}(p) = \frac{2}{c_p} \square_{\mu\nu}(p), \quad (2.31)$$

$$\hat{S}_{0\mu\nu}^{BB}(p) = \frac{2}{c_p} \square_{\mu\nu}(p) + \frac{4\Lambda^2}{\tilde{c}_p} \delta_{\mu\nu}, \quad (2.32)$$

$$\hat{S}_{0\mu}^{B\sigma D}(p) = \frac{2\Lambda^2 p_\mu}{\tilde{c}_p}, \quad (2.33)$$

$$\hat{S}_0^{DD}(p) = \frac{\Lambda^2 p^2}{\tilde{c}_p}, \quad (2.34)$$

<sup>9</sup>Up to instances which have been used to map is into the  $A^1, A^2$  basis, in the first place.

<sup>10</sup>Recall that one-point, seed action vertices exist only from the one-loop level.

$$\hat{S}_0^{CC}(p) = \frac{\Lambda^2 p^2}{\tilde{c}_p} + 2\lambda\Lambda^4, \quad (2.35)$$

where  $\lambda > 0$  is an undetermined constant. Since the actions in [57] were restricted to single supertrace terms,  $\hat{S}^{AA\sigma}$  and  $\hat{S}^{CC\sigma}$  vertices were forbidden, under  $\mathcal{C} \rightarrow -\mathcal{C}$  symmetry.<sup>11</sup> Note, though, that the  $\hat{S}^{DD\sigma}$  vertex is excluded more generally: cyclicity of the supertrace tells us that  $2\text{str } DD\sigma = \text{str } D\{D, \sigma\}$ , but this vanishes, since  $D$  and  $\sigma$  anti-commute; similarly for  $\hat{S}^{BB\sigma}$ . Due to the restriction to single supertrace terms, the vertices  $\hat{S}^{C,C}$ ,  $\hat{S}^{C,C\sigma}$  and  $\hat{S}^{C\sigma,C\sigma}$  were never considered.

It will be instructive to understand where expressions (2.31)–(2.35) come from, and so we repeat the analysis of [57]. First, let us focus on the  $A$ -sector. The Ward identity (1.48) tells us that  $p_\mu \hat{S}_{0\mu\nu}^{AA}(p) = 0$ . Given this and that the vertex is of mass dimension two it must, by Lorentz invariance, take the form given by equation (2.31). Now, since we have identified the two-point, tree level, seed action vertices with the corresponding Wilsonian effective action vertices, they are subject to the renormalisation conditions (1.33) and (2.23) (recall that we are working with  $\alpha = 1$ ).<sup>12</sup> These conditions, together with equation (1.54), tell us that  $c(0) = 1$ .

Next, we look at the pure  $D$  vertex. Goldstone's theorem [105] tells us that  $D$  is massless and so (2.34) follows by Lorentz invariance and dimensions. We can think of equation (2.34) as providing a definition of what we mean by  $\tilde{c}$ .

The  $B\sigma D$  vertex is determined by the Ward identity (1.50). Recalling that  $F = (B, \sigma D)$ , we have

$$p_\mu \hat{S}_{0\mu}^{B\sigma D}(p) = 2\hat{S}^{DD}(p).$$

Equation (2.33) therefore follows by Lorentz invariance. The longitudinal part of the pure  $B$  vertex now follows also from the Ward identity (1.50), since

$$p_\mu \hat{S}_{0\mu\nu}^{BB}(p) = 2\hat{S}_\nu^{B\sigma D}(p).$$

As for the transverse part of the pure  $B$  vertex, by Lorentz invariance and dimensions it must look like  $2\Box_{\mu\nu}(p)/f(p)$ , for the dimensionless function,  $f$ .

<sup>11</sup>In our treatment, these restrictions vanish, since we can always hide instances of  $\sigma$  on additional, otherwise empty, supertraces.

<sup>12</sup>Generally, of course, seed action vertices are independent of the renormalisation conditions.

However, to recover  $SU(N|N)$  invariance at high energies,  $f(p)$  must coincide with  $c(p)$ , in this regime. For the sake of simplicity, we choose  $f(p) = c(p)$ .

Finally, consider the  $C$ -sector vertex. Whereas the Goldstone mode  $D$  is massless,  $C$  is not and so we expect the kinetic terms of these two fields to differ by a mass term. In order that we recover  $U(N|N)$  invariance in the  $C$ -sector at sufficiently high energies, this mass term must be sub-leading, in this regime. We thus introduce the function  $\lambda_p$  of which we demand that it must not vanish at  $p = 0$  and that it ensures the mass term is sub-leading at high energies. The simplest choice is to take  $\lambda$  to be a positive constant.

Having justified the forms of the two-point, tree level vertices for when  $\alpha = 1$  and the actions are restricted to single supertrace terms, we must now generalise the analysis, for our current purposes.

We begin in the  $A$ -sector, where now we have two independent vertices to deal with,  $\hat{S}_{0\mu\nu}^{11}(p)$  and  $\hat{S}_{0\mu\nu}^{22}(p)$ .<sup>13</sup> As before, gauge invariance, Lorentz invariance and dimensions tell us that

$$\hat{S}_{0\mu\nu}^{11}(p) = A(p^2/\Lambda^2, \alpha)\square_{\mu\nu}(p), \quad (2.36)$$

$$\hat{S}_{0\mu\nu}^{22}(p) = \tilde{A}(p^2/\Lambda^2, \alpha)\square_{\mu\nu}(p), \quad (2.37)$$

where  $A(p^2/\Lambda^2, \alpha)$  and  $\tilde{A}(p^2/\Lambda^2, \alpha)$  are to be determined. Of these two functions, we know the following:

1.  $A(0, \alpha) = 2$ , due to the renormalisation condition (1.33);
2.  $\tilde{A}(0, \alpha) = 2/\alpha$ , due to the renormalisation condition (2.23);
3.  $A(p^2/\Lambda^2, 1) = \tilde{A}(p^2/\Lambda^2, 1) = 2/c_p$ , for consistency with [57];
4. At sufficiently high energies,  $SU(N|N)$  invariance is recovered and so the two functions must coincide, in this regime.

As mentioned already, these points do not unambiguously determine  $A(p^2/\Lambda^2, \alpha)$  and  $\tilde{A}(p^2/\Lambda^2, \alpha)$ . However, for definiteness, we make the following choices:

$$A(p^2/\Lambda^2, \alpha) = \frac{\alpha + 1 + c_p(\alpha - 1)}{\alpha c_p}, \quad (2.38)$$

$$\tilde{A}(p^2/\Lambda^2, \alpha) = \frac{\alpha + 1 + c_p(1 - \alpha)}{\alpha c_p}, \quad (2.39)$$

---

<sup>13</sup>These are linear combinations of  $\hat{S}_{0\mu\nu}^{AA}(p)$  and  $\hat{S}_{0\mu\nu}^{AA\sigma}(p)$ .

which gives

$$\hat{S}_{0\mu\nu}^{11}(p) = \frac{\alpha + 1 + c_p(\alpha - 1)}{\alpha c_p} \square_{\mu\nu}(p), \quad (2.40)$$

$$\hat{S}_{0\mu\nu}^{22}(p) = \frac{\alpha + 1 + c_p(1 - \alpha)}{\alpha c_p} \square_{\mu\nu}(p). \quad (2.41)$$

We will henceforth use the shorthand

$$A(p) \equiv A_p \equiv A(p^2/\Lambda^2, \alpha)$$

where we note that

$$A(0) = 2. \quad (2.42)$$

For future convenience, we define

$$B_p \equiv A_p^{-1}. \quad (2.43)$$

Now we move on to the pure  $D$ -sector. The only change we need make is that, rather than looking at both block off-diagonal components of  $\mathcal{C}$  together—what we have been calling  $D$ —we look at the two components  $\bar{D}$  and  $D$ , separately.

$$\hat{S}_0^{D\bar{D}}(p) = \hat{S}_0^{\bar{D}D}(p) = \frac{\Lambda^2 p^2}{\tilde{c}_p}. \quad (2.44)$$

Once again, the mixed  $BD$  vertex is now uniquely determined by gauge invariance. Hence,

$$\hat{S}_0^{D\bar{B}}{}_{\mu}(p) = -\hat{S}_0^{\bar{D}B}{}_{\mu}(p) = \frac{2\Lambda^2 p_{\mu}}{\tilde{c}_p}. \quad (2.45)$$

In turn, this now uniquely determines the longitudinal part of the pure  $B$  vertex, as before. For the transverse part of the pure  $B$  vertex, we note that  $SU(N|N)$  invariance demands that it is the same as the  $A^1$  and  $A^2$  vertices at sufficiently high energies. Thus, for simplicity, we choose

$$\hat{S}_{0\mu\nu}^{B\bar{B}}(p) = \hat{S}_{0\mu\nu}^{\bar{B}B}(p) = \frac{\alpha + 1}{\alpha c_p} \square_{\mu\nu}(p) + \frac{4\Lambda^2}{\tilde{c}_p} \delta_{\mu\nu}. \quad (2.46)$$

Finally, we deal with the  $C$ -sector. For the case where both fields are on the same supertrace we now have a new vertex, namely  $\hat{S}_0^{CC\sigma}$ . Linear combinations of  $\hat{S}_0^{CC}$  and  $\hat{S}_0^{CC\sigma}$  define the vertices  $\hat{S}_0^{C^1C^1}(p)$  and  $\hat{S}_0^{C^2C^2}(p)$ , which we take to be equal. As before, we take these vertices to be like the pure  $D$  vertices, plus a mass term. Thus we have

$$\hat{S}_0^{C^1C^1}(p) = \hat{S}_0^{C^2C^2}(p) = \frac{\Lambda^2 p^2}{\tilde{c}_p} + 2\lambda\Lambda^4, \quad (2.47)$$

where we note that  $\lambda$  can now depend on  $\alpha$ .

Since our current analysis includes multi-supertrace terms, there is nothing to prevent us from having  $S^{C^{1,2},C^{1,2}}(p)$  and  $\hat{S}^{C^{1,2},C^{1,2}}(p)$  vertices (we treat the  $A$ -sector shortly). At tree level, at any rate, it is useful to exclude these; for the seed action vertices, we simply set them to zero. To see whether the Wilsonian effective action vertices vanish, we must compute their flow, as shown in figure 2.21. We have used the old-style notation, as we wish to be specific about the supertrace structure.

$$\begin{array}{c}
 \left[ \begin{array}{c} \text{---} \circ \\ \vdots \\ \text{---} \circ \\ S_0 \\ \vdots \\ \text{---} \circ \\ \text{---} \circ \end{array} \right]^\bullet = - \begin{array}{c} \text{---} \circ \\ \vdots \\ \text{---} \circ \\ \hat{S}_0 \\ \vdots \\ \text{---} \circ \\ \text{---} \circ \\ S_0 \end{array} + \begin{array}{c} \text{---} \circ \\ \vdots \\ \text{---} \circ \\ S_0 \\ \vdots \\ \text{---} \circ \\ \text{---} \circ \\ S_0 \end{array} - 2 \begin{array}{c} \text{---} \circ \\ \vdots \\ \text{---} \circ \\ \hat{S}_0 \\ \vdots \\ \text{---} \circ \\ \text{---} \circ \\ S_0 \end{array}
 \end{array}
 \tag{2.48}$$

Figure 2.21: The flow of  $S_0^{C^{1,2},C^{1,2}}(p)$ .

Setting  $\hat{S}_0^{C^{1,2},C^{1,2}}(p) = 0$  causes diagrams 2.6 and 2.8 disappear. Equation (2.48) simplifies and we choose the solution  $S_0^{C^{1,2},C^{1,2}}(p) = 0$ .

Though we will return to the two-point, tree level vertices in more generality in section 2.5.5, we will henceforth always take the tree level  $C^{1,2}, C^{1,2}$  vertices to vanish.

Now, we can also have multi-supertrace terms in the  $A$ -sector, which must take the form  $\text{str } \sigma \mathcal{A} \text{ str } \sigma \mathcal{A}$ . These cannot be set to zero because they are related, by no- $\mathcal{A}^0$  symmetry, to single supertrace two-point vertices (see equation (2.14)). However, since we are working in the scheme where we cannot attach to  $\mathcal{A}^0$ , these terms will interest us no further. Thus, when we now refer to two-point, tree level vertices, we strictly mean only those with a single supertrace.

For ease of reference, we collect together all the new two-point, tree level vertices in appendix A.1.

It is worth remarking that we have checked that unbroken actions can be constructed which yield the above vertices, in the broken phase.

### 2.5.3 The Zero-Point Kernels and Effective Propagators

Having set the Wilsonian effective action and seed action two-point, tree level vertices equal to each other and having chosen their algebraic form, let us now return to equation (2.30). We can simplify this, since  $\Sigma_{0MN}^{XX}(p) = S_{0MN}^{XX}(p) - 2\hat{S}_{0MN}^{XX}(p)$  can be replaced by  $-S_{0MN}^{XX}(p)$ . This makes it clear that we have an equation involving only two-point, tree level vertices—which we know—and zero-point wines. We can thus determine these latter objects.

This is straightforward, and is presented in [57] for the special case of  $\alpha = 1$ . In the current case, we will just quote the new results. To this end, we define  $x = p^2/\Lambda^2$  and introduce two new functions:

$$f_p = \frac{(1 + \alpha)\tilde{c}_p}{(1 + \alpha)x\tilde{c}_p + 4\alpha c_p}, \quad (2.49)$$

$$g_p = \frac{2\alpha\tilde{c}_p}{(1 + \alpha)x\tilde{c}_p + 4\alpha c_p}. \quad (2.50)$$

These functions reduce to the definitions in [57] for  $\alpha = 1$  and, crucially, still satisfy the relationship

$$x f_p + 2g_p = 1. \quad (2.51)$$

As will become clear later, when we start to perform diagrammatic calculations, it is this relationship that is important to us, rather than the precise algebraic forms of  $f$  and  $g$ , which contain some degree of choice.

Denoting differentiation with respect to  $x$  by a prime, we are now ready to give the zero-point kernels:

$$\dot{\Delta}^{11}(p) = \frac{2}{\Lambda^2} \left[ \frac{\alpha c_p}{\alpha + 1 + c_p(\alpha - 1)} \right]', \quad (2.52)$$

$$\dot{\Delta}^{22}(p) = \frac{2}{\Lambda^2} \left[ \frac{\alpha c_p}{\alpha + 1 + c_p(1 - \alpha)} \right]', \quad (2.53)$$

$$\dot{\Delta}^{B\bar{B}}(p) = \frac{1}{\Lambda^2} [x\tilde{c}_p g_p]', \quad (2.54)$$

$$\dot{\Delta}^{D\bar{D}}(p) = \frac{2}{\Lambda^4} \frac{1}{x} [x^2 \tilde{c}_p f_p]', \quad (2.55)$$

$$\dot{\Delta}^{C^1 C^1}(p) = \frac{1}{\Lambda^4} \frac{1}{x} \left[ \frac{2x^2 \tilde{c}_p}{x + 2\lambda \tilde{c}_p} \right]', \quad (2.56)$$

$$\dot{\Delta}^{C^2C^2}(p) = \frac{1}{\Lambda^4} \frac{1}{x} \left[ \frac{2x^2 \tilde{c}_p}{x + 2\lambda \tilde{c}_p} \right]'. \quad (2.57)$$

Note that, in the  $B$  and  $D$ -sectors, it does not make any difference whether the barred or unbarred field comes first.

The next step we perform is absolutely central to the all that follows, and its importance cannot be over emphasised. We now determine the integrated kernels, where we note that their appearance has been anticipated by the notation  $\dot{\Delta} \equiv -\Lambda \partial_\Lambda |_\alpha \Delta$ . The integrated kernels are as follows:

$$\Delta^{11}(p) = \frac{1}{p^2} \frac{\alpha c_p}{\alpha + 1 + c_p(\alpha - 1)}, \quad (2.58)$$

$$\Delta^{22}(p) = \frac{1}{p^2} \frac{\alpha c_p}{\alpha + 1 + c_p(1 - \alpha)}, \quad (2.59)$$

$$\Delta^{B\bar{B}}(p) = \frac{1}{2\Lambda^2} \tilde{c}_p g_p, \quad (2.60)$$

$$\Delta^{D\bar{D}}(p) = \frac{1}{\Lambda^4} \tilde{c}_p f_p, \quad (2.61)$$

$$\Delta^{C^1C^1}(p) = \frac{1}{\Lambda^4} \frac{\tilde{c}_p}{x + 2\lambda \tilde{c}_p}, \quad (2.62)$$

$$\Delta^{C^2C^2}(p) = \frac{1}{\Lambda^4} \frac{\tilde{c}_p}{x + 2\lambda \tilde{c}_p}, \quad (2.63)$$

and are equivalent to those of [57] for  $\alpha = 1$ .

These objects have a very close relationship to the two-point, tree level vertices. In the  $C$ -sector, the integrated kernels are just the inverse of the corresponding two-point, tree level vertices:

$$S_0^{C^1C^1}(p) \Delta^{C^1C^1}(p) = S_0^{C^2C^2}(p) \Delta^{C^2C^2}(p) = 1 \quad (2.64)$$

In the  $A^{1,2}$  sectors, the integrated kernels are the inverses of the corresponding two-point, tree level vertices only in the transverse space:

$$S_{0\mu\nu}^{11}(p) \Delta^{11}(p) = \delta_{\mu\nu} - \frac{p_\mu p_\nu}{p^2}, \quad (2.65)$$

$$S_{0\mu\nu}^{22}(p) \Delta^{22}(p) = \delta_{\mu\nu} - \frac{p_\mu p_\nu}{p^2}. \quad (2.66)$$

In the  $B$  and  $D$  sectors, the results are most naturally phrased in terms of the composite field  $F$ . Following equation (1.44) we define

$$\Delta_{MN}^{F\bar{F}}(p) = \begin{pmatrix} \Delta^{B\bar{B}}(p) \delta_{\mu\nu} & 0 \\ 0 & -\Delta^{D\bar{D}}(p) \end{pmatrix}, \quad (2.67)$$

giving us

$$S_{0MS}^{F\bar{F}}(p)\Delta_{SN}^{\bar{F}F}(p) = S_{0MS}^{\bar{F}F}(p)\Delta_{SN}^{F\bar{F}}(p) = \delta_{MN} - p'_M p_N \quad (2.68)$$

where, as in the introduction (equation (1.49)),

$$p_N = (p_\nu, 2) \quad (2.69)$$

and we define

$$p'_M = \left( \frac{f_p p_\mu}{\Lambda^2}, g_p \right). \quad (2.70)$$

Note that equation (2.70) differs from the analogous definition of [57] by a sign in the fifth component. This can be traced back to our definition of  $F$  (see equation (1.43)).

We note that, when looking at components of the fields in equation (2.68) labelled by  $M$  and  $N$ , we must take particular care: whilst  $F = (B, D)$ ,  $\bar{F} = (\bar{B}, -\bar{D})$ . This extra sign can be easily forgotten.

Now, just as the integrated kernels in the  $A^{1,2}$  sectors are the inverses of the corresponding two-point, tree level vertices in the transverse space, so too in the  $F$ -sector. This follows upon contracting equation (2.68) with  $p_M$ :

$$p_M(\delta_{MN} - p'_M p_N) = p_N \left[ 1 - (p^2 f_p / \Lambda^2 + 2g_p) \right] = 0,$$

where we have used the definitions (2.69) and (2.70), have recognised that  $x = p^2 / \Lambda^2$  and have used equation (2.51).

In summary, we see that the  $C$ -sector integrated kernels are the inverses of the two-point, tree level vertex whereas, in the  $A$  and  $F$  sectors, the integrated kernels are the inverses of the two-point, tree level vertices in a restricted sense only. In recognition of the similarity of the integrated kernels to propagators, we will henceforth refer to them as effective propagators [57]. However, despite their similarities in both form and the role they play, we emphasise that they are not propagators in the usual sense. Indeed, since we never fix the gauge, we know that we cannot even define a propagator for the  $\mathcal{A}$ -sector fields.

The zero-point kernels and effective propagators are collected together in appendix A.2.

As a final remark, we note that we have not explicitly mentioned  $\dot{\Delta}_\sigma^{AA}$  in this analysis. Of course, it can be obtained from  $\dot{\Delta}^{11}$  and  $\dot{\Delta}^{22}$ , but this is

not really the point. As we will see in part III, diagrams containing explicit instances of  $\dot{\Delta}_\sigma^{AA}$  (as opposed to implicit instances, which have been absorbed when mapping to the  $A^1$ - $A^2$  basis) will always cancel and so the details of  $\dot{\Delta}_\sigma^{AA}$  need never concern us.

## 2.5.4 Diagrammatic Identities

We can phrase the relationship between the two-point, tree level vertices and the effective propagators in particularly concise form. In preparation, we consider more carefully the objects left over when a two-point, tree level vertex is contracted into an effective propagator. We use the  $F$ -sector relationship (2.68) as a template for *all* sectors, which we can do if we employ a prescription for allowing  $p'_M$  and  $p_N$  to depend on the sector of the calculation.

To be specific, we can take

$$S_{0MS}^{XY}(p)\Delta_{SN}^{YZ}(p) = \delta_{MN} - p'_M p_N \quad (2.71)$$

where the fields  $X, Z$  are any broken phase fields, the field  $Y$  is summed over and we identify the components of the r.h.s. according to table 2.1. (Note that the field  $Z$  must, in fact, be the same as  $Y$ , since ‘mixed’ effective propagators do not exist.)

	$\delta_{MN}$	$p'_M$	$p_N$
$F$	$\delta_{MN}$	$(f_k p_\mu / \Lambda^2, g_k)$	$(p_\nu, 2)$
$A$	$\delta_{\mu\nu}$	$p_\mu / p^2$	$p_\nu$
$C$	$\mathbb{1}$	—	—

Table 2.1: Prescription for unifying the relationships (2.64), (2.65), (2.66) and (2.68).

Henceforth, we refer to  $p'_M p_N$  as a ‘gauge remainder’ [57]. This captures the notion that the effective propagators generally leave something behind (other than a Kronecker  $\delta$ -function) when contracted into a two-point, tree level vertex. Moreover, if vertices or wines are struck by these objects, then

they can be processed via the gauge invariance identities (1.48) and (1.50). The algebraic details of the gauge remainders are reproduced in appendix A.3.

We now give a diagrammatic form for equation (2.71), using the convention that the diagrammatic form of the two-point, tree level vertices represents only the single supertrace components. The two supertrace contributions either vanish automatically ( $F$  sector) or by choice ( $C$  sector) or are not attached to ( $A$ -sector).

All diagrammatic identities are reproduced in appendix B, for easy reference.

**Diagrammatic Identity 1** *Consider a two point, tree level (single supertrace) vertex, attached to an effective propagator which, only ever appearing as an internal line, attaches to an arbitrary structure. This is shown diagrammatically in figure 2.22, where the effective propagator is denoted by a long, solid line.*

$$M-\textcircled{0}-\text{---}\langle \equiv M-\langle - M\blacktriangleright\langle \equiv M-\langle - M\triangleright\langle \quad (2.72)$$

Figure 2.22: The effective propagator relation.

The object  $\blacktriangleright$  decomposes into two constituents:

$$\frac{M}{p}\triangleright \equiv p'_M, \quad (2.73)$$

$$\frac{\triangleright}{p}^N \equiv p_N. \quad (2.74)$$

Diagrammatic identity 1 is one of the foundations of our entire diagrammatic approach and so we will give it a special name: the effective propagator relation. However, on closer inspection, it looks like we may have missed something. We know that, in the  $A$ -sector, there are attachment corrections. Thus, we might expect there to be  $1/N$  corrections to the effective propagator relation, arising from where the effective propagator attaches to the vertex (see figure 2.6). In practise, though, these corrections always vanish. This is

a consequence of the diagrammatic structure shown in figure 2.22 only ever appearing as an internal structure, in some larger diagram.

To understand why this is the case, consider a two-point, tree level vertex in the  $A^1$  sector (the same analysis can be repeated in the  $A^2$  sector). To one field we attach an effective propagator and to the other we attach a wine. The other ends of the effective propagator and wine are somehow tied up; we are not interested in these details or in any corrections to the corresponding attachments. This scenario is depicted in figure 2.23. On the l.h.s., we use compact notation, where any corrections to the attachments are packaged up. On the r.h.s., we make the corrections to the vertex attachments explicit. Note that, as in [57], an old-style wine with a line down its spine denotes an effective propagator.

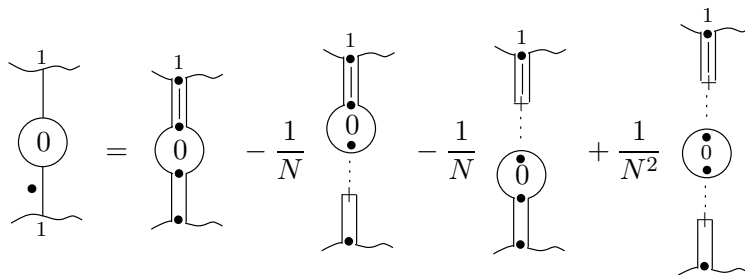


Figure 2.23: Showing how  $1/N$  corrections to the effective propagator relation vanish.

The crucial point is that, in the final diagram, the vertex—which attaches to other structures exclusively via false kernels—yields a factor of  $\text{str } \sigma_+ = N$ . Hence, the final diagram cancels either the second or third diagrams. Taking it to cancel the third diagram makes it clear that what we are effectively left with is just the  $1/N$  correction due to the attachment of the wine to the vertex. In other words, we can use the effective propagator relation as advertised.

Had we attached a second effective propagator to the vertex, rather than a wine, our argument still works. Though it is up to us to choose, we can only apply the effective propagator relation to one of the effective propagators. The remaining effective propagator plays the role of the wine, in the above

argument. Thus, it is not true to say that effective propagators only attach to two-point vertices directly (i.e. without any corrections). What is true is that the effective propagator relationship can be applied naïvely, without any consideration to possible  $1/N$  corrections.

Finally, notice how in diagrammatic identity 1 we have used the equivalence symbol in equation (2.72). In other words, we are taking the r.h.s. of equation (2.72) to define what we mean by the l.h.s..

There now follows a second diagrammatic identity, which follows from the properties of  $p'_M$  and  $p_N$ .

**Diagrammatic Identity 2** *Using the definitions (2.73) and (2.74), together with the information of table 2.1 and equation (2.51) gives us the diagrammatic identity below.*

$$\triangleright \triangleright = 1 \tag{2.75}$$

*The index at the apex of  $\triangleright$  is contracted into the index carried by  $>$ . Note that this relationship exists only in the  $A^{1,2}$  and  $F$ -sectors.*

*A number of corollaries follow from equation (2.75) and the fact that  $p_N$  is independent of both  $\Lambda$  and  $\alpha$ , in all sectors.*

### Corollaries

$$\begin{aligned} \left[ \triangleright \triangleright \right]^{\bullet} &= 0 \\ \Rightarrow \triangleright \triangleright^{\bullet} &= 0 \\ \frac{\partial}{\partial \alpha} \left[ \triangleright \triangleright \right] &= 0 \\ \Rightarrow \triangleright \frac{\partial}{\partial \alpha} > &\equiv \triangleright \triangleright^{\textcircled{\alpha}} = 0 \end{aligned}$$

*We have introduced  $\textcircled{\alpha}$  to represent  $\partial/\partial\alpha$ .*

In retrospect, diagrammatic identity 2 arises as a consequence of the effective propagator relation and gauge invariance. To see this, we note from the Ward identities (1.48) and (1.50) that

$$p_M S_{0MS}^{XX}(p) = 0. \tag{2.76}$$

This follows directly in the  $A$ -sector, since one-point  $A$ -vertices do not exist. In the  $F$ -sector, though, we are left with a one-point  $C$ -vertex. However, such vertices do not exist at tree level.

Now consider attaching an effective propagator to the vertex  $S_{0MS}^{XX}(p)$  in equation (2.76). Clearly, we must still be left with zero, but we have the option of utilising the effective propagator relation before the  $p_M$  has acted. Diagrammatically, this gives:

$$\triangleright \textcircled{0} \text{---} = 0 = \triangleright - \triangleright \triangleright \triangleright ,$$

which implies diagrammatic identity 2.

We conclude this section with a wonderful relationship between the effective propagators and the gauge remainders. To motivate this, consider an  $A^1$ -sector effective propagator attached to the  $p'_M$  part of a gauge remainder. Explicitly keeping track of which end of the effective propagator carries momentum  $p$  and which carries  $-p$ , we can write:

$$\Delta^{11}(-p, p) \frac{p_\mu}{p^2} = (-p)_\mu \tilde{\Delta}^{11}(-p, p)$$

where, trivially,  $\tilde{\Delta}^{11}(-p, p) = -\Delta^{11}(-p, p)/p^2 = -\Delta^{11}(p)/p^2$ . The point of doing this is that we have converted a  $p'_M$  like part of a gauge remainder attached to one end of an effective propagator into a  $p_M$  like part attached to the other end. The minus sign is inserted so that we have a consistent picture of the momentum flow.

We can thus think of components of gauge remainders at one end of an effective propagator as begin able to pass through the effective propagator, but inducing a change, in the process. We call the object  $\tilde{\Delta}$  a *pseudo effective propagator*.

The remarkable thing is that an equivalent relationship holds in the  $F$ -sector, too:

$$\Delta_{MN}^{F\bar{F}}(-p, p) p'_N = (-p)_M \tilde{\Delta}^{F\bar{F}}(-p, p),$$

where  $\tilde{\Delta}^{F\bar{F}}(p) = -\tilde{c}_p f_p g_p / 2\Lambda^4$  and we note that  $-p_M \neq (-p)_M$ . This leads us to another diagrammatic identity.

**Diagrammatic Identity 3** *Consider an effective propagator attached, at one*

end to the  $p'_M$  part of a gauge remainder. This can be redrawn as follow:

$$\longrightarrow = \triangleleft \dashrightarrow ,$$

where the dash-dot line represents the pseudo effective propagators.

### Corollary

$$\longrightarrow \blacktriangleright = \triangleleft \dashrightarrow \triangleright = \blacktriangleleft \longrightarrow$$

In retrospect, diagrammatic identity 3 can be deduced from the previous two diagrammatic identities. Diagrammatic identities 1 and 2 imply that

$$\textcircled{0} \longrightarrow = \triangleright - \triangleright \triangleright \triangleright = 0.$$

In other words, the (non-zero) structure  $\longrightarrow$  kills a two-point, tree level vertex. But, by equation (2.76), this implies that the structure  $\longrightarrow$  must be equal, up to some factor, to  $\triangleleft$ .

### 2.5.5 Universality

As we have pointed out already, the precise algebraic forms of the two-point, tree level vertices, effective propagators and gauge remainders have an element of choice in them. In this section, we wish to clarify precisely which parts are universal, which parts are forced upon us by the regularisation and which parts are purely down to choice. Similarly, we comment on whether or not we expect our diagrammatic identities to be generally true.

The entire purpose of our setup is ultimately to provide a means for computing physically observable quantities. Thus, despite the elaborate structure of the MGI-ERG, our real interest is in the physical field  $A^1$ .

All physically observable quantities must be controlled by the renormalisation condition for  $A^1$  (equation (1.33)), which is where the physics feeds in. Consequently, the single universal element of all that we have discussed in this section is the  $\mathcal{O}(p^2)$  part of the  $S_{0\mu\nu}^{11}(p)$  vertex:

$$S_{0\mu\nu}^{11}(p) = 2\Box_{\mu\nu}(p) + \mathcal{O}(p^4).$$

Now consider the actual computation of a (pseudo)-universal quantity within our framework. Whilst it is true that the final answer will be controlled by

the renormalisation condition for  $A^1$ , the extraction of a meaningful answer implicitly assumes that the framework is consistent. Thus, whilst a universal quantity cannot depend on the fact that we are using a spontaneously broken  $SU(N|N)$  regularisation scheme, within the ERG, the fact that we have chosen to compute in this way makes certain demands. We have seen a manifestation of these demands in the Ward identities and in constraints on the UV behaviour of the Wilsonian effective action and seed action, two-point, tree level vertices.

Generally speaking, there is no reason why the Wilsonian effective action and seed action two-point, tree level vertices need be identified with each other and so the fact that they are is purely down to choice. Having made this choice, we are still at liberty to choose the precise algebraic form of the two-point, tree level vertices, so long as this choice is consistent with the renormalisation condition, gauge invariance and preserves the regularisation. Irrespective of how we do this, we can ensure that the diagrammatic identities all still hold. We have seen that, given the effective propagator relationship and gauge invariance, all the other diagrammatic identities follow. However, the effective propagator relationship itself follows once we have set the Wilsonian effective action and seed action two-point, tree level vertices equal to each other.

Let us examine this statement in more detail. Having set the Wilsonian effective action and seed action two-point, tree level vertices equal we have, from equation (2.30)

$$\Lambda \partial_\Lambda |_\alpha S_0^{C^1 C^1}(p) = S_0^{C^1 C^1}(p) \dot{\Delta}^{C^1 C^1}(p) S_0^{C^1 C^1}(p).$$

Lorentz invariance demands that  $S_0^{C^1 C^1}(p)$  is an even function of  $p$  and so

$$\dot{\Delta}^{C^1 C^1}(p) = -\Lambda \partial_\Lambda |_\alpha \left[ S_0^{C^1 C^1}(p) \right]^{-1}.$$

Integrating up, we have

$$\Delta^{C^1 C^1}(p) = \left[ S_0^{C^1 C^1}(p) \right]^{-1} + \frac{\text{const}}{p^4}.$$

Let us examine the integration constant, in more detail. The only dimensionful quantities available are  $\Lambda$  and  $p$ . Since the integration constant is necessarily independent of the former it must go as  $1/p^4$ , by dimensions. The dimensionless constant which multiplies this, being independent of  $\Lambda$ , must be independent of  $p$  and so only function of  $\alpha$ .

Now,  $C^1$  is a massive field, so demanding that its effective propagator is well behaved as  $p \rightarrow 0$  uniquely fixes the integration constant to zero. The effective propagator relation follows, directly.

In the  $A^1$ -sector, equation (2.30) tells us that

$$\Lambda \partial_\Lambda |_\alpha S_{0\mu\nu}^{11}(p) = S_{0\mu\alpha}^{11}(p) \dot{\Delta}^{11}(p) S_{0\alpha\nu}^{11}(p).$$

Using equation (2.36) and the fact that  $\square_{\mu\alpha}(p)\square_{\alpha\nu}(p) = p^2\square_{\mu\nu}(p)$  we have:

$$-\Lambda \partial_\Lambda |_\alpha \frac{1}{A(p)} = p^2 \dot{\Delta}^{11}(p)$$

and, therefore, that

$$\frac{1}{A(p)} = p^2 \Delta^{11}(p) + p^2 \times \text{const.}$$

Demanding that the effective propagator vanishes in the limit  $p \rightarrow \infty$  [57] uniquely fixes the constant, which is dimensionless and independent of  $\Lambda$ , to be zero; the effective propagator relation follows.

Similar arguments to those above yield the effective propagator relation in the  $A^2$ ,  $C^2$  and  $F$ -sectors.

Now, given that we work in the scheme where the Wilsonian effective action and seed action two-point, tree level vertices are equal, there is a second place in which the  $A^1$  renormalisation condition is forced to feed in. Since,

$$S_{0\mu\nu}^{11}(p)\Delta^{11}(p) = \delta_{\mu\nu} - p_\mu p_\nu / p^2$$

and the  $\mathcal{O}(p^2)$  part of the vertex is universal, this implies that the  $\mathcal{O}(p^{-2})$  part of the effective propagator is universal, also.

To conclude this section, we introduce some nomenclature. Since we have furnished the two-point, tree level vertices and effective propagators with algebraic realisations, we will refer to such objects as ‘algebraic’. We note that components of these objects may be either universal or non-universal. These objects are the only ones for which we will ever introduce an algebraic realisation.<sup>14</sup>

Although we never introduce algebraic realisations for any other objects (i.e. higher point / higher loop order vertices and decorated wines) we note

---

<sup>14</sup>We do not count the zero-point wines separately, since they are just differentiated effective propagators.

that they may have components related, via gauge invariance, to our algebraic terms. In turn, this implies that such objects can have, buried in them, universal components.

### 2.5.6 Constraints in the $C$ -sector

We conclude our discussion of the weak coupling flow equations by giving the weak coupling version of the constraint (2.20) which, we recall, arises from demanding that all Wilsonian effective action one-point  $C^{1,2}$  vertices vanish.

Using the diagrammatic weak coupling flow equation (figure 2.19) we specialise  $\{f\}$  to  $C^{1,2}$ . Immediately, we find a number of simplifications, since all terms containing a vertex with a one-point Wilsonian effective action vertex (after decoration) vanish. Hence, the  $\beta$  and  $\alpha$  terms vanish. Expanding out the bar notation according to equation (2.27), the  $a_0[S_{n-r}, S_r]$  term dies, since one of the vertices is compelled to be a Wilsonian effective action one-point  $C^{1,2}$  vertex. The remaining two terms combine, and we note that here we are compelled to leave both the seed action vertex and wine undecorated.

There is an additional simplification. Since each diagram is decorated by a single field, this field must carry zero momentum. Now, it follows by dimensions (and is trivial to confirm) that

$$\dot{\Delta}^{C^1 C^1}(0) = 4\Delta^{C^1 C^1}(0),$$

and similarly for  $C^2$ . If we make this replacement when the wine attaches to a two-point, tree level vertex, then we can use the effective propagator relation. We thus arrive at the constraint for the  $n \geq 1$ -loop seed action, one-point vertices, shown in figure 2.24.<sup>15</sup>

Note that the  $n$ -loop seed action vertex is related to objects of loop order  $n - 1$  or lower. Thus, by appropriately tuning  $\hat{S}$ , we can satisfy the constraint order by order in perturbation theory.

---

<sup>15</sup>We recall that, at tree level, the one-point, seed action vertex is guaranteed to vanish because  $\mathcal{C}$  is dimensionless and the classical minimum of the Wilsonian effective action Higgs potential lies at  $\sigma$  [57].

$$4 \begin{array}{c} \hat{n} \\ | \\ \vdots \end{array} = - \sum_{r=1}^{n-1} \begin{array}{c} \hat{n}_r \\ \bullet \\ | \\ r \\ | \\ \vdots \end{array} - \frac{1}{2} \left[ \begin{array}{c} \bullet \\ \circ \\ \Sigma_{n-} \\ | \\ \vdots \end{array} + \begin{array}{c} | \\ \bullet \\ \circ \\ \Sigma_{n-} \end{array} \right] \quad (2.77)$$

Figure 2.24: The weak coupling regime constraint to ensure that the minimum of the superhiggs potential is not shifted by quantum corrections.

**Part II**

**Techniques**

## Chapter 3

# Further Diagrammatic Techniques

Having introduced both the new flow equation and the corresponding diagrammatic interpretation, we devote this chapter to describing a further set of diagrammatic techniques. The current state of affairs is that we can diagrammatically represent the flow of a vertex, and can process the result further by utilising the effective propagator relation.

The effective propagator relation allows us to replace a two-point vertex connected to an effective propagator with a Kronecker  $\delta$  and a ‘gauge remainder’. In section 3.1, we will see how we can deal with these remainders, diagrammatically. This will require that we broaden our understanding of both the Ward identities and no- $\mathcal{A}^0$  symmetry.

In section 3.2, we utilise the insights gained from the treatment of the gauge remainders to develop a diagrammatic technique for Taylor expanding vertices and wanes in momenta.

We round off the diagrammatic techniques with a further set of diagrammatic identities that will be heavily used in the computation of  $\beta$ -function coefficients.

### 3.1 Gauge Remainders

Up until now, we have referred to the composite object  $\triangleright\triangleright$  as a gauge remainder. Henceforth, we will often loosely refer to the individual components as gauge remainders. To make an unambiguous reference, we call  $\triangleright$  an active gauge remainder,  $\triangleright$  a processed gauge remainder and  $\triangleright\triangleright$  a full gauge remainder.

#### 3.1.1 Vertices

We begin by considering an arbitrary vertex, which is contracted with the momentum carried by one of its fields,  $X$ , as shown on the l.h.s. of figure 3.1. All of the fields shown are wildcards, though the field  $X$  has no support in the  $C$ -sector. To proceed, we use the Ward identities (1.48) and (1.50), which tell us that we either push forward or pull back (with a minus sign) the momentum of  $X$  to the next field on the vertex. We recall from section 1.2.3 that fields are read off a vertex in the counterclockwise sense; hence, we push forward counterclockwise and pull back clockwise.

Since the vertex contains all possible (cyclically independent) orderings of the fields, spread over all (legal) combinations of supertraces, any of the fields could precede or follow  $X$ . Hence, we must sum over all possible pushes forward and pulls back, as shown on the r.h.s. of figure 3.1.

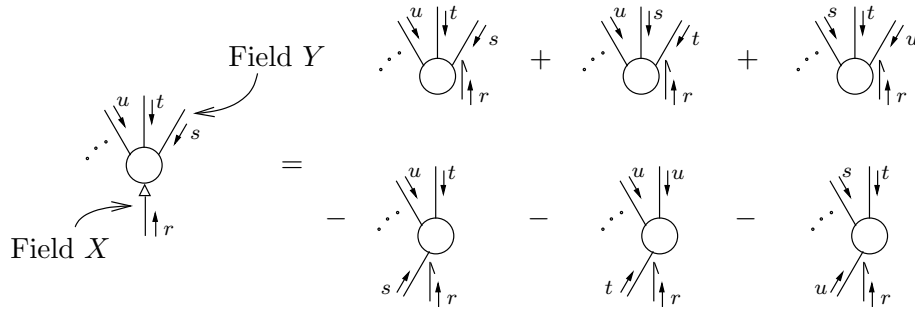


Figure 3.1: The l.h.s. shows the contraction of an arbitrary vertex with one of its momenta. On the r.h.s., the first row of diagrams shows all possible pushes forward on to the explicitly drawn fields and the second row shows all possible pulls back.

It is clear from the Ward identities (1.48) and (1.50) that the diagrams on the r.h.s. of figure 3.1 have no explicit dependence on the field  $X$ . Nonetheless, to interpret the diagrams on the r.h.s. unambiguously, without reference to the parent, we must retain information about  $X$ . This is achieved by keeping the line which used to represent  $X$  but which is now terminated by a half arrow, rather than entering the vertex. This line carries information about the flavour of  $X$  and its momentum, whilst indicating which field it is that has been pushed forward / pulled back on to. The half arrow can go on either side of the line.<sup>1</sup>

The diagrammatics we have been using has been, up until now, completely blind to details concerning the ordering of fields and the supertrace structure. If we are to treat gauge remainders diagrammatically, we can no longer exactly preserve these features. Let us suppose that we have pushed forward the momentum of  $X$  on to the field  $Y$ , as depicted in the first diagram on the r.h.s. of figure 3.1. Clearly, it must be the case that  $X$  and  $Y$  are on the same supertrace and that  $Y$  is immediately after  $X$ , in the counter-clockwise sense. The other fields on the vertex—which we will call spectator fields—can be in any order and distributed amongst any number of supertraces, up to the requirement that they do not come between the fields  $X$  and  $Y$ . To deduce the momentum flowing into the vertex along  $Y$ , we simply follow the indicated momentum routing. Hence, momentum  $r + s$  enters the vertex along  $Y$ , in the case that it is the field  $Y$  that has been pushed forward (pulled back) on to. Similarly, if we push forward on to the field carrying momentum  $t$ , then momentum  $r + t$  enters the vertex, along this field. We must also take into account that the flavour of  $Y$  will change if  $X$  is fermionic; these changes are given beneath (1.50).

However, our current form for the the Ward identities are in terms of the fields  $A$ ,  $C$  and  $F$ , whereas we want to be working with  $A^1$ s,  $A^2$ s and etc. This is easy enough to achieve: we can always project down to the required sub-sector using  $\sigma_{\pm}$  (see equation (2.10)). There is, though, one major subtlety: the fermionic gauge transformations can generate  $\mathcal{A}^0$ . Though we will see that,

---

<sup>1</sup>This should be borne in mind when we encounter pseudo effective propagators, attached to  $\triangleright$ .

for the calculations we wish to perform, we can adopt a prescription whereby we effectively remove  $\mathcal{A}^0$  once and for all, as an intermediate step we define

$$\begin{aligned}\tilde{A}^1 &\equiv A^1 + \sigma_+ \mathcal{A}^0 \\ \tilde{A}^2 &\equiv A^2 + \sigma_- \mathcal{A}^0.\end{aligned}$$

The flavour changes arising from pushing forward/ pulling back the (anti) fermionic field,  $X$  on to the field,  $Y$ , are summarised in table 3.1. Bosonic fields have been treated together. We note that the entries in the table contain some annoying signs. There is nothing that can be done about these; we simply incorporate them into the diagrammatic rules. Before any momenta have been contracted into vertices, the wildcard fields have neat interpretations in terms of  $F$ ,  $\bar{F}$ ,  $(A^1, C^1)$  and  $(A^2, C^2)$ . After such contractions have been performed, though, the precise meaning of the wildcard fields must be deduced from the field structure of the diagram.

$X$	$Y$	$\vec{Y}$	$\overleftarrow{Y}$
$\bar{F}$	$(A^1, C^1)$	$(\bar{B}, \bar{D})$	—
	$(A^2, C^2)$	—	$(\bar{B}, \bar{D})$
	$F$	$(\tilde{A}^2, C^2)$	$(\tilde{A}^1, C^1)$
$F$	$(A^2, C^2)$	$F$	—
	$(A^1, C^1)$	—	$F$
	$\bar{F}$	$(\tilde{A}^1, -C^1)$	$(\tilde{A}^2, -C^2)$

Table 3.1: The flavour changing effect of pushing forward and / or pulling back the momentum of the fermionic field  $X$  on to the field  $Y$ . If the field  $Y$  is bosonic, then the flavour of  $X$  and  $Y$  uniquely determine whether  $X$  must follow  $Y$ , or vice-versa. The empty entries correspond to the case where the required ordering of fields does not exist. The entries in this table do not include the relative minus sign always present between pushes forward and pulls back.

Let us suppose that we have some vertex which is decorated by, e.g., an

$F$  and a  $\bar{B}$  and that these fields are on the same supertrace. Now consider contracting the vertex with the momentum of the  $F$ . There are two cases to analyse. The first is where there are other fields on the same supertrace as the  $F$  and  $\bar{B}$ . For argument's sake, we will take them to be such that the  $\bar{B}$  follows the  $F$  (in the counterclockwise sense). Now the  $F$  can push forward on to the  $\bar{B}$ , generating a  $\tilde{A}^1$ . In this case, the vertex *coefficient function* is blind to whether its argument involves  $\tilde{A}^1$  or  $A^1$ : starting with a vertex containing  $\tilde{A}^1$ , we can always remove the  $\mathcal{A}^0$  part by no- $\mathcal{A}^0$  symmetry.

The second case to look at is where there are no other fields on the same supertrace as  $F$  and  $\bar{B}$ . Now the  $F$  can both push forward and pull back on to the  $\bar{B}$  generating, respectively,  $\tilde{A}^1$  and  $\tilde{A}^2$ . However, we cannot rewrite  $\tilde{A}^{1,2}$  as  $A^{1,2}$  since, whereas  $\text{str } \tilde{A}^{1,2} \neq 0$ ,  $\text{str } A^{1,2} = 0$ . Our strategy is to rewrite vertices involving a separate  $\text{str } \tilde{A}^{1,2}$  factor via no- $\mathcal{A}^0$  symmetry.

We have encountered a no- $\mathcal{A}^0$  relation already—see equation (2.14). Now we will generalise this relationship, which is most readily done by example. Consider the following part of the action, where we remember that all position arguments are integrated over:

$$\begin{aligned} & \cdots + \frac{1}{3} S_{\alpha\beta\gamma}^{111}(x, y, z) \text{str } \tilde{A}_\alpha^1(x) \tilde{A}_\beta^1(y) \tilde{A}_\gamma^1(z) \\ & + \frac{1}{2} S_{\alpha\beta,\gamma}^{11,A\sigma}(x, y, z) \text{str } \tilde{A}_\alpha^1(x) \tilde{A}_\beta^1(y) \text{str } A_\gamma(z) \sigma + \cdots \end{aligned}$$

We note that, in the second term, we have combined  $S^{AA,A}$  with  $S^{A,AA}$ , thereby killing the factor of  $1/2!$  associated with each of these vertices.

To determine the no- $\mathcal{A}^0$  relationship between these vertices, we shift  $A$ :  $\delta A_\mu(x) = \lambda_\mu(x) \mathbb{1}$ , and collect together terms with the same supertrace structure and the same dependence on  $\lambda_\mu$ . By restricting ourselves to the portion of the action shown, we only find common terms which depend on a single power of  $\lambda_\mu$ . By using a larger portion of the action we can, of course, obtain higher order relationships, though we will not require these. In the single supertrace vertex, this operation simply kills the factor of  $1/3$ ; in the double supertrace term, we focus on shifting the lone  $A$  which yields:

$$\begin{aligned} & \cdots + \lambda_\gamma(z) S_{\alpha\beta\gamma}^{111}(x, y, z) \text{str } \tilde{A}_\alpha^1(x) \tilde{A}_\beta^1(y) \\ & + \frac{1}{2} \lambda_\gamma(z) S_{\alpha\beta,\gamma}^{11,A\sigma}(x, y, z) \text{str } \tilde{A}_\alpha^1(x) \tilde{A}_\beta^1(y) \text{str } \sigma + \cdots \end{aligned}$$

Notice that we can rewrite the first term to recognise the invariance of the supertrace under cycling the remaining fields: we replace the existing vertex coefficient function by

$$\frac{1}{2} \left[ S_{\alpha\beta\gamma}^{111}(x, y, z) + S_{\alpha\gamma\beta}^{111}(x, z, y) \right].$$

Our no- $\mathcal{A}^0$  relation is, therefore:

$$S_{\alpha\beta\gamma}^{111}(x, y, z) + S_{\alpha\gamma\beta}^{111}(x, z, y) + 2NS_{\alpha\beta,\gamma}^{11,A\sigma}(x, y; z) = 0.$$

We now recast the final term, so that we work with  $\tilde{A}^1$ s and  $\tilde{A}^2$ s, rather than  $A\sigma$ . This is a little counterintuitive. At first, we recognise that  $A\sigma = \tilde{A}^1 - \tilde{A}^2$ . However,  $\tilde{A}^1$  and  $\tilde{A}^2$  are not independent. Specifically,

$$\text{str } \tilde{A}^1 = N\mathcal{A}^0 = -\text{str } \tilde{A}^2.$$

Consequently, we need to be careful what we mean by the vertex coefficient functions  $S^{\dots, \tilde{A}^1, 2}$ . If, as we will do, we treat the vertex coefficient functions  $S^{\dots, \tilde{A}^1}$  and  $S^{\dots, \tilde{A}^2}$  as independent then, by recognising that

$$S^{\dots, \tilde{A}^1}(\text{str } \dots)\text{str } \tilde{A}^1 + S^{\dots, \tilde{A}^2}(\text{str } \dots)\text{str } \tilde{A}^2$$

is equivalent to

$$S^{\dots, A\sigma}(\text{str } \dots)\text{str } A\sigma$$

and writing out the explicitly indicated supertraces in terms of  $\mathcal{A}^0$  and  $N$ , we find that

$$S^{\dots, \tilde{A}^1} - S^{\dots, \tilde{A}^2} = 2S^{\dots, A\sigma}.$$

The factor of two on the r.h.s. is, perhaps, unexpected; we emphasise that it comes from splitting up the variable  $\mathcal{A}^0$  between two other variables. In figure 3.2 we give a diagrammatic form for the subset of first order no- $\mathcal{A}^0$  relations which relate single supertrace vertices to two supertrace vertices.

A number of comments are in order. First, this relationship is trivially generalised to include terms with additional supertraces. Secondly, if we restrict the action to single supertrace terms, as in [57, 55], then the first two lines reproduce the no- $\mathcal{A}^0$  relations of [55]. Thirdly, the Feynman rules are such that

$$\begin{aligned}
& \begin{array}{c} S \\ \bullet \\ \text{---} \\ \bullet \\ A_\mu^1 \end{array} \begin{array}{c} \bullet \\ \text{---} \\ \bullet \\ R \end{array} + \dots + \begin{array}{c} R \\ \bullet \\ \text{---} \\ \bullet \\ A_\mu^1 \end{array} \begin{array}{c} \bullet \\ \text{---} \\ \bullet \\ S \end{array} + \begin{array}{c} A_\mu^1 \\ \bullet \\ \text{---} \\ \bullet \\ S \end{array} \begin{array}{c} \bullet \\ \text{---} \\ \bullet \\ R \end{array} \\
+ & \begin{array}{c} S \\ \bullet \\ \text{---} \\ \bullet \\ A_\mu^2 \end{array} \begin{array}{c} \bullet \\ \text{---} \\ \bullet \\ R \end{array} + \dots + \begin{array}{c} R \\ \bullet \\ \text{---} \\ \bullet \\ A_\mu^2 \end{array} \begin{array}{c} \bullet \\ \text{---} \\ \bullet \\ S \end{array} + \begin{array}{c} A_\mu^2 \\ \bullet \\ \text{---} \\ \bullet \\ S \end{array} \begin{array}{c} \bullet \\ \text{---} \\ \bullet \\ R \end{array} \\
+ & N \left[ \begin{array}{c} S \quad R \\ \bullet \quad \bullet \\ \text{---} \\ \bullet \quad \tilde{A}_\mu^1 \\ \bullet \end{array} - \begin{array}{c} S \quad R \\ \bullet \quad \bullet \\ \text{---} \\ \bullet \quad \tilde{A}_\mu^2 \\ \bullet \end{array} \right] \\
= & 0 \tag{3.1}
\end{aligned}$$

Figure 3.2: Diagrammatic form of the first order no- $\mathcal{A}^0$  relations.

some of the diagrams of figure 3.2 can be set to zero, for particular choices of the fields which decorate the vertex. For example, if all decorative fields are  $A^1$ s or  $C^1$ s, then the second row of diagrams effectively vanishes. Note, though, that if there are fermionic decorations, then there are guaranteed to be contributions from all rows.

In the calculations performed in this thesis, the only place we generate  $\tilde{A}^1$ s is as internal fields. Since internal fields are always attached to wines (or effective propagators), we can absorb the factors of  $N$  appearing in equation (3.1) into our rules for attaching wines / effective propagators to vertices. This is illustrated in figure 3.3, where the ellipsis denotes un-drawn pushes forward and pulls back, on to the remaining fields,  $\{f\}$ , which also decorate the vertex.

There are a number of things to note. First, the gauge remainder strikes the vertex and not the base of the wine; this is ambiguous from the way in which we have drawn the diagrams though this ambiguity is, in fact, deliberate, as we will discuss shortly. Thus, whilst the vertex now possesses an  $A^{1,2}$  field, the wine is still labelled by  $\bar{B}$ . Secondly—and this is the whole point of our prescription—the field struck by the gauge remainder becomes an  $A^{1,2}$ , and not an  $\tilde{A}^{1,2}$ ; the missing contributions to the vertex have been effectively absorbed into the wine Feynman rule. Thirdly, we implicitly sum over all possible ways in which the un-drawn fields,  $\{f\}$ , decorate the vertex in all diagrams (including

$$\begin{aligned}
\text{Diagram with } B \text{ and } F &= \text{Diagram with } A^1 - \text{Diagram with } A^2 + \dots \\
&\equiv \left[ \text{Diagram with } A^1 - \frac{1}{N} \text{Diagram with } A^1 \right] - \left[ \text{Diagram with } A^2 + \frac{1}{N} \text{Diagram with } A^2 \right] \\
&+ \dots
\end{aligned}$$

Figure 3.3: Prescription adopted for internal fermionic fields decorating a vertex struck by a gauge remainder.

those with the old-style notation). This ensures that all diagrams in the no- $\mathcal{A}^0$  relationship (3.1) are included. Lastly, we note once more that the Feynman rules are such that certain terms can be set to zero when we look at particular realisations of  $\{f\}$ .

We conclude our discussion of the effect of gauge remainders on vertices by considering diagrams generated by the new terms in the flow equation in which a component of  $\mathcal{A}$  decorating a vertex is replaced by a component of  $\mathcal{C}$ .<sup>2</sup> The situation is illustrated in figure 3.4 where, for reasons that will become apparent, we schematically indicate the type of vertex whose flow generates the terms we are interested in.

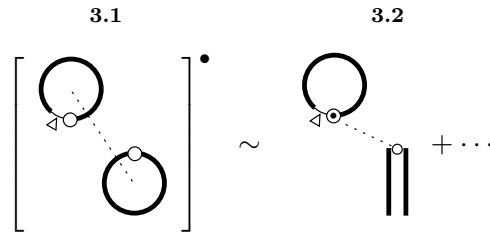


Figure 3.4: A gauge remainder strikes a vertex in which a component of  $\mathcal{A}$  has been replaced by a component of  $\mathcal{C}$ .

<sup>2</sup>Though not necessary for the following analysis, we recall from section 2.3.2 that, in the  $A^1, A^2$  basis, components of  $\mathcal{A}$  must be replaced by dynamical components of  $\mathcal{C}$ .

The effect of the gauge remainder requires a little thought. In diagram 3.1, the gauge remainder can clearly strike the  $\mathcal{C}$ . However, in diagram 3.2 the  $\mathcal{C}$  is not part of the vertex coefficient function and so is blind to the effects of the gauge remainder.

Allowing the  $\mathcal{C}$  of diagram 3.2 to strike the  $\mathcal{A}$ , which labels the vertex coefficient function, the vertex coefficient function changes. Now we have a strange situation: looking just at the coefficient functions of the diagrams (i.e. ignoring the implied supertrace structure), diagrams 3.1 and 3.2 are consistent, after the action of the gauge remainder. However, the implied supertrace structures of the two diagrams seems to differ, because the  $\mathcal{C}$  of diagram 3.2 is blind to the gauge remainder.

The solution is simple: we allow the effect of the gauge remainder striking the  $\mathcal{A}$  in diagram 3.2 to induce a similar change in the  $\mathcal{C}$ . This amounts to a diagrammatic prescription which ensures that all our diagrams continue to represent both numerical coefficients and implied supertrace structure. The key point is that we are free to do this with the  $\mathcal{C}$  since, not being part of a vertex (or, strictly, part of a wine) it does not contribute to the numerical value of the diagram but serves only to keep track of the supertraces which have been implicitly stripped off from the vertex whose flow we are computing.

Finally, we should take account of attachment corrections, if we are to work in the  $A^1, A^2$  basis. Attachment corrections effectively detach the embedded component of  $\mathcal{C}$  from the vertex, causing it to become an isolated  $\text{str}\mathcal{C}$ . In diagram 3.1, this field cannot now be struck by the gauge remainder. In diagram 3.2, when the gauge remainder acts, it no longer induces a change in the embedded component of  $\mathcal{C}$ . In fact, such contributions must cancel against other terms formed by the action of the gauge remainder; this is discussed further in section 3.1.3.

### 3.1.2 Wines

Thus far, we have been considering the effects of gauge remainders on vertices. It is straightforward to generalise this analysis to the effect on wines; the generic case is shown in Figure 3.5.

Figure 3.5: Contraction of an arbitrary wine with one of its momenta. The sense in which we will take pushes forward and pulls back is as in figure 2.14.

If the field whose momentum is contracted into the wine is fermionic, then pushes forward and pulls back will involve flavour changes. Let us begin by supposing that one of the fields hit decorates the wine (as opposed to being a derivative sitting at the end); in this case, the flavour changes are given by table 3.1. Note that instances of  $\mathcal{C}$  embedded at the ends of the wine behave like normal wine decorations, as far as gauge remainders are concerned. This follows from the gauge invariance of the flow equation and is natural if we view these embedded fields as behaving just like multi-supertrace components of the wine. Of course, if the gauge remainder does strike a component of  $\mathcal{C}$  which is really an embedded  $\mathcal{C}$  then it must be that this component of  $\mathcal{C}$  is forced to be on the same portion of supertrace as the rest of the wine. This is just a manifestation of the statement that the action of gauge remainders necessitates partial specification of the supertrace structure (cf. our treatment of vertices).

When we generate internal  $\tilde{A}^{1,2}$ s, we would like to attach to them according to the prescription of figure 3.3 i.e. we wish to extend this prescription such that the structure to which the wine attaches is generic, as opposed to being just a vertex. We can and will do this, though note that whether or not the  $1/N$  corrections actually survive depends on whether or not we endow our wines with completely general supertrace structure. If we do allow completely general wine decorations then the  $1/N$  corrections arise—as they did before—by combining terms with a lone  $\text{str } \tilde{A}^1$  (or  $\text{str } \tilde{A}^2$ ) with those without. If,

however, we take the only multi-supertrace terms of the wine to be those involving embedded  $\mathcal{C}$ s, then our no- $\mathcal{A}^0$  relations for the wine will cause the  $1/N$  corrections to vanish. Since these corrections are to be hidden in our Feynman rules, it does not matter which scheme we employ.

The next task is to consider what happens when we push forward (pull back) on to the end of a wine. This is straightforward: we know that  $\delta/\delta\mathcal{A}^0$  never attaches, irrespective of whether it has been generated by a fermionic gauge transformation. Using the prescription that we discard  $\delta/\delta\mathcal{A}^0$ , the flavour changes involved when a functional derivative sitting at the end of the wine is hit are summarised in table 3.2.

$X$	$Y$	$\vec{Y}$	$\overleftarrow{Y}$
$\bar{F}$	$\left(\frac{\delta}{\delta A^1}, \frac{\delta}{\delta C^1}\right)$	$\frac{\delta}{\delta F}$	—
	$\left(\frac{\delta}{\delta A^2}, \frac{\delta}{\delta C^2}\right)$	—	$\frac{\delta}{\delta F}$
	$-\frac{\delta}{\delta F}$	$\left(\frac{\delta}{\delta A^2}, -\frac{\delta}{\delta C^2}\right)$	$\left(\frac{\delta}{\delta A^1}, -\frac{\delta}{\delta C^1}\right)$
$F$	$\left(\frac{\delta}{\delta A^2}, \frac{\delta}{\delta C^2}\right)$	$-\left(\frac{\delta}{\delta B}, \frac{\delta}{\delta D}\right)$	—
	$\left(\frac{\delta}{\delta A^1}, \frac{\delta}{\delta C^1}\right)$	—	$-\left(\frac{\delta}{\delta B}, \frac{\delta}{\delta D}\right)$
	$\frac{\delta}{\delta F}$	$\left(\frac{\delta}{\delta A^1}, \frac{\delta}{\delta C^1}\right)$	$\left(\frac{\delta}{\delta A^2}, \frac{\delta}{\delta C^2}\right)$

Table 3.2: The flavour changing effect of pushing forward and / or pulling back the momentum of the fermionic field  $X$  on to the derivative,  $Y$ , at the end of a wine.

### 3.1.3 Gauge Invariance

We mentioned under figure 3.3 that the diagrams on the r.h.s. of the figure are ambiguous: if we ignore the l.h.s., it is not clear whether we have pushed forward around the bottom structure or pulled back down the wine. In this section we will argue that the two must be equivalent, by gauge invariance, and then demonstrate this to be the case.

Consider the flow of some vertex decorated by the fields  $f_1 \cdots f_n$ . Using the form of the flow equation given in figure 2.12, we explicitly decorate with

$f_1$ , but leave the other fields as unrealised decorations (see part III for much more detail concerning this procedure). This yields the diagrams of figure 3.6.

$$-\Lambda\partial_\Lambda \left[ \begin{array}{c} \textcircled{S} \\ | \\ f_1 \end{array} \right]^{f_2 \cdots f_n} = \frac{1}{2} \left[ \begin{array}{c} \textcircled{\Sigma_g} \\ \bullet \\ | \\ \textcircled{S} \\ | \\ f_1 \end{array} + \begin{array}{c} \textcircled{\Sigma_g} \\ | \\ \bullet - f_1 \\ | \\ \textcircled{S} \end{array} + \begin{array}{c} f_1 \\ | \\ \textcircled{\Sigma_g} \\ \bullet \\ | \\ \textcircled{S} \end{array} - \begin{array}{c} \bullet \\ \textcircled{\Sigma_g} \\ | \\ f_1 \end{array} - \begin{array}{c} f_1 \\ | \\ \bullet \\ \textcircled{\Sigma_g} \end{array} \right]^{f_2 \cdots f_n}$$

Figure 3.6: Flow of a vertex decorated by the fields  $f_1 \cdots f_n$ .

Now consider contracting each of the diagrams of figure 3.6 with the momentum of  $f_1$ . On the l.h.s., this generates the flow of a set of vertices decorated by  $m - 1$  fields. Amongst the diagrams generated on the r.h.s. are those for which we push forward / pull back on to fields to which the wine attaches. For each of these diagrams, there is then a corresponding diagram (with opposite sign) where we have pulled back / pushed forward on to the end of the wine. Such diagrams, in which we push forward / pull back on to an internal field cannot be generated by the l.h.s.; thus as a consequence of gauge invariance, it must be that they cancel amongst themselves.

**Proposition 3.1** *Consider the set of diagrams generated by the flow equation, each of which necessarily possesses a single wine that we will take to attach to the fields  $X_1$  and  $X_2$ . Suppose that we contract each of these diagrams with the momentum of one of the (external) fields,  $Y$ .*

*Of the resultant diagrams, we collect together those for which the momentum of  $Y$  is pushed forward and / or pulled back round a vertex, on to  $X_1$  ( $X_2$ ). We add to this set of diagrams all those for which the momentum of  $Y$  is pushed forward and / or pulled back along the wine on to the end attaching to  $X_1$  ( $X_2$ ).*

*We now split these sets into subsets, where the elements of each subset have exactly the same supertrace structure. The elements of each of these subsets cancel, amongst themselves.*

The proof of proposition 3.1 is essentially trivial. If we choose to work in the picture where we retain  $\mathcal{A}^0$ , then we know that there are no attachment corrections.<sup>3</sup> In this case, we can simply use tables 3.1 and 3.2 to demonstrate that proposition 3.1 is true.

Transferring to the  $A^1, A^2$  basis complicates matters by generating attachment corrections. However, we know that this picture is equivalent to the one in which we retain  $\mathcal{A}^0$ , and so the effects of these corrections cannot spoil the truth of proposition 3.1.

It is, though, instructive to see how proposition 3.1 can be demonstrated in the  $A^1, A^2$  basis, directly. However, rather than giving a complete exposition, we will demonstrate the truth of proposition 3.1 in the  $A^1, A^2$  basis for the original flow equation only (i.e. we neglect the effects of embedded components of  $\mathcal{C}$ ).

We begin by supposing that the field we are pushing forward / pulling back is in the  $A$ -sector. In this case, the effects of the attachment corrections are straightforward: irrespective of whether the field decorates the structure to which the wine attaches, or the wine itself, the flavour of the fields to which the wine attaches are the same, and so the attachment corrections are the same in both cases. Hence, proposition 3.1 is clearly true, in this case. The subtlety comes when the field we are pushing forward / pulling back is fermionic.

The first case that we will examine is shown in figure 3.7.

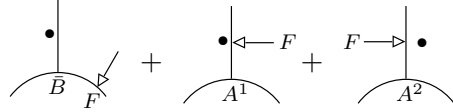


Figure 3.7: The push forward and / or pull back round the vertex cancels the pull back and / or push forward down the wine.

The potential problem arises because attachments to  $A^{1,2}$  come with a

---

<sup>3</sup>We recall from figure 1.8 that, in this picture, there is a correction to supersplitting. However, the structure which receives the correction is devoid of external fields and so cannot be struck by a gauge remainder.

correction, whereas attachments to  $\bar{B}$  do not. However, the first diagram has been discussed earlier in this chapter (see figure 3.3): when we push forward and / or pull back on to the field to which the wine attaches, this generates an effective attachment correction. These corrections are precisely the same as those present in the second and third diagrams (see figure 2.6) and so the cancellation required for proposition 3.1 to be true goes ahead as required!

The second case to deal with is shown in figure 3.8 (an identical analysis can be performed with  $A^2$  instead of  $A^1$ s).

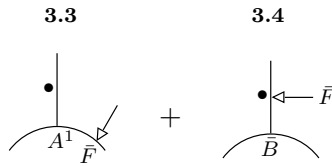


Figure 3.8: The push forward round the vertex does not quite cancel the pull back down the wine.

This is the most subtle case and so must be examined in some detail. The potential problem is clearly that there is an attachment correction where the bottom end of the wine attaches in diagram 3.3 but not in diagram 3.4.

Let us start by supposing that the wine of diagram 3.3 is undecorated and that the wine of diagram 3.4 has no additional decorations. The top ends of each wine must now attach to an  $A^1$ . However, we know that when an undecorated wine attaches at both ends to an  $A^1$ , there is effectively only an attachment correction at one end (see figures 2.8 and 2.9). Hence, in this case, the push forward round the vertex cancels the pull back down the wine.

Next, let us add an arbitrary number of bosonic decorations to the wines of each diagram (in diagram 3.4 we are clearly not interested in the case where any of the decorations come between the existing decoration and the bottom end of the wine). Now, let us focus on the correction term in at the bottom end of the wine in diagram 3.3. Since we plug the end of the wine with a  $\sigma_+$ , we can cycle the bosonic decorations around the end of the wine (remember that we are neglecting embedded components of  $\mathcal{C}$ ). The sum of all diagrams

thus obtained then vanishes by the coincident line identities, as is clear by considering the broken phase version of figure 1.9.

Having dealt with bosonic decorations, we now consider the case where the wines of diagrams 3.3 and 3.4 are decorated by a single additional (anti)fermion. In this case, it is not obvious that the attachment correction in diagram 3.3 vanishes by the coincident line identities: we cannot cycle the (anti)fermionic decoration around the  $\sigma_+$  plugging the wine. However, we have missed something. Consider the diagrams of figure 3.9.

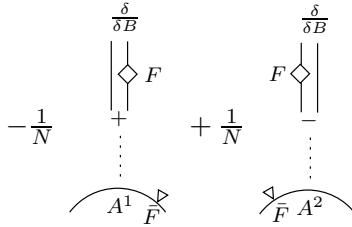


Figure 3.9: Two diagrams which, after the gauge remainders strike the explicitly drawn fields, cancel by the coincident line identities.

The pull back on to  $A^2$  in the second diagram generates the same field as the push forward on to  $A^1$  in the first diagram (see table 3.1). However, pulls back come with a relative minus sign, compared to pushes forward. This sign cancels the existing relative minus between the two diagrams and now the two diagrams cancel, courtesy of the coincident line identity shown in figure 2.10. This argument can be repeated for any number of fermionic decorations.

We have therefore demonstrated the truth of proposition 3.1, working explicitly in the  $A^1, A^2$  basis, for the original flow equation. It is straightforward, if tedious, to extend this proof to encompass the new terms in the flow equation, and so we omit the details; rather we argue that proposition 3.1 must be true, due to the equivalence of the  $A^1, A^2$  basis and the basis in which we retain  $\mathcal{A}^0$  (or simply as a consequence of supergauge invariance).

### 3.1.4 Cancellations Between Pushes forward / Pulls back

We saw in the previous section how, in certain circumstances, a push forward round a vertex could be cancelled by a pull back, also round the vertex (see figure 3.9). In this section, such cancellations are treated in complete generality.

Referring back to figure 3.1, we now ask when it is possible for the pulls back of the second row to cancel the pushes forward of the first row (this argument can be repeated for wines). It is clear that, if the field structure of corresponding terms is exactly the same, then they will cancel, due to the relative minus sign. For the purposes of this section, we wish to consider the case where any cancellations occur independently of the spectator fields. In other words, we will not consider cancellations which involve changing the ordering, flavour or indices of the spectator fields; this is delayed until the next section. Furthermore, whilst all the wildcard fields we are considering include all possible field choices, we do not sum over these choices, but consider each independently.

Let us temporarily suppose that  $X$  is in the  $A$ -sector and focus on the case where its momentum is pushed forward on to field  $Y$ . If both  $X$  and  $Y$  are bosonic, then the flavours of  $X$  and  $Y$  are independent of which field precedes the other. Moreover, for a given field arrangement, the flavours of the other fields will not change if the order of  $X$  and  $Y$  is swapped. In this case, the push forward on to  $Y$  will be exactly cancelled by the corresponding pull back.

However, if either  $X$  or  $Y$  is fermionic, then interchanging their order will necessarily change the field content of the vertex. This follows because a bosonic field in the 1-sector precedes an  $F$  and follows an  $\bar{F}$ , whereas a bosonic field in the 2-sector follows an  $F$  and precedes an  $\bar{F}$ . As an example, consider  $p_\mu S_{\mu RS\dots}^{1F\bar{F}\dots}(p, r, s, \dots)$ . To cancel the push forward on to  $F_R$  would require us to change the flavour of  $X$  to  $A^2$ :  $p_\mu S_{R\mu S\dots}^{F2\bar{F}\dots}(r, p, s, \dots)$ . Instead, we could try and cancel the push forward on to  $F_R$  by constructing the term  $p_\mu S_{SR\mu\dots}^{F\bar{F}1\dots}(s, r, p, \dots)$ , but now it is the  $\bar{F}$  carrying the index  $R$ , rather than the  $F$ . As we will see in the next section such a term can, in general, either cancel or double the original push forward. However, for the purposes of this section, we note that the spectator field  $\bar{F}_S$  has suffered a change and so we do not

consider this further.

Similarly, if both  $X$  and  $Y$  are fermionic, then interchanging them will alter the field content of the vertex, if other fields are present on the same supertrace. Then, we have the choice of altering the spectators or letting  $X, Y \rightarrow \bar{X}, \bar{Y}$ . The former case will be dealt with in the next section. In the latter case, we note from table 3.1 that pushing forward the momentum of  $F_R$  on to  $\bar{F}_S$  yields  $(A^1, C^1)_S$  whereas the pulling back the momentum of  $\bar{F}_R$  into  $F_S$  yields  $-(A^1, -C^1)_S$ . These contribution do produce a cancellation over the first four indices, but the fifth index contributions add.

In conclusion, when dealing with a single vertex, a push forward can only completely cancel a pull back, independently of the spectator fields, when both fields involved are bosonic. When we generalise this analysis to full diagrams, rather than individual vertices, we might expect this constraint to be relaxed: all internal fields will be summed over and we have seen how, for example, pushing forward the momentum of an  $A^1$  on to an  $F$  could be cancelled by pulling back the momentum of an  $A^2$ . Thus, if the  $A$  field is internal, then we will be including both cases, automatically. However, when dealing with full diagrams, we must be aware that interchanging fields can alter the supertrace structure of the diagram and so we will actually find that the conditions for cancellation between pushes forward and pulls back are even more stringent (see section 3.1.6).

### 3.1.5 Charge Conjugation

In the previous section we looked at whether pushes forward could cancel pulls back, independently of the spectator fields. If the properties of the spectator fields are allowed to change, then we find that every push forward is related to a pull back, by CC.

Referring back to equations (1.51)–(1.53) we can construct the following diagrammatic recipe for CC:

1. reverse the sense in which we read fields off from the vertices / wines,
2. pick up a minus sign for each field in the  $A$ -sector;
3. let  $\bar{F} \leftrightarrow -F$ ;

where we must remember that fields pushed forward / pulled back on to may have changed flavour and that the wildcard fields should be interpreted according to table 3.1. Rather than having to specify the sense in which fields are to be read off, we can instead replace a given diagram with its mirror image, whilst obeying points two and three above [51, 53, 57].

Now let us return to figure 3.1 and consider taking the mirror image of the bottom row of diagrams. Since the location and order of the spectator fields is unspecified we see that, up to a possible sign, the first and second rows are actually identical! However, whether corresponding entries in the two rows add or cancel, depends on whether the original vertex is even or odd under CC. In the former case, pushes forward and pulls back will add; in the latter case they will cancel.

It is important to note that this argument is separate from that of the previous section, as illustrated in figure 3.10. The diagrams of the first and fourth rows are equal, by CC, as are the diagrams of the second and third rows. However, diagrams 3.5 and 3.6, whose parents are not related by CC, cancel, as do diagrams 3.7 and 3.8.

### 3.1.6 Complete Diagrams

So far, we have just been concerned with isolated vertices and so now turn to full diagrams. We still wish to combine pushes forward and pulls back using CC but, to do so, we must look at the CC properties of whole diagrams, rather than the properties of individual vertices.

We begin by looking at the example illustrated in figure 3.11. Each diagram has two external fields, which we will choose to be  $A^1$ s, carrying indices  $\alpha$  and  $\beta$  and momenta  $p$  and  $-p$ . By Bose symmetry, the diagrams are symmetric under  $p_\alpha \leftrightarrow -p_\beta$ .

The first comment to make is that the diagrammatics is slightly different from the previous case. Rather than terminating the pushed forward / pulled back field-line with a half arrow, we just utilise the fact that the corresponding field line already ends in a  $>$  and use this to indicate the field hit.

$$\begin{array}{c}
\mathbf{3.5} \\
\begin{array}{c} \delta \\ \gamma \\ \alpha \quad \beta \end{array} \text{ (circle with gauge remainder on } \alpha) = \begin{array}{c} \delta \\ \gamma \\ \alpha \quad \beta \end{array} \text{ (circle with gauge remainder on } \beta) - \begin{array}{c} \delta \\ \gamma \\ \alpha \quad \beta \end{array} \text{ (circle with gauge remainder on } \alpha) \quad \text{FAS}
\end{array}$$

$$\begin{array}{c}
\mathbf{3.6} \\
\begin{array}{c} \delta \\ \gamma \\ \beta \quad \alpha \end{array} \text{ (circle with gauge remainder on } \beta) = - \begin{array}{c} \delta \\ \gamma \\ \beta \quad \alpha \end{array} \text{ (circle with gauge remainder on } \alpha) + \begin{array}{c} \delta \\ \gamma \\ \beta \quad \alpha \end{array} \text{ (circle with gauge remainder on } \alpha) \quad \text{FAS}
\end{array}$$

$$\begin{array}{c}
\mathbf{3.7} \\
\begin{array}{c} \gamma \\ \delta \\ \alpha \quad \beta \end{array} \text{ (circle with gauge remainder on } \alpha) = \begin{array}{c} \gamma \\ \delta \\ \alpha \quad \beta \end{array} \text{ (circle with gauge remainder on } \beta) - \begin{array}{c} \gamma \\ \delta \\ \alpha \quad \beta \end{array} \text{ (circle with gauge remainder on } \alpha) \quad \text{FAS}
\end{array}$$

$$\begin{array}{c}
\mathbf{3.8} \\
\begin{array}{c} \gamma \\ \delta \\ \beta \quad \alpha \end{array} \text{ (circle with gauge remainder on } \beta) = - \begin{array}{c} \gamma \\ \delta \\ \beta \quad \alpha \end{array} \text{ (circle with gauge remainder on } \alpha) + \begin{array}{c} \gamma \\ \delta \\ \beta \quad \alpha \end{array} \text{ (circle with gauge remainder on } \alpha) \quad \text{FAS}
\end{array}$$

Figure 3.10: Rows one and four are equal by CC; likewise for rows two and three. Independently of this, there are cancellations between diagrams of rows one and two and also diagrams of rows three and four.

Returning to the diagrams of figure 3.11 we see that, not only can we collect pushes forward and pulls back, but we can also exploit any symmetries of the diagrams to collect terms. Looking at diagram 3.9, it makes no difference whether the gauge remainder hits the field carrying  $\alpha$  or the field carrying  $\beta$ . Since we can push forward or pull back on to either of these fields, this accounts for the factor of four multiplying diagram 3.10.

Diagram 3.11 is interesting. Having used CC to collect the push forward and pull back, let us now suppose that all fields leaving the three-point vertex are in the  $A$ -sector. We note that the field struck by the gauge remainder has an  $\mathcal{A}^0$  component, but suppose that this has been absorbed into an attachment correction. In this picture, we cannot have an  $A^1$  alone on a supertrace and so all three fields must be on the same supertrace. However, we are still free to

$$\begin{array}{ccc}
\mathbf{3.9} & \mathbf{3.10} & \mathbf{3.11} \\
- \text{ (diagram 3.9) } & = 4 \text{ (diagram 3.10) } & - 2 \text{ (diagram 3.11) }
\end{array}$$

Figure 3.11: Example of a gauge remainder in a complete diagram. The dummy index  $R$  is given by  $\rho$ , if restricted to the first four indices.

interchange  $A_\alpha(p)$  and  $A_\beta(-p)$  and, summing over the two possible locations of these fields, we have:

$$\hat{S}_{\alpha\beta\rho}^{111}(p, -p, 0) + \hat{S}_{\beta\alpha\rho}^{111}(-p, p, 0).$$

These two terms cancel, as a result of CC.

We might wonder if CC causes components of diagram 3.10 to cancel. However, attachment corrections aside, the index structure  $\beta\alpha R$  corresponds to a different supertrace structure from the index structure  $\alpha\beta R$ . In the former case, the two  $A^1$ s are on different supertraces whereas, in the latter case, they are on the same supertrace. This is illustrated in figure 3.12.

$$\text{(diagram 3.10 left)} \text{ FAS} \neq \text{(diagram 3.10 right)} \text{ FAS}$$

Figure 3.12: Two components of diagram 3.10 which are not equal, due to their differing supertrace structure.

If we include attachment corrections (see figure 2.6), then the wine of diagram 3.10 can attach to the vertex via a false kernel. In this case, there is only one supertrace, and so all fields are necessarily on it. Such components of diagram 3.10 do cancel amongst themselves. However, these cancellations are generally hidden by our notation and are of no practical importance anyway, until we come to extracting numerical contributions to  $\beta$ -function coefficients.

Returning to diagram 3.11, for the diagram to survive, the field carrying momentum  $k$  must be in the  $F$ -sector. In this case, the gauge remainder can produce a  $C$ -sector field. Under interchange of  $\alpha$  and  $\beta$ , such a vertex is even and so survives.

This serves to illustrate a general feature of these diagrammatics, alluded to at the end of section 3.1.4. Suppose that we are pushing forward the momentum of a field  $X$  on to the field  $Y$ . If we can rearrange the diagram such that, leaving all other fields alone, we can place  $X$  on the other side of  $Y$ , then the resulting pull back on to  $Y$  will cancel the push forward, so long as no flavours or indices have changed in the rearrangement and the supertrace structure is still the same.

Here is how this applies to our examples. In the case of diagram 3.10, to convert a pull back on to  $A_\beta^1$  into a push forward, we must change the location of  $A_\alpha^1$ , to maintain the same supertrace structure (up to attachment corrections). The resulting term can then just be collected with the pull back, by CC. Hence the push forward on to  $A_\beta^1$  can never be completely cancelled by a pull back.

In the case of diagram 3.11 we can convert a push forward into a pull back without changing the locations of the spectator fields and without having to change the supertrace structure. If the fields carrying momentum  $k$  are in the  $A$ -sector, then interchanging them does not result in any flavour changes, and so the push forward cancels the pull back. However, if the fields carrying momentum  $k$  are fermionic, then interchanging them requires us to replace  $\bar{F} \leftrightarrow F$ . This constitutes a change of flavour and we find that the push forward does not completely cancel the pullback, since we are left with a contribution arising from the  $C$ -sector.

We note that, just as we can use CC to redraw vertices struck by gauge remainders, so too can we use CC to redraw entire diagrams. Given some diagram, the diagrammatic effect of CC is to replace a diagram by its mirror image, letting  $\bar{F} \leftrightarrow F$  (sic) and picking up a minus sign for each gauge remainder that has been performed.<sup>4</sup> Picking up a sign in this manner automatically

---

<sup>4</sup>So far, we have only encountered diagrams in which a single gauge remainder has acted, but we will come across more general cases later.



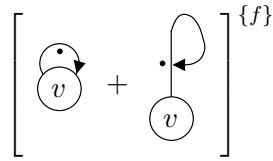


Figure 3.14: Two sub-diagrams between which, after the action of the gauge remainders, certain contributions are guaranteed to cancel.

*Allowing the gauge remainders to act, the push forward (pull back) around the vertex on to the field to which the wine attaches exactly cancels the pull back (push forward) along the wine on to the end to which the vertex attaches.*

Returning now to figure 3.13, it is worth making some comments about the structure at the top of diagram 3.13. First, the line segment which joins the top of the wine to the  $>$ —thereby forming a ‘hook’—performs no role other than to make this join. In other words, it is neither a section of wine nor an effective propagator. We could imagine deforming this line segment so that the hook becomes arbitrarily large. Despite appearances, we must always remember that this line segment simply performs the role of a Kronecker delta. When part of a complete diagram, this line segment can always be distinguished from an effective propagator, to which it can be made to look identical, by the context. This follows because hooks in which the line segment is a Kronecker  $\delta$  only ever attach to effective propagators or wines, whereas hook-like structures made out of an effective propagator only ever attach to vertices (this is particularly clear from the perspective of part III, but see diagram 3.14 for an example). When viewed in isolation, we will always take the hook structure to comprise just a line segment and so will draw the hook as tightly as possible.

Secondly, this hook structure—around which we will assume flows momentum  $l$ —is purely algebraic. To have any chance of surviving, the hook must be in either the  $D$  or  $\bar{D}$ -sector. This follows from referring to the algebraic form of the gauge remainders (appendix A.3) and noting that these are the only sectors for which  $l'$  is not an odd function of momentum. This is entirely

consistent with the structure of the rest of the diagram: to prevent the diagram from vanishing when we sum over independent permutations of fields on the vertex, the wine must be in the  $C$ -sector. Since gauge remainders have no support in the  $C$ -sector, and  $AC$  wines do not exist, this means that the field decorating the wine in the parent diagram 3.12 and, by the same reasoning, the hook must be fermionic.

When determining the algebraic form of the hook one must be very careful, due to the prevalence of awkward signs. The simplest way to get the right answer is to suppose that the hook is in either the full  $F$  or  $\bar{F}$  sector and project out later. With this way of looking at things, the gauge remainder forming the hook is given by  $g_l$ : since we have been using the full fermionic sector, there were no signs picked up when  $l'$  was originally generated by application of the effective propagator relation (see section 2.5.3). There may, however, be signs picked up at the end of the wine, which can be determined via table 3.2.

Appearance of these signs depends on whether the hook is in the  $F$  or  $\bar{F}$  sector which, in turn, depends on whether the field on the vertex to which the wine attaches is in the  $C^1$  or  $C^2$  sector, respectively.<sup>5</sup> We choose to use the prescription that whenever these signs appear, we will absorb them into the definition of the hook. This then allows us to take the wine to which the hook attaches to be just  $\hat{\Delta}^{C^1 C^1}(0)$  or  $\hat{\Delta}^{C^2 C^2}(0)$ , without the need to worry about signs.

The final ingredient we need to obtain the algebraic form for the hook is to realise that the inside of the hook constitutes an empty loop and so gives a group theory factor of  $\pm N$ , depending on flavour. Thus we have:

$$\mathcal{D}_1 = (-N) \int_l g_l \quad (3.2)$$

$$\mathcal{D}_2 = -(N) \int_l g_l. \quad (3.3)$$

The numbers at the base of the hook in the above equations indicate the sector of the wine to which the hooks attach. The overall minus sign in the second equation can be traced back to table 3.2, whereas the sign in the first equation is due to the group theory factor.

---

<sup>5</sup>Remember that the vertex could be, for example,  $\hat{S}_{0\mu\nu}^{11,C^2}(p, -p; 0)$ .

We now see a further advantage to having absorbed signs into the definition of the hook: we can trivially extend the diagrammatic effect of CC to cover its action on a disconnected hook. Quite simply, we have that

$$\mathcal{D} = - \mathcal{A} , \quad (3.4)$$

consistent with our previous definition that we take the mirror image, picking up a sign for every performed gauge remainder. Of course, had we not absorbed signs coming from the end of the wire to which the hook attaches, then it would only have made sense to apply our previous CC recipe to an entire diagram possessing a hook, rather than factorisable components.

We conclude this section by discussing a particular scenario—which will crop up repeatedly in our computation of  $\beta$ -function coefficients—in which it is possible to neglect attachment corrections.

Consider some complete diagram possessing a three-point vertex which is decorated by an external  $A^1$ -sector field and is struck by a gauge remainder. The type of diagram we are considering is represented in figure 3.15, where the fields  $\{f\}$  can attach anywhere except the bottom vertex, which must be three-point. If any of these fields are internal fields, then we take pairs of them to be connected by an effective propagator.

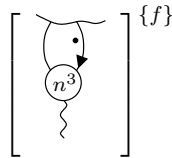


Figure 3.15: A diagram for which corrections to supersplitting / supersowing are restricted.

We now argue that we can forget about any attachment corrections. Let us start by supposing that the gauge remainder is in the  $F$ -sector. If the gauge remainder strikes the internal field, then it can generate an effective attachment correction. However this correction isolates the newly formed two-point vertex from the rest of the diagram, leaving us with  $\text{str } A^1 = 0$ .

Next, suppose that the gauge remainder is in the  $A$ -sector. Since two of the three fields entering the vertex are now in the  $A$ -sector, the third must also be bosonic. Moreover, the final field must be in the  $A$ -sector also, else the action of the gauge remainder will produce an  $AC$  vertex, which does not exist. Now, any attachment corrections would mean that all fields on the vertex are guaranteed to be on the same portion of supertrace, with respect to the diagram as a whole, irrespective of location. Summing over the independent locations of the fields causes the diagram to vanish, by CC.

Henceforth, whenever we deal with a three-point vertex decorated by an external field and struck by a gauge remainder, we will automatically discard all attachment corrections.

### 3.1.7 Socket Notation

If a gauge remainder hits a three-point vertex, then it will produce a two-point vertex. If one (or both) of the fields leaving the resulting two-point vertex are internal fields attached to effective propagators, then we will be able to use the effective propagator relation once more. An example is shown in figure 3.16.

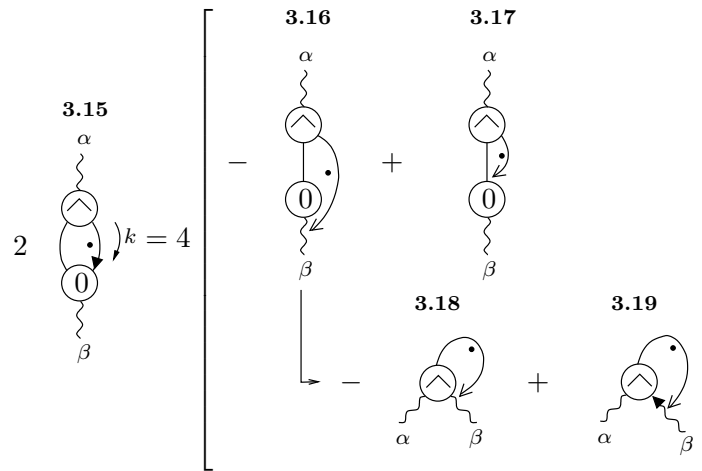


Figure 3.16: Gauge remainder which produces a diagram in which the effective propagator relation can be applied.

Referring also to figure 3.11, diagram 3.18 straightforwardly cancels diagram 3.10. Note that, this cancellation would have failed if the effective propagator relation were supplemented by  $1/N$  corrections (see section 2.5.4).

We are now interested in generalising this cancellation. In essence, what we are trying to demonstrate is that it does not matter how a diagram in which a gauge remainder has acted is formed: we should not be able to tell whether it has been formed directly or only after the application of the effective propagator relation.

This leads us to the socket notation: rather than specifying which field a gauge remainder has hit, instead we state that it has hit some socket which can be filled by any available field.<sup>6</sup> This is illustrated in figure 3.17. Note that whilst we allow sockets to represent fields which decorate wines, we do not take them to represent the derivatives at the end of a wine.

$$\begin{aligned}
 & \left[ \begin{array}{c} \mathbf{3.20} \\ \text{▼} \\ \textcircled{v} \end{array} \right] \{f\} = 2 \left[ \begin{array}{c} \mathbf{3.21} \\ \textcircled{v} \\ \text{↘} \end{array} \right] \{f\} \\
 & \left[ \begin{array}{c} \mathbf{3.22} \\ \text{•} \text{◀} \end{array} \right] \{f\} = 2 \left[ \begin{array}{c} \mathbf{3.23} \\ \text{•} \text{↙} \\ \text{↘} \end{array} \right] \{f\} + \left[ \begin{array}{c} \mathbf{3.24} \\ \text{•} \text{↖} \end{array} \right] \{f\} + \left[ \begin{array}{c} \mathbf{3.25} \\ \text{↘} \text{•} \end{array} \right] \{f\}
 \end{aligned}$$

Figure 3.17: Basic idea of socket notation.

Guided by the cancellation of diagrams 3.18 and 3.10, we are now led to consider the following diagrams: taking the parents in figure 3.17, we detach the gauge remainder from the structure it strikes and attach it instead to a three-point, tree level vertex. This vertex is now attached to the structure previously hit by the gauge remainder. Allowing the gauge remainder to act will produce the diagrams of figure 3.18.

Using table 3.1 and recalling that  $F = (B, D)$  and  $\bar{F} = (\bar{B}, -\bar{D})$ , it is straightforward to show that we can utilise the effective propagator relation to

---

<sup>6</sup>One may very well ask why we do not simply take gauge remainders to strike an arbitrary field, rather than an empty socket, which can be filled by an arbitrary field. We will see the value of the socket notation in part III.

$$2 \left[ \begin{array}{c} \textcircled{v} \\ | \\ \textcircled{0^2} \end{array} \right]^{\{f\}}, \quad 2 \left[ \begin{array}{c} \cdot \\ | \\ \textcircled{0^2} \end{array} \right]^{\{f\}}$$

Figure 3.18: Partner diagrams to diagrams 3.21 and 3.23.

demonstrate that, up to nested gauge remainders, the diagrams of figure 3.18 do, indeed, reduce to diagrams 3.21 and 3.23, irrespective of what we use to fill the sockets.

### 3.1.8 Nested Contributions

The basic methodology for nested gauge remainders is similar to the methodology just presented, but we must take account of the fact that the supertrace structure is now partially specified. In particular, this will generally mean that we cannot use CC to collect nested pushes forward and pulls back (the exception being if a gauge remainder produced in one factorisable sub-diagram hits a separate factorisable sub-diagram) and so must count them separately. Indeed, nested pushes forward and pulls back can have different supertrace structures as illustrated by considering the result of processing diagram 3.19, as shown in figure 3.19.

$$4 \left[ \begin{array}{cccc} \mathbf{3.26} & \mathbf{3.27} & \mathbf{3.28} & \mathbf{3.29} \\ \textcircled{0} & \textcircled{0} & \textcircled{0} & \textcircled{0} \end{array} \right]$$

Figure 3.19: Result of processing diagram 3.19.

We begin our analysis of the diagrams of figure 3.19 by noting that there are no attachment corrections. The first gauge remainder struck a three-point (tree level) vertex decorated by an external  $A$  to generate the nested gauge remainder. In turn, the nested gauge remainder has struck a three-point (tree level) vertex decorated by an external  $A$ . From our discussion at the end of

section 3.1.6 we thus deduce that all attachment corrections in the diagrams of figure 3.19 can be neglected.

Diagrams 3.26 and 3.28 have supertrace structure  $\pm N \text{str } A_\alpha^1 A_\beta^1$ , with the plus or minus depending on the sector of the wildcard fields. On the other hand, diagrams 3.27 and 3.29 have supertrace structure  $\text{str } A_\alpha^1 \text{str } A_\beta^1 = 0$ . Note in the latter case that the particular supertrace structure puts constraints on the field content of the diagram. Specifically, the wine in diagrams 3.27 and 3.29 cannot be fermionic. Let us suppose that it is. Then, the end which attaches to the vertex must be an  $F$  and so the end which attaches to the  $>$  must be an  $\bar{F}$ . However, referring to table 3.1 we see that an  $\bar{F}$  cannot pull back on to bosonic fields in the 1-sector. There is an inconsistency in such a diagram and so our original supposition that it exists must be wrong.

The diagrams of figure 3.19 are one-loop diagrams and it is clear that there is no way in which we can generate further gauge remainders. For calculations of arbitrary loop order, though, we can imagine generating arbitrarily nested diagrams. It would then be useful for us to know if there is any simple way of keeping track of which gauge remainders have pushed forward and which have pulled back. Of course, with sufficient thought, it is always possible to stare at a complicated diagram and deduce the pattern of pushes forward and pulls back. However, there is an easier way. Note in diagrams 3.26–3.29 that the nested gauge remainder is bitten on its right-hand edge by the original gauge remainder. Had we pushed forward, rather than pulled back with the initial gauge remainder, then this bite would have been to the left. With this in mind, consider a string of gauge remainders which bite a socket decorating either a wine or a vertex; the latter case is shown in figure 3.20.

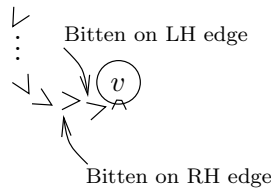


Figure 3.20: An arbitrarily nested gauge remainder bites a socket on a vertex.

The sense in which the socket on the vertex is bitten is obvious. To determine in which sense the nested gauge remainders are bitten, we simply equate bites on the left with pushes forward and bites on the right with pulls back. There is only one case where we must take a little care. Consider a nested version of the hook discussed in section 3.1.2. It is not surprising that we must take care here, as this is an example where the final gauge remainder in the string has bitten the end of a wine, rather than a socket. We can consider the gauge remainder that forms the un-nested hook of equations (3.2) and (3.3) to have bitten itself on the right. This, however, corresponds to a push forward and *not* a pull back. Thus, for the arbitrarily nested hook shown in figure 3.21, the number of pushes forward is equal to the number of bites on the left, plus one and the number of pulls back is equal to the number of bites on the right, minus one.



Figure 3.21: An arbitrarily nested version of the hook.

### 3.1.9 Double Gauge Remainders

We conclude our discussion of the gauge remainders by examining diagrams possessing two active gauge remainders. The techniques we use to process such terms are exactly the same as the ones detailed already in this chapter. There is, however, a qualitatively new type of diagram that arises, together with a source of possible ambiguity. To investigate both of these issues, we focus on a two-loop diagram, in which both gauge remainders bite the wine.<sup>7</sup> This is shown in figure 3.22.

We proceed by allowing first one gauge remainder to act and then, if possible, by allowing the second gauge remainder to act. The qualitatively new

---

<sup>7</sup>Double gauge remainder diagrams are not restricted to those in which both gauge remainders bite a wine; one or both of the gauge remainders can bite a vertex.

$$\frac{1}{2} \quad \mathbf{3.30} \quad \text{Diagram 3.30: A loop with a dot at the bottom and two arrows pointing towards each other from the top.$$

Figure 3.22: An example of a double gauge remainder diagram.

type of diagram arises because one of the effects of the first gauge remainder can be to ‘trap’ the second gauge remainder, by biting the field on the wine to which the second gauge remainder attaches. The active gauge remainder now does not have the same momentum flowing through it as the field it is trying to bite, and so it cannot act. The other diagrams generated are those in which the processed gauge remainder bites one of the ends of the wine. The result of allowing the first gauge remainder to act is shown in figure 3.23, where we have collected pulls back and pushes forward, as usual.

$$\mathbf{3.31} \quad \mathbf{3.32} \quad \mathbf{3.33} \\ \text{Diagram 3.31: A loop with a dot at the bottom and an arrow pointing left.} \quad - \quad \text{Diagram 3.32: A loop with a dot at the bottom and an arrow pointing left, with a second arrow pointing down from the top.} \quad + \quad \text{Diagram 3.33: A loop with a dot at the bottom and an arrow pointing left, with a second arrow pointing right from the top.$$

Figure 3.23: Result of allowing one gauge remainder in diagram 3.30 to act.

Diagram 3.32 possesses the trapped gauge remainder. In diagram 3.33 we have recognised that the wine ends where it attaches to the active gauge remainder and so this is where the processed gauge remainder bites. Note that we can trivially redraw this diagram, as shown in figure 3.24.<sup>8</sup>

Finally, consider allowing the active gauge remainder to act in diagrams 3.31 and 3.34. We are not interested in all the contributions. Rather, we just want to focus on

---

<sup>8</sup>Diagram 3.34 highlights how one must be very careful when drawing which end of an active gauge remainder a processed gauge remainder bites; diagrams 3.34 and 3.32 are clearly different.

3.34



Figure 3.24: A trivial redrawing of diagram 3.33.

1. the term produced by diagram 3.31 where the gauge remainder pulls back along the wine, to the same end as the hook;
2. the term produced by diagram 3.34 in which the gauge remainder pulls back to the bottom of the wine.

Reflecting the former diagram about a horizontal line, we arrive at the two diagrams of figure 3.25.<sup>9</sup>

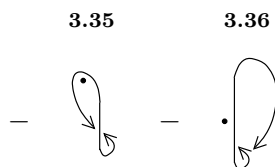


Figure 3.25: Two of the terms produced by processing diagrams 3.31 and 3.34.

From the way in which these two diagrams have been drawn, it is clear that they are distinct and that they must be treated as such. We can, however, redraw diagram 3.36 by sliding the outer gauge remainder round the hook to where the inner gauge remainder bites the wine. This is shown in figure 3.26.

Diagram 3.37 is, of course, still the same as diagram 3.36 but it is starting to look very similar to diagram 3.35. Indeed, we must make sure that we never slide the gauge remainder so far round the hook that it appears to bite the wine at the same point as the gauge remainder which forms the hook. If this were to happen, then such a diagram would be ambiguous.

---

<sup>9</sup>The reflection does not yield a net sign as we pick up one for each of the processed gauge remainders.

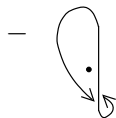


Figure 3.26: A trivial redrawing of diagram 3.36.

## 3.2 Momentum Expansions

The computation of  $\beta$ -function coefficients involves working at fixed order in external momentum. If a diagram contains a structure that is already manifestly of the desired order, then it is useful to Taylor expand at least some of the remaining structures in the external momentum. Vertices can always be expanded in momentum, as it is a requirement of the setup that such a step is possible [52, 53, 20]. Whereas wines, too, can always be Taylor expanded in momentum it is not necessarily possible to do so with effective propagators that form part of a diagram, as this step can introduce IR divergences. This will be discussed in detail in chapter 5.

In addition to allowing us to deal with diagrams possessing a structure already of the desired order in external momentum, the methodology of this chapter will also be of use in the extraction of universal coefficients from  $\Lambda$ -derivative terms. To this end, we will provide explicit lowest order expansions of certain vertices and discuss features of particular illustrative diagrams.

The key idea in what follows is that, if an  $A$ -field decorating an  $n$ -point vertex (wine) carries zero momentum, then we can relate this vertex (wine) to the momentum derivative of a set of  $(n - 1)$ -point vertices (wines). This relation arises as a consequence of the Ward identity (1.48) and so it is no surprise that the diagrammatics of this chapter is very similar to those of the last.

### 3.2.1 Basics

Consider the structure,  $U$ , which can be either a vertex or wine, the decorations of which include an  $A$ -field carrying zero momentum. Let us begin by

supposing that this  $A$ -field is sandwiched between the fields  $X$  and  $Y$ . By the Ward Identity (1.48), we have:

$$\begin{aligned} \epsilon_\mu U_{\dots R \mu S \dots}^{XAY \dots}(\dots, r, \epsilon, s - \epsilon, \dots) = \\ U_{\dots R S \dots}^{XY \dots}(\dots, r, s, \dots) - U_{\dots R S \dots}^{XY \dots}(\dots, r + \epsilon, s - \epsilon, \dots). \end{aligned} \quad (3.5)$$

Taylor expanding both sides in  $\epsilon$  and equating the  $\mathcal{O}(\epsilon)$  terms yields:

$$U_{\dots R \mu S \dots}^{XAY \dots}(\dots, r, 0, s, \dots) = \left( \partial_\mu^{s'} - \partial_\mu^{r'} \right) U_{\dots R S \dots}^{XY \dots}(\dots, r', s', \dots) \Big|_{r'=r, s'=s}. \quad (3.6)$$

This equation, for the case of a vertex, is represented diagrammatically in figure 3.27, which highlights the similarity between the momentum expansions and gauge remainders. The top row on the r.h.s. correspond to ‘push forward like’ terms, whereas those on the second row correspond to ‘pull back like’ terms. (As with the gauge remainders, pushes forward are performed in the counterclockwise sense.)

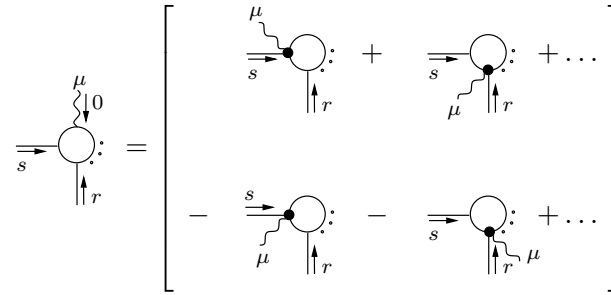


Figure 3.27: Diagrammatics expression for a vertex decorated by an  $A$ -field carrying zero momentum. The filled circle attached to the  $A$ -field line tells us to first replace all momenta with dummy momenta; then to differentiate with respect to the dummy momenta of the field hit, holding all other momenta constant and finally to replace the dummy momenta with the original momenta.

As with the gauge remainders, we must consider all possible independent locations of the  $A$ -field with respect to the other fields. Hence, terms between the first and second rows can cancel, if the field hit is bosonic.

We now want to convert derivatives with respect to the dummy momenta to derivatives with respect to the original momenta. There are two cases to

deal with. The first—in which we shall say that the momenta are paired—is where there are a pair of fields, carrying equal and opposite momentum. The second—in which we shall say that the momenta are coupled—is where there are three fields carrying, say,  $(r, s, -s - r)$ .

### Case I: Paired Momenta

This is the simplest case to deal with. If the momentum  $r$  has been replaced with dummy momentum  $r'$  and  $-r$  has been replaced with dummy momentum  $s'$  then

$$\left(\partial_\mu^{r'} - \partial_\mu^{s'}\right) \rightarrow \partial_\mu^r.$$

Hence, we can collect together a push forward like diagram with a pull back like diagram to give a derivative with respect to one of the original momenta. An example of this is shown in figure 3.28, for a field-ordered three-point vertex.

Figure 3.28: A field ordered three-point vertex with zero momentum entering along an  $A$ -field can be expressed as the momentum derivative of a two-point vertex. The open circle attached to the  $A$ -field line represents a derivative with respect to the momentum entering the vertex along the field hit.

### Case II: Coupled Momenta

The structures in this section contain momentum arguments of the form  $(r, s, -s - r)$ . Referring back to equation (3.6), we will denote the dummy momenta by  $(r', s', t')$ . We can make progress by noting that:

$$\left(\partial_\mu^{r'} - \partial_\mu^{s'}\right) \rightarrow \left(\partial_\mu^r \Big|_s - \partial_\mu^s \Big|_r\right) \quad (3.7)$$

and likewise, for all other combinations of  $(r', s', t')$ . Thus, as with the previous case, we need to combine a pair of terms differentiated with respect to dummy momenta to obtain a structure which is differentiated with respect to

its original momenta. The difference is that, whilst in the previous case the pair combined into one diagram, in this case they remain as a pair. An example is shown in figure 3.29.

The diagram shows an equation: a four-point vertex with a wavy line labeled '0' entering from the top, and two other lines labeled 'r' and 's' entering from the bottom left and bottom right respectively, is equal to the difference of two three-point vertices. The first three-point vertex has a wavy line on the left and two lines on the right, with a black dot on the left line. The second three-point vertex has a wavy line on the right and two lines on the left, with a black dot on the right line. This is followed by another equals sign, then two more three-point vertices: the first has a wavy line on the left and two lines on the right, with a white circle on the left line; the second has a wavy line on the right and two lines on the left, with a white circle on the right line. The entire right-hand side is labeled 'FAS'.

Figure 3.29: A field ordered four-point vertex with zero momentum entering along an  $A$ -field can be expressed as the momentum derivative of two three-point vertices.

The open circle attached to the  $A$ -field line represents a derivative with respect to the momentum entering the vertex along the field hit. However, this derivative is performed holding the momentum of the field hit in the partner diagram constant. Hence, the final two diagrams of figure 3.29 must be interpreted as a pair. The difference between this and the paired momentum case highlights the care that must be taken interpreting the new diagrammatics.

### 3.2.2 Wines

When we come to deal with wines, we must adapt the diagrammatic notation slightly. If the momentum derivative strikes a field decorating a wine, then we just use the current notation. However, it is desirable to change the notation when the momentum derivative strikes one of the ends a wine. In complete diagrams, placing the diagrammatic object representing a momentum derivative at the end of the wine becomes confusing; rather we place the object in middle and use an arrow to indicate which end of the wine it acts on, as shown in figure 3.30.

Hence, the second diagram denotes a derivative with respect to  $+k$ , whereas the third diagram denotes a derivative with respect to  $-k$ .

$$\frac{\text{Diagram 1}}{k} = \text{Diagram 2} = - \text{Diagram 3} \quad \text{FAS}$$

Figure 3.30: A field ordered one-point wine with zero momentum entering along a decorative  $A$ -field can be expressed as the momentum derivative of a zero-point wine.

### 3.2.3 Algebraic Expansions

In this section we provide the lowest order momentum expansions for the following:

1. a three-point, tree level vertex for which all fields are in the  $A^1$  sector;
2. a four-point, tree level vertex for which all fields are in the  $A^1$  sector.

The first case has already been partially examined in figure 3.28 and, algebraically, this reads:

$$S_{\mu RS}^{AXY}(0, s, -s) = \partial_{\mu}^s S_{RS}^{XY}(s, -s) \quad (3.8)$$

Using equation (A.1) and recalling that  $c(0) = 1$ , we obtain

$$\partial_{\mu}^k S_{0\alpha\beta}^{11}(k, -k) = 2(2k_{\mu}\delta_{\alpha\beta} - k_{\alpha}\delta_{\beta\mu} - k_{\beta}\delta_{\alpha\mu}) + \mathcal{O}(k^3). \quad (3.9)$$

The second case has already been partially examined in figure 3.29 and, algebraically, this reads:

$$S_{\alpha\beta\rho\sigma}^{1111}(l, -l - k, 0, k) = \partial_{\rho}^k \Big|_l S_{\alpha\beta\sigma}^{111}(l, -l - k, k).$$

Expanding both sides to zeroth order in momenta and utilising equation (3.9) yields:

$$S_{0\alpha\beta\rho\sigma}^{1111}(0, 0, 0, 0) \equiv S_{0\alpha\beta\rho\sigma}^{1111}(\underline{0}) = -2(2\delta_{\alpha\rho}\delta_{\beta\sigma} - \delta_{\beta\rho}\delta_{\alpha\sigma} - \delta_{\sigma\rho}\delta_{\alpha\beta}). \quad (3.10)$$

### 3.2.4 Complete Diagrams

The diagrams we deal with fall into two classes, depending on whether or not they possess a structure which is manifestly of the desired order in external momentum to which we wish to work. In the case that such a structure is

present, we will Taylor expand all components of the rest of the diagram that we are allowed to, in external momentum. The other case will arise in our discussion of  $\Lambda$ -derivatives (see chapters 5 and 13) and here, rather than being forced to Taylor expand certain structures, we choose which structures to Taylor expand.

### Forced Expansions

The generalisation to complete diagrams is straightforward and, as an example, figure 3.31 shows how we can manipulate diagram 3.17.

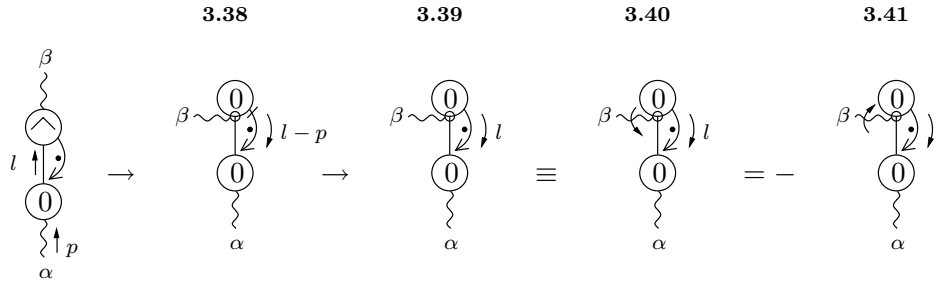


Figure 3.31: Manipulation of a diagram at  $\mathcal{O}(p^2)$ . Discontinuities in momentum flow are indicated by a bar.

The two-point vertex at the base of the diagram is  $\mathcal{O}(p^2)$ , which is the order in  $p$  to which we wish to work. We call this base structure an ‘ $\mathcal{O}(p^2)$  stub’. The first step is to Taylor expand the three-point vertex to zeroth order in  $p$ , as shown in diagram 3.38. There is now a discontinuity in momentum arguments, since although momentum  $l$  flows into and out of the differentiated two-point vertex, this vertex is attached to an effective propagator carrying momentum  $l$  and a wine carrying momentum  $l - p$ . This discontinuity is indicated by the bar between the vertex and the wine. We can Taylor expand the wine to zeroth order in momentum, too, and this is done in diagram 3.39. Since the discontinuity in momentum has now vanished, the bar is removed. We will encounter terms shortly in which the bar must be retained. Treatment of diagrams with an  $\mathcal{O}(p^2)$  stub in which the wine is decorated by an external field is exactly the same.

In diagram 3.40 we have introduced an arrow on the diagrammatic representation of the derivative. We have come across this arrow already the context of wines but have not yet required it for vertices. Indeed, in the current example, it is effectively redundant notation. We note, though, that we can reverse the direction of the arrow, at the expense of a minus sign, as in diagram 3.41. By reversing the direction of the arrow, we are now differentiating with respect to the momentum leaving the vertex along the struck field, rather than the momentum thus entering. We will require this notation shortly.

### Unforced Expansions

To illustrate the kind of diagrams in which we *choose* to Taylor expand structures, consider figure 3.32. The right-most vertex of the first diagrams is not forced to carry zero momentum along its external field; rather we construct this diagram, for reasons which will become apparent in section 13.3.2.

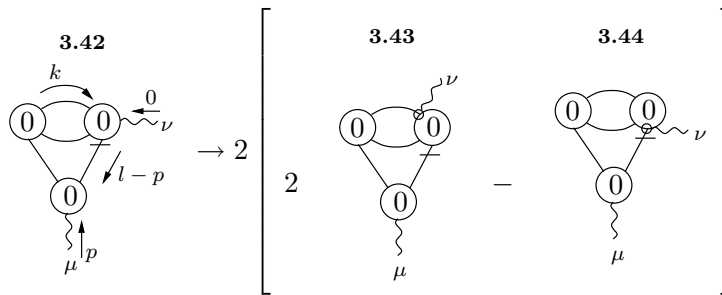


Figure 3.32: Example of a two-loop diagram in which we choose to Taylor expand in momenta, rather than this choice being forced upon us.

In direct analogy with the gauge remainders, the overall factor of two on the r.h.s. arises from collecting together CC pairs, and the additional factor of two in front of diagram 3.43 arises from invariance under swapping the two  $k$ -dependent internal fields. Now, however, we arrive at a potential source of confusion. We know that two diagrams on the r.h.s. must be interpreted as a pair. But, we are free to route momenta such that, in the first diagram, whilst holding  $l$  constant, we are either differentiating with respect to  $k$  or with respect to  $(l - k)$ . This choice, in turn, determines what must be held constant whilst differentiating with respect to  $l$  in the second diagram.

Noting that the relative factor of two between the two diagrams on the r.h.s. disappears if we choose an order for the interchangeable internal fields in the second diagram, the effect of the momentum derivatives on the right-most vertex is summarised in table 3.3. In the second column, we include the overall minus sign of the diagram (which arises from pulling back the momentum derivative).

Diagram 3.43	Diagram 3.44	Net Effect
$\partial_\nu^k _l$	$-\partial_\nu^{-l} _k$	$\partial_\nu^k _l + \partial_\nu^l _k$
$\partial_\nu^{(l-k)} _l$	$-\partial_\nu^{-l} _{(l-k)}$	$\partial_\nu^l _k$

Table 3.3: Algebraic realisation of the derivative striking the four-point vertices of diagrams 3.43 and 3.44, for different momentum routing.

It seems that the net effect on the right-most vertex depends on the choice of momentum routing. However, we do not expect individual elements of a diagram to be invariant under momentum rerouting; rather it is the diagram as a whole which is invariant under such a change. Thus, we can we choose to route  $k$  however we please in diagram 3.42 and need only ensure that diagrams 3.43 and 3.44 are consistent with this.

Note, though, that by performing the unforced Taylor expansion, diagram 3.42 is no longer invariant under rerouting the loop momentum  $l$ . As we will see in section 5.4, diagrams such as 3.42 are in fact constructed in actual calculations to facilitate extraction of numerical answers, rather than arising as a direct consequence of the flow equations. Hence, to incorporate such diagrams, we must add and subtract them from a calculation (i.e. we merely conveniently re-express zero). Diagrams genuinely generated by the flow equations are always invariant under momentum rerouting; indeed this is necessary for gauge invariance [6, 51].

There is a further subtlety concerning the treatment of diagrams in which we perform an unforced Taylor expansion, which can also be illustrated by our current example. When we come to extract the universal contribution from the

$\Lambda$ -derivative terms, it turns out the four-point vertex in diagram 3.42 will be Taylor expanded to zeroth order in all momenta, not just in  $p$ . Let us denote the field ordered four-point, tree level vertex (with all fields in the  $A^1$  sector) by:

$$S_{0\alpha\nu\rho\sigma}^{1111}(p-l, -p, k, l-k) \quad (3.11)$$

where  $\rho, \sigma$  are the indices corresponding to the indistinguishable internal fields. Given that, as a result of momentum rerouting invariance, the parent diagram is invariant under the interchange of these two internal fields and that the left-hand three-point vertex changes sign if we let  $\rho \leftrightarrow \sigma$ , the diagram is invariant under the addition of

$$a(\delta_{\nu\rho}\delta_{\alpha\sigma} + \delta_{\alpha\rho}\delta_{\nu\sigma}) + b\delta_{\sigma\rho}\delta_{\alpha\nu}, \quad (3.12)$$

to the four-point vertex, where  $a$  and  $b$  are arbitrary coefficients. This means that, when we Taylor expand the four-point vertex to zeroth order in momenta, there is a spectrum of equivalent forms that we can take.

In particular, we will obtain different forms depending on the order we choose for  $\rho$  and  $\sigma$ . These differences, of course, just give rise to a contribution of the form given by equation (3.12). However, to actually evaluate the  $\Lambda$ -derivative terms generally involves a complete loss of momentum rerouting invariance at a certain stage of the calculation (i.e. we ultimately lose the freedom to reroute  $k$ , as well as  $l$ ). At this point, the specific choice for a four-point vertex will become important.

We conclude this section by illustrating how certain groups of diagrams in which an unforced Taylor expansion has been performed can be combined. In chapter 13, we will be lead to consider the set of diagrams shown in the first row of figure 3.33.

We now fix the order of the interchangeable fields, choosing to do so in such a way that the momentum routing between pairs of diagrams is the same. Referring to the  $k$ -dependent sub-diagram, all structures are hit by a momentum derivative with the exception of the inner most effective propagator. We now analyse the two different momentum routings.

In the first instance, we will take momentum  $k$  to travel around the uppermost effective propagator. Noting that the inner-most effective propagator

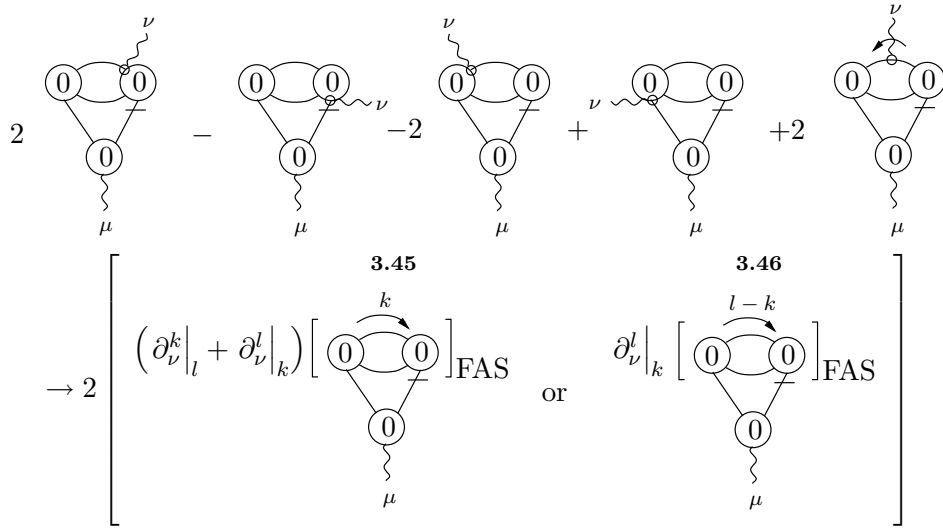


Figure 3.33: A set of diagrams which naturally combine.

carries momentum  $l-k$  and that  $(\partial_\nu^k|_l + \partial_\nu^l|_k) F(l-k) = 0$ , for any function  $F$ , we can take the momentum derivatives outside the  $k$ -dependent sub-diagram, to yield the first diagram 3.45.

In the second instance, we will take momentum  $(l-k)$  to flow around the upper-most effective propagator. The inner-most effective propagator now carries  $k$  and, referring to table 3.3, both vertices are hit by  $\partial_\nu^l|_k$ . Given that  $(\partial_\nu^{(l-k)} - \partial_\nu^l|_k) F(l-k) = 0$  we can take the momentum derivatives outside the  $k$ -dependent sub-diagram, to yield the second diagram 3.46.

It is apparent that these two diagrams differ by a total derivative with respect to  $k$ . This gives rise to a surface term which must be thrown away, for the consistency of the regularisation scheme [6]; thus, in this thesis, calculations are performed in general dimension  $D$ , so that such terms are automatically discarded. We can redraw both terms as the diagram shown in figure 3.34.

Now we see why we introduced arrows on momentum derivative striking vertices in figure 3.31. Let us return to diagram 3.47. Focusing on the structure enclosed by square brackets, we ignore its internal structure and note only that it carries external momentum  $l$ . The arrow on the derivative tells us to differentiate with respect to  $+l$  (with  $l$  routed as shown). This rule is consistent with the way in which we treat momentum derivatives of plain vertices.



way, then the derivative would be with respect to the momentum entering the structure from the right.

**Diagrammatic Identity 5** A sub-diagram comprising a two-point, tree level vertex, differentiated with respect to momentum and attached to two effective propagators can, using diagrammatic identity 4 and the effective propagator relation, be redrawn in the following way:

$$\begin{array}{c} \text{---} \textcircled{0} \text{---} \end{array} \equiv - \begin{array}{c} \text{---} \textcircled{0} \text{---} \end{array} + \frac{1}{2} \left[ \begin{array}{cc} \begin{array}{c} \text{---} \textcircled{0} \text{---} \\ \text{---} \textcircled{0} \text{---} \end{array} & - & \begin{array}{c} \text{---} \textcircled{0} \text{---} \\ \text{---} \textcircled{0} \text{---} \end{array} \\ \begin{array}{c} \text{---} \textcircled{0} \text{---} \\ \text{---} \textcircled{0} \text{---} \end{array} & - & \begin{array}{c} \text{---} \textcircled{0} \text{---} \\ \text{---} \textcircled{0} \text{---} \end{array} \end{array} \right].$$

We could re-express this in a less symmetric form by taking either of the two rows in the square brackets and removing the factor of half.

**Diagrammatic Identity 6** A sub-diagram comprising a two-point, tree level vertex, struck by  $\triangleright$  vanishes:

$$\begin{array}{c} \text{---} \textcircled{0} \text{---} \end{array} \triangleright = 0.$$

### Corollaries

$$\begin{array}{c} \begin{array}{c} \text{---} \textcircled{0} \text{---} \\ \text{---} \textcircled{0} \text{---} \end{array} \triangleright \equiv - \begin{array}{c} \text{---} \textcircled{0} \text{---} \\ \text{---} \textcircled{0} \text{---} \end{array} \triangleright \\ \begin{array}{c} \text{---} \textcircled{0} \text{---} \\ \text{---} \textcircled{0} \text{---} \end{array} \triangleright \equiv - \begin{array}{c} \text{---} \textcircled{0} \text{---} \\ \text{---} \textcircled{0} \text{---} \end{array} \triangleright = 0 \\ \begin{array}{c} \text{---} \textcircled{0} \text{---} \\ \text{---} \textcircled{0} \text{---} \end{array} \triangleright \equiv - \begin{array}{c} \text{---} \textcircled{0} \text{---} \\ \text{---} \textcircled{0} \text{---} \end{array} \triangleright = 0 \end{array}$$

Recall that  $\textcircled{\alpha}$  represents differentiation with respect to  $\alpha$ . We have used the independence of  $\triangleright$  on both  $\Lambda$  and  $\alpha$  (in all sectors).

**Diagrammatic Identity 7** A sub-diagram comprising a two-point, tree level vertex, differentiated with respect to momentum and attached to two effective propagators, one of which terminates with a  $>$  can, using diagrammatic identities 3 and 4, be redrawn in the following form:

$$\begin{array}{c} \text{---} \textcircled{0} \text{---} \end{array} \equiv - \begin{array}{c} \text{---} \textcircled{0} \text{---} \end{array}.$$

**Diagrammatic Identity 8** *A sub-diagram comprising a two-point, tree level vertex, attached to an un-decorated wavy line which terminates in a  $\triangleright$  can be redrawn, using diagrammatic identities 3 and 2, the effective propagator relation and the tree level flow equation:*

$$\begin{aligned}
 \text{---} \circlearrowleft \text{---} \triangleright &\equiv \left[ \text{---} \circlearrowleft \text{---} \right] \triangleright - \text{---} \circlearrowleft \text{---} \triangleright - \text{---} \circlearrowleft \text{---} \triangleright \\
 &\equiv \text{---} \triangleright
 \end{aligned}$$

**Diagrammatic Identity 9** *Consider the diagram shown on the l.h.s. of figure 3.35. We can redraw this as shown on the r.h.s. since, if the newly drawn  $\triangleright$  hits the external field, then the diagram vanishes.*

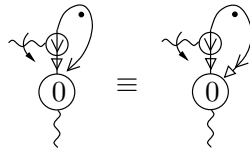


Figure 3.35: The first step in redrawing a diagram to yield a diagrammatic identity.

*We now allow the original  $\triangleright$  to act. It must trap the remaining  $\triangleright$ . Taking the CC of the resultant diagram, we reflect it but pick up no net sign, since we have both one processed gauge remainder and one momentum derivative. Having done this, we then reverse the direction of the arrow on the derivative, which does yield a minus sign. This gives us the diagrammatic identity, shown in figure 3.37.*

*We can, however, generalise this diagrammatic identity by stripping off the two-point, tree level vertices. We are justified in doing this: the integral over loop momentum will, by Lorentz invariance, yield a Kronecker  $\delta$  for both diagrams of figure 3.37. In other words, we need not worry that stripping off*

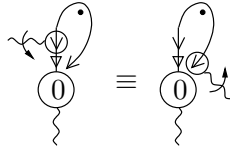


Figure 3.36: A diagrammatic identity.

*the two-point, tree level vertices is valid only up to some term which kills the vertex.*



Figure 3.37: Diagrammatic identity 9.

*Note that this identity holds if we replace the wavy line by an effective propagator.*

## Chapter 4

# One Loop Diagrammatics

In this chapter, we present the entire diagrammatics for the computation of  $\beta_1$ , arriving at a manifestly gauge invariant, diagrammatic expression, from which the universal value in  $D = 4$  can be immediately extracted. This computation of  $\beta_1$  not only serves as an illustration of the diagrammatic techniques of chapters 2 and 3, but is a necessary intermediate step in the computation of  $\beta_2$ . Much of the work presented in this chapter overlaps with the computation of  $\beta_1$  presented in [57]. However, there are a number of important differences, which we now outline.

First, the computation here is done for an unrestricted Wilsonian effective action. Previously, the action was restricted to just single supertrace terms; a consequence of which is that the single supertrace terms  $S_{0\mu\nu}^{AAC}(p, q, r)$  and  $S_{0\mu\nu}^{AAC\sigma}(p, q, r)$  can be set to zero (*ibid*). The second major difference is that the diagrammatics are no longer terminated after the use of the effective propagator relation. Gauge remainders and  $\mathcal{O}(p^2)$  manipulations are dealt with in an entirely diagrammatic fashion. Moreover, the diagrammatics are utilised even at the point where all quantities are ‘algebraic’ (see section 2.5.5).

We also choose to use a completely general  $\hat{S}$ , thereby demonstrating complete scheme independence. In fact, the inclusion of  $\hat{S}_1$  (higher loop vertices do not occur in the calculation) actually leads only to a trivial extension of the scheme independence. The instances of  $\hat{S}$  beyond tree level are restricted to those of the form  $\hat{S}_1^C$  (at  $\mathcal{O}(p^2)$ ), and are only ever involved in cancellations

via the constraint equation (2.77).<sup>1</sup> Nonetheless, it is instructive to see this occurring and to confirm that  $\beta_1$  is universal.

## 4.1 A Diagrammatic Expression for $\beta_1$

### 4.1.1 The Starting Point

The key to extracting  $\beta$ -function coefficients from the weak coupling flow equations (2.28) is to use the renormalisation condition (1.33), which places a constraint on the vertex  $S_{\mu\nu}^{11}(p)$ . From equations (1.54) and (A.1), this constraint is saturated at tree level:

$$S_{\mu\nu}^{11}(p) = \frac{2}{g^2} \square_{\mu\nu}(p) + \mathcal{O}(p^4) = \frac{1}{g^2} \mathbf{A}(0) \square_{\mu\nu}(p) + \mathcal{O}(p^4) = \frac{1}{g^2} S_{0\mu\nu}^{11}(p),$$

where we have used equation (2.42). Hence, all higher loop two-point vertices,  $S_{n \geq 1 \mu\nu}^{11}(p)$  vanish at  $\mathcal{O}(p^2)$ .

To utilise this information, we begin by specialising equation (2.28) to compute the flow of  $S_{1\mu\nu}^{11}(p)$ :

$$\Lambda \partial_\Lambda S_{1\mu\nu}^{11}(p) = 2\beta_1 S_{0\mu\nu}^{11}(p) - \gamma_1 \frac{\partial S_{0\mu\nu}^{11}(p)}{\partial \alpha} - \sum_{r=0}^1 a_0 [\bar{S}_{1-r}, \bar{S}_r]_{\mu\nu}^{11}(p) + a_1 [\Sigma_0]_{\mu\nu}^{11}(p). \quad (4.1)$$

The  $a_0$  term can be simplified. Defining  $\Pi_{RS}^{XY}(k) = S_{RS}^{XY}(k) - \hat{S}_{RS}^{XY}(k)$  and using the definition of the barred vertices, (2.27), we can write

$$- \sum_{r=0}^1 a_0 [\bar{S}_{1-r}, \bar{S}_r]_{\mu\nu}^{11}(p) = -2a_0 [\Pi_0, S_1]_{\mu\nu}^{11}(p) + 2a_0 [S_0, \hat{S}_1]_{\mu\nu}^{11}(p).$$

All the  $a_0$  terms generate two vertices, joined by a wine. Unless one of these vertices is decorated by a single field, both vertices must be decorated by an internal field and one of the external fields. Now, one-point  $\Pi_0$  vertices do not exist and two-point  $\Pi_0$  vertices vanish, since we have identified the two-point, tree level Wilsonian effective action vertices with the corresponding seed action vertices. We choose to discard one-point  $S_1^C$  vertices at this stage of the calculation and so  $a_0 [\Pi_0, S_1]_{\mu\nu}^{11}(p)$  does not contribute.

---

<sup>1</sup>In the one loop calculation we choose to set  $S_1^C = 0$  at the beginning of the calculation, rather than at the end. This means that we never compute the flow of this vertex in the current calculation and so must resort to the previously obtained constraints.

The next step is to focus on the  $\mathcal{O}(p^2)$  part of equation (4.1). Noting that  $S_{1\mu\nu}^{11}(p)$  is at least  $\mathcal{O}(p^4)$ , and that  $A(0)$  is independent of  $\alpha$ , we arrive at an algebraic expression for  $\beta_1$ :

$$-4\beta_1 \square_{\mu\nu}(p) + \mathcal{O}(p^4) = a_1[\Sigma_0]_{\mu\nu}^{11}(p) + 2a_0[S_0, \hat{S}_1]_{\mu\nu}^{11}(p), \quad (4.2)$$

which is shown diagrammatically in figure 4.1. It is implicit in all that follows that, unless otherwise stated, the external indices are  $\mu$  and  $\nu$  and we are working at  $\mathcal{O}(p^2)$ .

$$-4\beta_1 \square_{\mu\nu}(p) + \mathcal{O}(p^4) = \frac{1}{2} \left[ \begin{array}{ccc} \begin{array}{l} \mathbf{4.1} \rightarrow \mathbf{4.2} \\ \{ \mathbf{4.2} \ 4.22 \} \end{array} & \begin{array}{l} \{ \mathbf{4.3} \ 4.40 \} \\ \{ \mathbf{4.4} \ 4.24 \} \end{array} & \{ \mathbf{4.5} \ 4.26 \} \\ \begin{array}{c} \text{Diagram 1} \\ \Sigma_0 \end{array} & +2 & \begin{array}{c} \text{Diagram 2} \\ \Sigma_0 \end{array} & - & \begin{array}{c} \text{Diagram 3} \\ 0 \end{array} \\ \{ \mathbf{4.6} \ 4.32, 4.33 \} & & \mathbf{4.7} \rightarrow 0 & & \\ +2 & \begin{array}{c} \text{Diagram 4} \\ \hat{1} \\ 0 \end{array} & +4 & \begin{array}{c} \text{Diagram 5} \\ \hat{1} \\ 0 \end{array} & \end{array} \right]$$

Figure 4.1: A diagrammatic representation of the equation for  $\beta_1$ . On the r.h.s., we implicitly take the indices to be  $\mu$  and  $\nu$  and work at  $\mathcal{O}(p^2)$ .

The diagrams are labelled in boldface as follows: any diagram containing  $\Sigma$  as a vertex argument has two labels: the first corresponds to the Wilsonian effective action part and the second corresponds to the seed action part. Diagrams with only a Wilsonian effective action vertex or a seed action vertex have a single label. If the reference number of a diagram is followed by an arrow, it can mean one of two things:

1.  $\rightarrow 0$  denotes that the corresponding diagram can be set to zero, for some reason;
2.  $\rightarrow$  followed by a number (other than zero) indicates the number of the figure in which the corresponding diagram is processed.

If a diagram is cancelled, then its reference number is enclosed in curly braces, together with the reference number of the diagram against which it cancels. A diagram will not be taken as cancelled until the diagram against which it cancels has been explicitly generated. Thus, at various stages of the calculation where we collate surviving terms, we include those diagrams whose cancelling partner does not yet exist.

Returning to figure 4.1, the first three diagrams are formed by the  $a_1[\Sigma_0]$  term and the last two are formed by the  $a_0[S_0, \hat{S}_1]$  term. We do not draw any diagrams possessing either a one-point, tree level vertex or a wine which bites its own tail (see sections 1.2.1, 1.2.3 and 14.2). In the third diagram, we have used the equality between Wilsonian effective action and seed action two-point, tree level vertices to replace  $\Sigma_{0RS}^{XX}(k)$  with  $-S_{0RS}^{XX}(k)$ . The final diagram vanishes: the one-point vertex must be in the  $C$ -sector but, since an  $\dot{\Delta}^{AC,A}$  wine does not exist, it is not possible to form a legal diagram.

Note that we have not included the diagram which can be obtained from diagram 4.7 by taking the field on the wine and placing it on the top-most vertex, since such a term vanishes at  $\mathcal{O}(p^2)$ : the vertex  $S_{0\mu\alpha}^{11}(p)$  is, as we know already, at least  $\mathcal{O}(p^2)$ ; the same too applies to  $\hat{S}_{1\mu\alpha}^{11}(p)$ , as a consequence of the Ward identity (1.48).<sup>2</sup>

### 4.1.2 Diagrammatic Manipulations

As it stands, we cannot directly extract a value for  $\beta_1$  from equation (4.2). The r.h.s. is phrased in terms of non-universal objects. Whilst one approach would be to choose a particular scheme in which to compute these objects [53] we know from [57] that this is unnecessary: owing to the universality of  $\beta_1$ , all non-universalities must somehow cancel out. To proceed, we utilise the flow equations.

Our aim is to try and reduce the expression for  $\beta_1$  to a set of  $\Lambda$ -derivative terms—terms where the entire diagram is hit by  $\Lambda\partial_\Lambda|_\alpha$ —since, as we will see in chapter 5, such terms either vanish directly or combine to give only universal contributions (in the limit that  $D \rightarrow 4$ ).

---

<sup>2</sup>There is no argument that the  $\mathcal{O}(p^2)$  part of  $\hat{S}_{n \geq 1\mu\nu}^{11}(p)$  vanishes, since the renormalisation condition does not apply to the seed action.

The approach we use is to start with the term containing the highest point Wilsonian effective action vertex. By focusing on the term with the highest point vertex, we guarantee that the wine in the diagram is un-decorated. Now, we know that an un-decorated wine is  $-\Lambda\partial_\Lambda|_\alpha$  of an effective propagator. Hence, up to a term in which the entire diagram is hit by  $-\Lambda\partial_\Lambda|_\alpha$ , we can move the  $-\Lambda\partial_\Lambda|_\alpha$  from the effective propagator to the vertex. This step is only useful if the vertex is a Wilsonian effective action vertex, for now it can be processed, using the flow equations.

From figure 4.1 it is clear that the highest point Wilsonian effective action vertex in our calculation of  $\beta_1$  is the four-point, tree level vertex contained in diagram 4.1. The manipulation of this diagram is shown in figure 4.2. For the time being, we will always take the  $\Lambda$ -derivative to act before we integrate over loop momenta (this is fully discussed in chapter 5).

$$\frac{1}{2} \text{Diagram 4.1} = \frac{1}{2} \left[ \text{Diagram 4.8} \rightarrow \text{Diagram 4.13} \right] - \frac{1}{2} \text{Diagram 4.9} \rightarrow \text{Diagram 4.3}$$

Figure 4.2: The manipulation of diagram 4.1. In the final diagram, the  $\Lambda$ -derivative operates on just the four-point vertex.

We can now use the tree-level flow equation (2.29) to process the  $\Lambda$ -derivative of the four-point vertex. The flow of a four-point vertex with two  $A^1$  fields and two wildcards is shown in figure C.3. Throwing away all terms which vanish at  $\mathcal{O}(p^2)$  and joining the wildcards together with an effective propagator, we arrive at figure 4.3.

The diagrams have been arranged in a very specific way. The first eight diagrams have all had the loop of the parent diagram split open and joined back to the rest of the diagram with some other structure(s). The very first diagram contains the highest-point vertex of this subset. Moving along the first five diagrams, we take the basic structure of the first diagram and distribute the external fields in all possible ways, being careful to insert the correct vertex arguments. Having exhausted all possibilities, we move to the next three

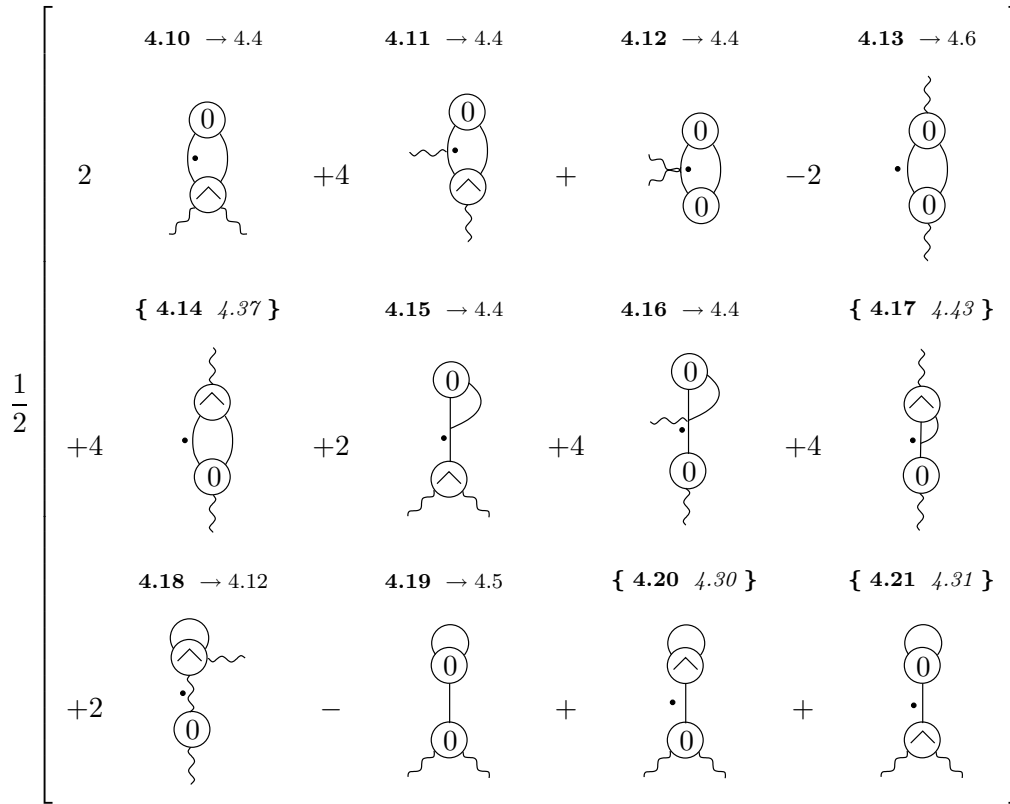


Figure 4.3: The re-expression of diagram 4.9, using the tree-level flow equation.

diagrams, where we take the first five diagrams but now demand that one end of the effective propagator attaches to the wine, rather than the bottom vertex (we discard any terms possessing one-point, tree level vertices). Finally, the bottom row contains all diagrams (which survive at  $\mathcal{O}(p^2)$ ) in which the loop of the parent diagram has not been split open.

Diagrams 4.10–4.12, 4.15 and 4.16 can be further manipulated using the effective propagator relation, since they contain a two-point, tree level vertex contracted into an effective propagator. The results of this procedure are shown in figure 4.4. Diagrams in which a wine bites its own tail have been discarded as have those in which a gauge remainder strikes a two-point vertex. Henceforth, we will assume that such terms have always been discarded.

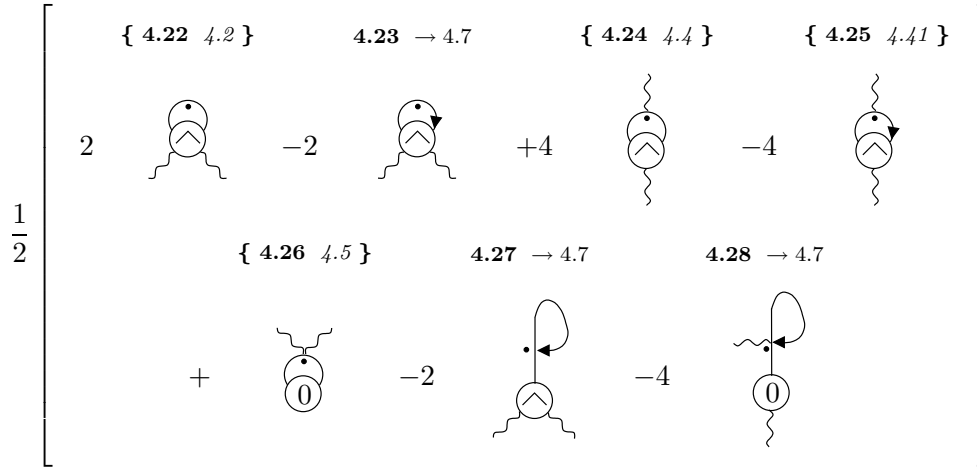


Figure 4.4: Manipulation of diagrams 4.10–4.12, 4.15 and 4.16.

Three of the diagrams generated exactly cancel the contributions in the first row of figure 4.1 containing seed action vertices (or Wilsonian effective action two-point, tree level vertices).

**Cancellation 4.1** *Diagram 4.22 exactly cancels diagram 4.2.*

**Cancellation 4.2** *Diagram 4.24 exactly cancels diagram 4.4.*

**Cancellation 4.3** *Diagram 4.26 exactly cancels diagram 4.5.*

Other than the  $\Lambda$ -derivative term, diagram 4.8, there are now only two diagrams left which contain four-point vertices. The first of these, diagram 4.18,

can be manipulated at  $\mathcal{O}(p^2)$  since the bottom vertex is at least  $\mathcal{O}(p^2)$  and the rest of the diagram can be Taylor expanded in  $p$ . Taking the zeroth order contribution from the differentiated effective propagator yields, by equation (A.13) (cf. equation (2.43)), the non-universal contribution  $B'(0)$ . If we were to take the zeroth order contribution from the four-point vertex<sup>3</sup>, it would reduce to the (double) momentum derivative of a two-point vertex. In the second of the diagrams containing a four-point vertex, diagram 4.23, the vertex is hit by a gauge remainder and so will automatically be reduced to a three-point vertex. Thus the effect of our manipulations is to ensure that all occurrences of the highest-point vertex in the calculation occur only in a  $\Lambda$ -derivative term.

Before moving on to the next stage of the calculation, we compare our current expression to that of reference [57]. Ignoring the multiple supertrace terms contained within each of our diagrams, the two expressions are superficially the same, up to diagrams 4.15 and 4.19–4.21. In each of these terms, the internal field joining the two three-point vertices must be in the  $C$ -sector. If it is in the  $F$ -sector, then each diagram vanishes because net fermionic vertices vanish. If it is in the  $A$ -sector, then charge conjugation invariance causes the diagrams to vanish when we sum over permutations of the bottom vertex (see section 3.1.5). Looking a little harder, we see a related difference between the current expression and that of reference [57]: amongst the components of diagrams 4.13 and 4.14 are diagrams possessing  $AAC$  vertices.

Now, with the aim of removing all three-point vertices from the calculation (up to  $\Lambda$ -derivative terms), we iterate the procedure. Referring to figure 4.3, only diagrams 4.19 and 4.13 possess exclusively Wilsonian effective action vertices and an un-decorated wine and so it is these which we manipulate.

Figure 4.5 shows the manipulation of diagram 4.19 which proceeds along exactly the same lines as the manipulations of figure 4.2. This time, however, we utilise figure C.1 for the flow of a three-point vertex with three wildcard fields and figure C.2 for the flow of a three-point vertex containing two external  $A^1$ s (which carry moment  $p$  and  $-p$ ). In this latter case, we discard all terms which vanish at  $\mathcal{O}(p^2)$ .

---

<sup>3</sup>As we will see in section 4.1.3 this manipulation is not necessary as there is a more elegant way to deal with the diagram.

$$\begin{aligned}
& -\frac{1}{2} \left[ \begin{array}{c} \text{4.29} \rightarrow \text{4.13} \\ \bullet \\ \text{Diagram 1} \end{array} \right] - \frac{1}{2} \left[ \begin{array}{cc} \{ \text{4.30} \ \text{4.20} \} & \{ \text{4.31} \ \text{4.21} \} \\ \text{Diagram 2} & + \text{Diagram 3} \end{array} \right] \\
& + \frac{1}{2} \left[ \begin{array}{cccc} \{ \text{4.32} \ \text{4.6} \} & | & \{ \text{4.33} \ \text{4.6} \} & \text{4.34} \rightarrow \text{4.7} & \text{4.35} \rightarrow \text{4.7} \\ \text{Diagram 4} & - & \text{Diagram 5} & +2 \text{Diagram 6} & +2 \text{Diagram 7} \end{array} \right]
\end{aligned}$$

Figure 4.5: Manipulation of diagram 4.19 using the tree level flow equations.

As with diagrams 4.2, 4.4 and 4.5, we find that diagrams of the same structure as the parent but containing a seed action vertex are cancelled.

**Cancellation 4.4** *Diagram 4.30 exactly cancels diagram 4.20.*

**Cancellation 4.5** *Diagram 4.31 exactly cancels diagram 4.21.*

We also find, as promised that the sole instance of a one-point, seed action vertex is cancelled.

**Cancellation 4.6** *Diagrams 4.32 and 4.33 exactly cancel diagram 4.6 by virtue of the constraint equation (2.77).*

In this context, the notation used in figure 4.5 to describe the cancellation of diagram 4.6 has an obvious interpretation. Note that the only surviving terms from figure 4.5 both contain gauge remainders.

Figure 4.6 shows the manipulation of diagram 4.13 (which first appears in figure 4.3), where the overall factor of  $1/2$  arises from the symmetry of the  $\Lambda$ -derivative term 4.36 under rotations by  $\pi$  (alternatively, the indistinguishability of the two internal fields). When we compute the flow of the vertices of diagram 4.36, we can utilise this symmetry to remove the factor of  $1/2$ .

We find a number of cancellations. The first of these is the expected cancellation of the partner of the parent diagram, possessing a seed action vertex.

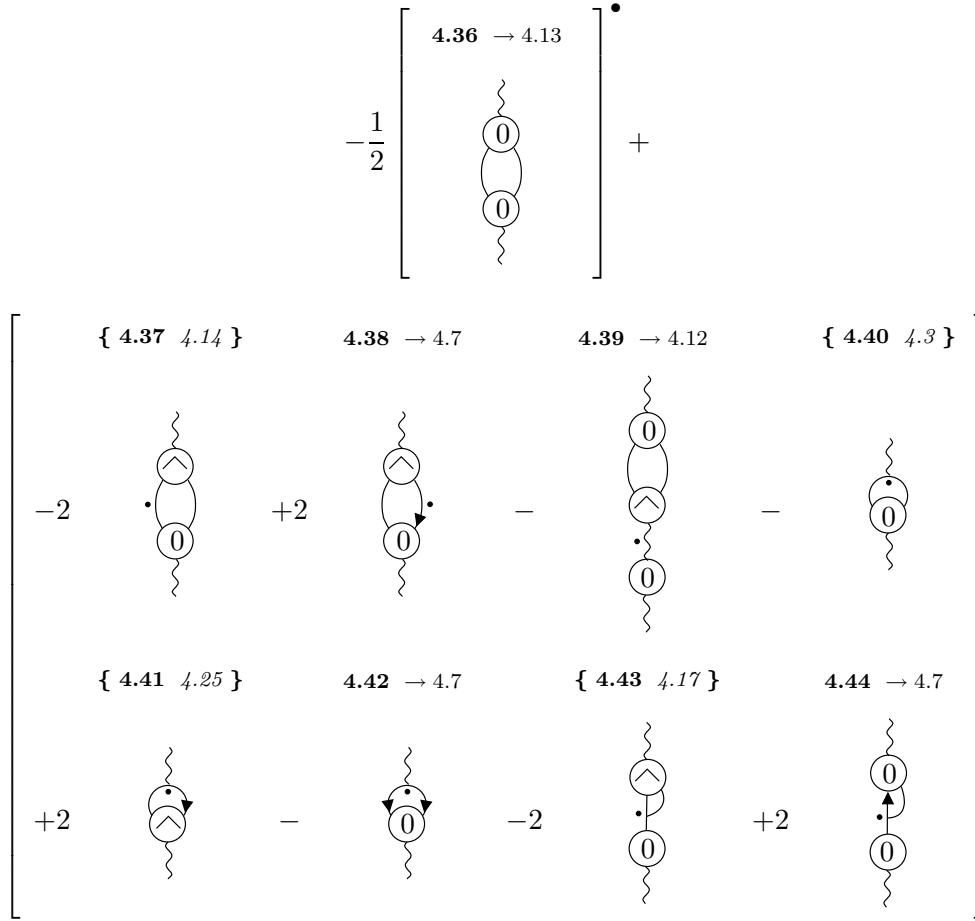


Figure 4.6: Manipulation of diagram 4.13 using the tree level flow equation.

**Cancellation 4.7** *Diagram 4.37 exactly cancels diagram 4.14.*

The next cancellation completes the removal of all terms from figure 4.1 formed by the action of  $a_0[\Sigma_0]$ .

**Cancellation 4.8** *Diagram 4.40 exactly cancels diagram 4.3.*

Of the remaining cancellations, one involves two diagrams, each possessing active gauge remainders, which we notice can be cancelled without the need to perform the gauge remainders. The final cancellation occurs only at  $\mathcal{O}(p^2)$ .

**Cancellation 4.9** *Diagram 4.41 exactly cancels diagram 4.25 since when a three-point tree level vertex is struck by a gauge remainder, it makes no difference whether it is a Wilsonian effective action vertex or a seed action vertex.*

**Cancellation 4.10** *Diagram 4.43 cancels diagram 4.17 at  $\mathcal{O}(p^2)$ . In each case, we Taylor expand the three-point, tree level vertex to zeroth order in external momentum, reducing it to the momentum derivative of a two-point, tree level vertex. It is then of no consequence that one of the three-point, tree level vertices was a seed action vertex whereas the other was a Wilsonian effective action vertex, since the two-point, tree level Wilsonian effective action vertices are identified with the corresponding seed action vertices.*

At this stage, up to diagrams in which the sole three-point vertex is hit by a gauge remainder, we have removed all three-point, tree level vertices from the calculation with the following exceptions:

1. the  $\Lambda$ -derivative terms, diagrams 4.36 and 4.29;
2. the  $B'(0)$  term, diagram 4.39;
3. three diagrams 4.27, 4.34 and 4.35, which are each left with a three-point, tree level vertex, even after the action of the gauge remainders.

The last three terms, which all possess an  $S_{0\mu\nu}^{11C^{1,2}}$  vertex, have no analogue in the version of the calculation presented in [57]. To make further progress, we must process the gauge remainders. In figure 4.7, we utilise the techniques of section 3.1 to manipulate the gauge remainders, stopping after the use of the effective propagator relation. We discard all terms which vanish due to their supertrace structure being  $\text{str } A_\mu^1 \text{str } A_\nu^1$ , and neglect attachment corrections to three-point vertices which are decorated by an external field and struck by a gauge remainder.

Note that diagram 4.58 is our first example of a diagram possessing a trapped gauge remainder. There is no corresponding diagram in which the gauge remainder bites the external field because then we are left with an *active* gauge remainder striking a two-point, tree level vertex. Note also that all diagrams which either cannot be processed further or do not contain an  $S_{0\mu\nu}^{11C^{1,2}}$  vertex cancel, amongst themselves.

**Cancellation 4.11** *Diagram 4.48 exactly cancels diagram 4.50.*

$$\begin{aligned}
4.23 &= 2 \left[ \begin{array}{cc} \{ 4.45 \ 4.52 \} & \{ 4.46 \ 4.49 \} \\ 2 \text{ (diagram)} & - \text{ (diagram)} \end{array} \right] \\
4.27 + 4.35 &= 2 \left[ \begin{array}{cc} \{ 4.47 \ 4.66 \} & \begin{array}{l} \{ 4.48 \ 4.50 \} \\ \{ 4.49 \ 4.46 \} \end{array} \\ \text{(diagram)} & - \text{(diagram)} \end{array} \right] \\
4.34 &= 2 \left[ \begin{array}{cc} \{ 4.50 \ 4.48 \} & 4.51 \rightarrow 4.9 \\ \text{(diagram)} & - \text{(diagram)} \end{array} \right] \\
4.38 &= -4 \left[ \begin{array}{ccc} \{ 4.52 \ 4.45 \} & 4.53 \rightarrow 4.8 & 4.54 \rightarrow 4.10 \\ \text{(diagram)} & - \text{(diagram)} & - \text{(diagram)} \end{array} \right] \\
4.28 &= 4 \left[ \begin{array}{ccc} 4.55 \rightarrow 4.10 & \{ 4.56 \ 4.59 \} & 4.57 \rightarrow 0 \\ \text{(diagram)} & + \text{(diagram)} & - \text{(diagram)} \end{array} \right] \\
4.42 &= 2 \left[ \begin{array}{c} 4.58 \rightarrow 4.10 \\ \text{(diagram)} \end{array} \right] \quad 4.44 = -4 \left[ \begin{array}{cc} \{ 4.59 \ 4.56 \} & 4.60 \rightarrow 4.8 \\ \text{(diagram)} & - \text{(diagram)} \end{array} \right]
\end{aligned}$$

Figure 4.7: Terms arising from processing the gauge remainders of the diagrams in figures 4.5 and 4.6.

**Cancellation 4.12** *Diagram 4.49 exactly cancels diagram 4.46.*

**Cancellation 4.13** *Diagram 4.52 exactly cancels diagram 4.45.*

**Cancellation 4.14** *Diagram 4.56 exactly cancels diagram 4.59.*

Whilst these cancellations are very encouraging, it is not clear that we are any closer to solving the mystery of the diagrams containing  $S_{0\mu\nu}^{11C^{1,2}}$  vertices. We will, however, persevere and process the nested gauge remainders arising from the previous procedure. The result of this is shown in figure 4.8.

$$\begin{aligned}
 4.53 = 4 & \left[ \begin{array}{cc} \{ 4.61 \ 4.64 \} & 4.62 \rightarrow 4.9 \\ \text{Diagram 1} & - \text{Diagram 2} \end{array} \right] \\
 4.60 = 4 & \left[ \begin{array}{cc} 4.63 \rightarrow 4.12 & \{ 4.64 \ 4.61 \} \\ \text{Diagram 3} & - \text{Diagram 4} \end{array} \right]
 \end{aligned}$$

Figure 4.8: Diagrams arising from processing the nested gauge remainders of figure 4.7.

Once again, we find a cancellation between a pair of the terms generated by this procedure.

**Cancellation 4.15** *Diagram 4.64 exactly cancels diagram 4.61.*

This exhausts the active gauge remainders and so is a good point to pause and collate the surviving terms. These fall into five sets:

1. The  $\Lambda$ -derivative terms, diagrams 4.8, 4.29 and 4.36;
2. The  $B'(0)$  terms, diagrams 4.18, 4.39 and 4.63. Notice that the last of these has been formed via the action of a nested gauge remainder;

3. Terms possessing an  $\mathcal{O}(p^2)$  stub formed by the action of a gauge remainder, diagrams 4.58, 4.55 and 4.54. Notice that the former of these has a trapped gauge remainder;
4. Terms possessing a  $S_{0\mu\nu}^{11C^{1,2}}$  vertex, diagrams 4.51 and 4.47;
5. Diagram 4.62.

We will leave the first three sets of diagrams, for the time being, and focus on the final two. Remarkably, diagram 4.51 from the fourth set and diagram 4.62 share a common feature! Both can be re-drawn via diagrammatic identity 8. Having thus re-drawn these diagrams, we then find that they can be converted into  $\Lambda$ -derivative terms. This whole procedure is shown in figure 4.9, where we have discarded any terms which vanish at  $\mathcal{O}(p^2)$ .

$$\begin{aligned}
4.51 &= 2 \text{ [Diagram: circle with 0, wavy lines, and a stub with a dot]} \\
&= 2 \left[ \text{ [Diagram: circle with 0, wavy lines, and a stub with a dot]} \right]^\bullet - \text{ [Diagram: circle with 0, wavy lines, and a stub with a dot]} - \text{ [Diagram: circle with 0, wavy lines, and a stub with a dot]} \\
&= 2 \left[ \begin{array}{c} \text{4.65} \rightarrow \text{4.13} \\ \text{ [Diagram: circle with 0, wavy lines, and a stub with a dot]} \end{array} \right]^\bullet - 2 \text{ [Diagram: circle with } \Pi_0 \text{, wavy lines, and a stub with a dot]} + \mathcal{O}(p^4) \\
4.62 &= 4 \text{ [Diagram: circle with 0, wavy lines, and a stub with a dot]} \\
&= 2 \left[ \begin{array}{c} \text{4.67} \rightarrow \text{4.13} \\ \text{ [Diagram: circle with 0, wavy lines, and a stub with a dot]} \end{array} \right]^\bullet
\end{aligned}$$

Figure 4.9: Re-drawing of diagrams 4.51 and 4.62 using diagrammatic identity 8 and their subsequent conversion into  $\Lambda$ -derivative terms.

Note how diagram 4.67 has a factor of  $1/2$ , relative to the parent diagram. This recognises the indistinguishability of the two processed gauge remainders possessed by this diagram.

Finally, we find the cancellation of the remaining diagrams possessing a  $S_{0\mu\nu}^{11C^{1,2}}$  vertex, up to those which are cast as  $\Lambda$ -derivative terms.

**Cancellation 4.16** *Diagram 4.66 exactly cancels diagram 4.47.*

Our next task is to analyse the surviving diagrams possessing an  $\mathcal{O}(p^2)$  stub formed by the action of a gauge remainder. This is a two-step process. First, we Taylor expand each of the sub-diagrams attached to the stub to zeroth order in  $p$ .<sup>4</sup> We then re-draw them, if possible, using various diagrammatic identities. The results of the complete procedure are shown in figure 4.10.

$$\begin{array}{l}
 \{ 4.68 \ 4.75 \} \\
 4.55 \rightarrow 4 \quad \begin{array}{c} \text{diagram} \\ \text{with a stub labeled } 0 \end{array} \\
 \\
 4.54 \rightarrow 4 \quad \begin{array}{c} \text{diagram} \\ \text{with a stub labeled } 0 \end{array} = -4 \left[ \begin{array}{c} 4.69 \rightarrow 4.11 \\ \text{diagram} \\ \text{with a stub labeled } 0 \end{array} + \begin{array}{c} 4.70 \rightarrow 4.11 \\ \text{diagram} \\ \text{with a stub labeled } 0 \end{array} + \begin{array}{c} \{ 4.71 \ 4.73 \} \\ \text{diagram} \\ \text{with a stub labeled } 0 \end{array} \right] \\
 \\
 4.58 \rightarrow -2 \quad \begin{array}{c} \text{diagram} \\ \text{with a stub labeled } 0 \end{array} = 2 \left[ \begin{array}{c} 4.72 \rightarrow 4.11 \\ \text{diagram} \\ \text{with a stub labeled } 0 \end{array} + 2 \begin{array}{c} \{ 4.73 \ 4.71 \} \\ \text{diagram} \\ \text{with a stub labeled } 0 \end{array} \right]
 \end{array}$$

Figure 4.10: Manipulations at  $\mathcal{O}(p^2)$ , followed by a re-expression of the resulting diagrams.

Some comments are in order. Having Taylor expanded diagram 4.54, we obtain the final set of diagrams by means of diagrammatic identity 4. In the case of diagram 4.58 the procedure after Taylor expansion is different: we re-express it as a total momentum derivative—which we discard—plus supplementary terms. These supplementary terms come with a relative minus sign

<sup>4</sup>As will become clear in chapter 5, this step can potentially generate IR divergence, in which case it is not legal. At the one-loop level, though, this never happens.

and correspond to the momentum derivative hitting all structures other than the wine. We then note that the two contributions in which the momentum derivative strikes a  $\triangleright$  can be combined, via diagrammatic identity 9. This gives a cancellation.

**Cancellation 4.17** *Diagram 4.73 exactly cancels diagram 4.71.*

The four surviving diagrams possessing an  $\mathcal{O}(p^2)$  stub formed by the action of a gauge remainder can now be combined into  $\Lambda$ -derivatives. Diagram 4.69 can be re-drawn via diagrammatic identity 8 and then, together with diagram 4.68 converted into a  $\Lambda$ -derivative term. Diagram 4.72 precisely halves the overall factor of diagram 4.70. The resultant diagram is then re-drawn via diagrammatic identity 9 which, upon inspection, is actually a  $\Lambda$ -derivative term (where we exploit the fact that  $\Lambda\partial_\Lambda$  kills  $\triangleright$ ). This is all shown in figure 4.11. Note that we have taken the  $\Lambda$ -derivative to strike entire diagrams rather than just the sub-diagram attached to the stub. This step is valid at  $\mathcal{O}(p^2)$ .

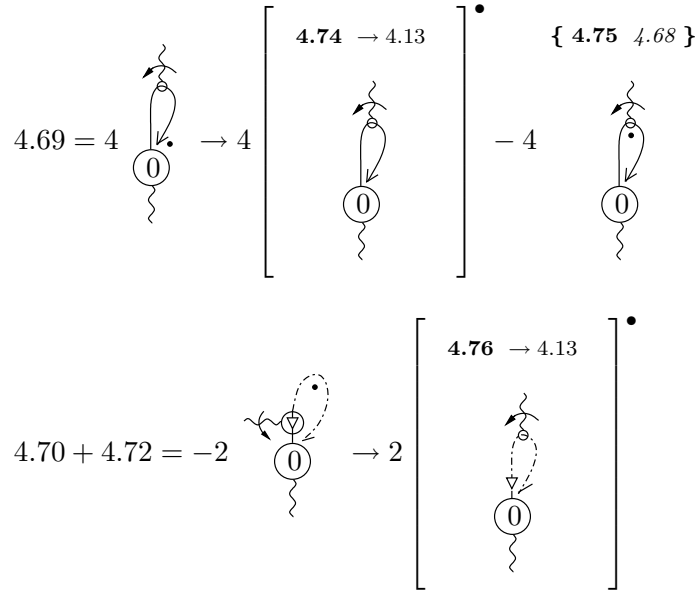


Figure 4.11: The final conversion into  $\Lambda$ -derivative terms.

In diagram 4.76 we have moved the momentum derivative from the  $\triangleright$  onto the pseudo effective propagator, discarding a total momentum derivative, in the process.

**Cancellation 4.18** *Diagram 4.75 exactly cancels diagram 4.68.*

We now find that all terms, other than the  $\Lambda$ -derivatives, have cancelled, with the sole exception of the  $B'(0)$  terms—which have been collected together in figure 4.12.

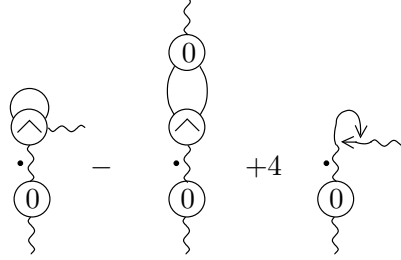


Figure 4.12: The set of  $B'(0)$  terms (which do not manifestly vanish at  $\mathcal{O}(p^2)$ ).

In anticipation of the cancellation of the  $B'(0)$  terms, the  $\Lambda$ -derivative terms have been collected together in figure 4.13 to give, for the first time, an entirely diagrammatic expression for  $\beta_1$ , in terms of  $\Lambda$ -derivatives.

$$4\beta_1 \square_{\mu\nu}(p) = -\frac{1}{2} \left[ \begin{array}{cccc} \text{4.77} & \text{4.78} & \text{4.79} & \text{4.80} \\ \text{Diagram 1} & - \text{Diagram 2} & +4 \text{ Diagram 3} & - \text{Diagram 4} \\ \text{4.81} & \text{4.82} & \text{4.83} & \\ +4 \text{ Diagram 5} & +8 \text{ Diagram 6} & +4 \text{ Diagram 7} & \end{array} \right] \bullet$$

Figure 4.13: Diagrammatic, gauge invariant expression for  $\beta_1$ , phrased entirely in terms of  $\Lambda$ -derivatives.

The diagrams in this expression will arise so many times in future that we will name them. The complete set of diagrams inside the square brackets will be referred to as  $\mathcal{D}_1$ . The first three of these are henceforth referred to as the standard set. The last two will be known as the little set.

### 4.1.3 The $B'(0)$ Terms

The first thing to notice about the  $B'(0)$  terms is that they are very similar to the first three diagrams of figure 4.13. Indeed, the  $B'(0)$  terms are very nearly just the standard set joined to an  $\mathcal{O}(p^2)$  stub, via an un-decorated wine. The only difference is that the standard set contains exclusively Wilsonian effective action vertices, whereas the  $B'(0)$  terms do not. However, we know that the  $B'(0)$  terms can be manipulated, at  $\mathcal{O}(p^2)$ . Doing this, we can replace the four-point (three-point) seed action vertex with a double (single) momentum derivative of a two-point, tree level vertex. Now, rather than making this replacement, we use the equality of the two-point, tree level Wilsonian effective action and seed action vertices to realise that, at  $\mathcal{O}(p^2)$ , we can trade the seed action vertices of the un-processed  $B'(0)$  terms for Wilsonian effective action vertices. Now the  $B'(0)$  terms take the form of the standard set attached to an  $\mathcal{O}(p^2)$  stub, via an un-decorated wine.

At this stage, we might wonder why the set of  $B'(0)$  terms does not contain diagrams like the fourth and fifth of figure 4.13. The answer is that we have discarded these terms already, on the basis that they vanish at  $\mathcal{O}(p^2)$ .<sup>5</sup>

There are several strategies to demonstrate that the  $B'(0)$  terms vanish. In reference [57], it was demonstrated algebraically that the  $B'(0)$  terms cancel, at  $\mathcal{O}(p^2)$ : Taylor expanding the standard set sub-diagrams to zeroth order in  $p$ , we can algebraically substitute for all constituent structures. There is, however, a much more elegant way to proceed which minimises the algebra and is more intuitive.

Let us assume for the moment that our calculation of  $\beta_1$  is consistent (of course, part of the purpose of having performed this calculation is to demonstrate this). Then we know that the set of diagrams contributing to  $\beta_1 \square_{\mu\nu}(p)$  must be transverse in  $p$ . The  $B'(0)$  terms are automatically transverse and so

---

<sup>5</sup> $B'(0)$  terms corresponding to the little set do not occur at all.

the only diagrams not manifestly transverse are those constituting the standard set. For the calculation to be consistent, then, the standard set must be transverse in  $p$  and hence at least  $\mathcal{O}(p^2)$ . This immediately tells us that the  $B'(0)$  terms are at least  $\mathcal{O}(p^4)$  and so can be discarded.

Hence, our task is to demonstrate the transversality of the standard set. Figure 4.14 shows the result of contracting one of the free indices of the standard set with its external momentum where, as usual, we have used the techniques of section 3.1.

$$= 4 \left[ - \text{diagram}_1 + \text{diagram}_2 + \text{diagram}_3 + \text{diagram}_4 \right]$$

Figure 4.14: The result of contracting the standard set with its external momentum. The first three diagrams on the r.h.s. cancel and the fourth vanishes by Lorentz invariance.

Now we analyse the diagrams on the right hand side. Algebraically, the first three terms go like:

$$\begin{aligned}
 A\text{-sector} &= 4N \int_l \frac{l_\alpha}{l^2} \left( -1 + \frac{l \cdot (l+p)}{(l+p)^2} + \frac{p \cdot (l+p)}{(l+p)^2} \right) \\
 F\text{-sector} &= 4(-N) \int_l \frac{f_l l_\alpha}{\Lambda^2} \left( -1 + \frac{l \cdot (l+p) f_{l+p}}{\Lambda^2} + 2g_{l+p} + \frac{p \cdot (l+p) f_{l+p}}{\Lambda^2} \right),
 \end{aligned}$$

where the  $UV$  finite sum vanishes after using the relationship (A.25) and shifting momenta. As we will see in section 9.1, this is a special case of diagrammatic identity 11. The final term of figure 4.14 vanishes by Lorentz invariance: the  $l$ -integral contains a single index and the only momentum available to carry this index, after integration over  $l$ , is  $p$ . However, this index is contracted into a vertex transverse in  $p$  and so the diagram vanishes.

Therefore, contracting the standard set with its external momenta yields zero. Since the standard set carries two Lorentz indices we have proven that it must be transverse in external momenta, as predicted. This, then, guarantees that the  $B'(0)$  terms vanish, at  $\mathcal{O}(p^2)$ , and also confirms the consistency of the calculation. At the two-loop level, we will find that the analogue of the  $B'(0)$  terms vanish for much the same reason.

## 4.2 Conclusions

The diagrammatic expression for  $\beta_1$  is one of the major results of this thesis and there are a number of comments worth making.

The first thing to do is to compare it to the expression for  $\beta_1$  obtained in [57]. Of those diagrams present in figure 4.13, only the single supertrace components of the first two, not possessing *AAC* vertices, are present in [57]. Diagrams 4.79, 4.82 and 4.83 are present in algebraic form and diagrams 4.80 and 4.81 are completely absent.

This is precisely what we expect: the treatment in [57] of gauge remainders was algebraic and single supertrace terms only were included; a consequence of this latter point being that *AAC* vertices—which diagrams 4.80 and 4.81 (and also components of 4.78) possess—can be set to zero.

Given the differences between the new approach and the old approach, an obvious question to ask is whether or not we obtain the expected universal coefficient in  $D = 4$ . The answer turns out to be trivially in the affirmative, as we will discuss in chapter 5. This is very encouraging, giving us faith that the changes we have made to the flow equation (see chapter 2) are consistent.<sup>6</sup>

One of the primary benefits of re-computing  $\beta_1$  has been the diagrammatic techniques which have been developed, as a by-product. The new techniques fall into two classes. First, there are those which enable us to process gauge remainders and to manipulate diagrams at  $\mathcal{O}(p^2)$ . Although not used originally, these methods can be applied to the old calculation of  $\beta_1$ , in exactly the same way as we have just applied them in the new calculation. Were we to return to

---

<sup>6</sup>Of course, given that we can obtain the universal one-loop coefficient using the old flow equation, the true test of the new flow equation is the computation of  $\beta_2$ .

the computation of  $\beta_1$  using the old flow equation, it would indeed be desirable to use the new techniques: the new approach is both considerably more efficient and more elegant than the old one.

Let us suppose that we were to re-do the old calculation in this way. The truly remarkable thing is that, up to diagrams possessing  $AAC$  vertices, the old calculation could be *exactly* mapped onto the new one: all we need do is replace the old style diagrams with the ‘supertrace blind’ diagrams. This use of supertrace blind diagrammatics represents the second class of new techniques. By allowing many diagrams to be processed in parallel, it hugely increases the efficiency of computations.

It is thus unarguably the case that much has been gained in the exercise of re-computing  $\beta_1$ . Indeed, such a step must be taken if we wish to compute  $\beta_2$ : though universal only in  $D = 4$ , the diagrammatic expression for  $\beta_1$  is valid in  $D = 4 - 2\epsilon$  dimensions and, as such, is necessary for the computation of  $\beta_2$ .

Whilst the exercise of re-computing  $\beta_1$  is necessary both to prepare for further calculations and to test the formalism, we should ask whether it has any merits on its own. Though we have made much of the efficiency and elegance of the approach, it perhaps does not compare all that well to traditional methods of computing  $\beta_1$ . Though, as we will see, the universal coefficient is extremely easy to extract from the final diagrammatic expression, we had to spend quite some time obtaining this expression. Nonetheless, once one knows the rules, the steps that take us from the initial diagrammatic expression of figure 4.1 to the final one are algorithmic. This suggests that our methodology is ideally suited for automation on a computer. We can, however, do very much better than this.

Re-examining the calculation, it becomes clear that, at each stage, we repeat the same steps numerous times. For example, the conversion of diagrams 4.19 and 4.13 into  $\Lambda$ -derivative terms mirror each other exactly (see figures 4.5 and 4.6). Both diagrams possess two three-point, tree level Wilsonian effective action vertices; upon their manipulation, the partner diagrams possessing seed action vertices are exactly cancelled. Indeed, thinking about this more carefully, if we take two three-point, tree level vertices, two effective propagators and two external fields, the only  $\Lambda$ -derivative terms we can con-

struct are precisely diagrams 4.29 and 4.36. This is starting to suggest that perhaps the generation of these  $\Lambda$ -derivative terms can be done in parallel.

These ideas will be developed in part III. Essentially, what we will find is that all the manipulations and cancellations seen in this chapter are merely special cases of more general mechanisms. Understanding these mechanisms completely will allow us to dispense with all the intermediate stages we have laboured through in going from our initial diagrammatic expression to the final one! The ramifications of this can hardly be over emphasised. If we could jump straight from equation (4.2) to the diagrammatic expression of figure 4.13, then suddenly our methodology becomes competitive with traditional ways of computing  $\beta_1$ .

# Chapter 5

## $\Lambda$ -Derivative Terms

In this chapter we detail the methodology used for treating  $\Lambda$ -derivative terms. Following a statement of the basic idea in section 5.1, the methodology is developed in section 5.2 by looking at the 1-loop integrals which contribute to  $\beta_1$ .

In section 5.3, we build on the 1-loop case to obtain the expected general form for 2-loop integrals. As preparation for the evaluation of  $\beta_2$ , we introduce an intermediate step which will allow us to explicitly demonstrate how non-universal contributions can cancel between diagrams. The methodology for this, which also has applications to terms which require manipulation at  $\mathcal{O}(p^2)$ , is presented in section 5.4.

We conclude the chapter by showing that certain running couplings which can spoil the universality of  $\beta_2$  can always be removed by a suitable choice of the seed action. This is an extension of work done in [57].

### 5.1 Introduction

The simplest  $\Lambda$ -derivative terms we will encounter are those contributing to  $\beta_1$ . From figure 4.13 we know that

$$4\beta_1 \square_{\mu\nu}(p) = -\frac{1}{2} [\mathcal{D}_1]^\bullet .$$

We now want to make the integral over loop momentum (which we will take to be  $k$ ) to be explicit and so, mindful that we will need to be more precise

about the r.h.s., write

$$4\beta_1 \square_{\mu\nu}(p) = -\frac{1}{2} \int_k [\mathcal{D}_1(k)]^\bullet. \quad (5.1)$$

The next step that we wish to perform is to interchange the order of the  $\Lambda$ -derivative and the momentum integral. This step is trivial only if the integral is convergent, even after this change. We temporarily ignore this subtlety and so now have

$$4\beta_1 \square_{\mu\nu}(p) = -\frac{1}{2} \left[ \int_k \mathcal{D}_1(k) \right]^\bullet.$$

Since the l.h.s. of this equation comprises a number times  $\mathcal{O}(p^2)$ , it follows that the coefficient multiplying the  $\mathcal{O}(p^2)$  part of the r.h.s. must be dimensionless. Consequently, we can schematically write

$$\beta_1 = \Lambda \partial_\Lambda |_\alpha (\text{Dimensionless Quantity}).$$

For the r.h.s. to survive differentiation with respect to  $\Lambda|_\alpha$ , it must either depend on some dimensionless running coupling—other than  $g$  and  $\alpha$ —or there must be some scale, other than  $\Lambda$ , available for the construction of dimensionless quantities. We show how we can avoid introducing such couplings in section 5.5.

One scale which is available is  $p$  and so we can envisage contributions to  $\beta_1$  of the form (in  $D = 4$ )

$$\Lambda \partial_\Lambda |_\alpha \ln p^2 / \Lambda^2.$$

Indeed, the standard set gives rise to contributions precisely of this type (see section 5.2.2). However, as we will see in section 5.2.3, we cannot form contributions of this type from the little set—but we know from [57] that the little set does contribute to  $\beta_1$ .

For the little set, then, what scales are there, other than  $\Lambda$ , available for the construction of dimensionless quantities? Courtesy of the  $SU(N|N)$  regularisation, we know that there are no scales in the UV.<sup>1</sup> Naïvely, we would not expect a scale to arise in the IR, either. However, we stated that interchanging the order of differentiation with respect to  $\Lambda \partial_\Lambda |_\alpha$  and loop integration in (5.1) is trivial only if the integral is convergent, even after this step. The

---

<sup>1</sup>Although we will find a subtle interplay between the IR and UV, which is commented on at the end of section 5.2.2.

key point is that performing this step has the capacity to introduce IR divergences. This is most easily appreciated by noting that  $\Delta_k^{11} \sim 1/k^2$ , whereas  $\dot{\Delta}_k^{11} \sim 1/\Lambda^2$ . Thus, to legally move  $\Lambda\partial_\Lambda|_\alpha$  outside of the loop integral, we must introduce some IR regulator, which then provides the scale necessary to form dimensionless quantities. After allowing  $\Lambda\partial_\Lambda|_\alpha$  to act, this unphysical scale will disappear. IR divergences introduced in this way will be called *pseudo-divergences*, since they are an artifact of the way in which we have chosen to perform the calculation.

Noting that in the case of the standard set it is effectively  $p$  which is providing the IR regularisation, our strategy for evaluating loop integrals is to look at the IR end. Scanning through the list of effective propagators (A.19)–(A.24), it is apparent that the leading contributions occur when all effective propagators are in the  $A$ -sector; likewise for any instances of  $\triangleright$ . Gauge invariance and considerations as to the supertrace structure will eventually determine that all contributions to  $\beta_1$  and  $\beta_2$  are ultimately limited to the lowest order momentum contributions from the  $A^1$  sector; it is precisely this regime—and this regime alone—that is universal.

## 5.2 1-loop Integrals

### 5.2.1 Vanishing Diagrams

We begin our analysis by looking at diagrams 4.80 and 4.81 which, up to an overall factor, are reproduced in figure 5.1. Recall that these two diagrams have no analogue in the computation of  $\beta_1$  presented in [57] and so we had better find that they vanish.

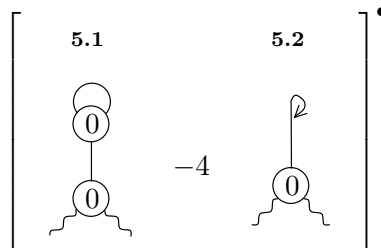


Figure 5.1: Two diagrams which give a vanishing contribution to  $\beta_1$  in  $D = 4$ .

We now focus on the IR end of the loop integral. The bottom vertex does not carry the loop momentum, nor does the effective propagator leaving it. However, we know that this effective propagator must be in the  $C$ -sector (else the bottom vertex vanishes by CC, when we sum over permutations of the fields). This immediately tells us that diagram 5.2 is IR safe, even if we interchange the order the  $\Lambda$ -derivative and the momentum integral: performing this step, the loop integral just goes as

$$\int_k gk.$$

Let us now focus on diagram 5.1. To try and find IR divergences, we take the fields involved in the loop integral to be in the  $A$ -sector. To deal with the top vertex, we recall that it is Taylor expandable in momenta [52, 53, 20]. Hence, to try and isolate the most IR divergent contribution from the loop integral, we take the minimum number of powers of momenta from the top vertex consistent with Lorentz invariance. Given that the field entering this vertex from beneath is in the  $C$ -sector, we can take  $\mathcal{O}(\text{mom}^0)$ .

Diagram 5.1 is clearly IR safe in  $D = 4$  since the loop integral looks at worst—without even taking into account the  $\Lambda$ -derivative—like

$$\int_k 1/k^2,$$

in the IR.

Thus we can safely interchange the order of integration and differentiation with respect to  $\Lambda|_\alpha$  for both diagrams 5.1 and 5.2. Having done so, we know that (the  $\mathcal{O}(p^2)$  parts of) both diagrams will vanish, when computed in  $D = 4$ . Bearing in mind that we must pre-regularise [51, 57] (see section 1.2.1) and in preparation for the 2-loop calculation, we ultimately want to be doing our computations in  $D = 4 - 2\epsilon$  dimensions. Rescaling our loop momenta  $k \rightarrow k/\Lambda$  we see that, at  $\mathcal{O}(p^2)$ , the diagrams acquire an overall factor of  $\Lambda^{-2\epsilon}$ . Working in this scheme, the  $\Lambda$ -derivative of the diagrams now  $\sim \epsilon$  which, of course, vanishes in the  $D = 4$  limit.

Note that diagram 4.77 (the first element of the standard set) also vanishes in  $D = 4$ , after differentiation with respect to  $\Lambda|_\alpha$ . However, we will always keep this term together with the other elements of the standard set. This is

done because we often exploit the fact that the set is transverse, and want to be able to do this irrespective both of  $D$  and whether or not it is struck by a  $\Lambda$ -derivative.

### 5.2.2 IR Regularisation Provided by $p$

In this section, we will encounter diagrams that survive differentiation with respect to  $\Lambda$  in  $D = 4$  and for which  $p$  plays a role in the IR regularisation. The only diagrams that fall into this class are diagrams 4.78 and 4.79. However, as just mentioned, diagram 4.77 will come along for the ride; a full understanding of the standard set is crucial for the 2-loop calculation. These three diagrams are reproduced, up to an overall factor, in figure 5.2. We henceforth take their loop momentum to be  $k$ .

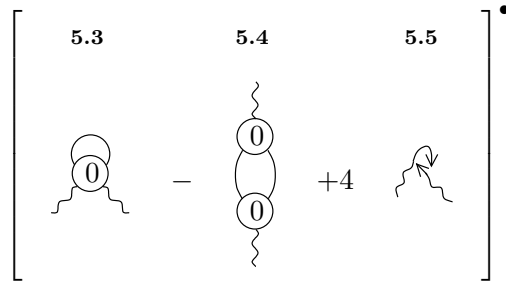


Figure 5.2: The standard set struck by  $\Lambda\partial_\Lambda|_\alpha$ .

Diagram 5.3 is IR safe. The second and third diagrams, before differentiation with respect to  $\Lambda|_\alpha$ , have the IR structure

$$\int_k \frac{\mathcal{O}(p^2, p \cdot k, k^2)}{k^2(k-p)^2}, \quad (5.2)$$

where we have taken a single power of momentum from each of the three-point vertices, have chosen all effective propagators to be in the  $A$ -sector and have evaluated any cutoff functions at zero momentum.

Note that choosing the effective propagators to be in the  $A$ -sector constrains diagram 5.4, considerably. For three-point vertices decorated exclusively by  $A$ -fields, it must be the case that all fields are on the same supertrace and hence in the same sub-sector. Consequently, for the contributions to diagram 5.4 with the severest IR behaviour, all fields must be in the  $A^1$ -sector.

Returning to equation (5.2), it is clear that the presence of  $p$  in the denominator is required to regulate the integral in the IR, at least when we choose to take  $\mathcal{O}(p^2)$  from the vertices. Performing the integral in  $D = 4$  will then give us something of the form

$$\mathcal{O}(p^2)(a \ln(p^2/\Lambda^2) + b).$$

When this is hit by the  $\Lambda$  derivative—which we can move outside the integral—only the first term will survive and so we will be left with a (universal) coefficient multiplying two powers of  $p$ .

That the final answer is Taylor expandable in  $p$  gives us an alternative way in which to evaluate  $\Lambda$ -derivative terms. Having moved the  $\Lambda$ -derivative outside the integral, we Taylor expand the denominator in  $p$ . Doing this,  $p$  will no longer act as a regulator and so we will then generate IR divergences, when we perform the integral. However, all divergences will be killed by the  $\Lambda$ -derivative. To parameterise these pseudo-divergences, we must introduce an IR regulator; it is natural to use dimensional regularisation.

It may, at this stage, seem a little perverse to have traded one IR regulator,  $p$ —which occurs naturally—for another. However, even for diagrams which are not Taylor expandable in  $p$ , it will turn out that we are often interested in the Taylor expandable part. By Taylor expanding in  $p$ , the resulting integrals tend to be easier to perform.

We now discuss how this procedure works, in more detail:

1. Take  $\mathcal{O}(\text{mom})$  from each of the vertices;
2. Taylor expand the denominator in  $p$ ;
3. replace the upper limit of the radial integral with  $\Lambda$ , thereby cutting off modes above this scale;
4. rescale  $k \rightarrow k/\Lambda$ , so that the diagram acquires an overall factor of  $\Lambda^{-2\epsilon}$ .

Having done the angular integral, we are left with an expression of the form:

$$\frac{(\Lambda^{-2\epsilon})^\bullet}{(4\pi)^{D/2}} \int_0^1 \frac{k^{D-1}}{k^4} dk \mathcal{O}(p^2).$$

Performing the integral gives us a factor of  $1/\epsilon$ , as expected. This is killed by a factor of  $\epsilon$  arising from differentiation with respect to  $\Lambda|_\alpha$ , confirming the consistency of the approach.

Before moving on, we must justify the validity of the third step. We know that the integral we are dealing with has support only in the IR. However,  $\int_k 1/k^4$  is not UV regulated and so we must incorporate the effects of the UV regularisation. Since the details of the regularisation will not affect the IR, at leading order, we choose the simplest form that cuts off momentum modes above the scale  $\Lambda$ . The non-universal corrections to this will necessarily remove any IR divergence, even before differentiation with respect to  $\Lambda|_\alpha$ , and so vanish in the limit that  $\epsilon \rightarrow 0$ . An implicit part of this step is that we now throw away all F-sector diagrams and evaluate any cutoff functions at zero momentum.

In readiness for the 2-loop calculation, we will now extend our analysis of the standard set, and will give its general form. We know the following facts about the standard set:

1. the sum of the diagrams is transverse;
2. when struck by  $\Lambda\partial_\Lambda|_\alpha$ , the coefficient of the  $\mathcal{O}(p^2)$  term is universal, up to  $\mathcal{O}(\epsilon)$  corrections (this follows from [57]);
3. in  $D = 4$ , the diagrams have the structure

$$\mathcal{O}(p^2) \ln(p^2/\Lambda^2) + \mathcal{O}(p^2) + \dots,$$

where the ellipsis denotes terms which are higher order in  $p$ .

From these three points and dimensions it follows that, in  $D = 4 - 2\epsilon$ , the standard set takes the algebraic form

$$\frac{N\Lambda^{-2\epsilon}}{(4\pi)^{D/2}} \left[ a_0 \left( 1 - \frac{p^{-2\epsilon}}{\Lambda^{-2\epsilon}} \right) \frac{1}{\epsilon} + \dots \right] \square_{\alpha\beta}(p) + \mathcal{O}(p^4, p^{4-2\epsilon}),$$

where  $a_0$  is a universal coefficient and the ellipsis denotes terms which are higher order in  $\epsilon$ .

We have no further interest in the  $\mathcal{O}(p^4, p^{4-2\epsilon})$  terms and so turn to the ellipsis. There are two ways in which we expect these terms to arise. On the

one hand, compared to equation (5.2), we can take additional powers of  $k$  in the numerator of the integrand, giving us non-universal contributions which are Taylor expandable in  $p$ . On the other hand, we generically expect the coefficient  $a_0$  to have arisen from some function of  $D$  in which we have taken  $D = 4$ . Expanding this function in  $\epsilon$  will give rise to sub-leading contributions. These contributions will be called computable. At the two-loop level, we will see how computable contributions can combine to give universal quantities.

Just as we talk of computable parts of some diagram, so too will we talk of the complimentary non-computable parts. We emphasise that by non-computable we really mean that the corresponding coefficients cannot be computed without specifying non-universal details of our set-up (i.e. cut-off functions and the precise form of the covariantisation); it is not that we cannot, in principle, calculate them.

Hence, the standard set takes the following form

$$\frac{N\Lambda^{-2\epsilon}}{(4\pi)^{D/2}} \left[ \sum_{i=0}^{\infty} \left( a_i + b_i \frac{p^{-2\epsilon}}{\Lambda^{-2\epsilon}} \right) \epsilon^{i-1} \right] \square_{\alpha\beta}(p) + \mathcal{O}(p^4, p^{4-2\epsilon}), \quad (5.3)$$

where  $b_0 = -a_0$ , the  $a_{i>0}$  are a mixture of computable and non-computable contributions and the  $b_i$  are entirely computable.

Notice that 1-loop computations are insensitive to the  $p^{-2\epsilon}/\Lambda^{-2\epsilon}$  terms: taking into account the additional factor of  $\Lambda^{-2\epsilon}$  sitting outside, such terms are independent of  $\Lambda$  and so will be killed by the  $\Lambda$ -derivative. At two-loops, where the standard set can occur as a sub-diagram, we expect such contributions to survive.

We now discuss how to calculate the coefficients  $b_i$ . It is convenient to begin by contracting the standard set with  $\delta_{\alpha\beta}$ . The  $b_i$  arise from integrals of the form

$$\int_k \frac{\mathcal{O}(p^2, p, k, k^2)}{k^2(k-p)^2}.$$

Note that the  $\mathcal{O}(k^2)$  term does not contribute to the  $b_i$ : the denominator becomes just  $1/(k-p)^2$  and so, by shifting momentum, we can remove  $p$  from the denominator entirely. It is now not possible to generate a power of  $p^{-2\epsilon}$ .

The next step is to combine denominators, using Feynman parameterisation [101]:

$$\int_0^1 da h(a) \int_k \frac{\mathcal{O}(p^2)}{(k^2 + K^2)^2},$$

where  $K^2 = a(1-a)p^2$  and  $h(a)$  is some function of  $a$ . At this stage, it is now tempting to proceed as before and restrict the range of the radial integral. However, this leaves us with an unpleasant calculation as we cannot use standard dimensional regularisation formulae. Besides, there is a much simpler way to proceed: we differentiate twice, with respect to  $p^2$ .

The effect on the integral is to ensure that it is UV regulated by the denominator of the integrand—without the need for any cutoff regularisation. We call this automatic UV regularisation (which will play an important role at two loops). Since we are interested in the part of the integral which has support in the IR, there is no need for us to restrict the range of integration, as doing so would only serve to make the calculation harder. Retaining just A-sector diagrams, we evaluate all cutoff functions at zero momentum, leaving us with an integral we can do using standard dimensional regularisation techniques (*ibid.*).

We perform the integral and compare it to the second derivative with respect to  $p^2$  of equation (5.3), contracted with  $\delta_{\alpha\beta}$ . This is one place where the value of keeping the standard set together manifests itself: because we know the standard set to be transverse, we know the effect of contracting with  $\delta_{\alpha\beta}$ . Equating powers of  $\epsilon$  allows us to determine the  $b_i$ . The first two coefficients are:

$$b_0 = -20/3 \tag{5.4}$$

$$b_1 = -124/9 + 20\gamma_{\text{EM}}/3 \tag{5.5}$$

where  $\gamma_{\text{EM}}$  is the Euler-Mascheroni constant.

At this point it is worth pausing to consider why the coefficients  $a_0$  and  $b_i$  have no dependence on  $N$ . We note in equation (5.3) that we have extracted an overall factor of  $N$ , but we might suspect that the  $a_i$  and  $b_i$  incorporate attachment corrections.<sup>2</sup> Let us look first at diagram 5.5. Since this is formed by the action of gauge remainders on three-point (tree level) vertices decorated

---

<sup>2</sup>The overall factor of  $N$  is what we expect for the diagrams if there are no attachment corrections. In this case, each diagram comprises one loop decorated by the two external fields and one empty loop. The empty loop yields  $\text{str } \sigma_+ = N$  if the internal fields are bosonic and  $\text{str } \sigma_- = -N$  if the internal fields are fermionic.

by an external field, we know from the end of section 3.1.6 that we can discard all  $1/N$  corrections.

Now consider diagram 5.4. The contributions to  $a_0$  and  $b_i$  come when all fields are in the  $A$ -sector. If either of the effective propagators attaches via a  $1/N$  correction, then the external fields are always guaranteed to be on the same supertrace, irrespective of location: the diagram vanishes by CC. However, we expect the  $a_{i \geq 1}$ , to be non-trivial functions of  $1/N$ , since these coefficients receive contributions in which the vertices of diagram 5.4 are each CC even (i.e.  $AAC$  vertices) and from diagram 5.3.

We conclude our analysis of the standard set by noting a beautiful interplay between the IR and the UV, illustrated by diagram 5.5. The strategy we have used is to pull the  $\Lambda$ -derivative outside of the momentum integral and then focus on the IR end. Focusing on the IR end allows us to throw away the regulating diagram. However, the regulating diagram was required to define the  $A$ -sector diagram when we interchanged the order of differentiation with respect to  $\Lambda$  and loop integration.

Now, suppose that we had left the  $\Lambda$ -derivative inside the integral. Then the  $A$ -sector diagram actually dies, since  $A$ -sector (processed) gauge remainders are independent of  $\Lambda$ . We are left with the  $B$ -sector diagram, which provides the same leading order contribution as the  $A$ -sector diagram, but arising from the UV!

Interplay such as this will only arise when the components of some diagram which gives a contribution in the IR are not regulated by cutoff functions, alone.

### 5.2.3 Loop Integrals Independent of $p$

We conclude our survey of 1-loop integrals by looking at the final two diagrams which contribute to  $\beta_1$ , as reproduced in figure 5.3, up to an overall factor.

The difference between these diagrams and the ones just analysed is that  $p$  is not involved in the IR regularisation. The integrals just go like

$$\int_k \frac{1}{k^4}$$

in the IR and we can use the techniques of the previous section to evaluate such terms. We thus expect the complete set of diagrams contributing to  $\beta_1$

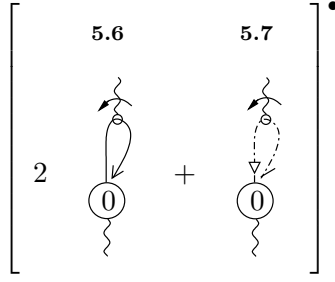


Figure 5.3: The little set struck by  $\Lambda\partial_\Lambda|_\alpha$ .

to take the following form, before differentiation with respect to  $\Lambda|_\alpha$ :

$$\frac{N\Lambda^{-2\epsilon}}{(4\pi)^{D/2}} \left[ \sum_{i=0}^{\infty} \left( A_i + B_i \frac{p^{-2\epsilon}}{\Lambda^{-2\epsilon}} \right) \epsilon^{i-1} \right] \square_{\mu\nu}(p) + \mathcal{O}(p^4, p^{4-2\epsilon}), \quad (5.6)$$

where the  $B_i$  are computable and the  $A_i$  generally contain both computable and non-computable parts. The universal coefficient  $A_0$  yields the sole contribution to  $\beta_1$ , in the  $\epsilon \rightarrow 0$  limit.

### 5.3 2-loop Integrals

In this section, we develop the machinery of the previous section to deal with two-loop  $\Lambda$ -derivative terms. The integrals we have to deal with fall into two classes: factorisable and non-factorisable. In the former case—dealt with in section 5.3.1—the loop-integrals are independent, whereas, in the latter case—dealt with in section 5.3.2—they are not.

Following on from the one-loop case we expect and, indeed, find—see chapters 12 and 13—that we can write<sup>3</sup>

$$4\beta_2 \square_{\mu\nu}(p) = -\frac{1}{2} [\mathcal{D}_2]^\bullet.$$

One of the main sources of complication in the two-loop case is that, even after differentiation with respect to  $\Lambda\partial_\Lambda|_\alpha$ , individual elements of  $\mathcal{D}_2$  can still possess IR divergences. It is only the sum of diagrams contributing to  $\mathcal{D}_2$  that we expect to give a finite (universal) contribution after differentiation with respect to  $\Lambda\partial_\Lambda|_\alpha$ .

Since we are interested in two-loop integrals which contribute to  $\beta_2$  we will, up to factors of  $p^{-2\epsilon}$ , work at  $\mathcal{O}(p^2)$ .

<sup>3</sup>In the limit that  $\alpha \rightarrow 0$ .

### 5.3.1 The Factorisable Case

To understand the algebraic form of two-loop diagrams, we need first to understand their structure. Since we are dealing with factorisable terms, we expect them to comprise two one-loop sub-diagrams, each of which carries external momentum  $p$ . These sub-diagrams must be connected to each other, and so we predict that they will be joined together by an effective propagator (for explicit examples, see chapter 12). This effective propagator just contributes powers of the external momentum and so we take the general form of a factorisable two-loop integral to be:

$$\frac{N^2 \Lambda^{-4\epsilon}}{(4\pi)^D} \sum_{i=0}^{\infty} \left( c_i + d_i \frac{p^{-2\epsilon}}{\Lambda^{-2\epsilon}} + e_i \frac{p^{-4\epsilon}}{\Lambda^{-4\epsilon}} \right) \frac{1}{\epsilon^{i-2}} \mathcal{O}(p^2), \quad (5.7)$$

where we obtain a power of  $p^{-2\epsilon}/\Lambda^{-2\epsilon}$  for each loop in which  $p$  provides IR regularisation.

### 5.3.2 The Non-Factorisable Case

To understand the non-factorisable case will require a little more work. We begin by trying to construct the most divergent possible type of diagram. To do this, we can adapt our study of factorisable diagrams. We know that factorisable diagrams constitute two one-loop sub-diagrams joined by an effective propagator. For a diagram constructed entirely of vertices and effective propagators this means that our most divergent (factorisable) two-loop diagram will comprise four three-point, tree level vertices and five effective propagators. (We can, of course, construct diagrams using processed gauge remainders, in addition to the other ingredients, but this will not tell us anything extra about the IR structure.)

We expect the most divergent non-factorisable diagrams to possess exactly the same ingredients, but joined together in a different way. Taking the loop momenta to be  $l$  and  $k$ , we know that one of the effective propagators must  $\sim 1/(l-k)^2$  (assuming it to be in the  $A$ -sector). Conservation of four-momentum at a vertex then implies that there must be at least one effective propagator carrying  $l$  and at least one carrying  $k$ . Knowing that, at  $\mathcal{O}(p^2)$  the integrand must be of mass dimension  $-8$ , we expect the most divergent type of diagram

we can construct (assuming no IR regularisation is provided by  $p$ ) to take the following form in the IR:

$$\mathcal{O}(p^2) \int_{l,k} \frac{\mathcal{O}(\text{mom}^2)}{k^2(l-k)^2 l^6}.$$

In fact, we will see in section 13.3.1 that, for the set of diagrams contributing to  $\beta_2$ , gauge invariance prevents the appearance of  $1/l^6$  and so we would find that, taking the above form, we would be forced to have  $l^2$  in the numerator. Hence, the most divergent type of integral we find has the following structure in the IR:

$$\mathcal{O}(p^2) \int_{l,k} \frac{1}{k^2(l-k)^2 l^4}. \quad (5.8)$$

To evaluate the contribution coming from the IR, we observe that the  $l$ -integral is automatically UV regulated. Thus, using dimensional regularisation, we perform the  $l$ -integral first, with unrestricted range of integration, and perform the  $k$ -integral second, with the range of radial integration restricted to  $\Lambda$ . We obtain one power of  $1/\epsilon$  from the Feynman parameter integral and a further power from the radial  $k$ -integral.

Doing the integrals the other way around would be awkward, as we cannot then use an un-restricted range of integration for the inner integral.

Had there been  $ps$  present in the denominators, providing regularisation, we would expect accompanying factors of  $p^{-2\epsilon}/\Lambda^{-2\epsilon}$ . Consequently, equation (5.7) is the form for a generic 2-loop integral.

### 5.3.3 Considerations for $\beta_2$

For the actual computation of  $\beta_2$ , we can constrain some of the coefficients in equation (5.7). Since the terms corresponding to the coefficients  $e_i$  are independent of  $\Lambda$ , we can drop them as they will vanish after differentiation. Given that we are comparing our final answer with the Taylor expandable, finite expression  $\beta_2 \square_{\mu\nu}(p)$ , it must be that the coefficients  $c_0$  and  $d_i$  vanish.

The coefficients  $c_0$  and  $d_0$  are entirely computable. The coefficient  $d_1$ , on the other hand, comprises both a purely computable part and a non-computable part multiplied by a computable coefficient. The computable part and the computable coefficient must both be zero.

Ultimately, we will be left with the coefficient  $c_1$  being the only contribution to the final answer. One of the primary tasks ahead is to show that the non-universal contributions to  $c_1$  cancel between diagrams.

This problem really has two sides. First, we must show that non-computable contributions from vertices etc. cancel out. Then we must show that the computable contributions to  $c_1$  combine to give the standard, universal answer.

## 5.4 Subtraction Techniques

### 5.4.1 Basics

Rather than attempting to process 2-loop diagrams directly, we perform an intermediate step whereby we add and subtract a set of terms designed to remove all non-computable contributions from the calculation. We illustrate this technique with a simple example. Consider the two-loop integral arising from the computation of the scalar two-loop  $\beta$ -function, within the ERG [25].

$$\int_{l,k} \left[ \Delta_l^2 \Delta_{l-k} \Delta_k - \frac{1}{2} \Delta_l^2 \Delta_k^2 \right]^\bullet,$$

where  $\Delta_l = c(l)/l^2$ . We can trivially rewrite this as

$$\int_{l,k} \left[ \Delta_l^2 \Delta_{l-k} \Delta_k - \Delta_l^2 \Delta_k^2 + \Delta_l^2 \Delta_k^2 - \frac{1}{2} \Delta_l^2 \Delta_k^2 \right]^\bullet,$$

where we call the second term a subtraction and the third term its corresponding addition. The addition trivially combines with the final term, though this is of no particular significance.

Now focus on the  $k$  integral, in the first term. Following [25, 9], we know that we can set  $c(l-k) = c(k)$ , as contributions higher order in  $l$  are killed in the  $\epsilon \rightarrow 0$  limit. Next, use the by now familiar prescription for the cutoff functions: if the integral is regulated without the cutoff functions, then we simply evaluate them at zero momentum, leaving the domain of integration unrestricted. If the integral requires the cutoff functions for regularisation, then restrict the domain of integration and evaluate the cutoff function at zero momentum. The sub-leading corrections to this will manifest themselves as additional powers of momenta, in the numerator.

If we were to start taking such sub-leading (non-computable) contributions under the  $k$ -integral, then this will allow us to Taylor expand the  $k$ -integral

in  $l$ . For the  $l$ -integral to still diverge in the IR—and thus survive differentiation with respect to  $\Lambda|_\alpha$  (in the limit that  $\epsilon \rightarrow 0$ )—we must take  $l^0$ . However, such non-computable contributions will be cancelled by exactly the same contributions coming from the second term, above. Hence we have, up to  $\mathcal{O}(\epsilon)$  corrections:

$$\int_{l,k} \left[ \Delta_l^2 (\Delta_{l-k} \Delta_k)_C - \Delta_l^2 (\Delta_k^2)_C + \frac{1}{2} \Delta_l^2 \Delta_k^2 \right]^\bullet,$$

where  $C$  tells us that, when considered as a pair, the first two  $k$ -integrals yield a computable contribution.

For the first term not to die in the  $\epsilon \rightarrow 0$  limit, we must set  $c(l) \rightarrow 1$  and so can extend the ‘ $C$ ’ to cover the whole term. We have:

$$\int_{l,k} \left( \left[ \Delta_l^2 \Delta_{l-k} \Delta_k \right]_C^\bullet - \left[ \Delta_l^2 \right]^\bullet \left[ \Delta_k^2 \right]_C - \Delta_l^2 \left[ \Delta_k^2 \right]_C^\bullet + \Delta_l^2 \left[ \Delta_k^2 \right]^\bullet \right), \quad (5.9)$$

where, in the final term, we have used the freedom to interchange  $l$  and  $k$ . Terms like the second and third, comprising a computable, factorisable sub-diagram, are to be called semi-computable. The third and fourth terms combine to give the non-computable (NC) contribution  $\Delta_l^2 [\Delta_k^2]_{\text{NC}}^\bullet$  which, up to  $\mathcal{O}(\epsilon)$  corrections, allows us to write

$$\int_{l,k} \left( \left[ \Delta_l^2 \Delta_{l-k} \Delta_k \right]_C^\bullet - \left[ \Delta_l^2 \right]^\bullet \left[ \Delta_k^2 \right]_C + \left[ \Delta_l^2 \right]_C \left[ \Delta_k^2 \right]_{\text{NC}}^\bullet \right).$$

Exploiting the freedom to interchange  $l, k$ , the second and third terms combine to leave us with a purely computable contribution:

$$\int_{l,k} \left[ \Delta_l^2 \Delta_{l-k} \Delta_k - \frac{1}{2} \Delta_l^2 \Delta_k^2 \right]_C^\bullet.$$

We have demonstrated that the original integral does, indeed, give something which is computable.

To calculate this integral, we can use a mixture of the techniques already discussed. In the factorisable case, we simply restrict the ranges of the integrals. In the non-factorisable case, we note that the  $l$ -integral is automatically UV regulated. Hence, we perform this integral first with an unrestricted domain of integration but then restrict the domain for the remaining  $k$ -integral. It is straightforward to confirm that we reproduce the expected, universal answer

$$-\frac{17}{3} \frac{1}{(4\pi)^4}.$$

### 5.4.2 Generalisation to the Gauge Case

Constructing subtractions in the gauge case is exactly analogous to the simpler case just analysed. In the same way, the subtractions are constructed such as to remove non-computable contributions, by noting that denominators can be Taylor expanded in momenta if sufficient powers of momentum are present in the numerator.

As the whole formalism is based around Taylor expansion, it is not surprising that we will need to use the techniques of section 3.2 to Taylor expand vertices in momenta. We know that the lowest order terms constitute derivatives of lower order vertices, and that the sign of this derivative depends on whether we have had to push forward or pull back. We define the subtraction to be the term which removes non-computable components from the parent diagram, and not by its sign. Hence, a subtraction involving a pull back will come with a positive sign.

The real subtlety in the gauge case comes from the diagrammatic manipulations that will be performed, subsequent to the construction of the subtractions. Recall from equation (5.9) that, after the construction of the subtraction, we arrive at a non-factorisable, computable term; two semi-computable, factorisable terms and a factorisable term. That this plain factorisable term is a combination of the addition and another term is besides the point; the point is that the addition is never under the influence of  $C$ . However, the semi-computable terms, which are of exactly the same form as the addition, are under the influence of  $C$ .

In the gauge case, we will encounter examples where the additions can be manipulated, using the diagrammatic techniques of section 3. We must now answer the question of whether the semi-computable terms—which are of exactly the same form—can be manipulated in the same way. As we will see, the answer depends on a choice we are free to make and, given that, on the precise structure of the diagrams in question.

The key to this problem is understanding exactly what it is that is meant by  $C$ . Let us suppose that we have taken a non-factorisable two-loop diagram and constructed a factorisable subtraction. We will suppose that the sub-diagram

of this latter term, to which we apply C, is just diagram 5.6.

The algebraic form of this diagram is (without the restriction to C)

$$\square_{\mu\beta}(p)(\Lambda^{-2\epsilon}) \bullet \int_k \partial_\alpha^k \left[ \frac{\mathbf{B}_k}{k^2} \right] \frac{k_\beta}{k^2}. \quad (5.10)$$

To compute the part of this diagram left over, after combining with our non-factorisable term we do the following: evaluate the cutoff function at zero momentum, restrict the range of the integral, and proceed as usual.

Next, suppose that we were to move the momentum derivative from the  $\mathbf{B}_k/k^2$  term to the  $k_\beta/k^2$  term, throwing away the total derivative, in the process. This yields

$$-\square_{\mu\beta}(p)(\Lambda^{-2\epsilon}) \bullet \int_k \frac{\mathbf{B}_k}{k^2} \partial_\alpha^k \left[ \frac{k_\beta}{k^2} \right]. \quad (5.11)$$

Evaluating this integral in the usual way gives a different contribution, at sub-leading order, than the integral of equation (5.10). What is going on? The point is, that whilst going from equation (5.10) to equation (5.11) is usually a perfectly valid step, it breaks down when these terms are under the influence of C. Specifically, because the effect of C has been to replace cutoff functions with a restricted range of integration, we are no longer justified in throwing away what would previously have been total momentum derivative terms.

Nonetheless, it is technically useful to be able to move the momentum derivative around, whilst being able to forget about any total momentum derivatives. We can do this if we employ the correct prescription: reinstate a term to both the parent and subtraction (after they are under the influence of C) such that, at sub-leading order, we can move momentum derivatives around with impunity. To understand what this term must be, let us return to equation (5.10). Rather than discarding the cutoff function straight away, we will first allow the momentum derivative to act.

Doing so, averaging over angle and substituting  $x = k^2$  yields:

$$\frac{N \mathcal{Q}_D}{D} \square_{\mu\alpha}(p)(\Lambda^{-2\epsilon}) \bullet \int dx x^{1-\epsilon} \left( \frac{\mathbf{B}'_x}{x} - \frac{\mathbf{B}_x}{x^2} \right).$$

Integrating the first term by parts, and discarding the resulting surface term gives:

$$\frac{N \mathcal{Q}_D}{D} \square_{\mu\alpha}(p) \int dx \frac{\mathbf{B}_x}{x^{1+\epsilon}} (\epsilon - 1).$$

Now if we remove the cutoff function and restrict the range of integration, it is apparent that the  $B'$  term has provided a sub-leading contribution; indeed, this is precisely the sub-leading contribution we are after!

We have seen how, when cutoff functions are necessary for UV regularisation, their derivatives can supply sub-leading contributions in the IR. This can be rephrased by saying that, under the influence of  $C$ , total momentum derivative contributions can no longer be discarded, at sub-leading order, unless we reinstate terms to parent and subtraction.

When dealing with automatically regulated integrals, however, total momentum derivatives can be thrown away, even under the influence of  $C$ . This follows because the range of integration need not be restricted, even after we have evaluated any cutoff functions at zero momentum. Equivalently, in this case, we can move momentum derivatives around without the need to reinstate the derivative of cutoff functions.

Returning to diagrams under the influence of  $C$  for which total momentum derivatives cannot be discarded, we note that there is a downside to the prescription that we reinstate derivatives of cutoff functions to both parent and subtraction. Let us suppose that the subtraction involves a momentum derivative striking an effective propagator and that it happens to be manipulable. If, under the influence of  $C$ , we do not reinstate any terms to the parent and subtraction, then we can perform all diagrammatic manipulations, since both the effective propagator relation and the gauge invariance identities hold. However, if we do reinstate terms, then we would have to supplement the usual diagrammatic identities with corrections. Generally, we will not perform any manipulations if this correction is present but will choose to do so, if it is not.

### 5.4.3 Application to Terms Manipulable at $\mathcal{O}(p^2)$

The application of the subtraction techniques we have described is not limited to  $\Lambda$ -derivative terms, but is useful for any class of terms in which we wish to perform Taylor expansions. We have already encountered such manipulations when we dealt with the  $\mathcal{O}(p^2)$  terms in the  $\beta_1$  diagrammatics. For example, the elements of the little set were derived from diagrams which were Taylor expanded in  $p$ . Let us return to this by considering one of the parents of the

little set, diagram 4.54, which is reproduced in figure 5.4.

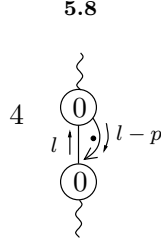


Figure 5.4: Reproduction of diagram 4.54, with explicit momentum routing.

Due to the fact that the structure carrying momentum  $l - p$  is a zero-point wine, rather than an effective propagator, it is clear that  $p$  is not required to regulate this diagram in the IR; hence we can expand not only the vertex but also the wine to zeroth order in  $p$ . For this diagram, there is no need to construct a subtraction. Indeed, at one-loop, there is never any need to construct subtractions for diagrams manipulable at  $\mathcal{O}(p^2)$ .

At two-loops, however, the situation is different. Consider the first diagram shown in figure 5.5. In anticipation of what follows, we have constructed a subtraction.

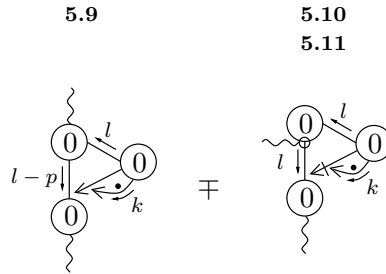


Figure 5.5: A two-loop diagram with an  $\mathcal{O}(p^2)$  stub, which cannot be Taylor expanded in  $p$ , and its subtraction.

Note that the second diagram comes with two labels, the first of which refers to the subtraction and the second of which refers to the addition.

We begin by focusing on diagram 5.9. Since we can always Taylor expand vertices in momenta, let us suppose that we take a power of  $l$  from the top-most

vertex (we cannot take any powers of  $p$ , at  $\mathcal{O}(p^2)$ ) and let us choose to take a power of  $k$  from the other vertex. The leading IR behaviour of the  $l$ -integral is now

$$\int_l \frac{1}{l^2(l-p)^2};$$

this is not Taylor expandable in  $p$ . Note that had we taken a power of  $l$  from the right-hand vertex, rather than a power of  $k$ , then the extra power of  $l$  in the integrand would render the diagram Taylor expandable in  $p$ .

Now let us consider the subtraction and addition. The addition (diagram 5.11) is manipulated in the usual way; this is basically what we would like to have done with diagram 5.9, in the first place. The effect of the subtraction on the parent is to cancel all those components which are Taylor expandable in  $p$ . This immediately tells us the following about any surviving contributions to diagram 5.9:

1. all fields carrying momentum  $l$  must be in the  $A$ -sector;
2. we must take  $\mathcal{O}(l^0)$  from the  $k$ -integral (note that the  $k$ -integral is Taylor expandable in  $l$ );
3. we must discard any remaining contributions to the  $l$  integral which do not  $\sim p^{-2\epsilon}$ .

The contributions to diagram 5.9 not removed by diagram 5.10 are shown in figure 5.6.

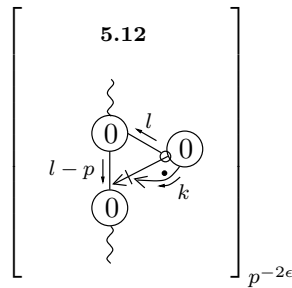


Figure 5.6: The contribution to diagram 5.9 not removed by its subtraction.

As required, we have taken the  $\mathcal{O}(l^0)$  from the  $k$ -integral. Though drawn as a dummy field, the field attached to the circle representing the derivative is

implicitly in the  $A$ -sector; this follows because the only derivatives of vertices we consider are those which arise from a field in the  $A$ -sector carrying zero momentum. The tag  $p^{-2\epsilon}$  demands that we take the  $p^{-2\epsilon}$  component of the diagram. Note, of course, that this tag implicitly assumes that we are using dimensional regularisation. However, were we to use some other means of regulating IR divergences, diagrams such as 5.12 would still exist, but the tag would be appropriately generalised.

## 5.5 Ensuring Universality

The central tenet of our analysis of the  $\Lambda$ -derivative terms has been that the derivative with respect to  $\Lambda|_{\alpha}$  of a dimensionless integral must vanish, unless there is a scale other than  $\Lambda$ , from which we can construct dimensionless quantities. Implicit in this is that there are no dimensionless running<sup>4</sup> couplings, hidden in the integrand.

The most obvious candidates for dimensionless running couplings can immediately be discounted:  $g$  counts the loop order, and so never appears in loop integrals and the presence of  $\alpha$  is irrelevant, since it is held constant, when differentiating with respect to  $\Lambda$ . The first question we must address is whether there are actually any other candidates for dimensionless running couplings.

To see how they could arise, in principle, consider the flow of any vertex, with mass dimension  $\geq 0$ . Now Taylor expand in momenta and focus on the term which is the same order in momenta as the mass dimension of the vertex. The coefficient of this term must be dimensionless; if this coefficient flows, then we have found what we are looking for.

As a first example, let us consider the flow of an  $m$ -loop vertex, decorated by an arbitrary number,  $q$ , of  $C$ s. We take the  $C$ s to carry momenta  $r_i$ . Recalling that  $C$ s are of mass dimension zero [57, 53], all such vertices are of mass dimension four. Hence, we are interested in the  $\mathcal{O}(\text{mom}^4)$  component of each of the vertices.

The crucial point for what follows is that, no matter what the value of  $m$ , the flow is guaranteed to produce a certain type of term: specifically, we will

---

<sup>4</sup>Where, strictly, we mean running with respect to  $\Lambda|_{\alpha}$ .



tex whose flow we compute, it is a different seed action vertex we tune. This ensures that we are never in the situation where we have to try and tune the same seed action vertex in two different directions.

Let us now move on to consider an  $m$ -loop vertex decorated by  $q$   $C$ s and also by a single  $A$  (we do not care which sub-sector this field is in). The vertex is now of mass dimension three and so it is the  $\mathcal{O}(\text{mom}^3)$  part we are interested in. This time, we are guaranteed to generate  $m$ -loop,  $q + 1$ -point seed action vertices, joined to a two-point, tree-level vertex by an undecorated wine. Now, however, we see a difference between this case and the previous one: the tree-level, two-point can be decorated by either an  $A$  or a  $C$ . We illustrate this in figure 5.8, where we take the  $A$  to carry momentum  $p$  and the  $C$ s to carry momenta  $r_i$ .

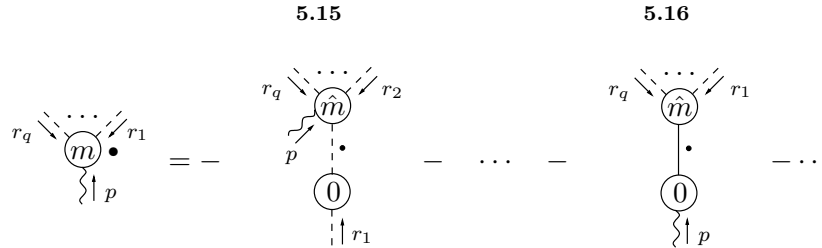


Figure 5.8: The flow of a vertex decorated by a single  $A$  and an arbitrary number of  $C$ s.

The first ellipsis denotes diagrams of the same structure as 5.15 but for which a different  $C$  decorates the two-point, tree level vertex. The final ellipsis denotes the remaining terms generated by the flow equation.

Having decorated with an  $A$ , we must now take account of gauge invariance. The most obvious effect is that the two-point, tree level vertex of diagram 5.16, unlike that of diagram 5.15, is forced to be  $\mathcal{O}(p^2)$ . Given that we are working at  $\mathcal{O}(\text{mom}^3)$ , this means that we must take a single power of momentum from the corresponding  $m$ -loop, seed action vertex. Now, if this single power of momentum is  $p$  then, by Lorentz invariance, its index must be contracted with the two-point, tree level vertex—killing it. Hence, this single power of momentum must be one of the  $r_i$ . In turn, this means that we can Taylor

expand the  $m$ -loop, seed action vertex of diagram 5.16 to zeroth order in  $p$ ; the effect of this is to reduce it to the derivative of an  $m - 1$ -point vertex. This means that gauge invariance has caused us to lose one of our  $m$ -loop,  $q + 1$ -point seed action vertices. We can still tune the flow of our Wilsonian effective action vertex to zero, though, by virtue of the presence of diagram 5.15 and the diagrams represented by the first ellipsis.

Let us examine the tuning of the seed action vertices in a little more detail. To do this, consider contracting the diagrams of figure 5.8 with the momentum carried by the  $A$ . On the l.h.s. of the equation, we now have the flow of (a set of)  $m$ -loop vertices, decorated by  $q$   $C$ s. Since we were working at  $\mathcal{O}(\text{mom}^3)$  but have contracted with a power of momentum, we should now be looking at  $\mathcal{O}(\text{mom}^4)$ . However, we know from our work on pure- $C$  vertices that the flow of such terms has already been tuned to zero. Thus, returning to the diagrams of figure 5.8, gauge invariance ensures that we need only tune the seed action vertices so as to remove those  $\mathcal{O}(\text{mom}^3)$  contributions transverse in  $p$ ! Note that this reproduces the conclusions of [57], in which the special case of the flow of a tree level  $ACC$  vertex was considered.

Next, we extend our analysis to a vertex decorated by two  $A$ s and  $q$   $C$ s. We now work at  $\mathcal{O}(\text{mom}^2)$ . If we take  $q > 0$ , then our analysis just mirrors what we have done: to avoid dimensionless, running couplings, gauge invariance ensures that we need only tune the seed action vertices transverse in the momenta of the  $A$ s. What if  $q=0$ ? Now the renormalisation condition guarantees that the flow of the vertex vanishes; this is, of course, exactly what we have been utilising to compute  $\beta$ -function coefficients.

In the case of a vertex decorated by three  $A$ s and  $q$   $C$ s, we work at  $\mathcal{O}(\text{mom}^1)$ . Any terms involving two-point, tree level vertices decorated by  $A$ s vanish, at the desired order in momentum. Consequently, irrespective of the value of  $q$ , gauge invariance—in conjunction with what we have just done—ensures that the flow of our vertex vanishes at  $\mathcal{O}(\text{mom}^1)$ , without the need for any further tuning. Similarly, this result implies that gauge invariance can be used to demonstrate that the flow of a vertex decorated by four  $A$ s and any number of  $C$ s vanishes, without the need for further tuning.

Our final task is to extend this analysis to include fermionic fields. To do

this, we will treat  $B$ s and  $D$ s separately, due to their differing mass dimensions. The point here is that neither  $S_{0\alpha\beta}^{B\bar{B}}(k)$  nor  $S_0^{D\bar{D}}(k)$  vanishes at zero momentum. Thus, whereas gauge invariance can force some or all of the highest loop order seed action vertices with the maximum number of legs to be written as derivatives of lower point vertices when  $A$ s are amongst the decorative fields, no such thing happens here. Thus, both  $B$ s and  $D$ s behave essentially like the  $C$ s, of the previous analysis.

As a final point, we might worry about the vertex  $S_{0\alpha}^{B\bar{D}}(k)$ —which vanishes at zero momentum. However, supposing that it is the  $B(\bar{D})$  that is the internal field, this vertex will always be accompanied by a term in which there is a  $D(\bar{B})$  as an internal field. It is the seed action vertex at the other end of the corresponding dumbbell which is the one we tune.

We have thus demonstrated that all dimensionless couplings, other than  $g$  and  $\alpha$ , can be prevented from running by a suitable choice of the seed action.

UNIVERSITY OF SOUTHAMPTON

FACULTY OF SCIENCE

School of Physics & Astronomy

**The Manifestly Gauge Invariant  
Exact Renormalisation Group**

Volume II of II

by

**Oliver Jacob Rosten**

Thesis for the degree of Doctor of Philosophy

March 2005

## Part III

# $\beta_{n+}$ Diagrammatics

# Chapter 6

## Introduction

In chapter 4, we saw how it is possible to derive an expression for  $\beta_1$  in terms of  $\Lambda$ -derivatives, with all other diagrams cancelling out. We noted how the structure of the calculation suggested that many of these cancellations could be done in parallel.

We now explore this idea in much greater depth, viewing the one-loop cancellations as a subset of the cancellations that take place in the computation of the arbitrary  $\beta$ -function coefficient,  $\beta_{n+1} \equiv \beta_{n+}$ .

The major difference between the diagrammatic methodology we will employ for the computation of  $\beta_{n+}$  compared to that used for  $\beta_1$  is the use of the generalised notation of figure 2.12. The idea behind this notation is to exploit one of the diagrammatic effects of manifest gauge invariance. When we compute the flow of a vertex decorated by some set of fields,  $\{f\}$ , manifest gauge invariance tells us that we can represent the resulting diagrams by some base structure which is then decorated in all possible ways by the fields  $\{f\}$ . In chapter 4, we performed all these decorations explicitly, generating a large number of diagrams. In the subsequent chapters, however, we will leave these decorations largely implicit and doing this will save us a huge amount of time.

Indeed, we will find that partial decoration, at most, is necessary for diagrammatic manipulations to be performed. As anticipated, this allows us to process large numbers of terms in parallel. Moreover, when we come to cancel these terms, we will find that we are able to do so without further decoration; the entire diagrammatic procedure is radically simplified.

However, in its current form, the generalised methodology is not sufficiently developed, for our purposes. Hence, in the initial stages, our approach is pedagogical. We start our computation of  $\beta_{n_+}$  in chapter 7, where we begin by explicitly converting diagrams into  $\Lambda$ -derivative terms, plus corrections. The first purpose this serves is to allow us to furnish the generalised methods with the desired set of features. Having done this, we then proceed with the usual diagrammatic procedure: we identify two-point, tree level vertices and apply the effective propagator relation, as appropriate. This then allows us to identify cancellations, a subset of which we could map back to the special case of  $n = 0$ .

However, as we iterate the procedure, it becomes clear that the cancellations we identify within our generalised framework are simply repeated with each iteration. This guides us from explicit cancellations to cancellation mechanisms, which guarantee that certain types of diagram will be cancelled in a calculation of  $\beta_{n_+}$ . Once we have identified these mechanisms, we can dispense with explicit computation; rather, we can immediately write down diagrammatic expressions, valid to all orders in perturbation theory, which give the result of iterating the diagrammatic procedure, until exhaustion.

In section 7.5 we arrive at a diagrammatic form for  $\beta_{n_+}$  in terms of  $\Lambda$ -derivative,  $\alpha$  and  $\beta$ -terms, up to gauge remainders and diagrams which require manipulation at  $\mathcal{O}(p^2)$ .

The next task is to examine the gauge remainder diagrams. Once again, the heavily compacted notation utilised in this chapter makes the problem tractable. The initial manipulation of the gauge remainders is done in chapter 8. Having found that many of the terms generated cancel amongst themselves, we then introduce a set of diagrammatic identities in chapter 9 to facilitate further progress. The validity of the final identity, which applies at three loops and beyond, is only partially demonstrated and so we make an unproven assertion that it is true in general. In chapter 10 we find that, aided by these identities, we can iterate the diagrammatic procedure, converting the surviving gauge remainder terms into further  $\Lambda$ -derivative,  $\alpha$  and  $\beta$  terms. This allows us to supplement our previous expression for  $\beta_{n_+}$ , to explicitly include the effects of processing all gauge remainders.

The final thing to be done is to process those terms which require manipu-

lation at  $\mathcal{O}(p^2)$ . Unfortunately, it is beyond the scope of this thesis to do this, though we comment on some of the associated issues in chapter 11.

Before embarking on the analysis, proper, some preliminary remarks are in order. We will encounter three types of labelled diagram in this chapter. The first type are those arising from the initial, step by step reduction of  $\beta_{n+}$  to  $\Lambda$ -derivatives and etc. These diagrams will be labelled **chapter.#**.

The second type are so called general diagrams which can arise from any level of iteration; special cases of these diagrams reduce to the explicitly generated diagrams. General diagrams are labelled **G.#**.

The third type are the illustrative diagrams and are labelled **I.#**.

In addition to diagrams being processed, discarded and cancelled we will encounter a further option: partial cancellation. If diagram  $Y$  is partially cancelled by diagram  $X$ , then the label above diagram  $X$  would be

$$\{\mathbf{X} Y(P)\}.$$

If the remaining part of diagram  $Y$  partially cancels a further diagram,  $W$ , then the label above diagram  $Y$  would be

$$\{\mathbf{Y} X, W(P)\}.$$

Unlabelled diagrams are those which are never referred to explicitly, though they are implicitly referred to in the generalised formalism which we develop.

# Chapter 7

## Initial Recasting

In this chapter we will generate an expression for  $\beta_{n_+}$  in terms of  $\Lambda$ -derivative,  $\alpha$  and  $\beta$ -terms, up to gauge remainders and diagrams with an  $\mathcal{O}(p^2)$  stub. The methodology we employ will be developed as we proceed; consequently, the ideas presented at the beginning of the chapter are refined, as we get deeper into the calculation.

Indeed, to begin with, we will mirror the calculation of  $\beta_1$ : starting from the flow equation (2.28), we write down a diagrammatic expression for  $\beta_{n_+}$ . We call this the zeroth level of the calculation. At the first level, we perform the usual diagrammatic procedure of converting manipulable diagrams into  $\Lambda$ -derivative terms, plus corrections. Iterating the procedure, we present the results of the second and third level manipulations. This is sufficient to enable us to refine the formalism and to deduce the result of manipulations performed at an arbitrary level.

### 7.1 Level-Zero Manipulations

To compute  $\beta_{n_+}$ , we start with flow equation (2.28) specialised to  $\{f\} = A_\mu^1(p), A_\nu^1(-p)$  and  $n = n + 1$  and work at  $\mathcal{O}(p^2)$ :

$$-4\beta_{n_+} \square_{\mu\nu}(p) + \mathcal{O}(p^4) = a_1 [\Sigma_n]_{\mu\nu}^{11}(p) - \sum_{r=0}^{n_+} a_0 [S_r, \Sigma_{n+r}]_{\mu\nu}^{11}(p) \quad (7.1)$$

This is represented in figure 7.1. Unless stated otherwise, we will take the indices of the two external fields to be  $\mu, \nu$  and work at  $\mathcal{O}(p^2)$ . In preparation for later, when we will encounter diagrams containing many vertices, it will

prove useful to have a tag for each vertex, independent of the vertex argument. Henceforth, we label vertices alphabetically, in the counter-clockwise sense; the bottom left vertex of a diagram being  $A$ .

$$-4\beta_{n_+} \square_{\mu\nu}(p) + \mathcal{O}(p^4) = \frac{1}{2} \left[ \begin{array}{c} \text{7.1} \rightarrow \text{7.2} \\ \text{\textcircled{\Sigma}_n} \\ \text{7.2} \rightarrow \text{7.7} \\ - \sum_{r=0}^{n_+} \begin{array}{c} \text{\textcircled{\bar{r}}} \\ \cdot \\ \text{\textcircled{\bar{n}_{+r}}} \end{array} \begin{array}{c} \text{B} \\ \text{A} \end{array} \end{array} \right]^{11}$$

Figure 7.1: A diagrammatic representation of the equation for  $\beta_{n_+}$ . Vertices are tagged alphabetically.

Although we will not perform any decorations at this stage, it is worth noting that the decoration of diagrams 7.1 and 7.2 is straightforward. Following section 2.4.2, if we were to place the two identical external fields on different structures we would pick up a factor of two whereas, if we were to place them on the same structure, we would not.

It is also worth examining the behaviour of the decorated diagrams at  $\mathcal{O}(p^2)$ .

Examining diagram 7.1 at  $\mathcal{O}(p^2)$  is trivial: none of the component diagrams vanish at  $\mathcal{O}(p^2)$  and so we need do nothing further. Diagram 7.2, however, is more subtle. If we attach one external field to each of the vertices, then the resulting diagram vanishes at  $\mathcal{O}(p^2)$ . Whilst it is completely legitimate to discard such terms, we choose to retain (some of) them. The reason for this is as follows.

The components of diagram 7.2 containing Wilsonian effective action vertices joined by an undecorated wine can be manipulated, using the flow equations. The salient point is that a set of the diagrams generated do not, individually, vanish at  $\mathcal{O}(p^2)$ . Of course, it must be the case the sum over the elements of this set has no  $\mathcal{O}(p^2)$  component. Crucially, we will see that these diagrams cancel diagrams arising from the manipulation of diagram 7.1. For the computation of  $\beta_2$ , at any rate, this allows us to bring the diagrammatic expression into a form from which we can extract the numerical value in  $D = 4$ .

These considerations are not restricted to the zeroth level of the calculation. At each level we will be confronted with terms that vanish at  $\mathcal{O}(p^2)$  and, rather than throwing them away, we choose to process the manipulable parts. The only exception to this rule concerns diagrams containing two-point, tree level vertices. Whilst it is possible to manipulate such diagrams, it is not useful to do so. The reason for this is easily seen by considering the  $r = 0$  component of diagram 7.2, with an external field attached to each of the vertices. If we were to manipulate this diagram, we just end up computing the flow of  $S_{n+\mu\alpha}^{11}(p)$  which is, of course, what we did to obtain equation (7.1), in the first place! Hence, this manipulation will just increase our work, without giving anything new.

Note that any terms which manifestly vanish at  $\mathcal{O}(p^2)$  and which cannot be manipulated can be discarded. However, we choose to retain a subset of them as it turns out that they are cancelled in parallel with terms that do not vanish in this way. Hence, it would be inefficient to try and separate them out.

Returning to diagram 7.2, if we do not attach any external fields to one (both) of the vertices, then the corresponding vertex is a one-point vertex and so has no Wilsonian effective action contribution [57]. However, just as we choose to manipulate the terms which vanish at  $\mathcal{O}(p^2)$ , so too do we choose to manipulate one-point vertices. Again, it is perfectly valid to discard such terms—indeed, this is the strategy employed in the one-loop calculation. On the other hand, by manipulating them we avoid having to enforce the constraint (2.77); rather, *all* diagrams involved in this constraint equation will be automatically cancelled by diagrams generated by the manipulation of one-point Wilsonian effective action vertices. When the dust has settled, all that we are left with is  $\Lambda$ -derivative terms containing one-loop Wilsonian effective action vertices. Now we utilise the fundamental constraint that such vertices vanish to remove these terms.

## 7.2 Level-One Manipulations

### 7.2.1 Diagram 7.1

We know from the one-loop calculation that if, in diagram 7.1, we take the Wilsonian effective action contribution and attach both external fields to the vertex, then we can process this diagram along the lines of figure 4.2.

The first step of this procedure is to isolate the manipulable component. Taking only the Wilsonian effective action contributions to the vertex is trivial. However, we now need to introduce some notation to denote whether or not the wine is decorated. To indicate an undecorated wine, we enclose the  $\Lambda\partial_\Lambda|_\alpha$  in a box, which we take to mean that we decorate *first* and then differentiate. Since it is illegal to decorate effective propagators, this has the desired effect.

To indicate a decorated wine, we define an object called the *reduced* wine:

$$\left(\dot{\Delta}\right)_R \equiv \overset{\circ}{\Delta} = \dot{\Delta} - \dot{\Delta}_{ST}^{XY}(k), \quad (7.2)$$

where we have suppressed all arguments of the generic wine,  $\dot{\Delta}$ , and its reduction. The isolation of the manipulable component of diagram 7.1 is shown in figure 7.2.

$$\frac{1}{2} \left[ \begin{array}{ccc} \overset{\square}{\text{7.3}} \rightarrow \text{7.3} & \{ \text{7.4} \text{ 7.36, 7.5(P)} \} & \{ \text{7.5} \text{ 7.11, 7.4(P)} \} \\ \begin{array}{c} \square \\ \circ \\ \text{\scriptsize } n \end{array} & + & \begin{array}{c} \circ \\ \circ \\ \text{\scriptsize } n \end{array} - 2 \begin{array}{c} \bullet \\ \circ \\ \text{\scriptsize } \hat{n} \end{array} \end{array} \right]^{11}$$

Figure 7.2: Isolation of the manipulable component of diagram 7.1.

We now process diagram 7.3, as shown in figure 7.3. The key thing to notice is that we have promoted the effective propagator of the  $\Lambda$ -derivative term, and the associated internal fields to which it attaches, to an unrealised decoration. This is denoted by  $\{I^2, \Delta\}$ . For the  $\Lambda$ -derivative term, decoration is performed *before* the diagram is hit by  $\Lambda\partial_\Lambda|_\alpha$ . Indeed, we remind ourselves of this by the square brackets around the  $\Lambda$ -derivative term. In the absence of these, we would decorate *after* the vertex is hit by  $\Lambda\partial_\Lambda|_\alpha$ . Henceforth, we will

often loosely refer to the promotion of objects to unrealised decorations simply as promotion to decorations.

$$\frac{1}{2} \left[ \left[ \textcircled{n} \right]^{\bullet} - \sum_{r=1}^n \left[ 2(n_r - 1)\beta_r \textcircled{n_r} + \gamma_r \frac{\partial}{\partial \alpha} \textcircled{n_r} \right] \right]^{11\{I^2, \Delta\}}$$

$$+ \frac{1}{2} \sum_{r=0}^n \begin{array}{c} \textcircled{\bar{r}} \\ \bullet \\ \textcircled{\bar{n}_r} \end{array} \quad \begin{array}{c} \text{7.6} \rightarrow \text{7.4} \\ \\ \end{array} \quad + \frac{1}{2} \begin{array}{c} \bullet \\ \textcircled{\Sigma_{n-}} \end{array} \quad \begin{array}{c} \text{7.7} \rightarrow \text{7.20} \\ \\ \end{array}$$

Figure 7.3: The result of processing diagram 7.3.

Comparing with the one-loop calculation this figure is, up to the  $\Lambda$ -derivative term, the analogue of figure 4.3. Note, though, that when we specialise the diagrams of figure 7.3 to  $n = 0$ , the second, third and fifth diagrams must be discarded, else they have an (illegal) negative vertex argument. Thus, all the diagrams of figure 4.3 are generated entirely by decorating diagram 7.6 (for  $n = 0$ ). This huge simplification has come about not just through leaving the external fields as unrealised decorations but also due to the similar promotion of the effective propagator. This latter step will prove central to the following analysis.

Our first task in analysing the diagrams of figure 7.3 is to determine the combinatorics associated with attaching the various fields to the diagram. We have already discussed the attachment of external fields, in the previous section. When we decorate with internal fields, what we will ultimately be doing is joining them together with an effective propagator. The rule is simply that, if the effective propagator starts on one structure and ends on another, then we must pick up a factor of two which recognises that we can choose which end of the effective propagator to attach to which structure. If both ends of the effective propagator attach to the same structure, then there is no such factor.

As an example of how this works, we will reproduce the factors of the diagrams 4.19 and 4.13, by attaching fields to (the Wilsonian effective action component of) diagram 7.6. To reproduce diagram 4.19, we must attach the

external fields to the same vertex and the effective propagator must start and end on the same vertex. However, we could have decorated either of the vertices with the external (internal) fields and so this gives us a factor of two. Taking into account the overall factor of  $-1/4$  in front of diagram 7.6 exactly reproduces diagram 4.19.

Now, to reproduce diagram 4.13, we must attach one external field and one internal field to each vertex. This gives a factor of four. However, due to the symmetry of the diagram, this exhausts all possibilities, yielding an overall factor of  $-1$ , as required.

We must now consider the implicit decoration of diagrams 7.6 and 7.7 with the two external fields and an effective propagator. The resultant terms will split into four classes:

1. terms which can be manipulated by applying the effective propagator relation;
2. terms which can be manipulated at  $\mathcal{O}(p^2)$ ;
3. terms which can be processed using the flow equations;
4. terms with which we can do nothing.

From our experiences with the one-loop calculation, we expect terms in the first class to cancel a subset of the un-manipulated contributions to diagram 7.1. We will see this explicitly below. Terms in the second class will be commented on in section 11. Terms in the third class will be dealt with in section 7.3, yielding diagrams which either directly, or through further manipulation, cancel the terms of the fourth class.

To prepare for the iteration of the diagrammatic procedure, we first want to split off all terms which can be manipulated directly i.e. without the need for using the flow equations. These terms are all those which contain a two-point, tree level vertex. If this vertex is decorated solely by internal fields, then the resulting diagram is in the first class above; if the vertex is decorated by an external field, then it is in the second class. All such terms are a subset of the components of diagram 7.6 that occur when the summed variable  $r$  takes its boundary values, zero or  $n$ .

To facilitate this separation, we define the reduced,  $n$ -loop vertex thus:

$$v_n^R = \begin{cases} v_n & n > 0 \\ v_0 - v_{0RS}^{XX}(k) & n = 0 \end{cases}$$

where we have suppressed all arguments of the generic vertex  $v_n$  and its reduction. By definition, the reduced vertex does not contain a two-point, tree level component.

We must take care rewriting diagram 7.6 in terms of reduced vertices since the  $n = 0$  case behaves slightly differently from the  $n > 0$  case. When  $n > 0$ , it is not possible for both vertices to be simultaneously tree level; hence we get only three terms. One contains two reduced vertices and two contain one reduced  $n$ -loop vertex and a two-point, tree level vertex. These latter two terms are identical and so can be combined. Moreover, in this case, the reduced  $n$ -loop vertex can be replaced by just an  $n$ -loop vertex. This step cannot be performed when  $n = 0$  since it will over-count the diagram comprising two two-point, tree level vertices—which do exist in this case—by a factor of two.

However, it is undesirable to explicitly draw the term comprising two two-point, tree level vertices since it is only present in the case when  $n = 0$ . Rather, we introduce the variable  $1/\vartheta_n$ , which takes the value of  $1/2$  when the following is satisfied: the  $n$ -loop vertex is both tree level and two-point. Now, in the terms containing one two-point, tree level vertex and one reduced vertex, we can replace the reduced vertex by a normal vertex for all  $n$ , so long as we multiply by a factor of  $1/\vartheta_n$ .<sup>1</sup>

Finally, then, the separation of terms is shown in figure 7.4

We now partially decorate diagram 7.9 by specifying which field attaches to the two-point, tree level vertex. To partially decorate with an external field, we simply attach one of them to the two-point, tree level vertex with a factor of unity. We will only pick up the factor of two arising from the attachment of the remaining external field<sup>2</sup> when the attachment is actually made.<sup>3</sup>

---

<sup>1</sup>As the calculation develops, we will find that there is a way to isolate all two-point, tree level vertices, irrespective of the value of  $n$ , in a unified manner. However, this relies on terms which have not yet been generated.

<sup>2</sup>Since one of the external fields has attached to the two-point, tree level vertex, the other must necessarily attach to a different structure.

<sup>3</sup>This prescription is designed to make partial decoration consistent with full decoration.

$$-\frac{1}{4} \left[ \sum_{r=0}^n \begin{array}{c} \text{7.8} \rightarrow \text{7.12} \\ \begin{array}{c} \textcircled{\bar{\tau}^R} \\ \cdot \\ \textcircled{\bar{n}_r^R} \end{array} \end{array} + \frac{2}{\vartheta_n} \begin{array}{c} \text{7.9} \rightarrow \text{7.5} \\ \begin{array}{c} \textcircled{\bar{0}^2} \\ \cdot \\ \textcircled{\bar{n}} \end{array} \end{array} \right]^{11\{I^2, \Delta\}}$$

Figure 7.4: Splitting off the tree level two-point, tree level vertices from diagram 7.6.

When we partially decorate with internal fields, what we choose to do is attach one end of the effective propagator. When we decorate with the other internal field—which in this case necessarily attaches to a different structure—we will pick up a factor of two, which recognises the indistinguishability of the internal fields. As with the external fields, this factor is suppressed until the final decoration is actually made. Figure 7.5 shows the result of this procedure, where we note that a dumbbell with barred arguments simplifies if one of vertices is a two-point, tree level vertex. This follows on account of

$$\begin{aligned} a_0[\bar{S}_m, \bar{S}_{0RS}^{XY}(k)] &= a_0[S_m, S_{0RS}^{XY}(k)] - a_0[S_m, \hat{S}_{0RS}^{XY}(k)] - a_0[\hat{S}_m, S_{0RS}^{XY}(k)] \\ &= -a_0[\hat{S}_m, S_{0RS}^{XY}(k)], \end{aligned}$$

where we have used the equality of the Wilsonian effective action and seed action two-point, tree level vertices.

In the case where we have attached one end of the effective propagator, the remaining decorative fields include the internal field to which the other end must attach. This is denoted by  $\{I\}$ . However, after this section we will drop this notation since, if there is a loose end of an effective propagator present, it is implicit that it must attach elsewhere. Moreover, when we decorate with an effective propagator, we will now drop the associated internal fields, since their presence is implied.

The next step is to attach the loose end of the effective propagator in diagram 7.10, as shown on the LHS of figure 7.6. Since the effective propagator is When decorating an arbitrary diagram with identical fields, we determine the associated factor only after completing the decoration.

$$\frac{1}{2i\vartheta_n} \left[ \left[ \begin{array}{c} \text{7.10} \rightarrow \text{7.6} \\ \circlearrowleft[0^2] \\ \bullet \\ \circlearrowleft[\hat{n}] \end{array} \right]^{11\{I\}} + \left[ \begin{array}{c} \circlearrowleft[0^2] \\ \bullet \\ \circlearrowleft[\hat{n}] \end{array} \right]^{1\{I^2, \Delta\}} \right]$$

Figure 7.5: Partial decoration of diagram 7.9 with either an external field or an effective propagator.

guaranteed to start and end on a different structure, this will necessarily yield a factor of two. On the RHS of figure 7.6, we apply the effective propagator relation, discarding the diagram in which the wine bites its own tail. Henceforth, we will automatically discard such diagrams.

$$\frac{1}{\vartheta_n} \left[ \begin{array}{c} \circlearrowleft[0] \\ \bullet \\ \circlearrowleft[\hat{n}] \end{array} - \begin{array}{c} \circlearrowleft[0] \\ \bullet \\ \circlearrowleft[\hat{n}] \end{array} \right]^{11} = \frac{1}{\vartheta_n} \left[ \begin{array}{c} \{ \text{7.11} \quad \text{7.5}(P) \} \\ \circlearrowleft[\hat{n}] \end{array} - \begin{array}{c} \bullet \\ \circlearrowleft[\hat{n}] \end{array} - \begin{array}{c} \bullet \\ \circlearrowleft[\hat{n}] \end{array} \right]^{11}$$

Figure 7.6: Result of tying up the loose end in diagram 7.10, followed by subsequent application of the effective propagator relation.

We now encounter our first cancellation. Having split diagram 7.1 into non-manipulable and manipulable parts we expect, from our experiences of the one-loop calculation, the former to be cancelled by manipulations of the latter.

**Cancellation 7.1** *Diagram 7.11 has the same structure as diagram 7.5. Irrespective of the value of  $n$ , diagram 7.11 exactly cancels the contributions to diagram 7.5, for which at least one of the external fields decorates the vertex. The only remaining contribution to diagram 7.5 is where both external fields decorate the wine i.e. the vertex is a two-point vertex. If  $n > 0$ , this contribution is exactly cancelled by diagram 7.11. However, when  $n = 0$ , the factor of  $1/\vartheta_n$  means that only half the contribution is removed. Hence, diagram 7.11 only partially cancels diagram 7.5.*

This first cancellation removes those components of the parent diagram whose vertices are uniquely seed action. (The only surviving component, occurring for  $n = 0$ , is a two-point, tree level vertex, for which the seed action contribution is just equal to the Wilsonian effective action contribution. Hence, we take such a contribution not to possess a uniquely seed action vertex.) As we will see throughout this chapter, this is a general feature of the diagrammatic method: starting from some parent diagram, we split off the non-manipulable terms from the manipulable ones. Diagrams in the former class can be further sub-divided, depending on whether or not they possess any seed action vertices. Upon manipulation of the parent diagram, these seed action vertices will be removed.

To cancel the remaining contributions to the parent diagram—i.e. those non-manipulable components possessing only uniquely Wilsonian effective action vertices—we will have to proceed to the next level of manipulation. The diagram which cancelled diagram 7.5 was one the components of diagram 7.6 which could be processed by using the effective propagator relation. It is the contributions to diagram 7.6 that must be manipulated via the flow equations which will generate the terms necessary to complete the cancellation (see section 7.3.1) of the non-manipulable components of diagram 7.1.

Again, we will find that this is a general feature of the diagrammatics. The non-manipulable contributions to some parent diagram will generally be completely removed after two levels of manipulation. At the first level, the uniquely seed action contributions will be cancelled whereas the uniquely Wilsonian effective action contributions will be cancelled at the second level.<sup>4</sup>

### 7.2.2 Diagram 7.2

We now process the components of diagram 7.2 containing Wilsonian effective action vertices and undecorated wines. As discussed in section 7.1 we do not manipulate any terms containing two-point, tree level vertices. Indeed, we can discard all terms containing such a vertex. The two-point, tree level vertex is

---

<sup>4</sup>In the case that there are any remaining contributions i.e. those containing a two-point, tree level vertex then, in the case where this vertex is decorated solely by internal fields, the corresponding diagrams will cancel among themselves.

$$-\frac{1}{2} \sum_{r=0}^{n_+} \left[ \begin{array}{ccc} \text{7.12} \rightarrow \text{7.8} & \{ \text{7.13} \text{ 7.46} \} & \{ \text{7.14} \text{ 7.22} \} \\ \begin{array}{c} \textcircled{r,R} \\ \square \\ \textcircled{n_{+r}^R} \end{array} & + & \begin{array}{c} \textcircled{r,R} \\ \circ \\ \textcircled{n_r^R} \end{array} & - 2 & \begin{array}{c} \textcircled{\hat{r},R} \\ \bullet \\ \textcircled{n_{+r}^R} \end{array} \end{array} \right]^{11}$$

Figure 7.7: Isolation of those components of diagram 7.2 which can be usefully processed.

necessarily decorated by an external field and so the diagram is at least  $\mathcal{O}(p^2)$ . Since any two-point vertex decorated by an external field is at least  $\mathcal{O}(p^2)$ , the diagram vanishes at  $\mathcal{O}(p^2)$  if the remaining external field decorates the other vertex. If, instead, the remaining external field decorates the wine, then the diagram vanishes in exactly the same way that the one-loop diagram 4.7 vanished.

Discarding all terms containing a two-point, tree level vertex, we isolate the remaining manipulable components, as shown in figure 7.7.

The next step is to convert diagram 7.12 into a  $\Lambda$ -derivative term. This procedure will turn the wine into an effective propagator and generate two correction terms, in which the  $\Lambda$ -derivative strikes each of the vertices. Due to the invariance of the parent diagram under interchange of the vertex arguments, we choose to compute the flow of only one of these vertices, but multiply by two.

Following our treatment of diagram 7.1 we want to convert the newly formed effective propagator into a decoration. However, when we come to reattach it, our current rule for attaching effective propagators will give us an extra factor of two.<sup>5</sup> We could demand that, for two unjoined structures, the first join does not come with a factor of two. Alternatively, as we choose to do, we simply allow all joins to come with a factor of two but include an ex-

<sup>5</sup>This follows because our current rule allows effective propagators joining two different structures to attach either way round. In the case under consideration, though, the effective propagator started out life as a wine, originally part of a dumbbell structure formed by the flow.

tra factor of 1/2 for each wine, originally part of a dumbbell structure, which becomes transformed into a decorative effective propagator.

To proceed further, we must know how to compute the flow of a reduced vertex. Consider for a moment the flow of a two-point, tree level vertex. From section 2.5.2, we know that this would produce a pair of two-point, tree level vertices joined together by an undecorated wine. This is precisely the diagram that must be excluded from the flow of a reduced vertex. To exclude such diagrams, we can extend the action of  $R$  such that it is defined to operate on a dumbbell structure in the following way. The action of  $R$  removes all terms for which the following are satisfied: both vertices are two-point, tree level vertices *and* the wine is undecorated. If a quantum term is generated by the action of the flow on a reduced vertex we can drop the  $R$ , as such terms appear only in the flow of  $(n > 0)$ -loop vertices.

The result of both promoting the effective propagator to a decorative field and computing the flow of the relevant vertex is shown in figure 7.8. Note that we adopt the rule that, upon decoration, there must be no disconnected structures.

$$\left[ \left[ \begin{array}{c} \textcircled{r^R} \\ \textcircled{n_{+r}^R} \end{array} \right] \bullet - 2 \sum_{t=1}^r \left[ 2(r_t - 1)\beta_t \left[ \begin{array}{c} \textcircled{r_t} \\ \textcircled{n_{+r}^R} \end{array} \right] + \gamma_t \left[ \begin{array}{c} \frac{\partial}{\partial \alpha} \textcircled{r_t} \\ \textcircled{n_{+r}^R} \end{array} \right] \right] \right]^{11\Delta} \\
 - \frac{1}{4} \sum_{r=0}^{n_+} \left( - \sum_{t=0}^r \left( \left[ \begin{array}{c} \text{7.15} \rightarrow \text{7.10} \\ \textcircled{\bar{t}} \text{---} \textcircled{\bar{r}_t} \\ \textcircled{n_{+r}^R} \end{array} \right]_R \right) + \left[ \begin{array}{c} \text{7.16} \rightarrow \text{7.9} \\ \textcircled{\Sigma_{r_-}} \\ \textcircled{n_{+r}^R} \end{array} \right] \right)$$

Figure 7.8: Result of processing diagram 7.12 by converting it into a  $\Lambda$ -derivative term, plus corrections.

The combinatorics associated with decorating the diagrams of figure 7.8 is very simple. We have a single effective propagator with which we must join

the bottom vertex to some other structure. This will produce a factor of two. Decoration with the external fields is equally straightforward though, of course, they can both attach to the same structure.

Before moving on, we note that we can rewrite diagram 7.16. Since we cannot have a vertex argument less than zero the sum over  $r$ , for this term, must start from one. Letting  $r \rightarrow r + 1$ , we can redraw diagram 7.16, as shown in figure 7.9.

$$-\frac{1}{4} \sum_{r=0}^n \left[ \begin{array}{c} \{ 7.17 \quad 7.53 \} \\ \text{Diagram 1} \\ \text{Diagram 2} \end{array} \right]^{11\Delta}$$



Figure 7.9: A re-expression of diagram 7.16.

As in section 7.2.1, we now remove from diagram 7.15 all those components which can be processed without using the flow equations i.e. all those containing two-point, tree level vertices. These terms occur when the summed variable  $t$  takes its boundary values; the isolation of two-point, tree level vertices is shown in figure 7.10. Note that, unlike the analogous case from the previous section, we do not need to include something like  $1/\vartheta_r$ : since the variable  $r$ , unlike  $n$ , is summed over, diagrams containing two two-point, tree level vertices necessarily occur and so can be included naturally.

In those diagrams for which one of the vertices attached to the dumbbell structure is reduced, we need not include the overall  $R$  (note, though, that it would be illegal to retain the overall  $R$  and remove the  $R$  from the vertices). Diagrams containing a single two-point, tree level vertex have been partially decorated.

Referring to the diagrams of figure 7.10, there are a number of comments to make. First, we note that we can discard diagram 7.19. If we attach the remaining external field to the wine, we know that such a diagram vanishes at  $\mathcal{O}(p^2)$ . If, instead, we attach the remaining external field to one of the vertices,

$$\begin{aligned}
& + \frac{1}{4} \sum_{r=0}^{n_+} \left[ \begin{array}{c} \left[ \begin{array}{c} \text{7.18} \rightarrow \text{7.11} \\ \begin{array}{c} \circlearrowleft{0^2} \\ | \\ \bullet \\ \circlearrowleft{\hat{r}^R} \end{array} \\ \circlearrowleft{n_{+r}^R} \end{array} \right]^{11} \\ -2 \left[ \begin{array}{c} \text{7.19} \rightarrow 0 \\ \begin{array}{c} \text{wavy line} \\ \circlearrowleft{0^2} \\ | \\ \bullet \\ \circlearrowleft{\hat{r}^R} \end{array} \\ \circlearrowleft{n_{+r}^R} \end{array} \right]^{1\Delta} \\ \\ \left[ \begin{array}{c} \text{7.20} \rightarrow \text{7.31} \\ \begin{array}{c} \circlearrowleft{\bar{t}^R} \text{---} \bullet \text{---} \circlearrowleft{\bar{r}_t^R} \\ \circlearrowleft{n_{+r}^R} \end{array} \end{array} \right]^{11\Delta} \\ \\ -\frac{1}{4} \left[ \begin{array}{c} \text{7.21} \rightarrow \text{7.11} \\ \begin{array}{c} \circlearrowleft{0^2} \\ | \\ \circ \\ \circlearrowleft{0^2} \\ \circlearrowleft{n_{+}^R} \end{array} \end{array} \right]^{11\Delta} \end{array} \right]
\end{aligned}$$

Figure 7.10: Isolation of the components of diagram 7.15 containing a two-point, tree level vertex. Dumbbells with a single two-point, tree level vertex have been partially decorated.

then this vertex must either be of the form  $S_{m\alpha\beta}^{11}(p)$  or  $S_{m\alpha\beta}^{\{11C\}}(p, -p, 0)$  (or the hatted versions of these vertices), for some loop order  $m$ . Either way, the vertex is  $\mathcal{O}(p^2)$  and so the diagram as whole is at least  $\mathcal{O}(p^4)$ . Since the diagram contains a seed action vertex, we cannot manipulate it—however we choose to decorate it—and so we can discard it.

Next, we further process diagrams 7.18 and 7.21. In the former case, we tie up the loose end noting that, to create a legal diagram, it must attach to the bottom vertex. This attachment yields a factor of two. In the latter case, we note that we must attach the effective propagator to one of the two-point, tree level vertices. If, instead, we attach an external field to each of these vertices then we can discard this diagram as it vanishes at  $\mathcal{O}(p^2)$  and cannot be usefully manipulated.<sup>6</sup> Having decorated one of the two-point, tree level vertices with the effective propagator, we now have no choice but to decorate both the wine and the remaining two-point, tree level vertex with external fields. This yields an additional factor of two.

Figure 7.11 shows how we tie up the loose end of the propagator in both of these cases and the subsequent application of the effective propagator relation. We are free to discard all gauge remainders, since they either strike a two-point vertex or have no support—as is the case when they attach to a one-point vertex. We can discard diagram 7.23

As expected, we now find another cancellation. Having split the parent diagram into manipulable and non-manipulable components (see figure 7.7), the seed action contributions to the latter are now removed.

**Cancellation 7.2** *Diagram 7.22 exactly cancels diagram 7.14.*

Note that, in this case, the issue of whether or not vertices of the parent diagram are uniquely seed action or Wilsonian effective action vertices never arises.

---

<sup>6</sup>In this particular case, the diagram can not be manipulated at all. The effective propagator is forced to decorate the wine. However, even if this were not the case, our prescription for treating such diagrams would demand that we throw it away, anyway.

$$-\sum_{r=0}^{n_+} \left[ \begin{array}{c} \{ 7.22 \quad 7.14 \} \\ \text{Diagram with } \hat{\gamma}^R \text{ and } n_{+r}^R \end{array} \right]^{11} - 2 \left[ \begin{array}{c} 7.23 \rightarrow 0 \\ \text{Diagram with } 0^2 \text{ and } n_+^R \end{array} \right]$$

Figure 7.11: Decoration of the two-point, tree level vertices of diagrams 7.18 and 7.21 and application of the effective propagator relation. In the final diagram, we complete the decoration as the remaining field is forced to decorate the wine.

Diagram	Level – 0	Level – 1
7.7	$a_1$	$a_1$
7.8	$a_1$	$a_0$
7.17	$a_0$	$a_1$
7.20	$a_0$	$a_0$

Table 7.1: The history of the four diagrams which are candidates for level-two manipulations.

### 7.3 Level-Two Manipulations

By processing diagrams 7.1 and 7.2, we have performed all possible level-one manipulations. At the second level, though, we must be more discerning about what we choose to manipulate. Ignoring gauge remainders and  $\mathcal{O}(p^2)$  manipulations, which will be dealt with later, there are four diagrams, components of which are candidates for manipulation: diagrams 7.7, 7.8, 7.17 and 7.20.

These diagrams are ones which have been formed by the action of either  $a_0$  or  $a_1$ , at each level of manipulation. The history of each of the diagrams is summarised in table 7.1.

Let us consider the effect of manipulating diagram 7.8. Suppose that we use the decorative effective propagator to form a loop on one of the vertices—in the

case that  $n = 0$ , this would correspond to diagram 4.19. We henceforth refer to loops formed by effective propagators attaching at both ends to the same vertex as simple loops. When we manipulate diagram 7.8, one of the diagrams produced will correspond to the  $\Lambda$ -derivative striking this simple loop. This diagram has the same topology as diagram 7.17—which is one of the other candidates for manipulation—and, as we will see, actually cancels part of it. Thus it is clear that we should not be manipulating both diagrams 7.8 and 7.17. The best way to proceed is to manipulate the first of these diagrams. We choose to do this because diagram 7.8 also contains a manipulable component with no simple loops—in the case that  $n = 0$ , this would be diagram 4.13—which must be manipulated, come what may.

As we iterate the diagrammatic procedure, we will generally find that diagrams with a structure formed by the action of  $a_1$  will cancel diagrams in which the  $\Lambda$ -derivative has been moved from effective propagators joining different vertices to a simple loop. There is, of course, one exception: diagrams formed by the (repeated) action of  $a_1$  possess only a single vertex and so cannot possess any effective propagators which join different vertices. These terms must be manipulated; indeed, we have already done so with diagram 7.1. Likewise, we must manipulate diagram 7.7.

Our final candidate for manipulation, diagram 7.20, is formed by the repeated action of  $a_0$ . This should be manipulated.

Upon manipulation of the diagrams in this section, we find, as expected, a number of cancellations. For some of these, a pattern is apparent, even at this level of manipulation and this leads us to the first generic cancellation mechanisms, of this chapter. As we build up the set of cancellation mechanisms, we can start to ask what happens when, starting with a certain diagram, we iterate the diagrammatic procedure, until exhausted. We find that, for diagram 7.2, we can describe the final result of this procedure in a remarkably compact form.

### 7.3.1 Diagram 7.8

We now iterate the diagrammatic procedure by processing the manipulable component of diagram 7.8. The isolation of those terms containing only Wilso-

nian effective action vertices and whose wine is undecorated is shown in figure 7.12.

$$-\frac{1}{4} \sum_{r=0}^n \left[ \begin{array}{ccc} \mathbf{7.24} \rightarrow \mathbf{7.15} & \{ \mathbf{7.25} \ \mathbf{7.51} \} & \{ \mathbf{7.26} \ \mathbf{7.33} \} \\ \begin{array}{c} \textcircled{r^R} \\ \square \\ \textcircled{n_r^R} \end{array} & + & \begin{array}{c} \textcircled{r^R} \\ \circ \\ \textcircled{n_r^R} \end{array} & - 2 & \begin{array}{c} \textcircled{\hat{r}^R} \\ \bullet \\ \textcircled{n_r^R} \end{array} \end{array} \right]^{11\Delta}$$

Figure 7.12: Isolation of the manipulable component of diagram 7.8.

The manipulations to be performed on diagram 7.24 are similar to those of the previous section but are complicated by the fact that the parent diagram is decorated by an effective propagator.

The first consideration is how this effective propagator attaches. In the current case of the wine being undecorated, the effective propagator can either join the two vertices or form a simple loop. This is shown in figure 7.13.

$$-\frac{1}{2} \sum_{r=0}^n \left[ \begin{array}{cc} \mathbf{I.1} & \mathbf{I.2} \\ \begin{array}{c} \textcircled{r^R} \\ \square \\ \textcircled{n_r^R} \end{array} & + & \begin{array}{c} \textcircled{r^R} \\ \textcircled{r^R} \\ \square \\ \textcircled{n_r^R} \end{array} \end{array} \right]^{11}$$

Figure 7.13: Attachment of the effective propagator to diagram 7.24.

In both cases, the attachment of the effective propagator yields a factor of two. In the former case, this is because we can choose which end of the effective propagator to attach to which vertex; in the latter case the factor arises since we can attach the simple loop to either vertex.

We denote the total number of simple loops by  $L$  (which, in this case is either zero or unity) which we decompose into the sum  $L_A + L_B$ , by looking at the number of simple loops on each vertex, separately. The quantity  $J_A$  denotes the total number effective propagators leaving the bottom vertex which attach

to a different structure. In this case, this reduces just to the total number of joins between the two vertices; being either one or two.

When we re-express our manipulable term as a  $\Lambda$ -derivative plus corrections, we must include an overall factor of  $1/J_A$  since the  $\Lambda$ -derivative can reproduce the parent diagram by striking any one of  $J_A$  indistinguishable effective propagators. Thus we see that diagram I.1 will pick up an extra factor of  $1/2$ , compared with diagram I.2. However, by choosing the canonical form for the  $\Lambda$ -derivative term we will find that, remarkably, this relative factor can be incorporated automatically! Consider the form for the  $\Lambda$ -derivative term, shown in figure 7.14.

$$-\frac{1}{16} \sum_{r=0}^n \left[ \begin{array}{c} \mathbf{I.3} \\ \textcircled{r^R} \\ \textcircled{n_r^R} \end{array} \right] \bullet^{11\Delta^2}$$

Figure 7.14: The canonical form of the  $\Lambda$ -derivative term for diagrams I.1 and I.2.

The first thing we must do is define the diagrammatic rules for attachment of the effective propagators. In accord with the discussion of section 7.2.1, each join between the two vertices yields a factor of two. Additionally, if we make  $J_A$  joins from a total of  $J$  effective propagators, then we will take there to be  ${}^J C_{J_A}$  different ways in which we can do this.

These rules now allow us to deduce the overall factor of diagram I.3. Starting from the factor of  $-1/4$  coming from the parent diagram 7.24, there are two additional contributions. First, the promotion of an effective propagator which was previously a wine gives a factor of  $1/2$ . Secondly, if we make just the single join between the vertices, we now have a choice of  $J = 2$  effective propagators with which to do this; we must compensate for this with a factor of  $1/J$ . If we make two joins between the vertices, then (up to interchanging the ends of each propagator), there is only one way we can do this. However, as we have just discussed, such a term must come with an additional factor of

$1/J$ .

Thus by giving the  $\Lambda$ -derivative term a overall factor of  $1/16$ , the contribution corresponding to diagram I.1 acquires a factor of  $1/2$ , relative to the one corresponding to diagram I.2.

Having arrived at a prescription for converting diagram 7.24 into a  $\Lambda$ -derivative term, we can now understand what we have done in a slightly different way, but one that will generalise readily to more complex diagrams.

Referring back to figure 7.14 let us now suppose that, having made the  $J_A$  joins between the two vertices, we allow the  $\Lambda$ -derivative to strike one of these  $J_A$  indistinguishable effective propagators. The resultant diagram, which possesses one wine and  $J_A - 1$  effective propagators, has an overall factor of

$$\frac{J!}{(J - J_A)!(J_A - 1)!} \times 2^{J_A}.$$

The next step is to ‘un-decorate’ by removing the  $J_A - 1$  effective propagators. This reduces the overall factor of the diagram by  $J^{-1}C_{J_A-1} \times 2^{J_A-1}$  which leaves

$$2J.$$

Crucially, the resultant diagram is of exactly the same topology as the parent diagram. In order for it to reproduce the parent diagram, then, we must simply compensate by a factor of  $1/2J$ .

The final ingredient we need to fully process diagram 7.24 is the correction terms to the  $\Lambda$ -derivative. These fall into two classes depending on whether the  $\Lambda$ -derivative strikes one of the vertices or one of the simple loops. In both cases, note that the  $\Lambda$ -derivative term is invariant under interchange of the vertex arguments.

In the latter case, let us suppose that we decorate one of the vertices—say vertex- $B$ —with  $L_B$  simple loops. This can be done in  $J C_{L_B}$  different ways. Allowing the  $\Lambda$ -derivative to strike one of these simple loops and un-decorating the diagram leaves over a factor of  $J$ . This is a very nice result, since it means that this correction term does not include the diagram specific term  $L_B$ . Since the  $\Lambda$ -derivative term is invariant under the interchange of its vertex arguments, we need only consider decorating one of the vertices with simple loops, so long as we multiply by two. The final point about diagrams

in which the  $\Lambda$ -derivative strikes a simple loop is that the effective propagator, forming the simple loop was, by definition, undecorated before being hit by the  $\Lambda$ -derivative. Consequently, it must be undecorated after differentiation, which we denote by enclosing the  $\Lambda$ -derivative in a box.

Finally, we process diagram 7.24 in figure 7.15.

$$\begin{aligned}
 & -\frac{1}{16} \sum_{r=0}^n \left[ \begin{array}{c} \left[ \begin{array}{c} \textcircled{r^R} \\ \textcircled{n_r^R} \end{array} \right] \bullet \\ - 2 \sum_{t=1}^r \left[ 2(r_t - 1)\beta_t \left[ \begin{array}{c} \textcircled{r_t} \\ \textcircled{n_r^R} \end{array} \right] + \gamma_t \left[ \begin{array}{c} \frac{\partial}{\partial \alpha} \textcircled{r_t} \\ \textcircled{n_r^R} \end{array} \right] \right] \\ - \sum_{t=0}^r \left( \left[ \begin{array}{c} \text{7.27} \rightarrow \text{7.17} \\ \textcircled{\tilde{t}} \text{---} \textcircled{\tilde{r}_t} \\ \textcircled{n_r^R} \end{array} \right]_R \right) + \left[ \begin{array}{c} \text{7.28} \\ \textcircled{\Sigma_{r-1}} \\ \textcircled{n_r^R} \end{array} \right] \end{array} \right]^{11\Delta^2} \\
 & + \frac{1}{4} \sum_{r=0}^n \left[ \begin{array}{c} \text{7.29} \rightarrow \text{7.40} \\ \textcircled{\square} \\ \textcircled{r^R} \\ \textcircled{n_r^R} \end{array} \right]^{11\Delta}
 \end{aligned}$$

Figure 7.15: Manipulation of diagram 7.24.

Our next task is to understand the combinatorics associated with decorating the diagrams of figure 7.15. This feature of the first three diagrams and diagram 7.29 has just been discussed, and leads us to the combinatorics for the attachment of effective propagators to diagrams 7.27 and 7.28. We will not explicitly analyse the latter case, since the arguments are just a simplified version of those which apply to the former.

Referring to diagram 7.27, let us consider making  $J_A$  joins between the dumbbell structure and the bottom vertex. For this to be consistent with the diagrammatics of the parent diagram, we know that this must come with a



1, 2, 3—as implied in figure 7.16—we denote the number of joins between the  $i^{\text{th}}$  and  $j^{\text{th}}$  structures by  $J_{ij}$ . Note that  $J_{ii}$  corresponds to a simple loop and that  $J_{ij} = J_{ji}$ . The sum over the total number of joins,  $\sum_{i \leq j} J_{ij}$  must equal  $L_B$ . We denote

$$\sum_{i < j} J_{ij} = L_{B'},$$

which represents the number of joins between separate structures on the dumbbell. The combinatoric factor for decorating the dumbbell structure with the  $L_B$  fields is

$$\begin{aligned} & {}^J C_{L_B} {}^{L_B} C_{L_{B'}} {}^{L_{B'}} C_{J_{12}} {}^{L_{B'}-J_{12}} C_{J_{13}} {}^{L_{B'}-J_{12}-J_{13}} C_{J_{23}} \\ & \times {}^{L_B-L_{B'}} C_{J_{11}} {}^{L_B-L_{B'}-J_{11}} C_{J_{22}} {}^{L_B-L_{B'}-J_{11}-J_{22}} C_{J_{33}} \\ & = \frac{J!}{(J-L_B)! \prod_{i \leq j} (J_{ij}!)} \end{aligned}$$

where we pick up an additional factor of

$$2^{L_{B'}}$$

from the freedom to interchange the ends of the effective propagators joining different structures. Here, too, if we were to attach just the set of effective propagators corresponding to  $J_{ij}$ , then this would come with a combinatoric factor of

$${}^J C_{J_{ij}}.$$

Now that we understand the combinatorics associated with decorating the diagrams of figure 7.15 we wish to identify cancellations. As in section 7.2.2, we begin by isolating two-point, tree level vertices, as shown in figure 7.17.

Diagram 7.30 is an example of the by now familiar case in which an effective propagator attaches to a two-point, tree level vertex. By equation (7.4) it comes with a combinatoric factor of  ${}^2 C_1$ , which has been incorporated.

We now attach the loose end of the effective propagator, which can be done in one of two ways: either we can attach it to the dumbbell structure, or we can attach it to the bottom vertex. Either way, we pick up a factor of two. The results of attaching the loose end, together with application of the effective propagator relation, are shown in figure 7.18.

$$\begin{aligned}
& + \frac{1}{16} \sum_{r=0}^n \left[ \begin{array}{c} \begin{array}{c} \text{7.30} \rightarrow \text{7.18} \\ \begin{array}{c} \circlearrowleft{0^2} \\ \bullet \\ \circlearrowleft{\hat{r}^R} \\ \\ \circlearrowleft{n_r^R} \end{array} \end{array} \right]^{11\Delta} \left[ \begin{array}{c} \begin{array}{c} \text{7.31} \rightarrow \text{7.38} \\ \begin{array}{c} \circlearrowleft{\bar{t}^R} \text{---} \bullet \text{---} \circlearrowleft{\bar{r}_t^R} \\ \\ \circlearrowleft{n_r^R} \end{array} \end{array} \right]^{11\Delta^2} \\
-4 \left[ \begin{array}{c} \begin{array}{c} \text{7.32} \rightarrow \text{7.19} \\ \begin{array}{c} \circlearrowleft{0^2} \\ \bullet \\ \circlearrowleft{0^2} \\ \\ \circlearrowleft{n^R} \end{array} \end{array} \right]^{11\Delta^2} \\
-2 \left[ \begin{array}{c} \begin{array}{c} \circlearrowleft{0^2} \\ \bullet \\ \circlearrowleft{\hat{r}^R} \\ \\ \circlearrowleft{n_r^R} \end{array} \end{array} \right]^{1\Delta^2} \\
- \frac{1}{16} \left[ \begin{array}{c} \begin{array}{c} \text{7.32} \rightarrow \text{7.19} \\ \begin{array}{c} \circlearrowleft{0^2} \\ \bullet \\ \circlearrowleft{0^2} \\ \\ \circlearrowleft{n^R} \end{array} \end{array} \right]^{11\Delta^2}
\end{aligned}$$

Figure 7.17: Isolation of those components of diagram 7.27 containing a two-point, tree level vertex.

Having performed manipulation via the flow equations and having processed one of the generated terms using the effective propagator relation, we find a cancellation, as expected.

**Cancellation 7.3** *Diagram 7.33 exactly cancels diagram 7.26.*

Now we return to diagram 7.32. Upon partial decoration, this will give us new types of diagram. Whilst we have encountered dumbbell structures comprising two two-point, tree level vertices, this is the first time we have also had more than just one effective propagator.

We follow the usual recipe: partially decorate the diagram by attaching fields / effective propagators to the two-point, tree level vertices; tie up all

$$-\frac{1}{2} \sum_{r=0}^n \left[ \begin{array}{c} \{ \text{7.33} \quad \text{7.26} \} \\ \begin{array}{c} \hat{r}^R \\ \bullet \\ n_r^R \end{array} \\ \begin{array}{c} \hat{r}^R \\ \bullet \\ n_r^R \end{array} \end{array} \right] - \begin{array}{c} \hat{r}^R \\ \bullet \\ n_r^R \end{array} \\
+ \left[ \begin{array}{c} \text{7.34} \rightarrow \text{7.40} \\ \begin{array}{c} \bullet \\ \hat{r}^R \end{array} \\ \begin{array}{c} \bullet \\ \hat{r}^R \end{array} \end{array} \right] - \begin{array}{c} \bullet \\ \hat{r}^R \end{array} - \begin{array}{c} \bullet \\ \hat{r}^R \end{array} \\
n_r^R \end{array} \Bigg]^{11\Delta}$$

Figure 7.18: Tying up the loose ends of diagram 7.30, together with application of the effective propagator relation.

loose ends and finally apply the effective propagator relation. The result of this procedure is shown in figure 7.19. Note that we do not include the diagram in which both two-point, tree level vertices are decorated by external fields, since this vanishes at  $\mathcal{O}(p^2)$  and cannot be usefully manipulated. Nor have we drawn those terms in which each of the two-point, tree level vertices is decorated by an effective propagator, the loose ends of which are both attached to the wine. Whilst there is nothing wrong with this, in principle, in this particular case such attachments will use up all the effective propagators but leave us with a loose vertex.

The terms generated fall into three classes, depending on how many times the effective propagator relation has been applied. Ignoring gauge remainders, we are interested in the terms for which it has been applied more than once. We will return to diagram 7.35, in which the relation has been applied once, in section 7.4.1. In the meantime, we focus on diagram 7.36, for which the relation has been applied twice.

**Cancellation 7.4** *Diagram 7.36 has the same structure as diagram 7.4. Irrespective of the value of  $n$ , diagram 7.36 exactly cancels the contributions to diagram 7.4, for which at least one of the external fields decorates the vertex.*

$$\begin{aligned}
& -\frac{1}{2} \left[ \begin{array}{c} \text{Diagram 1} \\ \text{Diagram 2} \\ \text{Diagram 3} \end{array} \right]^{1\Delta} - \frac{1}{4} \left[ \begin{array}{c} \{ 7.35 \quad 7.54 \} \\ \text{Diagram 4} \\ \text{Diagram 5} \end{array} \right]^{11\Delta} \\
& -\frac{1}{2} \left[ \begin{array}{c} \{ 7.36 \quad 7.4(P) \} \\ \text{Diagram 6} \\ -2 \text{ Diagram 7} + \text{Diagram 8} \\ -2 \left( \text{Diagram 9} - \text{Diagram 10} \right) \end{array} \right]^{11}
\end{aligned}$$

Figure 7.19: Partial decoration of diagram 7.32. All loose ends are tied up and the effective propagator relation is applied, as appropriate.

The only remaining contribution to diagram 7.4 is where both external fields decorate the wine i.e. the vertex is a two-point vertex. If  $n > 0$ , this contribution is exactly cancelled by diagram 7.36. However, when  $n = 0$ , this contribution survives, due to the reduction of the vertex in diagram 7.36. Hence, diagram 7.36 only partially cancels diagram 7.4.

This is the cancellation promised in section 7.2.1 in which the non-manipulable components of diagram 7.1 containing uniquely Wilsonian effective action vertices are removed. That the cancellation is between terms generated two levels apart makes perfect sense. We will assume—as will later be proven to be the case—that the cancellation of non-manipulable components of diagrams possessing vertices of unique character occurs due the generation of terms formed by the (repeated) action of  $a_0$  on the partner manipulable component.

Any term generated by the action of  $a_0$  possesses one more vertex than the parent diagram. If the dumbbell structure generated by the action of  $a_0$  contains a two-point, tree level vertex, then the other vertex—assuming, for the time being that it is not a two-point, tree level vertex—must be a seed action vertex. We can, of course, get rid of the two-point, tree level vertex by attaching it to another structure with an effective propagator. However, the remaining term necessarily contains a seed action vertex; indeed, it is this

contribution that cancels those partners of the parent diagram possessing a uniquely seed action vertex.

If we wish to cancel a diagram containing uniquely Wilsonian effective action vertices, then we must iterate the diagrammatic procedure. Focusing on those terms formed by the action of  $a_0$  at each level, we now arrive at diagrams with two more vertices than the original parent. We can choose these extra vertices to both be two-point, tree level vertices, joined by a wine. The remaining loose vertices are Wilsonian effective action vertices. We can now remove both two-point, tree level vertices by attaching different effective propagators to each. One of the resultant terms will cancel the non-manipulable, uniquely Wilsonian effective action contributions to the parent diagram.

We are now left to deal with the cancellation of those terms whose vertex does not have a unique character.

**Cancellation 7.5** *We have seen how diagrams 7.5 and 7.4 have been entirely cancelled by diagrams 7.11 and 7.36 for  $n > 0$  but only partially cancelled for  $n = 0$ . In the latter case, the surviving contributions to each diagram contain a two-point (tree level) vertex. In diagram 7.4, the whole of this contribution survives; in diagram 7.5 only half of it survives. Combining the two terms, we have  $\Pi_{0RS}^{XX}(k)$  which vanishes! Hence, diagram 7.5 partially cancels diagram 7.4.*

*In this way, we have removed all non-manipulable contributions to diagram 7.1.*

### 7.3.2 Diagram 7.7

Having processed the term formed by the action of  $a_1$  at the zeroth level and  $a_0$  at the first level, we now process the partner term, formed by the action of  $a_1$ , at the first level. The manipulable contribution to this diagram is, of course, the Wilsonian effective action contribution for which the wine is undecorated. This latter constraint forces the unattached effective propagator to form a simple loop, giving two simple loops, in total. Hence, when we re-express this term as a  $\Lambda$ -derivative term plus corrections, we must include an overall factor of  $1/2$ , to recognise the indistinguishability of the two simple

loops. The conversion of the manipulable component of diagram 7.7 into a  $\Lambda$ -derivative term plus corrections is shown in figure 7.20. However, since we have not explicitly isolated the manipulable component from the non-manipulable components, these latter diagrams must be included.

$$\begin{aligned}
& \frac{1}{8} \left[ \left[ \begin{array}{c} \textcircled{n_-} \end{array} \right]^\bullet - \sum_{r=1}^{n_-} \left[ 2(n_r - 2)\beta_{n_-} \textcircled{n_-} + \gamma_r \frac{\partial}{\partial \alpha} \textcircled{n_-} \right] \right]^{11\Delta^2} \\
& \quad - \frac{1}{2} \sum_{r=0}^{n_-} \begin{array}{c} \textcircled{\bar{r}} \\ \bullet \\ \textcircled{n_-} \end{array} + \frac{1}{2} \begin{array}{c} \bullet \\ \textcircled{\Sigma_{n-2}} \end{array} \\
& \quad + \frac{1}{4} \left[ \begin{array}{cc} \{ \textbf{7.39} \text{ ??}, \textbf{7.40}(P) \} & \{ \textbf{7.40} \text{ 7.41}, \textbf{7.39}(P) \} \\ \textcircled{n_-} & - 2 \textcircled{\hat{n}_-} \end{array} \right]^{11\Delta}
\end{aligned}$$

Figure 7.20: Result of processing the manipulable component of diagram 7.7. The incomplete cancellation of diagram 7.39 is due to the termination of the explicit computation of  $\beta_{n_+}$  before the diagram required to complete the cancellation is generated.

We see that this figure is similar to figure 7.3; the only differences being the vertex arguments, the number of decorative effective propagators and the relative factor between the diagrams and their corresponding parent. Nonetheless, we can split off the two-point, tree level vertices from diagram 7.37 in exactly the same way as we did with diagram 7.6. This procedure is shown in figure 7.21, where we have also used the effective propagator relation, wherever possible, and have tied up any loose ends.

Compared with the similar procedure performed on the previous level, there is one major difference: when we come to attach an effective propagator to the two-point, tree level vertex, there are two such objects from which to choose. The resulting factor of two will exactly cancel the factor of  $1/2$  arising from the indistinguishability of the simple loops of the parent diagram.

$$\begin{aligned}
& -\frac{1}{16} \sum_{r=0}^{n_-} \left[ \begin{array}{c} \textcircled{\bar{r}^R} \\ \cdot \\ \textcircled{\bar{n}_-^R} \end{array} \right]^{11\Delta^2} + \frac{1}{8\vartheta_{n_-}} \left[ \begin{array}{c} \textcircled{0^2} \\ \cdot \\ \textcircled{\hat{n}_-} \end{array} \right]^{1\Delta^2} \\
& + \frac{1}{2\vartheta_{n_-}} \left[ \begin{array}{c} \{ \textcircled{7.41} \quad \textcircled{7.40} \} \\ \textcircled{\hat{n}_-} \end{array} \right]^{11\Delta} - \left[ \begin{array}{c} \textcircled{\hat{n}_-} \\ \cdot \\ \textcircled{\hat{n}_-} \end{array} \right]^{11\Delta} - \left[ \begin{array}{c} \textcircled{\hat{n}_-} \\ \cdot \\ \textcircled{\hat{n}_-} \end{array} \right]^{11\Delta}
\end{aligned}$$

Figure 7.21: Result of splitting off two-point, tree level vertices from diagram 7.37.

We now find that all components of the parent diagram for which the vertex is uniquely seed action are removed.

**Cancellation 7.6** *Diagram 7.41 partially cancels diagram 7.40. The cancellation is complete for  $n_- > 0$ . In the case where  $n_- = 0$  the contribution containing a two-point vertex is only half removed; all other contributions being completely cancelled.*

Note that, although we have been performing second level manipulations, we only find cancellations that go back a single level. This is because the parent diagram was generated by the repeated action of  $a_1$  alone. Only by generating terms with  $a_0$  do we find cancellations and, since the terms in this section have a history involving at most one instance of  $a_0$ , the cancellations go back just a single level.

Cancellation 7.6 is simply a generalisation of cancellation 7.1 and leads us to the first of the general cancellation mechanisms, of this chapter. Our aim is to show how the non-manipulable components of a diagram formed by the exclusive and repeated action of  $a_1$  cancel. In the process, we will also see how the seed action contributions to a diagram comprising two vertices joined by a wine and decorated by arbitrary number of effective propagators cancel.

To begin, we consider the formation of a level- $J$  term by the repeated action of  $a_1$ . The very first instance of  $a_1$  in this calculation forms the diagram 7.1

which comprises a single vertex and a wine. When we convert this into a  $\Lambda$ -derivative term, this wine is promoted to an effective propagator. The daughter diagram formed by the action of  $a_1$ , diagram 7.7, has the same structure as the parent but is decorated by an additional effective propagator. The loop order of the vertex argument has reduced by one.

Iterating this procedure, it is clear that a level- $J$  term, formed by the repeated action of  $a_1$  comprises a single vertex, a wine and is decorated by the usual external fields and by  $J$  effective propagators. The loop order of this term is  $n - J$ . Consequently,  $J \leq n$  and so the generation of terms by the repeated action of  $a_1$  must ultimately terminate.

Figure 7.22 depicts the separation of the manipulable component of a level- $J$  term formed by the repeated action of  $a_1$ . The curious looking factor,  $\Upsilon_{J,0}$ , is an overall normalisation factor. The reason it is written in this apparently baroque form will become apparent later.

$$\begin{aligned}
 & -\Upsilon_{J,0} \left[ \begin{array}{c} \mathbf{G.1} \\ \text{diagram: two circles, top one has a dot, bottom one has } \Sigma_{n_J} \end{array} \right]^{11\Delta^J} = \\
 & -\Upsilon_{J,0} \left[ \begin{array}{c} \mathbf{G.2} \rightarrow 7.23 \\ \text{diagram: two circles, top one has a square, bottom one has } n_J \end{array} \right. + \left. \begin{array}{c} \{ \mathbf{G.3} \ G.12, G.4(P) \} \\ \text{diagram: two circles, top one has a dot, bottom one has } n_J \end{array} \right. \\
 & \left. - 2 \begin{array}{c} \{ \mathbf{G.4} \ G.8, G.3(P) \} \\ \text{diagram: two circles, top one has a dot, bottom one has } \hat{n}_J \end{array} \right]^{11\Delta^J}
 \end{aligned}$$

Figure 7.22: Isolation of the manipulable component of a level- $J$  diagram, formed by the repeated action of  $a_1$ .

We now manipulate diagram G.2, turning it into a  $\Lambda$ -derivative term plus corrections, as shown in figure 7.23.

Comparing diagrams G.1 and G.6 gives a recursion relation for the normalisation factor:

$$\Upsilon_{J+1,0} = \frac{1}{2} \frac{\Upsilon_{J,0}}{J+1}.$$

$$-\frac{\Upsilon_{J,0}}{J+1} \left[ \left[ \begin{array}{c} \bullet \\ \circlearrowleft n_J \end{array} \right] - \sum_{r=1}^{n_J} \left[ 2(n_J - r - 1)\beta_r - \gamma_r \frac{\partial}{\partial \alpha} \right] \left[ \begin{array}{c} \bullet \\ \circlearrowleft n_{J+r} \end{array} \right] \right]^{11\Delta^{J+1}}$$

$$- \frac{1}{2} \sum_{r=0}^{n_J} \begin{array}{c} \circlearrowleft \bar{r} \\ \bullet \\ \circlearrowleft \bar{n}_{J+r} \end{array} + \frac{1}{2} \begin{array}{c} \bullet \\ \circlearrowleft \Sigma n_{J+1} \end{array}$$

**G.5**  $\rightarrow$  7.24                      **G.6**

Figure 7.23: The result of processing diagram G.2.

Since the zeroth level diagram formed by  $a_1$ , diagram 7.1, has an overall factor of  $1/2$ , this fixes  $\Upsilon_{0,0} = -1/2$ , from which we can determine the normalisation factor:

$$\Upsilon_{J,0} = -\frac{1}{J!} \left(\frac{1}{2}\right)^{J+1}. \quad (7.5)$$

We now proceed in familiar fashion and strip off the two-point, tree level vertices from diagram G.5. Having done this, we partially decorate these vertices, tying up all loose ends and applying the effective propagator relation, as appropriate. The final result of this procedure is shown in figure 7.24

$$\Upsilon_{J+1,0} \left[ \sum_{r=0}^{n_J} \left[ \begin{array}{c} \bullet \\ \circlearrowleft \bar{r}^R \\ \bullet \\ \circlearrowleft \bar{n}_{J+r}^R \end{array} \right]^{11\Delta^{J+1}} - \frac{2}{\vartheta_{n_J}} \left[ \begin{array}{c} \text{wavy line} \\ \bullet \\ \circlearrowleft 0^2 \\ \bullet \\ \circlearrowleft \hat{n}_J \end{array} \right]^{1\Delta^{J+1}} \right]$$

$$- \frac{4(J+1)}{\vartheta_{n_J}} \left[ \begin{array}{c} \bullet \\ \circlearrowleft \hat{n}_J \end{array} \right]^{11\Delta^J} - \left[ \begin{array}{c} \bullet \\ \circlearrowleft \hat{n}_J \end{array} \right]^{11\Delta^J} - \left[ \begin{array}{c} \bullet \\ \circlearrowleft \hat{n}_J \end{array} \right]^{11\Delta^J} \right]$$

**{ G.8 G.4(P) }**

Figure 7.24: Isolation of the two-point, tree level vertices of diagram G.5 and etc.

Noting that  $2(J+1)\Upsilon_{J+1,0} = \Upsilon_{J,0}$ , we find a cancellation.

**Cancellation 7.7** *Diagram G.8 partially cancels diagram G.4. The cancellation is complete for  $n_J > 0$ . In the case where  $n_J = 0$  the contribution to diagram G.3 containing a two-point, tree level vertex is only half removed.*

Since this cancellation is guaranteed to happen, irrespective of the level,  $J$ , this gives our second cancellation mechanism (see section 3.1.6 for the first).

**Cancellation Mechanism 2** *Consider a level- $J$  diagram created by the repeated action of  $a_1$ . The component of this diagram for which the vertex is a Wilsonian effective action vertex and the wine is undecorated can be further manipulated, using the flow equations. This manipulation is guaranteed to produce a further set of terms generated by  $a_0$ . A subset of these terms contain a dumbbell structure for which at least one of the vertices is a two-point, tree level vertex. Attaching the two-point, tree level vertex to the other vertex generates a diagram which, up to gauge remainders, will partially cancel the seed action contributions to the parent diagram.*

*Ignoring these gauge remainders, the cancellation is complete for  $n_J > 0$ . In the case where  $n_J = 0$ , the contribution containing a two-point vertex is only half removed; all other contributions being completely cancelled.*

In order to complete the cancellation of the non-manipulable components of diagram G.1, we must manipulate diagram G.7. The first stage of this is shown in figure 7.25 in which, having separated the manipulable part, we perform the conversion into a  $\Lambda$ -derivative, plus corrections.

The final stage is to strip off the two-point, tree level vertices from diagram G.9, perform the partial decoration of these vertices, tie up all loose ends and apply the effective propagator relation, as appropriate. This is shown in figure 7.26 where, other than the diagram which does not possess any two-point, tree level vertices, we have retained only those diagrams which render diagrams generated earlier in this section completely cancelled.

**Cancellation 7.8** *Diagram G.11 exactly cancels diagram G.10.*

$$\begin{aligned}
& \left[ \begin{array}{c} \left[ \begin{array}{c} \textcircled{r^R} \\ \textcircled{n_{J+r}^R} \end{array} \right]^\bullet \\ -2 \sum_{t=0}^r \left[ 2(r_t - 1)\beta_t \left[ \begin{array}{c} \textcircled{r_t} \\ \textcircled{n_{J+r}^R} \end{array} \right] + \gamma_t \left[ \begin{array}{c} \frac{\partial}{\partial \alpha} \textcircled{r_t} \\ \textcircled{n_{J+r}^R} \end{array} \right] \right] \\ - \sum_{t=0}^r \left( \left[ \begin{array}{c} \mathbf{G.9} \rightarrow 7.26 \\ \textcircled{\bar{t}} \textcircled{\bar{r}_t} \\ \textcircled{n_{J+r}^R} \end{array} \right]_R \right) + \left[ \begin{array}{c} \textcircled{r^R} \\ \textcircled{\Sigma n_{J+r+1}} \end{array} \right] \end{array} \right]^{11\Delta^{J+2}} \\
& - \Upsilon_{J+1,0} \sum_{r=0}^{n_J} \left[ \left[ \begin{array}{c} \textcircled{r^R} \\ \textcircled{\square} \\ \textcircled{n_{J+r}^R} \end{array} \right] - \left[ \begin{array}{c} \textcircled{r^R} \\ \textcircled{\circ} \\ \textcircled{n_{J+r}^R} \end{array} \right] + 2 \left[ \begin{array}{c} \textcircled{\hat{r}^R} \\ \textcircled{\bullet} \\ \textcircled{n_{J+r}^R} \end{array} \right] \right]^{11\Delta^{J+1}}
\end{aligned}$$

Figure 7.25: Manipulation of diagram G.7.

$$\begin{aligned}
& - \Upsilon_{J+2,0} \sum_{r=0}^{n_J} \sum_{t=0}^r \left[ \begin{array}{c} \textcircled{\bar{t}^R} \textcircled{\bar{r}_t^R} \\ \textcircled{n_{J+r}^R} \end{array} \right]^{11\Delta^{J+2}} \\
& + 2\Upsilon_{J+1,0} \sum_{r=0}^{n_J} \left[ \begin{array}{c} \{ \mathbf{G.11} \ G.10 \} \\ \textcircled{\hat{r}^R} \\ \textcircled{\bullet} \\ \textcircled{n_{J+r}^R} \end{array} \right]^{11\Delta^{J+1}} + \Upsilon_{J,0} \left[ \begin{array}{c} \{ \mathbf{G.12} \ G.3(P) \} \\ \textcircled{\circ} \\ \textcircled{n_J^R} \end{array} \right]^{11\Delta^J} + \dots
\end{aligned}$$

Figure 7.26: Isolation of selected components of diagram G.9.

**Cancellation 7.9** *Diagram G.12 partially cancels diagram G.3. The cancellation is complete for  $n_J > 0$ . In the case where  $n_J = 0$  the contribution to diagram G.3 containing a two-point, tree level vertex survives.*

**Cancellation 7.10** *The components of diagrams G.3 and G.4 which survive from cancellations 7.7 and 7.9 exactly cancel.*

The cancellations shown in figure 7.26 give us further cancellation mechanisms. The first cancellation we will promote to a cancellation mechanism is the partial cancellation of diagram G.3 by diagram G.12.

**Cancellation Mechanism 3** *Consider a level- $J$  diagram created by the repeated action of  $a_1$ . Iterating the diagrammatic procedure twice creates a set of terms generated by two instances of  $a_0$  which possess a total of three vertices—two more than the parent diagram. Those terms for which the two extra vertices are both two-point, tree level vertices, each joined to the original vertex by an effective propagator, partially cancel the Wilsonian effective action contributions to the parent diagram, for which the wine is decorated, up to gauge remainders.*

*The cancellation is complete for  $n_J > 0$ . In the case where  $n_J = 0$ , the contribution to the parent diagram containing a two-point, tree level vertex survives; all other contributions being completely cancelled.*

This cancellation mechanism, combined with cancellation mechanism 2 leads to yet another cancellation mechanism.

**Cancellation Mechanism 4** *Consider a level- $J$  diagram created by the repeated action of  $a_1$ . By cancellation mechanisms 2 and 3, all non-manipulable components of this diagram are guaranteed to be cancelled for  $n_J > 0$ . For  $n_J = 0$ , two contributions survive, both of which possess a two-point, tree level vertex. One comes from the Wilsonian effective action contribution to the parent; the other is half of the seed action contribution to the parent. Given that the original vertex argument of the parent is  $\Sigma_{n_J}$ , these contributions are guaranteed to cancel since  $\Pi_{0RS}^{XX}(k) = 0$ .*

Cancellation mechanisms 2–4 thus guarantee that all non-manipulable components of a diagram formed by the repeated action of  $a_1$  are guaranteed to be cancelled, in the computation of  $\beta_{n+}$ .

The final cancellation mechanism of this section arises from the cancellation of diagram G.10 by diagram G.11. This cancellation is for the seed action contribution to a diagram containing a dumbbell structure decorated by any number of effective propagators, provided this number is greater than zero.<sup>7</sup> However, by combining this general cancellation with the specific cancellation 7.2, we can remove this restriction on the number of effective propagators.

**Cancellation Mechanism 5** *Consider a level- $J$  diagram formed by the action of a single instance of  $a_0$  preceded by  $J$  instances of  $a_1$ . Stripping off all two-point, tree level components of the vertices, we arrive at the parent diagram for what follows.*

*The component of this diagram for which both vertices are Wilsonian effective action vertices and the wine is undecorated can be further manipulated, using the flow equations. This manipulation is guaranteed to produce a further set of terms generated by  $a_0$ . A subset of these terms contain a dumbbell comprising a single two-point, tree level vertex and thus, necessarily, also a reduced seed action vertex. If we join this two-point, tree level vertex to the loose Wilsonian effective action vertex then the resulting diagram will exactly cancel the seed action contributions to the parent diagram, up to gauge remainders.*

### 7.3.3 Diagram 7.20

Processing the manipulable component of diagram 7.20 provides us with the first—and simplest—example of the manipulation of a diagram containing more than two vertices. That this diagram is the simplest of its type follows directly from its history: since it is formed by the repeated action of  $a_0$ , it has, upon decoration, the minimum number of joins between structures allowed. Since we will be focusing on the manipulable components of this diagram we do not decorate the wine and so the effective propagator must join one of the wines from the dumbbell structure to the bottom vertex. Although we will

---

<sup>7</sup>This restriction arises because of the way in which we have generated the diagrams: their history involves the action of a single instance of  $a_1$ .

ultimately undo this step, we will make this join, to get a better picture of the issues we will face in converting our diagram into a  $\Lambda$ -derivative term.

Due to the invariance of the dumbbell structure under the interchange of vertex arguments, we need only consider joining one of the constituent vertices to vertex- $A$ , so long as we multiply by two. Once the attachment is made, we will have an additional factor of two coming, as usual, from joining two different structures with an effective propagator. This is shown in figure 7.27.

$$\sum_{r=0}^{n_+} \sum_{t=0}^r \left[ \begin{array}{c} \text{I.4} \\ \textcircled{\overline{t}^R} \\ \square \\ \textcircled{t^R} \\ \textcircled{n_{+r}^R} \end{array} \right]^{11}$$

Figure 7.27: Attaching the effective propagator to the component of diagram 7.20 with an undecorated wine.

It is not immediately clear whether processing this term is of any use since, if we were to cast the manipulable term as a  $\Lambda$ -derivative, we would generate a term in which the  $\Lambda$ -derivative hits the effective propagator joining the bottom vertex to the middle vertex. This would just be of the same topology as the parent and so we would not have gained anything.

The solution is to consider two explicit pairs of values for  $\{r, t\}$ . Figure 7.28 shows diagram I.4 specialised to:

$$\{r, t\} = \{r', t'\}, \{n_+ - r' + t', t'\}.$$

where the constraints  $r \geq t$  and  $n_+ \geq r$  simply imply that  $r' \geq t'$  and that  $n_+ \geq r'$ . We assume, for the time being, that  $r' \neq n_+ - r' + t'$ .

Rotating diagram I.6 by  $\pi$ , it is clear that we can process the manipulable parts of diagrams I.5 and I.6, together. Note that if  $r' = n_+ - r' + t'$  then matters are more complicated. In this case, the two diagrams of figure 7.28 are

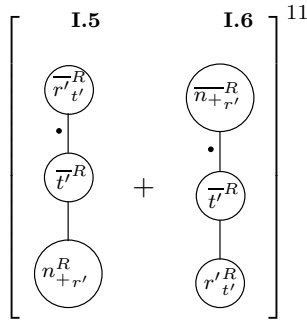


Figure 7.28: Specialisation of diagram I.4 to two specific realisations of  $\{r, t\}$ , which we assume to be different.

identical and, to prevent over-counting, we must multiply by a factor of  $1/2$ . Having included this factor, as appropriate, the manipulable components of diagrams I.5 and I.6 can be processed, irrespective of whether  $r' = n_+ - r' + t'$ . This is shown in figure 7.29, where  $S_{AC}$  is a function of the arguments of the top and bottom vertices; being  $1/2$  when they are the same and unity otherwise.

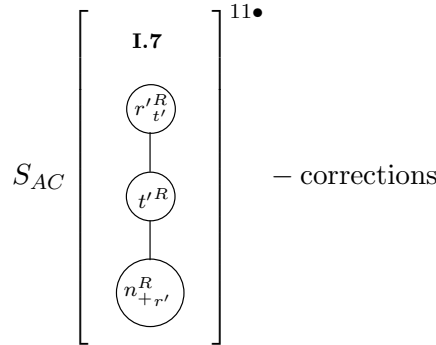


Figure 7.29: Conversion of diagrams I.5 and I.6 into a  $\Lambda$ -derivative term.

Note that we can interpret  $S_{AC}$  as arising due to symmetry properties of diagram I.7 *before we decorate with the external fields*. Diagram I.7 is only invariant under rotations by  $\pi$  when  $r' = n_+ - r' + t'$  and this is, of course, precisely when we must take  $S_{AC} = 1/2$ .

We can, however, be much more intelligent about  $S_{AC}$  and remove it completely by choosing the canonical form for the  $\Lambda$ -derivative term. Let us begin by considering the form for the  $\Lambda$ -derivative term shown in figure 7.30.

$$\frac{1}{16} \sum_{r=0}^{n_+} \sum_{t=0}^r \mathcal{S} \left[ \begin{array}{c} \text{I.8} \\ \circlearrowleft_{t^R} \quad \circlearrowleft_{r_t^R} \\ \circlearrowleft_{n_{+r}^R} \end{array} \right]^{11\Delta^2}$$

Figure 7.30: A trial form for the  $\Lambda$ -derivative term arising from diagram 7.20.

The operator  $\mathcal{S}$  is defined to operate after the attachment of all effective propagators joining different vertices but *before* the attachment of external fields or simple loops. For the time being, we leave it undefined but note that its action can, in principle, depend on any symmetries of the diagram. The overall factor of the diagram requires comment. Starting from the factor of  $1/4$  coming from the parent diagram, there are two additional contributions. First, the promotion of an effective propagator which was previously a wine gives a factor of  $1/2$ , as we know from section 7.2.2. Secondly, having chosen any pair of vertices, we now have a choice of two effective propagators with which to join them; we must compensate for this with a factor of  $1/2$ .

Let us now examine the diagrams corresponding to the following set of values for  $\{r, t\}$ .

$$\{r, t\} = (\{r', t'\}; \{n_+ - r' + t', t'\}; \{n_+ - t', n_+ - r'\}) + t' \rightarrow r' - t'. \quad (7.6)$$

If any particular ordered pair occurs more than once, we discard all but the first instance, to avoid over-counting. It is easy to check that these six realisations correspond to the six permutations of the ordered triplet

$$\{n'_r, t', r'_t\}.$$

where the condition that we do not over-count demands that any particular ordered triplet occurs only once. Hence, if  $m$  of the vertices have the same argument, there are a total of  $3!/m!$  distinct ordered triplets.

The next step is to join together the vertices in figure 7.30. There are  $3!$  ways to order the vertices in a line. Joining the vertices together, this over-counts the number of diagrams by a factor of two, since  $(A-B-C)$  is the same as  $(C-B-A)$ . We must now ascertain whether any of the remaining three

diagrams are indistinguishable. If a diagram has  $m$  vertices with identical argument, then permuting these vertices will produce a set of  $m!$  indistinguishable diagrams. However, if any of these permutations corresponds to rotating the diagram by  $\pi$ , then this permutation has already been counted. Consequently, diagrams not invariant under rotations by  $\pi$  come with a factor of two, relative to those which are thus invariant. Hence, we see that by representing the  $\Lambda$ -derivative term in the form of diagram 7.30, we can completely eliminate  $S_{AC}$ :  $\mathcal{S}$  just reduces to a constant factor,  $2/3!$ , since any symmetries of the diagrams are automatically taken care of!

Once again, having arrived at a prescription for converting diagram 7.20 into a  $\Lambda$ -derivative term, we can interpret the result in a more generalisable manner. To reproduce the manipulable component of diagram 7.20 from diagram I.8 (with  $\mathcal{S} = 2/3!$ ), consider joining any pair of vertices together with either of the effective propagators. There are  ${}^3C_2 \times 2$  different ways to do this, and each of them is identical. Up to an additional factor of two coming from the actual attachment, this is the factor we must take if we desire the  $\Lambda$ -derivative to strike the first effective propagator with which we decorate. Hence, compared to diagram 7.20, diagram I.8 has a relative factor of  $\frac{1}{{}^3C_2 \times 4}$ .

In figure 7.31 we finally process the manipulable components of diagram 7.20.

To isolate the two-point, tree level vertices and perform the subsequent attachments, we simply follow section 7.2.2. The only difference is that, rather than discarding the diagram containing a pair of two-point, tree level vertices, we keep it since the presence of  $> 1$  effective propagators means that we are not compelled to decorate at least one of these vertices with an external field. Figure 7.32 shows the result of proceeding along these lines.

As expected, we now find two cancellations. Since the parent diagram was formed by the action of at least one instance of  $a_0$  (two, in the current case), diagrams just generated cancel diagrams from both of the previous two levels.

**Cancellation 7.11** *Diagram 7.45 exactly cancels diagrams 7.43.*

**Cancellation 7.12** *Diagram 7.46 exactly cancels diagram 7.13.*

$$\begin{aligned}
& \left[ \begin{array}{c} \left[ \begin{array}{c} \textcircled{t^R} \quad \textcircled{r_t^R} \\ \textcircled{n_{+r}^R} \end{array} \right] \bullet \\ -3 \sum_{u=1}^t \left[ \begin{array}{c} (2(t_u - 1)\beta_u + \gamma_u) \frac{\partial}{\partial \alpha} \textcircled{t_u} \quad \textcircled{r_t^R} \\ \textcircled{n_{+r}^R} \end{array} \right] \\ -\frac{3}{2} \left( \sum_{u=0}^t \left[ \begin{array}{c} \textcircled{\bar{t}_u} \\ \bullet \\ \textcircled{\bar{u}} \end{array} \right]_R \textcircled{r_t^R} \textcircled{n_{+r}^R} - \left[ \begin{array}{c} \textcircled{t^R} \\ \textcircled{r_t} \\ \textcircled{\Sigma_{n_r}} \end{array} \right] \right) \end{array} \right]^{11\Delta^2} \\
& \frac{1}{4} \sum_{r=0}^{n_+} \sum_{t=0}^r \left[ \begin{array}{c} \left[ \begin{array}{c} \textcircled{\bar{t}^R} \textcircled{\bar{r}_t^R} \\ \textcircled{n_{+r}^R} \end{array} \right] - 2 \left[ \begin{array}{c} \{ \textcircled{\hat{t}^R} \textcircled{r_t^R} \} \\ \textcircled{n_{+r}^R} \end{array} \right] \end{array} \right]^{11\Delta}
\end{aligned}$$

Figure 7.31: The result of processing the manipulable part of diagram 7.20.

The cancellations we have seen in this section are easily generalised to diagrams containing an arbitrary number of vertices, say  $J+2$ . For our current purposes, we will assume that such diagrams are formed by the repeated action of  $a_0$  only; in other words, their lineage can be traced back to diagram 7.2. At each successive level of manipulation, the term whose manipulable component we will be processing has one more vertex and one more effective propagator compared to the analogous term from the previous level. It is thus the case that a level- $J$  term, formed exclusively by the action of  $a_0$ , possesses  $J+2$  vertices. Two of these vertices are barred and form a dumbbell structure. We take, as usual, the reduced component of these vertices. The remaining  $J$  vertices are all reduced Wilsonian effective action vertices. The diagram as a whole is decorated by the usual external fields and by  $J$  effective propagators.

Before moving on, it is worth discussing such diagrams in further detail.

$$\begin{aligned}
& -\frac{1}{32} \sum_{r=0}^{n_+} \sum_{t=0}^r \left[ \sum_{u=0}^t \left[ \begin{array}{c} \text{7.44} \\ \begin{array}{cc} \begin{array}{c} \bar{t}_u^R \\ \bullet \\ \bar{u}^R \end{array} & \begin{array}{c} r_t^R \\ \phantom{\bullet} \\ n_{+r}^R \end{array} \end{array} \right] \right]^{11\Delta^2} - 16 \left[ \begin{array}{c} \{ \text{7.45} \quad \text{7.43} \} \\ \begin{array}{cc} \begin{array}{c} i^R \\ \bullet \\ r_t^R \end{array} & \begin{array}{c} n_{+r}^R \end{array} \end{array} \right]^{11\Delta} \\
& + \frac{1}{2} \sum_{r=0}^{n_+} \left[ \begin{array}{c} \{ \text{7.46} \quad \text{7.13} \} \\ \begin{array}{c} r^R \\ \circ \\ n_{+r}^R \end{array} \end{array} \right]^{11}
\end{aligned}$$

Figure 7.32: Isolation of the two-point, tree level vertices in diagram 7.42 and etc.

Since the parent diagram has  $J + 2$  vertices and only  $J + 1$  objects with which to join them, (one wine and  $J$  effective propagators), it is not possible to avoid the presence of one-point and/or two-point vertices. This is not an issue, unless such a vertex is tree level, in which case, the diagram is to be discarded. This puts a constraint on the maximum level,  $J_{\max}$ , at which a manipulable diagram occurs. Since the sum of the vertex arguments always adds up to  $n_+$ , we will first be compelled to take a tree level vertex at level- $n$  (where there are  $n + 2$  vertices). With each additional level, we will be compelled to take one further tree level vertex. Hence, if a diagram is compelled to have  $T$  tree level vertices, it must be a level

$$J = n + T - 1 \tag{7.7}$$

diagram.

Since we do not allow one-point or two-point, tree level vertices, each tree level vertex must be decorated by three fields. To maximise the number of tree level vertices we are allowed requires that we minimise the number of fields decorating the remaining vertices. Hence, we suppose that these remaining vertices are each decorated by a single (necessarily internal) field. Temporarily ignoring the external fields, this means that we have  $J + 2 - T$  one point vertices

and  $T$  three-point vertices.

If we now include the two external fields, this allows us to decrease the number of internal fields attached to the tree level vertices by two.

Noting that we have  $2(J+1)$  internal fields, the condition that there be no one-point or two-point, tree level vertices implies that

$$(J+2-T) \times 1 + T \times 3 - 2 \leq 2(J+1)$$

Using equation (7.7) to substitute for  $T$  we obtain:

$$J \leq 2n, \tag{7.8}$$

telling us that  $J_{\max} = 2n$ ; this being last level where the candidate for manipulation is guaranteed not to possess one-point or two-point, tree level vertices. At the next level, however, we will be unable to avoid the appearance of such vertices. Thus, in summary, the final diagram to be manipulated occurs at level- $2n$ ; we call this the critical level. This generates level- $2n+1$  terms but none of these are then manipulated: the diagrammatic procedure terminates.

There is one further property of the level- $J_{\max}$  term whose components we manipulate. Since every field is required to decorate a vertex, for the diagram to survive, this implies that the wine must be undecorated. Hence, *all* Wilsonian effective action contributions to the level- $J_{\max}$  term are manipulable!

In figure 7.33, we show the conversion of a level- $J$  diagram, formed by the repeated action  $a_0$ , into a  $\Lambda$ -derivative term and a correction. Taking into account the factor of two yielded by joining two different vertices with an effective propagator, the parent diagram can be generated in

$$2(J+1)^{J+2} C_2 = (J+2)(J+1)^2$$

different ways from the  $\Lambda$ -derivative term. Hence, the  $\Lambda$ -derivative term comes with the inverse of this factor, relative to the parent. The overall factor of  $\Upsilon_{J,J}$  is a normalisation factor that we will determine at the end.

Notice, in the parent diagram, that we have chosen to join the bottom two vertices with the wine. This is, of course, a choice and is exactly equivalent to joining any other pair of vertices with the wine. However, by doing this,

$$\Upsilon_{J,J} \sum_{r=0}^{n_+} \sum_{t=0}^r \cdots \sum_{y=0}^x \left[ \begin{array}{c} \text{G.13} \\ \circlearrowleft y^R \\ \circlearrowleft x_y^R \\ \vdots \\ \circlearrowleft r_t^R \\ \square \\ \circlearrowleft n_{+r}^R \end{array} \right] + \left[ \begin{array}{c} \text{G.14} \\ \circlearrowleft y^R \\ \circlearrowleft x_y^R \\ \vdots \\ \circlearrowleft r_t^R \\ \circ \\ \circlearrowleft n_{+r}^R \end{array} \right] - 2 \left[ \begin{array}{c} \{ \text{G.15 } G.23 \} \\ \circlearrowleft y^R \\ \circlearrowleft x_y^R \\ \vdots \\ \circlearrowleft \hat{r}_t^R \\ \bullet \\ \circlearrowleft n_{+r}^R \end{array} \right] \Bigg]^{11\Delta^J}$$
  

$$\frac{\Upsilon_{J,J}}{(J+1)^2} \sum_{r=0}^{n_+} \sum_{t=0}^r \cdots \sum_{y=0}^x \left[ \frac{1}{J+2} \left[ \begin{array}{c} \text{G.16} \\ \circlearrowleft y^R \\ \circlearrowleft x_y^R \\ \vdots \\ \circlearrowleft r_t^R \\ \circlearrowleft n_{+r}^R \end{array} \right] \bullet - \left[ \begin{array}{c} \text{G.17} \rightarrow 7.34 \\ \circlearrowleft y^R \\ \circlearrowleft x_y^R \\ \vdots \\ \circlearrowleft r_t^R \\ \circlearrowleft n_{+r}^R \bullet \end{array} \right] \right] \Bigg]^{11\Delta^{J+1}}$$

Figure 7.33: Processing a level- $J$  diagram formed by the repeated action of  $a_0$ .

we make it clear that, in addition to the dumbbell structure, there can be an arbitrary number of additional vertices. Nonetheless, if we are to be absolutely rigorous about the interpretation of the diagrams of figure 7.33, we should really demand that there is a total of at least three vertices.

By demanding that we have at least the dumbbell structure and the vertex labelled by  $y$ , the ellipsis in the sequence of sums over vertex arguments makes sense: in the minimal case of three vertices, all we need do is identify the upper limit on the sum over  $y$  with  $t$ ; for terms with more vertices we simply replace the ellipsis with an appropriate number of extra sums. If we were to take only two vertices of the dumbbell structure, then we would actually have to remove the entire string of sums starting with the sum over  $t$  and ending with the sum over  $y$ . Furthermore, we would also have to remove the  $t$  from the vertex

argument  $r_t$ .

Indeed, since in what follows we will create a term for which the effective propagator relation can be used twice, we will be able to generate diagrams with one vertex less than the parent. If we want to be rigorous about this diagram, we should demand that it has at least three vertices, thereby forcing the parent to have at least four. These issues amount largely to pedantry. We will obtain the correct result by being lax and not worrying too much about the correctness of the notation. Nonetheless, since the cases in which the parent diagram has a total of either two and three vertices have been dealt with explicitly, the rigorous route will also take us where we want to go, so long as we supplement it with the necessary, earlier results.

In diagram G.17 we can allow the  $\Lambda\partial_\Lambda$  to strike any of the vertices; we choose the bottom one. However, upon processing this term, we rewrite the vertex arguments, to bring them into the same form as those of the parent. This is shown in figure 7.34.

The next step is to isolate the two-point, tree level vertices in diagram G.20. Discarding any terms in which two-point, tree level vertices are decorated by external fields, we arrive at the set of diagrams in figure 7.35.

Note that if we are to allow the parent diagram to possess any number of vertices greater than two, then we need to be careful with diagram G.24. This diagram cannot exist if the parent diagram is a zeroth level term and so should be discarded, in this case.

As expected, we find a cancellation.

**Cancellation 7.13** *Diagram G.23 exactly cancels diagram G.15.*

In turn, this cancellation implies a cancellation mechanism.

**Cancellation Mechanism 6** *A level- $J$  diagram formed by the repeated action of  $a_0$  comprises a total of  $J + 2$  vertices, two of which are barred and joined together by a wine. Stripping off all two-point, tree level vertices, we arrive at the parent, for what follows.*

$$\frac{-\Upsilon_{J,J}}{(J+1)^2} \sum_{r=0}^{n_+} \sum_{t=0}^r \cdots \sum_{y=0}^x \left[ \begin{array}{c} \sum_{z=1}^y 2(y_z - 1)\beta_z \left[ \begin{array}{c} \text{G.18} \\ \circlearrowleft y_z \\ \circlearrowleft x_y^R \\ \vdots \\ \circlearrowleft r_t^R \\ \circlearrowleft n_{+r}^R \end{array} \right] + \gamma_z \left[ \begin{array}{c} \text{G.19} \\ \circlearrowleft y_z \\ \circlearrowleft x_y^R \\ \vdots \\ \circlearrowleft r_t^R \\ \frac{\partial}{\partial \alpha} \circlearrowleft n_{+r}^R \end{array} \right] \\ \\ + \frac{1}{2} \sum_{z=0}^y \left( \left[ \begin{array}{c} \text{G.20} \rightarrow 7.35 \\ \circlearrowleft z^R \\ \circlearrowleft y_z^R \\ \circlearrowleft x_y^R \\ \vdots \\ \left[ \begin{array}{c} \circlearrowleft \bar{r}_t \\ \bullet \\ \circlearrowleft \bar{n}_{+r} \end{array} \right]_R \end{array} \right] - \left[ \begin{array}{c} \text{G.21} \\ \circlearrowleft y^R \\ \circlearrowleft x_y^R \\ \vdots \\ \circlearrowleft r_t^R \\ \circlearrowleft \Sigma_{n_r} \end{array} \right] \right) \end{array} \right]^{11\Delta^{J+1}}$$

Figure 7.34: The result of processing diagram G.17.

The component of this diagram for which all vertices are Wilsonian effective action vertices and the wine is undecorated can be further manipulated, using the flow equations. This manipulation is guaranteed to produce a further set of terms generated by  $a_0$ . A subset of these terms contain a dumbbell comprising a single two-point, tree level vertex and thus, necessarily, also a reduced seed action vertex. If we sum over the identical diagrams formed upon joining this two-point, tree level vertex to each of the loose Wilsonian effective action vertices then the resulting diagram will exactly cancel the seed action contributions to the parent diagram. In this scenario, gauge remainders automatically vanish.

Our next task is to find an expression for  $\Upsilon_{J,J}$ . Comparing diagrams G.22

$$2\Upsilon_{J,J} \sum_{r=0}^{n_+} \sum_{t=0}^r \cdots \sum_{x=0}^w \left[ -\frac{1}{4(J+1)^2} \sum_{y=0}^x \sum_{z=0}^y \begin{array}{c} \text{G.22} \\ \circlearrowleft z^R \\ \circlearrowleft y_z^R \\ \circlearrowleft x_y^R \\ \vdots \\ \circlearrowleft \hat{r}_t^R \\ \bullet \\ \circlearrowleft \hat{n}_{+r}^R \end{array} \right]^{11\Delta^{J+1}} \\
+ \sum_{y=0}^x \left[ \begin{array}{c} \{ \text{G.23 } G.15 \} \\ \circlearrowleft y^R \\ \circlearrowleft x_y^R \\ \vdots \\ \circlearrowleft \hat{r}_t^R \\ \bullet \\ \circlearrowleft \hat{n}_{+r}^R \end{array} \right]^{11\Delta^J} + J^2 \left[ \begin{array}{c} \text{G.24} \\ \circlearrowleft x^R \\ \circlearrowleft w_x^R \\ \vdots \\ \circlearrowleft r_t^R \\ \circ \\ \circlearrowleft n_{+r}^R \end{array} \right]^{11\Delta^{J-1}}$$

Figure 7.35: Isolation of two-point, tree level vertices in diagram G.20, and the results of their subsequent decoration. Diagrams possessing a two-point, tree level vertex decorated by an external field have, together with any gauge remainders, been discarded.

and G.13, we see that

$$\Upsilon_{J+1,J+1} = -\frac{\Upsilon_{J,J}}{2(J+1)^2}. \quad (7.9)$$

Since diagram 7.2 tells us that  $\Upsilon_{0,0} = -1/2$ , it follows that

$$\Upsilon_{J,J} = \frac{1}{(J!)^2} \left(-\frac{1}{2}\right)^{J+1}. \quad (7.10)$$

Let us now consider iterating the diagrammatic procedure by processing the manipulable component of diagram G.22. In making this step, we have implicitly assumed that  $J < J_{\max}$ .

The result of this manipulation is simply to reproduce figures 7.33–7.35 but with  $J \rightarrow J+1$ . The level- $J+1$  version of diagram G.23 will just cancel the seed action components of diagram G.22, by cancellation mechanism 6. The level- $J+1$  version of diagram G.24 comes with an overall factor of  $2(J+1)^2 \Upsilon_{J+1,J+1}$  which, by equation (7.9) is just equal to  $-\Upsilon_{J,J}$ . Hence, this diagram exactly cancels diagram G.14.

The cancellation of seed action contributions is always guaranteed to occur. Even if it is the case that we are manipulating a level- $J_{\max}$  term, we still generate level- $J_{\max} + 1$  terms, one of which will cancel the seed action contributions to the parent. However, the level- $J_{\max} + 1$  candidate for manipulation will vanish, apparently meaning that we will not generate the diagrams to cancel the remaining Wilsonian effective action contribution to the level- $J_{\max}$  parent. However, as we have already noted, all Wilsonian effective action contributions to a level- $J_{\max}$  diagram are manipulable! Hence, the cancellation of all non-manipulable Wilsonian effective action contributions is guaranteed, also.

With these points in mind, we arrive at another cancellation mechanism.

**Cancellation Mechanism 7** *A level- $J$  diagram formed by the repeated action of  $a_0$  comprises a total of  $J + 2$  vertices, two of which are barred and joined together by a wine. Stripping off all two-point, tree level vertices, we arrive at the parent, for what follows.*

*Assuming that we can iterate the diagrammatic procedure twice then, amongst the terms we generate, is a diagram with  $J + 2$  reduced vertices plus an additional dumbbell structure. Focusing on the case where the two vertices comprising the dumbbell are two-point, tree level vertices, we now join each of these*

to a different, loose vertex. Summing over all ways of doing this, the resulting term will exactly cancel the remaining Wilsonian effective action contributions to the original parent diagram.

*In case that the diagrammatic procedure terminates with the generation of level- $J+1$  terms, the only Wilsonian effective action contributions to the parent diagram are those without a decorated wine i.e. those which have already been manipulated.*

*In this scenario, gauge remainders automatically vanish.*

We can now use cancellation mechanisms 6 and 7 to describe the ultimate fate of diagram 7.2 and all of its children. When the diagrammatic procedure has been iterated until exhaustion, only four types of term will remain: those at each level which are analogous to diagrams G.16, G.18, G.19 and G.21. All the rest are either processed, cancelled or discarded. Those in the latter class have been discarded either at  $\mathcal{O}(p^2)$  or as a consequence of the constraint  $S_m^1(0) = 0$ . It is actually the case that certain components of the surviving diagrams could also be discarded, for just these reasons. However, as certain components of such diagrams do survive, we choose to keep the entire diagram, for the time being.

This allows us to write the result of exhaustively manipulating diagram 7.2 in a fantastically compact form. We begin by introducing the vertex arguments,  $V^J$ , where upper roman indices act simply as labels. To make contact with the current computation,  $V^{J=0} = n_+$ . Next, we introduce the compact notation

$$V^{J,J_+} \equiv V^J - V^{J+1} \quad (7.11)$$

$$V^{J,J_+;R} = V^{J;R} - V^{J+1;R} \quad (7.12)$$

where

$$V^{J;R} = (V^J)^R.$$

Finally, we define

$$\bigcirc_{n_+, J} \equiv \prod_{I=0}^J \sum_{V^{I_+}=0}^{V^I} \bigcirc_{V^{I,J_+;R}} \quad (7.13)$$

where the first argument gives the value of  $V^0$ .

Now we can give a diagrammatic expression for the result of exhaustively manipulating diagram 7.2, as shown in figure 7.36.

$$\sum_{J=0}^{2n} \frac{\Upsilon_{J,J}}{(J+1)^2} \left[ \begin{array}{c} \frac{1}{J+2} \left[ \begin{array}{c} \textcircled{V^{J+1;R}} \\ \textcircled{n_+, J} \end{array} \right] \bullet \\ - \sum_{V^{J+2}=1}^{V^{J+1}} 2(V^{J+1, J+2} - 1) \beta_{V^{J+2}} \left[ \begin{array}{c} \textcircled{V^{J+1, J+2}} \\ \textcircled{n_+, J} \end{array} \right] \\ - \sum_{V^{J+2}=1}^{V^{J+1}} \gamma_{V^{J+2}} \left[ \begin{array}{c} \frac{\partial}{\partial \alpha} \textcircled{V^{J+1, J+2}} \\ \textcircled{n_+, J} \end{array} \right] \\ - \left[ \begin{array}{c} \textcircled{\bullet} \\ \textcircled{\Sigma_{V^{J+1}-1}} \\ \textcircled{n_+, J} \end{array} \right] \end{array} \right]^{11\Delta^{J+1}}$$

Figure 7.36: Final result of the exhaustive manipulation of diagram 7.2.

## 7.4 Level-Three Manipulations

As with the previous level of manipulation, we find that there is an excess of candidates for manipulation. In keeping with what went before, we use the following prescription for choosing which terms to manipulate. We begin by only considering terms formed by the exclusive action of  $a_0$  and  $a_1$  (as opposed to e.g. terms formed by the  $\Lambda\partial_\Lambda$  striking a simple loop). Of these, we further restrict our choice to those for which the final operation was by an  $a_0$  unless

the diagram was formed exclusively by the action of  $a_1$ .

This leaves us with three candidates for manipulation: diagrams 7.31, 7.38 and 7.44. All but the first of these have been implicitly dealt with as a consequence of the generalised manipulations of the previous section and so are not considered further.

As for diagram 7.31 we find, as we might suspect, that its seed action contributions are cancelled upon processing the manipulable part. This leaves over the non-manipulable, Wilsonian effective action contribution. Again, we suspect that this will be cancelled upon iterating the diagrammatic procedure, but we will not get to see this explicitly. Rather, the initial manipulation of diagram 7.31 will guide us toward a set of cancellation mechanisms, one of which guarantees the cancellation of the remaining Wilsonian effective action contribution to diagram 7.31.

Indeed, the cancellation mechanisms obtained in the section will complete the set of rules required to show that  $\beta_{n_+}$  can, up to gauge remainders and terms which require manipulation at  $\mathcal{O}(p^2)$ , be expressed as a set of  $\Lambda$ -derivative,  $\alpha$  and  $\beta$ -terms.

#### 7.4.1 Diagram 7.31

We will now use the insights of section 7.3.3, in which we processed diagram 7.20, to process diagram 7.31. These two diagrams are of a very similar structure. However, in the latter case, we have an additional effective propagator with which to decorate. This greatly increases the number of different topologies which can be constructed. The compensation for this is that the sum over vertex arguments decreases by one.

Let us consider the manipulable component of diagram 7.31. Since, in this case, the wine is undecorated, we must use one of the effective propagators to make a join between the loose vertex and either of the other two. So far, this is just the same as with diagram 7.20. The real difference occurs with the attachment of the remaining effective propagator, with which we can do one of two things: form a simple loop or join any pair of vertices. However, despite this apparent complexity, the conversion into a  $\Lambda$ -derivative term is remarkably simple.

As we did with diagram 7.20, let us try constructing the  $\Lambda$ -derivative term by promoting the wine to a decorative effective propagator, as shown in figure 7.37. The currently undetermined parameter,  $\mathcal{S}'$ , could, in principle, depend on the structure of the diagram after all joins between vertices have been made.

$$\frac{1}{16} \sum_{r=0}^n \sum_{t=0}^r \mathcal{S}' \left[ \left[ \begin{array}{cc} \textcircled{t^R} & \textcircled{r_t^R} \\ & \textcircled{n_r^R} \end{array} \right] \right]^{\bullet 11\Delta^3}$$

Figure 7.37: A trial form for the  $\Lambda$ -derivative term arising from diagram 7.31.

From this diagram, the can generate the parent diagram in

$${}^3C_2 \times 2 \times {}^3C_1 = 18$$

different ways. (We choose two vertices from three, and one effective propagator from three, which can attach either way round) Thus  $\mathcal{S}'$  just reduces to a constant factor of  $1/18$ . In figure 7.38 we process diagram 7.31. Due to the indistinguishability of the three vertices of the  $\Lambda$ -derivative term, we need only compute the flow of one of these, so long as we multiply by three.

The correction term formed by the  $\Lambda\partial_\Lambda$  striking a simple loop, diagram 7.48, can be formed in nine ways as we can choose any one of three effective propagators to decorate any of the three vertices. The final two diagrams in the figure are just the un-manipulated components of the parent diagram.

In figure 7.39, we show the effect of isolating the two-point, tree level vertices belonging to diagram 7.47. These vertices have been decorated, any loose ends tied up and the effective propagator relation has been applied.

As expected, we find a number of cancellations between diagrams from this level and the previous two. The first two cancellations, as we will see shortly, can be described by the generalisation of cancellation mechanisms 6 and 7.

$$\begin{aligned}
& \frac{1}{288} \sum_{r=0}^n \sum_{t=0}^r \left[ \begin{array}{c} \left[ \begin{array}{cc} t^R & r_t^R \\ & n_r^R \end{array} \right] \bullet \\ -3 \sum_{u=1}^t \left[ 2(t_u - 1) \beta_u \left[ \begin{array}{cc} t_u & r_t^R \\ & n_r^R \end{array} \right] + \gamma_u \left[ \begin{array}{cc} \frac{\partial}{\partial \alpha} t_u & r_t^R \\ & n_r^R \end{array} \right] \right] \\ -\frac{3}{2} \left( \sum_{u=0}^t \left[ \begin{array}{cc} \tilde{t}_u & r_t^R \\ \bullet & n_r^R \\ \bar{u} & \end{array} \right] - \left[ \begin{array}{c} t^R \\ r_t^R \\ \bullet \\ \Sigma_{n_{r+1}} \end{array} \right] \right) \end{array} \right]^{11\Delta^3} \\
& -\frac{1}{16} \sum_{r=0}^n \sum_{t=0}^r \left[ \frac{1}{2} \left[ \begin{array}{c} \mathbf{7.48} \\ t^R \\ r_t^R \\ \square \\ \text{---} \\ n_r^R \end{array} \right] - \left[ \begin{array}{cc} \bar{t}^R & \bar{r}_t^R \\ & n_r^R \end{array} \right] + 2 \left[ \begin{array}{c} \{ \mathbf{7.49} \quad \mathbf{7.50} \} \\ \hat{t}^R \bullet r_t^R \\ n_r^R \end{array} \right] \right]^{11\Delta^2}
\end{aligned}$$

Figure 7.38: The result of processing diagram 7.31.

$$\begin{aligned}
& -\frac{1}{192} \sum_{r=0}^n \sum_{t=0}^r \sum_{u=0}^t \left[ \begin{array}{c} \overline{t}_u^R \\ \bullet \\ \overline{u}^R \end{array} \quad \begin{array}{c} r_t^R \\ n_r^R \end{array} \right]^{11\Delta^3} - 24 \left[ \begin{array}{c} \{ 7.50 \quad 7.49 \} \\ \hat{t}^R \\ \bullet \\ r_t^R \\ n_r^R \end{array} \right] - \left[ \begin{array}{c} \hat{t}^R \\ \bullet \\ r_t^R \\ n_r^R \end{array} \right]^{11\Delta^2} \\
& + \frac{1}{16} \sum_{r=0}^n \sum_{t=0}^r \frac{1}{6} \left[ \begin{array}{c} \hat{t}^R \\ \bullet \\ 0^2 \\ \text{wavy} \end{array} \quad \begin{array}{c} r_t^R \\ n_r^R \end{array} \right]^{1\Delta^3} + \left[ \begin{array}{c} \hat{t}^R \\ \bullet \\ \hat{t}^R \\ \bullet \\ r_t^R \\ n_r^R \end{array} \right]^{11\Delta^2} \\
& + \frac{1}{16} \sum_{r=0}^n \left[ \begin{array}{c} 0^2 \\ r^R \\ n_r^R \end{array} \right]^{11\Delta^2} + 4 \left[ \begin{array}{c} \{ 7.51 \quad 7.25 \} \\ r^R \\ \bullet \\ n_r^R \end{array} \right] - 2 \left[ \begin{array}{c} r^R \\ \bullet \\ n_r^R \end{array} \right] + \left[ \begin{array}{c} r^R \\ \bullet \\ n_r^R \end{array} \right]^{11\Delta} \\
& + \frac{1}{4} \sum_{r=0}^n \left[ \begin{array}{c} \text{7.52} \rightarrow 7.40 \\ \hat{t}^R \\ \bullet \\ r^R \\ n_r^R \end{array} \right] - 2 \left[ \begin{array}{c} \hat{t}^R \\ \bullet \\ r^R \\ n_r^R \end{array} \right] + \left[ \begin{array}{c} \hat{t}^R \\ \bullet \\ r^R \\ n_r^R \end{array} \right] - 2 \left( \left[ \begin{array}{c} \bullet \\ \hat{t}^R \\ r^R \end{array} \right] - \left[ \begin{array}{c} \bullet \\ \hat{t}^R \\ r^R \end{array} \right] \right) \\
& + \frac{1}{16} \sum_{r=0}^n \left[ \begin{array}{c} \left[ \begin{array}{c} \bullet \\ 0^2 \\ \text{wavy} \end{array} \right] \\ r^R \\ n_r^R \end{array} \right] - \left[ \begin{array}{c} \left[ \begin{array}{c} \bullet \\ 0^2 \\ \text{wavy} \end{array} \right] \\ r^R \\ n_r^R \end{array} \right] + 2 \left[ \begin{array}{c} \left[ \begin{array}{c} \bullet \\ 0^2 \\ \text{wavy} \end{array} \right] \\ r^R \\ n_r^R \end{array} \right] - \left[ \begin{array}{c} \left[ \begin{array}{c} \bullet \\ 0^2 \\ \text{wavy} \end{array} \right] \\ r^R \\ n_r^R \end{array} \right] \right]^{1\Delta^2}
\end{aligned}$$

Figure 7.39: Isolation of two-point, tree level vertices in diagram 7.47 and etc.

**Cancellation 7.14** *Diagram 7.50 exactly cancels diagram 7.49.*

**Cancellation 7.15** *Diagram 7.51 exactly cancels diagram 7.25.*

The remaining cancellation is similar to something we have already seen, but in a different context—as we will discuss shortly. First, though, recall how, in section 7.3, we chose not to manipulate diagram 7.17 since we claimed that it would be partially cancelled by terms arising from the manipulation of diagram 7.8. We now see that this diagram is, in fact, *completely* cancelled by terms arising from the *iterated* manipulation of diagram 7.8.

**Cancellation 7.16** *Diagram 7.52 is very similar to diagram 7.29. They have the same vertex arguments, the same overall factor and are decorated by the same set of fields. However, in the former case, the explicitly drawn wine—which forms a simple loop—must be undecorated. In the latter case, this wine must be decorated. Hence, we can combine the diagrams by taking either one of them and removing the restriction on the decoration of the wine. This new diagram can then be combined with diagram 7.34 to give the first diagram in figure 7.40.*

*Let us analyse the topmost vertex. The restriction that this vertex be reduced excludes the case  $\Sigma_0^2 = -S_0^2$ . However, this contribution is exactly provided by diagram 7.35. By including this term, we are left with only the first diagram on the second line of figure 7.40. Finally, then, this diagram exactly cancels diagram 7.17.*

It is apparent that cancellation 7.16 has much in common with the combination of cancellations 7.1, 7.4 and 7.5. In each case we are cancelling components of a diagram containing a structure formed by the action of  $a_1$ . In the latter case, this is all that the diagram contains and so the cancellations arise from manipulating this structure directly. In the former case, however, the structure is formed after the action of an  $a_0$  on the previous level and so we have chosen not to manipulate it.

Had we chosen to manipulate it, the cancellation of the seed action contribution and the Wilsonian effective action contributions with decorated wine

$$\begin{aligned}
7.52 + 7.29 + 7.34 &= \frac{1}{4} \sum_{r=0}^n \left[ \begin{array}{c} \textcircled{\Sigma_r^R} \\ \textcircled{n_r^R} \end{array} \right]^{11\Delta} \\
&= \frac{1}{4} \sum_{r=0}^n \left[ \begin{array}{c} \{ 7.53 \quad 7.17 \} \\ \textcircled{\Sigma_r} \\ \textcircled{n_r^R} \end{array} \right] - \left[ \begin{array}{c} \{ 7.54 \quad 7.35 \} \\ \textcircled{\Sigma_0^2} \\ \textcircled{n^R} \end{array} \right]^{11\Delta}
\end{aligned}$$

Figure 7.40: Showing how diagrams 7.52, 7.29, 7.34 and 7.35 combine to cancel diagram 7.17.

would then have proceeded in exactly the same way as cancellations 7.1, 7.4 and 7.5. However, there would be additional contributions arising from the  $\Lambda\partial_\Lambda$  striking other structures in the diagram. This, in turn, would then have affected our manipulation of diagram 7.8, since it would have removed the manipulable contributions containing simple loops.

To generalise the cancellations just seen, we will again consider a level- $J$  diagram, but this time allow decoration by any (legal) number of effective propagators. To ensure that the relationship between the number of vertices, the vertex arguments and the number of effective propagators is correct, we will start by analysing the way in which manipulable diagrams are formed.

We assume that we have a manipulable diagram and that we have promoted the wine to a decorative effective propagator, thereby converting the diagram into a  $\Lambda$ -derivative term. We know that the diagram has been formed by the repeated action of  $a_1$ s and  $a_0$ s but assume that any instances of  $a_1$ s are consecutive and not preceded by any instances of  $a_0$ .

In terms of the  $\Lambda$ -derivative term that has been formed, it is the case that each instance of  $a_0$  has contributed a vertex and an effective propagator, whilst leaving the sum of the vertex arguments the same. Each instance of  $a_1$  has contributed an effective propagator, has decreased the sum of the vertex arguments by one but left the number of vertices the same. Both  $a_0$  and  $a_1$

contribute a factor of  $1/2$  each time they act. The former comes with a relative factor of  $-1$ .

If we define  $s$  to be the number of times  $a_1$  has acted, then a generic level- $J$   $\Lambda$ -derivative term possesses  $J + 2 - s$  vertices, the sum of whose arguments adds up to  $n_+ - s$ . These vertices are decorated by the usual external fields and by  $J + 1$  effective propagators.

Since we have already considered, in section 7.3.2, diagrams formed by the exclusive action of  $a_1$ , we consider in this section those diagrams for which  $a_0$  has acted at least once.

The treatment of these terms is simply a generalisation of what we did in section 7.3.3. The first thing to note is that the presence of more than one vertex implies the action of at least one instance of  $a_0$ , which gives the condition that

$$J \geq s. \quad (7.14)$$

Compared to the case in section 7.3.3, there are a number of changes we must make. First, we replace  $\Upsilon_{J,J}$  by  $\Upsilon_{J,J-s}$  where it is straightforward to show that

$$\Upsilon_{J,J-s} = \frac{1}{J!(J-s)!} \left(\frac{1}{2}\right)^s \left(-\frac{1}{2}\right)^{J+1-s}. \quad (7.15)$$

It is clear that this expression is consistent with our previous expression of both  $\Upsilon_{J,J}$  and  $\Upsilon_{J,0}$  (see equations 7.10 and 7.5).

The second change that we must make is to the level at which the diagrammatics terminates. Compared to the terms in section 7.3.3, a manipulable diagram now has  $J + 2 - s$  vertices, rather than  $J + 2$ . Thus, from equation 7.8, such a diagram will last appear at level

$$J \leq 2n + s, \quad (7.16)$$

meaning that the diagrammatic procedure terminates at level  $2n + s + 1$ . We emphasise that the critical level now depends on  $s$ .

Thirdly, after casting the manipulable term as a  $\Lambda$ -derivative, we must now admit the possibility of the  $\Lambda\partial_\Lambda$  striking a simple loop. Lastly, we can no longer discard either gauge remainders or two-point, tree level vertices decorated by external fields.

Figure 7.41 shows the starting point for the manipulations: a level- $J$  diagram for which the manipulable term has been isolated. Again, to be rigorous, the diagrams of this figure should, strictly speaking, possess at least three vertices and to be rigorous in what follows, at least four. However, it is clear by now that the results we obtain will be valid, so long as we are careful with how we interpret the diagrams. We note further that the case of just two vertices has, of course, been treated in complete generality in section 7.3.2.

$$\Upsilon_{J,J-s} \sum_{r=0}^{n_{s-1}} \sum_{t=0}^r \cdots \sum_{y=0}^x$$

$$\times \left[ \begin{array}{c} \text{G.25} \rightarrow 7.42 \\ \circlearrowleft y^R \\ \circlearrowleft x_y^R \\ \vdots \\ \circlearrowleft r_t^R \\ \square \\ \circlearrowleft n_{s+r-1}^R \end{array} \right] + \left[ \begin{array}{c} \text{G.26} \\ \circlearrowleft y^R \\ \circlearrowleft x_y^R \\ \vdots \\ \circlearrowleft r_t^R \\ \circ \\ \circlearrowleft n_{s+r-1}^R \end{array} \right] - 2 \left[ \begin{array}{c} \{ \text{G.27} \ \text{G.30} \} \\ \circlearrowleft y^R \\ \circlearrowleft x_y^R \\ \vdots \\ \circlearrowleft r_t^R \\ \bullet \\ \circlearrowleft \hat{n}_{s+r-1}^R \end{array} \right] \Bigg]^{11\Delta^J}$$

Figure 7.41: Isolation of the manipulable part of a level- $J$  diagram.

Figure 7.42 shows the result of performing the manipulations (including isolation of two-point, tree level vertices and etc.) where we have not explicitly drawn the  $\Lambda$ -derivative,  $\beta$  and  $\gamma$ -terms, gauge remainders and diagrams which require manipulation at  $\mathcal{O}(p^2)$ .

**Cancellation 7.17** *Diagram G.30 exactly cancels diagram G.27.*

A cancellation mechanism follows trivially from cancellation G.30.

**Cancellation Mechanism 8** *A level- $J$  diagram formed by  $s$  consecutive instances of  $a_1$  followed by  $J-s+1$  instances of  $a_0$  possesses a dumbbell structure and an additional  $J-s$  reduced vertices. The diagram as a whole is decorated by the usual external fields and  $J+1$  effective propagators. Stripping off any*

$$\begin{aligned}
& \Upsilon_{J+1, J+1-s} \sum_{r=0}^{n_{s-1}} \sum_{t=0}^r \cdots \sum_{z=0}^y \left[ \begin{array}{c} \text{G.28} \\ \circlearrowleft z^R \\ \circlearrowleft y_z^R \\ \vdots \\ \circlearrowleft \bar{r}_t^R \\ \bullet \\ \circlearrowleft \bar{n}_{s+r-1}^R \end{array} \right] - \sum_{r=0}^{n-s} \sum_{t=0}^r \cdots \sum_{y=0}^x \left[ \begin{array}{c} \text{G.29} \\ \circlearrowleft y^R \\ \circlearrowleft x_y^R \\ \vdots \\ \circlearrowleft r_t^R \\ \bullet \\ \circlearrowleft \Sigma_{n_{s+r}} \end{array} \right] \Bigg]^{11\Delta^{J+1}} \\
& + \Upsilon_{J, J-s} \sum_{r=0}^{n_{s-1}} \sum_{t=0}^r \cdots \sum_{y=0}^x 2 \left[ \begin{array}{c} \{ \text{G.30 } G.27 \} \\ \circlearrowleft y^R \\ \circlearrowleft x_y^R \\ \vdots \\ \circlearrowleft r_t^R \\ \bullet \\ \circlearrowleft \hat{n}_{s+r-1}^R \end{array} \right] - \frac{1}{J+1-s} \left( \left[ \begin{array}{c} \text{G.31} \\ \circlearrowleft y^R \\ \circlearrowleft x_y^R \\ \vdots \\ \circlearrowleft r_t^R \\ \bullet \\ \circlearrowleft \Sigma_{n_{s+r-1}} \end{array} \right] - \left[ \begin{array}{c} \text{G.32} \\ \circlearrowleft y^R \\ \circlearrowleft x_y^R \\ \vdots \\ \circlearrowleft r_t^R \\ \circ \\ \circlearrowleft n_{s+r-1}^R \end{array} \right] \right) \Bigg]^{11\Delta^J} \\
& + \sum_{r=0}^{n_{s-1}} \sum_{t=0}^r \cdots \sum_{x=0}^w 2J \Upsilon_{J, J-s} \left[ \begin{array}{c} \text{G.33} \\ \circlearrowleft x^R \\ \circlearrowleft w_x^R \\ \vdots \\ \circlearrowleft r_t^R \\ \circ \\ \circlearrowleft n_{s+r-1}^R \end{array} \right] - \Upsilon_{J-1, J-1-s} \left[ \begin{array}{c} \text{G.34} \\ \circlearrowleft x^R \\ \circlearrowleft w_x^R \\ \vdots \\ \circlearrowleft r_t^R \\ \circ \\ \circlearrowleft n_{s+r-1}^R \end{array} \right] \Bigg]^{11\Delta^{J-1}} + \cdots
\end{aligned}$$

Figure 7.42: Selected terms arising from the manipulation of diagram G.25.

remaining two-point, tree level vertices, we arrive at the parent diagram for what follows.

The component of this diagram for which the vertices are Wilsonian effective action vertices and the wine is undecorated can be further manipulated, using the flow equations. This manipulation is guaranteed to produce a further set of terms generated by  $a_0$ . A subset of these terms contain a dumbbell comprising a single two-point, tree level vertex and thus, necessarily, also a reduced, seed action vertex. If we join this two-point, tree level vertex to one of the loose (reduced) Wilsonian effective action vertices then the resulting diagram will exactly cancel the seed action contributions to the parent diagram, up to gauge remainders.

The remaining cancellation mechanisms require a little more work. First, consider diagram G.34. The level- $J + 1$  version of this diagram, assuming that it exists, will exactly cancel diagram G.26. This is what we expect, since we know that diagrams containing exclusively Wilsonian effective action vertices and decorated wines always cancel diagrams coming two levels down the line. Again, if the diagrammatic procedure terminates at level- $J + 1$ , then this implies that the only Wilsonian effective action contributions to the parent diagram are manipulable.

**Cancellation Mechanism 9** *A level- $J$  diagram formed by  $s$  consecutive instances of  $a_1$  followed by  $J - s + 1$  instances of  $a_0$  possesses a dumbbell structure and an additional  $J - s$  reduced vertices. The diagram as a whole is decorated by the usual external fields and  $J + 1$  effective propagators. Stripping off any remaining two-point, tree level vertices, we arrive at the parent diagram for what follows.*

*Assuming that we can iterate the diagrammatic procedure twice then, amongst the terms we generate, is a diagram with  $J - s + 2$  reduced vertices plus an additional dumbbell structure. Focusing on the case where the two vertices comprising the dumbbell are two-point, tree level vertices, we now join each of these to a different, loose vertex. Summing over all ways of doing this, the resulting term will exactly cancel the remaining Wilsonian effective action contributions to the original parent diagram, up to gauge remainders.*

*In case that the diagrammatic procedure terminates with the generation of level- $J+1$  terms, the only Wilsonian effective action contributions to the parent diagram are those without a decorated wine i.e. those which have already been manipulated.*

The next cancellation mechanism follows by comparing diagrams G.29 and G.31 and G.32 and G.33. Looking at the first pair of diagrams we note that, from equation 7.15,

$$\frac{\Upsilon_{J+1, J-s}}{J+1-s} = -\Upsilon_{J+1, J-s+1}.$$

Consequently, the version of diagram G.31 for which  $(J, J-s) \rightarrow (J+1, J-s)$  exactly cancels diagram G.29.

Due to these diagrams occurring for different values of  $J$  and  $s$ , we must check that the cancellation occurs for all values of  $J, s$  and not just over some range between the boundaries. At the bottom end, we note that diagram G.31 does not exist for  $s = 0$  (after decoration we would be left with a loose vertex, in this case). Thus, by equation 7.14, this diagram first exists for  $(J, s) = (1, 1)$  which cancels the  $(0, 0)$  instance of diagram G.29. These cancellations continue all the way up to the version of diagram G.29, spawned from the critical level. Recalling from equation 7.16 that the critical level depends on  $s$ , it is clear that the final instance of diagram G.29 is exactly cancelled by the final instance of diagram G.31.

Looking at diagrams G.32 and G.33 we note that, from equation 7.15,

$$2J\Upsilon_{J, J-s} = -\frac{\Upsilon_{J-1, J-s-1}}{J-s}.$$

Consequently, the level- $J+1$  version of diagram G.33 exactly cancels diagram G.32. Again, we must check that this cancellation occurs over the complete range of values of  $J$  ( $s$  is the same for both diagrams).

At the bottom end, we know that the first instance of diagram G.33 occurs one level after the first instance of diagram G.32, since the former requires the action of two instances of  $a_0$ , rather than just one. Hence, the first instances of these diagrams cancel. At the top end, however, we are left over with the version of diagram G.32 spawned from the critical level: the version of

diagram G.33 which should cancel it is never generated, since the diagrammatic procedure will have terminated.

Let us consider the level- $J_{\max} + 1$  version of diagram G.32 in more detail. To maximise the number of vertices and hence the level, the structure at the bottom of this diagram must contain a tree level vertex, being formed by processing a tree level vertex decorated by a simple loop, and attached to one other vertex. Hence, the structure at the bottom of the diagram is decorated by a single field. The constraint that both the wine and the vertex are reduced cannot be satisfied: the diagram vanishes. Consequently, the set of diagram G.29, G.31, G.32 and G.33 are always guaranteed to disappear from the calculation.

**Cancellation Mechanism 10** *Consider a level- $J$  diagram formed by  $s$  consecutive instances of  $a_1$  followed by  $J - s + 1$  instances of  $a_0$ . After stripping off any remaining two-point, tree level vertices, we arrive at the parent diagram for what follows.*

*Processing the manipulable component of the parent diagram yields (amongst others) a term formed by the action of  $a_1$  and a term formed by the action of  $a_0$ . In the case that  $s > 0$ , a diagram in which the  $\Lambda\partial_\Lambda$  strikes a simple loop is also generated. This term can be combined with terms arising from the  $a_0$  term in which the wine is made to form a simple loop (which can only be formed for  $s > 0$ ).*

*Up to a correction term, this combination precisely cancels the diagram formed by the action of  $a_1$  arising from a parent diagram if we let  $(J, s) \rightarrow (J + 1, s + 1)$ .*

*Returning to the parent diagram, we assume that we can iterate the diagrammatic procedure twice. We focus on the term formed by two instances of  $a_0$ ; specifically, the component of the resulting dumbbell comprising two two-point, tree level vertices. If we join these two vertices together, then the resulting diagram exactly cancels the above correction term.*

*In the case that the diagrammatic procedure terminates before the second iteration, the correction term vanishes!*

## 7.5 The Critical Level

The cancellation mechanisms 2–10 can now be used to give, up to gauge remainders and terms possessing an  $\mathcal{O}(p^2)$  stub, an extremely compact expression for  $\beta_{n_+}$ . In fact, we need not even use all of the cancellation mechanisms, since mechanisms 5–7 are contained within mechanisms 8 and 9.

The effect of the minimal set of cancellation mechanisms is very simple: iterating the diagrammatic procedure until exhaustion, the only terms which survive, up to gauge remainders and terms possessing an  $\mathcal{O}(p^2)$  stub are  $\Lambda$ -derivative terms,  $\beta$ -terms and  $\gamma$ -terms. Using the methodology of section 7.3.3 in which we gave a diagrammatic expression for the result of exhaustively manipulating diagram 7.2, we can arrive at a similar expression for exhaustively manipulating both diagrams 7.2 and 7.1. The only change that we must make is to take

$$V^0 = n_+ - s. \quad (7.17)$$

This gives us the extremely compact diagrammatic expression for  $\beta_{n_+}$ , shown in figure 7.43, where we have used the compact notation defined by 7.13.

A word should be said about how to simplify this expression, yet further. Up until now, we have been keeping all one-point Wilsonian effective vertices, unless they occur at tree level. However, it is inevitable that, at some stage, we must implement the requirement that one-point Wilsonian effective vertices are required to vanish and it is here that we must do it. Our aim is to maximise the number of vertices each of the diagrams of figure 7.43 can possess, so long as none of these vertices are one-point.

Once more, let us suppose that there are  $T$  tree level vertices. In the case of the  $\Lambda$ -derivative terms, each of these must be decorated by at least three fields. The remaining vertices must be decorated by at least two fields.

Thus, for the  $\Lambda$ -derivative terms, we can obtain a constraint on the maximum value of  $J$  by equating the number of fields required to produce a diagram with no one-point vertices with the total number of available fields:

$$2(J + 2 - s - T) + 3T \leq 2(J + 1) + 2.$$

$$\begin{aligned}
-4\beta_{n_+} \square_{\mu\nu}(p) &= -2 \sum_{s=1}^{n_+} \sum_{J=s}^{2n_+} \Upsilon_{J+1, J+1-s} \\
&\times \left[ - \sum_{\substack{V^{J+1-s} \\ V^{J+2-s}=1}} \left[ \begin{array}{c} \frac{1}{J+2-s} \left[ \begin{array}{c} \textcircled{V^{J+1-s}; R} \\ \textcircled{n_+ - s, J - s} \end{array} \right] \bullet \\ \left[ 2 \left( V^{J+1-s, J+2-s} - 1 \right) \beta_{V^{J+2-s}} + \gamma_{V^{J+2-s}} \frac{\partial}{\partial \alpha} \right] \textcircled{V^{J+1-s, J+2-s}} \\ \textcircled{n_+ - s, J - s} \end{array} \right] \right]^{11\Delta^{J+1}} \\
&- 2 \sum_{J=0}^n \Upsilon_{J+1, 0} \left[ \left[ \textcircled{n_J^R} \right] \bullet - \sum_{r=0}^{n_J} \left[ 2(n_J - r - 1) \beta_r + \gamma_r \frac{\partial}{\partial \alpha} \right] \textcircled{n_{J+r}} \right]^{11\Delta^{J+1}} \\
&+ \dots
\end{aligned}$$

Figure 7.43: Diagrammatic expression for  $\beta_{n_+}$  arising from the exhaustive manipulation of diagrams 7.2 and 7.1. The ellipsis denotes gauge remainders and terms with an  $\mathcal{O}(p^2)$  stub.

Using equation 7.7 to substitute for  $T$  we obtain:

$$J \leq n + 2s - 1. \tag{7.18}$$

The new maximum value of  $J$  can be used to replace the upper limit for the sum over  $J$  in figure 7.43. This limit coincides with the old one when  $s$  takes its maximum value,  $n_+$ , but is lower for all other values.

For the  $\alpha$  and  $\beta$ -terms we might worry that there could be a higher maximum value of  $J$ , since both of these terms possess a single full vertex. Such a vertex can be tree level, but needs only two decorative fields. However, if this vertex is tree level, then this necessarily reduces the sum over vertex arguments from  $n_+ - s$  to  $n_+ - s - V^{J+2-s}$ , where  $V^{J+2-s} > 0$ . This ensures that the maximum value of  $J$  for the  $\alpha$  and  $\beta$ -terms is not higher than corresponding value for the  $\Lambda$ -derivative terms.

At this stage, a final comment about the diagrams of figure 7.43 is in order. When we come to decorate these diagrams, terms which vanish at  $\mathcal{O}(p^2)$  will be generated. It is finally time to discard such diagrams, just as it is now time to discard diagrams with one-point vertices.

## Chapter 8

# Gauge Remainders

In this chapter, we show how to deal with gauge remainder terms, whilst using the heavily compacted notation developed in chapter 7. The very first thing that we must do is identify all terms containing gauge remainders.

Figure 7.39 provides an example of all the different types of terms we will encounter. On the first and second lines, we see gauge remainders arising from a single application of the effective propagator relation. Such terms—which we will call Type-Ia terms—have a seed action vertex joined to wine which ends in a gauge remainder. On the third and fourth lines, we see gauge remainders arising from two applications of the effective propagator relations. Such terms do not have any seed action vertices. If the necessarily decorated wine ends in a gauge remainder at one end only, then it is a gauge remainder of Type-Ib. If the wine ends in a gauge remainder at both ends, then it is a gauge remainder of Type-II.

Finally, on the last line, we find gauge remainders formed by a single application of the effective propagator relation but which also possess an  $\mathcal{O}(p^2)$  stub. These terms are of Type-III.

We will find that the majority of cancellations occur between terms in the same class. Nonetheless, as we will see, there are important cancellations between the various classes, allowing us to incorporate the gauge remainder terms into our compact expression for  $\beta_{n+}$ .

## 8.1 Type-Ia Gauge Remainders

A number of specific examples of Type-Ia gauge remainders are present, throughout this chapter. The only ones which have been presented in complete generality are those arising from the manipulation of diagrams formed by the exclusive use of  $a_1$ , which appear in figure 7.24. We combine these with those formed from the manipulation of terms generated by the action of at least one instance of  $a_0$  in figure 8.1.

There are several aspects of figure 8.1 that deserve comment. First, in the last two lines, we have separated off those diagram containing two vertices or fewer from those containing more than two. It is easy to see why: referring to the first set of diagrams, if we were to allow the sum over  $J$  to start from  $s$ , then the product over  $I$  does not make sense. Thus, we separate off the  $J = s$  case, which corresponds to there being two vertices. Similarly, the single vertex terms must be treated separately. Note also that we have not used the compact notation (7.13) since this can only be used when the sum over the dummy index  $I$  starts from zero.

Secondly, despite the comments made under figure 7.43 we use  $2n + s$  as the upper limit for the sum over  $J$ . We know that such diagrams can contain one-point Wilsonian effective action vertices. However, we wish to keep them right up until the stage where the conversion of gauge remainder diagrams into  $\Lambda$ -derivatives has been achieved.

Thirdly, we know that gauge remainders arising from terms formed by the exclusive action  $a_0$  kill the diagram. Thus we need not consider diagrams for which  $s = 0$ : the sum over  $s$  starts from one.

We now want to generate the diagrams formed by the action of the gauge remainders. Since these will be the very first gauge remainders performed we recall, from section 3.1, that we can collect together pushes forward and pulls back by using charge conjugation.

In keeping with what we have done already in this chapter, we want to isolate two-point, tree level vertices. The isolation of two-point, tree level vertices is trivial, even in the case where the gauge remainder strikes a reduced vertex.

$$\begin{aligned}
& -2 \sum_{s=1}^{n_+} \sum_{J=s+1}^{2n+s} \Upsilon_{J,J-s} \\
& \times \left[ \begin{array}{c} \text{G.35} \rightarrow 8.7 \\ \begin{array}{c} \text{Circle } V^{J+1-s;R} \\ \uparrow \bullet \\ \text{Circle } \hat{V}^{0,1;R} \end{array} \\ + \frac{1}{J+1-s} \left[ \begin{array}{c} \text{G.36} \rightarrow 8.7 \\ \begin{array}{c} \text{Circle } \hat{V}^{0,1;R} \text{ with self-loop} \\ + \\ \text{Circle } \hat{V}^{0,1;R} \text{ with self-loop} \end{array} \\ \text{Circle } V^{J+1-s;R} \end{array} \right] \\ \text{G.37} \rightarrow 8.7 \\ \begin{array}{c} \text{Circle } \hat{V}^{0,1;R} \text{ with self-loop} \\ + \\ \text{Circle } \hat{V}^{0,1;R} \text{ with self-loop} \end{array} \end{array} \right]^{11\Delta^J} \\
& \left[ \prod_{I=1}^{J-s} \sum_{V^{I+}=0}^{V^I} \text{Circle } V^{I,I+;R} \right] \\
& -2 \sum_{J=1}^{n_+} \sum_{r=0}^{n_{J-1}} \Upsilon_{J,0} \left[ \begin{array}{c} \text{G.38} \rightarrow 8.4 \\ \begin{array}{c} \text{Circle } r^R \\ \uparrow \bullet \\ \text{Circle } \hat{n}_{J+r-1}^R \end{array} \\ + \left[ \begin{array}{c} \text{G.39} \rightarrow 8.6 \\ \begin{array}{c} \text{Circle } \hat{n}_{J+r-1}^R \text{ with self-loop} \\ + \\ \text{Circle } \hat{n}_{J+r-1}^R \text{ with self-loop} \end{array} \\ \text{Circle } r^R \end{array} \right] \\ \text{G.40} \rightarrow 8.6 \\ \begin{array}{c} \text{Circle } \hat{n}_{J+r-1}^R \text{ with self-loop} \\ + \\ \text{Circle } \hat{n}_{J+r-1}^R \text{ with self-loop} \end{array} \end{array} \right]^{11\Delta^J} \\
& + 2 \sum_{J=0}^n \frac{\Upsilon_{J,0}}{\vartheta_{n_J}} \left[ \begin{array}{c} \text{G.41} \rightarrow 8.2 \\ \begin{array}{c} \text{Circle } \hat{n}_J \text{ with self-loop} \\ + \\ \text{Circle } \hat{n}_J \text{ with self-loop} \end{array} \\ \text{G.42} \rightarrow 8.2 \\ \begin{array}{c} \text{Circle } \hat{n}_J \text{ with self-loop} \\ + \\ \text{Circle } \hat{n}_J \text{ with self-loop} \end{array} \end{array} \right]^{11\Delta^J}
\end{aligned}$$

Figure 8.1: Type-Ia gauge remainders.

Consider a gauge remainder which strikes a reduced vertex, but which has not yet acted. Since the gauge remainder kills two-point (tree level) vertices, we can promote the reduced vertex to a full vertex. Then, after the gauge remainder has acted, we simply split the resulting vertex into a reduced part and a two-point, tree level part.

The field that the gauge remainder strikes will be represented using the ‘socket’ notation of section 3.1.7. When the socket decorates a two-point, tree level vertex, we will partially decorate this vertex, not by specifying the field which fills the socket, but by specifying the other field that decorates the vertex.<sup>1</sup>

We will start by dealing with the simplest terms: diagrams G.41 and G.42. In the case of the former diagram we can drop the  $\vartheta_{n_J}$  since, if the vertex is two-point and tree level, then it is killed by the gauge remainder anyway. In the latter case, something a little odd is going on. Irrespective of whether or not we allow the gauge remainder to act, the vertex of this diagram has a two-point, tree level component. The reason that this has arisen relates to how we have organised the calculation. Since, when we introduced the entire  $\beta_{n_+}$  diagrammatics we generated diagrams such as G.42 with specific value of  $J$ , we were unable to separate off two-point, tree level components cleanly as this would have required treating diagrams with different values of  $n$ , differently. Now, with our more sophisticated treatment where  $J$  is summed over, we can happily separate off the two-point, tree level contribution to the vertex in diagram G.42, noting that this simply occurs for  $J = n$ . We do this in figure 8.2 where we recall that when we do take the two-point, tree level contribution,  $\vartheta_{n_J} = 2$ . We also redraw diagram G.41, removing the  $\vartheta_{n_J}$  altogether.

The effects of our operations are now clear. The two diagrams G.43 and G.44 now take exactly the same form as the remaining diagrams in figure 8.1, just with fewer vertices. The other two diagrams, G.45 and G.46 are more properly classified as type-II and type-III diagrams, respectively. These will be returned

---

<sup>1</sup>This field carries the same momentum as the vertex, and so we can use the effective propagator relation.

$$\begin{aligned}
& +2 \sum_{J=0}^n \Upsilon_{J,0} \left[ \begin{array}{c} \text{G.43} \rightarrow 8.3 \\ \text{G.44} \rightarrow 8.3 \end{array} \right]^{11\Delta^J} \\
& - \Upsilon_{n-1,0} \left[ \begin{array}{c} \text{G.45} \rightarrow 8.24 \end{array} \right]^{11\Delta^{n-1}} + \Upsilon_{n,0} \left[ \begin{array}{c} \text{G.46} \rightarrow 8.35 \end{array} \right]^{1\Delta^n}
\end{aligned}$$

Figure 8.2: Re-expression of diagrams G.41 and G.42.

to in later sections. Note that diagram G.45 does not make sense for  $n = 0$  and so our prescription is simply to discard it, in this case.

We now focus on diagrams G.43 and G.44 and allow the gauge remainder to act. First, we will look at the case where, in the former diagram, the gauge remainder bites the field to which the wine attaches and, in the latter diagram, the gauge remainder bites the base of the wine. These two terms exactly cancel, via cancellation mechanism 1. In addition to this, we must of course take into account account terms formed by the gauge remainders striking other locations. The result of processing diagrams G.43 and G.44 is shown in figure 8.3.

The usual procedure, from here, would be to decorate all those two-point, tree level vertices to which we can attach a field which carries the same momentum as the vertex. However, we will see later that the candidate for decoration, diagram G.47, is cancelled, wholesale, and so there is no need to perform the decoration, in this case.

Next, we process diagram G.38, letting  $J \rightarrow J + 1$ . This is shown in figure 8.4.

We now follow the usual diagrammatic procedure of decorating two-point, tree level vertices, tying up any loose ends and then applying the effective

$$\begin{aligned}
& 4\Upsilon_{n,0} \left[ \begin{array}{c} \{ \text{G.47 } G.100 \} \\ \text{Diagram 1} \end{array} + \begin{array}{c} \{ \text{G.48 } G.101 \} \\ \text{Diagram 2} \end{array} \right]^{11\Delta^n} \\
& + 4 \sum_{J=0}^n \Upsilon_{J,0} \left[ \begin{array}{c} \{ \text{G.49 } G.318 \} \\ \text{Diagram 3} \end{array} + \begin{array}{c} \{ \text{G.50 } G.55 \} \\ \text{Diagram 4} \end{array} + \begin{array}{c} \{ \text{G.51 } G.57 \} \\ \text{Diagram 5} \end{array} \right]^{11\Delta^J}
\end{aligned}$$

Figure 8.3: Result of processing diagrams G.43 and G.44.

$$-4 \sum_{J=0}^n \Upsilon_{J+1,0} \left[ \sum_{r=0}^{n_J} \left[ \begin{array}{c} \{ \text{G.52 } G.75 \} \\ \text{Diagram 6} \end{array} \right] + \begin{array}{c} \text{G.53} \rightarrow 8.5 \\ \text{Diagram 7} \end{array} \right]^{11\Delta^{J+1}}$$

Figure 8.4: Result of processing diagram G.38.

propagator relation, as appropriate, to give the diagrams of figure 8.5. Notice that we have not drawn those diagrams in which the loose end of the effective propagator has been attached to the socket. To form such a diagram we would have to start with a three-point (tree level) vertex decorated by a simple loop. The gauge remainder would strike the vertex along the third field. This gauge remainder could not be fermionic since then the three-point vertex would have an odd number of fermions. Since gauge remainders have no support in the  $C$ -sector, this forces it to be in the  $A$ -sector; but now the diagram vanishes by charge conjugation invariance!

The validity of using the effective propagator relation in the situation where one of the fields of the two-point, tree level vertex has been pushed forward (pulled back) on to has been discussed in section 3.1.7.

Immediately, we find cancellations.

$$\begin{aligned}
& -4 \sum_{J=0}^n \Upsilon_{J+1,0} \left[ \begin{array}{c} \text{G.54} \\ \text{Diagram with } 0^2 \text{ and } \hat{n}_J^R \end{array} \right]^{1\Delta^{J+1}} \\
& -4 \sum_{J=0}^n \Upsilon_{J,0} \left[ \begin{array}{cccc} \{ \text{G.55 } \text{G.50} \} & \text{G.56} & \{ \text{G.57 } \text{G.51} \} & \text{G.58} \\ \text{Diagram 1} & - \text{Diagram 2} & + \text{Diagram 3} & - \text{Diagram 4} \end{array} \right]^{11\Delta^J}
\end{aligned}$$

Figure 8.5: Partial decoration of diagram G.53, in which all loose ends have been tied up and the effective propagator relation has been applied.

**Cancellation 8.1** *Diagram G.55 exactly cancels diagram G.50.*

**Cancellation 8.2** *Diagram G.57 exactly cancels diagram G.51.*

These two cancellations remove all contributions arising from diagram G.43 in which the gauge remainder strikes a socket, up to terms in which the socket decorates a two-point, tree level vertex. From our experiences with the calculation so far, this is both what we expect and require if we are to be able, ultimately, to cast the gauge remainder diagrams as  $\Lambda$ -derivative terms.

Currently, the only term left containing a reduced vertex decorated by a socket which has been struck by a gauge remainder is diagram G.52. We can guess that this diagram will be cancelled by terms coming from processing a term with one more vertex i.e. the three vertex component of diagram G.35. However, before doing this, we process the partners of diagram G.38: diagrams G.39 and G.40.

The treatment of these diagrams is almost identical to the previous treatment of diagrams G.43 and G.44 and is shown in figure 8.6. The only difference is that an additional vertex, unaffected by the action of the gauge remainder, must be included.

$$\begin{aligned}
& -4 \sum_{J=0}^n \Upsilon_{J+1,0} \left[ \left[ \begin{array}{c} \text{G.59} \rightarrow 8.17 \quad \text{G.60} \rightarrow 8.17 \\ \text{Diagram 1} + \text{Diagram 2} \\ n_J^R \end{array} \right] \right]^{11\Delta^{J+1}} \\
& -4 \sum_{J=0}^n \sum_{r=0}^{n_J} \Upsilon_{J+1,0} \left[ \left[ \begin{array}{c} \{ \text{G.61} \text{ } G.77 \} \quad \{ \text{G.62} \text{ } G.79 \} \quad \text{G.63} \\ \text{Diagram 3} + \text{Diagram 4} + \text{Diagram 5} \\ r^R \end{array} \right] \right]^{11\Delta^{J+1}}
\end{aligned}$$

Figure 8.6: Result of processing diagrams G.39 and G.40.

Now, in addition to diagram G.52, we have two further diagrams containing two reduced vertices and a socket which has been hit by a gauge remainder; namely diagrams G.61 and G.62. To remove these three diagrams, we must complete our treatment of the diagrams of figure 8.1 by processing those containing three or more vertices. These are of course those terms which have been represented using a very compact notation. It would be nice to maintain the compact notation for all of the daughter diagrams, but this is not quite possible. If, after the gauge remainder has acted, we take the two-point, tree level component of the vertex with argument  $V^{J+1-s}$ , then this causes the argument of the final vertex in the product over  $I$ ,  $V^{J-s, J+1-s; R}$ , to reduce to just  $V^{J-s; R}$ . If the parent diagram had only three vertices, then this means that the daughter has no product over  $I$ . Hence, when taking the two-point, tree level contribution from a vertex, only those diagrams with more than three vertices can still be represented using the compact notation.

The first stage of the treatment of diagrams G.35–G.37 is shown in figure 8.7. We have simplified the diagrams by letting  $J \rightarrow J + s$ . The final row of diagrams correspond (after shifting) to  $J = 1$ . In this case, we have let

$s \rightarrow s + 1$  and then changed the dummy variable  $s$  to  $J$ .

Note that, for diagrams G.64–G.67, we have reduced the upper limit of the sum over  $J$  by one. The reason is simple: when  $J = 2n$ , the parent diagram is the highest level manipulable diagram and hence contains only three-point, tree level vertices and one-point higher loop vertices. If the gauge remainder strikes a vertex, then this vertex must be one of the three-point, tree level vertices. The effect of this is to produce a two-point, tree level vertex and so does not leave behind any reduced components. Since all the vertices of diagrams G.64–G.67 are reduced, such a term cannot exist for  $J = 2n$ . If, instead, the gauge remainder strikes the wine, then this means that, in processing the parent, one of the fields attached to one of the three-point, tree level vertices has been moved on to a wine. Again, this leaves behind a two-point, tree level vertex, but no reduced component.

In figure 8.8 we process diagram G.71 by partially decorating the two-point, tree level vertices, tying up any loose ends and applying the effective propagator relation, as appropriate.

As we predicted earlier, by processing the three-vertex terms, we generate diagrams to cancel the only remaining diagrams possessing less than three reduced vertices, one of which is decorated by a socket, hit by a gauge remainder.

**Cancellation 8.3** *Diagram G.75 exactly cancels diagram G.52*

**Cancellation 8.4** *Diagram G.77 exactly cancels diagram G.61.*

**Cancellation 8.5** *Diagram G.79 exactly cancels diagram G.62.*

This then leaves behind diagrams G.64–G.66 as the only remaining diagrams at this stage of the calculation possessing only reduced vertices and a socket struck by a gauge remainder. The structure of the cancellations is now becoming clear. Gauge remainder diagrams of Type-Ia come in three types, as we know already from figure 8.1, with the first of these being absent when there is only a single vertex.

$$\begin{aligned}
& -4 \sum_{s=1}^{n_+} \sum_{J=1}^{2n-1} \Upsilon_{J+s,J} \\
& \times \left[ \begin{array}{c} \{ \text{G.64 G.82} \} \\ \begin{array}{c} \text{V}^{J+1;R} \\ \uparrow \\ \hat{\text{V}}^{0,1;R} \end{array} \\ + \frac{1}{J+1} \left[ \begin{array}{c} \{ \text{G.65 G.84} \} \\ \begin{array}{c} \text{V}^{J+1;R} \\ \uparrow \\ \hat{\text{V}}^{0,1;R} \end{array} \\ + \begin{array}{c} \{ \text{G.66 G.86} \} \\ \begin{array}{c} \text{V}^{J+1;R} \\ \uparrow \\ \hat{\text{V}}^{0,1;R} \end{array} \\ + \begin{array}{c} \text{G.67} \\ \begin{array}{c} \text{V}^{J+1;R} \\ \uparrow \\ \hat{\text{V}}^{0,1;R} \end{array} \end{array} \right] \end{array} \right]^{11\Delta^{J+s}} \\
& \left[ \prod_{I=1}^J \sum_{V^{I+}=0}^{V^I} \text{V}^{I,I+;R} \right] \\
& -4 \sum_{s=1}^{n_+} \sum_{J=2}^{2n} \Upsilon_{J+s,J} \\
& + \frac{1}{J+1} \left[ \begin{array}{c} \text{G.68} \rightarrow 8.9 \\ \begin{array}{c} 0^2 \\ \uparrow \\ \hat{\text{V}}^{0,1;R} \end{array} \\ + \begin{array}{c} \text{G.69} \rightarrow 8.19 \\ \begin{array}{c} 0^2 \\ \uparrow \\ \text{V}^{0,1;R} \end{array} \\ + \begin{array}{c} \text{G.70} \rightarrow 8.19 \\ \begin{array}{c} 0^2 \\ \uparrow \\ \text{V}^{0,1;R} \end{array} \end{array} \right]^{11\Delta^{J+s}} \\
& \left[ \prod_{I=1}^J \sum_{V^{I+}=0}^{V^I} \text{V}^{I,I+;R} \right] \text{V}^{J;R} \\
& -4 \sum_{J=0}^n \sum_{r=0}^{n_J} \Upsilon_{J+2,1} \\
& + \frac{1}{2} \left[ \begin{array}{c} \text{G.71} \rightarrow 8.8 \\ \begin{array}{c} 0^2 \\ \uparrow \\ \hat{n}_{J+r}^R \end{array} \\ + \begin{array}{c} \text{G.72} \rightarrow 8.19 \\ \begin{array}{c} 0^2 \\ \uparrow \\ n_{J+r}^R \end{array} \\ + \begin{array}{c} \text{G.73} \rightarrow 8.19 \\ \begin{array}{c} 0^2 \\ \uparrow \\ n_{J+r}^R \end{array} \end{array} \right]^{11\Delta^{J+2}} \\
& \text{V}^{r,R}
\end{aligned}$$

Figure 8.7: Separating off the two-point, tree level vertices from diagrams G.35–G.37, after the action of the gauge remainder.

$$4 \sum_{J=0}^n \sum_{r=0}^{n_J} \Upsilon_{J+1,0}$$

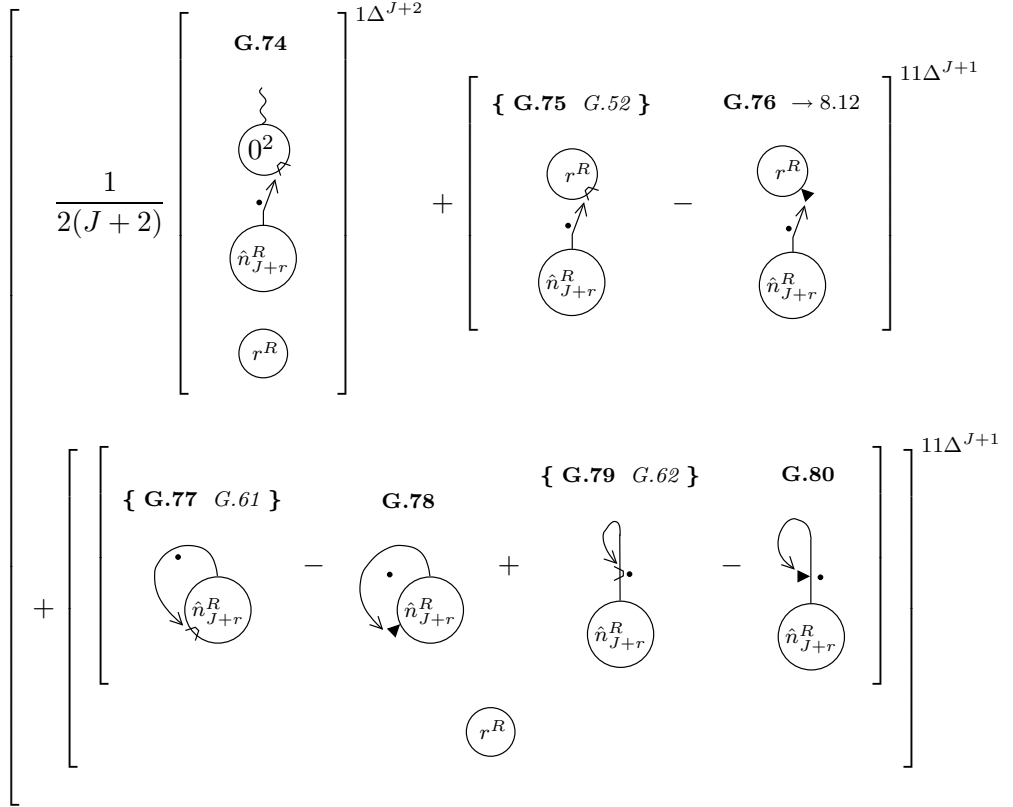


Figure 8.8: Partial decoration of diagram G.71. All loose ends have been tied up and the effective propagator relation applied.

Processing the one vertex terms,<sup>2</sup> we find that the contribution in which a gauge remainder strikes the field on the vertex to which the wine attaches cancels the contribution in which a gauge remainder strikes the base of the wine. Among the surviving terms, we are left with diagrams with reduced vertices and a socket struck by a gauge remainder.

Processing the two vertex terms, we find that diagrams of the second and third topologies exactly repeat the cancellations seen with the one vertex terms. However, we also have a diagram of the first topology to process. When the gauge remainder acts in diagrams of the first topology, it generates either a two-point, tree level vertex or a reduced vertex. Let us consider the former case and suppose that we join the two-point, tree level vertex to some other structure, with an effective propagator. With the term under consideration, we must make this join either to the wine or to the vertex from which the wine leaves. We have seen how this then cancels (up to nested gauge remainders) the remaining one vertex terms in which the vertex is reduced and the diagram possess a socket struck by a gauge remainder.

Processing the three vertex terms repeats the cancellations seen with the two vertex terms but gives us something extra. Now when we process the diagram of the first topology and generate a two-point, tree level vertex, we can join this not only to the wine and the vertex to which the wine attaches but also to the loose vertex. We have seen how this then cancels (up to nested gauge remainders) the remaining two vertex term formed from the diagram of the first topology in which the gauge remainder acts to produce a reduced vertex.

As we iterate the diagrammatic procedure, we expect that this pattern of cancellations will just repeat, until the procedure terminates. We now demonstrate that this expectation is indeed true, by processing diagram G.68—the result of which is shown in figure 8.9.

**Cancellation 8.6** *Diagram G.82 cancels diagram G.64.*

**Cancellation 8.7** *Diagram G.84 cancels diagram G.65.*

---

<sup>2</sup>Having removed any terms which are properly classed as gauge remainders of type-II of III.

$$4 \sum_{s=1}^{n+} \sum_{J=2}^{2n} \Upsilon_{J+s-1, J-1}$$

$$\left[ \frac{1}{2J(J+s)} \left[ \begin{array}{c} \text{G.81} \\ \begin{array}{c} \text{Diagram: } \hat{V}^{0,1;R} \text{ with a wavy line and a dot, connected to } 0^2 \text{ and } V^{J;R} \\ \left[ \prod_{I=1}^{J-1} \sum_{V^{I+}=0}^{V^I} V^{I, I+; R} \right] \end{array} \end{array} \right] \right]^{1\Delta^{J+s}}$$

$$+ \left[ \begin{array}{c} \text{Diagram: } V^{J;R} \text{ with a dot, connected to } \hat{V}^{0,1;R} \\ \text{Diagram: } V^{J;R} \text{ with a dot, connected to } \hat{V}^{0,1;R} \\ \text{Diagram: } V^{J;R} \text{ with a dot, connected to } \hat{V}^{0,1;R} \\ \left[ \prod_{I=1}^{J-1} \sum_{V^{I+}=0}^{V^I} V^{I, I+; R} \right] \end{array} \right]^{11\Delta^{J+s-1}}$$

$$+ \frac{1}{J} \left[ \begin{array}{c} \text{Diagram: } \hat{V}^{0,1;R} \text{ with a dot and a loop} \\ \text{Diagram: } \hat{V}^{0,1;R} \text{ with a dot and a loop} \\ \text{Diagram: } \hat{V}^{0,1;R} \text{ with a dot and a loop} \\ \text{Diagram: } \hat{V}^{0,1;R} \text{ with a dot and a loop} \\ \left[ \prod_{I=1}^{J-1} \sum_{V^{I+}=0}^{V^I} V^{I, I+; R} \right] \\ V^{J;R} \end{array} \right]$$

Figure 8.9: The result of processing diagram G.68.

**Cancellation 8.8** *Diagram G.86 cancels diagram G.66.*

This completes the cancellation of all terms arising from Type-Ia gauge remainders in which the gauge remainder strikes a socket and for which all vertices are reduced. It is apparent that there is a cancellation mechanism at work.

**Cancellation Mechanism 11** *Consider a diagram, to be denoted by  $X$ , possessing two arbitrary structures,  $A$  and  $B$ . These two structures can, but need not be, identified with each other. Additionally, the diagram possesses  $N_V$  reduced vertices and is decorated by the usual external fields and by  $N_P$  effective propagators.*

*A wine leaves the structure  $B$  and attaches, via a gauge remainder with an arbitrary number of nestings, to the structure  $A$ . We are free to place any restrictions we choose on the decoration of the wine. Note that the attachment to  $B$  need not be direct: it can, in principle, be via a (nested) gauge remainder. Furthermore, both of the structures  $A$  and  $B$  can be associated with the wine. Hence, diagram  $X$  represents not only gauge remainders of type-I but also of type-II (and type-III). An example of diagram  $X$  is shown in figure 11 where we have taken  $N_V = 0$ , the attachment to  $B$  to be direct, the wine to be full and no nesting in the attachment to  $A$ .*

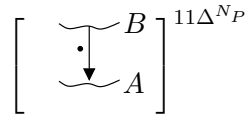


Figure 8.10: An example of diagram  $X$ .

*Suppose now that the structure  $A$  is actually just one of  $N_A$  identical structures. For example, suppose that  $A$  is just a reduced vertex. Then if  $B$  is some other structure, we know that we could equally have hit any of the other  $N_V$  vertices with the gauge remainder. Therefore, in this case,  $N_A = N_V + 1$ . If, however,  $B$  and  $A$  are identified as being the same vertex, then  $N_A = 1$ . Likewise, if  $A$  represents the wine, then  $N_A = 1$ .*

Finally, we allow the gauge remainder to act. We are interested in the case where it strikes a socket on  $A$ . Thus, if  $A$  is to be identified with the wine, this excludes the case where the gauge remainder strikes the end of the wine. If  $A$  is identified with a vertex, we do not allow the socket to be filled by the other end of the wine. For the purposes of this analysis, the case where the gauge remainder generates a two-point, tree level vertex is ignored.

Let us now consider a second diagram  $Y$ . It possesses both the structures  $A$  and  $B$ , but this time the wine ends in a gauge remainder which strikes a vertex (it makes no difference whether or not the vertex is reduced). Any restrictions placed on the decoration of the wine of diagram  $X$  apply to the wine of diagram  $Y$ . Additionally, diagram  $Y$  possesses a further  $N_V$  vertices and is decorated by the usual external fields and by  $N_P+1$  effective propagators. An example of diagram  $Y$  is shown in figure 11.

$$\frac{1}{2(N_P + 1)N_A} \left[ \begin{array}{c} \text{---} B \\ \cdot \\ \downarrow \\ \bigcirc \\ \text{---} A \end{array} \right]^{11\Delta^{N_P+1}}$$

Figure 8.11: An example of diagram  $Y$ .

Allowing the gauge remainder to act, this time it is the two-point, tree level component of the struck vertex that we focus on. We now decorate this vertex with one of the effective propagators and tie up the loose end. Since  $A$  can be identified with any of the other structures, we only need join the loose end to  $A$ . Up to further nestings this will precisely cancel the contribution we took from diagram  $X$ , so long as, before any manipulation, diagram  $X$  has a factor of  $2(N_P + 1)N_A$ , relative to diagram  $Y$ .

The combination of cancellation mechanisms 1 and 11 are sufficient to account for all the cancellations seen in this section.

We will now collate the terms that have survived up to this stage of the calculation.<sup>3</sup> The terms fall very neatly into five set, the elements of which are given below:

1. diagrams G.45 and G.46;
2. diagrams G.47 and G.48; diagrams G.59 and G.60; diagrams G.69 and G.70; and diagrams G.72 and G.73;
3. diagrams G.54, G.74 and G.81;
4. diagrams G.49, G.63 and G.67;
5. diagrams G.56 and G.58; diagrams G.76, G.78 and G.80; and diagrams G.83, G.85 and G.87.

The first set stands somewhat apart from the rest since, as we have already noted, the diagrams contained therein should be reclassified as gauge remainders of a different type.

The remaining four sets have a very nice structure. Recall how we arranged the original type-Ia gauge remainders in figure 8.1. However, we then noted that the final two elements should really be replaced, in the context of bona-fide type-Ia gauge remainders, by diagrams G.43 and G.44. We call this new set the set of proper type-Ia gauge remainders. The set of proper type-Ia gauge remainders essentially consists of diagrams G.43 and G.44 and their multiple vertex analogues. As we arrange the gauge remainders in this way, so we can do likewise with the terms that survive their manipulation.

The elements set 2 will be combined with similar diagrams formed from gauge remainders of type-Ib.

Set 3 comprises those diagrams which require manipulation at  $\mathcal{O}(p^2)$ , the  $\mathcal{O}(p^2)$  stub of which has been formed by the action of a gauge remainder. These terms will be commented on in chapter 11.

Set 4 is of particular interest. Whereas the elements of the previous two sets contain two-point, tree-level vertices, the elements of this set do not. Rather, it is as if the gauge remainder has ‘reached the end of line’, by biting the end

---

<sup>3</sup>Generally, these terms will be processed or cancelled but, since this occurs at a later stage in the calculation, these actions should be ignored for the collation of current survivors.

of the wine. The corresponding diagrams escape cancellation since there is, at this point in the calculation, no other way to generate them. As we have already seen in the one-loop calculation, such terms play a crucial role, being reducible to  $\Lambda$ -derivative terms (cf. diagram 4.27 and its children).

The final set comprises nested gauge remainders which, up to the nesting, take an identical form to the set of proper type-Ia gauge remainders.

Thus, with a bit of care, we can deduce the result of processing the nested gauge remainders. Noting that we can not collect the nested push forward with the nested pull back, we will simply generate the nested versions of the sets 2–4 and a doubly nested version of set 5. There is no analogue of set 1 since its formation would require the presence of a full vertex in the nested versions of diagram G.44.

There is, however, one more type of diagram we can generate. To see this, consider processing diagram G.76, as shown in figure 8.12.

$$\begin{aligned}
 & -4 \sum_{J=0}^n \Upsilon_{J+1,0} \\
 & \times \left[ \sum_{r=0}^{n_J} \left[ \begin{array}{c} \text{Diagram 1} \\ \text{Diagram 2} \end{array} \right] + \begin{array}{c} \text{Diagram 3} \\ \text{Diagram 4} \end{array} \right]^{11\Delta^{J+1}}
 \end{aligned}$$

Figure 8.12: Result of processing diagram G.76.

So far, this is exactly what we expect, where the nested push forward has been performed independently of the nested pull back and we have separated off the two-point, tree level component of the vertex struck by the gauge remainder. However, when we come to decorate the two-point, tree level vertex, we encounter something new. If we decorate this vertex with an effective propagator, then we can tie up the loose ends in the usual ways (as before, we can discard the case where we join the two-point, tree level vertex to itself). Additionally, though, we can attach the loose end to the nested gauge remainder. We show this explicitly in figure 8.13.

$$-4 \sum_{J=0}^n \Upsilon_{J,0} \left[ \begin{array}{c} \{ \text{G.88 } G.349 \} \quad \{ \text{G.89 } G.348 \} \\ \begin{array}{c} \text{Diagram 1: } \hat{n}_J^R \text{ vertex with a loop labeled } 0^2 \\ \text{Diagram 2: } \hat{n}_J^R \text{ vertex with a loop labeled } 0^2 \end{array} \end{array} \right]^{11\Delta^J}$$

Figure 8.13: An example of the new types of diagram arising from processing nested gauge remainders. These terms represent the only surviving contributions from diagrams 8.1 and 8.2 after all nested gauge remainders have been processed.

Since these diagrams are formed by attaching the loose end to a single specific structure (as opposed to one of many identical structures), they come with a factor of  $2(J + 1)$ . Although we can apply the effective propagator relation, we cannot employ the diagrammatic identity 3, since the gauge remainder attached to the wine bites the effective propagator at the point where it joins to the other gauge remainder. Hence, this latter gauge remainder has a different momentum flowing through it than the effective propagator.

Analogous diagrams at a higher level of nesting behave in a very similar manner. Now, though, we have a choice about which of the unattached gauge remainders to join to the two-point, tree level vertex. Each of these cases must be treated individually.

It is thus apparent that we can iterate the diagrammatic procedure, at each stage generating ever more nested versions sets 2–5, together with diagrams of the type just discussed. The procedure will terminate: each successive nesting reduces the maximum number of vertices by one.

It is straightforward to compute the maximum number of nestings. We must maximise the number of three-point, tree level vertices; since it is these that a gauge remainder must strike to have any hope of producing further levels of nesting.

Referring back to diagram G.35, to maximise the number of nestings, we require two fields to decorate the struck vertex and three fields to decorate the loose vertices. The vertex to which the wine is attached must be decorated

by at least one additional field. Since we assume that all other vertices are tree level, the argument of this vertex is just  $n_+ - s$ . Hence, the number of fields required to decorate this vertex,  $E(s)$ , depends on  $s$ : if  $s < n_+$ , then we require only one additional field to decorate this vertex whereas, if  $s = n_+$ , we require two additional fields, on account of the vertex being reduced.

Letting  $J \rightarrow J + s$ , the number of vertices included in the sum over  $I$  is now just  $J$ . It is thus apparent that, ] of all  $J + 2$  vertices,  $J + 1$  of them could potentially increment the level of nesting by one. However, for each of these vertices to actually be able to increase the level of nesting, we require that there be sufficient decorative fields. The value of  $J$  corresponding to the maximum number of nestings,  $J_{MN}$ , can thus be found by equating the number of required fields with the number of decorative fields:

$$2 + 3J_{MN} + E(s) = 2(J_{MN} + s) + 2.$$

It is clear that to maximise  $J_{MN}$ , we should maximise  $s$ . We thus find that  $J_{MN} = 2n$  and so the maximum number of nestings is  $2n + 1$ .

Since, to maximise the number of nestings requires that we maximise  $s$  then, at the final level of nesting, we produce (nested) versions of diagrams G.56 and G.58, for which the vertices are tree level (i.e.  $J = n$ ). The wines, in both cases, have the minimal number of decorations—being zero in the first case and one in the second. Allowing the final gauge remainder to act will produce diagrams like those of sets 2–4, above.

## 8.2 Type-Ib Gauge Remainders

The treatment of type-Ib gauge remainders is very similar to those of type-Ia. Figure 8.14 shows all gauge remainders of type-Ib.

Comparing figures 8.1 and 8.14 it is clear that the primary differences between gauge remainders of type-Ia and Ib are as follows. First, in the latter case, the wine leaves a Wilsonian effective action vertex, rather than a seed action vertex. Secondly, this wine must be decorated. Of course, this latter restriction is automatically satisfied in the case where the gauge remainder bites the wine. It is also clear that our set of type-Ib diagrams really are type-Ib diagrams: there are no diagrams of types-II and III hiding, as there were for the original set of type-Ia diagrams.

When we allow the gauge remainders to act, it is apparent what the result will be. All diagrams possessing only reduced vertices and in which the gauge remainder hits a socket will cancel, via cancellation mechanism 11. However, the surviving terms will be of a slightly different form to the analogous type-Ia survivors, due to the reduction of the wine. In figure 8.15, we show the terms arising from diagrams G.96 and G.97 that are not cancelled via cancellation mechanism 11.

Diagram G.98 is something we have not seen before, arising due to the reduction of the wine in diagram G.96. When the gauge remainder in diagram G.97 pulls back on to the base of the wine, there is no contribution from diagram G.96 to cancel the term with an undecorated wine.

The next diagram is familiar from our analysis of the type-Ia terms. Indeed, we can combine it with diagram G.49 simply by replacing the vertex argument  $n_j^R$  with  $\Pi_{n_j^R}$ .

The final two diagrams also are of a familiar structure though the wines of the analogous type-Ia terms, diagrams G.47 and G.48, are not explicitly reduced. However, since these diagrams contain a single, two-point vertex, we are very restricted in the decorations we can perform. Indeed, irrespective of the value of  $n$ , we always have at least two fields with which to decorate (i.e.

$$\begin{aligned}
& 2 \sum_{s=1}^{n_+} \sum_{J=2}^{2n} \Upsilon_{J+s-1, J-1} \\
& \times \left[ \begin{array}{c} \text{G.90} \rightarrow 8.19 \\ \begin{array}{c} \textcircled{V^{J;R}} \\ \uparrow \circ \\ \textcircled{V^{0,1;R}} \end{array} \\ + \frac{1}{J} \left[ \begin{array}{c} \text{G.91} \rightarrow 8.19 \\ \begin{array}{c} \textcircled{V^{0,1;R}} \\ \circ \rightarrow \end{array} \\ + \begin{array}{c} \text{G.92} \rightarrow 8.19 \\ \begin{array}{c} \bullet \rightarrow \\ \textcircled{V^{0,1;R}} \end{array} \end{array} \right] \\ \textcircled{V^{J;R}} \end{array} \right] \Bigg|^{11\Delta^{J+s-1}} \\
& \left[ \prod_{I=1}^{J-1} \sum_{V^{I+}=0}^{V^I} \textcircled{V^{I, I+; R}} \right] \\
& + 2 \sum_{J=1}^{n_+} \sum_{r=0}^{n_{J-1}} \Upsilon_{J,0} \left[ \begin{array}{c} \text{G.93} \rightarrow 8.16 \\ \begin{array}{c} \textcircled{r^R} \\ \uparrow \circ \\ \textcircled{n_{J+r-1}^R} \end{array} \\ + \left[ \begin{array}{c} \text{G.94} \rightarrow 8.16 \\ \begin{array}{c} \textcircled{n_{J+r-1}^R} \\ \circ \rightarrow \end{array} \\ + \begin{array}{c} \text{G.95} \rightarrow 8.16 \\ \begin{array}{c} \bullet \rightarrow \\ \textcircled{n_{J+r-1}^R} \end{array} \end{array} \right] \\ \textcircled{r^R} \end{array} \right] \Bigg|^{11\Delta^J} \\
& - 2 \sum_{J=0}^n \Upsilon_{J,0} \left[ \begin{array}{c} \text{G.96} \rightarrow 8.15 \\ \begin{array}{c} \textcircled{n_J^R} \\ \circ \rightarrow \end{array} \\ + \begin{array}{c} \text{G.97} \rightarrow 8.15 \\ \begin{array}{c} \bullet \rightarrow \\ \textcircled{n_J^R} \end{array} \end{array} \right] \Bigg|^{11\Delta^J}
\end{aligned}$$

Figure 8.14: Type-Ib gauge remainders.

$$\begin{aligned}
& 4 \sum_{J=0}^n \Upsilon_{J,0} \left[ \begin{array}{c} \{ \text{G.98 } G.111 \} \quad \text{G.99} \rightarrow 10.1 \\ \begin{array}{c} \square \\ \downarrow \\ \textcircled{n_J^R} \end{array} \quad - \quad \begin{array}{c} \bullet \\ \downarrow \\ \textcircled{n_J^R} \end{array} \end{array} \right]^{11\Delta^J} \\
& - 4 \Upsilon_{n,0} \left[ \begin{array}{c} \{ \text{G.100 } G.47 \} \quad \{ \text{G.101 } G.48 \} \\ \begin{array}{c} \circ \\ \downarrow \\ \textcircled{0^2} \end{array} \quad + \quad \begin{array}{c} \circ \\ \downarrow \\ \textcircled{0^2} \end{array} \end{array} \right]^{11\Delta^n}
\end{aligned}$$

Figure 8.15: Diagrams arising from processing diagrams G.96 and G.97 that are not cancelled when diagram G.93 is processed.

the two external fields). This in fact forces us to decorate wines of the type-Ia terms, giving two cancellations.

**Cancellation 8.9** *Diagram G.100 cancels diagram G.47, the cancellation being forced as a consequence of the diagrammatic structure and the specific set of decorative fields.*

**Cancellation 8.10** *Diagram G.101 cancels diagram G.48, the cancellation being forced as a consequence of the diagrammatic structure and the specific set of decorative fields.*

The next stage is to process diagrams G.93–G.95, the result of which which is shown in figure 8.16. Once again, we have retained only those terms which are not involved in cancellations against other diagrams generated from figure 8.14.

We now uncover a wonderful interplay between the type-Ia and type-Ib gauge remainders. First, we note that diagrams G.102 and G.54 are very similar. Indeed, we can decompose diagram G.54 into a component with a decorated wine and a component with an undecorated wine. The former can then be combined with diagram G.102 if we simply replace the argument  $n_J$  with  $\Pi_{n,J}$ . We will comment on these diagrams in chapter 11.

$$\begin{aligned}
& 4 \sum_{J=0}^n \Upsilon_{J+1,0} \left[ \begin{array}{c} \mathbf{G.102} \\ \text{Diagram: } 0^2 \text{ with wavy line and arrow from } n_J^R \end{array} \right]^{1\Delta^{J+1}} + \left[ \begin{array}{cc} \mathbf{G.103} \rightarrow 8.17 & \mathbf{G.104} \rightarrow 8.17 \\ \text{Diagram: } 0^2 \text{ with loop} & + \text{Diagram: } 0^2 \text{ with loop and arrow} \\ & \text{Diagram: } n_J^R \end{array} \right]^{11\Delta^{J+1}} \\
& + 4 \sum_{J=0}^n \sum_{r=0}^{n_J} \Upsilon_{J+1,0} \left[ \begin{array}{cc} \mathbf{G.105} \rightarrow 8.19 & \mathbf{G.106} \rightarrow 8.19 \\ \text{Diagram: } n_{J+r}^R \text{ with loop and dot} & - \text{Diagram: } n_{J+r}^R \text{ with loop and square} \\ & \text{Diagram: } r^R \end{array} \right]^{11\Delta^{J+1}} \\
& - 4 \sum_{J=0}^n \Upsilon_{J,0} \left[ \begin{array}{cc} \mathbf{G.107} & \mathbf{G.108} \\ \text{Diagram: } n_J^R \text{ with loop and arrow} & + \text{Diagram: } n_J^R \text{ with loop and dot} \end{array} \right]^{11\Delta^J}
\end{aligned}$$

Figure 8.16: Diagrams arising from processing diagrams G.93–G.95 that are not cancelled by other diagrams arising from figure 8.14.

Secondly, we note that we can combine diagrams G.105 and G.63. This is simply the two vertex generalisation of the combination of diagrams G.99 and G.49

Lastly, diagrams G.103 and G.104 can be combined, respectively, with diagrams G.59 and G.60. The former diagrams remove from the latter diagrams all contributions in which the wine is decorated.

This is exactly what we saw when we combined diagrams G.100, G.101 with diagrams G.47, G.48. In this case, however, the combination of diagrams vanished since, irrespective of the value of  $n$ , there was no way for the requirement that the wine be undecorated to be reconciled with the number of decorative fields. In the current case, this issue is circumvented by the presence of an additional vertex.

Focusing on the remainder of diagrams G.103 and G.59, we recognise that joining the two-point, tree level vertex to the other vertex allows us to use the effective propagator relation, once more. In the case of the remainder of diagrams G.104 and G.60, the two-point, tree level vertex is already joined to a structure which carries the same momentum (an undecorated wine) and it is clear, in this case, that we cannot use the effective propagator relation. We *can*, however, use diagrammatic identity 8. After utilising this identity, we then decorate the socket of the two-point, tree level vertex in all possible ways.

The result of the above operations is shown in figure 8.17.

**Cancellation 8.11** *Diagram G.111 exactly cancels diagram G.98.*

We can make further progress, since a number of diagrams can be discarded. We focus first on diagram G.109 and G.110. In both cases, the diagrams are disconnected. In the former case, this is a consequence of the wine not being decorated; in the latter case it is trivial. Hence, these diagrams can be discarded. We do, however, make the very important observation that, at higher levels of nesting, we must keep the analogues of these diagrams; in this circumstance, the additional gauge remainder(s) provide a socket(s) to which we can attach the loose vertex.

Diagram G.112, too, can be discarded. The gauge remainder striking the vertex must be bosonic, else the vertex to which it attaches will be decorated



by an odd number of fermions. This restriction can only be satisfied in the  $A$ -sector since gauge remainders have no support in the  $C$ -sector. However, this then causes the diagram to vanish (when we sum over all independent permutations of the fields) by charge conjugation invariance.

In this case, though, it is useful to retain the diagram. By processing diagram G.112, we will find that the generated terms manifestly remove contributions from diagrams later in the calculation. In some sense, this point is moot, since we know that these contributions must vanish anyway. The real point is that we will encounter nested versions of diagram G.112 that do not vanish and so must be processed. Processing the simplest instance of such diagrams i.e. diagram G.112, itself, will illuminate the pattern of cancellations we expect for the more complicated terms.

Returning to figure 8.17, we note that diagrams G.113 and G.99 have a very similar structure and can be combined to give a  $\Lambda$ -derivative term, plus corrections. This observation will prove central to our subsequent analysis (see chapter 10).

We now complete our treatment of the terms of figure 8.14. Using the results of the previous section and the cancellations seen in this section, we can jump straight to the final set of terms. Thus, to generate these terms, we include not only diagrams G.90–G.92<sup>4</sup> but also diagrams G.69, G.70, G.72, G.73, G.105 and G.106. The result of combining these terms is shown split between figures 8.18 and 8.19. The former of these shows the nested gauge remainder terms.

We now collate all surviving terms—including those remaining from the type-Ia sector of the calculation—which fall neatly into three sets:

1. Diagrams which comprise an  $\mathcal{O}(p^2)$  stub, formed by the action of a gauge remainder: G.54, G.74, G.81, G.102, G.122 and G.127;
2. Diagrams which possess the structure  $\text{---}\curvearrowright$  : G.49, G.63, G.67, G.99, G.105, G.113, G.123, G.124, G.125 and G.126;

---

<sup>4</sup>Strictly speaking, some terms arising from the manipulation of these diagrams have already been cancelled by the some of the terms generated by the manipulation of diagrams G.93–G.95.

$$\begin{aligned}
& 4 \sum_{J=0}^n \sum_{r=0}^{n_J} \Upsilon_{J+1,0} \left[ \begin{array}{c} \text{G.114} \\ \begin{array}{c} \circlearrowleft \\ \uparrow \\ \circlearrowleft \\ n_{J+r}^R \end{array} \\ + \\ \text{G.115} \\ \begin{array}{c} \circlearrowleft \\ \circlearrowleft \\ n_{J+r}^R \end{array} \\ + \\ \text{G.116} \\ \begin{array}{c} \circlearrowleft \\ \bullet \\ n_{J+r}^R \end{array} \\ - \\ \text{G.117} \\ \begin{array}{c} \square \\ \circlearrowleft \\ n_{J+r}^R \end{array} \\ \\ \circlearrowleft \\ r, R \end{array} \right]^{11\Delta^{J+1}} \\
& + 4 \sum_{s=1}^{n+} \sum_{J=2}^{2n-1} \Upsilon_{J+s-1, J-1} \\
& \times \left[ \begin{array}{c} \text{G.118} \\ \begin{array}{c} \circlearrowleft \\ \uparrow \\ \circlearrowleft \\ V^{0,1;R} \\ V^{J;R} \end{array} \\ \\ \left[ \prod_{I=1}^{J-1} \sum_{V^{I+}=0}^{V^I} \circlearrowleft \right] \\ V^{I, I+; R} \end{array} \right] + \frac{1}{J} \left[ \begin{array}{c} \text{G.119} \\ \begin{array}{c} \circlearrowleft \\ \circlearrowleft \\ V^{0,1;R} \end{array} \\ \\ \left[ \prod_{I=1}^{J-1} \sum_{V^{I+}=0}^{V^I} \circlearrowleft \right] \\ V^{I, I+; R} \end{array} \right] \left[ \begin{array}{c} \text{G.120} \\ \begin{array}{c} \circlearrowleft \\ \bullet \\ V^{0,1;R} \end{array} \\ \\ \circlearrowleft \\ V^{J;R} \end{array} \right] - \left[ \begin{array}{c} \text{G.121} \\ \begin{array}{c} \square \\ \circlearrowleft \\ V^{0,1;R} \end{array} \\ \\ \circlearrowleft \\ V^{J;R} \end{array} \right] \right]^{11\Delta^{J+s-1}}
\end{aligned}$$

Figure 8.18: Nested gauge remainder contributions arising from the manipulation of diagrams G.90–G.92.

$$\begin{aligned}
& 4 \sum_{J=0}^n \sum_{r=0}^{n_J} \\
& \times \left[ \Upsilon_{J+2,1} \left[ \begin{array}{c} \text{G.122} \\ \text{Diagram: } 0^2 \text{ with wavy line, } n_{J+r}^R \text{ with arrow, } r^R \end{array} \right]^{1\Delta^{J+2}} \right. \\
& \quad \left. + \Upsilon_{J+1,0} \left[ \begin{array}{cc} \text{G.123} \rightarrow 10.1 & \text{G.124} \rightarrow 10.1 \\ \text{Diagram: } n_{J+r}^R \text{ with arrow} & + \text{Diagram: } n_{J+r}^R \text{ with arrow} \\ & \text{Diagram: } r^R \end{array} \right]^{11\Delta^{J+1}} \right] \\
& \quad + 4 \sum_{s=1}^{n_+} \sum_{J=2}^{2n} \frac{\Upsilon_{J+s-1, J-1}}{J} \left[ \begin{array}{cc} \text{G.125} \rightarrow 10.1 & \text{G.126} \rightarrow 10.1 \\ \text{Diagram: } V^{0,1;R} \text{ with arrow} & + \text{Diagram: } V^{0,1;R} \text{ with arrow} \\ \left[ \prod_{I=1}^{J-1} \sum_{V^{I+}=0}^{V^I} V^{I, I+; R} \right] & V^{J; R} \end{array} \right]^{11\Delta^{J+s-1}} \\
& \quad + 4 \sum_{s=1}^{n_+} \sum_{J=2}^{2n-1} \Upsilon_{J+s, J} \left[ \begin{array}{c} \text{G.127} \\ \text{Diagram: } 0^2 \text{ with wavy line, } V^{0,1;R} \text{ with arrow, } \left[ \prod_{I=1}^{J-1} \sum_{V^{I+}=0}^{V^I} V^{I, I+; R} \right] \\ V^{0,1;R} & V^{J; R} \end{array} \right]^{1\Delta^{J+s}}
\end{aligned}$$

Figure 8.19: Result of combining (the surviving contributions to) diagrams G.90–G.92 with diagrams G.69, G.70, G.72, G.73, G.105 and G.106.

3. Nested gauge remainders: G.56, G.58; G.76, G.78, G.80; G.83, G.85, G.87; G.107, G.108, G.112 and G.114–G.121.

We discussed, in some detail, the result of processing nested gauge remainders at the end of the section on type-Ia gauge remainders. We will now add to this, by including the analysis of the nested gauge remainders of type-Ib.

The first thing we note is that, among the set of nested gauge remainders are a set of diagrams which have no analogue in the original set of gauge remainders: namely diagrams G.112, G.117 and G.121. We will put these to the side for one moment.

In preparation for processing the other nested gauge remainders, let us recall the pattern of cancellations in the un-nested case. The bulk of terms generated by the type-Ia and type-Ib parent diagrams cancelled among themselves, courtesy of cancellation mechanisms 1 and 11. Such cancellations will go through in exactly the same way in the nested case. There were then those terms that are cancelled only as a result of combining terms formed by type-Ia gauge remainders with those formed by type-Ib gauge remainders. Examples of this are given by cancellations 8.9–8.11. In the nested case, too, these cancellations will go through just the same, with one exception. At the final level, the analogues of diagrams G.47 and G.48 will have, in addition to the socket on the vertex, an additional  $2n + 1$  locations to which a field must be attached (i.e. corresponding to the  $2n + 1$  nested gauge remainders). To fill these slots, there are precisely the correct number of fields. Now, the type-Ib versions of these diagrams must die at this level of nesting, since we cannot both decorate the wine and leave no empty slots.

Note that this nicely confirms that, at any other level of nesting, the analogue of cancellations 8.9 and 8.10 work: other than at the final level, diagrams G.47 and G.48 always have more decorative fields than empty slots, meaning that the wine must be decorated. This guarantees cancellation against type-Ib terms which necessarily possess a reduced wine.

However, rather than performing these cancellations it will prove useful to retain the components of diagrams G.47 and G.48 which die only as a consequence of our particular choice of decorations i.e. those components with an un-decorated wine. Doing so, we will find a manifest cancellation against

components of other diagrams, coming from later in the calculation.<sup>5</sup>

When dealing with nested terms, though, we must be aware that new types of diagram can arise. There are two ways in which this can happen. First, diagrams, or particular decorations of diagrams, that were legitimately discarded in the un-nested case may survive in the nested case: we have commented already that this is precisely the case with diagrams G.109 and G.110.

Secondly, when a nested gauge remainder generates a two-point, tree level vertex, we now have the option of attaching it to one of the nested gauge remainders. We have encountered this already with the type-Ia gauge remainders, which yielded diagrams of the type shown in figure 8.13. Noting that we will find further examples of such terms shortly, we show the type-Ib analogue of the aforementioned diagrams in figure 8.20.

$$-4 \sum_{J=0}^n \Upsilon_{J,0} \left[ \begin{array}{c} \{ \text{G.128 } G.367 \} \quad \{ \text{G.129 } G.368 \} \\ \begin{array}{c} \text{Diagram 1: } \text{A circle labeled } n_J^R \text{ with an arrow pointing to a circle labeled } 0^2 \text{ which has a self-loop.} \\ \text{Diagram 2: } \text{A circle labeled } n_J^R \text{ with an arrow pointing to a circle labeled } 0^2 \text{ which has a self-loop and a small dot on the arrow.} \end{array} \end{array} \right]^{11\Delta^J}$$

Figure 8.20: Analogues of the diagrams of figure 8.13 generated by type-Ib gauge remainders.

We now return to the three diagrams that we temporarily put to one side, diagrams G.112, G.117 and G.121. However, we note that these now have partner diagrams which are nested with respect to the already processed gauge remainder; these additional terms coming, of course, from having manipulated the other nested gauge remainders.

Processing this set of diagrams is actually very easy, requiring a minor generalisation of cancellation mechanism 11. Recall the set-up for cancellation mechanism 11: a wine, whose join to the arbitrary structure  $B$  can be via nested gauge remainders, attaches to the structure  $A$  via nested gauge remainders. Allowing the gauge remainder hitting  $A$  to act, we assume that it strikes a

<sup>5</sup>At the un-nested level, there is no mileage in keeping the vanishing terms.

socket. Up until now, we have demanded that this socket could not be filled by the other end of the wine. Now, we simply relax this assumption, though we need to do so with care.

By allowing the socket to be filled by the wine, we are implicitly identifying the structures  $A$  and  $B$ . In the case that  $A$  and  $B$  are both reduced vertices, this step would be illegal for type-Ia gauge remainders since  $B$  would have to have been a seed action vertex whereas  $A$  would have to have been a Wilsonian effective action vertex. (Note that this problem does not arise for type-Ib gauge remainders). In the case that  $A$  and  $B$  are both identified with the wine, we would discard the result in both the type-Ia and type-Ib cases, since it would correspond to a wine biting its own tail. However, in the type-II case, we note that the attachment of the wine to the structure  $B$  is non-trivial i.e. is via a gauge remainder. In the case that we identify both  $A$  and  $B$  with the wine, this prevents the wine from biting its own tail.

Next we must consider a similar diagram in which the gauge remainder which previously attached to  $A$  now attaches to a vertex, instead. In the case that the gauge remainder strikes a socket and this socket is filled by the wine, we are now identifying the *vertex* with structure  $B$ . When we take the two-point, tree level part of this vertex, we still go ahead and attach it to the structure  $A$  with an effective propagator. We are then free to identify  $A$  as either a vertex or the wine.

With these thoughts in mind, we now supplement cancellation mechanism 11.

**Cancellation Mechanism 12** *Cancellation mechanism 11 holds exactly if we allow the socket struck by the gauge remainder to be filled by the wine, so long as the implicit identification of structures involved does not lead to an inconsistency.*

Thus, cancellation mechanism 12 now guarantees that contributions from diagrams G.112, G.117, G.121 and their analogues possessing additional vertices in which the gauge remainder bites a socket which decorates anything other than a two-point, tree level vertex will cancel. This equally applies to the version of these diagrams in which the gauge remainder biting the base of

the wine is nested.

Iterating the diagrammatic procedure once, we obtain nested versions of the parents, diagrams possessing an  $\mathcal{O}(p^2)$  stub and diagrams in which the two-point, tree level vertex has been joined to a bitten gauge remainder. Note that the nesting is now with respect to the gauge remainder we are currently performing.

Iterating the diagrammatic procedure until exhaustion, we obtain either diagrams with an  $\mathcal{O}(p^2)$  stub or diagrams in which the two-point, tree level vertex has been joined to a bitten gauge remainder. In figure 8.21 we give examples of these latter terms. The diagrams that we choose to draw are the simplest that can exist in the sense that we choose to draw the ones with the minimum number of vertices and the minimum level of nesting. We henceforth call such a set of diagrams a minimal set. (We no longer explicitly draw diagrams with an  $\mathcal{O}(p^2)$  stub, since we will not be doing a complete treatment of them, within this thesis.)

We can now group all terms which survive upon processing the nested gauge remainders.

1. Diagrams which comprise an  $\mathcal{O}(p^2)$  stub, formed by the action of a gauge remainder;
2. Diagrams which comprise a nested version of  $\mathfrak{R}$ , including those diagrams in which one of the gauge remainders in this structure is hit by  $\Lambda\partial_\Lambda$ ;
3. Diagrams in which a two-point, tree level vertex is attached to one of the nested gauge remainders;

To conclude this section, we analyse those diagrams in which the string of nested gauge remainders bite each other, in a loop i.e. the second set above. In the case of such terms formed by type-Ia gauge remainders this is trivial: we just generate nested versions of diagrams G.49, G.63, and G.67. In the case of such terms formed by type-Ib gauge remainders, alone, things are exactly the same i.e. we simply generate nested versions of diagrams G.105, G.123 and G.125.

$$\begin{aligned}
& +4\Upsilon_{n-1,0} \\
& \left[ \begin{array}{cccc}
\text{G.130} \rightarrow 9.21 & & \text{G.131} \rightarrow 9.21 & \\
- \text{ (diagram)} & + & \text{ (diagram)} & \\
\text{G.132} \rightarrow 9.24 & \text{G.133} \rightarrow 9.24 & \text{G.134} \rightarrow 9.24 & \text{G.135} \rightarrow 9.24 \\
+ \text{ (diagram)} & - \text{ (diagram)} & - \text{ (diagram)} & - \text{ (diagram)} \\
\text{G.136} \rightarrow 9.24 & \text{G.137} \rightarrow 9.24 & \text{G.138} \rightarrow 9.24 & \text{G.139} \rightarrow 9.24 \\
- \text{ (diagram)} & + \text{ (diagram)} & + \text{ (diagram)} & - \text{ (diagram)}
\end{array} \right] 11\Delta^{n-1}
\end{aligned}$$

Figure 8.21: The simplest versions of diagrams in which a two-point, tree level vertex is attached to a bitten gauge remainder.





and  $L$ s to represent ones and zeros:

$$\begin{aligned} &RR \cdots RR \\ &RR \cdots RL \\ &RR \cdots LR \\ &\vdots \end{aligned}$$

Next, imagine that we cyclically permute each of the above strings. After a suitable vertical re-ordering of terms, we just reproduce the above sequence. Thus, when singling out one of the gauge remainders of diagram I.11—for example to attach a wine to or to hit with  $\Lambda \partial_\Lambda|_\alpha$ —we can do this in  $m$  equivalent ways. Therefore, the conversion of diagrams I.9 and I.10 into diagram I.11 works, irrespective of the precise arrangement of the gauge remainders.

### 8.3 Type-II Gauge Remainders

All gauge remainders of type-II have been collected together in figure 8.24. The general pattern of terms is similar to those for the gauge remainders of types-Ia and Ib, but with some marked differences.

The most obvious difference in the pattern of terms is the appearance of diagrams G.143, G.147, G.150 and G.151. However, we also see that diagrams G.149, G.146 and G.142 come with factor of two, relative to their partner diagrams. This makes sense: for these diagrams, we have correctly counted separately the case where each of the gauge remainders attaches to the wine.

We must now decide how to process these diagrams. The first thing we note is that we are guaranteed to encounter trapped gauge remainders in diagrams G.148, G.151 and their analogues possessing additional vertices. In each of these cases, we can choose to act with either of the gauge remainders first, and one of the things it will do is bite the field on the structure to which the tip of the other gauge remainder is attached. If, on the other hand, the first action of one of the gauge remainders is to bite a socket or the end of a wine, then we are free to perform the other gauge remainder as well. However, as we will see shortly, it is inefficient to do this: we will be able to cancel a set of diagrams in which an active gauge remainder is un-processed.

Given that we are only going to process one gauge remainder, for the time being, we must decide what to do with diagrams G.149, G.146 and G.142. The answer is to be democratic: we take one instance of these diagrams where one gauge remainder acts and one instance where the other acts, dividing by two to avoid over-counting.

Once a gauge remainder has acted, we proceed in exactly the same way as we did with the gauge remainders of types-Ia and Ib: we isolate any two-point, tree level vertices, decorate them and apply the effective propagator relation, as appropriate. This procedure is trivial for diagrams in which a single vertex is hit by both gauge remainders: if one of the gauge remainders hits a socket, then the vertex must still be reduced, else it will be killed by the remaining gauge remainders (indeed, the vertex must actually be three-point or greater,

$$\begin{aligned}
& - \sum_{s=1}^{n_+} \sum_{J=2}^{2n} \Upsilon_{J+s-1, J-1} \\
& \times \left[ \begin{array}{c} \text{G.140} \\ \begin{array}{c} \textcircled{V^{J;R}} \\ \updownarrow \\ \textcircled{V^{0,1;R}} \end{array} \\ \end{array} \right] + \frac{1}{J} \left[ \begin{array}{c} \text{G.141} \\ \begin{array}{c} \textcircled{V^{0,1;R}} \\ \circlearrowleft \end{array} \end{array} \right] + 2 \left[ \begin{array}{c} \text{G.142} \\ \begin{array}{c} \bullet \\ \downarrow \\ \textcircled{V^{0,1;R}} \\ \textcircled{V^{J;R}} \end{array} \end{array} \right] + \frac{1}{J+1} \left[ \begin{array}{c} \text{G.143} \\ \begin{array}{c} \textcircled{V^{0,1;R}} \\ \bullet \\ \textcircled{V^{0,1;R}} \end{array} \end{array} \right] \\
& \left[ \prod_{I=1}^{J-1} \sum_{V^{I+}=0}^{V^I} \textcircled{V^{I, I+; R}} \right] \Bigg]^{11\Delta^{J+s-1}} \\
& - \sum_{J=0}^n \sum_{r=0}^{n_J} \Upsilon_{J+1, 0} \\
& \times \left[ \begin{array}{c} \text{G.144} \rightarrow 8.27 \\ \begin{array}{c} \textcircled{r^R} \\ \updownarrow \\ \textcircled{n_{J+r}^R} \end{array} \end{array} \right] + \left[ \begin{array}{c} \text{G.145} \rightarrow 8.27 \\ \begin{array}{c} \textcircled{n_{J+r}^R} \\ \circlearrowleft \end{array} \end{array} \right] + 2 \left[ \begin{array}{c} \text{G.146} \rightarrow 8.27 \\ \begin{array}{c} \bullet \\ \downarrow \\ \textcircled{n_{J+r}^R} \\ \textcircled{r^R} \end{array} \end{array} \right] + \frac{1}{2} \left[ \begin{array}{c} \text{G.147} \\ \begin{array}{c} \textcircled{n_{J+r}^R} \\ \bullet \\ \textcircled{n_{J+r}^R} \end{array} \end{array} \right] \\
& + \sum_{J=0}^n \Upsilon_{J, 0} \left[ \begin{array}{c} \text{G.148} \rightarrow 8.26 \\ \begin{array}{c} \textcircled{n_J^R} \\ \circlearrowleft \end{array} \end{array} \right] + 2 \left[ \begin{array}{c} \text{G.149} \rightarrow 8.26 \\ \begin{array}{c} \bullet \\ \downarrow \\ \textcircled{n_J^R} \end{array} \end{array} \right] + \left[ \begin{array}{c} \text{G.150} \rightarrow 8.27 \\ \begin{array}{c} \textcircled{n_J^R} \\ \bullet \\ \textcircled{n_J^R} \end{array} \end{array} \right] \\
& - \Upsilon_{n-1, 0} \left[ \begin{array}{c} \text{G.151} \rightarrow 8.26 \\ \begin{array}{c} \textcircled{n_J^R} \\ \bullet \\ \textcircled{n_J^R} \end{array} \end{array} \right] \Bigg]^{11\Delta^{n-1}} \\
& \Bigg]^{11\Delta^{J+1}}
\end{aligned}$$

Figure 8.24: Type-II gauge remainders.

irrespective of loop order, though we will not make use of this). On the other hand, if one of the gauge remainders traps the other, then a reduction of the vertex is no longer forced.

We now see the benefit both of performing only one of the gauge remainders and of treating the gauge remainders in diagrams G.149, G.146 and G.142 democratically. Starting with diagram G.151 let us suppose that we process one of the gauge remainders and it strikes a socket. By cancellation mechanism 11 this will be cancelled by a contribution arising from diagram G.149. To be precise, this contribution will be killed if we take one half of diagram G.149 and allow the bottom gauge remainder to act, creating a two-point, tree level vertex, which we then join to the wine with an effective propagator.

Staying with diagram G.149, the next thing to do is to find the contributions in which one of the gauge remainders strikes a socket on anything other than a two-point, tree level vertex. There are two ways in which this can happen. Either the bottom gauge remainder can strike a socket on the vertex or the top gauge remainder can strike a socket on the wine. Let us now add this collection of diagrams to those generated by the gauge remainders of diagrams G.148 and G.150 striking a socket.<sup>7</sup> It is not hard to check that the complete set of these diagrams is cancelled by terms coming from diagrams G.144 and G.146. This only works if we treat the gauge remainders in the latter diagram democratically. Moving on to diagrams G.140–G.143, it is clear that all contributions in figure 8.24 for which a gauge remainder strikes a socket are removed by cancellation mechanism 11.

We must now address the question of the types of term that will be left over, after we allow one of the gauge remainders to act. As usual, we will be left with terms possessing an  $\mathcal{O}(p^2)$  stub, nested gauge remainders and terms in which a gauge remainder strikes the end of a wine. Additionally, as mentioned previously, we will find trapped gauge remainders.

Consider allowing one of the gauge remainders in diagram G.145 to act, trapping the other gauge remainder and creating a two-point tree level vertex.

---

<sup>7</sup>In the former case, if the socket decorates a two-point, tree level vertex, then the diagram dies whereas, in the latter case, it is impossible to generate a socket on a two-point, tree level vertex.

Now join this vertex to either the wine or the other vertex, with one of the effective propagators. This procedure is shown in figure 8.25.

$$\begin{aligned}
 & -2 \sum_{J=0}^n \Upsilon_{J+1,0} \left[ \begin{array}{c} \text{Diagram 1} \\ \text{Diagram 2} \end{array} \right]^{11\Delta^{J+1}} \\
 & \rightarrow -2 \sum_{J=0}^n \Upsilon_{J,0} \left[ \begin{array}{c} \text{Diagram 3} \\ \text{Diagram 4} \end{array} \right]^{11\Delta^J} + \dots
 \end{aligned}$$

Figure 8.25: Some of the terms generated by processing diagram G.145.

The terms on the second line of figure 8.25 will cancel against trapped gauge remainder terms generated by diagrams G.148 and G.150. These cancellations are an example of cancellation mechanism 12.

Indeed, cancellation mechanism 12 now guarantees that all diagrams arising from figure 8.24 possessing a trapped gauge remainder are cancelled, up to nested gauge remainders and terms with an  $\mathcal{O}(p^2)$  stub.

We are almost ready to process the diagrams of figure 8.24, but there are a couple of further observations we can make to simplify things. We have noted that, among the terms left over are those in which a gauge remainder strikes the end of a wine. Depending on which end of the wine the gauge remainder bites will determine how we treat the corresponding term. If the gauge remainder bites the end of the wine to which the remaining, active gauge remainder attaches, then we will go ahead and process the active gauge remainder. If, on the other hand, the first gauge remainder bites the other end of the wine, then we will leave the remaining active gauge remainder unprocessed, for the time being. The reason for this is that, later in the calculation, we will find terms that combine with the diagrams possessing unprocessed gauge remainders; by leaving these gauge remainders unprocessed, until that stage, we save ourselves

some work.

In the case where we do allow the second gauge remainder to act, cancellation mechanism 11 ensures that terms in which this gauge remainder bites a socket that decorates anything other than a two-point, tree level vertex will cancel.<sup>8</sup> Hence, in cases where both gauge remainders strike the wine, we are ultimately left only with those terms in which both gauge remainders hit the ends of the wine.

Finally, then, figure 8.26 shows the result of processing diagrams G.148, G.149 and G.151, where all terms which would be cancelled by cancellation mechanisms 11 and 12 have been omitted.

Having done all that we can with diagrams G.148, G.149 and G.151, up to processing nested gauge remainders, we now move on to diagrams G.144–G.146 and G.150.

We can immediately write down the result of processing these diagrams, by using cancellation mechanisms 11 and 12 and by using the preceding analysis as a template. Most straightforwardly, we obtain a copy of figure 8.26, but where each diagram contains an extra vertex, with argument  $n_J^R$ , and where the factor of  $-\Upsilon_{n-1,0}$  is replaced by  $\Upsilon_{J,0}$ ;  $J$  being summed over in the usual manner. In addition to these terms, we obtain a further set of nested gauge remainders, which are shown in figure 8.27

Clearly, the result of processing the remaining diagrams of figure 8.24 is just to create versions of figures 8.26 and 8.27 with greater number of vertices. In the new versions of the latter figure we will, of course, also have a nested version of diagram G.144.

Our task now is to understand what happens when we allow the gauge remainders in these diagrams to act, recalling that we choose to hold back with diagrams G.152 and G.153. To do this, it is useful to split the diagrams into different classes, listed below. Each class constitutes a minimal set of

---

<sup>8</sup>If we were to allow the gauge remainder to act in the terms were we have withheld its action, cancellation mechanism 11 would ensure the usual cancellation of diagrams in this case, too.

$$\begin{aligned}
& 2 \sum_{J=0}^n \Upsilon_{J,0} \left[ \begin{array}{c} \mathbf{G.152} \rightarrow 10.7 \\ \cdot \downarrow \uparrow \\ \textcircled{n^R_J} \end{array} \right]^{11\Delta^J} - 2\Upsilon_{n-1,0} \left[ \begin{array}{c} \mathbf{G.153} \rightarrow 10.7 \\ \cdot \downarrow \uparrow \end{array} \right]^{11\Delta^{n-1}} \\
& - 2\Upsilon_{n-1,0} \\
& \times \left[ \begin{array}{cccc} \mathbf{G.154} \rightarrow 8.30 & \mathbf{G.155} \rightarrow 8.29 & \mathbf{G.156} \rightarrow 8.28 & \mathbf{G.157} \rightarrow 8.28 \\ \cdot \downarrow \uparrow & \cdot \downarrow \uparrow & \cdot \downarrow \uparrow & \cdot \downarrow \uparrow \\ + & + & - & \\ \mathbf{G.158} \rightarrow 8.33 & \mathbf{G.159} \rightarrow 8.33 & \{ \mathbf{G.160} \ G.352 \} & \{ \mathbf{G.161} \ G.353 \} \\ + & - & + & - \\ \cdot \downarrow \uparrow & \cdot \downarrow \uparrow & \cdot \downarrow \uparrow & \cdot \downarrow \uparrow \end{array} \right]^{11\Delta^{n-1}} \\
& + 2\Upsilon_{n,0} \left[ \begin{array}{cccc} \mathbf{G.162} & \mathbf{G.163} & \mathbf{G.164} & \mathbf{G.165} \\ \cdot \downarrow \uparrow & \cdot \downarrow \uparrow & \cdot \downarrow \uparrow & \cdot \downarrow \uparrow \\ \textcircled{0^2} & \textcircled{0^2} & \textcircled{0^2} & \textcircled{0^2} \\ \cdot \downarrow \uparrow & \cdot \downarrow \uparrow & \cdot \downarrow \uparrow & \cdot \downarrow \uparrow \end{array} \right]^{1\Delta^n}
\end{aligned}$$

Figure 8.26: Result of processing diagrams G.148, G.149 and G.151, up to terms which are guaranteed to cancel, via cancellation mechanisms 11 and 12.

$$2 \sum_{J=0}^n \Upsilon_{J,0} \left[ \begin{array}{c}
\begin{array}{ccc}
\text{G.166} \rightarrow 8.30 & \text{G.167} \rightarrow 8.30 & \text{G.168} \rightarrow 8.30 \\
\begin{array}{c} \circ \\ \downarrow \\ \circ \\ \downarrow \\ n_J^R \end{array} & + & \begin{array}{c} \circ \\ \downarrow \\ \bullet \\ \downarrow \\ n_J^R \end{array} & + & \begin{array}{c} \circ \\ \downarrow \\ \bullet \\ \downarrow \\ n_J^R \end{array} \\
\text{G.169} \rightarrow 8.29 & \text{G.170} \rightarrow 8.28 & \text{G.171} \rightarrow 8.28 \\
+ & \begin{array}{c} \circ \\ \downarrow \\ n_J^R \end{array} & + & \begin{array}{c} \circ \\ \downarrow \\ n_J^R \end{array} & - & \begin{array}{c} \circ \\ \downarrow \\ n_J^R \end{array}
\end{array} \right] 11\Delta^J$$

Figure 8.27: Nested gauge remainder terms generated from diagrams G.144–G.146 and G.150.

diagrams, which we give explicitly, together with copies of the diagrams of this minimal set supplemented by additional vertices.

1. Diagrams possessing a single, unprocessed gauge remainder, which is active. The minimal set of such term constitutes diagrams G.156, G.157, G.170 and G.171;
2. Diagrams possessing two unprocessed gauge remainders, one of which is active and the other of which is inactive. The minimal set of such terms constitutes diagrams G.155 and G.169;
3. Diagrams possessing two unprocessed, active gauge remainders. The minimal set such terms constitutes diagrams G.154, G.166–G.168 and the nested version of diagram G.144.

Allowing the gauge remainders to act, we will find that all terms in which the gauge remainder strikes a socket will cancel by cancellation mechanisms 11 and 12, unless the socket decorates a two-point, tree level vertex. Furthermore, these cancellations occur within the above classes.

For the diagrams of the final class—in each of which there are two active gauge remainders, one of which is nested—we might suspect that, once more

we should be diplomatic and take contributions in which each of the gauge remainders act. However, it is unnecessary to do this.

We can understand the need for our original diplomacy as being down to the indistinguishability of the two gauge remainder structures i.e. each of these structures constitutes an un-nested, single gauge remainder. In the current case, however, the two structures are distinguishable, since one is nested whilst one is not. If we consistently allow just one of these structures to act, then cancellation mechanisms 11 and 12 will guarantee that all contributions in which the gauge remainder bites a socket (unless the socket is on a two-point, tree level vertex), including the case where the socket is filled by the wine, cancel among themselves. The question is with which gauge remainder structure should we act? Of course, either choice is equivalent though we can hope that a judicious choice will simplify the rest of the calculation.

We choose to allow the nested structure to act. As we will see, this does generate a particularly appealing set of diagrams. Moreover, had we allowed the un-nested gauge remainder to act then, among the diagrams of the next level of nesting, we would have found terms possessing two identical (nested) gauge remainder structures. In this case, we would once again have had to turn to diplomacy; by always choosing to process the nested contribution, we avoid ever having to do this again.

We now describe the terms which survive the action of the gauge remainders, up to those diagram with an  $\mathcal{O}(p^2)$  stub which is generated by the action of a gauge remainder. Let us begin with those coming from the first class, above, which are shown in figure 8.28.

Despite the apparent slew of terms, what we have is actually very simple. Diagrams G.172–G.179 are just nested versions of the parent diagrams; diagrams G.180–G.183 are further cases of the by-now-familiar diagrams in which a two-point, tree level vertex is joined to a bitten gauge remainder and diagrams G.184–G.191 are just nested versions of diagrams G.158–G.161.

The sense in which we can consider certain diagrams of figure 8.28 to be nestings of old diagrams is very precise. To see this let us consider first diagrams G.172–G.175 as nestings of diagrams G.170 and G.171. In this case

$$\begin{aligned}
& 2 \sum_{J=0}^n \Upsilon_{J,0} \left[ \begin{array}{cccc} \text{G.172} & \text{G.173} & \text{G.174} & \text{G.175} \\ \text{Diagram 1} & \text{Diagram 2} & \text{Diagram 3} & \text{Diagram 4} \end{array} \right]^{11\Delta^J} \\
& - 2\Upsilon_{n-1,0} \\
& \times \left[ \begin{array}{cccc} \text{G.176} & \text{G.177} & \text{G.178} & \text{G.179} \\ \text{Diagram 5} & \text{Diagram 6} & \text{Diagram 7} & \text{Diagram 8} \\ \text{G.180} \rightarrow 9.23 & \text{G.181} \rightarrow 9.23 & \text{G.182} \rightarrow 9.23 & \text{G.183} \rightarrow 9.23 \\ \text{Diagram 9} & \text{Diagram 10} & \text{Diagram 11} & \text{Diagram 12} \\ \text{G.184} \rightarrow 9.22 & \text{G.185} \rightarrow 9.22 & \text{G.186} & \text{G.187} \\ \text{Diagram 13} & \text{Diagram 14} & \text{Diagram 15} & \text{Diagram 16} \\ \text{G.188} \rightarrow 9.22 & \text{G.189} \rightarrow 9.22 & \text{G.190} & \text{G.191} \\ \text{Diagram 17} & \text{Diagram 18} & \text{Diagram 19} & \text{Diagram 20} \end{array} \right]^{11\Delta^{n-1}}
\end{aligned}$$

Figure 8.28: The minimal set of terms arising from processing diagrams G.156, G.157, G.170 and G.171 and their analogues with additional vertices, up to terms with an  $\mathcal{O}(p^2)$  stub.

the rule to take us from the old diagram to the new diagram is simple: we insert an additional gauge remainder between the active gauge remainder and the preceding processed gauge remainder, picking up a sign if the insertion corresponds to a pull back. In the parent diagrams there is, however, a second processed gauge remainder and we might well wonder whether this can become nested as well. The answer is yes: we will see how this comes about shortly.

Similarly, all other diagrams which we have said can be thought of as nestings of earlier diagrams can, at this stage of the calculation, only be thought of as nestings with respect to a particular processed gauge remainder. With our experiences of the calculation thus far, it is not surprising that we will find that this restriction can be lifted, upon continuing with the diagrammatic procedure.

Next, we move on to consider the surviving terms coming from the second class of diagrams, above, collecting together all such terms in figure 8.29, up to diagrams with an  $\mathcal{O}(p^2)$  stub.

$$\begin{aligned}
& 2 \sum_{J=0}^n \Upsilon_{J,0} \left[ \begin{array}{c} \text{G.192} \\ \text{G.193} \end{array} \right]^{11\Delta^J} + 2\Upsilon_{n-1,0} \left[ \begin{array}{c} \text{G.194} \\ \text{G.195} \end{array} \right]^{11\Delta^{n-1}} \\
& \qquad \qquad \qquad + 2\Upsilon_{n-1,0} \\
& \times \left[ \begin{array}{c} \text{G.196} \rightarrow 8.33 \quad \text{G.197} \rightarrow 8.33 \quad \text{G.198} \rightarrow 9.21 \quad \text{G.199} \rightarrow 9.21 \\ \text{diagram 1} \quad \text{diagram 2} \quad \text{diagram 3} \quad \text{diagram 4} \end{array} \right]^{11\Delta^{n-1}}
\end{aligned}$$

Figure 8.29: Surviving contributions from diagrams G.155 and G.169, modulo terms with an  $\mathcal{O}(p^2)$  stub.

Once again, we have generated nested versions of the parent diagrams but, once again, we have generated only one of the possible types of nesting. Re-

ferring back to the parents, diagrams G.155 and G.169, we note that each has one active gauge remainder, one performed gauge remainder and one trapped gauge remainder. Diagrams G.192–G.195 are nested with respect to the active gauge remainder. We will shortly generate the nestings with respect to the performed gauge remainder; trapped gauge remainders will never become nested since, by definition, they are unable to act.

The final four diagrams of figure 8.29 will prove to be of particular interest. Notice that diagram G.197 (G.196) naturally combines with diagram G.159 (G.158); we return to this at the end of the section. Having combined terms in this manner, we will find in section 9.1 that they can be redrawn via diagrammatic identity 11. The resultant diagram will then take the same form as diagram G.198 (G.199) but with the gauge remainder on the other end of the wine.<sup>9</sup> We will return to this observation in section 9.2.

Finally, then, we can treat the surviving terms coming from the third class of diagrams, above, for which we recall that the minimal set comprises diagrams G.154, G.166–G.168 and the nested version of diagram G.144. Remembering to perform, undemocratically, the nested gauge remainder first, we split the resultant terms into three sets.

First, we have those diagrams with an  $\mathcal{O}(p^2)$  stub, which we comment on in chapter 11. Secondly, we have diagrams with a further level of nesting. As usual, we produce nested versions of the parent diagrams, where we note that the nesting is with respect to the already nested gauge remainder. There are, however, additional nested diagrams, as we should expect. Returning to the original set of type-II gauge remainders in figure 8.24, we know that among the nested gauge remainders generated are diagrams with a different structure to the parents: namely diagrams G.155–G.157 and G.169–G.171. Thus, we expect nested versions of these to be produced when we process nested versions of the original gauge remainders.

Now we can start to see how everything meshes together. We have already seen that by processing diagrams G.155–G.157 and G.169–G.171, we generate their nested counterparts, but that this nesting is with respect to the active

---

<sup>9</sup>The two diagrams with a gauge remainder on either end of the wine can actually be shown to be equivalent to each other, by a trivial redrawing.

gauge remainder. By processing the diagrams of the third class, above, we now generate nested versions of diagrams G.155–G.157 and G.169–G.171 where the nesting is with respect to the gauge remainder which bites the wine.

The third set of terms—which constitutes all those diagrams not in the first or second sets—is shown in figure 8.30. As with that which was done previously, if the first gauge remainder bites the opposite end of the wine to the one which the other gauge remainder attaches, then we delay further manipulation. We show the resultant diagrams in figure 8.30.

There are a number of comments worth making. First, note how diagrams G.202–G.205 are nested versions of diagrams G.152 and G.153, respectively, where the nesting is with respect to the performed gauge remainder. These diagrams, like diagrams G.200, G.201, G.216 and G.217, still possess an active gauge remainder, which we choose not to process, for the time being.

Secondly, diagrams G.206–G.213 naturally combine with diagrams G.184–G.191. Together, we can think of these as nested versions of diagrams G.158–G.161 where now we perform the nesting in all possible ways. Note that these diagrams—or, at any rate, their analogues possessing additional vertices—are precisely the type of diagrams we alluded to at the end of section 8.2. Taking the undecorated component of the wines, we see that we produce the diagrams necessary to exactly cancel a special case of diagram I.12<sup>10</sup> i.e. the case where  $m = 3$ .

We are now in a position to deduce the diagrams that remain once we have iterated the diagrammatic procedure, until exhaustion, which we list below.

1. terms with an  $\mathcal{O}(p^2)$  stub, which has been formed by the action of a gauge remainder;
2. Diagrams possessing a wine which has been bitten by two gauge remainders. To generate the terms this set comprises, we start with just diagrams G.158–G.161 and G.196–G.199. For each of these terms, we now include nested versions where the nesting is respect to either of the performed gauge remainders. Note, of course, that we have already explicitly

---

<sup>10</sup>Recalling that, in diagram I.12 we must pick up a minus sign for each pull back and that we sum over all realisations of the un-drawn gauge remainders.

$$\begin{aligned}
& -2 \sum_{J=0}^n \Upsilon_{J,0} \\
& \times \left[ \begin{array}{cccc}
\text{G.200} \rightarrow 10.20 & \text{G.201} \rightarrow 10.20 & \text{G.202} \rightarrow 10.20 & \text{G.203} \rightarrow 10.20 \\
\begin{array}{c} \text{Diagram 1} \\ \text{Diagram 2} \end{array} & - \begin{array}{c} \text{Diagram 3} \\ \text{Diagram 4} \end{array} & + \begin{array}{c} \text{Diagram 5} \\ \text{Diagram 6} \end{array} & - \begin{array}{c} \text{Diagram 7} \\ \text{Diagram 8} \end{array} \\
\end{array} \right] 11\Delta^J \\
& -2\Upsilon_{n-1,0} \\
& \times \left[ \begin{array}{cccc}
& \text{G.204} \rightarrow 10.20 & \text{G.205} \rightarrow 10.20 & \\
& - \begin{array}{c} \text{Diagram 9} \\ \text{Diagram 10} \end{array} & + \begin{array}{c} \text{Diagram 11} \\ \text{Diagram 12} \end{array} & \\
\text{G.206} \rightarrow 9.22 & \text{G.207} \rightarrow 9.22 & \text{G.208} & \text{G.209} \\
+ \begin{array}{c} \text{Diagram 13} \\ \text{Diagram 14} \end{array} & - \begin{array}{c} \text{Diagram 15} \\ \text{Diagram 16} \end{array} & + \begin{array}{c} \text{Diagram 17} \\ \text{Diagram 18} \end{array} & - \begin{array}{c} \text{Diagram 19} \\ \text{Diagram 20} \end{array} \\
\text{G.210} \rightarrow 9.22 & \text{G.211} \rightarrow 9.22 & \text{G.212} & \text{G.213} \\
- \begin{array}{c} \text{Diagram 21} \\ \text{Diagram 22} \end{array} & + \begin{array}{c} \text{Diagram 23} \\ \text{Diagram 24} \end{array} & - \begin{array}{c} \text{Diagram 25} \\ \text{Diagram 26} \end{array} & + \begin{array}{c} \text{Diagram 27} \\ \text{Diagram 28} \end{array} \\
\{ \text{G.214 } G.365 \} & \{ \text{G.215 } G.366 \} & \text{G.216} \rightarrow 10.20 & \text{G.217} \rightarrow 10.20 \\
+ \begin{array}{c} \text{Diagram 29} \\ \text{Diagram 30} \end{array} & - \begin{array}{c} \text{Diagram 31} \\ \text{Diagram 32} \end{array} & - \begin{array}{c} \text{Diagram 33} \\ \text{Diagram 34} \end{array} & + \begin{array}{c} \text{Diagram 35} \\ \text{Diagram 36} \end{array} \\
\text{G.218} \rightarrow 8.33 & \text{G.219} \rightarrow 8.33 & \text{G.220} \rightarrow 8.33 & \text{G.221} \rightarrow 8.33 \\
- \begin{array}{c} \text{Diagram 37} \\ \text{Diagram 38} \end{array} & + \begin{array}{c} \text{Diagram 39} \\ \text{Diagram 40} \end{array} & + \begin{array}{c} \text{Diagram 41} \\ \text{Diagram 42} \end{array} & - \begin{array}{c} \text{Diagram 43} \\ \text{Diagram 44} \end{array} \\
\end{array} \right] 11\Delta^{n-1}
\end{aligned}$$

Figure 8.30: Surviving terms from diagrams G.154, G.166–G.168 and the nested version of diagram G.144, up to additionally nested diagrams and terms with an  $\mathcal{O}(p^2)$  stub.

encountered some of these diagrams. For every diagram now in the set, we include copies possessing additional vertices.

3. Diagrams possessing a wine bitten by a single gauge remainder at one end and having an active gauge remainder at the other. To generate the terms this set comprises, we start with just diagrams G.152 and G.153. For both of these terms, we now include nested versions where the nesting is respect to either of the performed gauge remainder and etcetera;
4. Diagrams possessing a two-point, tree level vertex joined to a bitten gauge remainder. The examples of this we have seen so far are: diagrams G.180–G.183, G.200, G.201 and G.214–G.221.

Whereas we have stated how to generate the complete set of diagrams for the second and third sets above, we have not done so with the fourth set. The reason is that, whilst we certainly expect the fourth set of terms to contain nestings of the diagrams already listed, there are additional terms that we have not yet encountered.

The diagrams we are considering occur whenever a diagram possesses the following: a two-point, tree level vertex, formed by the action of a gauge remainder, and a nested gauge remainder, which is not attached to anything. This tells us that, indeed, there is a diagram of the form we are interested in that we are yet to encounter. To see this, return to the diagrams of figure 8.27. With the exception of diagram G.169 all these diagrams possess a nested gauge remainder, which is not attached to anything. Hence, after processing the gauge remainder(s) of these diagrams, we will generate two-point, tree level vertices, which can give us diagrams of the type we are currently studying. However, in the case of diagram G.169 we must wait until the next level of nesting until we are able to generate a two-point, tree level vertex which is joined to a bitten gauge remainder. The additionally nested versions of this diagram have actually been generated—see diagrams G.192 and G.193—but are yet to be processed. When we do process them, among the terms generated will be those in figure 8.31.



Now we have all the diagrams we need from which we generate the complete set of diagrams comprising a two-point, tree level vertex attached to a bitten gauge remainder. Starting from diagrams G.180–G.183, G.200, G.201, G.214–G.221 and G.222–G.229 we now include all possible nestings of each of these terms. Finally, for every diagram now in the set, we include copies possessing additional vertices.

We might worry that the considerations that led us to the diagrams of figures 8.31 and 8.32 imply that we are missing contributions that could arise from e.g. diagram G.167. If we allow the nested gauge remainder to act first and it bites an end of the wine, then we know we must allow the un-nested gauge remainder to act. If this second gauge remainder were nested, then when we generate a two-point tree level vertex, we would have a new option of where to attach it. Since we have not explicitly gone to this level of nesting in the calculation, we might worry that we are missing such terms. They are, however, taken care of by diagrams G.170 and G.171. Upon processing these terms we generate, among others, diagrams G.180–G.183. Provided that we consider all possible nestings of these diagrams, then we will generate the terms we were worrying about.

At this stage, it perhaps seems that the set of diagrams comprising a two-point, tree level vertex joined to a bitten gauge remainder form a disparate set of terms. There is, however, a deep and illuminating relationship between them which we now begin to explore.

First, we look at diagrams G.204, G.205 G.216 and G.217. Suppose that we were to allow the active gauge remainder in these diagrams to act: then the diagrams in which the gauge remainder strikes a socket decorating anything other than a two-point, tree level vertex would cancel, courtesy of cancellation mechanism 11. We return to this in chapter 10.

Secondly, we look at diagrams G.180–G.183 and diagrams G.218–G.221. To this set of eight terms, we now add diagrams G.158, G.159, G.196 and G.197. We have already recognised that these latter four diagrams can be combined, in pairs. If we do this, then we generate a two-point, tree level vertex joined to a bitten gauge remainder i.e. we generate two terms of the same type as the other eight! We collect together all ten diagrams in figure 8.33.

$$-2\Upsilon_{n-1,0}$$

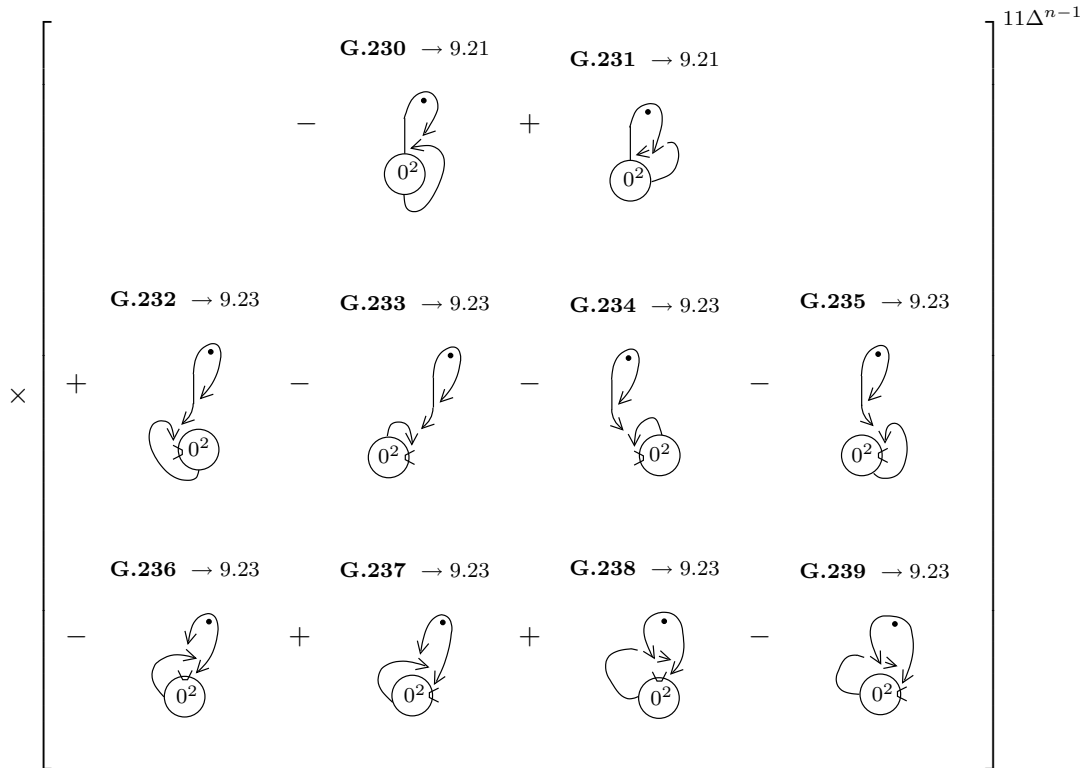


Figure 8.33: Collecting together diagrams G.158, G.159, G.196 and G.197, which have been combined in pairs, and diagrams G.180–G.183, and G.218–G.221.

Note that, in the second row of diagrams, we have used CC to replace a bite on one side of the wine with a bite on the other side.

The most striking feature of figure 8.33 is its similarity to figure 8.21. Indeed, there is a one-to-one correspondence between the diagrams of these two figures: to generate the diagrams of the latter figure from those of the former, we simply remove the restriction that the wines be un-decorated and multiply by  $-1/2$ .

To understand the interrelationship between the diagrams of figure 8.33, let us start by taking diagrams G.230 and G.231 and perform the following operations: we strip off the effective propagator and detach the end of the wine attached to the vertex. This gives us the diagrams of figure 8.34.

$$-2\Upsilon_{n,0} \left[ - \begin{array}{c} \text{I.13} \\ \text{Diagram I.13} \end{array} + \begin{array}{c} \text{I.14} \\ \text{Diagram I.14} \end{array} \right] 11\Delta^n$$

Figure 8.34: Resulting of promoting the effective propagator of diagrams G.230 and G.231 to a decoration and detaching the wine from the vertex.

We now consider adding an additional level of nesting to diagrams I.13 and I.14. Then we reattach the wine—but let it join to any available socket. If it attaches to the vertex, then we just generate nested versions of diagrams G.230 and G.231. If, instead, it attaches to one of the nested gauge remainders then, upon joining the other gauge remainder to the un-drawn socket of the vertex, we simply generate diagrams G.232–G.239. This deep relationship between the diagrams of figure 8.33 will be exploited in section 9.2 and chapter 10.

To conclude this section, we comment on the final set of diagrams comprising a two-point, tree level vertex joined to a bitten gauge remainder. This set constitutes diagrams G.214, G.215 and G.222–G.229. We can arrange these diagrams as we arranged those in figure 8.33, providing we make three minor changes: first, change the overall sign; secondly, include a trapped gauge remainder; thirdly reduce the wine.

## 8.4 Type-III Gauge Remainders

All gauge remainders of type-III have been collected together in figure 8.35.

Given what we have done already in this chapter, we can immediately deduce the diagrams that will remain, after we allow the gauge remainders to act. Diagrams in which the gauge remainder strikes a socket which decorates anything other than a two-point, tree level vertex will be cancelled, via cancellation mechanism 11. The surviving diagrams will either be nested versions of the parents or diagrams in which the gauge remainder strikes an end of the wine. Note that when we create a two-point, tree level vertex, we cannot decorate it with the remaining external field, since then the diagram as a whole will vanish at  $\mathcal{O}(p^2)$ .

Iterating the diagrammatic procedure, we will ultimately be left with only two types of diagram:

1. diagrams in which an arbitrarily nested gauge remainder bites either end of the wine;
2. diagrams in which a two-point, tree level vertex (formed by the action of a gauge remainder) is joined to a bitten gauge remainder.

We give the minimal set of these terms in figure 8.36. We recall that, to obtain the complete set we do the following. For each diagram, include versions in which the level of nesting is arbitrarily higher and nest in all possible ways. Finally, for every diagram now in the set, we include copies possessing additional vertices.

$$\begin{aligned}
& -2 \sum_{s=1}^{n_+} \sum_{J=2}^{2n} \Upsilon_{J+s,J} \left[ \begin{array}{c} \text{G.240} \\ \begin{array}{c} \text{V}^{0,1;R} \\ \uparrow \\ \circ \\ \uparrow \\ 0^2 \\ \uparrow \\ \text{wavy} \end{array} \\ \text{G.241} \\ \begin{array}{c} \text{loop} \\ \uparrow \\ 0^2 \\ \uparrow \\ \text{wavy} \\ \text{V}^{0,1;R} \end{array} \end{array} \right] \begin{array}{c} \\ \\ \\ \text{V}^{I,I+;R} \\ \text{V}^{J;R} \end{array} \Bigg] 1\Delta^{J+s} \\
& + 2 \sum_{J=0}^n \sum_{r=0}^{n_J} \Upsilon_{J+2,0} \left[ \begin{array}{c} \text{G.242} \\ \begin{array}{c} n_{J+r}^R \\ \uparrow \\ \circ \\ \uparrow \\ 0^2 \\ \uparrow \\ \text{wavy} \end{array} \\ \text{G.243} \\ \begin{array}{c} \text{loop} \\ \uparrow \\ 0^2 \\ \uparrow \\ \text{wavy} \\ n_{J+r}^R \end{array} \end{array} \right] \begin{array}{c} \\ \\ \\ r^R \end{array} \Bigg] 1\Delta^{J+2} \\
& - 2 \sum_{J=0}^n \Upsilon_{J+1,0} \left[ \begin{array}{c} \text{G.244} \\ \begin{array}{c} n_J^R \\ \uparrow \\ \circ \\ \uparrow \\ 0^2 \\ \uparrow \\ \text{wavy} \end{array} \\ \text{G.245} \\ \begin{array}{c} \text{loop} \\ \uparrow \\ 0^2 \\ \uparrow \\ \text{wavy} \\ n_J^R \end{array} \end{array} \right] \Bigg] 1\Delta^{J+1} \\
& + 2 \Upsilon_{n,0} \left[ \begin{array}{c} \text{G.246} \\ \begin{array}{c} \text{loop} \\ \uparrow \\ 0^2 \\ \uparrow \\ \text{wavy} \end{array} \end{array} \right] 1\Delta^n
\end{aligned}$$

Figure 8.35: Type-III gauge remainders.

$$\left[ \begin{array}{cccc}
& & 4\Upsilon_{n,0} & \\
& & \{ \text{G.249 } G.353 \} & \{ \text{G.250 } G.352 \} \\
\text{G.247} & \{ \text{G.248 } G.323 \} & & \\
\begin{array}{c} \circ \\ \downarrow \\ \circ \\ \downarrow \\ \text{0}^2 \\ \downarrow \\ \text{wavy} \end{array} & + & \begin{array}{c} \bullet \\ \downarrow \\ \circ \\ \downarrow \\ \text{0}^2 \\ \downarrow \\ \text{wavy} \end{array} & - & \begin{array}{c} \circ \\ \downarrow \\ \circ \\ \downarrow \\ \text{0}^2 \\ \downarrow \\ \text{wavy} \end{array} & + & \begin{array}{c} \circ \\ \downarrow \\ \circ \\ \downarrow \\ \text{0}^2 \\ \downarrow \\ \text{wavy} \end{array}
\end{array} \right] 1\Delta^n$$

Figure 8.36: The minimal set of terms produced by applying the diagrammatic procedure, until exhaustion, to diagrams G.240–G.246.

## Chapter 9

# Further Diagrammatic Identities

### 9.1 The New Identities

In order to make further progress, one of the things that we must do is introduce a new set of diagrammatic identities. These will enable us to treat diagrams like the ones in figure 8.13. Rather than simply stating the diagrammatic identities, it will prove more illuminating to provide some motivation, by sketching how the terms involved arise.

We know already that we plan to convert certain diagrams possessing processed gauge remainders into  $\Lambda$ -derivative terms; we have, of course, seen an explicit example of this in the one-loop calculation. Whilst we are yet to demonstrate that we can, in the general case, make this conversion, let us suppose that we are able to do so. An example of the types of term that we expect to encounter is shown in figure 9.1.

We now iterate the usual diagrammatic procedure but with one crucial difference: every time we generate a two-point, tree level vertex—whether it be via the flow equations, the action of a gauge remainder or manipulations at  $\mathcal{O}(p^2)$ —we have the new option of attaching it to the gauge remainder structure depicted in the diagrams of figure 9.1. In figure 9.2 we schematically represent examples of the types of diagram we expect to arise in the former two cases.

$$- \sum_{J=0}^n \Upsilon_{J+1,0} \left[ \left[ \begin{array}{c} \mathbf{I.15} \\ \wedge_{> <}^V \\ \textcircled{n_J^R} \end{array} \right] \bullet - \left[ \begin{array}{c} \mathbf{I.16} \\ \wedge_{> <}^V \\ \textcircled{n_J^R} \bullet \end{array} \right] - \dots \right]^{11\Delta^{J+1}}$$

Figure 9.1: An example of the type of  $\Lambda$ -derivative term we expect to arise from the gauge remainder sector of the calculation.

$$\left[ \begin{array}{c} \mathbf{I.17} \\ \wedge_{> <}^V \\ \bullet \\ \textcircled{\hat{V}^R} \end{array} - \begin{array}{c} \mathbf{I.18} \\ \wedge_{> <}^V \\ \bullet \\ \textcircled{\hat{V}^R} \end{array} \right], \left[ \begin{array}{c} \mathbf{I.19} \\ \wedge_{> <}^V \\ \bullet \\ \curvearrowright \end{array} - \begin{array}{c} \mathbf{I.20} \\ \wedge_{> <}^V \\ \bullet \\ \curvearrowright \end{array} \right]$$

Figure 9.2: Examples of some of the new types of term we expect to generate when we process diagrams like I.16.

These examples are not exhaustive. For instance, there are diagrams similar to I.17 and I.18 in which the vertex is a Wilsonian effective action vertex, and the wine is reduced. Similarly, we have implicitly assumed that diagrams I.19 and I.20 have been created by an un-nested type-Ia gauge remainder. Nonetheless, these example diagrams capture all the features that we require. The first diagrammatic identity follows from considering a version of sub-diagram I.19 in which the gauge remainder structure at the top is not nested. For the sake of clarity, we will be more explicit about where this sub-diagram comes from.

To this end, consider decoration of two-point, tree level vertices by  $\curvearrowright$ . We will not specify the number of vertices in the diagram and will suppose that the decorations include the usual external fields and  $M \geq 1$  effective propagators. This is illustrated in figure 9.3, where we use the effective propagator relation and note that the gauge remainder vanishes, since it must be in the  $C$ -sector.

Further progress can be made with the final diagram. The socket must

$$\left[ \begin{array}{c} \text{loop} \\ \text{circle with } 0^2 \\ \text{arrow} \end{array} \right]^{11\Delta^M} = \left[ \begin{array}{c} \text{loop} \\ \text{arrow} \\ \text{dot} \end{array} \right]^{11\Delta^M}$$

Figure 9.3: A two-point, tree level vertex, generated by the action of a gauge remainder and decorated by  $\text{---}\curvearrowright$ .

be decorated by one of the effective propagators,<sup>1</sup> since the gauge remainder does not carry a Lorentz index. We perform this decoration and assume, for simplicity, that the loose ends are both joined to the same, lone vertex (whose argument is irrelevant) and that the only remaining decorations are the external fields. This is shown in figure 9.4 where the second diagram has just been obtained by charge conjugation of the first.

$$\left[ \begin{array}{c} \text{loop} \\ \text{dot} \\ \text{arrow} \\ \text{circle} \end{array} \right]^{11} = \left[ \begin{array}{c} \text{loop} \\ \text{arrow} \\ \text{dot} \\ \text{circle} \end{array} \right]^{11}$$

Figure 9.4: Further decoration of the previous diagram.

We now consider specific decorations of these diagram and order the fields. We decorate the first diagram by placing both external fields on the ‘outside’ of the vertex, so that the ordering of the fields on the vertex is  $11F\bar{F}$ . We decorate the second diagram by placing both external fields on the ‘inside’ of the vertex. This is shown in figure 9.5, where we also indicate the flavour of the empty loops.

The ordering of the fields is the same in both cases. Indeed, the bottom parts of the diagrams are the same in each case: the (field ordered) vertices

---

<sup>1</sup>We suppose that the wine is attached to one of the un-drawn vertices, rather than the socket, but this restriction is unnecessary for the argument that follows.

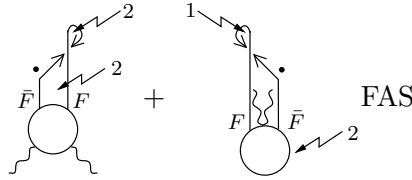


Figure 9.5: A possible pair of field ordered diagrams formed from a term in which the structure  $\curvearrowright$  is attached to a two-point, tree level vertex which has been formed by the action of a gauge remainder.

are identical, as is the wine, the gauge remainder it goes into and the effective propagator. Moreover, in both cases there is any empty loop giving a factor of  $-N$ . The difference occurs in the top part of the diagram.

We focus first on the push forward / pull back on to the top of the effective propagator. The two cases correspond to pushing forward / pulling back an  $F$  on to an  $\bar{F}$ . Referring to table 3.1, we see that both cases come with the same sign, but generate a different field. However, this field has been removed by the effective propagator relation! Finally, then, all that remains is the hook at the top of the diagram, around which we assume flows momentum  $l$ . Up to group theory, they both reduce to  $\int_l g_l$ , as we know from equations (3.2)–(3.4). However, in one case the hook encloses a loop in the two-sector, whereas in the other case, it enclose a loop in the one-sector. These come with opposite signs, causing the two terms to cancel.

It should be clear that the various restrictions we have imposed, such as there only begin on vertex, do not affect the final conclusion: whenever a diagram possesses a component like that of figure 9.3, it is guaranteed to vanish. This provides us with a new diagrammatic identity.

**Diagrammatic Identity 10** *Consider a vertex attached to an effective propagator, which ends in a hook. Suppose that a gauge remainder strikes this vertex. Focusing on the terms produced when the gauge remainder pushes forward / pulls back on to a socket, we suppose that a two-point, tree level vertex is generated. Applying the effective propagator relation, the gauge remainder dies, leaving us with the diagrammatic identity shown in figure 9.6.*

$$\mathcal{G}_{\uparrow} - \mathcal{G}_{\downarrow} = 0$$

Figure 9.6: Diagrammatic identity 10.

**Corollary** *The diagrammatic identity immediately implies that  $\mathcal{G}_{\uparrow}$ , alone, vanishes; this follows because we can re-express this sub-diagram as:*

$$1/2 \left[ \mathcal{G}_{\uparrow} - \mathcal{G}_{\downarrow} \right]$$

(see section 3.1.2).

The next diagrammatic identity is more interesting, finally resolving the issue of what to do with the diagrams of figure 8.13. We do not consider these diagrams on their own, but rather combine them with two diagrams which are special cases of diagram I.18. These latter two diagrams are shown in figure 9.7.

$$4 \sum_{J=0}^n \Upsilon_{J,0} \left[ \begin{array}{c} \text{I.21} \quad \text{I.22} \\ \begin{array}{c} \text{Diagram 1} \\ \uparrow \\ \hat{n}_J^R \end{array} \quad - \quad \begin{array}{c} \text{Diagram 2} \\ \uparrow \\ \hat{n}_J^R \end{array} \end{array} \right]^{11\Delta^J}$$

Figure 9.7: Two diagrams which are special cases of diagram I.18.

For the purposes of the imminent diagrammatic identity, we strip off the common structures from diagrams I.21, I.22, G.88 and G.89.

The resulting sub-diagrams corresponding to diagrams G.89 and I.22 are collected together in figure 9.8.<sup>2</sup>

The letters  $U-Z$  will be used to denote field flavour, and the subscripts  $S$  and  $R$  represent indices. Each of these sub-diagrams is really part of a complete diagram and so the loose ends are somehow tied up. This immediately tells us that  $W$  and  $X$  must both be either bosonic or fermionic. In the former case,

<sup>2</sup>The remaining sub-diagrams will be treated later.

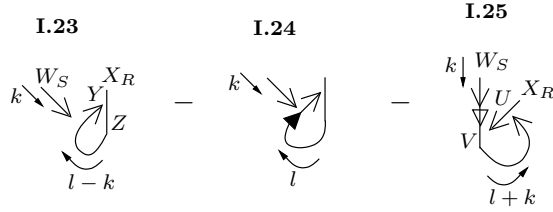


Figure 9.8: The first two sub-diagrams show the algebraic part of diagram G.89, where we have used the effective propagator relation. The final sub-diagram shows the algebraic part of diagram I.22.

$W_S$	$X_R$	$Y$	$Z$	$U$	$V$
$A_\sigma^1$	$A_\rho^1$	$A^1$	$A^1$	$A^1$	$A^1$
		$F$	$B$	$\bar{B}$	$\bar{B}$
$A_\sigma^2$	$A_\rho^2$	$A^2$	$A^2$	$A^2$	$A^2$
		$\bar{F}$	$\bar{B}$	$B$	$B$
$\bar{F}_S$	$F_R$	$A^2$	$F$	$A^2$	$\bar{F}$
		$\bar{B}$	$A^1$	$F$	$A^1$
$F_S$	$\bar{F}_R$	$A^1$	$\bar{F}$	$A^1$	$F$
		$B$	$A^2$	$\bar{F}$	$A^2$

Table 9.1: Possible flavours of the fields of the diagrams of figure 9.8.

they must both be in the  $A$ -sector: gauge remainders have no support in the  $C$ -sector, and the mixed case—where  $W$  is in the  $A$ -sector and  $X$  is in the  $C$ -sector—will vanish, due to charge conjugation invariance. Depending on how we tie the legs up determines how many closed loops each diagram possesses, which in turn affects the group theory factors. This is only important when both the fields  $W$  and  $X$  are fermionic, as we will see below. In table 9.1, the possible sets of field flavours are listed.

We now evaluate the three diagrams of figure 9.8, algebraically, in the different sectors. The easiest case to do is when all of the fields are in one of the  $A$ -sectors, say  $A^1$ . Strictly speaking, we should not look at this case on

its own, as it is UV divergent; rather, we should look at it together with its partner, in which the fields  $U, V, Y, Z$  are fermionic.

Treating these contributions together, we can express the sub-diagrams thus:

$$N \frac{k_\sigma}{k^2} \int_l \left\{ \begin{array}{l} \frac{l_\rho}{l^2} \left[ 1 - \frac{l \cdot (l+k)}{(l+k)^2} - \frac{k \cdot (l+k)}{(l+k)^2} \right] \\ - \frac{f l_\rho}{\Lambda^2} \left[ 1 - \frac{l \cdot (l+k)}{\Lambda^2} - 2g_{l+k} - \frac{k \cdot (l+k)}{\Lambda^2} \right] \end{array} \right\} = 0, \quad (9.1)$$

where the group theory factors of  $\pm N$  arise from the explicitly drawn loop and we have used equation (A.25).

It is trivial to show that we obtain the same overall result when we take the fields  $W$  and  $X$  to be in the  $A^2$  sector. The remaining sectors are more subtle and must, in fact, all be treated together. At first, this looks a little strange, since we cannot obviously combine the case where  $W, X = \bar{F}, F$  with  $W, X = F, \bar{F}$ : when we tie up all the loose ends, it looks as though we are trying to equate diagrams possessing arbitrary structure that are clearly different. However, as we will now demonstrate, we can take these structures to be the same by utilising charge-conjugation invariance.

In figure 9.9, we have taken sub-diagram I.25, with fermionic external fields and have redrawn it. The first step is done by using charge-conjugation invariance. The second step is just a trivial redrawing.

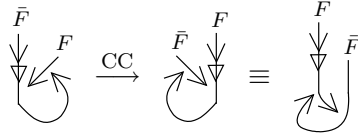


Figure 9.9: Sub-diagram 9.9 with specific field content.

The point is that we should now consider together the final diagram of figure 9.9 with a copy of the first diagram for which we take the fields  $W, X$  to be not  $\bar{F}, F$  but  $F, \bar{F}$ . To this pair of diagrams, we can now attach exactly the same arbitrary structure.

There is one final subtlety. From table 9.1 it is apparent that, for a given fermionic choice of  $W$  and  $X$  we can, in each of the sub-diagrams I.23–I.25,

choose one of the internal fields to be either an  $A^1$  or an  $A^2$ . These two choices come with different group theory factors. Once all loose ends are tied up, we are interested in the flavours of the loops carrying momenta  $l$  and  $k$ . There are three such loops and we denote their flavours by an ordered triplet.<sup>3</sup> In the case that we choose one of the fields to be an  $A^1$ , the loop flavours are  $\{1, 1, 2\}$  whereas, if we choose one of the field to be an  $A^2$ , then the loop flavours are  $\{2, 2, 1\}$ . If all loops are empty, then the group theory factors are  $-N^3$  and  $N^3$ , respectively. If one of the loops is decorated by the external fields, then this loop contributes  $\text{str } A^1 A^1$  and so the group theory factors are just  $-N^2$  and  $N^2$ , respectively. Either way, the two choices of the flavour of the bosonic fields give rise to opposite signs.

With these points in mind, we can evaluate diagrams I.23–I.25 when the external fields are fermionic: it is straightforward to show that they sum to zero. Combining this with the similar result from the  $A$ -sector, we have a diagrammatic identity, since the diagrams of figure 9.8 sum to zero.

However, we are not quite done. Referring back to figure 9.8, we should also analyse the case in which the nested gauge remainder is either a push forward, rather than a pull back or vice-versa, as appropriate. The corresponding diagrams are shown in figure 9.10



Figure 9.10: Partner diagrams to those of figure 9.8, in which the nested gauge remainder has changed character.

These sub-diagrams are even easier to analyse than the previous set: we know from trivial extension of the arguments presented in section 3.1.8 that the external fields cannot be fermionic and so we need take them only in the  $A$ -sector. Note, however, that the internal fields can be fermionic. In this case,

<sup>3</sup>There can, of course, be additional loops, but they will contribute a group theory factor common to both cases.

one of the external fields must be in the  $A^1$  sector, whilst the other must be in the  $A^2$ -sector. Taking this into account, it is easy to show that the two diagrams of figure 9.10 sum to zero. This completes our analysis and yields the required diagrammatic identity.

**Diagrammatic Identity 11** *Consider a two-point, tree level vertex, attached to an effective propagator and then to a gauge remainder. The gauge remainder bites the remaining socket of the vertex in either sense. A second gauge remainder bites the first gauge remainder. These sub-diagrams can be redrawn as shown in figure 9.11.*

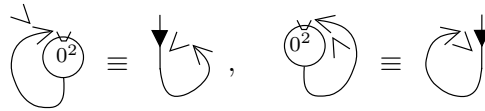


Figure 9.11: Diagrammatic identity 11.

The next logical step is to generalise this relationship to one that is suitable for an arbitrary level of nesting. To begin with, we will increase the level of nesting by one. Before stating the new diagrammatic identity, we will indicate where the terms involved come from.

Let us start by considering nested versions of diagrams G.88 and G.89. The extra gauge remainder can either go inside or outside the loop, as shown in figure 9.12.

The diagrams of figure 9.12 leave us with two problems. On the one hand, whilst diagrams I.26, I.27, I.30 and I.31 can be redrawn using diagrammatic identity 11, we need to find the terms against which they cancel. On the other hand, we suspect that diagrams I.28, I.29, I.32 and I.33 will somehow cancel against nested versions of diagrams I.21 and I.22. As it stands, this cancellation does not quite work: we need further diagrams.

The solutions to both of these two problems are intimately related. The terms we require to make both sets of cancellations work are generated by the

$$4 \sum_{J=0}^n \Upsilon_{J,0} \left[ \begin{array}{cccc} \mathbf{I.26} & \mathbf{I.27} & \mathbf{I.28} & \mathbf{I.29} \\ \begin{array}{c} \text{Diagram I.26} \\ \text{Diagram I.27} \\ \text{Diagram I.28} \\ \text{Diagram I.29} \end{array} & + & \begin{array}{c} \text{Diagram I.27} \\ \text{Diagram I.28} \\ \text{Diagram I.29} \\ \text{Diagram I.30} \end{array} & - & \begin{array}{c} \text{Diagram I.28} \\ \text{Diagram I.29} \\ \text{Diagram I.30} \\ \text{Diagram I.31} \end{array} & + & \begin{array}{c} \text{Diagram I.29} \\ \text{Diagram I.30} \\ \text{Diagram I.31} \\ \text{Diagram I.32} \end{array} & - & \begin{array}{c} \text{Diagram I.30} \\ \text{Diagram I.31} \\ \text{Diagram I.32} \\ \text{Diagram I.33} \end{array} \end{array} \right] 11\Delta^J$$

Figure 9.12: The nested versions of diagrams G.88 and G.89.

same set of diagrams. Imagine converting a diagram containing a singly nested version of  $\curvearrowright$  into a  $\Lambda$ -derivative term. Among the corrections generated will be the (processed) type-Ia gauge remainders of figure 9.13.

$$4 \sum_{J=0}^n \Upsilon_{J,0} \left[ \begin{array}{cccc} \mathbf{I.34} & \mathbf{I.35} & \mathbf{I.36} & \mathbf{I.37} \\ \begin{array}{c} \text{Diagram I.34} \\ \text{Diagram I.35} \\ \text{Diagram I.36} \\ \text{Diagram I.37} \end{array} & - & \begin{array}{c} \text{Diagram I.35} \\ \text{Diagram I.36} \\ \text{Diagram I.37} \end{array} & - & \begin{array}{c} \text{Diagram I.36} \\ \text{Diagram I.37} \end{array} & + & \begin{array}{c} \text{Diagram I.37} \end{array} \end{array} \right] 11\Delta^J$$

Figure 9.13: Particular type-Ia gauge remainders arising from the conversion of diagrams possessing a nested version of  $\curvearrowright$  into a  $\Lambda$ -derivative term.

Utilising the effective propagator relation, we generate eight terms. The two not involving further gauge remainders are precisely those that we need for the next diagrammatic identity. What of the other terms? These cancel diagrams I.26, I.27, I.30 and I.31 via diagrammatic identity 11!

Now we are in a position to uncover the new diagrammatic identity. Consider the set of diagrams shown in figure 9.14.

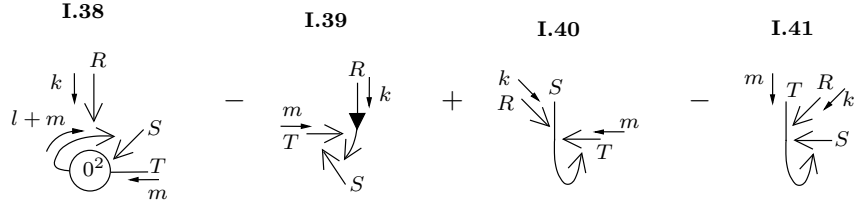


Figure 9.14: A set of diagrams, possessing three performed gauge remainders, which sum to zero.

The first sub-diagram has been stripped off from diagram I.33; the second sub-diagram has been stripped off from a nested version of diagram I.21 and the final two sub-diagrams have been stripped off from diagrams I.36 and I.37.

It intuitively makes sense that these four diagrams sum to zero: suppose that we remove a nested gauge remainder from each diagram.<sup>4</sup> The set of four diagrams would then decompose: the first two would cancel via diagrammatic identity 11, whereas the last two would cancel via diagrammatic identity 10!

Let us now examine the sub-diagrams of figure 9.14 in more detail. Ultimately, these sub-diagrams must form full diagrams and so all empty sockets or loose ends will be tied up. Cancellations will occur between terms for which the field ordered structure which completes the diagram is the same. It is clear that if we attach a given field ordered structure to these sub-diagrams, then the group theory factors will be the same for each of the complete diagrams. This is, of course, crucial.

We will now compute these diagrams, taking all fields to be in the  $A$ -sector (it does not matter whether they are  $A^1$ s or  $A^2$ s). Up to the common structure and a common group theory factor, we have:

$$\frac{k_\rho}{k^2} \int_l \frac{l_\sigma}{l^2} \left[ \begin{array}{l} \frac{(l+m+k)_\tau}{(l+m+k)^2} - \frac{(l+m)_\tau}{(l+m)^2} \frac{(l+m) \cdot (l+m+k)}{(l+m+k)^2} \\ - \frac{(l+m)_\tau}{(l+m)^2} \frac{k \cdot (l+m+k)}{(l+m+k)^2} \\ + \frac{(l+m)_\tau}{(l+m)^2} - \frac{(l+m+k)_\tau}{(l+m+k)^2} \end{array} \right] = 0, \quad (9.2)$$

<sup>4</sup>In the last two diagrams, the top-most gauge remainder is independent of the other two; it is certainly not nested in the usual sense and it is not this that we remove.

where we have implicitly assumed that the individual terms are regulated by diagrams in which the internal fields of the sub-diagrams are fermionic. This is straightforward to show; these regulating diagrams also sum to zero. Finally, we must consider diagrams in which two of the external fields are fermionic. As with diagrammatic identity 11, we must use charge conjugation to identify all those diagrams with the same common structure. Though the pattern of cancellations is different from that of equation (9.2), we have verified that the diagrams sum to zero.

This completes the analysis of the diagrams of figure 9.14 and so now we should consider the partner diagrams which have different patterns of pushes forward and pulls back. This is subtle. The salient points are most easily introduced by focusing on diagram I.39. As drawn, each of the three gauge remainders in the loop is bitten on the right and it is implicitly assumed that this diagram has been combined with its charge conjugate, in which each of the gauge remainders is bitten on the left.

By changing pushes forward into pulls back—or, equivalently, bites on the right (left) to bites on the left (right)—we can generate three independent new diagrams. We can characterise this by the sense in which each of the gauge remainders is bitten. We have  $-RRL$ ,  $-RLR$ ,  $+RLL$ , where we have picked up a sign for each change from right to left. Using charge conjugation to rewrite the final term as  $-LRR$ , we see that set of three terms are related to each other by cyclic permutations. This leads us to consider the three diagrams of figure 9.15, together.

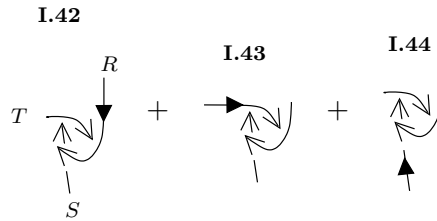


Figure 9.15: The three partner diagrams to diagram I.39.

Now we encounter a potential problem. Whilst diagram I.38, too, has three partner diagrams, diagrams I.40 and I.41 have only one, each. It is thus clear

that we will not be able to show that the sum of these diagrams vanishes via a direct analogue of equation 9.2.

The key to understanding how these diagrams do cancel revolves around understanding both the group theory factors of the diagrams and the flavours of the external legs. We examine the former first.

Returning to diagram I.42, let us suppose that all three legs are attached to the same field-ordered structure. Attaching the legs in the order shown, i.e. without crossing any of them over, the order on the structure is  $RST$ , in the counter-clockwise sense. Now, however, consider crossing the leg labelled  $S$  with the leg labelled  $R$ . Naïvely, one might expect this to change the group theory but this is not the case. The diagram can be untied, as illustrated in figure 9.16.

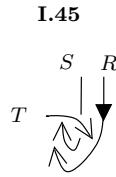


Figure 9.16: A trivial redrawing of sub-diagram I.42.

Similar considerations apply to the partners of diagrams I.38, I.40 and I.41: crossing over legs which attach to the same structure does not, counter intuitively, change the group theory factor.

Next, we examine the flavours of the external legs. First, we note that the external legs cannot be fermionic (in just the same way that the external legs of the analogous diagrams involved in diagrammatic identity 11 could not be fermionic). Hence, the external legs must be either  $A$ s or  $C$ s.

If an odd number of the external legs are  $A$ s then forming a complete diagram will give us something which vanishes by CC when we sum over field ordered structures. This follows because, even if the three external legs attach to the same structure, we can interchange two of them without changing the group theory factors (and we will not get any flavour changes, since the fields are bosonic).

Now, due to gauge remainders having no support in the  $C$ -sector, it must be the case that at least one of the external fields is an  $A$ ; for complete diagrams not to vanish by CC, it follows that there must be precisely two  $A$ s. But, if any of the legs are  $C$ s, then a pair of the internal lines must be fermionic, since gauge remainders have no support in the  $C$ -sector. This then means that whilst two of the bosonic external legs must be in the 1(2) sector, the remaining one must be in the 2(1) sector. However, the single field in the 2(1) sector must be on a different supertrace from the other two; if this field is an  $A$ , then once more the diagram vanishes by CC. This thus leaves only those sub-diagrams with two external  $A^{1,2}$ s and one external  $C^{2,1}$ . We see how this applies to the partners of diagrams I.40 and I.41 in figure 9.17.

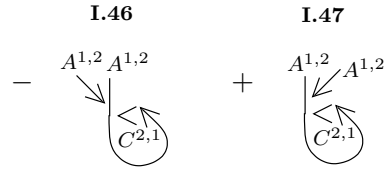


Figure 9.17: The two partners of sub-diagrams I.40 and I.41. Any other combination of external fields will cause the diagrams to vanish.

The crucial point is that sub-diagrams I.46 and I.47 simply cancel: the un-nested pull back of the first diagram cancels the corresponding push forward of the second. Now let us examine diagrams I.42–I.44. The final one of these vanishes; the trapped gauge remainder cannot be in the  $C$ -sector, but since the field that attaches to this must be on a different supertrace from the other two, the diagram vanishes by CC. This then leaves diagrams I.42 and I.43. Similarly, of the partners to diagram I.38, only two survive. Evaluating these four surviving diagrams, algebraically, yields zero.

We have demonstrated that the set of diagrams in figure 9.14 sums to zero and that this still holds if we change pushes forward into pulls back (or *vice-versa*) in all independent ways. Having made these changes, whilst it is true that the complete set of diagrams sum to zero, it is also true that there are more stringent relationships. However, we are not interested in these relationships,

as such. For the purposes of this thesis, we require only the weaker constraint. With this in mind, we obtain a further diagrammatic identity.

**Diagrammatic Identity 12** *Consider the diagrams of figure 9.18. This equality holds, if we change nested gauge remainders from being struck on the left (right) to being struck on the right (left), in all independent ways.*

$$\text{Diagram 1} - \text{Diagram 2} + \text{Diagram 3} - \text{Diagram 4} = 0$$

Figure 9.18: Diagrammatic identity 12.

We conclude our discussion of diagrammatic identities, for the time being, by going some way towards generalising diagrammatic identity 12. Our aim is to show that an analogous relation holds for sub-diagrams with arbitrarily nested gauge remainders. Of course, if this nesting is with respect to the gauge remainder that we have been taking to carry index  $R$ , then we can still use diagrammatic identity 12. Rather, we are interested in the case where the nesting is within the loops formed out of gauge remainders.

We will not, however, rigorously demonstrate the resulting identity to be true. Rather, what we will do is demonstrate it to be true for the following case: first, we will take all gauge remainders in a loop to bite each other in the same sense (i.e. all to the right (left)); second, we will demand that all fields are in the  $A$ -sector. Having done this, we will then assert, without proof, that if it is true in this case, then it is generally true. The specific case we will consider is depicted in figure 9.19.

**Assertion 1** *If the diagrams of figure 9.19 can be shown to sum to zero in the  $A$ -sector then we assert the following, without proof:*

1. *these diagrams will sum to zero in all sectors;*

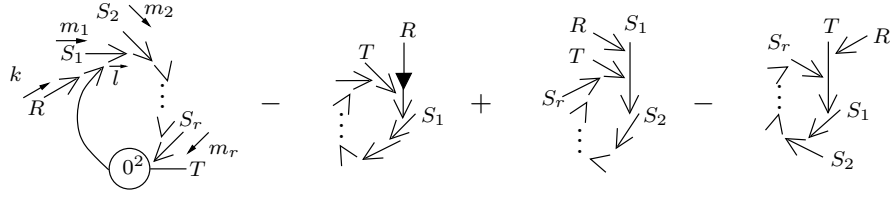


Figure 9.19: Four diagrams which sum to zero when all fields are in the  $A$ -sector.

2. the sets of partner diagrams in which we exchange pushes forward for pulls back (and vice-versa) also sum to zero.

It is worth emphasising that there is no particular barrier to proving this assertion. Indeed, intuitively it makes sense and a future task is to demonstrate it explicitly.

We now take all fields in the diagrams of figure 9.19 to be in the  $A$ -sector. In this sector, the roman indices reduce to Latin indices *viz.*  $S_j \rightarrow \sigma_j$ . Assuming that these sub-diagrams attach to the same common structure, we can combine them, algebraically:

$$\frac{k_\rho}{k^2} \int_l \frac{l_{\sigma_1}}{l^2} \prod_{j=2}^r \frac{(l + \sum_{i=2}^j m_i) \sigma_j}{(l + \sum_{i=2}^j m_i)^2} \left[ \begin{array}{l} \frac{(l-m_1)_\tau}{(l-m_1)^2} - \frac{(l-m_1-k)_\tau}{(l-m_1-k)^2} \frac{(l-m_1-k) \cdot (l-m_1)}{(l-m_1)^2} \\ - \frac{(l-m_1-k)_\tau}{(l-m_1-k)^2} \frac{k \cdot (l-m_1)}{(l-m_1)^2} \\ + \frac{(l-m_1-k)_\tau}{(l-m_1-k)^2} \\ - \frac{(l-m_1)_\tau}{(l-m_1)^2} \end{array} \right] = 0. \quad (9.3)$$

Combining this result with assertion 1 gives us a diagrammatic identity.

**Diagrammatic Identity 13** *The set of sub-diagrams of figure 9.19 sum to zero. The complimentary sets of diagrams in which arbitrary numbers of pushes forward (pulls back) are consistently changed to pulls back (pushes forward) also sum to zero.*

## 9.2 Application

We now apply the new diagrammatic identities to the types of diagram that arise in our computation of  $\beta_{n+}$ . This is actually extremely easy! In figure 9.20

we show how to re-express a typical series of sub-diagrams. By enclosing each sub-diagram by  $[ ]_{ES}$ , we mean that we should sum over Every Sense (*ES*) in which the gauge remainders can push forward or pull back on to the designated location.

For example, sub-diagram I.48 which has two gauge remainders—one of which is a push forward and the other of which is a pull back—is taken to represent four diagrams. The other three can be characterised by  $PF/PF$ ,  $PB/PF$  and  $PB/PB$ . Note that we do not combine the very first push forward with the corresponding pull back. This is because we are dealing with sub-diagrams, and it is quite possible that we have already ‘used up’ this luxury, elsewhere in the diagram.

It is worth clarifying the diagrams represented by the various ellipses. The ellipsis following diagram I.49 denotes additionally nested diagrams, where the two-point, tree level vertex is still joined to the innermost gauge remainder. The ellipsis after diagram I.50 denotes additionally nested diagrams, where the two-point, tree level vertex joins to the innermost but one gauge remainder. The vertical dots on the next line represent additionally nested diagrams in which the two-point, tree level vertex joins to gauge remainders successively further away from the innermost one. Note, though, that we never make the join to the outermost gauge remainder.

The meaning of the remaining ellipses should be clear. We draw attention to the fact that  $[ ]_{ES}$  refers to *all* gauge remainders. Thus, for example, in diagram I.53 we must sum over not just the different senses in which the two gauge remainders at the top of the diagram can bite each other, but also the sense in which the other gauge remainder strikes the vertex. Diagrams related to each other by the diagrammatic identities are those which possess the same total number of processed gauge remainders.

The relationship shown in figure 9.20 can now be directly applied to specific diagrams, coming from the computation of  $\beta_{n+}$ . There are two cases to deal with. Focusing on the sub-diagrams enclosed by the first  $[ ]_{ES}$ , we can either attach the bottommost gauge remainder to some independent structure or to one of the empty sockets in the sub-diagrams.

$$\begin{aligned}
& \left[ \begin{array}{c} \text{I.48} \\ \text{Diagram I.48} \end{array} + \left[ \begin{array}{c} \text{I.49} \\ \text{Diagram I.49} + \dots \\ \text{I.50} \\ \text{Diagram I.50} + \dots \\ \vdots \end{array} \right] \right]_{ES} \\
= & \left[ \begin{array}{c} \text{I.51} \\ \text{Diagram I.51} \end{array} + \left[ \begin{array}{c} \text{I.52} \\ \text{Diagram I.52} + \dots \\ \text{I.53} \\ \text{Diagram I.53} + \text{I.54} \\ \text{Diagram I.54} + \dots \\ \text{I.55} \\ \text{Diagram I.55} + \dots \end{array} \right] \right]_{ES}
\end{aligned}$$

Figure 9.20: A re-expression of a series of diagrams, using diagrammatic identities 11–13.

To obtain the set of terms in the first class, we start with diagrams G.88, G.89, G.130 and G.131. We then add their analogues with a higher level of nesting. Finally, for each diagram now in the set, we include their analogues possessing additional vertices.

To obtain the set of terms in the second class we start with: diagrams G.130–G.139, diagrams G.230–G.239 and the version of the final set possessing a trapped gauge remainder. To generate the complete set of terms, we now employ the usual procedure of including additional levels of nesting and extra vertices, as appropriate.

Redrawing the terms of the first class is trivial. The second class is not much harder but, having applied the diagrammatic identities, some of the resulting terms can be combined both with other redrawn terms and also terms from elsewhere in the calculation. Consequently, it is the second set of terms we will focus on.

We start by looking at diagrams G.230 and G.231. Redrawing these terms using diagrammatic identity 11 leads them to take a very similar form to diagrams G.198 and G.199—they look identical but for the fact that the trapped gauge remainder is on the other side of the wine. In fact, it makes no difference which side of the wine the trapped gauge remainder lies; the two cases are identical as can be demonstrated by a trivial redrawing.

To the four diagrams comprising the two we have redrawn and diagrams G.198 and G.199 we now add diagrams G.130 and G.131. This has the effect of removing the undecorated component of the wine.<sup>5</sup> The result is shown in figure 9.21.

Now we want to move on to see what happens in the additionally nested case. Our first task is to generate the nested versions of diagrams G.230 and G.231. This is done by combining the diagram G.184, G.185, G.188 and G.189; G.206, G.207, G.210 and G.211 and the nested versions of diagrams G.196 and G.197. Combining terms with trapped gauge remainders

---

<sup>5</sup>At this level of nesting, the wine must be decorated, irrespective of the value of  $n$ . This is an example of how retaining terms which can be argued to vanish, obviates the need to make such an argument.

$$\begin{array}{c}
2\Upsilon_{n-1,0} \\
\times \left[ \begin{array}{cccc}
\{ \mathbf{G.251} \ G.361 \} & \{ \mathbf{G.252} \ G.362 \} & \{ \mathbf{G.253} \ G.363 \} & \{ \mathbf{G.254} \ G.364 \} \\
\begin{array}{c} \text{Diagram 1} \\ \text{Diagram 2} \\ \text{Diagram 3} \\ \text{Diagram 4} \end{array} & - & + & - \\
\end{array} \right]^{11\Delta^{n-1}}
\end{array}$$

Figure 9.21: Combining diagrams G.198, G.199, G.230 and G.231 with diagrams G.130 and G.131.

with the corresponding terms that do not gives us the eight diagrams of figure 9.22.

$$\begin{array}{c}
2\Upsilon_{n-1,0} \\
\times \left[ \begin{array}{cccc}
\mathbf{G.255} \rightarrow 9.23 & \mathbf{G.256} \rightarrow 9.23 & \mathbf{G.257} \rightarrow 9.23 & \mathbf{G.258} \rightarrow 9.23 \\
- \begin{array}{c} \text{Diagram 1} \\ \text{Diagram 2} \end{array} & + \begin{array}{c} \text{Diagram 3} \\ \text{Diagram 4} \end{array} & + \begin{array}{c} \text{Diagram 5} \\ \text{Diagram 6} \end{array} & - \begin{array}{c} \text{Diagram 7} \\ \text{Diagram 8} \end{array} \\
\mathbf{G.259} \rightarrow 9.23 & \mathbf{G.260} \rightarrow 9.23 & \mathbf{G.261} \rightarrow 9.23 & \mathbf{G.262} \rightarrow 9.23 \\
- \begin{array}{c} \text{Diagram 9} \\ \text{Diagram 10} \end{array} & + \begin{array}{c} \text{Diagram 11} \\ \text{Diagram 12} \end{array} & + \begin{array}{c} \text{Diagram 13} \\ \text{Diagram 14} \end{array} & - \begin{array}{c} \text{Diagram 15} \\ \text{Diagram 16} \end{array}
\end{array} \right]^{11\Delta^{n-1}}
\end{array}$$

Figure 9.22: Result of combining the nested versions of diagrams G.158 and G.159 with the nested versions of diagrams G.196 and G.197.

The eight diagrams of figure 9.22 naturally combine with diagrams G.232–G.239. We now apply diagrammatic identity 12 to diagrams G.255–G.258 and G.236–G.239 and diagrammatic identity 11 to diagrams G.259–G.262 and G.232–G.235. The result of these redrawing is shown in figure 9.23 where, in particular cases, we have collected terms together to recreate a two-point, tree level vertex attached to an effective propagator.

$$2\Upsilon_{n-1,0}$$

$$\begin{array}{cccc}
 \mathbf{G.263} \rightarrow 9.24 & \mathbf{G.264} \rightarrow 9.24 & \mathbf{G.265} \rightarrow 9.24 & \mathbf{G.266} \rightarrow 9.24 \\
 \begin{array}{c} \cdot \\ \downarrow \\ \curvearrowright \end{array} & + & \begin{array}{c} \cdot \\ \uparrow \\ \curvearrowleft \end{array} & - & \begin{array}{c} \cdot \\ \uparrow \\ \curvearrowright \end{array} & - & \begin{array}{c} \cdot \\ \downarrow \\ \curvearrowleft \end{array} \\
 \\
 \mathbf{G.267} \rightarrow 9.24 & \mathbf{G.268} \rightarrow 9.24 & \mathbf{G.269} \rightarrow 9.24 & \mathbf{G.270} \rightarrow 9.24 \\
 - & \begin{array}{c} \cdot \\ \downarrow \\ \curvearrowleft \end{array} & - & \begin{array}{c} \cdot \\ \uparrow \\ \curvearrowright \end{array} & - & \begin{array}{c} \cdot \\ \downarrow \\ \curvearrowleft \end{array} & - & \begin{array}{c} \cdot \\ \uparrow \\ \curvearrowright \end{array} \\
 \\
 \mathbf{G.271} \rightarrow 9.24 & \mathbf{G.272} \rightarrow 9.24 & \mathbf{G.273} \rightarrow 9.24 & \mathbf{G.274} \rightarrow 9.24 \\
 - & \begin{array}{c} \cdot \\ \downarrow \\ \curvearrowright \\ \circlearrowleft \\ 0^2 \end{array} & + & \begin{array}{c} \cdot \\ \downarrow \\ \curvearrowleft \\ \circlearrowright \\ 0^2 \end{array} & + & \begin{array}{c} \cdot \\ \downarrow \\ \curvearrowleft \\ \circlearrowleft \\ 0^2 \end{array} & - & \begin{array}{c} \cdot \\ \downarrow \\ \curvearrowright \\ \circlearrowright \\ 0^2 \end{array} \\
 \\
 \{ \mathbf{G.275} \ G.383 \} & \{ \mathbf{G.276} \ G.384 \} & \{ \mathbf{G.277} \ G.385 \} & \{ \mathbf{G.278} \ G.386 \} \\
 - & \begin{array}{c} \cdot \\ \downarrow \\ \curvearrowleft \end{array} & + & \begin{array}{c} \cdot \\ \downarrow \\ \curvearrowright \end{array} & + & \begin{array}{c} \cdot \\ \downarrow \\ \curvearrowleft \end{array} & - & \begin{array}{c} \cdot \\ \downarrow \\ \curvearrowright \end{array} \\
 \\
 \{ \mathbf{G.279} \ G.387 \} & \{ \mathbf{G.280} \ G.388 \} & \{ \mathbf{G.281} \ G.389 \} & \{ \mathbf{G.282} \ G.390 \} \\
 + & \begin{array}{c} \cdot \\ \downarrow \\ \curvearrowleft \\ \curvearrowright \end{array} & - & \begin{array}{c} \cdot \\ \downarrow \\ \curvearrowright \\ \curvearrowleft \end{array} & - & \begin{array}{c} \cdot \\ \downarrow \\ \curvearrowleft \\ \curvearrowright \end{array} & + & \begin{array}{c} \cdot \\ \downarrow \\ \curvearrowright \\ \curvearrowleft \end{array}
 \end{array}
 \Bigg]^{11\Delta^{n-1}}$$

Figure 9.23: Result of applying diagrammatic identities 11 and 12, as appropriate, to diagrams G.255–G.262 and G.232–G.239.

We are nearly at the nested version of figure 9.21. To get there, there are two more things we must do. First, we need to include the nested versions of diagrams G.198 and G.199. This will simply have the effect of doubling the contribution coming from diagrams G.263–G.270. Secondly, we should add diagrams G.132–G.139 and the nested version of diagrams G.130 and G.131, having redrawn the lot via diagrammatic identity 11. The combined result of both of these procedures is shown in figure 9.24.

It is now straightforward to predict the result of going to arbitrarily higher levels of nesting: we generate ever more nested versions of diagrams G.275–G.302. This, in turn, tells us what to expect from those diagrams possessing both a two-point, tree level vertex attached to a bitten gauge remainder and a trapped gauge remainder (e.g. diagrams G.214, G.215 and G.222–G.229). At the lowest level of nesting, we will generate versions of diagrams G.251 and G.252 with an additional trapped gauge remainder and the opposite sign. At the next level of nesting, we simply generate a version of figure 9.23 where we make the following changes: first, change the overall sign; secondly, include a trapped gauge remainder; thirdly reduce the wine. For successive levels of nesting, we take the set of diagrams just generated and add further nested gauge remainders.

$$\begin{array}{c}
 \left[ \begin{array}{cccc}
 \text{G.283} & \text{G.284} & \text{G.285} & \text{G.286} \\
 \text{G.287} & \text{G.288} & \text{G.289} & \text{G.290} \\
 \text{G.291} & \text{G.292} & \text{G.293} & \text{G.294}
 \end{array} \right] \\
 \times \left[ \begin{array}{cccc}
 \{ \text{G.295 } G.399 \} & \{ \text{G.296 } G.400 \} & \{ \text{G.297 } G.401 \} & \{ \text{G.298 } G.402 \} \\
 \{ \text{G.299 } G.403 \} & \{ \text{G.300 } G.404 \} & \{ \text{G.301 } G.405 \} & \{ \text{G.302 } G.406 \}
 \end{array} \right] \\
 \left. \begin{array}{c}
 2 \\
 + \\
 -
 \end{array} \right] 11\Delta^{n-1}
 \end{array}$$

Figure 9.24: Result of combining diagrams G.263–G.274, nested versions of diagrams G.198 and G.199, diagrams G.132–G.139 and the nested version of diagrams G.130 and G.131. We have concluded that there is only one thing more tedious than drawing a thousand diagrams by hand; and that is drawing them on a computer.

## Chapter 10

# Iterating the Diagrammatic Procedure

The next phase of the calculation is to convert sets of surviving gauge remainder diagrams into  $\Lambda$ -derivative terms, plus corrections. This is essentially an iteration of what we have done already: we expect the first  $\Lambda$ -derivative terms to spawn further  $\Lambda$ -derivative terms, together with gauge remainders and etc. This part of the calculation will just draw on the techniques given in chapter 7. Then we can process these new gauge remainders, using the techniques of chapter 8, ultimately arriving at a set of terms we can once more convert into  $\Lambda$ -derivatives, and so forth.

The advantage of having left this phase until now is that the diagrammatic identities of the chapter 9 will enable us to immediately identify cancellations which would otherwise have remained hidden. We begin by collecting terms spawned by gauge remainders of types-Ia, Ib and II, components of which naturally combine to give  $\Lambda$ -derivative terms.

The first case we will examine is the very simplest, corresponding to diagrams in which the gauge remainder structure is un-nested. Starting from diagrams G.99, G.113 and G.123–G.126 we re-express them as shown in figure 10.1.

We note in passing that we can remove the restriction that the vertex of diagram G.303 be reduced, as the decorations force it to be at least three-point,

$$\begin{aligned}
& -4 \sum_{J=0}^n \Upsilon_{J,0} \left[ \begin{array}{c} \mathbf{G.303} \rightarrow 10.2 \quad \{ \mathbf{G.304} \ G.327 \} \\ \left[ \begin{array}{c} \text{Diagram 1} \\ \text{Diagram 2} \end{array} \right] \bullet + \text{Diagram 3} \\ \text{Diagram 1: } \left[ \begin{array}{c} \text{Loop} \\ \text{Line} \end{array} \right] \text{ on } n_J^R \\ \text{Diagram 2: } \left[ \begin{array}{c} \text{Loop} \\ \text{Line} \end{array} \right] \text{ on } n_J^R \\ \text{Diagram 3: } \text{Loop on } n_J^R \end{array} \right]^{11\Delta^J} \\
& 4 \sum_{J=0}^n \sum_{r=0}^{n_J} \Upsilon_{J+1,0} \left[ \begin{array}{c} \{ \mathbf{G.305} \ G.326 \} \quad \mathbf{G.306} \\ \left[ \begin{array}{c} \text{Diagram 4} \\ \text{Diagram 5} \end{array} \right] \bullet + \text{Diagram 6} \\ \text{Diagram 4: } \left[ \begin{array}{c} \text{Loop} \\ \text{Line} \end{array} \right] \text{ on } n_{J+r}^R \\ \text{Diagram 5: } \left[ \begin{array}{c} \text{Loop} \\ \text{Line} \end{array} \right] \text{ on } n_{J+r}^R \\ \text{Diagram 6: } \text{Loop on } r^R \end{array} \right]^{11\Delta^{J+1}} \\
& +4 \sum_{s=1}^{n_+} \sum_{J=2}^{2n} \frac{\Upsilon_{J+s-1, J-1}}{J} \left[ \begin{array}{c} \mathbf{G.307} \quad \mathbf{G.308} \\ \left[ \begin{array}{c} \text{Diagram 7} \\ \text{Diagram 8} \end{array} \right] \bullet + \text{Diagram 9} \\ \text{Diagram 7: } \left[ \begin{array}{c} \text{Loop} \\ \text{Line} \end{array} \right] \text{ on } V^{0,1;R} \\ \text{Diagram 8: } \left[ \begin{array}{c} \text{Loop} \\ \text{Line} \end{array} \right] \text{ on } V^{0,1;R} \\ \text{Diagram 9: } \text{Loop on } V^{0,1;R} \\ \left[ \begin{array}{c} \prod_{I=1}^{J-1} \sum_{V^{I+}=0}^{V^I} \text{Diagram 10} \\ \text{Diagram 10: } \text{Loop on } V^{I,I+;R} \end{array} \right] \text{Diagram 11} \\ \text{Diagram 11: } \text{Loop on } V^{J;R} \end{array} \right]^{11\Delta^{J+s-1}}
\end{aligned}$$

Figure 10.1: Combination of diagrams G.99, G.113 and G.123–G.126.

irrespective of the value of  $n$ . However, we will not perform this step as we will then have to undo it, when we come to deal with diagrams in which the gauge remainder structure is nested. As we iterate the diagrammatic procedure, though, we will encounter diagrams for which such restrictions can be removed, irrespective of the level of nesting of the gauge remainder structure.

Diagram G.303 is converted into a  $\Lambda$ -derivative term, as shown in figure 10.2.

To prepare for the treatment of the diagrams of figure 10.2 and, in the process, for the treatment of terms containing nested gauge remainders, we can guess from our earlier work that it will be desirable to promote  $\rightarrow$

$$-4 \sum_{J=0}^n \Upsilon_{J,0} \left[ \left[ \left[ \begin{array}{c} \text{G.309} \rightarrow 10.3 \\ \bullet \\ \curvearrowright \\ n_J^R \end{array} \right] - \left[ \begin{array}{c} \text{G.310} \rightarrow 10.3 \\ \bullet \\ \curvearrowright \\ n_J^R \bullet \end{array} \right] \right]^{11\Delta^J} \\
- J \left[ \begin{array}{c} \text{G.311} \rightarrow 10.3 \\ \curvearrowright \\ n_J^R \\ \square \end{array} \right]^{11\Delta^{J-1}}$$

Figure 10.2: Converting diagram G.303 into a  $\Lambda$ -derivative term.

into a decoration.

Having done this, we will detach the gauge remainder from the effective propagator. Since it can now attach to either end of any of the effective propagators, we must compensate for this step with a factor of  $1/2(J+1)$ . The rule for its attachment is that it must either bite another gauge remainder (the nested case) or the end of a wire. Furthermore, it can attach either as a push-forward or a pull-back. Since, for the term under consideration these add, we must compensate by a further factor of two.

Figure 10.3 shows the re-expression of the diagrams of figure 10.2 using the new notation, where the vertex struck by the  $\Lambda$ -derivative has been processed.

In the final diagram, we start the sum over  $J$  from one, rather than from zero, since we must have at least one effective propagator available with which to attach the gauge remainder to some other structure. Furthermore, we have removed the restriction that the vertex be reduced. We do this because the vertex must be at least three-point, irrespective of both how many gauge remainders decorate the diagram and the value of  $n$ .

This is looking extremely familiar. What we have here is essentially a version of what we were doing in chapter 7. The crucial difference is the presence of the decorative structure  $\curvearrowright$ . Its behaviour is somewhere between that

$$\begin{aligned}
& -2 \sum_{J=0}^n \Upsilon_{J+1,0} \left[ \left[ \begin{array}{c} \text{G.312} \\ \circlearrowleft{n_J^R} \end{array} \right] \bullet - \sum_{r=1}^{n_J} \left[ 2(n_{J+r} - 1)\beta_r + \gamma_r \frac{\partial}{\partial \alpha} \right] \circlearrowleft{n_{J+r}^R} \right] \left. \vphantom{\sum} \right]^{11\Delta^{J+1}\rangle} \\
& - \frac{1}{2} \sum_{r=0}^{n_J} \left[ \begin{array}{c} \text{G.313} \rightarrow 10.4 \\ \circlearrowleft{\bar{r}} \\ \bullet \\ \circlearrowleft{\bar{n}_{J+r}} \end{array} \right]_R + \frac{1}{2} \circlearrowleft{\Sigma_{n_{J+1}}} \\
& + \sum_{J=1}^n \Upsilon_{J,0} \left[ \begin{array}{c} \square \\ \circlearrowleft{n_J} \end{array} \right] \left. \vphantom{\sum} \right]^{11\Delta^J\rangle}
\end{aligned}$$

Figure 10.3: Re-expression of the diagrams of figure 10.2.

of the usual (internal) effective propagators and the usual external fields. Like the former, it can be struck by  $\Lambda \partial_\Lambda |_\alpha$  but, like the latter, it cannot be used to join different structures.

It is not hard to predict what our strategy will be: we will process diagram G.313 using the usual diagrammatic procedure. However, compared to the analogous manipulations performed at the beginning of this chapter, we will have extra terms, arising from the presence of the structure  $\curvearrowright$ .

First, we isolate the two-point, tree level vertices in diagram G.313. As usual, we can decorate such vertices with external fields or use an effective propagator to join them to some other structure. Now, however, we have the additional choice of decorating with the structure  $\curvearrowright$ . This is where all the subtleties in converting terms containing gauge remainders into  $\Lambda$ -derivative terms arise: our entire diagrammatic procedure revolves around isolating two-point, tree level vertices and attaching them to other structures. Now, every time we create such a vertex, we can join it to the decorative gauge remainder, which was never previously an option.

In this particular case, though, there is very little complication, since an effective propagator which attaches to the (un-nested) gauge remainder must be in the  $C$ -sector. Hence, if this effective propagator attaches at the other

end to a two-point, tree level vertex then, after application of the effective propagator relation, there will be no additional gauge remainders. When we move on to diagrams where we can join two-point, tree level vertices to nested gauge remainders, however, the full effective propagator relation must be used.

Returning to the case in hand, we iterate the usual diagrammatic procedure. The intermediate step of stripping off the two-point, tree level vertices from diagram G.313 is shown in figure 10.4.

$$\begin{aligned}
 & \sum_{J=0}^n \Upsilon_{J+1,0} \left[ \sum_{r=0}^{n_J} \begin{array}{c} \text{G.314} \\ \circlearrowleft \bar{r}^R \\ \bullet \\ \circlearrowleft \bar{n}_{J+r}^R \end{array} - 2 \begin{array}{c} \text{G.315} \rightarrow 10.5 \\ \circlearrowleft 0^2 \\ \bullet \\ \circlearrowleft \hat{n}_J^R \end{array} \right]^{11\Delta^{J+1} >} \\
 & - \Upsilon_{n+1,0} \left[ \begin{array}{c} \text{G.316} \rightarrow 10.5 \\ \circlearrowleft 0^2 \\ \circ \\ \circlearrowleft 0^2 \end{array} \right]^{11\Delta^{n+1} >}
 \end{aligned}$$

Figure 10.4: Isolation of the two-point, tree level vertices of diagram G.313.

The partial decoration of diagrams G.315 and G.316, followed by the tying together of any loose ends and the application of the effective propagator relation, as appropriate, is shown in figure 10.5. Note that the attachment of  $\text{---}\curvearrowright$  to a two-point, tree level vertex will come with a factor of  $2 \times 2(J+1)$ , corresponding to the number of different ways in which we can create  $\text{---}\curvearrowright$ .

Diagrams G.317, G.319–G.321 G.322 and G.325 are the types of diagram we were obtaining in chapter 7 with the difference that, amongst the decorative fields, we have  $>$ . Again, the constraint that there must be an effective propagator with which to attach the gauge remainder to some other structure means that for diagrams G.319–G.321 we start the sum over  $J$  from one, rather than zero. Encouragingly, we find cancellations against terms generated by the original set of gauge remainders.

$$\begin{aligned}
& -2 \sum_{J=0}^n \Upsilon_{J+1,0} \left[ \begin{array}{c} \text{G.317} \\ \begin{array}{c} \text{---} \\ | \\ \circlearrowleft{0^2} \\ | \\ \bullet \\ | \\ \circlearrowleft{\hat{n}_J^R} \end{array} \end{array} \right]^{1\Delta^{J+1}\rangle} + 2\Upsilon_{J,0} \left[ \begin{array}{c} \{ \text{G.318 } G.49 \} \\ \begin{array}{c} \text{---} \\ | \\ \bullet \\ | \\ \circlearrowleft{\hat{n}_J^R} \end{array} \end{array} \right]^{11\Delta^J} \\
& -2 \sum_{J=1}^n \Upsilon_{J,0} \left[ \begin{array}{c} \text{G.319} \quad \text{G.320} \quad \text{G.321} \\ \frac{1}{\vartheta_{n_J}} \begin{array}{c} \bullet \\ | \\ \circlearrowleft{\hat{n}_J} \end{array} - \begin{array}{c} \bullet \\ | \\ \circlearrowleft{\hat{n}_J^R} \end{array} - \begin{array}{c} \bullet \\ | \\ \circlearrowleft{\hat{n}_J^R} \end{array} \end{array} \right]^{11\Delta^J} \\
& 2\Upsilon_{n,0} \left[ \begin{array}{c} \text{G.322} \\ \begin{array}{c} \text{---} \\ | \\ \bullet \\ | \\ \circlearrowleft{0^2} \\ | \\ \text{---} \end{array} \end{array} \right]^{1\Delta^n} - 2 \left[ \begin{array}{c} \{ \text{G.323 } G.248 \} \\ \begin{array}{c} \text{---} \\ | \\ \bullet \\ | \\ \circlearrowleft{0^2} \\ | \\ \text{---} \end{array} \end{array} \right]^{1\Delta^n} \\
& + \Upsilon_{n-1,0} \left[ 4 \left[ \begin{array}{c} \text{G.324} \rightarrow 10.7 \\ \begin{array}{c} \bullet \\ | \\ \circlearrowleft{\hat{n}_J} \end{array} \end{array} \right]^{11\Delta^{n-1}} - \left[ \begin{array}{c} \text{G.325} \\ \begin{array}{c} \bullet \\ | \\ \circlearrowleft{\hat{n}_J} \end{array} \end{array} \right]^{11\Delta^{n-1}\rangle} \right]
\end{aligned}$$

Figure 10.5: The result of processing diagrams G.315 and G.316.

**Cancellation 10.1** *Diagram G.318 exactly cancels diagram G.49.*

**Cancellation 10.2** *Diagram G.323 cancels diagram G.248 by virtue of the fact that the decorations force the wine of the latter diagram to be decorated, for all values of  $n$ .*

We now consider continuing with the usual diagrammatic procedure, by processing the manipulable part of diagram G.314. It is clear that this will just give us a version of figure 7.25, so long as we include the gauge remainder in the decorations and add one extra term, corresponding to the  $\Lambda$ -derivative striking  $\text{---}\curvearrowright$ .

Let us compute the factor of this extra term, compared to the parent diagram. First of all, being a correction term, it will come with a relative minus sign. Promoting the wine to a decorative effective propagator will have yielded a factor of  $1/2(J+2)$ . This  $J$  dependence is compensated for by the  $4(J+2)$  different ways in which we can create  $\text{---}\curvearrowright$ . We then have a choice of two vertices to which to attach the structure  $\left[ \text{---}\curvearrowright \right]^\bullet$ . Hence, the overall factor, relative to the parent diagram, is  $-4$ . The corresponding term is the first diagram in figure 10.6.

At the next stage of the diagrammatic procedure, too, we will have new diagrams. These arise from attaching  $\text{---}\curvearrowright$  to two-point, tree level vertices. Two such diagrams we have essentially encountered already, as these are just versions of diagrams G.318 and G.324 possessing an additional vertex. There are two more that we have not yet encountered: taking the usual dumbbell structure with a two-point, tree level vertex at either end, these correspond to attaching  $\text{---}\curvearrowright$  to one of the vertices and joining the other vertex to a reduced Wilsonian effective action vertex. The resulting terms correspond to the final two diagrams of figure 10.6.

**Cancellation 10.3** *Diagram G.326 exactly cancels diagram G.305.*

**Cancellation 10.4** *Diagram G.327 exactly cancels diagram G.304.*

Iterating the diagrammatic procedure, it is apparent that the four cancellations 10.1–10.4 will go through just the same at each level of manipulation.

$$\begin{aligned}
& -4 \sum_{J=0}^n \sum_{r=0}^{n_J} \Upsilon_{J+1,0} \left[ \begin{array}{c} \{ \mathbf{G.326} \ G.305 \} \\ \left[ \begin{array}{c} \text{loop} \\ \bullet \end{array} \right] \\ \text{circle } n_{J+r}^R \\ \text{circle } r^R \end{array} \right]^{11\Delta^{J+1}} \\
& +4 \sum_{J=0}^n \Upsilon_{J,0} \left[ \begin{array}{cc} \{ \mathbf{G.327} \ G.304 \} & \mathbf{G.328} \rightarrow 10.7 \\ \text{circle } n_J^R \text{ with loop} & - \text{circle } n_J^R \text{ with loop} \end{array} \right]^{11\Delta^J}
\end{aligned}$$

Figure 10.6: New types of diagram arising from iterating the diagrammatic procedure.

Given the cancellation of these terms, cancellation mechanisms 2–10 now guarantee that we can reduce this sector of the calculation to  $\Lambda$ -derivative,  $\beta$  and  $\gamma$  terms, up to further gauge remainders and terms that require manipulation at  $\mathcal{O}(p^2)$ .

Processing the new gauge remainders is easy! We have copies of all of the old gauge remainder diagrams, with the only difference that we must include  $\triangleright$  as a decoration. There is also an additional set of type-Ib gauge remainders, corresponding to diagrams G.324 and G.328 and their analogues possessing additional vertices.

Before doing anything with these terms, we note that we can combine them with two diagrams coming from the *original* set of type-II gauge remainders; namely, diagrams G.152 and G.153. The result of this is shown in figure 10.7.

We can discard diagram G.329 since the wine, not being decorated, is forced to be in the  $C$ -sector: it is clear that the unprocessed gauge remainder has no support. However, it is illuminating to keep this diagram since it will serve to illustrate the structure of cancellations in the case where the processed gauge remainder is nested.

$$\begin{aligned}
& 2 \sum_{J=0}^n \Upsilon_{J,0} \left[ \begin{array}{cc} \text{G.329} \rightarrow 10.8 & \text{G.330} \rightarrow 10.8 \\ \begin{array}{c} \square \downarrow \\ \textcircled{n_J^R} \end{array} & - \begin{array}{c} \circ \downarrow \\ \textcircled{n_J^R} \end{array} \end{array} \right]^{11\Delta^J} \\
& + 2\Upsilon_{n-1,0} \left[ \begin{array}{c} \text{G.331} \rightarrow 10.8 \\ \begin{array}{c} \bullet \leftarrow \\ \textcircled{\phantom{n_J^R}} \end{array} \end{array} \right]^{11\Delta^{n-1}}
\end{aligned}$$

Figure 10.7: Result of combining diagrams G.324 and G.328 with diagrams G.152 and G.153.

Allowing the gauge remainder to act in diagrams G.329–G.331, it is apparent that all generated terms in which the gauge remainder strikes a socket which decorates anything other than a two-point, tree level vertex will simply cancel, via cancellation mechanism 11.

Remembering to include terms that survive from the manipulation of diagrams G.329–G.331, our analysis of the complete set of gauge remainders goes through almost exactly as it did before. We might worry that there are new terms which arise when we decorate a two-point, tree level vertex generated by a gauge remainder with  $\curvearrowright$ . Upon utilising the effective propagator relation, however, these terms vanish, courtesy of diagrammatic identity 10. The set of surviving terms is then just given by the survivors from sections 8.1–8.4—where we include  $>$  in the decorations—and by the diagrams of figure 10.8 and their analogues containing greater number of vertices.

As we will see later, diagram G.333 will be cancelled, completely. What, however, are we to do with diagram G.332? The answer is that this diagram vanishes via diagrammatic identity 10.

Now we process the gauge remainders in diagrams G.334–G.336 and their analogues containing additional vertices. All contributions in which a gauge remainder strikes a socket which decorates anything other than a two-point,

$$\begin{aligned}
& 4\Upsilon_{n-1,0} \left[ \begin{array}{ccc} \mathbf{G.332} \rightarrow 0 & \{ \mathbf{G.333} \ G.354 \} & \mathbf{G.334} \rightarrow 10.9 \\ \text{Diagram 1} & + & \text{Diagram 2} + \text{Diagram 3} \end{array} \right]^{11\Delta^{n-1}} \\
& 4 \sum_{J=0}^n \Upsilon_{J,0} \left[ \begin{array}{cc} \mathbf{G.335} \rightarrow 10.9 & \mathbf{G.336} \rightarrow 10.9 \\ \text{Diagram 4} & - & \text{Diagram 5} \end{array} \right]^{11\Delta^J}
\end{aligned}$$

Figure 10.8: The minimal set of new types of diagram arising from processing the gauge remainders spawned by terms with  $>$  among the decorations.

tree level vertex will cancel, via cancellation mechanism 11. Iterating the diagrammatic procedure once will give us:

1. versions of the parent diagrams, nested with respect to the already nested gauge remainder;
2. terms with an  $\mathcal{O}(p^2)$  stub;
3. the diagrams of figure 10.9 and their analogues, containing additional vertices.

Diagrams G.337 and G.338 vanish by virtue of diagrammatic identity 10.

Iterating the diagrammatic procedure until exhaustion will give us, up to terms with an  $\mathcal{O}(p^2)$  stub, increasingly nested versions of the diagrams of figure 10.9, together with versions of these diagrams accompanied by additional vertices, as appropriate. The nesting is with respect to the already nested gauge remainder and so we need not bother considering the nested versions of diagrams G.337 and G.338 in this sense, since they will still vanish.

Having processed the gauge remainders, we arrive inevitably (for generic  $n$ ) at yet another set of terms which can be converted into  $\Lambda$ -derivatives: we obtain a copy of figure 10.1 but where we have a  $>$  among the decorations. The analogue of diagram G.303 is shown in figure 10.10.

$$\left[ \begin{array}{cccc}
 \mathbf{G.337} \rightarrow 0 & \mathbf{G.338} \rightarrow 0 & \mathbf{G.339} \rightarrow 10.23 & \mathbf{G.340} \rightarrow 10.23 \\
 \begin{array}{c} \bullet \\ \downarrow \\ \curvearrowright \end{array} & - & \begin{array}{c} \bullet \\ \downarrow \\ \curvearrowright \end{array} & + & \begin{array}{c} \bullet \\ \downarrow \\ \curvearrowright \end{array} & - & \begin{array}{c} \bullet \\ \downarrow \\ \curvearrowright \end{array} \\
 \\
 \mathbf{G.341} \rightarrow 10.23 & \mathbf{G.342} \rightarrow 10.23 & \mathbf{G.343} \rightarrow 10.23 & \mathbf{G.344} \rightarrow 10.23 \\
 \begin{array}{c} \square \\ \downarrow \\ \curvearrowright \\ \circlearrowleft \\ 0^2 \end{array} & - & \begin{array}{c} \square \\ \downarrow \\ \curvearrowright \\ \circlearrowleft \\ 0^2 \end{array} & - & \begin{array}{c} \circ \\ \downarrow \\ \curvearrowright \\ \circlearrowleft \\ 0^2 \end{array} & + & \begin{array}{c} \circ \\ \downarrow \\ \curvearrowright \\ \circlearrowleft \\ 0^2 \end{array}
 \end{array} \right] 11\Delta^{n-1}$$

Figure 10.9: The minimal set of terms spawned by diagrams G.334–G.336, up to nested versions of the parent diagrams and diagrams with an  $\mathcal{O}(p^2)$  stub.

We see that we must take some care converting such a term into a  $\Lambda$ -derivative term, since the structure  $\curvearrowright$  is repeated. The new rule is simple to guess: to convert the first diagram into a  $\Lambda$ -derivative term, promote  $\curvearrowright$  to a decoration and divide not only by a factor of  $4(J+1)$ , but also by an additional factor of two. This extra factor recognises that we now have two gauge remainders with which to decorate the effective propagators. The resulting  $\Lambda$ -derivative term is shown in figure 10.11.

$$-4 \sum_{J=0}^n \Upsilon_{J,0} \left[ \left[ \left[ \curvearrowright \right] \bullet \right] \left[ \begin{array}{c} \bullet \\ \downarrow \\ \curvearrowright \\ \circlearrowleft \\ n_J^R \end{array} \right] \right]^{11\Delta^J} = -8 \sum_{J=1}^n \Upsilon_{J-1,0} \left[ \left[ \left[ \curvearrowright \right] \bullet \right] \left[ \begin{array}{c} \bullet \\ \downarrow \\ \curvearrowright \\ \circlearrowleft \\ n_J^R \end{array} \right] \right]^{11\Delta^{J-1}}$$

Figure 10.10: An example of a candidate for conversion into a  $\Lambda$ -derivative term, possessing the structure  $\curvearrowright$  both as a decoration and as the component of the diagram hit by  $-\Lambda\partial_\Lambda$ .

$$- \sum_{J=0}^n \Upsilon_{J+1,0} \left[ \left[ \begin{array}{c} \mathbf{G.345} \\ \textcircled{n_J^R} \end{array} \right] \bullet \right]^{11\Delta^{J+1} > 2} + \dots$$

Figure 10.11: A  $\Lambda$ -derivative term for a diagram decorated by two gauge remainders.

To check that we can correctly reproduce the parent diagram, we will try to recreate the rightmost diagram of figure 10.10. To generate this term, we must choose two effective propagators from  $(J + 1)$  and two gauge remainders from two. We then use the gauge remainders to decorate the ends of the effective propagators in all possible ways. This gives a factor of

$$\frac{(J + 1)(J)}{2} \times 8.$$

Adding the push-forward to the pull-back—which, we recall, is legal for both gauge remainders in this case—gives a further factor of four. Combining with the factor in front of the  $\Lambda$ -derivative term and including an extra factor of two since the  $\Lambda$ -derivative can hit either of the  $\text{---}\curvearrowright$  structures, it is clear that the parent diagram is reproduced.

There is, needless to say, a subtlety in what we have done that has not been explored. Whilst the notation we have employed for the  $\Lambda$ -derivative term most certainly includes decoration by two instances of the structure  $\text{---}\curvearrowright$ , it is natural to allow it to include also decoration with a structure in which one of the effective propagators is bitten by a nested gauge remainder. This would correspond to the diagrams of figure 10.12.

Note the overall factor of diagrams I.56 and I.57: given that we collect together the first push-forward and pull-back, yielding a factor of two, there is only one independent way to generate each of these diagrams.

Wonderfully, we see that such  $\Lambda$ -derivative terms arise, naturally, from the nested version of diagram G.303. (Note that the nested version of diagram G.303 are derived from diagrams G.108, G.115 and G.78.) This is, of course, no coincidence. Before we process diagram G.345, we would first like



$$-\frac{2}{m!} \sum_{J=0}^n \Upsilon_{J+1,0} \left[ \left[ \begin{array}{c} \mathbf{I.58} \\ \textcircled{n_J^R} \end{array} \right] \right]^{11\Delta^{J+1} > m}$$

Figure 10.13: The candidate for a  $\Lambda$ -derivative term with  $m$  decorative gauge remainders.

Our task now is to show that diagram I.58 is the correct representation for a  $\Lambda$ -derivative term comprising a single vertex and  $m$  decorative gauge remainders, however we choose to arrange the gauge remainders. In actual fact, our aim at this stage is not quite this grand. In  $\Lambda$ -derivative terms where effective propagators join gauge remainders, we know that parent diagrams of the form of diagram I.12 should exist. We are yet to show this even for the case where the gauge remainders form a single structure and for the time being just assume that these terms will come with the correct factors.

To begin our analysis of diagram I.58, we must first ask what constitutes a valid arrangement of gauge remainders. A valid arrangement possesses an arbitrary number of clusters of gauge remainders. In each cluster, every gauge remainder is bitten by another gauge remainder, from the same cluster. (In the case of  $\textcircled{\cdot}$ , we consider the gauge remainder to be biting itself.) This means that diagrams such as  are excluded, since the rightmost gauge remainder does not bite another gauge remainder (see also section 3.1.9).

We can deduce the maximum value of  $m$  (note that this will change for diagrams with additional vertices). For every instance of  $>$ , there must be a field to which it can be attached. The maximum number of available fields occurs when  $J = n$ . In this case, we require a minimum of three fields to decorate the vertex<sup>1</sup>. Therefore,

$$m_{\max} = 2n + 1.$$

The first arrangement of gauge remainders we will look at is one in which we suppose that each of the gauge remainders forms an independent structure

---

<sup>1</sup>If  $J < n$ , we need one less field to decorate the vertex, but the number of total available fields decreases by at least two.

$\ni$  . We will now suppose that diagram I.58 correctly represents such terms for some value of  $m < m_{\max}$ , say  $m'$ . Following through the formation of diagram G.345, it is apparent the corrections generated by the formation of diagram I.58 yield, amongst others, the term shown in figure 10.14

$$-\frac{4}{m'!} \sum_{J=0}^n \Upsilon_{J,0} \left[ \begin{array}{c} \mathbf{I.59} \\ \left[ \begin{array}{c} \ni \\ \bullet \end{array} \right] \\ \left( n_J^R \right) \end{array} \right]^{11\Delta^J > m'}$$

Figure 10.14: A term generated by the corrections to diagram I.58 for  $m = m' < m_{\max}$ .

Converting diagram I.59 into a  $\Lambda$ -derivative term, and promoting  $\ni$  to a decoration yields a version of diagram I.58 in which  $m = m' + 1$ . Given that diagram I.58 correctly represents a term in which all decorative gauge remainders form a  $\ni$  for  $m = 1$ , it therefore follows by induction that diagram I.58 correctly represents such terms for all  $m$ .

We now generalise this argument to confirm that diagram I.58 works, however we arrange the gauge remainders. To this end, let us suppose that we form  $r$  clusters, each containing  $q_i$  gauge remainders. The first thing we note is that there are

$$\frac{m!}{\sum_{i=1}^r q_i!}$$

ways of partitioning  $m$  gauge remainders into these  $r$  clusters. Assuming that we do not collect together any pushes-forward with pulls-back, the actual formation of each cluster yields a factor of  $(q_i - 1)!$ . Supposing now that for one and only one of the clusters we combine the first push-forward with the corresponding pull-back, it is clear that we can redraw diagram I.58, as shown in figure 10.15.

It may of course be possible to simplify diagram I.60 in cases where further pushes-forward and pulls-back can be combined; for our current purposes, however, there is no need to do this.

$$-\frac{2}{\sum_{i=1}^r q_i} \sum_{J=0}^n \Upsilon_{J+1,0} \left[ \begin{array}{c} \text{I.60} \\ \underbrace{\begin{array}{c} \wedge \quad \vee \\ \circ \quad \circ \end{array}}_{q_1} \quad \underbrace{\begin{array}{c} \wedge \quad \vee \\ \circ \quad \circ \end{array}}_{q_2} \quad \dots \\ \circlearrowleft_{n_J^R} \end{array} \right] \bullet^{11\Delta^{J+1}}$$

Figure 10.15: A generic form of diagram I.58, in which the decorative  $\triangleright$ s have been explicitly arranged. One push-forward has been implicitly combined with the corresponding pull-back, via CC.

We now assume that diagram I.60 has the correct factor for some value of  $m < m_{\max}$ , say  $m'$ . There are two types of diagram possessing  $m' + 1$  gauge remainders, which we must consider. The first is where the extra gauge remainder forms  $\triangleright$ . The second is where this gauge remainder supplements one of the existing gauge remainder clusters.

In the former case, we need to find the factor for the diagrams in which:

1. the new gauge remainder, which forms  $\triangleright$ , is hit by  $\Lambda\partial_\Lambda|_\alpha$ ;
2. the effective propagator leaving (the new)  $\triangleright$  is struck by  $\Lambda\partial_\Lambda|_\alpha$ ;
3. one of the other gauge remainder structures is hit by  $\Lambda\partial_\Lambda|_\alpha$ ;
4. an effective propagator leaving one of the gauge remainders of one of the original structures is hit by  $\Lambda\partial_\Lambda|_\alpha$ .

This task is made somewhat easier by the fact that, for the time being, we will not worry about the factor of diagrams in which differentiated effective propagators join two gauge remainders. Our hope is that the sum of the four diagrams above is consistent with a version of diagram I.58 with  $m = m' + 1$ .

Following our earlier analysis, it is trivial to show that the first two diagrams come with the correct factor. Our strategy for the remaining two diagrams is as follows. Returning to diagram I.60, consider extracting a gauge remainder from the  $i$ th structure—which we assume to possess  $q_i = q'_i > 1$  gauge remainders—and using it to form  $\triangleright$ . Such a diagram still possesses  $m'$  gauge remainders and so, under our initial assumption, still comes with the correct factor.



to the first two items above, which we have done already. If all of the  $q_i$  are unity, then we are just back to the case of  $m$  instances of  $\curvearrowright$ ; again, which has already been analysed.

Our penultimate task is to look at the case where one of the existing structures of diagram I.60—for the case that this diagram possesses  $m'$  gauge remainders—is supplemented by an additional gauge remainder. The procedure is very similar to what we have just done. We suppose that it is the  $i$ th structure that we supplement. First, we show that the supplemented  $i$ th structure, struck by  $\Lambda\partial_\Lambda|_\alpha$ , comes with the correct factor. Next, we return to the diagram with just  $m'$  gauge remainders and remove a gauge remainder from the  $j$ th structure, adding it to the  $i$ th structure. Then we increase the number of gauge remainders in the  $j$ th structure by one and suppose that it is this structure that is struck by  $\Lambda\partial_\Lambda|_\alpha$ . It is straightforward to show that the resulting terms can be combined into a  $\Lambda$ -derivative term, consistent with a version of diagram I.58 for which  $m = m' + 1$ .

To complete the proof by induction that diagram I.58 is correct for all  $m$ , we must explicitly show that it is actually correct for  $m = 3$  and where there are two gauge remainder structures. This is very easy to do and will not be presented here; suffice to say that it has been checked.

We now return to diagram G.345 and analyse what happens when it is processed. First of all, we obtain a version of figure 10.3 where the diagrams come with a relative factor of  $1/2$  and have an extra decorative  $>$ . Similarly, with figure 10.4. The next step is to decorate the two-point, tree level vertices of the diagrams in the new version of this figure. When we decorate the diagram like G.315, there are four things we can do:

1. decorate the two-point, tree level vertex with an external field;
2. attach the two-point, tree level vertex to either the wine or a vertex, using an effective propagator;
3. decorate the two-point, tree level vertex with  $\curvearrowright$ ;
4. decorate the two-point, tree level vertex with the nested version of  $\curvearrowright$ .

The first option will reproduce diagram G.317 but with a relative factor of

1/2 and an additional decorative  $>$ . The second option will do likewise with diagrams G.319–G.321. The third option will reproduce diagram G.318 with the same factor but with an additional decorative  $>$ . The reason that the factor is the same is because the relative factor of 1/2 we were expecting is cancelled out by the choice of two  $>$ s with which we can form  $\curvearrowright$ . The fourth option will yield a version of diagram G.318, with the same factor and the same decorations, but in which the  $\curvearrowright$  has been replaced by the two independent, singly nested versions. These two terms are depicted by the first two diagrams of figure 10.17. Additionally, these diagrams will come with gauge remainder contributions, where the gauge remainder is trapped by the nested structure, as depicted by the third and fourth diagrams of figure 10.17.

$$4 \sum_{J=0}^n \left[ \begin{array}{cccc} \mathbf{G.346} & \mathbf{G.347} & \{ \mathbf{G.348} \ G.89 \} & \{ \mathbf{G.349} \ G.88 \} \\ \begin{array}{c} \downarrow < \\ \bullet \\ \hat{n}_J^R \end{array} & - \begin{array}{c} \downarrow < \\ \bullet \\ \hat{n}_J^R \end{array} & - \begin{array}{c} \downarrow < \\ \bullet \\ \hat{n}_J^R \end{array} & + \begin{array}{c} \downarrow < \\ \bullet \\ \hat{n}_J^R \end{array} \end{array} \right]^{11\Delta^J}$$

Figure 10.17: New types of diagram arising from the decoration of version of diagram G.315.

Having considered the decoration of the diagram like G.315, we move on to consider the decoration of the diagram like G.316. From our previous arguments it is clear that we will produce:

1. versions of diagrams G.322 and G.325 with a relative factor of 1/2 and an additional decorative  $>$ ;
2. versions of diagrams G.323 and G.324 with the same factor and a decorative  $>$ ;
3. versions of diagrams G.323 and G.324 with the same factor, the same decorations but in which the  $\curvearrowright$  has been replaced by the two independent, singly nested versions. These contributions have partners possessing gauge remainders;

4. an entirely new type of term in which we attach an instance of  $\curvearrowright$  to both of the two-point, tree level vertices;
5. an entirely new type of term in which we attach each of the two-point, tree level vertices to one of the gauge remainders which constitute the nested versions of  $\curvearrowright$ .

The diagrams described in the last three items are shown in figure 10.18.

We now find a number of cancellations, some implicit and others explicit. Turning first to the former, we see that there will be a repetition of cancellation 10.1. To be precise, diagrams G.346 and G.347 will cancel against the nested versions of diagram G.49. Similarly, the nested version of cancellations 10.3 and 10.4 go through just the same. We must be more careful with the nested version of cancellation 10.2, since it occurs only as a consequence of the particular diagrammatic structure and set of decorative fields. The nested version of this cancellation will fail in the following circumstances: at the final level of nesting and at any level of nesting beyond the current one (but before the final level) when there are additional vertices.

From cancellations 10.1 and 10.4 we will derive another cancellation mechanism. (Cancellation 10.2 involves diagrams possessing an  $\mathcal{O}(p^2)$  stub; since these will not be fully treated in this thesis, we do not worry about cancellation mechanisms for such terms.)

**Cancellation Mechanism 13** *Consider a manipulable diagram comprising gauge remainder structures and a single vertex: this is the parent for what follows. Iterating the diagrammatic procedure, amongst the correction terms generated at each stage are those diagrams possessing a dumbbell structure with at least one two-point, tree level vertex.*

*In the case where there is a single two-point, tree level vertex, we will attach it to a gauge remainder structure. In the case that there are two such vertices, we will attach one to a gauge remainder structure and the other to a vertex. For the purposes of this cancellation mechanism, we utilise the effective propagator relation, wherever possible, but retain only the Kronecker delta*

$$\begin{aligned}
& 4\Upsilon_{n,0} \\
& \times \left[ \begin{array}{cccccc}
\mathbf{G.350} & \mathbf{G.351} & \{ \mathbf{G.352} \ G.250 \} & \{ \mathbf{G.353} \ G.249 \} & & \\
\begin{array}{c} \circ \\ \downarrow \\ \circ^2 \\ \downarrow \end{array} & \begin{array}{c} \circ \\ \downarrow \\ \circ^2 \\ \downarrow \end{array} & \begin{array}{c} \circ \\ \downarrow \\ \circ^2 \\ \downarrow \end{array} & \begin{array}{c} \circ \\ \downarrow \\ \circ^2 \\ \downarrow \end{array} & + & \begin{array}{c} \circ \\ \downarrow \\ \circ \\ \downarrow \end{array} \\
\end{array} \right]^{1\Delta^n} \\
& -4\Upsilon_{n-1,0} \\
& \times \left[ \begin{array}{cccc}
\mathbf{G.355} \rightarrow 10.20 & \mathbf{G.356} \rightarrow 10.20 & \mathbf{G.357} \rightarrow 10.20 & \mathbf{G.358} \rightarrow 10.20 \\
\begin{array}{c} \circ \\ \downarrow \\ \bullet \\ \downarrow \end{array} & \begin{array}{c} \circ \\ \downarrow \\ \bullet \\ \downarrow \end{array} & \begin{array}{c} \circ \\ \downarrow \\ \bullet \\ \downarrow \end{array} & \begin{array}{c} \circ \\ \downarrow \\ \bullet \\ \downarrow \end{array} \\
\end{array} \right]^{11\Delta^{n-1}} \\
& +2\Upsilon_{n-1,0} \\
& \times \left[ \begin{array}{cccc}
\{ \mathbf{G.359} \ G.160 \} & \{ \mathbf{G.360} \ G.161 \} & \{ \mathbf{G.361} \ G.251 \} & \{ \mathbf{G.362} \ G.252 \} \\
\begin{array}{c} \circ \\ \downarrow \\ \bullet \\ \downarrow \end{array} & \begin{array}{c} \circ \\ \downarrow \\ \bullet \\ \downarrow \end{array} & \begin{array}{c} \circ \\ \downarrow \\ \bullet \\ \downarrow \end{array} & \begin{array}{c} \circ \\ \downarrow \\ \bullet \\ \downarrow \end{array} \\
\{ \mathbf{G.363} \ G.253 \} & \{ \mathbf{G.364} \ G.254 \} & \{ \mathbf{G.365} \ G.214 \} & \{ \mathbf{G.366} \ G.215 \} \\
- & + & + & - \\
\begin{array}{c} \circ \\ \downarrow \\ \bullet \\ \downarrow \end{array} & \begin{array}{c} \circ \\ \downarrow \\ \bullet \\ \downarrow \end{array} & \begin{array}{c} \circ \\ \downarrow \\ \bullet \\ \downarrow \end{array} & \begin{array}{c} \circ \\ \downarrow \\ \bullet \\ \downarrow \end{array} \\
\end{array} \right]^{11\Delta^{n-1}}
\end{aligned}$$

Figure 10.18: New types of diagram arising from the decoration of version of diagram G.316.

part. The resulting diagrams are guaranteed to exactly cancel against identical terms generated earlier in the calculation, together with the parent diagram.

A further cancellation mechanism follows from cancellation 10.3

**Cancellation Mechanism 14** *Consider the conversion of diagrams possessing gauge remainder structures and at least one vertex into  $\Lambda$ -derivative terms. For what follows, we take the parent diagrams to have only manipulable components; i.e. a decomposition like that of figure 10.1 has been performed.*

*For a given set of gauge remainder structures, there is a tower of manipulable terms; each successive term possessing an additional vertex.*

*Starting from the single vertex term, we apply the diagrammatic procedure. This generates a diagram which cancels the two vertex term coming from the tower. Successive iterations generate diagrams which cancel successive terms from the tower.*

The explicit cancellations are more exciting as a selection of them involve the first use of one of the diagrammatic identities.

**Cancellation 10.5** *Diagram G.348 exactly cancels diagram G.89 via diagrammatic identity 11.*

**Cancellation 10.6** *Diagram G.349 exactly cancels diagram G.88 via diagrammatic identity 11.*

**Cancellation 10.7** *Diagram G.352 exactly cancels diagram G.250 via diagrammatic identity 11.*

**Cancellation 10.8** *Diagram G.353 exactly cancels diagram G.249 via diagrammatic identity 11.*

**Cancellation 10.9** *Diagram G.354 exactly cancels diagram G.333 by virtue of the fact that the decorations force the wine of the latter diagram to be decorated, for all values of  $n$ .*

**Cancellation 10.10** *Diagram G.359 cancels diagram G.160, by virtue of the fact that the decorations force the wine of the latter diagram to be decorated, for all values of  $n$ .*

**Cancellation 10.11** *Diagram G.360 cancels diagram G.161, by virtue of the fact that the decorations force the wine of the latter diagram to be decorated, for all values of  $n$ .*

**Cancellation 10.12** *Diagrams G.361–G.364 exactly cancel diagrams G.251–G.254.*

**Cancellation 10.13** *Diagram G.365 exactly cancels diagram G.214 via diagrammatic identity 11.*

**Cancellation 10.14** *Diagram G.366 exactly cancels diagram G.215 via diagrammatic identity 11.*

Taking into account cancellation mechanisms 2–10, 13 and 14, we can deduce the terms we will be left with after iterating the procedure of converting terms into  $\Lambda$ -derivatives. The above cancellations are repeated, at every stage of the calculation. This includes cancellations 10.10 and 10.11: even in the versions of diagrams G.160 and G.161 with additional vertices, we are still forced to decorate the wine, as this is the only way to ensure that there are no disconnected structures. Note, though, that at higher levels of nesting, decoration of the wine is not necessarily forced, as sockets are available for the decorative fields.

Thus, we will reduce this sector of the cancellation to  $\Lambda$ -derivative,  $\beta$  and  $\gamma$  terms, up to further gauge remainders and terms that require manipulation at  $\mathcal{O}(p^2)$ . The gauge remainder terms are as follows. First, we have a copy of the original set of gauge remainders, which come with a relative factor of  $1/2$  and two decorative  $\triangleright$ s. Secondly, we have copies of diagrams G.329–G.331 with an additional decorative gauge remainder<sup>2</sup>. Lastly, we have an entirely new set of terms, shown in figure 10.19.

**Cancellation 10.15** *Diagram G.367 exactly cancels diagram G.128 via diagrammatic identity 11.*

---

<sup>2</sup>Obtaining these terms involves partial cancellations against diagrams generated by manipulating gauge remainders of type-II, possessing a single, decorative gauge remainder.

$$4 \sum_{J=0}^n \Upsilon_{J,0}$$

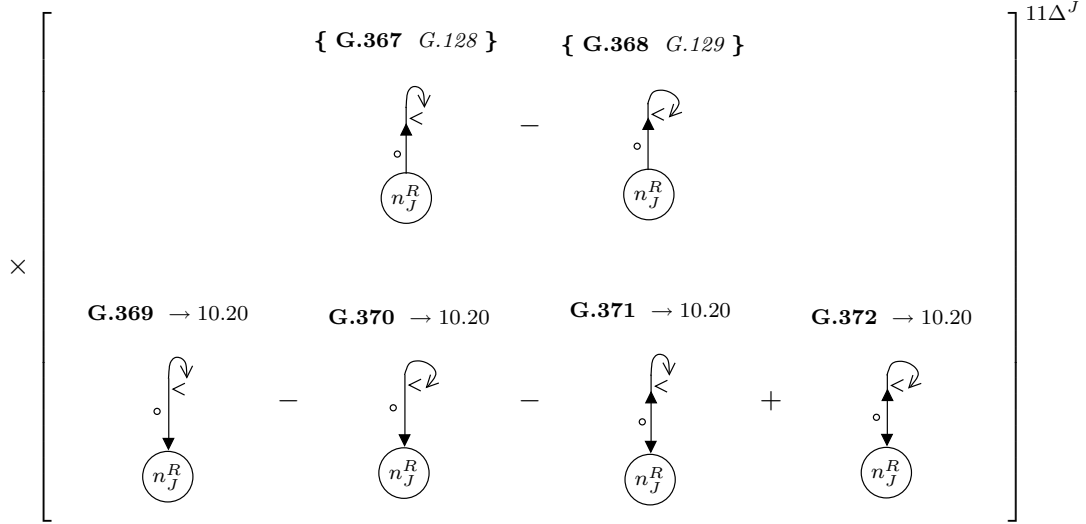


Figure 10.19: New types of gauge remainder diagrams arising from iterating the diagrammatic procedure.

**Cancellation 10.16** *Diagram G.368 exactly cancels diagram G.129 via diagrammatic identity 11.*

Notice that diagrams G.369 and G.370 are just nested versions of diagram G.328 and that diagrams G.355 and G.356 are just nested versions of diagram G.324. Just as the un-nested diagrams combined with diagrams generated by the original type-II gauge remainders, so too in the nested case.

We can do more than this: precisely half of the contributions to diagrams G.357, G.358, G.371 and G.372 are cancelled, respectively, by diagrams G.217, G.216, G.201 and G.200. This is courtesy of diagrammatic identity 11.

Figure 10.20 shows the results of combining terms, in the manner discussed, above.

This time around, processing the gauge remainders requires a little more thought. When we process the copy of the original set of gauge remainders, we must now take seriously those terms in which we attach a nested gauge remainder to a two-point, tree level vertex; unlike the un-nested case, such

$$\begin{aligned}
& -2 \sum_{J=0}^n \Upsilon_{J,0} \\
& \times \left[ \begin{array}{ccc}
\text{G.373} \rightarrow 10.24 & \text{G.374} \rightarrow 10.24 & \text{G.375} \rightarrow 10.24 \\
\begin{array}{c} \square \\ \downarrow \\ \circlearrowleft \\ n_J^R \end{array} & - \begin{array}{c} \square \\ \downarrow \\ \circlearrowleft \\ n_J^R \end{array} & - \begin{array}{c} \circ \\ \downarrow \\ \circlearrowleft \\ n_J^R \end{array} \\
\text{G.376} \rightarrow 10.24 & \text{G.377} \rightarrow 10.24 & \text{G.378} \rightarrow 10.24 \\
+ \begin{array}{c} \circ \\ \downarrow \\ \circlearrowleft \\ n_J^R \end{array} & + \begin{array}{c} \circ \\ \downarrow \\ \circlearrowleft \\ n_J^R \end{array} & - \begin{array}{c} \circ \\ \downarrow \\ \circlearrowleft \\ n_J^R \end{array}
\end{array} \right] 11\Delta^J \\
& -2\Upsilon_{n-1,0} \\
& \times \left[ \begin{array}{cccc}
\text{G.379} \rightarrow 10.22 & \text{G.380} \rightarrow 10.22 & \text{G.381} \rightarrow 10.22 & \text{G.382} \rightarrow 10.22 \\
\begin{array}{c} \circlearrowleft \\ \bullet \\ \downarrow \\ \circlearrowleft \end{array} & - \begin{array}{c} \circlearrowleft \\ \bullet \\ \downarrow \\ \circlearrowleft \end{array} & - \begin{array}{c} \circlearrowleft \\ \bullet \\ \downarrow \\ \circlearrowleft \end{array} & + \begin{array}{c} \circlearrowleft \\ \bullet \\ \downarrow \\ \circlearrowleft \end{array}
\end{array} \right] 11\Delta^{n-1}
\end{aligned}$$

Figure 10.20: The result of combining diagrams G.355–G.358 and G.369–G.372 with diagrams G.202–G.205, G.200, G.201, G.216 and G.217.



*At the next level of nesting, the corresponding terms do not quite cancel. The term required to complete the cancellation is closely related to the second ingredient, above. Given that a diagram like the second ingredient exists, it then follows that a similar diagram must exist, in which the two-point, tree level vertex has been formed by the action of an un-nested gauge remainder (and is yet to be attached to anything). Now consider the version of this diagram with two decorative gauge remainders (this will exist if the additionally nested version of the first and second ingredients exist). Joining these gauge remainders to the two-point, tree level vertex, we create the term we require for our cancellation to go ahead.*

*Additionally nested versions of this supplementary diagram now ensure, via diagrammatic identities 12 and 13 that the original cancellation is guaranteed to occur, at all levels of nesting.*

Consequently, not only are analogues of cancellations 10.5, 10.6, 10.15 and 10.16 guaranteed to go ahead at all levels of nesting but so to are analogues of cancellations 10.7, 10.8, 10.13 and 10.14.

Moreover, diagrammatic identity 11 was applied in the generation of the diagrams of figure 10.20. Thus, the additionally nested version of this figure is generated also, so long as we incorporate the the correct set of terms in which a two-point, tree level vertex generated by a type-II gauge remainder is attached to a nested gauge remainder structure.

With this in mind, let us now analyse the diagrams of figure 10.20. This is easy, because there are no remaining decorative gauge remainders, in this case. Allowing the gauge remainder to act in these diagrams, it is apparent that all generated terms in which the gauge remainder strikes a socket which decorates anything other than a two-point, tree level vertex will simply cancel, via cancellation mechanism 11. Iterating the diagrammatic procedure until exhaustion, we focus first on the surviving terms coming from diagrams G.379–G.382. The minimal set of such terms with the lowest level of nesting, is shown in figure 10.22 up to diagrams with an  $\mathcal{O}(p^2)$  stub. We note that the additionally nested diagrams are nested with respect to the currently un-nested, processed gauge remainder.

$$2\Upsilon_{n-1,0}$$

$$\begin{array}{c}
 \left[ \begin{array}{ccc}
 \{ \mathbf{G.383} \ G.275 \} & \{ \mathbf{G.384} \ G.276 \} & \{ \mathbf{G.385} \ G.277 \} \\
 \begin{array}{c} \cdot \\ \downarrow \\ \curvearrowright \end{array} & - & \begin{array}{c} \curvearrowright \\ \downarrow \\ \cdot \end{array} & - & \begin{array}{c} \cdot \\ \downarrow \\ \curvearrowright \end{array} \\
 \\
 \{ \mathbf{G.386} \ G.278 \} & \{ \mathbf{G.387} \ G.279 \} & \{ \mathbf{G.388} \ G.280 \} \\
 + & \begin{array}{c} \curvearrowright \\ \downarrow \\ \cdot \end{array} & - & \begin{array}{c} \cdot \\ \downarrow \\ \curvearrowright \end{array} & + & \begin{array}{c} \cdot \\ \downarrow \\ \curvearrowright \end{array} \\
 \\
 \{ \mathbf{G.389} \ G.281 \} & \{ \mathbf{G.390} \ G.282 \} & \mathbf{G.391} \rightarrow 10.23 \\
 + & \begin{array}{c} \cdot \\ \downarrow \\ \curvearrowright \end{array} & - & \begin{array}{c} \cdot \\ \downarrow \\ \curvearrowright \end{array} & + 2 & \begin{array}{c} \cdot \\ \downarrow \\ \curvearrowright \end{array} \\
 \\
 +2 \left[ \begin{array}{ccc}
 \mathbf{G.392} \rightarrow 10.23 & \mathbf{G.393} \rightarrow 10.23 & \mathbf{G.394} \rightarrow 10.23 \\
 - & \begin{array}{c} \cdot \\ \downarrow \\ \curvearrowright \end{array} & - & \begin{array}{c} \cdot \\ \downarrow \\ \curvearrowright \end{array} & + & \begin{array}{c} \cdot \\ \downarrow \\ \curvearrowright \end{array}
 \end{array} \right]
 \end{array} \right] 11\Delta^{n-1}
 \end{array}$$

Figure 10.22: The minimal set of diagrams surviving diagrams arising from diagrams G.379–G.382.

Directly, we find a very encouraging set of cancellations.

**Cancellation 10.17** *Diagrams G.383–G.386 exactly cancel diagrams G.275–G.278.*

**Cancellation 10.18** *Diagrams G.387–G.390 exactly cancel diagrams G.279–G.282.*

Focusing now on the terms that survive, we can combine them with diagrams coming from earlier in the calculation. Diagrams G.391 and G.392 are identical to diagrams G.339 and G.340 and can be combined directly. All four diagrams G.341–G.344 can be redrawn, using diagrammatic identity 11. The first two now manifestly remove from diagrams G.393 and G.394 the components in which the wine is undecorated.<sup>3</sup> The resultant diagrams take exactly the same form as the final two redrawn diagrams and so can be combined. The end product of these procedures is shown in figure 10.23

$$8\Upsilon_{n-1,0} \left[ \begin{array}{cccc} \mathbf{G.395} & & \mathbf{G.396} & & \mathbf{G.397} & & \mathbf{G.398} \\ \begin{array}{c} \text{Diagram G.395} \\ \text{Diagram G.396} \\ \text{Diagram G.397} \\ \text{Diagram G.398} \end{array} \end{array} \right]^{11\Delta^{n-1}}$$

Figure 10.23: Combination of diagrams G.391–G.394 and G.339–G.344.

This kind of pattern of terms is precisely what we anticipate needing. Consider the kind of terms we expect to arise when we manipulate diagrams with three decorative gauge remainders. Amongst these terms will be those formed by decorating a version of diagram G.316. This version of diagram G.316 will come with an overall factor of 1/6 and two additional decorative gauge remainders.

Now, if we attach a  $\curvearrowright$  to one of the two-point, tree level vertices and the nested version of  $\curvearrowleft$  to the other, then we will generate terms very

---

<sup>3</sup>As we noted earlier, this contribution vanishes anyway, since gauge remainders have no support in the  $C$ -sector. However, this illustrates the kind of cancellations which are necessary at higher levels of nesting.

similar to those in figure 10.23. Indeed, the diagram with the trapped gauge remainder, G.397 and G.398 will be removed completely, as we would hope. The components of the other two diagrams, in which the wine is un-decorated will, however survive. But this is exactly what we want: these are precisely the terms we need in order to construct  $\Lambda$ -derivative terms in which gauge remainder structures are joined by effective propagators!

Next, we consider the result of processing diagrams G.373–G.378. We need not explicitly give all of the resultant terms, since many of them are just nestings of earlier diagrams. In particular, diagrams G.373–G.376 are just the nested versions of diagrams G.329–G.330. Thus, we can follow through the manipulation of the latter diagrams to deduce the result of manipulating the former.

First, we will produce nested versions of diagrams G.335 and G.336. Iterating the diagrammatic procedure until exhaustion, the minimal set of terms will be given by a version of diagrams G.341–G.344, where the nesting is with respect to  $\text{---}\curvearrowright$ . We must be careful with the overall factor: the factor of four in front of diagrams G.341–G.344 arises because we have been able to collect pushes-forward and pulls-back twice. With the new diagrams, we can do it only once. Hence, the overall factor is just two, but each of the original diagrams will now have four nested versions.

Going beyond the minimal set, we include diagrams possessing additional vertices and diagrams additionally nested, with respect to the top-most gauge remainder structure.

These points will be illuminated when we consider diagrams G.377 and G.378. Although these diagrams have a virtually identical structure to the ones just discussed, they do not have analogues with a lower degree of nesting, earlier in the calculation, since such terms die. Hence, we should include the result of processing these diagrams, explicitly.

Together with this, we will include the other terms spawned by diagrams G.373–G.378 which have no analogue earlier in this section of the calculation. These are those for which the active gauge remainder generates a two-point, tree level vertex which we then join to the nested gauge remainder at the top of the diagram. The resulting collection of terms is shown in figure 10.24.

**Cancellation 10.19** *Diagrams G.399–G.402 exactly cancel diagrams G.295–G.298.*

**Cancellation 10.20** *Diagrams G.403–G.406 exactly cancel diagrams G.299–G.302.*

These are the final cancellations we will explicitly need to see to complete the treatment of the gauge remainders! The pattern of cancellations is now clear. Each gauge remainder that strikes a vertex can generate a two-point, tree level vertex. We already know that if we attach this vertex to another vertex or a wine, the resulting diagrams are guaranteed to cancel, via cancellation mechanisms 11 and 12. There are now only two things we can do with the two-point, tree level vertex (up to generating terms with an  $\mathcal{O}(p^2)$  stub): either we can attach it to one of the gauge remainders which explicitly strikes some structure, or we can use the decorative gauge remainders to create a structure to which to attach it.

In the former case, we can then re-express the diagrams using diagrammatic identities 10–13. From figure 9.20, we know that amongst the redrawn terms are those necessary to cancel the diagrams of the latter case, up to terms possessing sub-diagrams like I.51, I.52 and etcetera. But these are cancelled also. Here, the cancellation is not against terms formed by active gauge remainders. Rather, it occurs when one or more of the two-point, tree level components of dumbbell structures, generated by the flow equation are joined to decorative gauge remainders. The trapped gauge remainder term generated is the term we require for the cancellation to work.

Let us illustrate this further by showing how some diagrams which we have not explicitly cancelled will disappear. Diagrams G.291–G.294 will vanish once we come to process the versions of the type-Ia and Ib gauge remainder terms with two decorative gauge remainders.

Next, consider diagrams G.407–G.410. These will be cancelled by diagrams G.222–G.225, G.226–G.229 and the nested versions of diagrams G.206 and G.207. From this we will be left over with the nested version of diagrams G.214 and G.215—ready for cancellation when we process the  $\Lambda$ -derivative terms for diagrams with three decorative gauge remainders!

$$-2\Upsilon_{n-1,0}$$

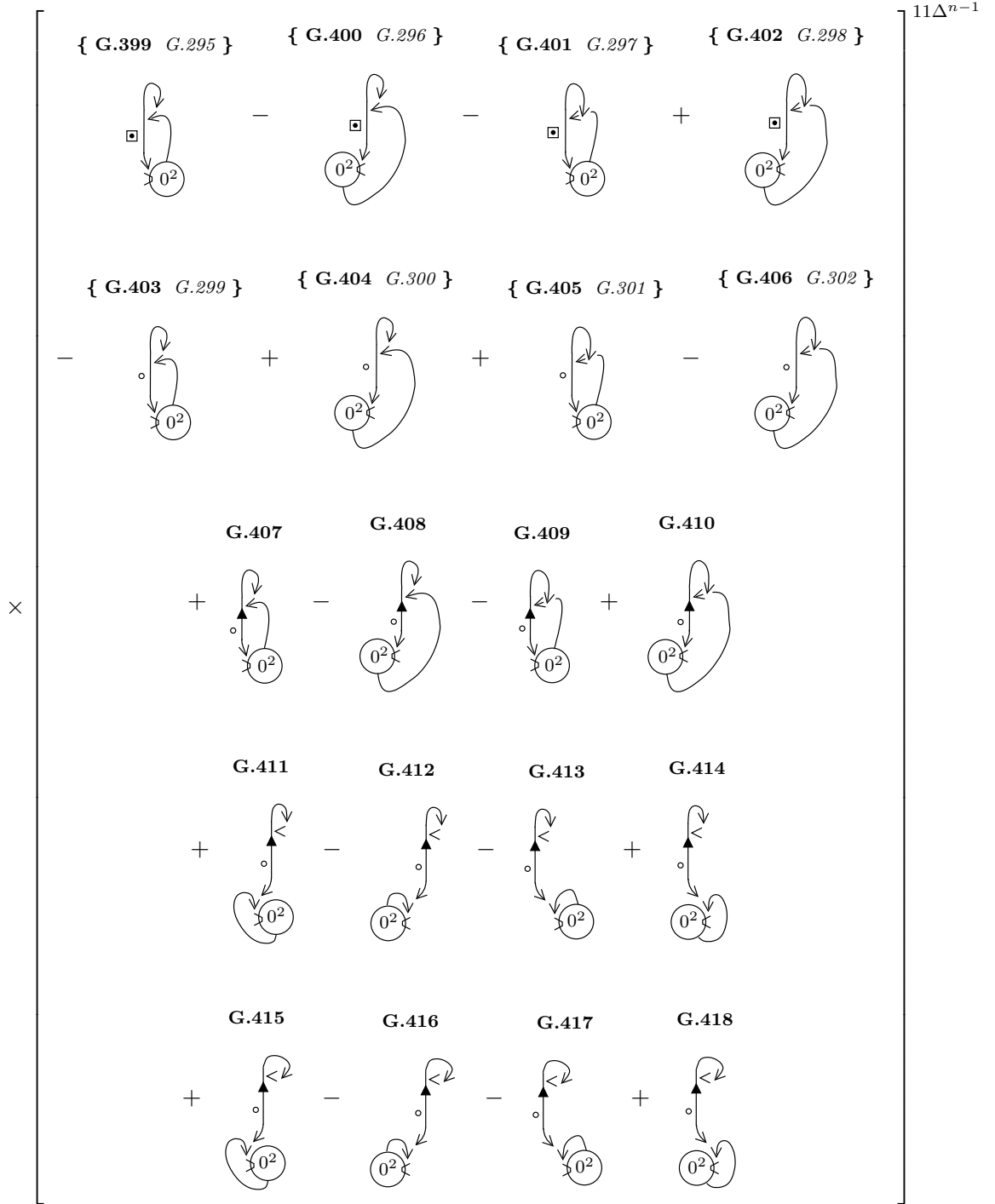


Figure 10.24: The minimal set of diagrams surviving diagrams arising from diagrams G.373–G.378, which cannot be written as nestings of terms generated earlier in this section, up to diagrams with an  $\mathcal{O}(p^2)$  stub.

Finally, diagrams G.411–G.418 will cancel terms in which a singly nested version of  $\wp$  is attached to each of the two-point, tree level vertices of a dumbbell structure formed by a  $\Lambda$ -derivative term with four decorative gauge remainders.

With these myriad cancellations, the question of course arises as to what are we actually left with. There are a number of cancellations in this section which are not exact, but dependent on the precise diagrammatic structure and the decorative fields; namely, cancellations 10.9–10.11 and 10.2. These cancellations fail in the following circumstances: at the final level of nesting and at any level of nesting beyond the current one (but before the final level) when there are additional vertices. In this case, the surviving terms comprise an un-decorated, differentiated wine. The terms surviving from the failure of the first three cancellations are exactly the terms we require in order to be able to perform the conversion into  $\Lambda$ -derivative terms, as anticipated in figure 8.23. The terms surviving from the failure of the cancellation 10.2 possess an  $\mathcal{O}(p^2)$  stub. Since they also possess an undecorated wine, attached to this stub, it is apparent that they are higher loop manifestations of the  $B'(0)$  terms that we encountered in the one-loop calculation. These will be commented on in chapter 11.

Indeed, we can now write down the final result of processing the gauge remainders, up to terms with an  $\mathcal{O}(p^2)$  stub. This is shown in figure 10.25 where, once again, we have used the compact notation defined by (7.13).

Comparing this expression to that of figure 7.43, the most striking thing is how similar they are. Whilst processing the gauge remainders took a huge amount of time and effort, the final result can be represented in an incredibly concise fashion. This is a compelling indication of the potential of this formalism.

We now conclude this chapter by re-deriving the expression for  $\beta_1$ , in terms

$$\begin{aligned}
-4\beta_{n_+} \square_{\mu\nu}(p) &= -2 \sum_{s=1}^{n_+} \sum_{m=0}^{2(s-1)} \sum_{J=0}^{2n-m} \frac{\Upsilon_{J+s+1, J+1}}{m!} \\
&\times \left[ \frac{1}{J+2} \left[ \begin{array}{c} \textcircled{V^{J+1;R}} \\ \textcircled{n_+-s, J} \end{array} \right]^\bullet \right]^{11\Delta^{J+s+1} > m} \\
&- \sum_{\substack{V^{J+1} \\ V^{J+2}=1}} \left[ \begin{array}{c} \left[ 2(V^{J+1, J+2} - 1) \beta_{V^{J+2}} + \gamma_{V^{J+2}} \frac{\partial}{\partial \alpha} \right] \textcircled{V^{J+1, J+2}} \\ \textcircled{n_+-s, J} \end{array} \right] \\
&- 2 \sum_{J=0}^n \sum_{m=0}^{2J+1} \frac{\Upsilon_{J+1, 0}}{m!} \\
&\times \left[ \left[ \textcircled{n_J^R} \right]^\bullet - \sum_{r=1}^{n_J} \left[ 2(n_J - r - 1) \beta_r + \gamma_r \frac{\partial}{\partial \alpha} \right] \textcircled{n_{J+r}} \right]^{11\Delta^{J+1} > m} \\
&+ \frac{2\Upsilon_{n, 0}}{(2n+2)!} \left[ \left[ \right]^\bullet \right]^{11\Delta^n > 2n+2} \\
&+ \dots
\end{aligned} \tag{10.1}$$

Figure 10.25: Diagrammatic expression for  $\beta_{n_+}$  including gauge remainder terms. The ellipsis denotes terms with an  $\mathcal{O}(p^2)$  stub.

of  $\mathcal{D}_1$ , up to  $\mathcal{O}(p^2)$  terms. In equation (10.1), we set  $n = 0$  to yield:

$$-4\beta_1 \square_{\mu\nu}(p) = \left[ \begin{array}{c} -\Upsilon_{2,1} \left[ \begin{array}{c} \textcircled{0^R} \\ \textcircled{0^R} \end{array} \right]^{11\Delta^2} \\ -2 \sum_{m=0}^1 \frac{\Upsilon_{1,0}}{m!} \left[ \textcircled{0^R} \right]^{11\Delta > m} \\ + \Upsilon_{0,0} \square^{11 > 2} \end{array} \right]^{\bullet} + \dots$$

From equation (7.15) we have:

$$\Upsilon_{2,1} = 1/16, \quad \Upsilon_{1,0} = -1/4, \quad \Upsilon_{0,0} = -1/2$$

Let us start by analysing the pure gauge remainder term. Given that the two external fields must be on the same supertrace, we can only form a gauge remainder structure in which both gauge remainders are bitten in the same sense (both on the left or both on the right). Since there are an even number of gauge remainders we will pick up a minus sign (see section 3.1.8), whichever sense we choose.

Combining the two different senses via CC yields a factor of two. We can now choose to attach either of the external fields to either of the gauge remainders; this yields a further factor of two. Thus, including the  $\Upsilon_{0,0}$ , the overall factor of the diagram is +2, as it should be.

Next we look at the single vertex term. First, suppose that  $m = 0$ . Attaching all fields to the vertex comes with a factor of unity; including the  $-2\Upsilon_{1,0}$  the overall factor of the diagram is +1/2. Secondly, suppose that  $m = 1$ . We must attach the decorative gauge remainder to the effective propagator. There are four ways to do this, corresponding to the two ends of the effective propagator and the equality of the push-forward and pull-back. Hence, the overall factor of this diagram is +2.

Finally, we look at the double vertex term. We discussed, in detail, in section 7.3.1 that the two possible ways of performing the decorations (i.e. with or without a simple loop) both come with a factor of eight. Thus, including the factor of  $-\Upsilon_{2,1}$ , the overall factor of both fully decorated diagrams is  $-1/2$ .

Summing up all terms, it is clear that we have correctly reproduced the diagrammatic expression for  $\beta_1$  in terms of  $\mathcal{D}_1$ , up to the  $\mathcal{O}(p^2)$  terms.

# Chapter 11

## Terms with an $\mathcal{O}(p^2)$ Stub

It is, unfortunately, beyond the scope of this thesis to give a complete treatment of diagrams possessing an  $\mathcal{O}(p^2)$  stub. This is due to constraints of time and space, rather than any particular conceptual difficulty; indeed, certain terms possessing an  $\mathcal{O}(p^2)$  stub—the type-III gauge remainders—have already been processed. Moreover, as we will sketch below, the full treatment of such terms just reuses many of the techniques that we have already introduced.

To begin, it is useful to split the terms with an  $\mathcal{O}(p^2)$  stub into two groups, one of which further sub-divides. To make the initial distinction between terms, we focus on the wine / effective propagator leaving the  $\mathcal{O}(p^2)$  stub. If the field attached to the stub carries the same momentum as the stub—i.e. it has not been bitten by a gauge remainder—then we call the corresponding diagrams ‘ $\mathcal{O}(p^2)$  terms of type-I’. If, on the other hand, the field attached to the stub has been hit by a gauge remainder then we call the corresponding diagrams ‘ $\mathcal{O}(p^2)$  terms of type-II’.

Let us now focus on the terms of type-I. If the wine is undecorated, then we will call the corresponding diagrams terms of type-Ia. If the wine is decorated, then they will be called terms of type-Ib.

### 11.1 $\mathcal{O}(p^2)$ Terms of Type Ia

The terms of type-Ia are the higher loop analogues of the  $B'(0)$  terms that we encountered in the one-loop calculation. We recall here the reason why the one-loop  $B'(0)$  terms vanish (see section 4.1.3).

The final form of  $\beta_1$  is, up to a factor, the  $\Lambda$ -derivative of  $\mathcal{D}_1$ . For what follows, we will define  $\mathcal{P}_1$  to be  $\mathcal{D}_1$ , modulo the terms with an  $\mathcal{O}(p^2)$  stub. Let us now go back a step in the computation of  $\beta_1$  and reinstate the  $\mathbf{B}'(0)$  terms. These comprise an  $\mathcal{O}(p^2)$  stub attached to an undecorated wine, the other end of which attaches to something very similar to  $\mathcal{P}_1$ ; to be specific, it attaches to a version of  $\mathcal{P}_1$  where, in each diagram, one of the vertices decorated by an external field is replaced by a seed action version of that vertex. However, at  $\mathcal{O}(p^2)$ , we can replace this seed action vertex with a Wilsonian effective action vertex, thereby forming an instance of  $\mathcal{P}_1$ . Now, the transversality of  $\mathcal{P}_1$  guarantees that the  $\mathbf{B}'(0)$  terms vanish at  $\mathcal{O}(p^2)$ .

At higher loops, we expect something similar to happen. Indeed, every time we form a  $\Lambda$ -derivative term, we will generate an  $\mathbf{B}'(0)$  term amongst the corrections. Whilst we no longer expect to be able to always replace seed action vertices by Wilsonian effective action vertices at  $\mathcal{O}(p^2)$ , we do expect the  $\mathbf{B}'(0)$  sub-diagrams to which the undecorated wine attaches to be transverse, nonetheless. Though it will not be as direct as in the one-loop case, we predict that this transversality to be related to the transversality of the  $\Lambda$ -derivative terms. This has been explicitly checked at two-loop order; we intend to prove that the  $\mathbf{B}'(0)$  terms are guaranteed to vanish at any loop-order in [59].

## 11.2 $\mathcal{O}(p^2)$ Terms of Types Ib and II

Whilst we can argue that terms of type-Ia must vanish we have no choice but to manipulate terms of types-Ib and II. The basic idea is that, since the diagram possess an  $\mathcal{O}(p^2)$  stub and we are working to  $\mathcal{O}(p^2)$ , we hope be able to Taylor expand the rest of the diagram in  $p$ . There are, of course, a number of very important caveats. The first is that, just because a diagram possess an  $\mathcal{O}(p^2)$  stub, does not necessarily mean that it is at least  $\mathcal{O}(p^2)$ . For example, consider the diagram in figure 11.1.

The key point about this diagram is that, if the decorative effective propagators form simple loops, it possesses an effective propagator carrying the external momentum. This, of course, goes as  $1/p^2$ , nullifying the effect of the  $\mathcal{O}(p^2)$  stub. What, then, are we to do with such diagrams? We note that, if

$$-8 \sum_{J=0}^n \Upsilon_{J,0} \left[ \begin{array}{c} \mathbf{I.64} \\ \text{Diagram with } n_j^R \text{ and } 0^2 \text{ components} \end{array} \right] \Delta^J$$

Figure 11.1: An example of a diagram which, whilst possessing an  $\mathcal{O}(p^2)$  stub has  $\mathcal{O}(p^0)$  components.

the decorative effective propagators do not decorate the top vertex, then this vertex must be at least  $\mathcal{O}(p^2)$ , washing out the effect of the  $1/p^2$ . Of course, if the effective propagators do form simple loops on the vertex, then the vertex is no longer manifestly transverse in external momentum, and so we are back to the original problem. The solution is to combine sets of diagrams. Referring to diagram I.64 we want to keep the bottom sub-diagram exactly the same and sum over all the different things we can attach to the top end of the effective propagator. We expect this sum to be transverse in external momentum—something which is borne out at the two-loop level.

The reason for this expectation is that, by summing over all legal sub-diagrams we can attach to the top end of the effective propagator, we expect to reproduce sets of diagrams which contribute to the final expression for  $\beta$ -function coefficients. The transversality of these diagrams will then guarantee that the effect of the  $1/p^2$  is compensated for. Once more, a complete proof of this will have to wait until [59].

The second caveat is as to the validity of Taylor expanding a diagram in external momentum. Whilst we can always Taylor expand vertices [57] we have seen already in section 5.4.3 that, at the two-loop level, we encounter diagrams which, as a whole, cannot be Taylor expanded in  $p$ . The solution here is to construct subtractions, an example of which was given in the aforementioned section. It is interesting to note that in the calculation of  $\beta_2$ , it is only a tiny fraction of terms with an  $\mathcal{O}(p^2)$  stub for which it is necessary to construct

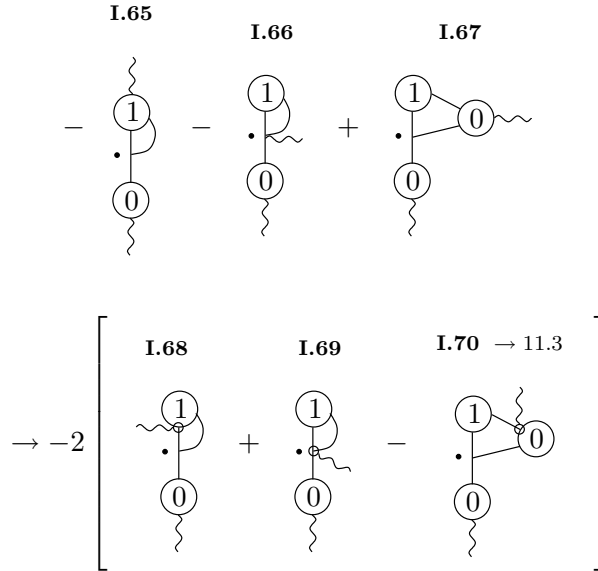


Figure 11.2: Example of three two-loop diagrams, components of which can be combined into total momentum derivatives, at  $\mathcal{O}(p^2)$ .

subtractions; the vast majority can just be blindly Taylor expanded.

Irrespective of whether we Taylor expand directly, or construct subtractions, the strategy then is to try and combine diagrams either into total momentum derivatives or into  $\Lambda$ -derivatives. We have seen an example of how the latter works in the one-loop calculation. To get a feel for how the former works, consider the three two-loop diagrams shown in the first row of figure 11.2.

To go from the first row to the second row, we have set  $p = 0$  everywhere except in the  $\mathcal{O}(p^2)$  stub, which is a perfectly valid step, in these cases. We have then diagrammatically expanded to  $\mathcal{O}(p^0)$ , using the techniques of section 3.2. The next step is to apply diagrammatic identity 5 to diagram I.70, as shown in figure 11.3, where we note that any gauge remainder which hits the two-point, one-loop vertex will kill it.

Now we see that the combination of diagrams I.68, I.69 and I.71 can be rewritten as a total momentum derivative. We have commented already how total momentum derivatives can be discarded, since all integrals are pre-regularised using dimensional regularisation. This then leaves the gauge remainder terms, diagrams I.72 and I.73. At first sight, it looks as though we are

$$- 2 \left[ \begin{array}{ccc} \mathbf{I.71} & \mathbf{I.72} & \mathbf{I.73} \\ \begin{array}{c} \textcircled{1} \\ \cdot \\ \textcircled{0} \\ \text{wavy line} \end{array} & \begin{array}{c} \textcircled{1} \\ \cdot \\ \textcircled{0} \\ \text{wavy line} \end{array} & \begin{array}{c} \textcircled{1} \\ \cdot \\ \textcircled{0} \\ \text{wavy line} \end{array} \end{array} \right]$$

Figure 11.3: Result of processing diagram I.70, using diagrammatic identity 5.

stuck, since the gauge remainders are differentiated with respect to momentum. However, trivially redrawing

$$\begin{array}{c} \textcircled{1} \\ \cdot \\ \textcircled{0} \\ \text{wavy line} \end{array} = \begin{array}{c} \textcircled{1} \\ \cdot \\ \textcircled{0} \\ \text{wavy line} \end{array} \leftarrow + \begin{array}{c} \textcircled{1} \\ \cdot \\ \textcircled{0} \\ \text{wavy line} \end{array} \leftarrow$$

it is clear that progress can be made. In the case that the derivative hits the  $\triangleright$ , the  $\triangleright$  is just a perfectly normal, active gauge remainder which can be treated in the usual manner. In the case that the derivative hits  $\triangleleft$ , we then use diagrammatic identity 3 to redraw

$$\begin{array}{c} \textcircled{1} \\ \cdot \\ \textcircled{0} \\ \text{wavy line} \end{array} \leftarrow \equiv \begin{array}{c} \textcircled{1} \\ \cdot \\ \textcircled{0} \\ \text{wavy line} \end{array} \cdots \triangleright$$

Now in this case, too, we have an active gauge remainder which, again, can be processed in the usual way.

When we do process these gauge remainders we expect one of three things to occur. First, the usual gauge remainder cancellation mechanisms occur via cancellation mechanisms 11 and 12. Secondly, processed gauge remainder terms can, themselves, be combined into total momentum derivatives. Thirdly, processed gauge remainder terms can be converted into  $\Lambda$ -derivative terms. It is instructive to see this latter operation in action, particularly as it gives a flavour for how  $\mathcal{O}(p^2)$  terms of types-Ib and II interact.

Our starting point is diagram I.72 which, of course, is derived from an  $\mathcal{O}(p^2)$  term of type-Ib. Focusing on the case in which the momentum derivative hits  $\triangleright$ <sup>1</sup>, we will further restrict ourselves to considering the diagram formed when the gauge remainder pulls-back along the wine, to meet the two-point tree level

<sup>1</sup>Indeed, if the momentum derivative hits  $\triangleleft$ , then we can allow  $\triangleright$  to act backwards, through the wine, courtesy of diagrammatic identity 3. The diagram then dies, since  $\triangleright$  strikes a two-point Wilsonian effective action vertex.

vertex.<sup>2</sup> We now combine the resultant diagram with two  $\mathcal{O}(p^2)$  diagrams of type-II, as shown in figure 11.4.

$$2 \left[ \begin{array}{ccc} \mathbf{I.74} \rightarrow 11.5 & \mathbf{I.75} \rightarrow 11.5 & \mathbf{I.76} \rightarrow 11.5 \\ \begin{array}{c} \text{Diagram 1: Two vertices labeled 1 and 0. A wavy line enters vertex 0 from below. A line connects 1 and 0. A wavy line exits vertex 1 to the right. A dot is on the line between 1 and 0.} \\ \text{Diagram 2: Two vertices labeled 1 and 0. A wavy line enters vertex 0 from below. A line connects 1 and 0. A wavy line exits vertex 1 to the right. A dot is on vertex 1.} \\ \text{Diagram 3: Two vertices labeled 1 and 0. A wavy line enters vertex 0 from below. A line connects 1 and 0. A wavy line exits vertex 0 to the right. A dot is on vertex 1.} \end{array} \end{array} \right]$$

Figure 11.4: Combination of a diagram derived from I.72 and two  $\mathcal{O}(p^2)$  diagrams of type-II.

Diagrammatically Taylor expanding the final two diagrams, we can then combine diagrams into a  $\Lambda$ -derivative. The easiest way to see this is to note that

$$\begin{aligned} \leftarrow \text{Diagram 1} &= \text{Diagram 2} - \text{Diagram 3} - \text{Diagram 4} \\ &= - \text{Diagram 5} - \text{Diagram 6} + \text{Diagram 7} - \text{Diagram 8} + \text{Diagram 9} . \end{aligned}$$

The first diagram on the second line is obtained from the diagram above by means of diagrammatic identity 8. The other diagrams on the second line are simply obtained by using the effective propagator relation. Applying the above relation to diagram I.76 we will generate five diagrams. The third and fifth involve an active gauge remainder striking the two-point, one-loop vertex and so die. The second diagram exactly cancels diagram I.75. The remaining two diagrams combine with diagram I.74 to form a  $\Lambda$ -derivative term, as shown in figure 11.5.

To conclude this section, we give a final diagrammatic identity, which the two-loop calculation taught us is necessary for the treatment of terms with an  $\mathcal{O}(p^2)$  stub.

---

<sup>2</sup>We do not consider the partner push-forward on to the two-point vertex, since this corresponds to the two external fields being on different supertraces.

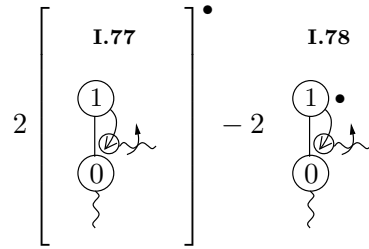


Figure 11.5: Rewriting diagrams I.74–I.76 as a  $\Lambda$ -derivative term.

**Diagrammatic Identity 14** *It is true in all sectors for which the gauge remainder is not null that*

$$\begin{array}{c} \nu \\ \swarrow \\ \text{wavy line} \\ \oplus \\ \alpha \end{array} = \delta_{\alpha\nu}.$$

*It therefore follows that*

$$\begin{array}{c} \text{wavy line} \\ \oplus \\ \bar{k} \end{array} = \left. \begin{array}{c} k \\ \text{wavy line} \end{array} \right\}.$$

## Part IV

# Computation of $\beta_2$ and Conclusions

## Chapter 12

# Two Loop Diagrammatics

The principle result of the last chapter is the reduction of  $\beta_{n+}$  to  $\Lambda$ -derivative,  $\alpha$  and  $\beta$ -terms, up to diagrams with an  $\mathcal{O}(p^2)$  stub. In this chapter, we specialise equation (10.1) to help us generate a manifestly gauge invariant, diagrammatic expression for  $\beta_2$ , from which we can readily extract the numerical coefficient.

Of course, due to the incompleteness of equation (10.1), we will have to do some additional work. Though the details will not be presented here, we have completed the diagrammatic procedure for the  $\mathcal{O}(p^2)$  terms for the specific case of  $\beta_2$ . Rather than using the highly efficient techniques of the previous chapter, this has been done exactly along the lines of our computation of  $\beta_1$  (see also chapter 11). Indeed, it should be noted that the entire  $\beta_2$  calculation was originally done in this manner. The arduous nature of this approach cannot be over emphasised. Whereas the 1-loop calculation generates less than 100 diagrams, of which only seven survive, the two loop calculation generates of  $\mathcal{O}(10^4)$  diagrams, of which  $\mathcal{O}(100)$  survive.

In addition to the extra work required to treat the  $\mathcal{O}(p^2)$  terms, the  $\alpha$  and  $\beta$ -terms require further processing. As we have noted previously, diagrams of these types possess a full vertex which, necessarily, has a two-point, tree level component. Hence, we can play diagrammatic games with these terms, reducing them to a simpler form.

The first section will give the  $\Lambda$ -derivative diagrams obtained by specialising equation (10.1) to the form corresponding to  $\beta_2$ . We note that, at the two-loop level, assertion 1 is unnecessary: we never employ diagrammatic iden-

tity 13. Hence, the expression we obtain is not reliant on any assumptions. In section 12.2 the  $\Lambda$ -derivative terms obtained by processing the terms with an  $\mathcal{O}(p^2)$  stub are given.

Accompanying the diagrams of section 12.1 and 12.2 are  $\alpha$  and  $\beta$ -terms. To perform manipulations on the  $\beta$ -terms does not require any new methodology and so, in section 12.3, we jump straight to the final set of diagrams. To manipulate the  $\alpha$ -terms, on the other hand, requires some new diagrammatic identities. These identities are presented in section 12.4, together with both the original and recast  $\alpha$ -terms.

We conclude this chapter by utilising the diagrammatic expression for  $\beta_1$  to simplify the diagrammatic expression for  $\beta_2$ . This will allow us to cast  $\beta_2$  as a set of  $\Lambda$ -derivative terms, for every one of which the whole diagram—as opposed to just a factorisable sub-diagram—is hit by  $\Lambda\partial_\Lambda|_\alpha$ , and  $\alpha$ -terms.

## 12.1 Specialising Equation (10.1)

To extract the numerical coefficient for  $\beta_2$ , we need to go from equation (10.1) to a set of fully decorated diagrams. Since we must sum over all independent decorations, this generates a large number of terms. There are, however, several simplifications—which fall into three classes. First, there are those diagrams which vanish, for some reason. Secondly, there are pairs of diagrams which exactly cancel. Lastly, we can compact our notation to reduce the number of diagrams we must draw.

### 12.1.1 Diagrams which can be Discarded

For what follows, we will take a diagram to be fully decorated, a consequence of which is that the sense in which any gauge remainders act is completely determined. With this in mind, we are able to discard any diagrams for which:

1. there is manifestly no contribution at  $\mathcal{O}(p^2)$ ;
2. the two external  $A^1$ s are forced to be on different supertraces.

The first characteristic is straightforward, and will not be discussed further. The second characteristic has been discussed already in the context of gauge

remainders (see section 3.1.8): certain patterns of pushes forward and pulls back can force the external  $A^1$ s to be on different supertraces, if at least one nested gauge remainder is decorated by an external field. We choose only to discard complete diagrams for this reason, as opposed to explicitly discarding components of diagrams for which certain choices of field ordering cause the  $A^1$ s to be on different supertraces.

### 12.1.2 Cancellations Between Diagrams

The cancellations in this section are between pushes forward and pulls back. If we can find a pair of diagrams, identical in every way, up to the sense in which one of the gauge remainders acts, then these will cancel. Such diagrams are non-planar. It is only in this case that we have any hope of finding the desired cancellations; changing the sense in which any of the gauge remainders act in a planar diagram generates either a non-planar diagram or a planar diagram in which the external fields are on different supertraces or a planar diagram, the non-vanishing components of which have a changed field content. As an example, consider the diagrams of figure 12.1.

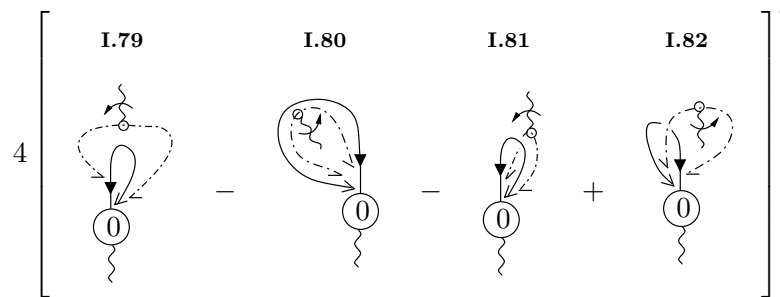


Figure 12.1: Four diagrams, two of which cancel and two of which do not.

Diagrams I.79 and I.80 have the same pattern of pushes forward and pulls back, up to the gauge remainder which bites the vertex; similarly with diagrams I.81 and I.82. In the latter case, there is only one supertrace: the pair of diagrams cancel. In the former case, the external fields are on separate supertraces: diagram I.80 vanishes and diagram I.79 survives.

### 12.1.3 Compact Notation

There are two ways in which we can compact our notation. First, having identified pairs of gauge remainder diagrams which cancel, we now recombine sets of those which survive, to avoid having to explicitly draw all patterns of pushes forward and pulls back. Let us consider a diagram possessing several, independent, nested gauge remainder structures. Now consider also those partner diagrams in which the nestings are performed in different senses. For each of these structures, we will draw only one possible arrangement of the gauge remainders but will take this to stand for all possible arrangements, with one proviso: we will use CC to collect together the first push forward from any *one* of the structures with the corresponding pull back. This yields a factor of two and so we must be careful not to double count if we ever want to expand the diagram out to explicitly show all possible arrangements of the gauge remainders. In diagrams possessing instances of the un-nested structure  $\curvearrowright$  we will always combine the push forward and pull back for each and every instance. To distinguish diagrams where we employ these conventions from diagrams in which we have actually made a specific choice about the pattern of pushes forward and pulls back, we will tag them with  $[ \ ]_{ES'}$  (cf.  $[ \ ]_{ES}$  defined in section 9.2.).

Secondly, we can use equation (10.1) to show that certain sub-diagrams always occur together. In fact, we will use only the simplest manifestation of this; fully exploiting the dependence of  $\beta_{n+}$  on the diagrammatic expressions for all  $\beta_{m \leq n}$  will be saved for the future [59]. Let us focus on a diagram possessing  $J' + 1$  vertices, for  $J' > 1$ . We now suppose that one of the vertices is a three-point, tree level vertex, decorated by a simple loop. Next, we focus on a diagram with  $J'$  vertices, to one of which we attach  $\text{---}\curvearrowright$ . It is easy to check that the two diagrams thus described always come with a relative factor of  $-4$ . We represent the combination of these two diagrams, as shown in figure 12.2.

$$\text{hatched circle on line} \equiv \text{circle with 0 and loop on line} - 4 \text{ hook on line}$$

Figure 12.2: Shorthand for two diagrams always guaranteed to occur together.

### 12.1.4 Generation of Terms

We now generate the explicitly decorated terms contributing to  $\beta_2$ , derived from equation (10.1). Since there are so many diagrams, we will split them into sets. These sets will be designed so that either each element is transverse in  $p$  on its own, but shares some common feature with the other elements, or only the sum over elements is transverse.

All  $\Lambda$ -derivative terms which vanish in the  $\epsilon \rightarrow 0$  limit and which are not involved in the simplifications of section 12.5 are tagged  $\rightarrow 0$ . The reasons for which they vanish are dealt with in section 13.1. We could, of course, immediately discard all diagrams which vanish in the  $\epsilon \rightarrow 0$  limit. However, for possible future work, we want the expression obtained after the simplifications to be valid in  $D = 4 - 2\epsilon$ .

The first set of terms comprises those that contain a one-loop vertex but are not transverse in  $p$ , alone. These are shown in figure 12.3.

$$\frac{1}{2} \left[ \begin{array}{ccccccc} \{ & \mathbf{12.1} & & \mathbf{12.2} & & \mathbf{12.3} & & \mathbf{12.4} & \} & \rightarrow 0 & \bullet \\ & \text{diagram 12.1} & - & \text{diagram 12.2} & - 2 & \text{diagram 12.3} & + 2 & \text{diagram 12.4} & & & \end{array} \right]$$

Figure 12.3: The set of diagrams possessing one-loop vertices, the elements of which are not individually transverse in  $p$ .

To demonstrate that the sum of diagrams 12.1–12.4 is transverse in  $p$ , we use a modified version of the technique we employed to demonstrate the transversality of the standard set. To understand why a modification is neces-

sary, it is instructive to compare diagram 12.3 with the second element of the standard set. Now consider contracting these diagrams with the momentum of one of the external fields, and processing them using the techniques of section 3.1. Due to the symmetry of the second element of the standard set, it is manifestly clear that it does not matter which of the external fields we choose. For diagram 12.3, on the other hand, separately contracting momenta with each of the external fields does not manifestly yield the same set of terms.<sup>1</sup> The solution is to be democratic: we take one instance of diagram 12.3 where we contract with the momentum of the external field decorating the one loop vertex and one instance where we contract with the momentum of the external field decorating the tree level vertex, dividing by two to avoid overcounting. Proceeding in this manner, it is straightforward to demonstrate the transversality of diagrams 12.1–12.4.

We now move to the second set of terms derived from equation (10.1). These are shown in figure 12.4 and comprise two one-loop sub-diagrams, both of which are present in the diagrammatic expression for  $\beta_1$ , modulo the little set. The nested gauge remainders are particularly simple in this case: the only ones that survive are those drawn, as all others vanish by group theory considerations.

Notice the suggestive way in which these terms have been arranged. We could fill in the blank entries in the ‘matrix’ of figure 12.4 by halving the values of the off-diagonal elements and then reflecting about the diagonal. This highlights that the terms of figure 12.4 can be obtained by ‘squaring’ the diagrammatic expression for  $\beta_1$ , modulo the little set, and joining pairs of diagrams together with an effective propagator.

Let us be more precise with what we mean by ‘squaring’. Consider extracting the diagrams which gives us  $\beta_1 \square_{\mu\alpha}(p)$ , modulo the little set, from under the  $\Lambda$ -derivative. Now join these, via  $\Delta_{\alpha\beta}^{11}(p)$ , to the analogous set of diagrams extracted from  $\beta_1 \square_{\nu\beta}(p)$ . Enclosing the resultant diagrams under a  $\Lambda$ -derivative, we simply obtain the diagrams of figure 12.4, up to a factor of

---

<sup>1</sup>Though Lorentz invariance or Bose symmetry tells us that the sum of the two sets of terms must be equivalent.

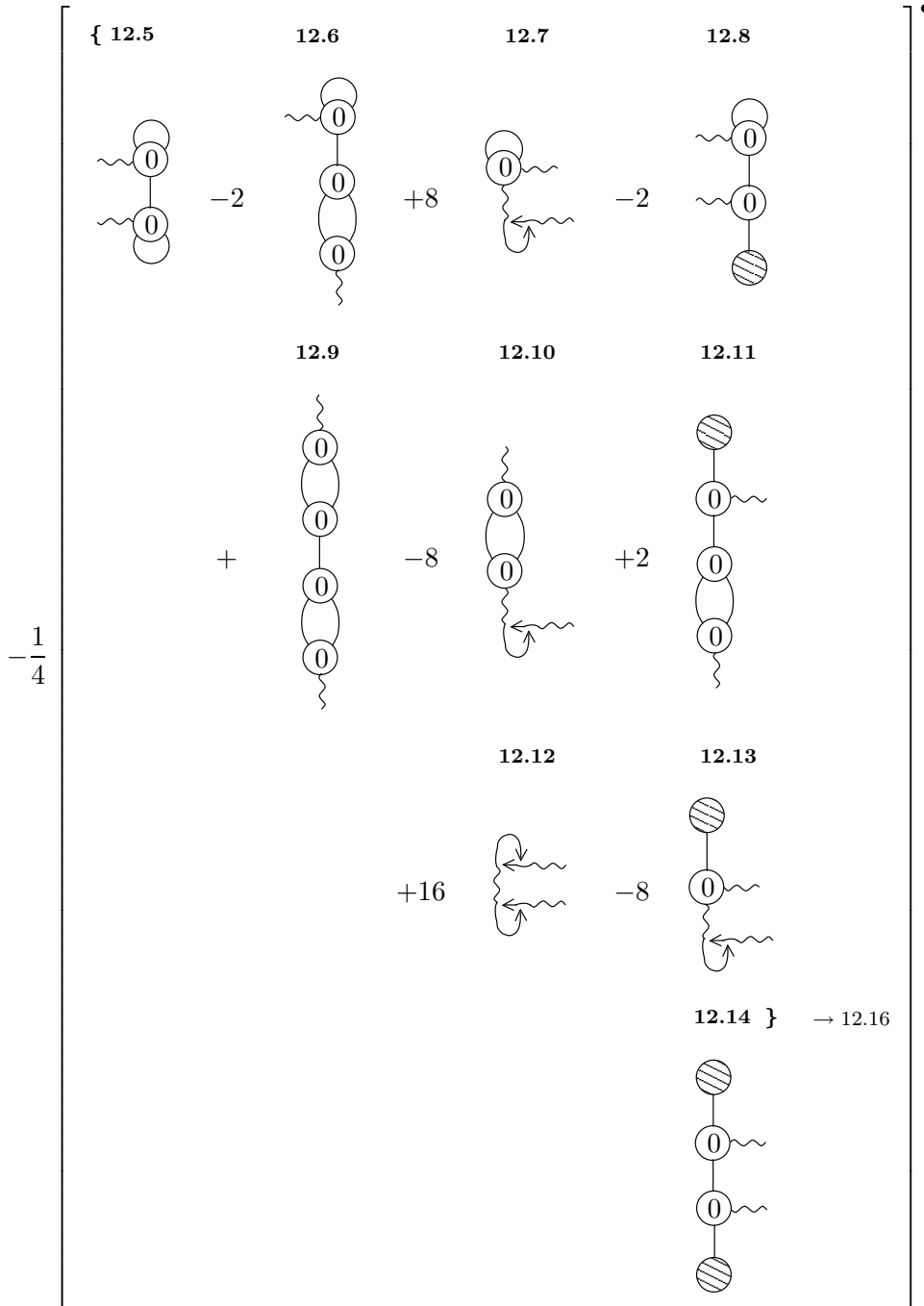


Figure 12.4: Diagrams for which both one-loop sub-diagrams are found in the diagrammatic expression for  $\beta_1$ .

–16. Trivially, this makes it immediately apparent that the sum over diagrams of figure 12.4 is transverse in  $p$ .

The third set of terms derived from equation (10.1), shown in figure 12.5, comprises all diagrams with an  $A_\mu^1 A_\nu^1 C$  vertex. Each of these terms is automatically transverse.

The fourth set of terms, split between figures 12.6 and 12.7, is the final set of  $\Lambda$ -derivatives which we obtain directly from equation (10.1).

To demonstrate that the set of diagrams 12.29–12.51 is transverse is not too difficult. For diagrams where there is no symmetry ensuring that contraction with the momentum of one of the external fields gives a set of terms manifestly the same as those obtained by contracting with the momentum of the other external field, we should once more be democratic. To complete the demonstration of transversality, it is necessary to utilise diagrammatic identities 10–12.

Note that whilst we sum over different nestings in diagram 12.48 some, but not all, of these will cancel in pairs. Specifically, if we take the gauge remainder attached to the effective propagator to bite the external field on the other side, then this will ensure that the external fields are on the same supertrace, irrespective of they sense in which their associated gauge remainders act. Pairs of such diagrams will cancel.

## 12.2 Terms with an $\mathcal{O}(p^2)$ Stub

As anticipated in chapter 11, the result of processing all diagrams with an  $\mathcal{O}(p^2)$  stub ultimately yields terms of four types: the two-loop analogue of the  $B'(0)$  terms and  $\Lambda$ -derivative,  $\alpha$  and  $\beta$ -terms. The set of  $B'(0)$  terms simply comprises an  $\mathcal{O}(p^2)$  stub joined, via a zero-point wine, to the complete set of diagrams coming from the previous section. We have commented already that this set of diagrams is transverse in  $p$ ; in turn, this guarantees that the  $B'(0)$  terms can be discarded at  $\mathcal{O}(p^2)$ .

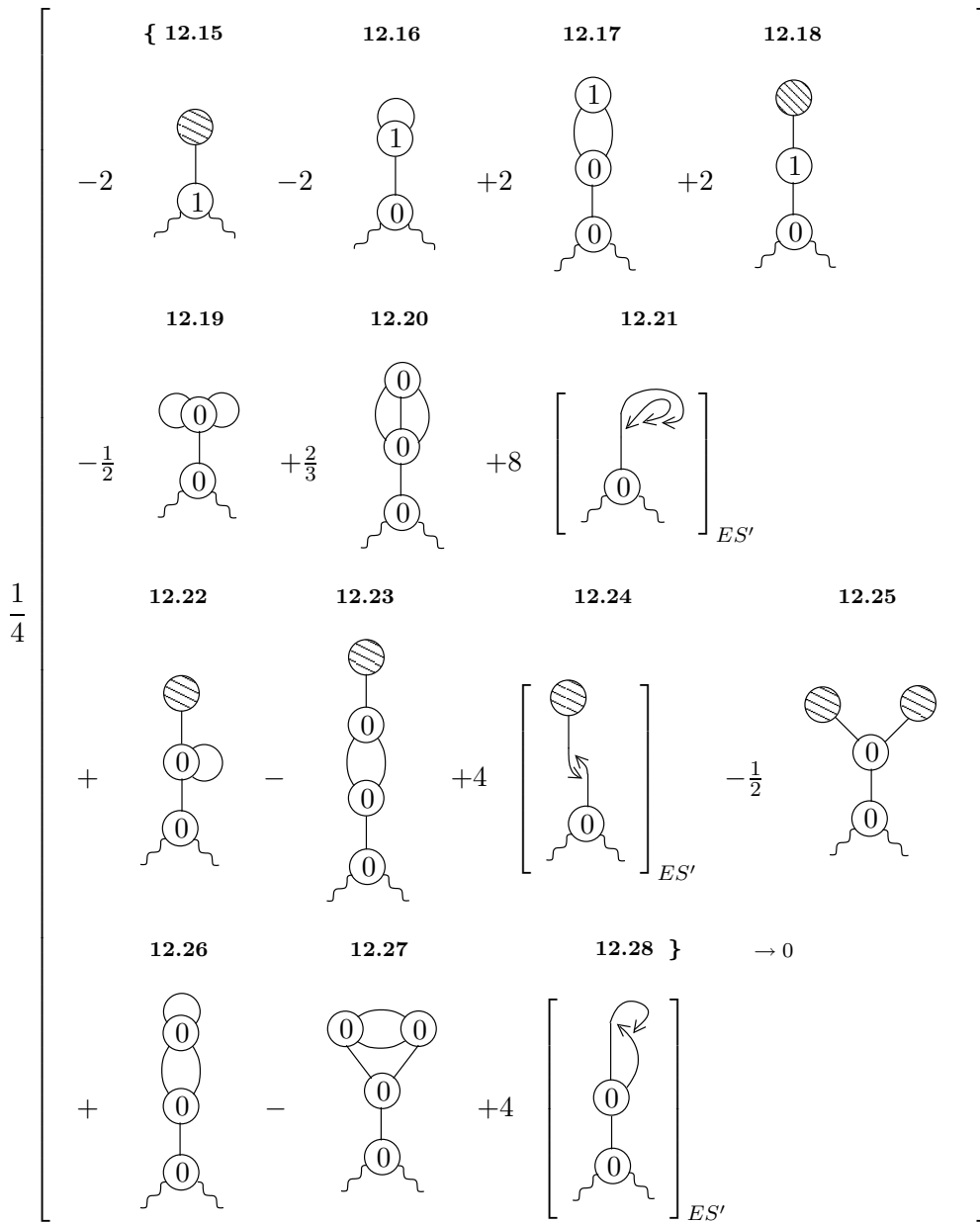


Figure 12.5: Diagrams with an  $A_\mu^1 A_\nu^1 C$  vertex.

$$\left[ \begin{array}{c}
\{ \mathbf{12.29} \quad \mathbf{12.30} \quad \mathbf{12.31} \} \rightarrow \mathbf{13.1} \\
- \begin{array}{c} \text{Diagram 12.29} \\ \text{Diagram 12.30} \end{array} + \begin{array}{c} \text{Diagram 12.30} \\ \text{Diagram 12.31} \end{array} - 4 \left[ \begin{array}{c} \text{Diagram 12.31} \\ \text{Diagram 12.32} \end{array} \right]_{ES'} \\
\mathbf{12.32} \rightarrow 0 \quad \mathbf{12.33} \rightarrow \mathbf{13.5} \\
+ \begin{array}{c} \text{Diagram 12.32} \\ \text{Diagram 12.33} \end{array} - 2 \begin{array}{c} \text{Diagram 12.33} \\ \text{Diagram 12.34} \end{array} \\
\{ \mathbf{12.34} \quad \mathbf{12.35} \\
+ 2 \begin{array}{c} \text{Diagram 12.34} \\ \text{Diagram 12.35} \end{array} - 2 \begin{array}{c} \text{Diagram 12.35} \\ \text{Diagram 12.36} \end{array} \} \rightarrow \mathbf{13.8} \\
+ 8 \left[ \begin{array}{c} \text{Diagram 12.36} \\ \text{Diagram 12.37} \end{array} \right]_{ES'}
\end{array} \right] \bullet$$

Figure 12.6: The final set of  $\Lambda$ -derivatives which can be obtained directly from equation (10.1): part I.

	{ <b>12.37</b>	<b>12.38</b>	<b>12.39</b>	<b>12.40</b> } $\rightarrow 0$				
		$-\frac{2}{3}$		$-$		$+\frac{1}{2}$		
	<b>12.41</b> $\rightarrow$ 13.3	<b>12.42</b> $\rightarrow$ 13.9	<b>12.43</b> $\rightarrow$ 13.10					
	$-\frac{2}{3}$		$-2$		$+4$			
	<b>12.44</b> $\rightarrow$ 13.5	<b>12.45</b> $\rightarrow$ 13.12	<b>12.46</b> $\rightarrow$ 13.14					
$\frac{1}{4}$	$+2$		$+$		$-2$			
	<b>12.47</b> $\rightarrow$ 13.16	<b>12.48</b> $\rightarrow$ 0						
	$+16$		$-8$	$\left[ \begin{array}{c} \text{shaded circle} \\ \text{wavy line} \end{array} \right]_{ES'}$				
	<b>12.49</b> $\rightarrow$ 13.24	<b>12.50</b> $\rightarrow$ 13.24	<b>12.51</b> $\rightarrow$ 13.25					
	$+16$		$+16$		$+8$			

Figure 12.7: The final set of  $\Lambda$ -derivatives which can be obtained directly from equation (10.1): part II.

We will deal with all  $\alpha$  and  $\beta$ -terms—including those generated directly from equation (10.1)—together; hence, in this section, we will present only those  $\mathcal{O}(p^2)$  terms which can be cast as  $\Lambda$ -derivatives. These terms break down into four sets.

The first set of terms is shown in figure 12.8. This set comprises those diagrams for which the  $\mathcal{O}(p^2)$  stub is formed by the action of an un-nested gauge remainder and for which the field attached to this gauge remainder does not join directly to the free socket on the  $\mathcal{O}(p^2)$  stub. Note also that the aforementioned gauge remainder is differentiated with respect to its momentum.

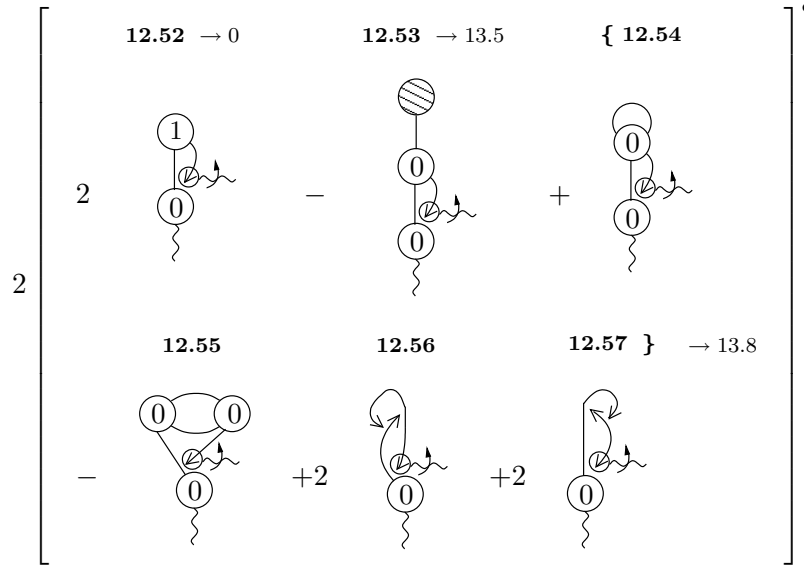


Figure 12.8: The first set of  $\Lambda$ -derivative terms with an  $\mathcal{O}(p^2)$  stub.

There is a clear pattern to the terms of figure 12.8, with each possessing a sub-diagram familiar from our calculation of  $\beta_1$ . Upon examination of diagram 12.52, this comes as no surprise. Diagram 12.52 contains a two-point, one loop vertex; given that  $\beta_1$  is obtained by computing the flow of just such a vertex (but with the fields in the  $A^1$ -sector) this explains how the remaining terms are generated.

There are, however, some differences between the sub-diagrams formed by computing the flow of the two-point, one-loop vertex of diagram 12.52 and the diagrams which contribute to  $\beta_1$ . These differences arise because, in the current case, the two-point, one-loop vertex is decorated by internal,

as opposed to external fields. This immediately explains why there are no diagrams possessing little set-like sub-diagrams: the parents of the little set possess two-point, tree level vertices; if this vertex is decorated by an internal field then, not only are we no longer required to Taylor expand the rest of the diagram, but we can also simply utilise the effective propagator relation.

Furthermore, notice that there are two diagrams, 12.56 and 12.57, containing sub-diagrams like the third element of the standard set. If the external fields of these sub-diagrams were in the  $A$ -sector, then we could simply combine diagrams 12.56 and 12.57. This would then give the third element of the standard set with the correct relative factor, compared to diagrams 12.54 and 12.55.

Returning to diagram 12.52, and taking all fields to be in the  $A$ -sector, the renormalisation condition forces the two-point, one loop vertex to go at least as the fourth power of momentum. This ensures that the Taylor expansion in  $p$  which was performed to derive this diagram is valid. Since diagrams 12.53–12.57 are spawned by diagram 12.52 it immediately follows that  $p$  is set to zero everywhere other than the  $\mathcal{O}(p^2)$  stub, in these diagrams.

The second set of  $\Lambda$ -derivative terms with an  $\mathcal{O}(p^2)$  stub is shown in figure 12.9. As with the previous set, the  $\mathcal{O}(p^2)$  stub is formed by the action of an un-nested gauge remainder. This time, however, the effective propagator attached to the gauge remainder loops round to decorate the free socket of the stub.

There are a number of things to note about the diagrams of figure 12.9, which we list below.

1. Though we have chosen to label the sub-diagrams carrying index  $\alpha$ , these labels refer to complete diagrams; thus each label refers to two diagrams.
2. The set of sub-diagrams carrying index  $\alpha$  is *not* the same as the set obtained in our computation of  $\beta_1$ : the final two diagrams come with a relative factor of  $1/2$ .
3. Upon attaching the effective propagator,  $\Delta_{\alpha\beta}^{11}(p)$ , in diagrams 12.62 and 12.63, we can use the effective propagator relation but are free to discard the

$$\begin{aligned}
& - \left[ 2 \begin{array}{c} \beta \\ \downarrow \\ \textcircled{0} \\ \uparrow \\ \beta \end{array} + \begin{array}{c} \beta \\ \downarrow \\ \textcircled{0} \\ \uparrow \\ \beta \end{array} \right] \bullet \Delta_{\alpha\beta}^{11}(p) \\
& \times \left[ \begin{array}{cccc} \{ \text{12.58} & \text{12.59} & \text{12.60} & \text{12.61} \} \rightarrow \text{12.16} \\ \begin{array}{c} \textcircled{0} \\ \uparrow \\ \alpha \end{array} & - & \begin{array}{c} \textcircled{0} \\ \uparrow \\ \alpha \end{array} & + 4 \begin{array}{c} \textcircled{0} \\ \uparrow \\ \alpha \end{array} & - & \begin{array}{c} \textcircled{0} \\ \uparrow \\ \alpha \end{array} \\ \{ \text{12.62} & \text{12.63} \} \rightarrow \text{12.17} \\ +4 \begin{array}{c} \textcircled{0} \\ \uparrow \\ \alpha \end{array} & + 2 \begin{array}{c} \textcircled{0} \\ \uparrow \\ \alpha \end{array} \end{array} \right]
\end{aligned}$$

Figure 12.9: The second set of  $\Lambda$ -derivative terms with an  $\mathcal{O}(p^2)$  stub.

gauge remainder. This follows as a consequence of Lorentz invariance and the transversality of the  $\mathcal{O}(p^2)$  stub. To see this, start by looking at the diagrams carrying index  $\beta$ , and suppose that the contracted index of the  $\mathcal{O}(p^2)$  stub is just  $\gamma$ . Then, by Lorentz invariance, the loop integral must yield the index structure  $\delta_{\beta\gamma}$ . Now, the gauge remainder generated by the application of the effective propagator relation is  $p_\alpha p_\beta / p^2$ ; the  $\delta_{\beta\gamma}$  ensures that the  $p_\beta$  is contracted into the  $\mathcal{O}(p^2)$  stub, killing the diagram.

4. Diagrams 12.62 and 12.63 can be cast, at  $\mathcal{O}(p^2)$ , such that  $\Lambda\partial_\Lambda|_\alpha$  strikes a set of whole diagrams (rather than just factorisable sub-diagrams). This follows because the combination of the two sub-diagrams with index  $\alpha$  take exactly the same form as the sub-diagrams struck by  $\Lambda\partial_\Lambda|_\alpha$ .
5. The Taylor expansion in  $p$  used to derive the two diagrams carrying index  $\beta$  is valid. The steps are just a repetition of some of the one loop diagrammatics and we know this to be legal.

The third set of  $\Lambda$ -derivative terms with an  $\mathcal{O}(p^2)$  stub is shown in figure 12.10. These are distinguished by the fact the the  $\mathcal{O}(p^2)$  stub is formed by the action of a nested gauge remainder.

A subset of the parent diagrams for these terms are not Taylor expandable to the desired order in  $p$ . As detailed in section 5.4.3 it is necessary to construct subtractions, in this case. Manipulation of the additions helps generate the diagrams of figure 12.10; the parents and subtractions combine to give the diagrams of figure 12.11.

### 12.3 $\beta$ -Terms

In this section, we collect together all  $\beta$ -terms, as shown in figure 12.12.

There is a great temptation to try and manipulate diagrams 12.81 and 12.82 at  $\mathcal{O}(p^2)$ . However, we must be extremely careful: when all fields are in the  $A$ -sector, the loop integral has components which are not Taylor expandable

$$\begin{array}{c}
\left[ \begin{array}{cccc}
\{ 12.64 & 12.65 & 12.66 & 12.67 \} \rightarrow 13.22 \\
- \text{diagram} & - \text{diagram} & + \text{diagram} & + \text{diagram} \\
\{ 12.68 & 12.69 & 12.70 & 12.71 \} \rightarrow 13.27 \\
+ \text{diagram} & + \text{diagram} & - \text{diagram} & + \text{diagram} \\
12.72 \rightarrow 13.27 & \{ 12.73 & 12.74 \} \rightarrow 0 \\
-\frac{1}{2} \text{diagram} & -\frac{1}{2} \left[ \text{diagram} \right]_{ES'} & +\frac{1}{2} \left[ \text{diagram} \right]_{ES'} & 
\end{array} \right.
\end{array}$$

Figure 12.10: The third set of  $\Lambda$ -derivative terms with an  $\mathcal{O}(p^2)$  stub.

$$-4 \left[ \left[ \begin{array}{c} \beta \\ \text{diagram} \\ \text{diagram} \end{array} \right] + \left[ \text{diagram} \right] \right]_{p^{-2\epsilon}} \times \Delta_{\alpha\beta}^{11}(p) \left[ \begin{array}{cc} \{ 12.75 & 12.76 \} \rightarrow 12.18 \\ 2 \text{diagram} & + \text{diagram} \\ \alpha & \alpha \end{array} \right]$$

Figure 12.11: Terms with an  $\mathcal{O}(p^2)$  stub which are not Taylor expandable to the desired order in  $p$ .

$$\begin{array}{c}
-2\beta_1(\alpha) \\
\left[ \begin{array}{cccc}
\{ \mathbf{12.77} & \mathbf{12.78} & \mathbf{12.79} & \mathbf{12.80} \} \rightarrow 12.16 \\
\begin{array}{c} \text{Diagram 12.77} \\ \text{Diagram 12.78} \\ \text{Diagram 12.79} \\ \text{Diagram 12.80} \end{array} \\
\{ \mathbf{12.81} & \mathbf{12.82} & \mathbf{12.83} & \mathbf{12.84} \} \rightarrow 12.17 \\
\begin{array}{c} \text{Diagram 12.81} \\ \text{Diagram 12.82} \\ \text{Diagram 12.83} \\ \text{Diagram 12.84} \end{array}
\end{array} \right]
\end{array}$$

Figure 12.12: All  $\beta$ -terms.

to the desired order in  $p$ . Thus, whilst we can Taylor expand the three point vertex of diagram 12.81, we cannot set  $\Delta^{11}(l-p)$  to  $\Delta^{11}(l)$ . Nonetheless, we can make progress with these terms, as we will see in section 12.5.

## 12.4 $\alpha$ -Terms

The  $\alpha$ -terms split naturally into two sets, shown in figures 12.13 and 12.14. The first set are those for which the  $\alpha$ -derivative strikes an  $\mathcal{O}(p^2)$  stub. The second set are those for which the  $\alpha$ -derivative strikes any other vertex.

It is straightforward to argue that terms of the first type vanish, at  $\mathcal{O}(p^2)$ . The  $\mathcal{O}(p^2)$  stub of diagrams 12.85–12.88 is attached, via an effective propagator, to something we know to be transverse in  $p$ . Hence, the  $1/p^2$  coming from the effective propagator is ameliorated. Given that the  $\mathcal{O}(p^2)$  part of the vertex  $S_{0\mu\alpha}^{11}(p)$  is independent of  $\alpha$ , the diagrams can be discarded.

We conclude this section by developing—and then applying—a set of diagrammatic identities to enable us to process the remaining  $\alpha$ -terms. The first

$$\gamma_1(\alpha) \left[ \begin{array}{cccc} \{ \text{12.85} & \text{12.86} & \text{12.87} & \text{12.88} \} \rightarrow 0 \\ \frac{\partial}{\partial\alpha} \text{diagram 1} & - \frac{\partial}{\partial\alpha} \text{diagram 2} & + 4 \frac{\partial}{\partial\alpha} \text{diagram 3} & - \frac{\partial}{\partial\alpha} \text{diagram 4} \end{array} \right]$$

Figure 12.13:  $\alpha$ -terms of the first type.

$$\frac{1}{2}\gamma_1(\alpha) \left[ \begin{array}{ccc} \{ \text{12.89} & \text{12.90} & \text{12.91} \\ - \frac{\partial}{\partial\alpha} \text{diagram 1} & + \frac{\partial}{\partial\alpha} \text{diagram 2} & + 2 \frac{\partial}{\partial\alpha} \text{diagram 3} \\ \text{12.92} & \text{12.93} & \text{12.94} \\ + \frac{\partial}{\partial\alpha} \text{diagram 4} & + \frac{\partial}{\partial\alpha} \text{diagram 5} & - \frac{\partial}{\partial\alpha} \text{diagram 6} \\ \text{12.95} & \text{12.96} & \text{12.97} \} \rightarrow \text{12.15} \\ - \frac{\partial}{\partial\alpha} \text{diagram 7} & - 2 \frac{\partial}{\partial\alpha} \text{diagram 8} & - 8 \frac{\partial}{\partial\alpha} \text{diagram 9} \end{array} \right]$$

Figure 12.14:  $\alpha$ -terms of the second type.

key ingredient is the observation that  $\triangleright$  is independent of  $\alpha$  and so is killed by  $\alpha$ -derivatives. Recall that we can use  $\odot$  as shorthand for differentiation with respect to  $\alpha$ .

**Diagrammatic Identity 15** *A sub-diagram comprising a two-point, tree level vertex, differentiated with respect to  $\alpha$  and attached to an effective propagator can, using the effective propagator relation, be redrawn, in the following form:*

$$-\overset{\odot}{\textcircled{0}} \equiv -\overset{\odot}{\textcircled{0}} - \overset{\odot}{\triangleright}.$$

**Diagrammatic Identity 16** *A sub-diagram comprising a two-point, tree level vertex, differentiated with respect to  $\alpha$  and attached to two effective propagators can, using diagrammatic identity 15 and the effective propagator relation, be redrawn in the following form:*

$$-\overset{\odot}{\textcircled{0}} \equiv -\overset{\odot}{\textcircled{0}} + \frac{1}{2} \left[ \begin{array}{c} \overset{\odot}{\leftarrow} - \overset{\odot}{\triangleright} \\ \overset{\odot}{\rightarrow} - \overset{\odot}{\triangleleft} \end{array} \right].$$

We could re-express this in a less symmetric form by taking either of the two rows in the square brackets and removing the factor of half.

**Diagrammatic Identity 17** *A sub-diagram comprising a two-point, tree level vertex, differentiated with respect to  $\alpha$  and attached to an effective propagator which terminates in a  $\triangleright'$  vanishes:*

$$\overset{\odot}{\leftarrow}\textcircled{0} \equiv \overset{\odot}{\triangleright'}\textcircled{0} = 0,$$

as follows from diagrammatic identities 3 and 6.

**Diagrammatic Identity 18** *A sub-diagram comprising a two-point, tree level vertex attached to an effective propagator, differentiated with respect to  $\alpha$ , which terminates in a  $\triangleright$  can be redrawn, using diagrammatic identity 17, the effective propagator relation diagrammatic identity 2:*

$$\overset{\odot}{\leftarrow}\textcircled{0} \equiv -\overset{\odot}{\triangleleft}.$$

$$-\frac{1}{2}\gamma_1\frac{\partial}{\partial\alpha}
\left[
\begin{array}{cccc}
\text{12.98} & \text{12.99} & \text{12.100} & \text{12.101} \\
\begin{array}{c} \text{Diagram 12.98} \\ \text{0} \end{array} & - \begin{array}{c} \text{Diagram 12.99} \\ \text{0} \\ \text{0} \end{array} & +4 \begin{array}{c} \text{Diagram 12.100} \end{array} & - \begin{array}{c} \text{Diagram 12.101} \\ \text{0} \end{array} \\
\text{12.102} & \text{12.103} \\
+8 \begin{array}{c} \text{Diagram 12.102} \\ \text{0} \end{array} & +4 \begin{array}{c} \text{Diagram 12.103} \\ \text{0} \end{array}
\end{array}
\right]$$

Figure 12.15: All remaining  $\alpha$ -terms.

Applying the new diagrammatic identities to diagrams 12.90–12.97 and their daughters, as appropriate, we obtain the terms of figure 12.15.

It is thus apparent that the  $\alpha$ -terms arising from the computation of  $\beta_2$  can be reduced to the  $\alpha$ -derivative of the set of terms which we differentiate with respect to  $\Lambda|_\alpha$  to give  $\beta_1$ !

## 12.5 Simplifications

In this section we simplify the diagrammatic expression for  $\beta_2$  by utilising our diagrammatic expression for  $\beta_1$ . We begin by examining diagrams 12.77–12.80 which, having re-expressed, we will combine with the diagrams of figure 12.4 and diagrams 12.58–12.61

Referring to diagrams 12.77–12.80, the first thing to note is that we can use the effective propagator relation to get rid of the  $\mathcal{O}(p^2)$  stub and the effective propagator to which it attaches. Having done this, we can discard the resulting gauge remainder, as it strikes a set of diagrams transverse in  $p$ . The next step is to expand the overall factor of  $\beta_1$ , using our earlier diagrammatic expression. To do this, we perform two intermediate steps. First, change the index  $\nu$  to  $\alpha$  and multiply by  $\delta_{\alpha\nu}$ . Secondly, we use the fact that diagrams 12.77–

12.80 are transverse in  $p$  to recognise that, at  $\mathcal{O}(p^2)$ , we can replace  $\delta_{\alpha\nu}$  by  $\square_{\beta\nu}(p)2\Delta_{\alpha\beta}^{11}(p)$ . We now insert our diagrammatic expression for  $\beta_1\square_{\beta\nu}(p)$  and, having done this, join together one-loop sub-diagrams with the effective propagator,  $\Delta_{\alpha\beta}^{11}(p)$ . Now we are ready to identify cancellations.

At  $\mathcal{O}(p^2)$ , the diagrams of figure 12.4 are completely cancelled. The remaining terms are shown in figure 12.16; they are the same as diagrams 12.58–12.61, but with opposite sign.

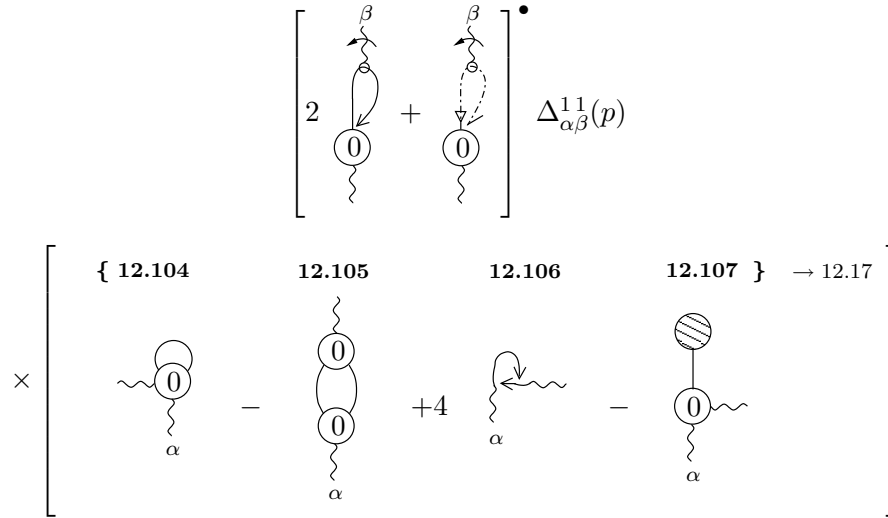


Figure 12.16: Result of combining the diagrams of figure 12.4, diagrams 12.58–12.61 and 12.77–12.80.

The next step is to examine diagrams 12.81–12.84. Replacing  $\beta_1$  proceeds exactly as before: first we change the index  $\nu$  to  $\alpha$  and multiply by  $2\square_{\beta\nu}(p)\Delta_{\alpha\beta}^{11}(p)$ ; secondly, we substitute for  $\beta_1\square_{\beta\nu}(p)$ .

Noting that the diagrams contributing to  $\beta_1$  are hit by  $\Lambda\partial_\Lambda|_\alpha$  but the one-loop sub-diagrams to which they are joined by the effective propagator,  $\Delta_{\alpha\beta}^{11}(p)$ , are not, we now move the  $\Lambda\partial_\Lambda|_\alpha$ . At  $\mathcal{O}(p^2)$ , this will generate a set of terms where whole two-loop diagrams are hit by  $\Lambda\partial_\Lambda|_\alpha$  minus a correction in which the explicitly drawn sub-diagrams of diagrams 12.81–12.84 are hit by  $\Lambda\partial_\Lambda|_\alpha$ . This is precisely what we want: with these sub-diagrams now under a  $\Lambda$ -derivative, they are Taylor expandable to the desired order in  $p$ . Performing this Taylor expansion, we can reduce the four sub-diagrams to an instance of the little set, struck by  $\Lambda\partial_\Lambda|_\alpha$ . We now find cancellations. First, those terms

formed from  $\beta_1$  modulo the little set exactly cancel diagrams 12.104–12.107. Secondly, those diagrams from the little set contribution to  $\beta_1$  can be combined with diagrams 12.62–12.63.

The set of surviving terms are shown in figure 12.17. The labels for the first set of terms each refer to four diagrams. Upon attachment of the effective propagator to a two-point, tree level vertex, the resulting gauge remainder can be thrown away.

There is now one final step to perform. We focus on diagrams 12.112 and 12.113. We know that the first two diagrams which they multiply (carrying index  $\beta$ ) have components which are not Taylor expandable to the desired order in  $p$ . These components are exactly removed by diagrams 12.75–12.76. With these components removed, we now Taylor expand these diagrams in  $p$  and perform the usual diagrammatic manipulations, reducing the four diagrams carrying index  $\beta$  to an instance of the standard set. The resulting diagrams can then be combined with diagrams 12.114–12.116, to yield the diagrams of figure 12.18.

We have thus demonstrated that  $\beta_2$  can be reduced to a set of  $\Lambda$ -derivative terms, where the entire diagram is hit by  $\Lambda\partial_\Lambda|_\alpha$ , and  $\alpha$ -terms. For ease of future reference, we present the simplified diagrammatic expression for  $\beta_2$  in appendix D.

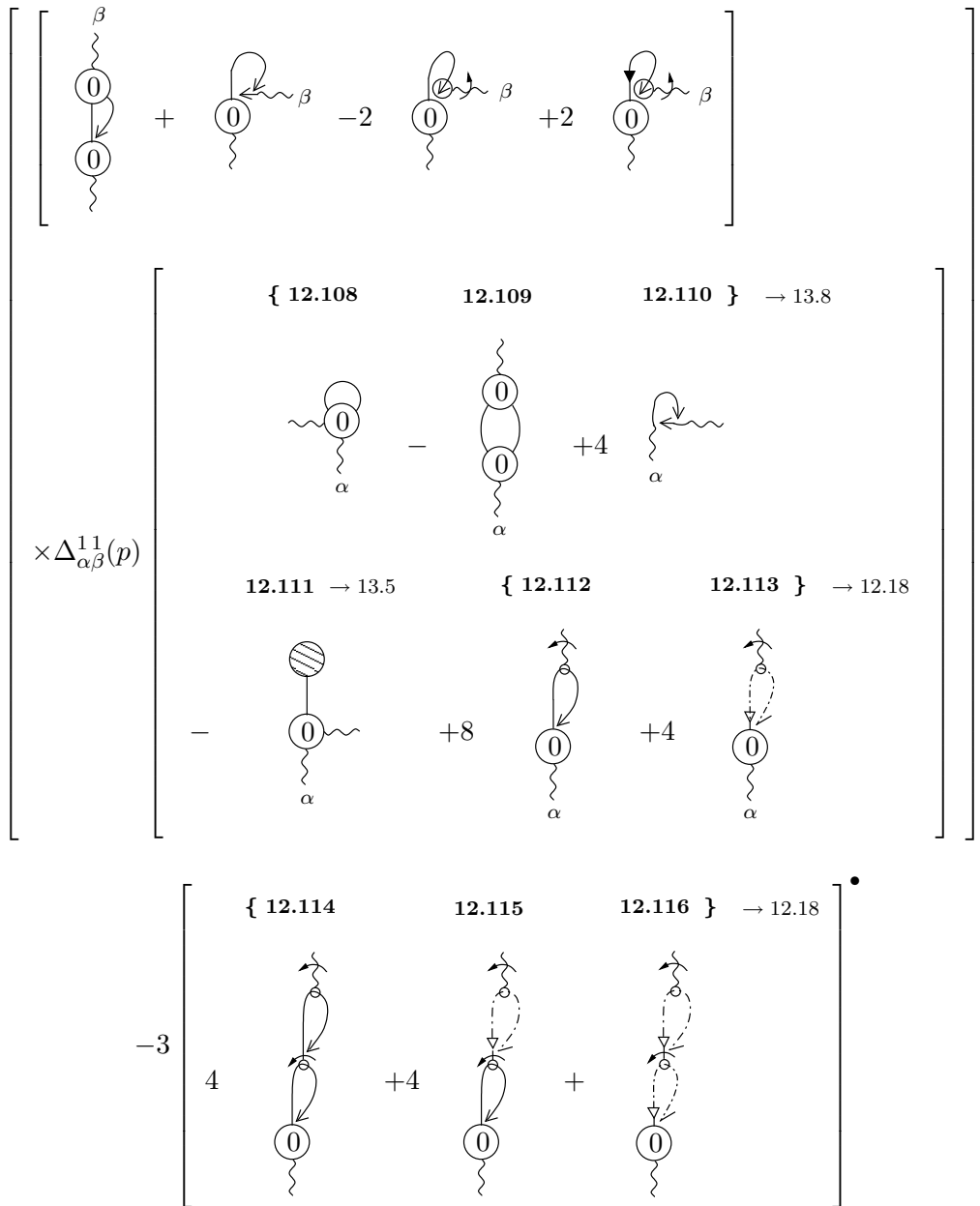


Figure 12.17: Result of combining diagrams

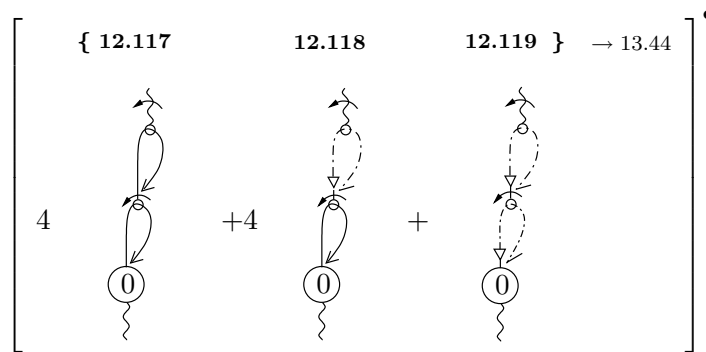


Figure 12.18: Result of combining diagrams 12.112 and 12.113 with 12.75–12.76 and then combining the result with diagrams 12.114–12.116.

# Chapter 13

## Numerical Evaluation of $\beta_2$

In this chapter we apply the methodology of chapter 5 to the computation of  $\beta_2$ . The starting point is the set of diagrams left over from chapter 12, which we will call the original set (see also appendix D).

There are three things we must do. First, ignoring the  $\alpha$ -terms, we must demonstrate that all non-computable contributions cancel, between diagrams. Secondly, we must show that the  $\alpha$ -terms vanish in the limit that  $\alpha \rightarrow 0$ . Lastly, we must evaluate  $\beta_2$ .

We begin our first task in section 13.1 with the simplest diagrams to treat—those which vanish in the  $\epsilon \rightarrow 0$  limit—and build up in complexity from there. In section 13.2 we treat a sub-set of those diagrams which are manifestly finite.<sup>1</sup> There are two types of such terms that we will encounter. First, we treat a non-factorisable diagram which yields a computable contribution to  $\beta_2$ . Secondly, we treat a set of factorisable diagrams which, up to  $\mathcal{O}(\epsilon)$  corrections, give a computable coefficient multiplying the fourth and fifth diagrams of  $\mathcal{D}_1$ . This computable coefficient turns out to vanish, as a consequence of the transversality of the non-universal one-loop sub-diagrams it multiplies.

We can guess from the pattern of terms that cancel in this way that we expect similar cancellations involving the members of the standard set. This is one of the things we investigate in section 13.3. As we see in subsection 13.3.1,

---

<sup>1</sup>There are some diagrams which, although they appear to contain IR divergences, turn out not to, for purely numerical reasons. It is not useful to treat such diagrams in this section as they are more naturally dealt with in conjunction with those that do contain IR divergences.

the cancellations of section 13.2 are indeed mirrored, though things are much more complex. This complexity arises, on the one hand, because the standard set comprises not only Taylor expandable, finite parts but also both Taylor and non-Taylor expandable IR divergent coefficients. On the other hand, the complete set of terms we seek in order to mirror the earlier cancellations is not manifestly present in the original set. The philosophy we take is to add zero to the calculation by constructing the terms we are missing, together with identical diagrams with opposite sign. Our next task is to try and cancel these latter diagrams.

This is trivial for those diagrams involving the first element of the standard set, which is not surprising, since such diagrams are manifestly finite. We choose not to treat these terms in section 13.2, with the other manifestly finite diagrams, but treat them in subsection 13.3.2, in order to keep the standard set together.

Also in this section, we generate the required diagrams involving the second and third members of the standard set. This is harder: we must construct subtractions for a subset of the original set; upon the manipulation of the additions, we generate the terms we are after, and many more, besides. We conclude section 13.3 by manipulating the semi-computable partners of the additions.

In section 13.4 we construct a further set of subtractions. First, we do this, as appropriate, for the un-treated terms in the original set. Secondly, we construct subtractions for a subset of the diagrams resulting from the manipulation of the additions generated in section 13.3. In section 13.5 we perform a final set of manipulations, which remove all remaining non-computable contributions.

In section 13.6 we treat the  $\alpha$ -terms; in section 13.7 we give the result of our numerical evaluation of  $\beta_2$  and in section 13.8, we conclude this chapter.

## 13.1 Vanishing Diagrams

There are a number of diagrams in the original set which are IR safe, even before differentiation with respect to  $\Lambda|_\alpha$ . After differentiation, such terms will vanish in the  $\epsilon \rightarrow 0$  limit. In almost all cases, diagrams vanish on an

individual level and, in this case, have been tagged  $\rightarrow 0$  in chapter 12. Whilst there are many diagrams which are trivially IR safe, there are cases in which it is necessary to use some property of the diagram in question to demonstrate this, as we will discuss in section 13.1.1.

In section 13.1.2 we encounter diagrams which can only be shown to vanish in the  $\epsilon \rightarrow 0$  limit when combined into a set. In section 13.1.3 we recognise that for certain diagrams possessing gauge remainders, the  $ES'$  tag can be removed.

### 13.1.1 Diagrams which Vanish Individually

To check that individual diagrams tagged  $\rightarrow 0$  do indeed vanish, the first thing we do is put all fields carrying loop momenta<sup>2</sup> in the  $A$ -sector; if a diagram is IR safe in this sector then it will be IR safe in all sectors.

There are now three observations which are necessary to show that certain  $\Lambda$ -derivative terms vanish in the  $\epsilon \rightarrow 0$  limit:

1. the renormalisation condition (1.33), together with the form for  $S_{0\alpha\beta}^{11}(q)$  (equation (A.1)) demands that  $S_{1\alpha\beta}^{11}(q) \sim \mathcal{O}(q^4)$ , which is sufficient to guarantee that all diagrams containing one-loop vertices vanish;
2. gauge invariance forces  $S_{\alpha\beta}^{AAC}(q) \sim \mathcal{O}(q^2)$  which is sufficient to guarantee that diagrams such as 12.32 vanish;
3. sub-diagrams which are divergent as a consequence of all fields being in the  $A$ -sector but that attach to a  $C$ -sector effective propagator no longer diverge because, since  $A$ -fields do not carry a fifth index, the sub-diagram has no support in the divergent sector (e.g. diagram 12.48).

### 13.1.2 Diagrams which Vanish as a Set

Diagrams 12.29–12.31 have been reproduced in figure 13.1.

For the individual diagrams to have any chance of surviving differentiation with respect to  $\Lambda\partial_\Lambda|_\alpha$ , the internal legs leaving the common four-point vertex must be in the  $A$ -sector (and we must take only the  $\mathcal{O}(p^2)$  part of this vertex).

---

<sup>2</sup>This excludes fields forced to carry zero momentum which must be  $C$ s.

$$-\frac{1}{4} \left[ \begin{array}{c} \{ \text{13.1} \quad \text{13.2} \quad \text{13.3} \} \rightarrow 0 \\ \begin{array}{c} \text{Diagram 13.1} \\ \text{Diagram 13.2} \\ \text{Diagram 13.3} \end{array} \end{array} \right]_{ES'}$$

Figure 13.1: Three diagrams which do not separately vanish as  $\epsilon \rightarrow 0$ , but vanish when combined into a set related by gauge invariance.

However, if these legs are in the  $A$ -sector then, summing over the three diagrams, it is clear that the common four-point vertex attaches to the standard set. Since the standard set is transverse in momentum, the IR behaviour of the diagrams is improved—to the extent that the set of diagrams clearly vanishes in the  $\epsilon \rightarrow 0$  limit. Note that diagrams 12.26–12.28 combine into a set in exactly the same way. However, these diagrams actually vanish on an individual level, anyway, by virtue of the second point above.

### 13.1.3 Diagrams which Possess Vanishing Components

Particular patterns of pushes forward and pulls back in diagrams possessing nested gauge remainder structures can be discarded, up to  $\mathcal{O}(\epsilon)$  corrections. To illustrate this, consider the diagrams shown in figure 13.2.

$$2 \left[ \begin{array}{c} \text{Diagram} \\ \text{ES}' \end{array} \right] = 2 \left[ \begin{array}{c} \text{I.83} \quad \text{I.84} \\ \text{Diagram I.83} \quad - \quad \text{Diagram I.84} \end{array} \right]$$

Figure 13.2: Two components of a diagram, one of which can and one of which cannot be discarded.

Taking diagrams I.83 and I.84 to have their fields as shown (FAS), let us now suppose that we move the external field on, say, the left hand vertex to the ‘inside’ of each diagram. The key point is that the only components of these diagrams which survive in the  $\epsilon \rightarrow 0$  limit are those for which all fields leaving

the three-point vertices are in the  $A^1$ -sector; for what follows, we discard all other contributions. Thus, moving one field from the ‘outside’ to the ‘inside’, whilst temporarily ignoring the group theory factors, produces a relative minus sign and a possible change to the flavours of the gauge remainders.

Now consider the components of diagram I.83 where there are attachment corrections. The supertrace structure of the diagram as a whole is  $\text{str } A_\mu^1(p)A_\nu^1(-p)$ , irrespective of the location of the external fields. Hence, in this case, components with the left-hand external field ‘inside’ are exactly cancelled by the corresponding components with the left-hand field ‘outside’. However, for the components of diagram I.83 for which both all attachments are direct, moving the left-hand external field ‘inside’ the diagram will cause it to be on a different supertrace from the other external field. In this case, there can be no cancellation.

Turning now to diagram I.84, things are different for the case where all attachments are direct: the diagram has no empty supertraces; the external fields are always on the same supertrace, irrespective of location. Note that this further implies that all internal fields must be bosonic: fermionic fields separate a portion of supertrace in the 1-sector from a piece in the 2-sector, but the latter does not exist, in this scenario! Thus, all components with the left-hand external field ‘inside’ are exactly cancelled by the corresponding components with the left-hand field ‘outside’. Hence, whilst we keep diagram I.83, mindful that certain components cancel but some survive, we discard diagram I.84. In other words, we can drop the  $ES'$  of the parent.

## 13.2 Finite Diagrams

In this section, we deal with some, but not all, of the manifestly finite diagrams. First, we will encounter a single diagram which yields a computable contribution to  $\beta_2$ . Next, we will examine a set of diagrams which result in a computable coefficient times a non-universal, one loop diagram; the computable coefficient will be shown to vanish. The one-loop diagram is none other than the usual combination of the two diagrams possessing an  $A_\mu^1 A_\nu^1 C$  vertex that contribute to  $\mathcal{D}_1$ .

With this in mind, we expect to find a set of diagrams in which the stub is the standard set. Though some of the resulting contributions are manifestly finite, we choose not to treat them in this section, so that we can keep the standard set intact.

### 13.2.1 Universal Diagrams

Diagram 12.41 is the sole  $\Lambda$ -derivative term which yields simply a finite, universal contribution to  $\beta_2$ .<sup>3</sup> We reproduce this diagram, having chosen a particular momentum routing, in figure 13.3.

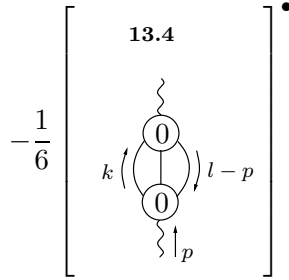


Figure 13.3: Reproduction of diagram 12.41.

The requirement that we take contributions which survive the  $\epsilon \rightarrow 0$  limit places useful constraints on the diagram. First, all fields must be in the  $A$ -sector; given this, we are compelled to take  $\mathcal{O}(\text{mom}^0)$  from each of the vertices. In turn, this forces both vertices to comprise a single supertrace: it is forbidden to have a single gauge field on a supertrace; if we take two supertraces, each with two gauge fields, then gauge invariance demands that we cannot take  $\mathcal{O}(\text{mom}^0)$  from such a vertex.

Now that we know that both vertices have only a single supertrace, all fields are forced to be in the  $A^1$  sector. Temporarily ignoring attachment corrections, the group theory factor of the diagram must be either  $N^2$  or unity. However, we can show that contributions of the latter type cancel. To see this, recall

---

<sup>3</sup>Since the leading order contribution to this diagram is finite, it is not merely computable but actually universal: it is independent of the way in which we compute it (see [25] for a different way of evaluating this diagram).

from equation (3.10) that

$$\begin{aligned} S_{\mu\alpha\beta\gamma}^{1111}(\underline{0}) &= -2(2\delta_{\mu\beta}\delta_{\alpha\gamma} - \delta_{\alpha\beta}\delta_{\mu\gamma} - \delta_{\mu\alpha}\delta_{\beta\gamma}) \\ S_{\nu\gamma\beta\alpha}^{1111}(\underline{0}) &= -2(2\delta_{\nu\beta}\delta_{\alpha\gamma} - \delta_{\gamma\beta}\delta_{\nu\alpha} - \delta_{\nu\gamma}\delta_{\beta\alpha}). \end{aligned}$$

Focusing on the component of diagram 13.4 with a group theory factor of unity, the locations of the external fields are independent, since they are always guaranteed to be on the same supertrace. Summing over all independent locations of the external fields yields something proportional to

$$S_{\mu\alpha\beta\gamma}^{1111}(\underline{0}) + S_{\alpha\mu\beta\gamma}^{1111}(\underline{0}) + S_{\alpha\beta\mu\gamma}^{1111}(\underline{0}) = 0. \quad (13.1)$$

Similarly, all attachment corrections can be ignored. If we suppose that one of the effective propagators attaches via a correction (see figure 2.9) then the supertrace structure of the diagram is left invariant under independently placing the ends of this effective propagator in all independent locations. Hence the diagram vanishes courtesy of (13.1). Increasing the number of effective propagators which attach via a correction clearly does not change this result.

Returning to the case of direct attachment, if the group theory goes as  $N^2$ , then the locations of the external gauge fields are dependent, since it must be ensured that they are on the same supertrace. Up to insertions of  $A_{\mu,\nu}^1$ , we can use charge conjugation invariance to fix the order of the three internal fields so long as we multiply by two. Now, there are three identical pairs of locations that we can place the pair of fields  $A_{\mu,\nu}^1$ . Including the diagram's overall factor of  $-1/6$  we have:

$$-N^2 \times S_{\mu\alpha\beta\gamma}^{1111}(\underline{0})S_{\nu\gamma\beta\alpha}^{1111}(\underline{0}) = -72N^2\delta_{\mu\nu} + \mathcal{O}(\epsilon). \quad (13.2)$$

To obtain the contribution to  $\beta_2$  coming from diagram 13.4, we must multiply the above factor by the number obtained from the loop integral. Since the integral yields a finite contribution, we simply Taylor expand the effective propagator  $\Delta^{11}(l-p)$  to  $\mathcal{O}(p^2)$ . Remembering to evaluate the cutoff functions at zero momentum—which yields a factor of  $1/2$  for each of the effective propagators—we have:

$$\frac{1}{8} \left[ \int_{l,k} \frac{1}{k^2(l-k)^2l^4} \left( p \cdot p - \frac{4(l \cdot p)^2}{l^2} \right) \right]^\bullet,$$

Looking at this expression, we might worry that the presence of  $l^4$  in the denominator means that the integral is actually IR divergent, even after differentiation with respect to  $\Lambda\partial_\Lambda|_\alpha$ . However, due to the form of the  $\mathcal{O}(p^2)$  contributions, averaging over angles in the  $l$ -integral will produce a factor of

$$1 - \frac{4}{D} \sim \epsilon,$$

in addition to the power of  $\epsilon$  coming from the  $\Lambda$ -derivative. This renders the contribution from diagram 13.4 finite.

To evaluate the integral, we use the techniques of chapter 5. Specifically, we perform the  $l$  integral first, with unrestricted range of integration, and then perform the  $k$ -integral with the radial integral cutoff at  $\Lambda$ . After differentiation with respect to  $\Lambda\partial_\Lambda|_\alpha$ , the integral gives  $\mathcal{Q}_D^2 p^2/32$ . Combining this with the factor coming from equation (13.2) yields:

### 13.5

$$\text{diagram 13.4} = -\frac{9N^2}{(4\pi)^4} p^2 \delta_{\mu\nu} + \mathcal{O}(\epsilon).$$

Before moving on, it is worth commenting further on the fact that all attachment corrections in diagram 12.41 effectively vanish. When we finally come to evaluate the numerical value of  $\beta_2$ , we will be dealing with diagrams for which all fields are in the  $A^1$  sector. The highest point vertex that we will encounter is four-point: we have already seen how attachment corrections to such a vertex vanish. Three-point vertices are even easier to treat. Suppose that an effective propagator attaches via a correction to a three-point vertex, decorated exclusively by  $A$ s. We can sum over the two locations to which the effective propagator can attach, but these two contributions cancel, by CC.

If nested gauge remainders are in the  $A$ -sector, we know from the analysis of section 3.1.6 that we can ignore attachment corrections.

Thus, when we come to extract numerical contributions to  $\beta_2$ , we will neglect attachment corrections. Similarly, for direct attachments, we need focus only on the cases where the group theory goes as  $N^2$ .

### 13.2.2 Non-Universal Diagrams

In this section, we treat all diagrams which possess the one-loop diagram shown in figure 13.4. We use the fact that gauge invariance forces the diagram to be transverse in its external momentum, to extract the momentum dependence: the bottom structure of the diagram on the r.h.s. of the figure represents the  $\mathcal{O}(q^2)$  coefficient of the bottom vertex of the diagram on the l.h.s.

$$\begin{array}{c} \text{shaded circle} \\ | \\ \text{0} \\ / \quad \backslash \\ \alpha \quad \beta \\ \nearrow \quad \searrow \\ q \end{array} = \begin{array}{c} \text{shaded circle} \\ | \\ \text{0} \\ / \quad \backslash \\ \nearrow \quad \searrow \end{array} \times \square_{\alpha\beta}(q) + \mathcal{O}(q^4)$$

Figure 13.4: Extracting the dependence of a transverse one-loop diagram on its external momentum.

The diagram of figure 13.4 will turn up in one of two ways: either with its external momentum being  $p$  or with its external momentum being a loop momentum. The key point is that, in both cases, we can discard contributions higher order in momentum. In the former case, this is because we are working at  $\mathcal{O}(p^2)$  whereas, in the latter case, it is because additional powers of loop momentum will kill the divergence that keeps the diagram alive. Stripping off this  $\mathcal{O}(\text{mom}^2)$  part leaves behind the same coefficient function.

The set of diagrams containing the diagram of figure 13.4 as a common one-loop sub-diagram is shown in figure 13.5. Whilst it is not immediately apparent that all the diagrams of this set possess the common one-loop sub-diagram, we will find that they can be shown to do so in the  $\epsilon \rightarrow 0$  limit.

A number of comments are in order. First is that diagrams 13.9–13.12 manifestly contain the desired one-loop sub-diagram. Upon restricting the internal fields carrying a loop momentum to the  $A$ -sector, it is clear that diagrams 13.7 and 13.8 also possess the one-loop sub-diagram. What about the first diagram? Let us denote the loop momentum by  $k$ . Given that the fields carrying  $k$  are in the  $A$ -sector, we must take a single power of momentum from the

$$\begin{aligned}
& \left[ \begin{array}{ccc}
\{ \mathbf{13.6} & \mathbf{13.7} & \mathbf{13.8} \\
\frac{1}{2} \text{ (diagram)} - \frac{1}{2} \text{ (diagram)} & & -2 \text{ (diagram)}
\end{array} \right] \\
& - \left[ \begin{array}{cccc}
\mathbf{13.9} & \mathbf{13.10} & \mathbf{13.11} & \mathbf{13.12} \\
\text{(diagram)} + \text{(diagram)} - 2 \text{(diagram)} + 2 \text{(diagram)}
\end{array} \right] = \\
& \quad \times \Delta_{\alpha\beta}^{11}(p) \text{ (diagram)} \\
& = \left[ \begin{array}{c}
\mathbf{13.13} \\
\frac{N\Lambda^{-2\epsilon}}{(4\pi)^{D/2}} \left( u + v \frac{p^{-2\epsilon}}{\Lambda^{-2\epsilon}} \right) \frac{1}{\epsilon} \times \text{(diagram)} \square_{\mu\nu}(p)
\end{array} \right] + \mathcal{O}(\epsilon)
\end{aligned}$$

Figure 13.5: The complete set of diagrams which contain the one-loop diagram shown in figure 13.4.

four-point vertex. This means that we can Taylor expand this vertex to zeroth order in either  $k$  or  $p$ . The result will be a momentum derivative of an  $AAC$  vertex, carrying either  $p$  or  $k$ , respectively; we show this diagrammatically in figure 13.6.

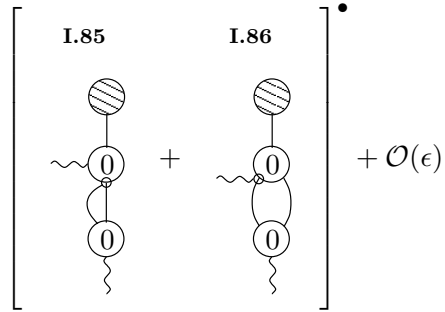


Figure 13.6: Taylor expanding the four-point vertex of diagram 13.6.

Diagrams I.86 and I.85 now contain the desired one-loop sub-diagram, albeit differentiated with respect to its external momentum. However, since we know the momentum dependence of the differentiated vertex, we can strip it off, all the same.

Having stripped the momentum dependence off the common one-loop sub-diagram, we find that the sum of diagrams in figure 13.5, given by contribution 13.13, is transverse in  $p$ . Hence, we could, if we wanted, reabsorb the  $\square_{\mu\nu}(p)$  of this term into the diagrammatic part.

The coefficients  $u$  and  $v$  are to be determined. There are two ways to do this. First, it is straightforward, using the techniques of chapter 5 to show that

$$u = 0, \quad v = 0.$$

It is important that  $v = 0$ : hidden inside the common one-loop diagram is a factor of  $\Lambda^{-2\epsilon}$ ; hence, the  $p^{-2\epsilon}$  terms survive for generic  $v$ .

However, it is also possible to demonstrate that  $u$  and  $v$  vanish, diagrammatically! First, recall that we take all internal fields in the diagrams of figure 13.5 to be in the  $A$ -sector. Secondly, note that when our common stub attaches to an internal field, we can use the fact that it is transverse in momentum to apply the effective propagator relation, so long as we compensate with a factor of  $1/A_k$ .

In this way, diagram 13.8 reduces to diagrams 13.11 and 13.12, up to a relative factor of  $-A(k)/A(p)$ . However, at  $\mathcal{O}(p^2)$ , we can evaluate  $A(p)$  at zero momentum. Up to  $\mathcal{O}(\epsilon)$  correction, we can do likewise with  $A(k)$ . Thus, at leading order, diagram 13.8 cancels diagrams 13.11 and 13.12.

Now let us turn to diagram 13.7. Applying the effective propagator relation, remembering to compensate with  $1/A(k)$ , the Kronecker delta contribution gives a diagram which cancels diagram 13.6, at leading order. Processing the gauge remainder we get three terms. The first cancels diagram 13.9, at leading order. The second and third involve the iterated use of the effective propagator relation. The Kronecker delta contribution can be processed by noting that the processed gauge remainder can act backwards, through the effective propagator, by means of diagrammatic identity 3. This gives two contributions, which cancel each other at  $\mathcal{O}(p^2)$ . The gauge remainder contribution gives one diagram which cancels 13.10, at leading order and a second which vanishes via diagrammatic identity 6.

We conclude this section with an observation that will prove very useful, in the next section.

**Comment 1** *The cancellations in figure 13.5 are guaranteed to occur at, leading order in  $\epsilon$ , for any choice of common one-loop sub-diagram, so long as the sub-diagram is both transverse and Taylor expandable in its external momentum. This latter requirement can be understood as follows. Suppose that the external momentum of the one-loop sub-diagram corresponds to a loop momentum of the complete diagram,  $k$ . If the one-loop sub-diagram is not Taylor expandable, then powers of  $k^{-2\epsilon}$  will affect the loop integral over  $k$ , spoiling the cancellations.*

### 13.3 The Standard Set as a Sub-Diagram

Inspired by comment 1, we try and repeat the cancellations of the previous section but with the one-loop diagram of figure 13.4 replaced by the standard set. Immediately, we know that life is going to get harder: the standard set has contributions which are not Taylor expandable in momentum; moreover, the standard set is IR divergent, so even if we do manage to repeat the cancellations

of the previous section, the sub-leading contributions will not necessarily vanish as  $\epsilon \rightarrow 0$ . Nonetheless, the pattern of cancellations we have just observed will be mirrored; the difference is that there will be terms that survive.

The first challenge is to identify the analogues of the diagrams of figure 13.5. This is easy for all but the first diagram. Putting this diagram temporarily to one side, the diagrams we will need are: 12.34–12.36, 12.54–12.57 and 12.108–12.110.<sup>4</sup>

As for the first diagram, we need to think what it is that we really want. The cancellations of the last section involved us partially Taylor expanding this diagram, to produce diagrams I.86 and I.85. Now, the key point is that the momentum derivative acting in these diagrams hits a structure which is transverse. Given that the standard set is transverse, it is thus apparent that we want to find a set of diagrams in which the whole of the standard set is hit by a momentum derivative; it is no use if the momentum derivative strikes just the vertices of the standard set but not the effective propagators or gauge remainders as well.

It is immediately clear that the set of such diagrams do not exist. Particularly, there are no diagrams which, after Taylor expansion, directly yield momentum derivatives striking effective propagators or gauge remainders. In section 13.3.1, we will simply construct the diagrams that we need, both adding and subtracting<sup>5</sup> them from the calculation. One set of terms will be involved in cancellations similar to those of the previous section; the complementary set with opposite sign will cancel against terms generated in section 13.3.2.

### 13.3.1 Mirroring the Cancellations of Section 13.2.2

The terms we need to construct to mirror the cancellations of section 13.2.2 are shown in figure 13.7. Since each diagram is both added to and subtracted from the calculation, each diagram comes with two labels.

---

<sup>4</sup>Diagrams 12.34–12.36 appear to be highly IR divergent. However, the degree of divergence is lessened by the transversality of the standard set.

<sup>5</sup>These subtractions are distinct from those discussed in section 5.4: we are not starting from some parent diagram and constructing a set of terms directly derived from the parent to cancel all Taylor expandable components. Rather, we are using an empirical observation to find a set of diagrams for which certain Taylor expandable components cancel.

We can now ask what happens when we combine the diagrams of figure 13.7 with the overall minus sign with diagrams 12.34–12.36, 12.54–12.57 and 12.108–12.110.

Our starting point is equation (5.3), the algebraic form of the standard set. Given comment 1, we know that the coefficients  $a_i$ —which correspond to the parts of the standard set, Taylor expandable in external momentum—will be involved in cancellations. Specifically, the leading order contributions involving the  $a_i$  will cancel exactly. Hence, terms involving  $a_1$  will disappear completely, in the  $\epsilon \rightarrow 0$  limit. Terms involving  $a_0$ , on the other hand, will leave behind  $\mathcal{O}(1)$ , as opposed to  $\mathcal{O}(\epsilon)$  contributions, which will survive.

Let us examine these surviving terms in more detail. We begin by noting that, in the case that the external momentum of the standard set corresponds to a loop momentum, the standard set must attach to something computable, as all other contributions will die in the  $\epsilon \rightarrow 0$  limit. Surviving sub-leading corrections will arise from the expansion of functions of  $D$  in  $\epsilon$ .<sup>6</sup>

When the standard set has external momentum  $p$ , we are free to pick up any sub-leading contributions from the one-loop sub-diagrams to which it attaches; we are not restricted to computable contributions only.

We must now move on to consider the  $b_i$  contributions to the standard set. Once again, if the external momentum of the standard set is a loop momentum, then the standard set must attach to something computable. Next, let us suppose that the external momentum of the standard set is  $p$ . Since all the  $b_i$  are computable, if we take the most divergent part of the sub-diagram to which the standard set is attached, then we have computable contributions. If we take the sub-leading part of the diagram to which the standard set attaches, we will be left with a mixture of computable and non-computable contributions.

We represent all the surviving terms using a mixture of algebra and diagrams in figure 13.8. Contributions containing non-computable parts are represented diagrammatically; these are combined with computable contributions

---

<sup>6</sup>If the standard set has external momentum  $l$ , we might worry that we could pick up momentum derivative contributions in the  $l$ -integral from expanding, say,  $A(l-p)$  in  $p$ . However, we could always ensure that the  $l$ -integral is done first in which case, as we know from section 5.4.2, such contributions will vanish.

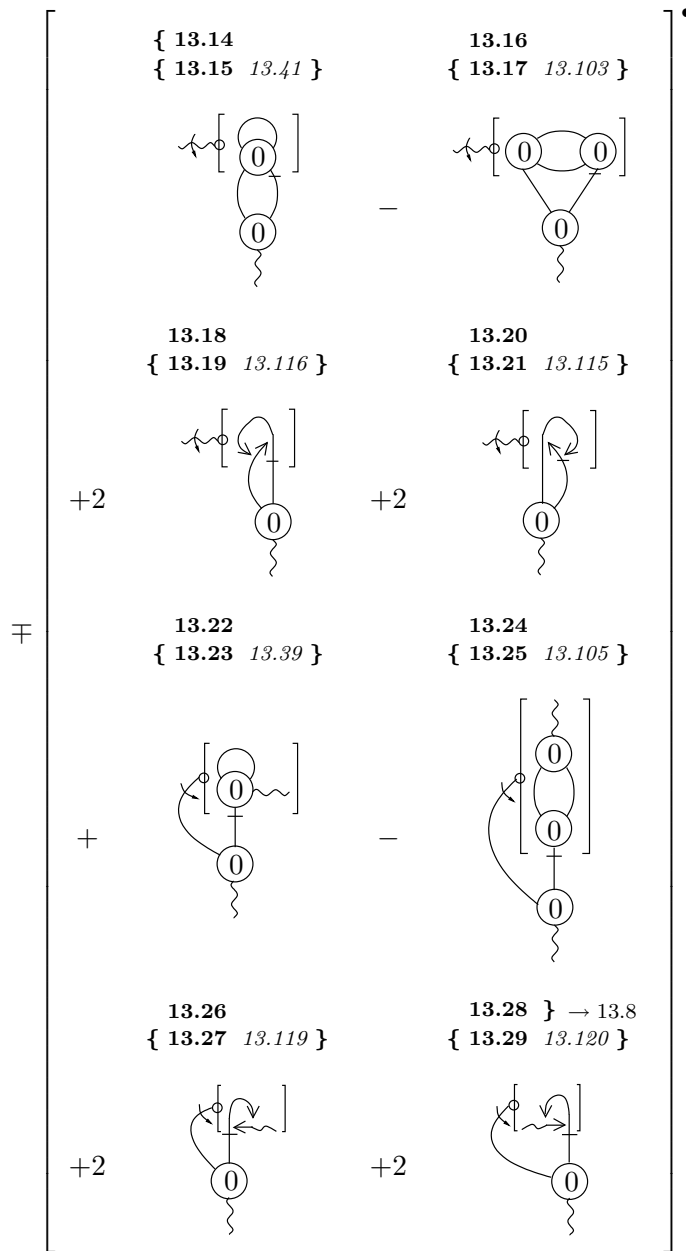


Figure 13.7: Terms we construct to allow us to mirror the cancellations of the previous section.

which take the same diagrammatic form. The remaining computable contributions are represented algebraically, in terms of the undetermined coefficients  $U_i^{a,b}$  and  $V_i^{a,b}$ .

Since non-computable contributions occur only at sub-leading order, we must take a sub-leading contribution from the sub-diagrams to which the standard set attaches. This is denoted by the tag  $\mathcal{O}(\epsilon^0)$ .

There are several things to note. First, is that in all diagrams possessing the tag  $\mathcal{O}(\epsilon^0)$ , we must take the most divergent part of the instance of the standard set to which they attach. Although some of the contributions corresponding to the  $\mathcal{O}(\epsilon^{-1})$  parts of the tagged sub-diagrams are included in 13.37, we cannot include them in the diagrams tagged by  $\mathcal{O}(\epsilon^0)$  by simply removing the tag: this would cause  $a_1$  terms contributing to the standard set to spuriously reappear.

Secondly, the coefficients  $U_0^{a,b}$  and  $V_0^{a,b}$  both vanish, by construction.

Lastly, the coefficients  $U_1^{a,b}$  are easy to compute, since each of the diagrams contributing involves the computable part of the standard set, for which we know the algebraic form. Moreover, to extract these coefficients we can Taylor expand the sub-diagram to which the standard set attaches, in  $p$  (we can not do this for  $V_1^{a,b}$ , which would make life harder if we were to ever evaluate these coefficients).

Using our knowledge of the standard set coefficients  $a_0$ ,  $b_0$  and  $b_1$  (see equations (5.3), (5.4) and (5.5)) we find:

$$U_1^a = \frac{571}{36} - \frac{80\gamma_{\text{EM}}}{3} \quad (13.3)$$

$$U_1^b = -\frac{451}{36} + \frac{80\gamma_{\text{EM}}}{3}. \quad (13.4)$$

It may seem a little odd that  $\gamma_{\text{EM}}$  appears here; this is an artifact of the way in which we have chosen to split up the computable contributions in figure 13.8 between diagrams and algebra. Thus, the diagrams tagged  $\mathcal{O}(\epsilon^0)$ , contain  $\gamma_{\text{EM}}$  in such a way as to exactly cancel the contributions contained in the algebraic coefficients.

### 13.3.2 Generating the Constructed Diagrams

Referring back to the constructed diagrams of the previous section, we show how to cancel the unprocessed diagrams of figure 13.7; in other words, we

$$\begin{aligned}
& \left[ \begin{aligned}
& \mathbf{13.30} \rightarrow 0 \\
& - \left[ \begin{array}{c} \text{Diagram 13.30} \\ \mathcal{O}(\epsilon^0) \end{array} \right] \\
& + \left\{ \mathbf{13.31} \quad \mathbf{13.32} \quad \mathbf{13.33} \right\} \rightarrow \mathbf{13.38} \\
& + \left[ \begin{array}{c} \text{Diagram 13.31} \\ \mathcal{O}(\epsilon^0) \end{array} \right] - 2 \left[ \begin{array}{c} \text{Diagram 13.32} \\ \mathcal{O}(\epsilon^0) \end{array} \right] - 2 \left[ \begin{array}{c} \text{Diagram 13.33} \\ \mathcal{O}(\epsilon^0) \end{array} \right] \\
& + \left[ \begin{array}{c} \left[ \begin{array}{c} \text{Diagram 13.34} \\ \mathcal{O}(\epsilon^0) \end{array} \right] + \left[ \begin{array}{c} \text{Diagram 13.35} \\ \mathcal{O}(\epsilon^0) \end{array} \right] - 2 \left[ \begin{array}{c} \text{Diagram 13.36} \\ \mathcal{O}(\epsilon^0) \end{array} \right] + 2 \left[ \begin{array}{c} \text{Diagram 13.37} \\ \mathcal{O}(\epsilon^0) \end{array} \right] \\
& \times \Delta_{\alpha\beta}^{11}(p) \left[ \begin{array}{c} \left\{ \mathbf{13.34} \quad \mathbf{13.35} \quad \mathbf{13.36} \right\} \rightarrow \mathbf{13.39} \\ \text{Diagram 13.34} - \text{Diagram 13.35} + 4 \text{Diagram 13.36} \\ \alpha \qquad \qquad \qquad \alpha \qquad \qquad \qquad \alpha \end{array} \right] \\
& + \frac{N^2 \Lambda^{-4\epsilon}}{(4\pi)^D} \sum_{i=0}^1 \frac{1}{\epsilon^{i-2}} \left[ \begin{array}{c} \mathbf{13.37} \\ \left( U_i^a + V_i^a \frac{p^{-2\epsilon}}{\Lambda^{-2\epsilon}} \right) p^2 \delta_{\mu\nu} + \left( U_i^b + V_i^b \frac{p^{-2\epsilon}}{\Lambda^{-2\epsilon}} \right) p_\mu p_\nu \end{array} \right]
\end{aligned} \right]
\end{aligned}$$

Figure 13.8: The terms surviving from the analogue of figure 13.5, in which the common one-loop sub-diagram is the standard set.

demonstrate how the constructed diagrams can be generated, naturally.

This generation of terms requires two steps. We begin by processing a set of  $\Lambda$ -derivative diagrams. The simplest of these—the IR finite diagram 12.42—can be dealt with by diagrammatic Taylor expansion. Having been manipulated, we immediately find two of the desired cancellations.

However, the remaining diagrams of this section are not manifestly finite and so we must construct subtractions (see section 5.4). The corresponding additions are not of the right form to cancel the rest of the unprocessed terms of the previous section, and so we must move on to the second step of our procedure. This involves the diagrammatic manipulation of a subset of the additions. This completes the generation of the terms we are looking for.

We conclude this section by manipulating the semi-computable terms formed by combining parent diagrams with their subtractions. We choose to do this here, as these manipulations are very similar to those which we perform on the additions.

### Manipulation of $\Lambda$ -derivative Terms

The first diagram aside, the treatment of terms in this section requires the construction of subtractions. As we will see, for certain diagrams there is no unique way in which to do this. However, since we know the set of terms we are ultimately trying to generate, we can use this as a guide. Of course, the ultimate effect of constructing any particular set of subtractions and their corresponding additions must be the same: all we are really doing is adding zero to the calculation in a convenient form. The point is that by a cunning choice of subtraction, we can generate a set of terms which are manifestly of the form we desire.

**Diagram 12.42** To manipulate diagram 12.42, we note that it is manifestly finite, after differentiation with respect to  $\Lambda|_\alpha$ . Taking the simple loop of this diagram to carry momentum  $k$  and the other loop to carry  $l$ , we are forced to take a single power of either  $l$  or  $p$  from both the three-point and five-point vertices. This is shown in figure 13.9.

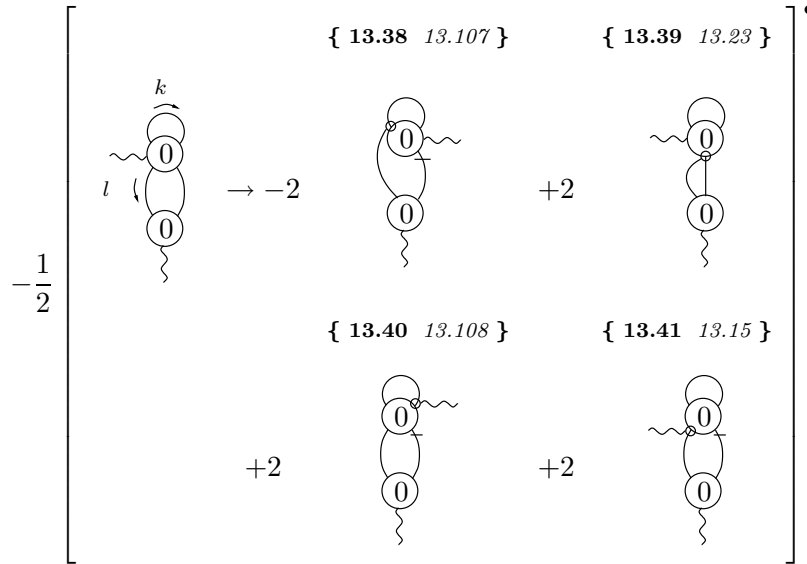


Figure 13.9: Manipulation of diagram 12.42 under  $\Lambda\partial_\Lambda|_\alpha$ .

Diagrams 13.38–13.41 constitute a momentum derivative of a vertex which belongs to an instance of the first element of the standard set. Diagrams 13.39 and 13.41 are the analogues of diagrams I.86 and I.85 and, as we might hope, are involved in cancellations against some of the terms that we constructed in the last section. We note that a key feature of the first element of the standard set is that the effective propagator forming the loop does not carry the external momentum of the diagram. Hence, the momentum derivatives in diagrams 13.39 and 13.41 can be taken to strike the whole of the sub-diagram of which they currently strike only part.

**Cancellation 13.1** *Diagram 13.39 exactly cancels diagram 13.23.*

**Cancellation 13.2** *Diagram 13.41 exactly cancels diagram 13.15.*

Diagrams 13.38 and 13.40, on the other hand, have no analogue that we have encountered already: the momentum derivative in these diagrams is not with respect to the external momentum of the one-loop sub-diagram which they strike.

**Diagram 12.43** Diagram 12.43 is the first term for which we construct subtractions, and it is one for which we can choose different ways in which to do

this. Rather than considering diagram 12.43 as is, we will—for reasons which will become apparent—explicitly consider two different momentum routings. Whilst these diagrams are, of course, equivalent by momentum rerouting invariance, they guide us to different subtractions, as shown in figure 13.10.

The reason for constructing the subtractions in this manner is now hopefully apparent: diagrams 13.44, 13.46, 13.51 and 13.53 can be very nearly combined into a momentum derivative of the second element of the standard set (we are currently missing the diagram in which the momentum derivative strikes the effective propagators). Had we only constructed subtractions 13.43–13.47, this would not have been manifestly obvious.

To begin the analysis of diagram 13.42 and its subtractions, we focus on the three-legged sub-diagram carrying loop momentum  $k$ . For the diagram as a whole to have any chance of surviving in the  $\epsilon \rightarrow 0$  limit, the (internal) legs leaving the sub-diagram must be in the  $A$ -sector. Thus, by Lorentz invariance, the sub-diagram carrying loop momentum  $k$  must go as odd powers of momentum (up to additional non-Taylor expandable functions of  $l$ ). Noting that, in  $D = 4$ , the sub-diagram carrying loop momentum  $k$  goes as, at worst,  $(\ln l) \times \mathcal{O}(\text{mom}, \dots)$  in the IR, it is clear that we must take only the  $\mathcal{O}(\text{mom})$  part of the sub-diagram.

The effect of diagrams 13.43 and 13.45 is now immediately clear: they completely remove from diagram 13.42 all contributions in which the sub-diagram carrying loop momentum  $k$  goes as  $l$ .

Let us now suppose that we take  $\mathcal{O}(p)$  from the sub-diagram carrying loop momentum  $k$ . We start by noting that the only place for this power of  $p$  to come from is the four-point vertex. Now, if all the fields leaving the four-point vertex are in the  $A$ -sector, then Lorentz invariance forces us to take an additional power of momentum from the four-point vertex. Recalling that we should not take any further powers of  $l$  or  $p$ , we see that we must take (at least) one power of  $k$  from the four-point vertex (and a further power of  $k$  from the 3pt). The  $k$ -integral is now Taylor expandable in  $l$ . In the case that the  $k$ -dependent fields leaving the four-point vertex are not in the  $A$ -sector, the  $k$ -integral is trivially Taylor expandable in  $l$ .

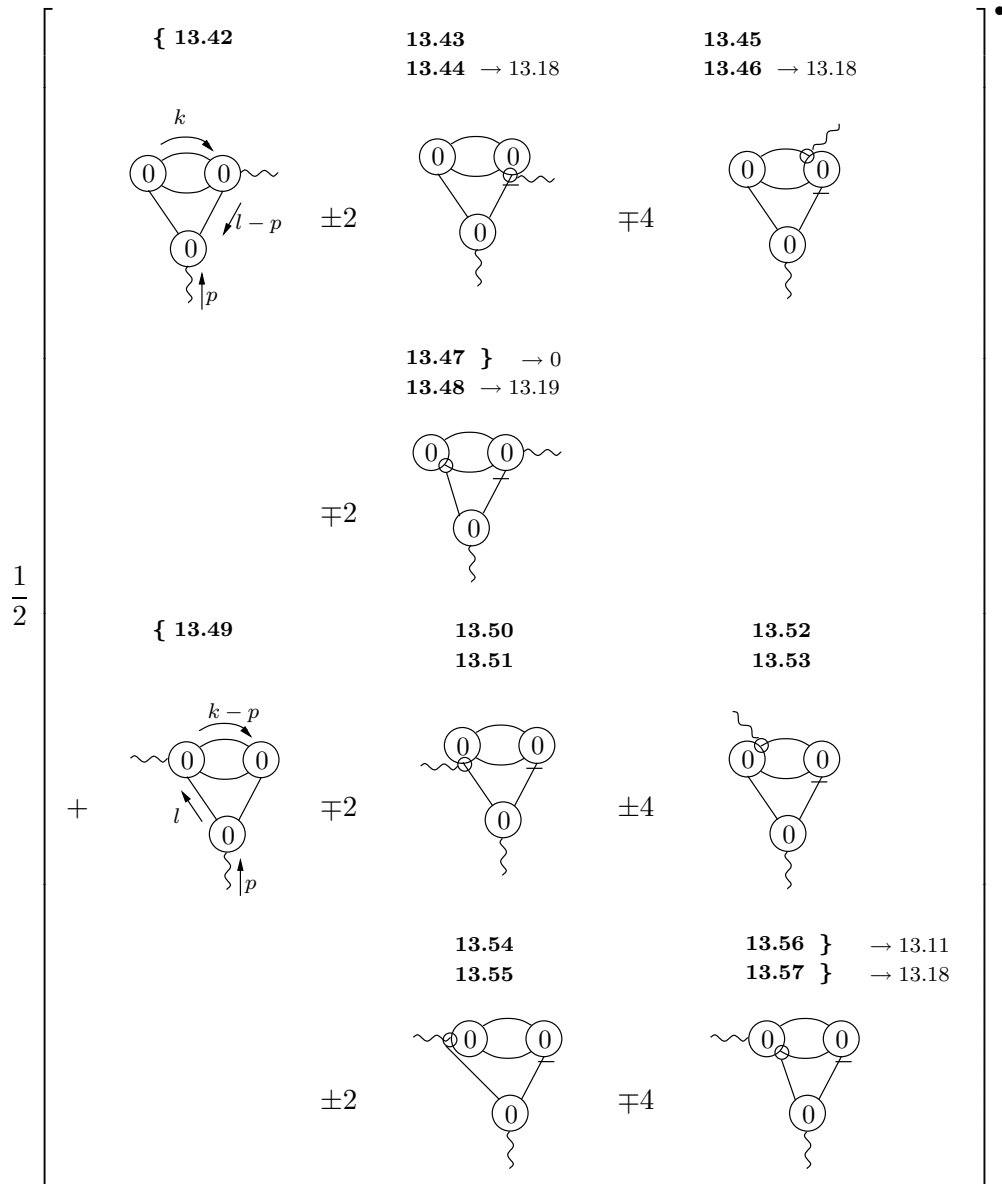


Figure 13.10: Diagram 12.43 and its subtractions. The two diagrams on the LHS are copies of diagram 12.43 with differing momentum routings (hence the overall factor of  $1/2$ ).

The remaining subtraction, diagram 13.47, removes all these contributions; hence diagram 13.42 turns out to be completely cancelled by its subtractions.

The same cannot, however, be said for diagram 13.49. It is clear that whilst diagrams 13.50 and 13.52 remove from 13.49 all contributions from the  $k$ -integral that are Taylor expandable in  $p$ , these diagrams possess components which are not Taylor expandable in  $p$  and so will survive. Diagrams 13.54 and 13.56 remove all contributions that are Taylor expandable in  $l$  (as always, this statement is correct only up to contributions that vanish anyway in the  $\epsilon \rightarrow 0$  limit). Non-computable contributions from the  $k$ -integral are precisely those which are Taylor expandable in  $l$  and  $p$  and so cancel between the parent diagram and its subtractions.

Figure 13.11 shows the surviving contributions to diagrams 13.49, 13.50, 13.52, 13.54 and 13.56.

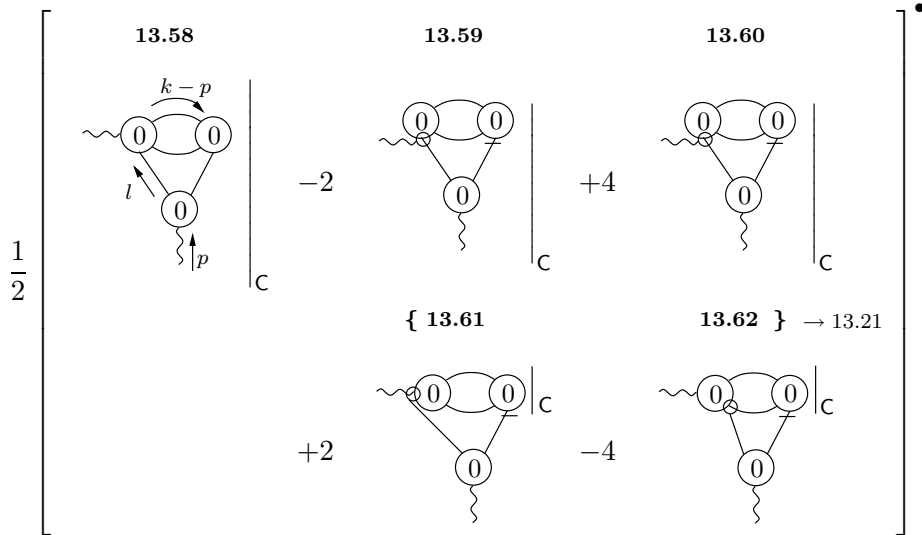


Figure 13.11: The cancellation of non-computable contributions between diagram 13.49 and its subtractions. The C symbol has been expanded to cover the whole of the first three diagrams, which is valid up to corrections which vanish in the  $\epsilon \rightarrow 0$  limit.

We conclude the treatment of diagram 12.43 by discussing whether or not it is necessary to consider derivatives of cutoff functions (or other functions), since we found in section 5.4.2 that such objects can, in principle, contribute.

Any such derivatives arising from the sub-diagram carrying loop momentum  $k$  will cancel between parent and subtractions, since the accompanying powers of momentum render the  $k$  integral Taylor expandable in  $l$  and  $p$ .

Next, we must consider derivatives arising in the  $l$ -integral. If we Taylor expand the  $p$  dependent cutoff function to yield  $p.lA'(l)$ , then the  $k$  integral becomes Taylor expandable in  $p$ , to the order in  $p$  to which we are working. Hence, such contributions will have been cancelled.

These points lead us directly to consider some of the subtleties involved in precisely what we mean by C. As we have just discussed, there is no need for us to consider derivatives of cutoff functions. Now, if the  $k$ -integral is the outer integral, then it is regulated by  $A(k-p)A(l-k)$  which we can simply Taylor expand to zeroth order in  $p$  and  $l$ . Doing this, of course, causes the diagram to lose invariance under momentum routing. Indeed, to maintain this invariance—at least up to  $\mathcal{O}(\epsilon^0)$ —it would be necessary for us to keep the terms  $l.kA'(k)$  and  $k.pA'(k)$  (which will provide a computable contribution at  $\mathcal{O}(\epsilon^0)$ ) from the Taylor expansion of the cutoff functions.<sup>7</sup>

Knowing that the contributions from these terms will be removed by the subtractions, we can drop them as long as we ensure that the form we choose for the four-point vertex is consistent between parent diagram and subtractions. This last point is important. We know from section 3.2.4 that the differences between the alternative forms of the four-point vertex disappear as a consequence of the freedom to reroute momenta. Here, then, we must take real care.

There are several ways to proceed. On the one hand, we could ensure that the choice of four point vertex must be consistent between parent and *both* the factorisable and non-factorisable subtractions which involves making sure that all dummy indices match up, in all diagrams. On the other hand, we can make sure that we keep the first order terms in the Taylor expansion of both  $A(k-p)$  and  $A(l-k)$  so that then we can forget about the consistency of the four-point vertices, as we have restored momentum rerouting invariance up to the required order in  $\epsilon$ . Alternatively, we could Taylor expand (say)  $A(l-k)$

---

<sup>7</sup>Recall that taking more than a single power of either  $l$  or  $p$  from the sub-diagram carrying loop momentum  $k$  will kill the diagram as a whole.

to zeroth order only and choose the four-point vertex to be consistent between parent and non-factorisable subtraction. Then we would only need to keep  $k.pA'(k)$ . Either way, these points demonstrate the subtleties of interpreting C and the danger of trying to apply C to a single diagram.

**Diagram 12.45** Diagram 12.45 is shown, together with its subtractions, in figure 13.12.

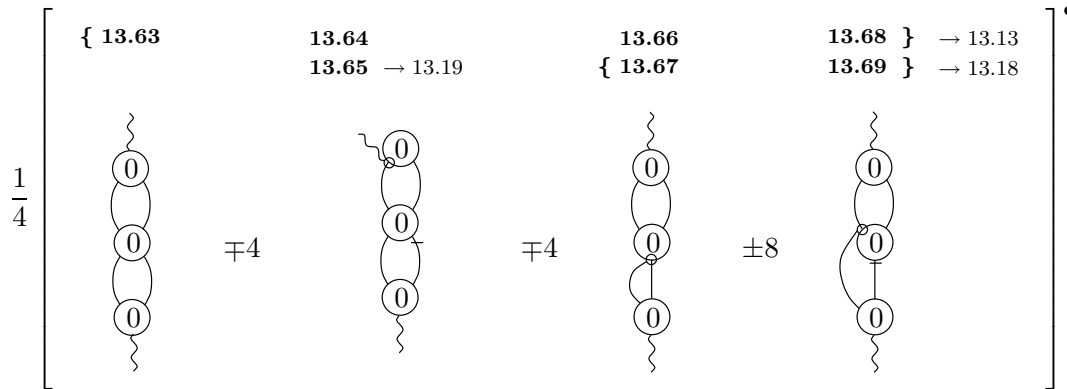


Figure 13.12: Diagram 12.45 and its subtractions.

To construct the subtractions, we must take into account the symmetry of the parent diagram. For example, the first subtraction, diagram 13.64, is designed to remove non-computable contributions arising when one of the sub-diagrams is Taylor expandable in  $p$ . Since it could be either of the sub-diagrams which is Taylor expandable in  $p$ , this gives rise to factor of two in addition to the usual factor coming from charge conjugation symmetry. The effect of the subtractions is shown in figure 13.13.

**Diagram 12.46** As in the previous case, we must take into account the symmetry of the diagram, when constructing the subtractions. Figures 13.14 and 13.15 show the construction of the subtractions and their effects on the parent diagram. Note that we have extended the influence of C to cover the whole of diagrams 13.78 and 13.79, which is valid up to  $\mathcal{O}(\epsilon)$  corrections.

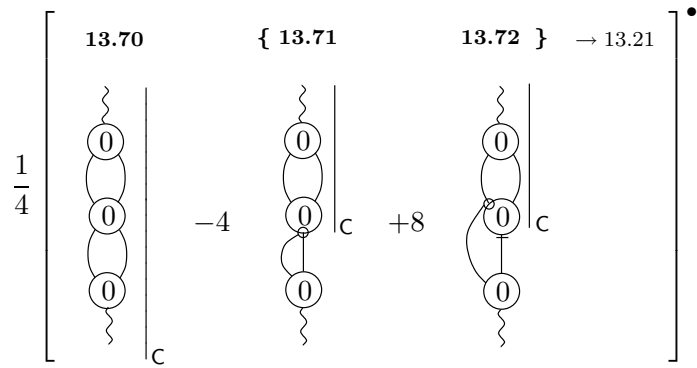


Figure 13.13: The cancellation of non-computable contributions between diagram 13.63 and its subtractions.

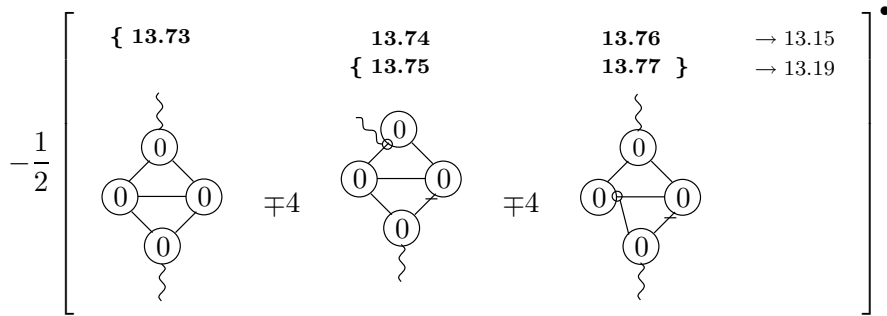


Figure 13.14: Diagram 12.46 and its subtractions.

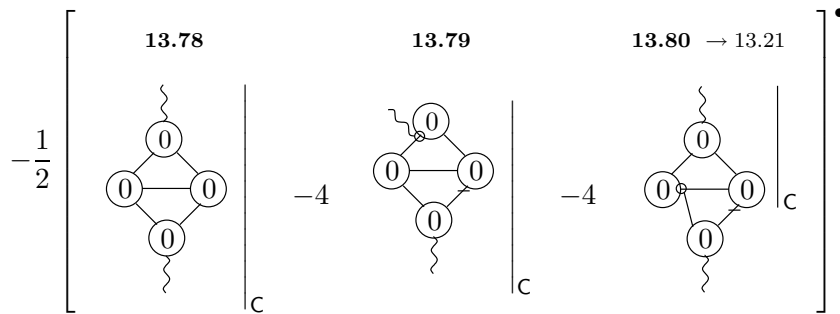


Figure 13.15: The cancellation of non-computable contributions between diagram 13.73 and its subtractions.

**Diagram 12.47** Diagram 12.47 is another example of a case where we must be somewhat sneaky in the choice our subtractions. As with diagram 12.43, we split the parent diagram into two copies, with differing momentum routings, and construct subtractions for each. This is shown in figure 13.16. Note that, although the diagrammatics is unambiguous, we have explicitly indicated the momentum routing for the subtractions.

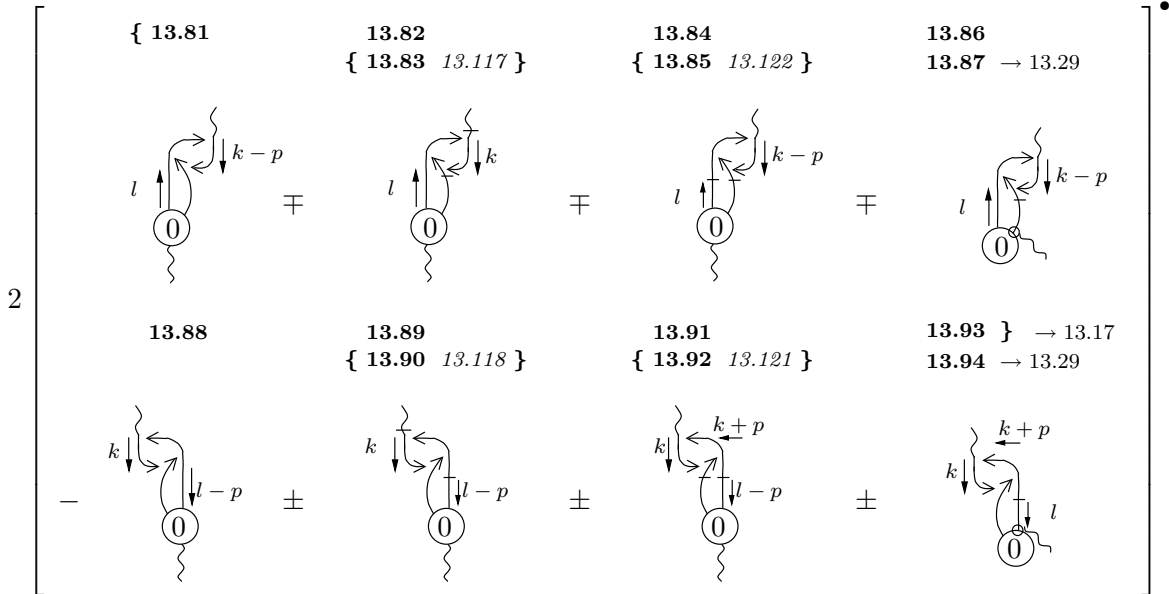


Figure 13.16: Diagram 12.47 and its subtractions.

The pattern of subtractions demands comment. To understand them, it suffices to focus on the three-legged sub-diagram, carrying loop momentum  $k$ , of diagram 13.81. The components of this diagram that are Taylor expandable in  $p$  or  $k$  are subtracted off by diagrams 13.82 and 13.84, respectively. The surviving non-Taylor expandable components fall into two classes. First, there are those which survive only at small  $l$ —in this case, the entire diagram gives a computable contribution, up to  $\mathcal{O}(\epsilon)$  corrections. However, there are also contributions which survive at large  $l$ . These non-computable contributions are removed by diagram 13.86.

The structure of subtractions perhaps seems different from the previous two cases. However, for diagrams 12.45 and 12.46 we were able to exploit symmetry to reduce the number of subtractions; in other words, the analogue

of diagram 13.86 exists in these cases, but can simply be combined with the analogue of diagrams 13.82 and 13.84.

Figure 13.17 shows the cancellation of non-computable contributions between the parents and subtractions of figure 13.16. Notice that, in all bar diagrams 13.97 and 13.101 we are able to extend the influence of  $C$  to cover the entire diagram, up to terms which vanish as  $\epsilon \rightarrow 0$ .

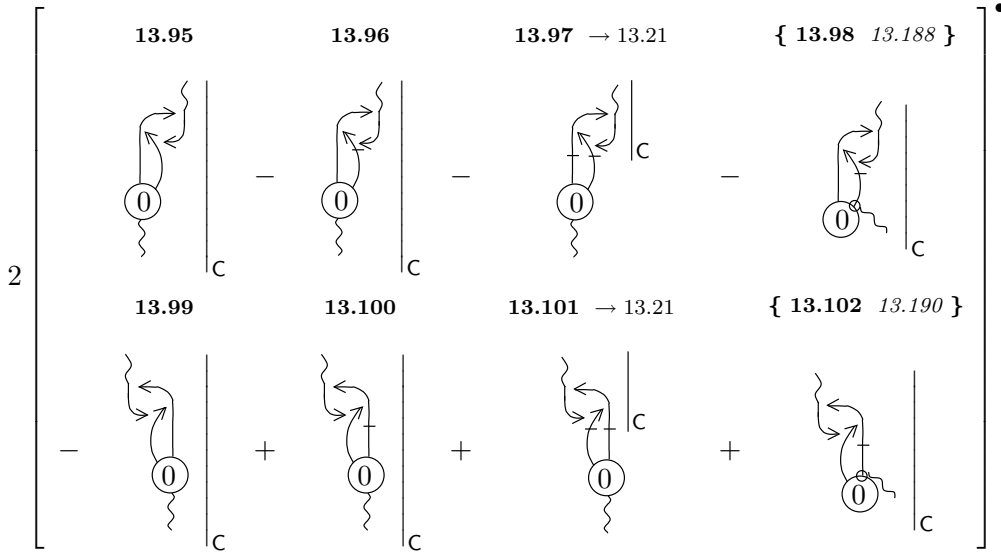


Figure 13.17: The terms remaining after cancellation of non-computable contributions to diagrams 13.81 and diagram 13.88 by their subtractions.

### Manipulation of Additions

Having completed the construction of subtractions for this section, we note that diagrams 13.48, 13.65, 13.75 and 13.77 can be manipulated, using diagrammatic identity 5.<sup>8</sup> However, in preparation for this, we choose first to combine some of the non-manipulable additions.

We can, up to a missing term and a discarded total momentum derivative, combine diagrams 13.44, 13.46, 13.51 and 13.53 such that they cancel diagram 13.17. In turn, this missing term will be generated when we process

<sup>8</sup>It is also true that diagrams 13.87 and 13.94 could be manipulated in this way. However, the resulting gauge remainders are trapped. It is more efficient to construct subtractions for these diagrams first, and then manipulate them, rather than doing things the other way around.

the manipulable additions. Likewise, we can combine diagrams 13.55, 13.57, 13.67 and 13.69 such that they cancel diagram 13.25, up to a missing term which will shortly be generated and a discarded total momentum derivative. This recasting of terms is shown in figure 13.18.

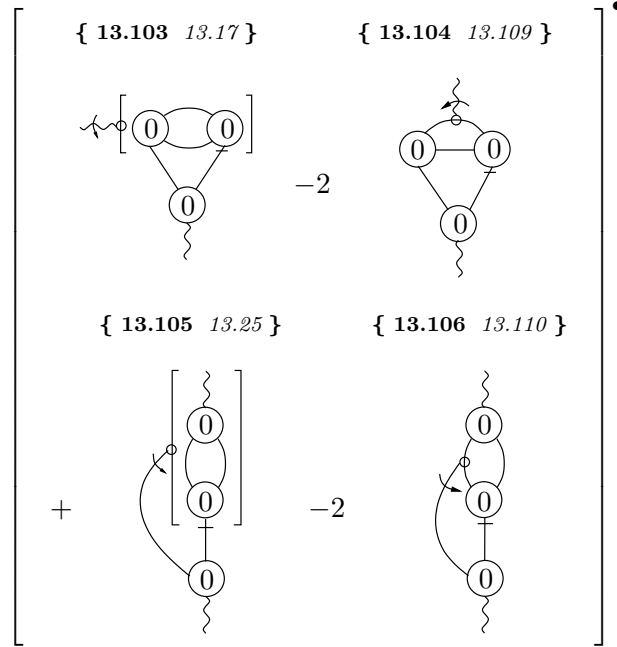


Figure 13.18: The first two diagrams are a re-expression of diagrams 13.44, 13.46, 13.51 and 13.53 and the final two are a re-expression of diagrams 13.55, 13.57, 13.67 and 13.69.

As hoped, we find two cancellations.

**Cancellation 13.3** *Diagram 13.103 exactly cancels diagram 13.17.*

**Cancellation 13.4** *Diagram 13.105 exactly cancels diagram 13.25.*

Now we turn to the diagrammatic manipulation of the aforementioned additions. The final result of this procedure—where we have processed all gauge remainders—is split between figures 13.19 and 13.20.

It looks as though we may have missed some simplifications. In particular, diagrams 13.134–13.137 possess an  $\mathcal{O}(p^2)$  stub, which we might hope will allow

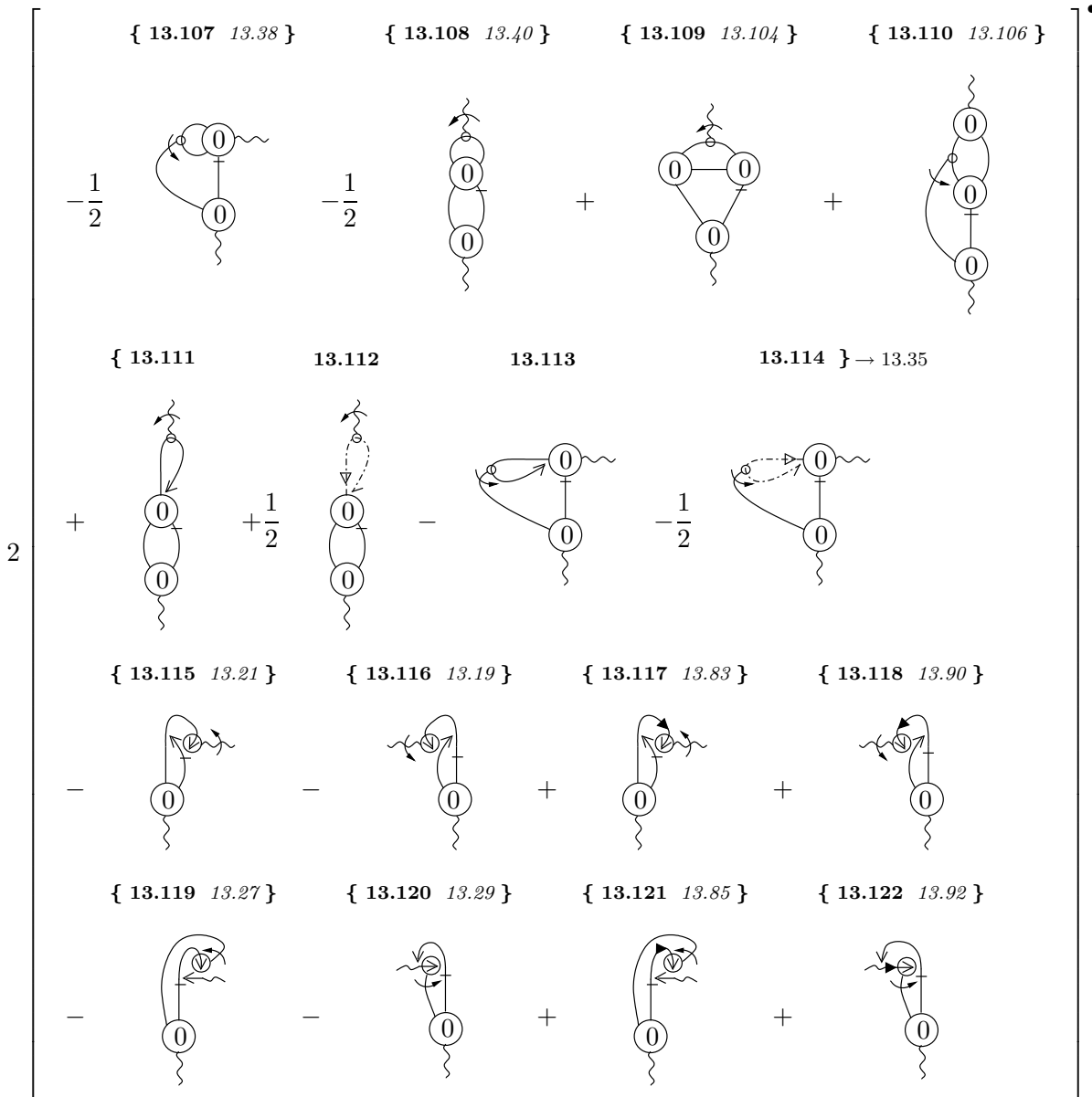


Figure 13.19: The result of the diagrammatic manipulation of diagrams 13.48, 13.65, 13.75 and 13.77—part I.

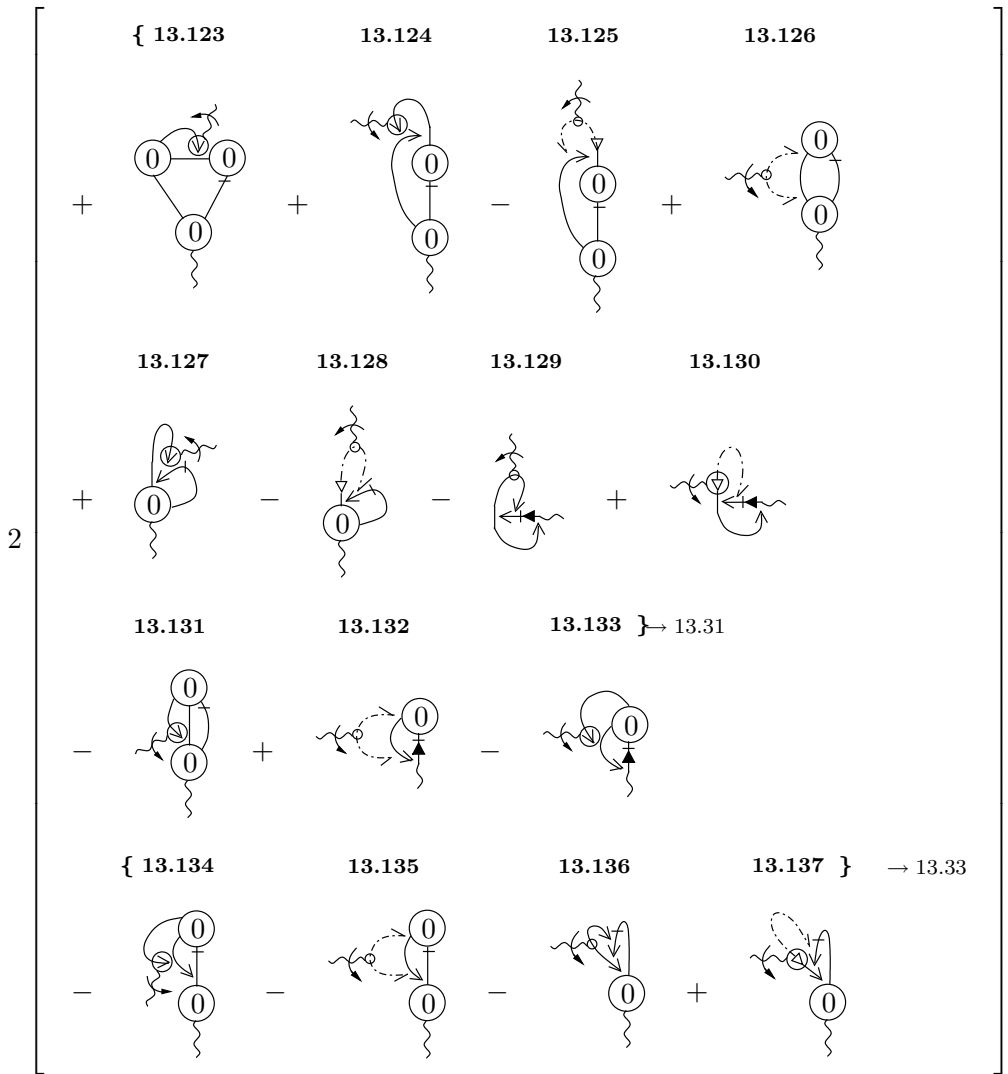


Figure 13.20: The result of the diagrammatic manipulation of diagrams 13.48, 13.65, 13.75 and 13.77—part II.

us to remove the discontinuity in momentum arguments. This discontinuity occurs where an effective propagator carrying momentum, say  $k - p$ , attaches to structures which have been Taylor expanded in  $p$ . However, we cannot set  $p = 0$  in the denominator of the effective propagator, since  $p$  provides IR regularisation for the  $k$ -integral. Hence, we cannot simplify these diagrams.

As promised, we cancel the remaining unprocessed diagrams from figure 13.7.

**Cancellation 13.5** *Diagram 13.115 cancels diagram 13.21, up to a discarded total momentum derivative.*

**Cancellation 13.6** *Diagram 13.116 cancels diagram 13.19, up to a discarded total momentum derivative.*

**Cancellation 13.7** *Diagram 13.119 cancels diagram 13.27, up to a discarded total momentum derivative.*

**Cancellation 13.8** *Diagram 13.120 cancels diagram 13.29, up to a discarded total momentum derivative.*

A comment about these cancellations is in order. Consider the momentum derivative in diagrams 13.115, 13.116, 13.119 and 13.120. As drawn, each momentum derivative strikes part of the sub-diagram. However, we can take this momentum derivative to strike the whole of the sub-diagram, where this derivative is with respect to the sub-diagram's external momentum. This step is correct up to a total momentum derivative with respect to the sub-diagram's loop momentum (see section 3.2.4). However, we know that such total momentum derivative terms can be discarded [6].

The two surviving diagrams from figure 13.18 are removed.

**Cancellation 13.9** *Diagram 13.109 exactly cancels diagram 13.104.*

**Cancellation 13.10** *Diagram 13.110 exactly cancels diagram 13.106.*

Finally, we get six bonus cancellations.

**Cancellation 13.11** *Diagram 13.107 cancels diagram 13.38, up to a discarded total momentum derivative.*

**Cancellation 13.12** *Diagram 13.108 cancels diagram 13.40, up to a discarded total momentum derivative.*

**Cancellation 13.13** *Diagram 13.117 exactly cancels diagram 13.83 courtesy of diagrammatic identity 14.*

**Cancellation 13.14** *Diagram 13.118 exactly cancels diagram 13.90 courtesy of diagrammatic identity 14.*

**Cancellation 13.15** *Diagram 13.121 exactly cancels diagram 13.85 courtesy of diagrammatic identity 14.*

**Cancellation 13.16** *Diagram 13.122 exactly cancels diagram 13.92 courtesy of diagrammatic identity 14.*

### **Manipulation of Semi-Computable Terms**

We conclude this section by manipulating the semi-computable partners of the additions which were manipulated in the previous section. Note, though, that not all of the additions have semi-computable partners: in the case where the loop integrals of a semi-computable diagram do not factorise, the  $\mathbb{C}$  can be extended to cover the entire diagram. We choose not to manipulate these terms as we can just compute them, directly; we comment on this further in section 13.5.3.

For the terms whose loop integrals factorise, we focus on the computable sub-diagrams. Ideally, we would like to manipulate these. However, by doing so we generate diagrams where we would like to have kept momentum derivatives of cutoff functions (see section 5.4.2). Hence, what we choose to do is split the computable part of the semi-computable terms into  $\mathcal{O}(\epsilon^{-1})$  and  $\mathcal{O}(\epsilon^0)$  components. We can then manipulate the former, keeping only the  $\mathcal{O}(\epsilon^{-1})$  part of the resultant terms. We leave the  $\mathcal{O}(\epsilon^0)$  components un-manipulated. Again, this will be commented on in section 13.5.3.

Figure 13.21 shows the result of this procedure.

Since, in diagrams 13.143–13.149 we take the  $\mathcal{O}(\epsilon^0)$  part of the topmost sub-diagram, we are compelled to take the most divergent contribution from

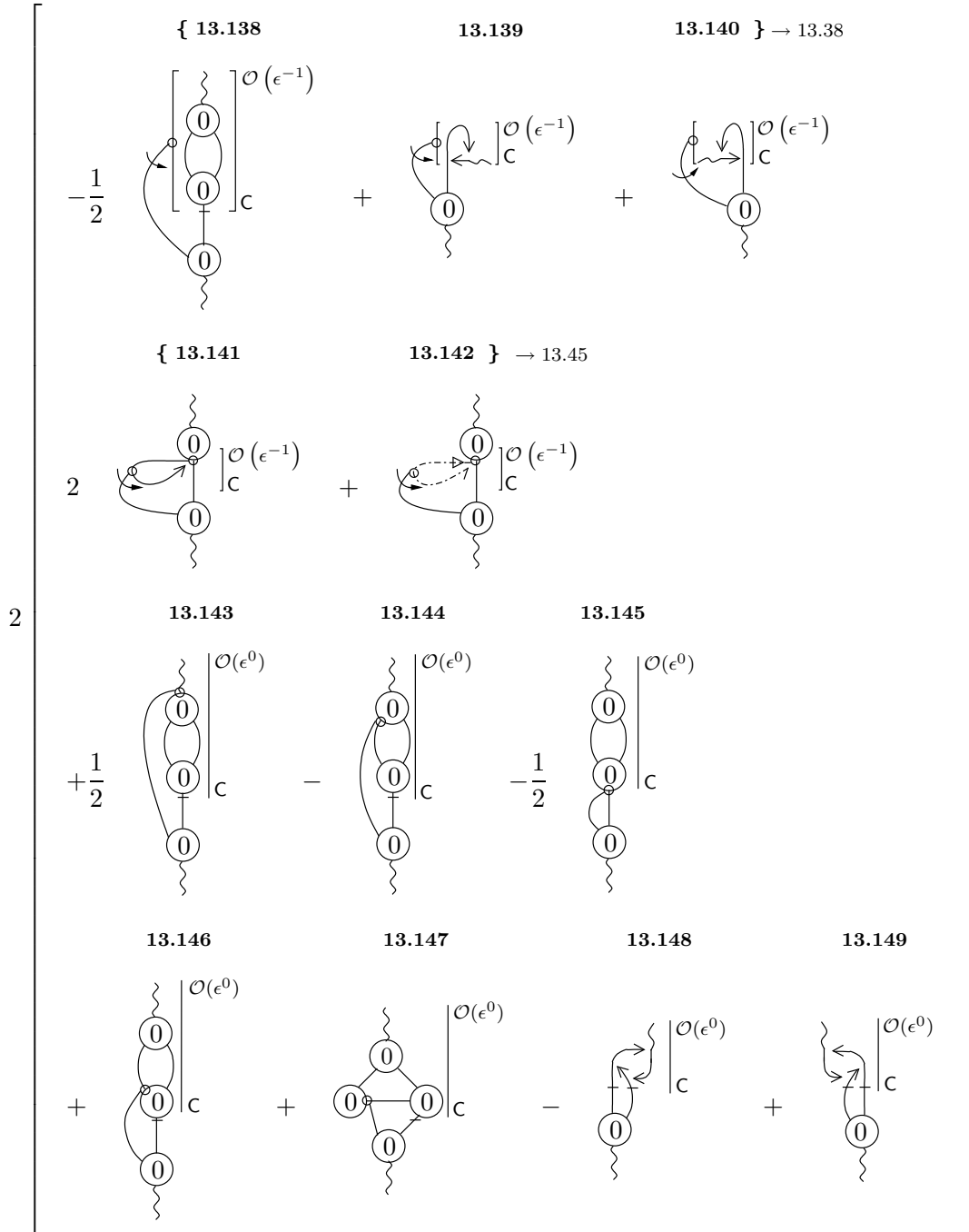


Figure 13.21: The result of processing diagrams 13.61, 13.62, 13.71, 13.72, 13.80, 13.97 and 13.101.

the bottom diagram, up to terms which vanish as  $\epsilon \rightarrow 0$ . Consequently, these seven diagrams are computable.

## 13.4 Further Subtractions

In this section, we construct two further sets of subtractions. First, we do this for the remaining  $\Lambda$ -derivative terms generated in chapter 12. Secondly, we note that we can construct ‘second level’ subtractions, for a number of the terms generated in section 13.3.

### 13.4.1 Subtractions for Terms Generated in Chapter 12

**Diagrams 12.64–12.67** To generate the subtractions for the four diagrams analysed in this section will require a minor development of the current formalism.

In the subsequent analysis, we need look only at the first two diagrams, since all conclusions drawn will apply to the other pair, as well. We will suppose that the effective propagator which terminates in a processed gauge remainder which is differentiated with respect to momentum carries loop momentum  $l$ . We will take the other loop momentum to be  $k$ . (See also figure 13.22.) In order for the diagrams to have any chance of surviving, the effective propagator carrying momentum  $l$  must be in the  $A$ -sector. If this is the case, then diagrams 12.64 and 12.65 become algebraically equivalent; likewise for diagrams 12.66 and 12.67. Consequently, for the following analysis, we will replace diagram 12.65 (12.67) with twice diagram 12.64 (12.66). This step is valid, up to  $\mathcal{O}(\epsilon)$  corrections.

With the diagrams partially in the  $A$ -sector—as just described—it is clear that, by Lorentz invariance, the  $k$ -integral must go as odd powers of  $l$  (up to additional factors of  $l^{-2\epsilon}$ ). For the diagram to survive, we take just the single power of  $l$ . Given that we wish to cancel off terms for which the  $k$ -integral is Taylor expandable in  $l$ , we construct our subtraction such that it contains

$$l \cdot \partial^l F(l - k)|_{l=0}. \quad (13.5)$$

where  $F$  is the structure which depends on  $l - k$ ; precisely which structure this

is will depend on the momentum routing. This expression can be rewritten as

$$-l \cdot \partial^k F(-k).$$

Given that we want to be able to construct the same subtraction, irrespective of the momentum routing of the parent, we must use the prescription that, in the  $k$ -integral, *we keep derivatives of cutoff functions, if they appear*. Hence, we construct the subtractions as shown in figure 13.22; we are free to move the  $\partial^k$  from gauge-remainder to effective propagator at the expense of a minus sign.

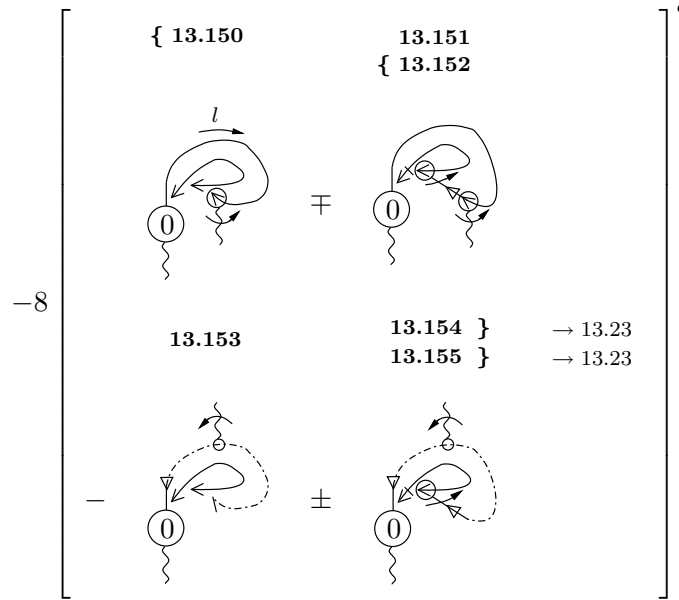


Figure 13.22: Diagrams 12.65, 12.64, 12.67 and 12.66 and their subtractions. The first pair of diagrams have been combined into a single term, with an additional factor of two. Likewise, for the second pair.

Note that in the subtractions, the dummy field leaving the vertex is implicitly in the  $A$ -sector. This is because the only fields which can attach to circles denoting momentum derivatives are in the  $A$ -sector.

Figure 13.23 shows both the cancellation of non-computable components between parent and subtraction and the subsequent cancellation between the computable part of the subtraction and the addition. This is different from the way in which we treated additions and subtractions in the previous section,

where we chose to keep them apart. Note that the NC of diagrams 13.157 and 13.159 refers just to the ‘innermost’ sub-diagram.

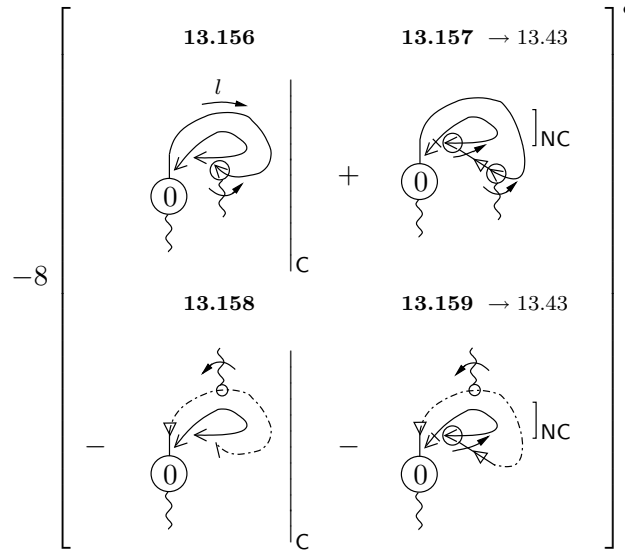


Figure 13.23: The cancellation of contributions between the diagrams of figure 13.22. Two steps have been performed on the RHS: first, non-computable contributions have been cancelled between parent and subtraction; second, diagrams 13.152 and 13.155 have been added.

**Diagrams 12.49 and 12.50** The analysis of diagrams 12.49 and 12.50 requires the techniques of the previous section. Similarly, we can choose to keep just one of the diagrams (12.49) and multiply by two. This is because the two gauge remainders attached to external fields must be in the  $A^1$ -sector for the diagrams not to vanish. Now let us examine the consequences of this for the remaining gauge remainders, both of which are attached to an internal field. The one which bites a gauge remainder attached to an external field must also be in the  $A^1$  sector. The final gauge remainder can either be in the  $A^1$  or  $B$ -sector.

Once again, it is necessary for the subtraction to contain a term of the form given by equation (13.5). We can simplify the diagrammatics using a trick most easily seen with the momentum routing such that the gauge remainder on the ‘inside’ of diagram 12.49 carries  $l - k$  (see also figure 13.24). This gauge remainder, which can be in any sector, is contracted into the gauge remainder

$l_\alpha/l^2$ , at the other end of the effective propagator. Now,

$$l \cdot \partial^l [(l-k)'_\alpha]_{l=0} \frac{l_\alpha}{l^2} = \partial^k \cdot (k').$$

Rather than constructing the subtraction such that the  $k$ -integral contains no indices whereas the  $l$ -integral possesses both  $\mu$  and  $\nu$ , we use Lorentz invariance to draw the diagram in an equivalent, but more intuitive form. Figure 13.24 comprises two separate parts. The first part shows the construction of the subtraction. The second part shows both the cancellation of non-computable components between parent and subtraction and the subsequent cancellation between the computable part of the subtraction and the addition.

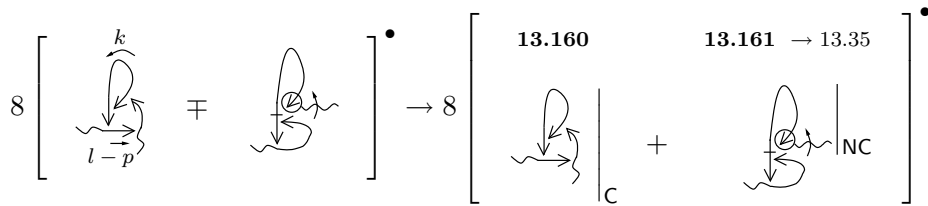


Figure 13.24: The LHS of the figure shows diagrams 12.49, 12.50 and their subtractions. The parent diagrams have been combined into a single term, with an additional factor of two. The right hand side shows the cancellation of contributions between the three diagrams of the RHS.

There is a curious feature to the parent and its subtraction that deserves comment. In the parent, the gauge remainders carrying  $l$  or  $l-p$  can always be chosen to be in the  $A$ -sector. UV regularisation is provided by the  $l-k$  gauge-remainder being in the  $F$ -sector. However, in the subtraction term, we cannot throw away the  $F$ -sector part of the  $l$ -dependent (factorisable) sub-diagram. Such details concerning the regularisation will not, of course affect the universal quantity which we ultimately compute.

**Diagram 12.51** Due to the symmetry of diagram 12.51, the subtraction comes with a relative factor of two. Figure 13.25 shows both the construction of the subtraction and the cancellation of terms between parent, subtraction and addition.

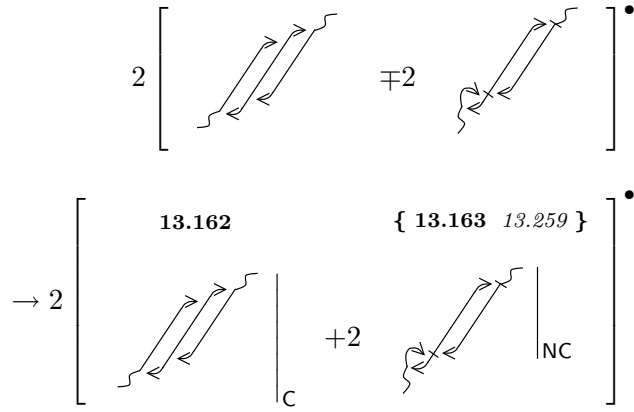


Figure 13.25: The top row of the figure shows diagram 12.51 and its subtraction. The bottom shows the cancellation of contributions between all three diagrams of the top row.

**Diagrams 12.68–12.72** The subtractions for diagrams 12.68–12.72 are shown in figure 13.26.

In figure 13.27 we combine both the subtractions and additions with their corresponding parent diagrams.

### 13.4.2 Subtractions for Terms Generated in Section 13.3

**Diagrams 13.87 and 13.94** Figure 13.28 shows the subtractions for diagrams 13.87 and 13.94.

Figure 13.29 shows the result of adding the subtractions of figure 13.28 to their parents.

At this stage, we find two cancellations. Whilst cancellations are always welcome, these turn out to be between diagrams under the influence of  $C$ ; hence, they do not help us to demonstrate the computability of  $\beta_2$ .

**Cancellation 13.17** *Diagram 13.188 exactly cancels diagram 13.98.*

**Cancellation 13.18** *Diagram 13.190 exactly cancels diagram 13.102.*

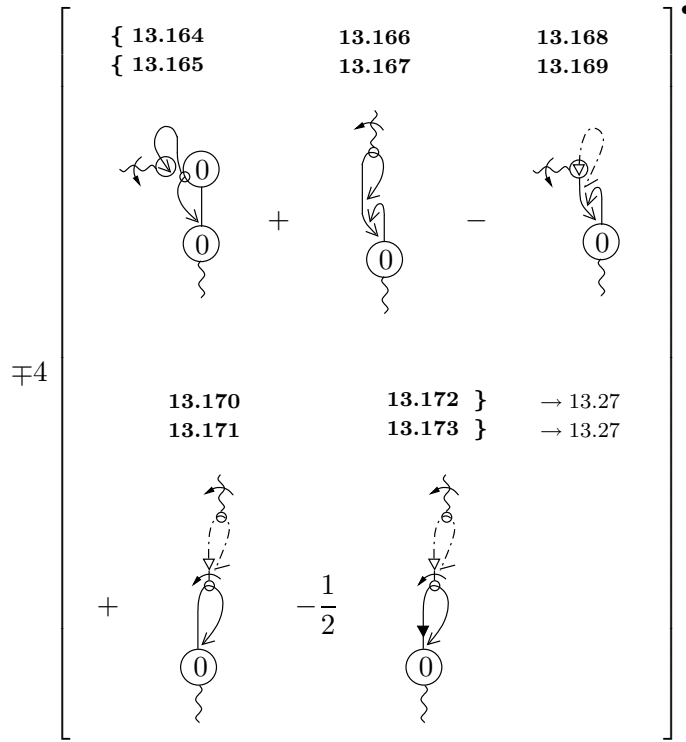


Figure 13.26: Subtractions (and additions) for diagrams 12.68–12.72.

**Diagrams 13.123–13.133** Figure 13.30 shows the construction of subtractions for diagrams 13.123–13.133.

Figures 13.31 and 13.32 show the result of combining both the subtractions and additions of figure 13.30 with their parents.

**Diagrams 13.134–13.137** The construction of subtractions for diagrams 13.134–13.137 is straightforward, since it almost exactly mirrors the construction of subtractions for diagrams 12.68–12.72, which we have done already. The primary difference between the diagrams we treat here and those we have treated already is the presence of a discontinuity in momentum arguments. Specifically, diagrams 13.134–13.137 each possess a bar, indicating that we have not set  $p = 0$  in the denominator of the ( $A$ -sector) effective propagator joined to the two-point, tree level vertex.

However, we can ignore the bar, for the purposes of constructing subtractions. The point is that  $p$  acts as an IR regulator only if we take computable

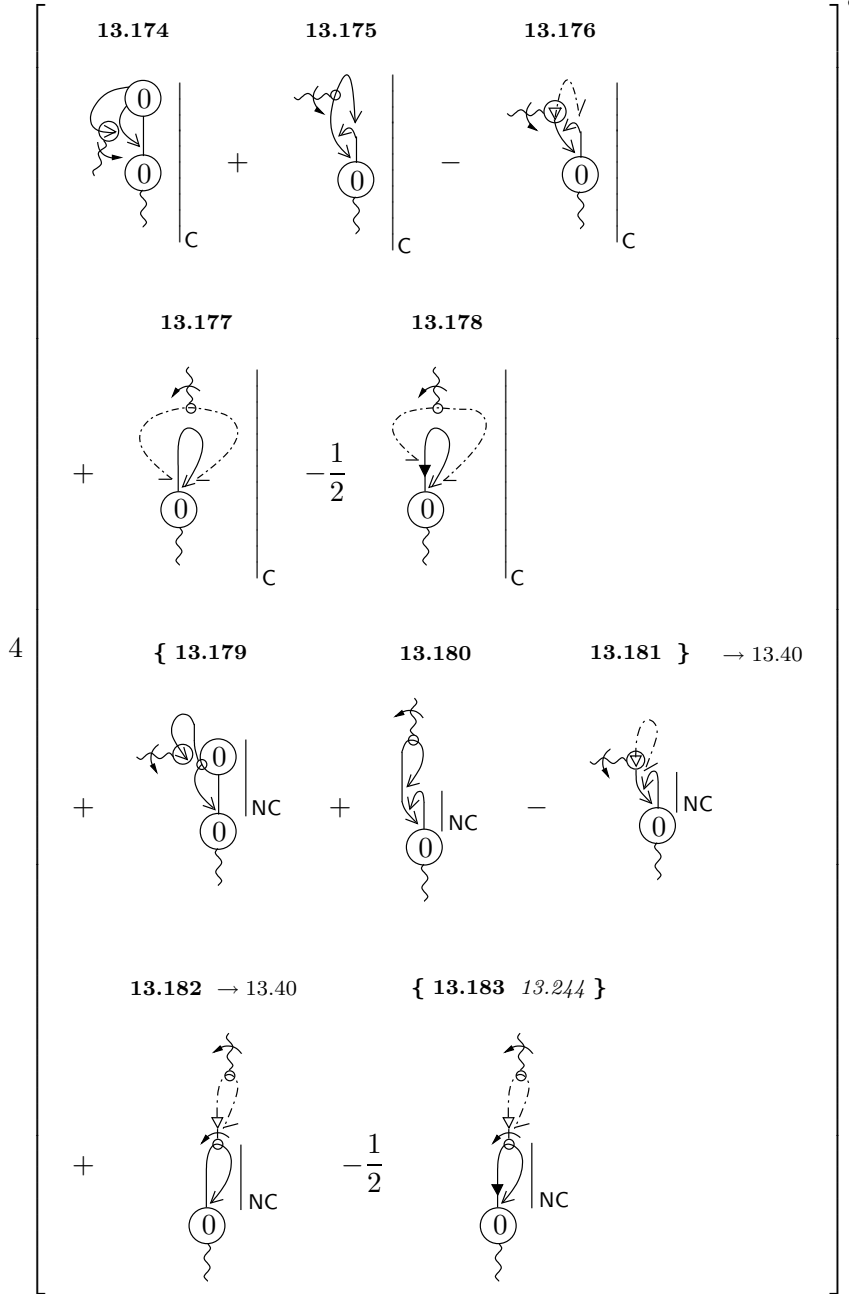


Figure 13.27: Result of combining diagrams 12.68–12.72 with both their subtractions and additions.

$$\mp 2 \left[ \begin{array}{cc} \{ 13.184 & 13.186 \} \rightarrow 13.29 \\ \{ 13.185 & 13.187 \} \rightarrow 13.29 \end{array} \right] \bullet$$

Figure 13.28: Subtractions for diagrams 13.87 and 13.94.

$$2 \left[ \begin{array}{cccc} \{ 13.188 & 13.98 \} & 13.189 \rightarrow 13.35 & \{ 13.190 & 13.102 \} & 13.191 \rightarrow 13.35 \end{array} \right] \bullet$$

Figure 13.29: The result of combining diagrams 13.87 and 13.94 with their subtractions.

contributions. For non-computable contributions, we can just set  $p = 0$  in the effective propagator and hence remove the bar. Since it is these contributions that our subtractions are designed to remove, we can just construct our subtractions without any discontinuity in momentum arguments. Note that if we were to remove the bar from diagram 13.135, then we could apply the effective propagator relation. We will exploit this, shortly.

Rather than explicitly constructing the subtractions and additions, we use our experience to jump straight to the set of terms arising from combining these diagrams with their parents. This is shown in figure 13.33.

**Cancellation 13.19** *Diagram 13.244 exactly cancels diagram 13.183.*

## 13.5 Further Manipulations

In this section, we complete the demonstration that all non-computable contributions to the original set (ignoring the  $\alpha$ -terms) cancel. To do this, we

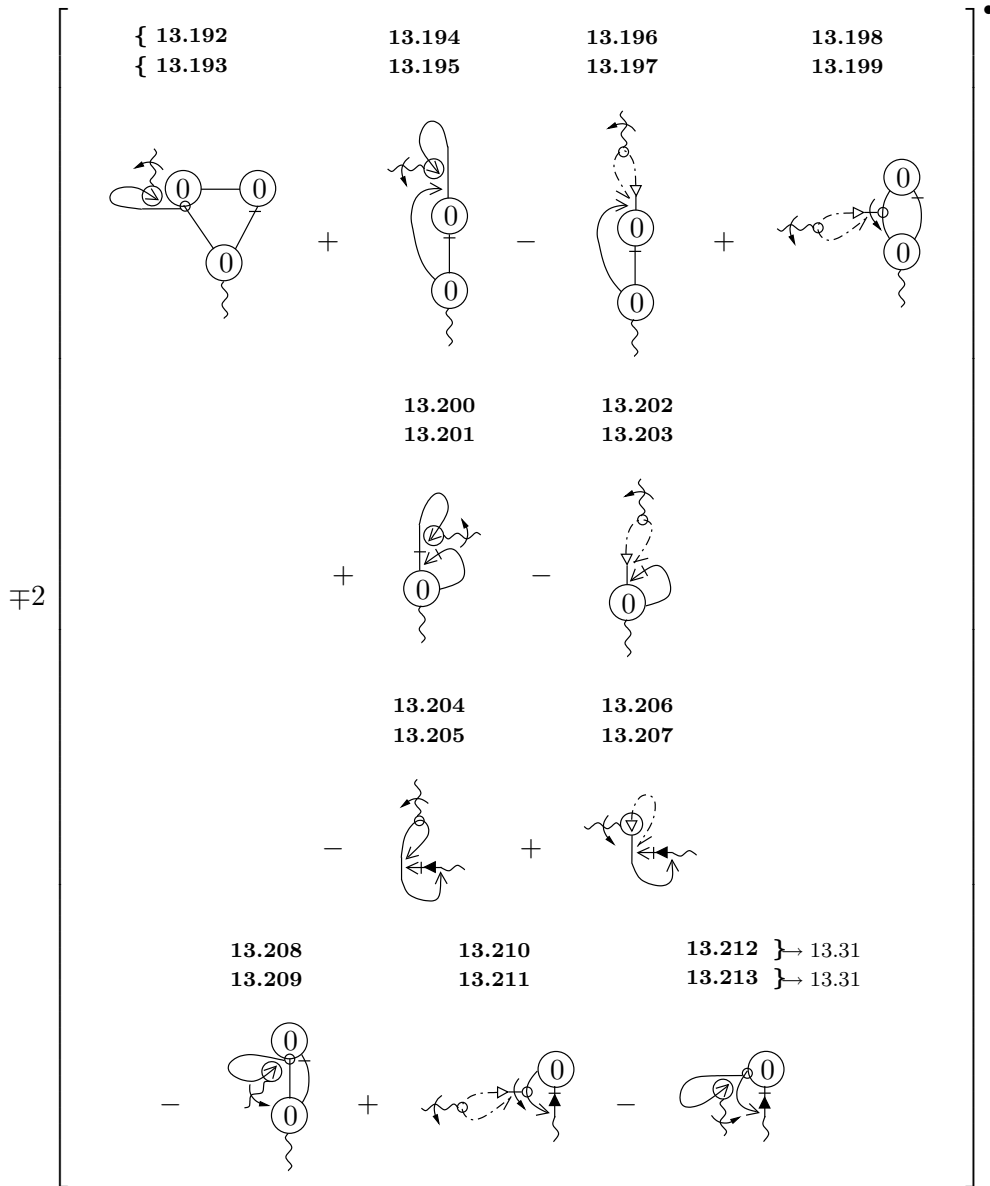


Figure 13.30: Subtractions for diagrams 13.123–13.133.

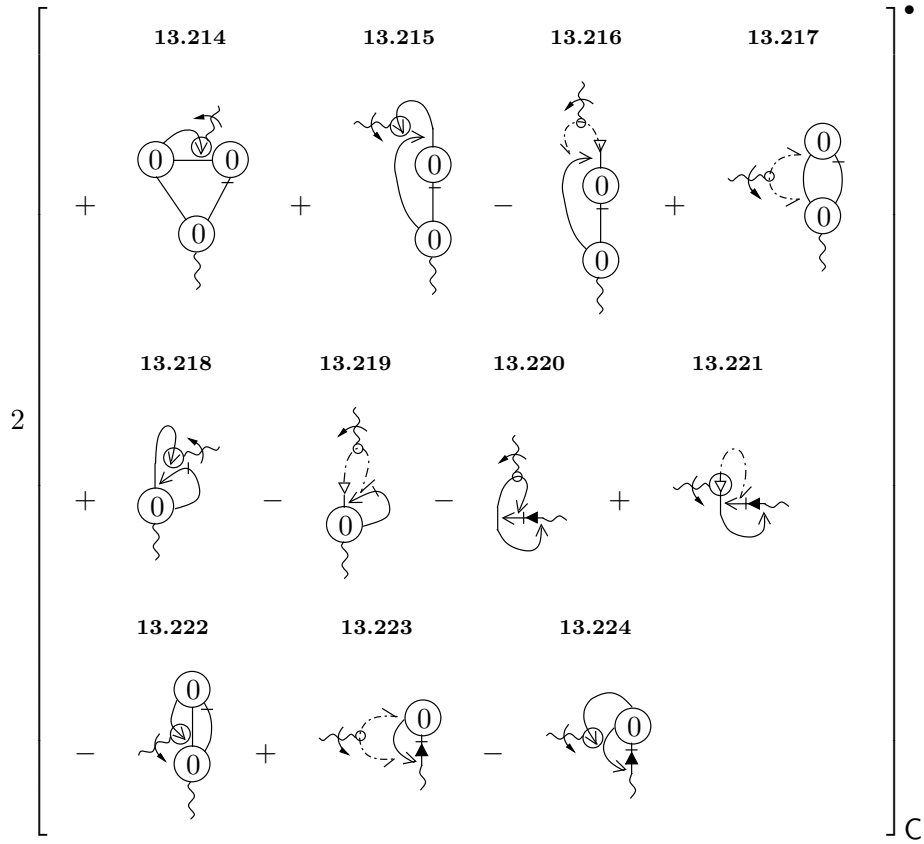


Figure 13.31: Result of the cancellation of components between diagrams 13.123–13.133 and both the subtractions and additions of figure 13.30—part I.

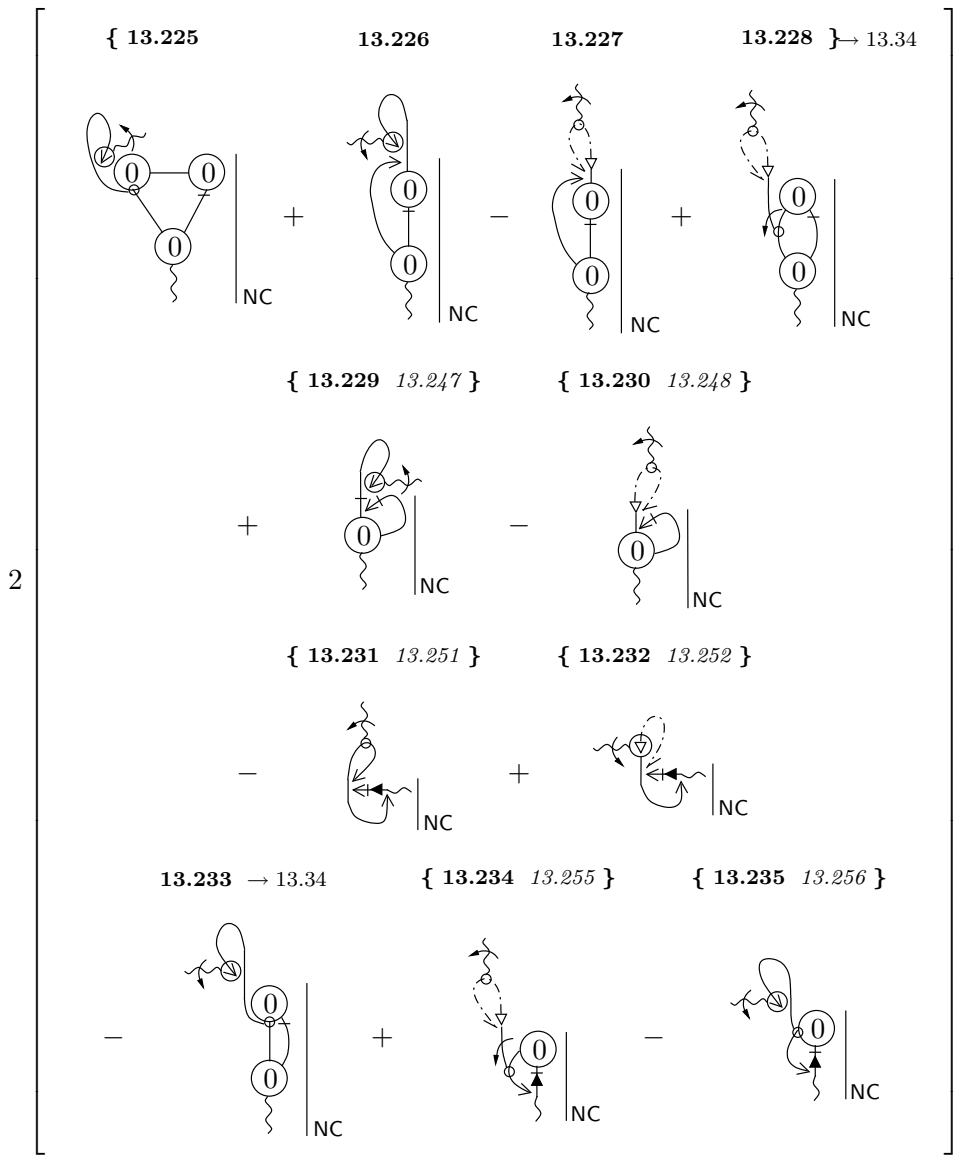


Figure 13.32: Result of the cancellation of components between diagrams 13.123–13.133 and both the subtractions and additions of figure 13.30—part II.

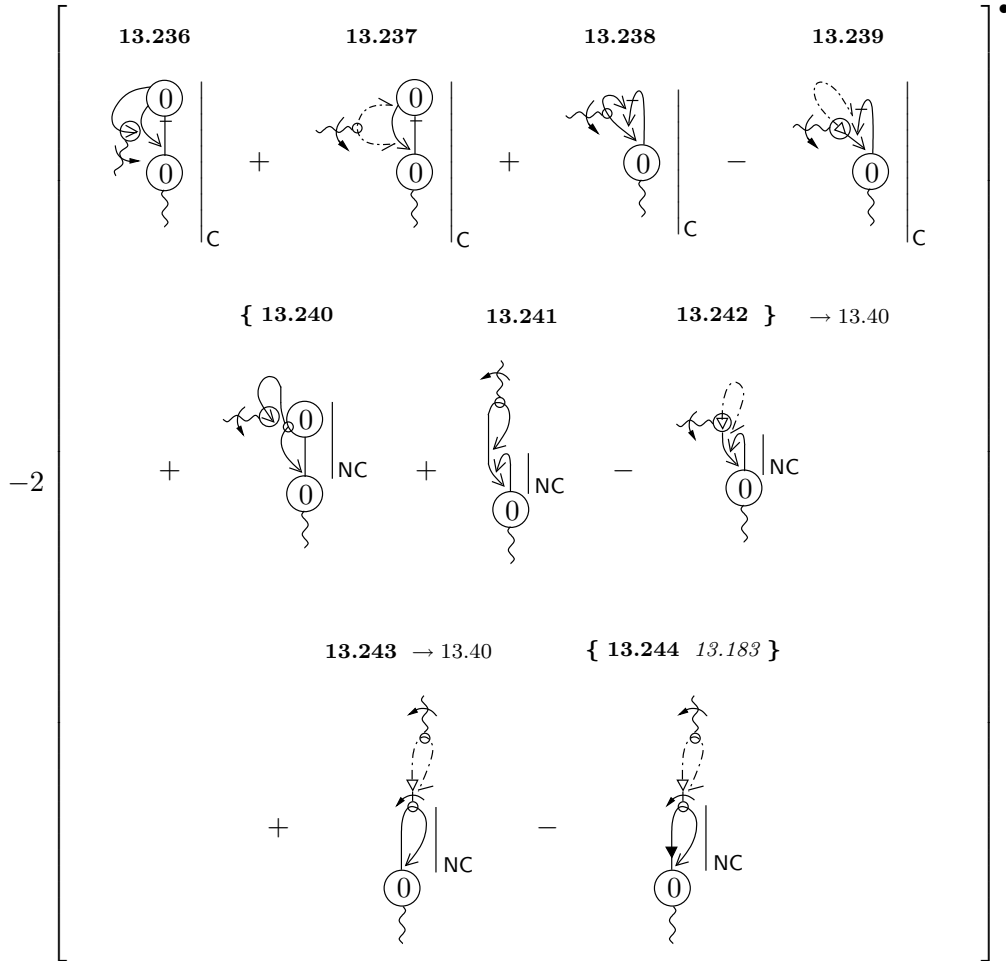


Figure 13.33: Result of isolating computable and non-computable contributions to diagrams 13.134–13.137, achieved via an implicit intermediate step involving the construction of subtractions.

organise the calculation in a specific way. First, we recognise that by manipulating certain diagrams, we can completely remove all non-computable contributions arising from instances of the standard set. Secondly, we remove all remaining non-computable contributions arising from instances of the little set. Finally, we demonstrate that the small number of remaining non-computable contributions to  $\beta_2$  cancel, amongst themselves.

### 13.5.1 Removal of Non-Computable Contributions to the Standard Set

In this section, we process a subset of the terms of figure 13.32, which we note are under the influence of NC. To make progress, we can interpret NC as the identity minus C; thus, if we are happy manipulating diagrams under C, then we are happy manipulating them under NC.

For the diagrams we wish to manipulate, it turns out that the manipulations do not generate diagrams for which we would, according to our current prescription, have to reinstate derivatives of cutoff functions; hence we proceed.

Diagram 13.225 can be processed using the effective propagator relation, since the rightmost two-point, tree level vertex is attached to an effective propagator carrying the same momentum. If we take the Kronecker delta arising from the effective propagator relation, then we note that we can combine this term with diagram 13.233. If we take the gauge remainder part, then the  $\triangleright$  strikes a two-point, tree level vertex differentiated with respect to its momentum. We can move this derivative from the vertex to the  $\triangleright$ , by means of diagrammatic identity 6. This then allows us to use the effective propagator relation, once more.

Both diagrams 13.226 and 13.227 possess, amongst other structures, an undifferentiated  $>$  which attaches to a wine carrying the same momentum. Such structures can be redrawn using diagrammatic identity 3 to give a pseudo effective propagator ending in a  $\triangleright$ . This  $\triangleright$  strikes the three-point vertex, and this can just be processed in the usual way.

Diagram 13.228 can be processed using diagrammatic identity 4. It is not obvious that we should be performing this manipulation, since one of the resulting diagrams has the same complexity as its parent. The reason that we choose

to do this is to bring diagram 13.228 into the same form as diagram 13.233—and, by doing so, we will find a number of cancellations. This illustrates a key tenet of the diagrammatics, in general: if it is possible to bring the common sub-diagram of two full diagrams into the same form, it is always right to do so!

As usual, a subset of the diagrams produced by the manipulations cancel between themselves. The remaining terms are shown in figure 13.34.

As expected, many of the diagrams cancel against un-manipulated terms from figure 13.32.

**Cancellation 13.20** *Diagram 13.247 exactly cancels diagram 13.229.*

**Cancellation 13.21** *Diagram 13.248 exactly cancels diagram 13.230.*

**Cancellation 13.22** *Diagram 13.251 exactly cancels diagram 13.231.*

**Cancellation 13.23** *Diagram 13.252 exactly cancels diagram 13.232.*

**Cancellation 13.24** *Diagram 13.255 exactly cancels diagram 13.234.*

**Cancellation 13.25** *Diagram 13.256 exactly cancels diagram 13.235.*

The next step is to collect together a set of terms, possessing non-universal sub-diagrams which are related by gauge invariance. Up to  $\mathcal{O}(\epsilon)$  corrections, we will be able to recast this set as a computable term plus a set of diagrams comprising the standard set atop the little set. The set of diagrams is shown in figure 13.35. For all sub-diagrams possessing the tag NC, we are using the prescription that we keep derivatives of cutoff functions; hence we are free to move the momentum derivative around this sub-diagram at will, discarding any total momentum derivatives.

Diagram 13.257 is (up to a discarded total momentum derivative) simply diagram 13.161, which we have moved here to make the subsequent steps clearer. The next two diagrams are obtained by manipulating diagrams 13.189 and 13.191.

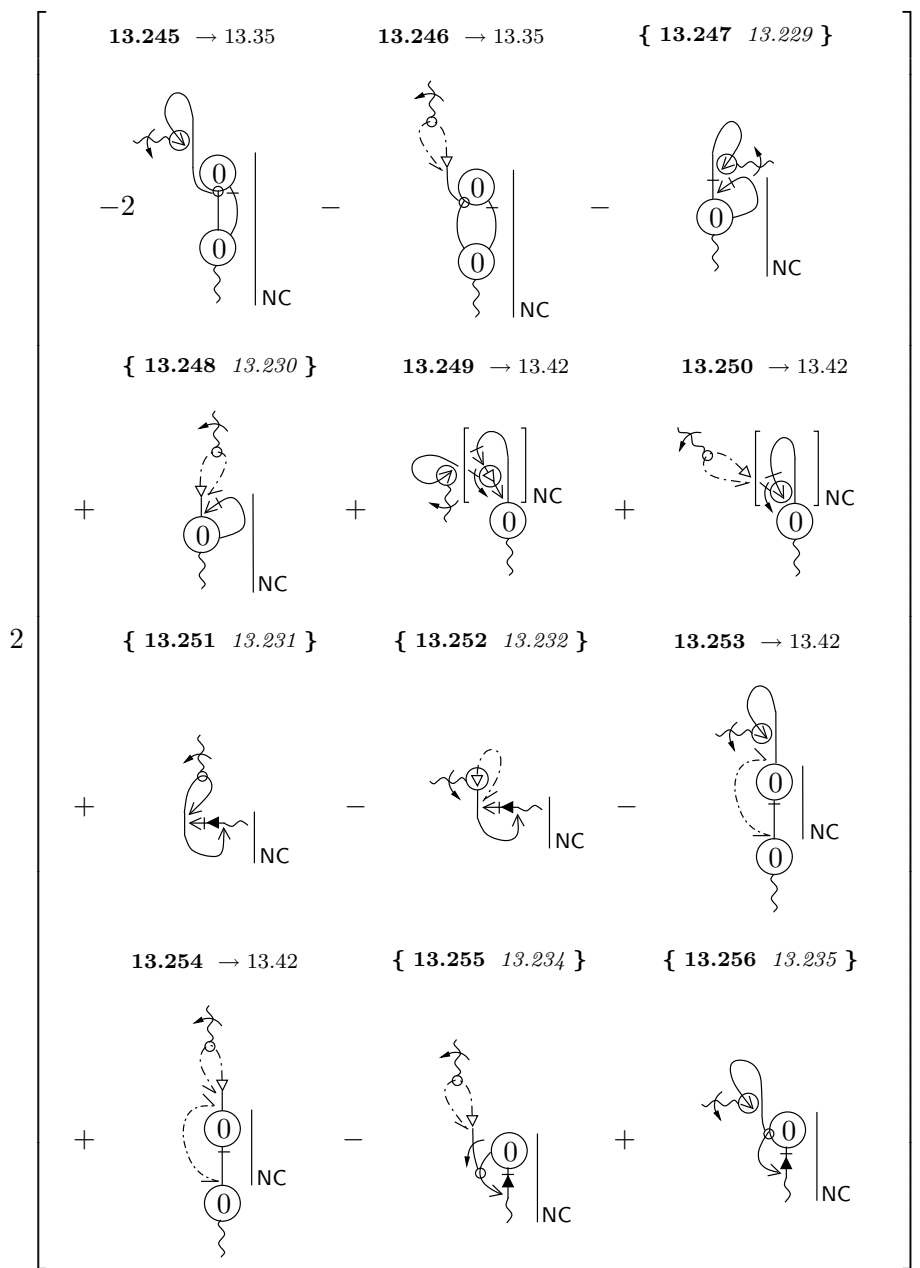


Figure 13.34: The result of manipulating diagrams 13.225–13.228. The factor of two in front of the first diagram arises from combining one of the generated terms with diagram 13.233.

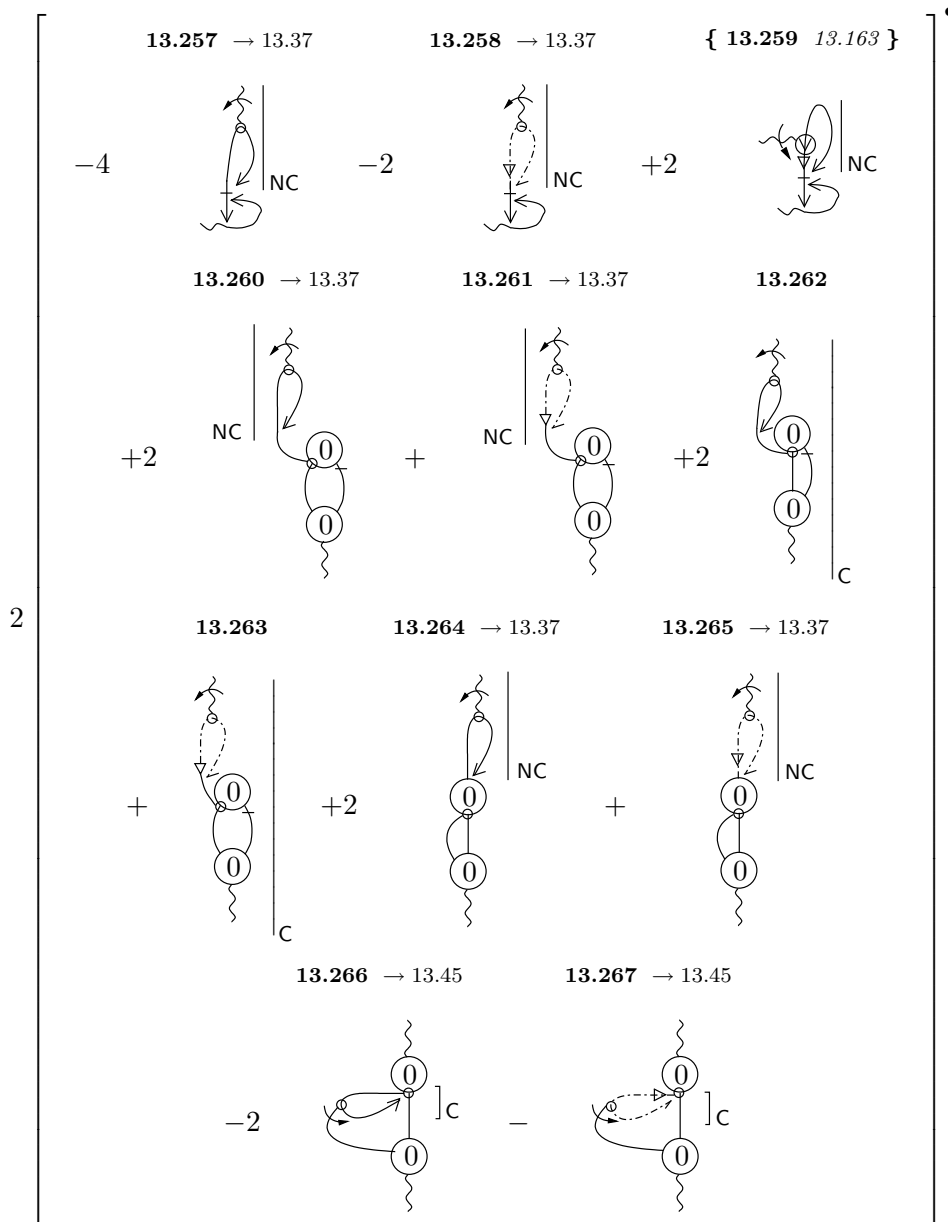


Figure 13.35: The rearrangement of diagrams 13.161, 13.113 and 13.114; the cancellation of components between 13.111, 13.112 and 13.245, 13.246; the manipulation of diagrams 13.189 and 13.191.

**Cancellation 13.26** *Diagram 13.259 exactly cancels diagram 13.163, though this is not immediately obvious. First, redraw the topmost sub-diagram of diagram 13.163 using diagrammatic identity 14 and use CC to reflect the bottom sub-diagram. This yields the the first diagram shown in figure 13.36.*

$$4 \left[ \text{Diagram 1} \right]_{\text{NC}} \equiv -4 \left[ \text{Diagram 2} \right]_{\text{NC}} \equiv -4 \left[ \text{Diagram 3} \right]_{\text{NC}}$$

Figure 13.36: Showing how we can redraw diagram 13.163.

*In turn, we redraw this once using diagrammatic identity 2 and then again using diagrammatic identity 3. Finally, the cancellation works courtesy of diagrammatic identity 9.*

Diagrams 13.260–13.263 come from combining diagrams 13.111 and 13.112 with diagrams 13.245 and 13.246, where we have discarded terms which vanish in the  $\epsilon \rightarrow 0$  limit.

Diagrams 13.264–13.267 come from re-expressing diagrams 13.113 and 13.114. Although it may not look like it, diagram 13.264 (13.265) is actually the same as diagram 13.266 (13.267). This follows because Lorentz invariance demands that the little set goes as  $\delta_{\alpha\beta}$ , allowing us to redraw the diagrams in the manner shown. Summing diagram 13.264 (13.266) and 13.266 (13.267) simply sums  $\text{NC} + \text{C}$  and so reproduces the parent diagram.

Having described the origin of the diagrams in figure 13.35 we move on to why they have been collected in this manner. Start by focusing on the first column of diagrams. It is apparent that the NC part is common between all three. Furthermore, if we are to take the NC part as shown, then for the contribution not to vanish in the  $\epsilon \rightarrow 0$  limit, we must take the divergent part of the bottom sub-diagram. However, when we sum over all three diagrams, the divergent part of the bottom sub-diagrams is none other than the divergent part of the standard set!

Since the standard set is transverse, and the little set goes as  $\delta_{\alpha\beta}$ , we can redraw this set of diagrams to take form shown in figure 13.37. At  $\mathcal{O}(\epsilon)$ , we must take the divergent—and hence universal—part of the standard set.

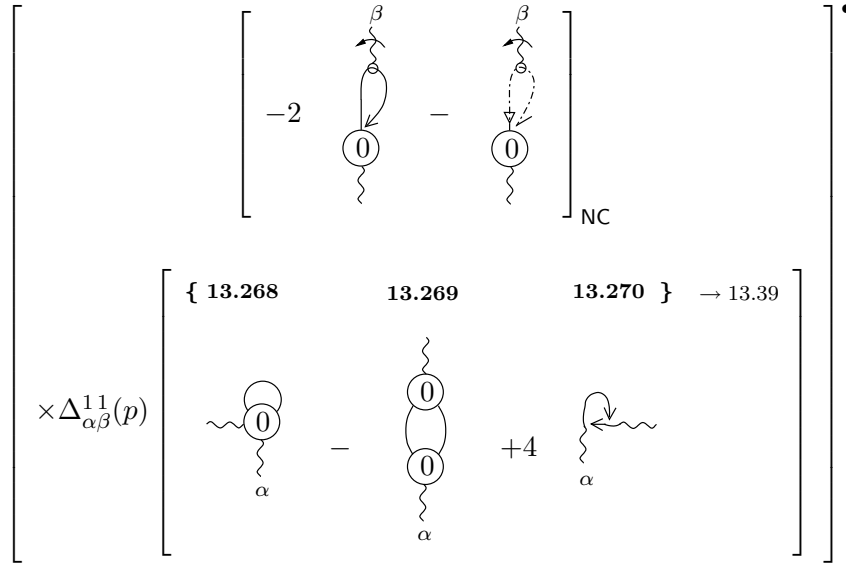


Figure 13.37: A redrawing of the first two columns of figure 13.35 (up to  $\mathcal{O}(\epsilon)$  corrections).

We conclude this section by completing the removal of all non-computable contributions which come from the standard set. In figure 13.38, we combine diagrams 13.138–13.140 with diagrams 13.31–13.33.

### 13.5.2 Removal of Non-Computable Contributions to the Little Set

Diagrams 13.268–13.270 cancel components of diagrams 13.34–13.36, to leave behind a computable contribution. To be specific, let us focus on the sub-diagrams multiplying the standard set, for diagrams 13.34–13.36. The non-computable parts of these diagrams are completely cancelled, to leave behind the components shown in figure 13.39.

Note that the final two sub-diagrams on the first row of figure 13.39 can be discarded, as they do not possess an  $\mathcal{O}(p^{-2\epsilon})$  component

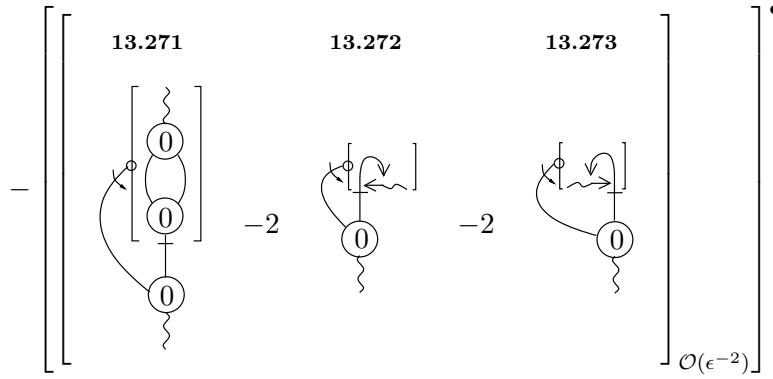


Figure 13.38: Result of combining diagrams 13.138–13.140 with diagrams 13.31–13.33.

To complete the removal of the non-computable contributions to the little set, there are a number of intermediate steps we must perform. First, we can simplify the remaining terms by recognising that diagrams 13.240–13.243 exactly halve the overall factor of diagrams 13.179–13.182. The resulting partial cancellations yield the diagrams of figure 13.40.

Immediately, we will process diagram 13.277. The simplest way to do this is to use diagrammatic identity 4 to redraw the differentiated two-point, tree level vertex and the effective propagator to which it attaches on the *right*. The term in which the momentum derivative is moved from the vertex to the effective propagator just dies: the  $\triangleright$  now acts backwards along the other effective propagator to kill the vertex. Hence, we are left only with the term in which the momentum derivative strikes a (trapped) gauge remainder. We draw the diagrams in which this derivative strikes  $\triangleright$  and  $\triangleright$  separately, in figure 13.41.

Note that these manipulations are valid under NC, without the need to reinstate derivatives of cutoff functions.

The next step is to recognise that there are four diagrams whose momentum discontinuity can be removed. First, look at diagram 13.249. Having removed the momentum discontinuity, we will recast this diagram. In the sub-diagram under the influence of NC, we move the momentum derivative which strikes  $\triangleright$



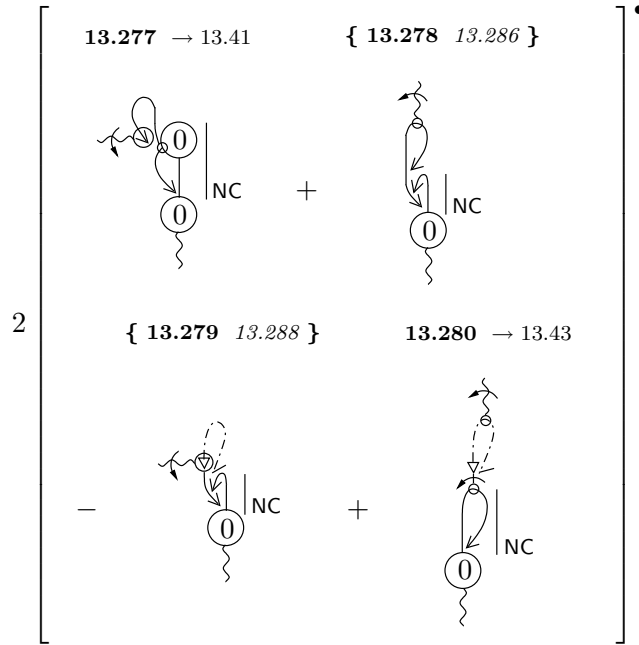


Figure 13.40: The result of combining diagrams 13.179–13.182 with diagrams 13.240–13.243.

There are five such diagrams coming from this section: 13.280, 13.282, 13.284, 13.285 and 13.287. In addition, there are two more coming from earlier in the calculation: diagrams 13.157 and 13.159.

We can redraw these latter diagrams. If we take the indices of the sub-diagram under the influence of NC to be  $\alpha$  and  $\beta$ , then Lorentz invariance forces this sub-diagram to go like  $\delta_{\alpha\beta}$ . This then contracts together a  $\triangleright$  with a  $\triangleright$  giving unity. Thus, these diagrams look like the little set, under the influence of NC, joined to a set of sub-diagrams best described as a ‘stretched out’ version of the little set; these diagrams are actually just elements of the little set restricted to the  $A^1$ -sector. Noting that we must take the divergent part of these stretched out sub-diagram, we can just redraw them to take the form of the little set, up to  $\mathcal{O}(\epsilon)$  corrections.

We now combine the redrawn versions of diagrams 13.157 and 13.159 with the five diagrams coming from this section. We always take momentum derivatives to strike (pseudo) effective propagators, rather than gauge remainders. This means that will need to include derivative of cutoff functions, as appropriate. The resulting diagrams are shown in figure 13.43.

$$-2 \left[ \begin{array}{c} \{ 13.281 \quad 13.283 \} \\ \text{Diagram 1} \\ \text{NC} \\ 0 \end{array} + \begin{array}{c} 13.282 \rightarrow 13.43 \\ \text{Diagram 2} \\ \text{NC} \\ 0 \end{array} \right] \bullet$$

Figure 13.41: Result of manipulating diagram 13.277.

Diagrams 13.289–13.292 are precisely those we need to remove the non-computable components from diagrams 12.117–12.119 (up to  $\mathcal{O}(\epsilon)$  corrections). The remaining computable contributions are shown in figure 13.44.

### 13.5.3 Final Reminders

Diagrams 13.266 and 13.267 combine with diagrams 13.141 and 13.142 to give the diagrams of figure 13.45

This completes the demonstration that, up to the  $\alpha$ -terms, all non-computable contributions to the original set cancel. The surviving diagrams are either explicitly under the influence of  $\mathbb{C}$  or contain a factorisable sub-diagram from which we take the  $\mathcal{O}(\epsilon^0)$ , computable coefficient. In the latter case we are forced to take the (computable) divergent part of the other sub-diagram, as all other contributions die in the  $\epsilon \rightarrow 0$  limit.

Although we are left with a large number of computable contributions to  $\beta_2$ , it is possible to simplify our expression. For example, we can manipulate diagrams such as 13.79. This would reproduce many of the cancellations that we saw when we manipulated the addition, corresponding to this diagram. However, not all of the cancellations would go through. Specifically, those which involved throwing away total momentum derivative contributions will survive, since we are working under the influence of  $\mathbb{C}$  (see section 5.4.2). Consequently, we choose not to perform these manipulations, for the time being. However, we return to this issue in the conclusions of this chapter and envisage a thorough treatment in [60].

$$\begin{aligned}
& \left[ \begin{array}{cc}
\{ 13.283 \ 13.281 \} & 13.284 \rightarrow 13.43 \\
\text{[Diagram 1]} - \text{[Diagram 2]} & \\
13.285 \rightarrow 13.43 & \{ 13.286 \ 13.278 \} \\
+ \text{[Diagram 3]} + \text{[Diagram 4]} & \\
13.287 \rightarrow 13.43 & \{ 13.288 \ 13.279 \} \\
- \text{[Diagram 5]} - \text{[Diagram 6]} &
\end{array} \right] \bullet
\end{aligned}$$

Figure 13.42: Result of redrawing diagrams 13.249, 13.250, 13.253 and 13.254.

## 13.6 The $\alpha$ -terms

### 13.6.1 The Problem

Before computing the numerical value of  $\beta_2$ , we must analyse the  $\alpha$ -terms. Our aim is to show that, as anticipated in section 2.1, this set of terms vanishes in the  $\alpha \rightarrow 0$  limit.

Our starting point is the simplified set of  $\alpha$ -terms, collected together in figure 12.15. As recognised already, we can write the contribution to  $\beta_2 \square_{\mu\nu}(p)$  coming from the  $\alpha$ -terms in the following form:

$$\frac{1}{8} \gamma_1 \frac{\partial \mathcal{D}_1}{\partial \alpha}, \tag{13.6}$$

where, of course,

$$4\beta_1 \square_{\mu\nu}(p) = -\frac{1}{2} [\mathcal{D}_1]^\bullet. \tag{13.7}$$

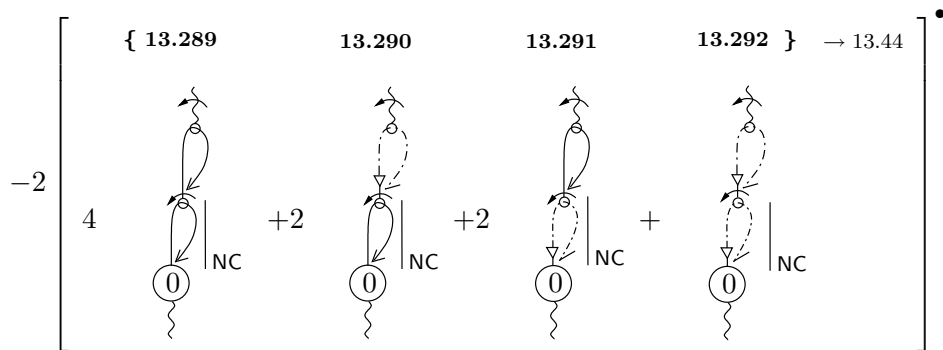


Figure 13.43: Combining the remaining terms which possess an element of the little set explicitly under the influence of NC.

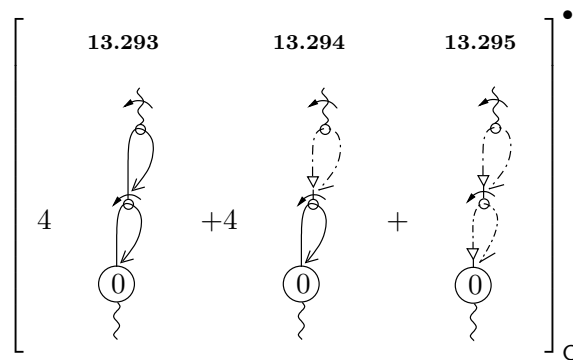


Figure 13.44: Cancellation of non-computable contributions between diagrams 13.289–13.292 and 12.117–12.119.

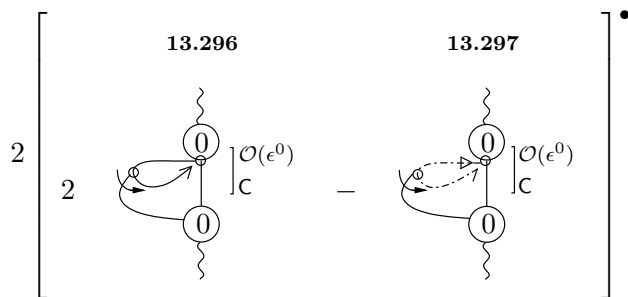


Figure 13.45: Showing diagrams 13.266 and 13.267 combine with diagrams 13.141 and 13.142.

Since we know from equation (2.25) that  $\gamma_1 \sim \alpha$ , for small  $\alpha$ , it is clear that the  $\alpha$ -terms will not vanish as required, if  $\partial\mathcal{D}_1/\partial\alpha \sim 1/\alpha$ , or worse. The task, then, is to analyse the  $\alpha$ -dependence of  $\mathcal{D}_1$ .

Whilst we have an explicit algebraic form for three of the diagrams (the final member of the standard set and the two members of the little set), the rest contain either three-point or four-point vertices, for which we do not have an explicit algebraic realisation. It is not our aim to choose specific forms for these structures (i.e. through a choice of seed action etc.); rather we wish to focus on general properties that will tell us all we need to know about the  $\alpha$ -dependence.

We note that the issue is complicated by the fact that in deducing the  $\alpha$ -dependence of  $\mathcal{D}_1$ , we must perform a loop integral. This integral must be done before we take the  $\alpha \rightarrow 0$  limit, as the two procedures do not commute. However, whilst we cannot set  $\alpha \rightarrow 0$  too soon, we can work at small  $\alpha$ , and we will do so henceforth.

From our work in chapter 5, we know how to parameterise the  $\alpha$ -dependence of  $\mathcal{D}_1$ . For our purposes, this is most easily done in  $D = 4$ :

$$\mathcal{D}_1 = \left[ 4\beta_1 \ln \left( \frac{(\text{IR scale})^2}{\Lambda^2} \right) + H(\alpha) \right] \square_{\mu\nu}(p). \quad (13.8)$$

The non-universal function  $H(\alpha)$  is independent of  $\Lambda$ . We now choose to recast this equation. When constructing the (dimensionless) argument of the logarithm, we divide the IR scale by the only other scale available,  $\Lambda$ .

Let us examine this in the context of actually performing the loop integrals to obtain (13.8). The appearance of the IR scale has been discussed, in depth, in chapter 5. The scale  $\Lambda$  has a natural interpretation as the scale at which the loop integrals are effectively cutoff. However, we should not preclude the possibility that the loop integrals are actually cutoff at some scale  $h(\alpha)\Lambda$ , where  $h(\alpha)$  is a dimensionless function, independent of  $\Lambda$ . Of course, this has no effect on the value of  $\beta_1$  obtained by differentiating  $\mathcal{D}_1$  with respect to  $\Lambda|_\alpha$ . With this in mind, we rewrite equation (13.8) as follows:

$$\mathcal{D}_1 = \left[ 4\beta_1 \ln \left( \frac{(\text{IR scale})^2}{\Lambda^2 h(\alpha)} \right) + \tilde{H}(\alpha) \right] \square_{\mu\nu}(p). \quad (13.9)$$

This recasting now allows us to break the problem of the  $\alpha$ -terms into two parts. On the one hand, we have potential  $\alpha$ -dependence coming from any

non-trivial  $\alpha$ -dependence of the effective cutoff scale, parameterised by  $h(\alpha)$ . On the other hand, we have  $\alpha$ -dependence coming from the region of the loop integral with support, parameterised by  $\tilde{H}(\alpha)$ . We deal with these cases in turn.

### 13.6.2 Behaviour of $h(\alpha)$

The treatment of this problem is slightly easier than one might expect. The crucial point is that the logarithm term in equation (13.9) comes only from (UV regulated) terms with non-trivial IR behaviour. There are four diagrams with non-trivial IR behaviour: the final two elements of the standard set and both elements of the little set. Our strategy is to examine these diagrams and, through a choice of cutoff functions, ensure that the momentum integrals are cutoff at  $\Lambda$ ; equivalently that  $h(\alpha)$  is independent of  $\alpha$ .

Sufficient UV regularisation can be provided by cutoff regularisation alone—e.g. for the little set—or entirely by the regulating sector—e.g. for the final element of the standard set. In the latter case, we are interested simply in the scale at which the  $B$ -sector diagrams regulate the  $A^1$ -sector diagrams. In the former case we are interested not only in this, but also the scale at which the  $A^1$  sector diagrams die off on their own.

For all that follows, we assume that the momentum of the cutoff functions  $c(k^2/\Lambda^2)$  and  $\tilde{c}(k^2/\Lambda^2)$  crosses over from large to small for  $x \equiv k^2/\Lambda^2 \sim \mathcal{O}(1)$ . This amounts to an implicit choice of the non-universal details of the set-up. In this section, we will demonstrate that, given this choice, we can consistently arrange for all momentum integrals to be cutoff at  $x \sim \mathcal{O}(1)$ .

We start by looking at the final element of the standard set, which we recall has the algebraic form

$$4N \int_k \left( \frac{(k-p)_\nu k_\mu}{(k-p)^2 k^2} - \frac{f_{k-p}(k-p)_\nu f_k k_\mu}{\Lambda^2 \Lambda^2} \right), \quad (13.10)$$

where

$$f_k = \frac{(1+\alpha)\tilde{c}_x}{(1+\alpha)x\tilde{c}_x + 4\alpha c_x}. \quad (13.11)$$

At large  $x$ , where  $f_k = 1/x$  (see equation (1.28)), we recover unbroken  $SU(N|N)$ , as we must, for the theory to be regularised. Given our assumption that  $\tilde{c}_x$

crosses over at  $x \sim \mathcal{O}(1)$ , we need only ensure that the denominator of  $f_k$  crosses over at  $x \sim \mathcal{O}(1)$ . The crossover of the denominator occurs at

$$x\tilde{c}_x \sim 4\alpha c_x.$$

Now, since we are working at small  $\alpha$  (and  $x\tilde{c}_x \gg c_x$  for large  $x$ ), the crossover must happen for small values of  $x$ . Taylor expanding, we therefore find that the crossover occurs at

$$x\tilde{c}_0 \sim \alpha c_0,$$

(in the limit of small  $\alpha$ ). Now, we know that  $c_0$  is fixed to be unity; however, there is no such constraint on  $\tilde{c}_0$ . In turn, this implies that the momentum integral for the third element of the standard set is cutoff at  $x \sim \mathcal{O}(\alpha/\tilde{c}_0)$ . Note that if we set  $\tilde{c}_0 \sim 1$ , then we would indeed find the problem that  $\partial\mathcal{D}_1/\partial\alpha \sim 1/\alpha$ . Demanding that the cutoff scale occurs at  $x \sim \mathcal{O}(1)$  then forces us to choose

$$\tilde{c}_0 \sim \mathcal{O}(\alpha), \tag{13.12}$$

(which is perfectly compatible with  $\tilde{c}_x$  crossing over at  $x \sim \mathcal{O}(1)$ ).

Let us now turn to the remaining three diagrams with non-trivial IR behaviour. The treatment of these is somewhat different from what we have just done, as we have regularisation provided not only by the  $B$ -sector, but also by cutoff function regularisation. The crossover scale in the  $B$ -sector follows trivially from the observation that

$$\Delta^{B\bar{B}}(k) = \frac{\alpha c_x f_x}{(1 + \alpha)\Lambda^2}.$$

Hence, we immediately know that, given the choice  $\tilde{c}_0 \sim \mathcal{O}(\alpha)$ , the crossover occurs at  $x \sim \mathcal{O}(1)$ , in this sector.

However, we now need to show that the scale at which the cutoff regularisation kicks in in the  $A^1$ -sector also occurs at this scale. If a diagram is sufficiently regulated by cutoff regularisation alone, then the  $B$ -sector becomes effectively redundant. If the  $B$ -sector is required, in addition to cutoff regularisation, then there can be two scales in the problem: the first is where the momentum in the  $A^1$ -sector can be considered large and the second is where the momentum in the  $B$ -sector can be considered large. The  $A^1$  and  $B$ -sectors cancel each other at the highest of these scales.

Turning now to the  $A^1$ -sector, we recall that

$$\Delta^{11}(k) = \frac{1}{k^2} \frac{\alpha c_x}{(\alpha + 1) + c_x(\alpha - 1)},$$

which goes as  $\alpha c_x/x$  for large  $x$  and as  $1/2x$  for small  $x$ . The crossover occurs, for small  $\alpha$ , at

$$\alpha(c_x + 1) \sim 1 - c_x.$$

(Note that the l.h.s. dominates at sufficiently small  $x$ , whereas the r.h.s. dominates at large  $x$ .) Again, due to the smallness of  $\alpha$ , we can Taylor expand in  $x$  to find the crossover point, which occurs at

$$\frac{x |c'_0|}{\alpha} \sim \mathcal{O}(1).$$

This implies that, for the effective cutoff to be at  $x \sim \mathcal{O}(1)$ , we must choose  $|c'_0| \sim \mathcal{O}(\alpha)$ .

This actually completes the analysis necessary to show that  $h(\alpha)$  can always be arranged to be independent of  $\alpha$ . However, for the purposes of the next section, it is useful to show that we can, in fact, ensure that all momentum integrals are cutoff at  $x \sim \mathcal{O}(1)$ . The reason that this is useful is because we expect a one dimensional integral with an integrand of  $\mathcal{O}(1)$  but with support only over a range  $\Delta x$  to go like  $\Delta x$ . Hence, it is desirable for this range to be  $\mathcal{O}(1)$  as opposed to, e.g.,  $\mathcal{O}(\alpha^{-1})$ .

In the  $A^2$  sector, recalling that

$$\Delta^{22}(k) = \frac{1}{k^2} \frac{\alpha c_x}{\alpha + 1 + c_x(1 - \alpha)},$$

we see that the large momentum behaviour is  $\alpha c_x/x$ , whereas the small momentum behaviour is  $\alpha/2x$ . Since the  $\alpha$ -dependence is the same for both, the crossover scale is clearly set by  $c$ , which is assumed to crossover at  $x \sim \mathcal{O}(1)$ .

In the  $D$  sector, given that

$$\Delta^{D\bar{D}}(k) = \frac{\tilde{c}_x f_x}{\Lambda^4},$$

our choice that  $\tilde{c}_0 \sim \mathcal{O}(\alpha)$  ensures that the crossover occurs at  $x \sim \mathcal{O}(1)$ , assuming that  $\tilde{c}_x$  crosses over at  $x \sim \mathcal{O}(1)$ .

In the  $C$ -sector, we recall that

$$\Delta^{CC}(k) = \frac{1}{\Lambda^4} \frac{\tilde{c}_x}{x + 2\lambda\tilde{c}_x},$$

from which it is clear that the crossover scale is controlled by  $\tilde{c}$  and  $\lambda$ ; we use this freedom to ensure that the crossover occurs at  $x \sim \mathcal{O}(1)$ .

We have thus demonstrated that, by suitable choices of the behaviours of our cutoff functions, we can guarantee that all momentum integrals are cutoff at the scale  $x \sim \mathcal{O}(1)$  (working at small  $\alpha$ ); one consequence of this is that  $h(\alpha)$  is independent of  $\alpha$  and so does not generate a contribution to  $\beta_2$  in the  $\alpha \rightarrow 0$  limit.

We conclude this section with an interesting comment on universality. It is clear from our analysis so far that the freedom to choose the non-universal parts of our cutoff functions enables us to choose  $h(\alpha)$ . Returning to equation (13.9), it thus looks like we could generate a universal contribution to  $\beta_2$  by choosing e.g.  $h(\alpha) = \alpha^m$ , for some  $m \neq 0$ . However, the universal appearance of this contribution is accidental, as can be appreciated from the fact that it arises from a particular choice of a non-universal function. Indeed, the universal  $\beta_2$  will only be obtained by arranging things so that all contributions from the running of  $\alpha$  can be removed in the  $\alpha \rightarrow 0$  limit.

### 13.6.3 Behaviour of $\tilde{H}(\alpha)$

To start our analysis of  $\tilde{H}(\alpha)$ , we begin by returning to the third element of the standard set. We know that the integrand of equation (13.10) effectively has support only over the region  $0 \leq x < \mathcal{O}(1)$ . Moreover, any non-trivial  $\alpha$ -dependence of  $\tilde{H}(\alpha)$  must come from the  $B$ -sector, as  $A$ -sector (processed) gauge remainders are independent of  $\alpha$ .

From our algebraic choice for  $f$  (see equation (13.11)), the most obvious possible source of problematic  $\alpha$ -behaviour comes when  $x$  is small. However, this is ameliorated by our previous choice of  $\tilde{c}_0$ . To complete our analysis of this diagram, we must now perform the loop integral but we already know that, since the effective cutoff of this integral is  $\mathcal{O}(1)$  as opposed to, say,  $\mathcal{O}(\alpha^{-1})$ , we do not expect the loop integral to generate any bad  $\alpha$ -dependence (i.e. dependence which diverges as  $\alpha \rightarrow 0$ ).

Looking now at the little set, the situation is similar: in the  $B$ -sector, our choice of  $\tilde{c}_0$  cures any bad  $\alpha$ -dependence; in the  $A^1$ -sector there is not even a potential problem. In both cases, the effective cutoff for the loop integral is

$\mathcal{O}(1)$ .

This exhausts the analysis of the diagrams for which we have an explicit algebraic form and so now we turn to the diagrams possessing three and four-point vertices.

First, we will look at the diagrams with an  $A_\mu^1 A_\nu^1 C$  vertex. Neither this vertex nor the effective propagator to which it attaches carries the loop momentum of the diagram and so we analyse them separately. The effective propagator—which carries zero momentum—goes as

$$\frac{1}{2\lambda\Lambda^4}.$$

We see that the  $\alpha$ -dependence of this can always be controlled by a suitable choice of  $\lambda$ . (It can always be ensured that this choice of  $\lambda$  is compatible with the choice which guarantees that the crossover for the  $C$ -sector effective propagator occurs at  $x \sim \mathcal{O}(1)$ .)

What about the  $A_\mu^1 A_\nu^1 C$  vertex? We have encountered this already in section 5.5: at  $\mathcal{O}(p^2)$  it is a dimensionless coupling and so we tune its flow to zero. This means that the flow equations tell us nothing about its  $\alpha$ -dependence: this dependence is a boundary condition. The solution is simply to choose the boundary condition to have sufficiently good  $\alpha$ -dependence, which is something we are always at liberty to do.

Now let us examine the remaining part of these diagrams. Attached to the other end of the  $C$ -sector effective propagator is either a hook or a three-point vertex, decorated by a simple loop. Since the hook simply goes as

$$N \int_k g_k,$$

where  $g_x = (1 - xf)/2$ , it is clear that the loop integral does not produce any troublesome  $\alpha$ -dependence.

The case where the top part of the diagram constitutes a three-point vertex is almost as easy to treat. Let us consider the flow of this vertex. If we take the dimensionless part, then we know that the flow has already been tuned to zero; in this case, we choose the boundary condition, appropriately. Taking the flow of the dimensionful part of the vertex we once again tune the seed action. This time, though, we do so to ensure sufficiently good  $\alpha$ -dependence. Note

that we need not worry about constraints coming from gauge invariance. If the top vertex contains two fields in the  $A$ -sector (it cannot contain a single one) then gauge invariance simply tells us that the vertex is transverse; it is not related to lower point vertices. Performing the loop integral does not generate any bad  $\alpha$ -dependence.

The penultimate diagram to deal with is the second element of the standard set, which comprises two three-point vertices, joined together by two effective propagators. Once again, our aim is to choose the seed action such that the  $\alpha$ -dependence of the three-point vertices is sufficiently good. This time, however, we must worry about gauge invariance.

The first effect of gauge invariance is to relate the longitudinal part of each of these vertices to two-point, tree level vertices. Referring to our list of two-point, tree level vertices (equations (A.1)–(A.10)), it is clear that our three-point vertices have buried in them, necessarily, components which go as  $\mathcal{O}(\alpha^{-1})$ .

To examine the transverse components of these vertices, we must use the flow equations. Figure 13.46 shows the flow of a three-point vertex comprising one external field and two identical internal fields (i.e. this vertex should be viewed as part of a whole diagram).

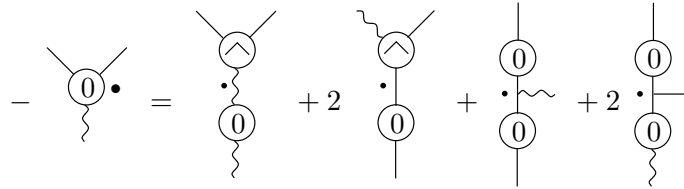
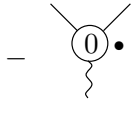


Figure 13.46: Flow of a three-point, tree level vertex viewed as part of a whole diagram.

We expect the critical case to occur when all three fields are in the  $A$ -sector, since gauge invariance will then force us to take  $\mathcal{O}(\text{mom}^2)$  from each two-point, tree level vertex. In particular, this means that we will be unable to tune the three-point seed action vertices if we take the  $\mathcal{O}(\text{mom}^3)$  part of the

vertex whose flow we are computing (the  $\mathcal{O}(\text{mom}^1)$  part is, of course, universal and independent of  $\alpha$ ).

Given our choice that  $c'_0 \sim \mathcal{O}(\alpha)$ , it is straightforward to show that

$$- \left[ \text{Diagram} \right]_{\mathcal{O}(\text{mom}^3)} \sim \frac{\mathcal{O}(\alpha^0) \mathcal{O}(\text{mom}^3)}{\Lambda^2}.$$


Thus it is clear that we can always tune the seed action to ensure that worst behaviour of the three-point, tree level vertices is the  $\mathcal{O}(\alpha^{-1})$  dependence forced by gauge invariance. This leading  $\alpha$ -dependence now cancels between the vertices and effective propagators of the second element of the standard set. The loop integral does not generate any bad  $\alpha$ -dependence

The treatment of the first element of the standard set follows, similarly: by tuning the seed action (and choosing suitable boundary conditions for the flow) we can ensure that the worst  $\alpha$ -dependence is that forced on us by gauge invariance. This dependence is then cancelled by the effective propagator. The loop integral does not generate any bad  $\alpha$ -dependence.

We have thus demonstrated that, by suitable choice of seed action, the non-universal details of the cutoff functions and the boundary conditions for our flow, we can ensure that  $\tilde{H}(\alpha) \sim \mathcal{O}(\alpha^0)$ . It therefore follows that we can always arrange for the  $\alpha$ -terms to vanish in the  $\alpha \rightarrow 0$  limit.

## 13.7 Computation of $\beta_2$

We are now in a position to compute  $\beta_2$ . Recalling the form for a generic two loop integral, given by equation (5.7), we expect to be able to write:

$$-4\beta_2 \square_{\mu\nu}(p) = \left[ \frac{\Lambda^{-4\epsilon}}{4} \sum_{i=0}^1 \left( C_i + D_i \frac{p^{-2\epsilon}}{\Lambda^{-2\epsilon}} \right) \frac{1}{\epsilon^{i-2}} \right] \square_{\mu\nu}(p) + \mathcal{O}(\epsilon). \quad (13.13)$$

As we have argued already, it must be the case that  $C_0$  and  $D_i$  vanish, else the r.h.s. of equation (13.13) is not compatible with the l.h.s. Since we have shown that the non-computable contributions to  $C_1$  cancel, we could just compute the surviving, computable contributions to  $C_1$  and hence obtain  $\beta_2$ . However, as a check on the consistency of the formalism, we will do more than this. We have, in fact, already shown that the non-computable contributions to  $D_1$

cancel. We will now also check that  $C_0$  vanishes. (We could demonstrate that  $D_0$  and the computable part of  $D_1$  vanish, too.)

To collate the contributions to  $C_0$  and  $C_1$ , it is easier to introduce a slightly different form for  $\beta_2$ :

$$-4\beta_2 \square_{\mu\nu}(p) = \frac{N^2}{(4\pi)^D} \left[ \left( \frac{1}{\epsilon} C_0^a + C_1^a \right) p^2 \delta_{\mu\nu} + \left( \frac{1}{\epsilon} C_0^b + C_1^b \right) p_\mu p_\nu \right] + \mathcal{O}(\epsilon) \quad (13.14)$$

We now split up the contributions to  $C_0^{a,b}$  and  $C_1^{a,b}$  into five sets,  $A$ – $E$ , as follows:

$A$  contribution 13.5;

$B$  contribution 13.37;

$C$  diagrams 13.143–13.149, 13.296 and 13.297;

$D$  diagrams 13.271–13.273;

$E$  diagrams 13.58–13.60; 13.70; 13.78 and 13.79; 13.95, 13.96, 13.99 and 13.100; 13.156 and 13.158; 13.160; 13.162; 13.174–13.178; 13.214–13.224; 13.236–13.239; 13.293–13.295.

The result of numerically evaluating the contribution to  $C_0^{a,b}$  and  $C_1^{a,b}$  is summarised in table 13.1.

The null entries correspond to terms which are restricted to a specific order in  $\epsilon$ ; this is distinct from an entry of zero. We note that the evaluation of the elements of sets  $A$ ,  $B$  and  $D$  is independent of the prescription we choose for treating derivatives of cutoff functions, total momentum derivatives and etc. However, the remaining two sets are, individually, susceptible to this prescription.

Inserting the net contributions to  $C_0^{a,b}$  and  $C_1^{a,b}$  into equation (13.14) we find that, in the  $\epsilon \rightarrow 0$  limit,

$$\beta_2 = -\frac{34}{3} \frac{N^2}{(4\pi)^4}, \quad (13.15)$$

thereby recovering the standard result [102].

	$C_0^a$	$C_0^b$	$C_1^a$	$C_1^b$
$A$	0	0	-9	0
$B$	0	0	$\frac{571}{9} - \frac{80\gamma_{\text{EM}}}{3}$	$-\frac{451}{9} + \frac{80\gamma_{\text{EM}}}{3}$
$C$	—	—	$-\frac{111}{2} + 60\gamma_{\text{EM}}$	$\frac{111}{2} - 60\gamma_{\text{EM}}$
$D$	$-\frac{50}{3}$	$\frac{50}{3}$	—	—
$E$	$\frac{50}{3}$	$-\frac{50}{3}$	$\frac{835}{18} - \frac{100\gamma_{\text{EM}}}{3}$	$-\frac{913}{18} + \frac{100\gamma_{\text{EM}}}{3}$
	0	0	$\frac{136}{3}$	$-\frac{136}{3}$

Table 13.1: Contributions to  $\beta_2$ .

## 13.8 Conclusions

The correct numerical evaluation of  $\beta_2$  represents the final result of this thesis—and perhaps the most important. More than anything else, this demonstrates beyond all reasonable doubt the consistency of the formalism, thereby fulfilling the fundamental aim of this piece of work.

With this in mind, it is worth now looking at the calculation—as we did in the one-loop case—as a piece of work in its own right, particularly in regard to its complexity. Our starting point will be the starting point for this chapter: the set of diagrams in appendix D, which we denote by  $\mathcal{D}_2$ . By beginning our evaluation of the complexity here, we are essentially assuming that this set of diagrams can be trivially generated.<sup>9</sup> We know that this is true for those not involving  $\mathcal{O}(p^2)$  stubs; it is certainly reasonable to expect that our  $n_+$ -loop formula (10.1) can be extended to include the missing diagrams.

Even given our starting point, it still seems that we had to work very hard to actually extract the numerical value of  $\beta_2$ . However, as I will argue here, I believe this to be an artifact of being the very first time a two-loop calculation has been performed, within this framework. Let us analyse the extraction of

<sup>9</sup>The actual generation of decorated diagrams should be natural to implement on a computer, removing the need to do it by hand.

$\beta_2$ , in more detail.

The set  $\mathcal{D}_2$  contains 83 terms.<sup>10</sup> Including the  $\alpha$ -terms, 35 of these can be discarded. Of those that remain, there are 19 factorisable diagrams which explicitly contain elements of  $\mathcal{D}_1$ . There are 10 non-factorisable diagrams which also explicitly contain elements of  $\mathcal{D}_1$ , once we realise that survival in the  $\epsilon \rightarrow 0$  limit forces certain internal fields to be in the  $A$ -sector. The remaining 19 diagrams are what we will refer to as the irreducible two-loop diagrams.

Much of the work in this chapter went into constructing subtractions for the irreducible diagrams and then performing manipulations on either the additions or the NC diagrams resulting from combining parent, subtraction and addition. However there is a very clear pattern to both the construction of the subtractions, their subsequent manipulation and the diagrams we are left with.

Indeed, recall that when we reached the end of the one-loop calculation, we concluded that we had been essentially repeating the same steps, over and over again; this led us to the vastly more powerful formalism of part III. I believe the situation here to be somewhat analogous: to me, the structure of the computation of  $\beta_2$  is highly suggestive of a greatly simplified, underlying formalism.

Further support for this is given by the set of diagrams from which we ultimately evaluate the computable parts. We will denote this set of terms by  $\mathcal{D}_2|_U$ . To generate this set, we can start by simply taking each of the irreducible two-loop diagrams and placing it, wholesale, under the influence of  $C$ . We then do likewise with the three factorisable diagrams whose two sub-diagrams are each elements of the little set. As we have noted already, many of the remaining diagrams of  $\mathcal{D}_2|_U$  can be cancelled if we are willing to perform manipulations under the influence of  $C$ . Up until now, we have been hesitant to do this, but it is clear that this is the natural way to proceed. This would enable us to replace 20 of the diagrams under the influence of  $C$  with a small set of total momentum derivative terms (which, of course, generically survive in this scenario).

---

<sup>10</sup>We are counting diagrams in which we must sum over  $ES'$  only once, but this makes no difference to our argument as all these terms vanish, anyway.

Indeed, if we were always to manipulate diagrams under the influence of  $\mathbb{C}$ , then this suggests a different way to organise the calculation. Given that these manipulations just mirror those performed on the corresponding additions, we should *always* combine parent, subtraction *and* addition to yield the parent under the influence of  $\mathbb{C}$  and a term under the influence of  $\mathbb{NC}$ . This will give the simplifications just discussed; it will also affect our treatment of the remaining elements of  $\mathcal{D}_2|_U$ .

The remaining elements are basically those which we recognised could be combined into finite sets (see sections 13.2.2 and 13.3.1). Now, however, the combination of terms is slightly different: all the cancellations we saw will still occur. However, the set of surviving terms will be smaller, with some of them having been involved in the aforementioned simplifications.

Ultimately, we are left with  $\mathcal{O}(30)$  contributions to  $\beta_2$ , all of which are very easy to compute. Thus, if the procedure of going from  $\mathcal{D}_2$  to  $\mathcal{D}_2|_U$  can be greatly simplified—as I believe to be the case—then the extraction of  $\beta_2$  within this framework could be reduced to a remarkably straightforward calculation. These ideas will be further explored in [60].

# Chapter 14

## Conclusion

### 14.1 Summary

The basis of all new work done in this thesis is the new flow equation, 2.7–2.9. Like the flow equation which it replaces (equations 1.30–1.32), the new flow equation is manifestly gauge invariant. Where it differs is in its ability to distinguish the two fields  $A^1$  and  $A^2$ . In turn, this enables us to isolate the effects of the unphysical field  $A^2$  and thus to compute useful quantities beyond one loop.

The computational method draws its inspiration from the diagrammatic techniques of [57] and [25]. The former paper presents a computation of the one-loop Yang-Mills  $\beta$ -function using the (old) MGI-ERG whereas the latter paper presents a computation of the scalar two-loop  $\beta$ -function. (Henceforth, we will use  $\beta_n$  to refer to Yang-Mills  $\beta$ -function coefficients.) In both papers, it was recognised that the ERG provides a natural framework for isolating universal contributions to universal objects. By leaving all non-universal quantities unspecified, the calculational procedure becomes so constrained that computation can be done diagrammatically.

Given that the form of the flow equation has changed from that of [57], the first challenge was to see whether diagrammatic techniques can still be employed. As discussed in section 2.3, the diagrammatics of [57] can indeed be extended, at the expense of additional complication. The essence of this complication is that wines—which had previously only ever comprised single

supertrace components—are effectively generalised to multi-supertrace objects.

Whilst the initial reaction was that this had made life harder, such multi-supertrace objects can, in fact, be naturally absorbed into the diagrammatics. Indeed, in section 2.4 we developed an entirely new form of diagrammatics, in which single and multi-supertrace objects are treated in parallel, having been absorbed into a composite object.

In retrospect, that such a simplification is possible is hardly surprising. Although all ingredients in the treatment of [57] were restricted to single supertrace terms, the structure of the diagrammatic cancellations strongly suggested that multi-supertrace terms, if included, would cancel in the same way. Indeed, since all non-universal contributions must cancel anyway, it is natural that sets of them can be packaged up together and thus removed in one go.

Moreover, our scheme now amounts to using standard Feynman diagrammatic expansions, except that the Feynman rules are novel and, embedded within the diagrams, there is a prescription for automatically evaluating the group theory factors.

An immediate consequence of these new diagrammatics is that the calculation of [57] can be essentially repeated, line for line. However, in the new way of doing things, multi-supertrace terms come along for the ride, without really adding any complication.<sup>1</sup>

Now, although much of the calculation of  $\beta_1$  in [57] was done diagrammatically, these techniques were not pushed to their limit, since gauge remainders and  $\mathcal{O}(p^2)$  terms were treated algebraically.

In section 3.1 we showed how the gauge remainders, too, can be treated diagrammatically. The  $\mathcal{O}(p^2)$  terms are those possessing a manifestly  $\mathcal{O}(p^2)$  stub. Since we work at  $\mathcal{O}(p^2)$ , other structures in the diagram carrying momentum  $p$  can be Taylor expanded to zeroth order in  $p$ , assuming that this step does not generate any IR divergences. In section 3.2 we showed how to perform these Taylor expansions diagrammatically.

With the techniques for treating gauge remainders and Taylor expansions,

---

<sup>1</sup>Effectively, the only additional terms arise from the existence of *AAC* vertices, which could be discarded in the original treatment, as a consequence of the action being restricted to single supertrace terms.

diagrammatically, under our belts, we illustrated their use by applying them to the calculation of  $\beta_1$ . In chapter 4 we showed, for the first time, that  $\beta_1$  can be reduced to a set of  $\Lambda$ -derivative terms. This represents a radical improvement over the approach in [57] and proves crucial for performing calculations beyond one-loop.

Given the reduction of  $\beta_1$  to  $\Lambda$ -derivative terms, in chapter 5 we discussed how to numerically evaluate them. This is easy for those diagrams contributing to  $\beta_1$ , and serves as a warm-up exercise for a more general treatment of  $\Lambda$ -derivative terms, suitable for two-loop calculations.

At the two-loop level, there are a number of novelties. The first is that individual diagrams may possess genuine IR divergences (as opposed to *pseudo* IR divergences, which arise as a consequence of the way in which we evaluate  $\Lambda$ -derivative terms). The second is that individual diagrams generically possess non-universal contributions which do not die in the limit that we take  $D \rightarrow 4$ .

To demonstrate that these non-universal contributions cancel amongst themselves, we developed the subtraction techniques of section 5.4. Wonderfully, even these have a diagrammatic interpretation, which can be applied not only to  $\Lambda$ -derivative terms but also to  $\mathcal{O}(p^2)$  terms which are not Taylor expandable in  $p$ .

However, despite the appeal and elegance of the diagrammatic techniques developed in chapters 2–5 there is a problem when it comes to actually using them to compute  $\beta$ -function coefficients. Although the final expression for  $\beta_1$  is both small and extremely easy to extract the answer from, it requires a considerable amount of work to actually derive it. Part III is devoted to finding the solution to this problem.

The principle behind the methodology of part-III is an extension of the idea that non-universal contributions cancel in parallel. In the development of the new diagrammatics of section 2.4 it was recognised that the flow of a vertex decorated by some set of fields  $\{f\}$  can be represented by leaving the elements of  $\{f\}$  as implicit (or unrealised) decorations. In the computation of  $\beta_1$ , this was not exploited, and we explicitly performed all these decorations. This, of course, generated many terms, since the rule for performing explicit decorations is that one does so in all possible, independent ways. However, when applying

the diagrammatic procedure to these myriad diagrams, it became apparent that exactly the same steps were being performed on sets of diagrams. Thus, it made sense to try and perform these steps in parallel.

The key to doing this, as first discussed in chapter 7, is to make use of the fact that we can leave decorations unrealised. Let us review the diagrammatics for  $\beta_{n+}$ . We start by computing the flow of  $S_{n+\mu\nu}^{11}(p)$ , at  $\mathcal{O}(p^2)$ . However, rather than explicitly decorating our diagrams with the two external fields  $A_\mu^1(p)$  and  $A_\nu^1(p)$ , we leave them as unrealised decorations. The diagrammatic procedure now proceeds as follows:

1. isolate any two-point, tree level vertices and fully decorate them, applying the effective propagator relationship, if possible, and identify any cancellations;
2. of the terms that remain, isolate the manipulable components i.e. those comprising only Wilsonian effective action vertices, effective propagators and an undecorated wine;
3. convert the manipulable diagrams into  $\Lambda$ -derivative terms, plus corrections, having promoted the wine of the parent into an unrealised decoration;
4. repeat the procedure.

Thus, as we iterate the procedure, the only decorations we perform (of two-point, tree level vertices) all facilitate further manipulation—either because we can apply the effective propagator relation or because we can perform manipulations at  $\mathcal{O}(p^2)$ . For the  $\Lambda$ -derivative terms, we go the other way, promoting explicit decorations to unrealised decorations. Since this is done at each stage of the calculation, the  $\Lambda$ -derivative terms in fact possess only unrealised decorations.

Let us now consider the partner non-manipulable diagrams to a  $\Lambda$ -derivative term. Since these were spawned by a  $\Lambda$ -derivative term from the previous level of manipulation, they each possess only one explicit decoration: the wine formed by the action of  $a_0$  or  $a_1$ . At each stage of the calculation, these non-manipulable terms cancel without the need for any further decoration, which

represents a massive simplification of the calculational procedure.

By iterating the diagrammatic procedure until exhaustion we were able to show that an arbitrary  $\beta_{n+}$  can be reduced to  $\Lambda$ -derivative,  $\beta$  and  $\alpha$ -terms, up to gauge remainders and  $\mathcal{O}(p^2)$  terms (figure 7.43).

Chapter 8 is dedicated to the initial processing of the gauge remainders. Again, this procedure can be performed without the need to fully decorate diagrams. As with our initial strategy, we decorate only two-point, tree level vertices. This procedure generates further  $\mathcal{O}(p^2)$  terms, diagrams which cancel non-manipulable terms and nested gauge remainders. These latter terms are then processed.

By iterating this procedure until exhaustion, entire sets of gauge remainder terms are shown to cancel, to all orders in perturbation theory. In preparation for the treatment of those diagrams which remain, we introduced a new set of diagrammatic identities in chapter 9. We note that the last of these, which is applicable to calculations at the three-loop level and beyond remains to be proven. However, that it is plausible has been demonstrated by proving its validity in a special case and so we made the unproven assertion that it is true in all cases.

Armed with these diagrammatic identities, we showed in chapter 10 how the remaining gauge remainder terms can be converted into  $\Lambda$ -derivative,  $\alpha$  and  $\beta$ -terms, thereby supplementing the expression of figure 7.43. In this way, we arrived at figure 10.25 which gives an incredibly compact form for any  $\beta_{n+}$ , given our earlier assertion, up to  $\mathcal{O}(p^2)$  terms.

The full treatment of the  $\mathcal{O}(p^2)$  terms, though not conceptually of any greater difficulty than the preceding analysis is beyond the scope of this thesis. A discussion of the general principles is given in chapter 11.

The final part of the thesis is devoted to the computation of  $\beta_2$ . Up to  $\mathcal{O}(p^2)$  terms, we jumped straight to the  $\Lambda$ -derivative,  $\beta$  and  $\alpha$ -terms by specialising the expression of figure 10.25 to  $n = 1$ . The explicit treatment of the  $\mathcal{O}(p^2)$  terms is not presented in this thesis but it turns out that, by following chapter 11, such terms can be reduced to  $\Lambda$ -derivative,  $\beta$  and  $\alpha$ -terms, also.

Having done this, we then used our earlier diagrammatic expression for  $\beta_1$  to simplify the expression for  $\beta_2$ . The set of diagrams from which we extract

the numerical coefficient comprises just  $\Lambda$ -derivative and  $\alpha$ -terms and is given in appendix D.

In chapter 13 we used the techniques of chapter 5 to numerically evaluate  $\beta_2$ . After demonstrating that the  $\alpha$ -terms vanish in the  $\alpha \rightarrow 0$ , subject to constraints on the  $\alpha$  dependence of the cutoff functions and seed action, we obtained

$$\beta_2 = -\frac{34}{3} \frac{N^2}{(4\pi)^4},$$

thereby reproducing the standard result.

## 14.2 Discussion

In terms of the original aims of the thesis, the computation of  $\beta_2$  is the most important result of this work. That this highly non-trivial calculation produced the correct answer surely confirms the consistency of the approach, beyond reasonable doubt. Moreover, it should be emphasised that this is the very first analytical, continuum calculation of a two-loop quantity to be performed without fixing the gauge.

However, we have achieved very much more than this. As mentioned in chapter 12, this two-loop calculation was initially performed in a very arduous fashion, since it was first done before the discovery of the methods of part III. Consequently, every single decoration was performed explicitly, generating  $\mathcal{O}(10^4)$  diagrams, almost all of which cancelled, to leave the diagrams of chapter 12.

At this stage, the status of continuum, manifestly gauge invariant calculations was in a peculiar state. On the one hand, leaving the gauge unfixed had guided us to a set of powerful and elegant diagrammatic techniques. On the other hand, the sheer number of diagrams produced was almost overwhelming. Certainly, for perturbative computation, these methods could not be considered anything other than a curiosity.

However, the discoveries of part III have changed everything. Although the work started in part III is yet to be completed (assertion 1 must be proven and the  $\mathcal{O}(p^2)$  terms must be treated), it is quite clear there is a deep structure underlying our original computations of  $\beta_1$  and  $\beta_2$ .

It is certainly my belief that it should be straightforward to complete the work of part III and thus to arrive at an expression for  $\beta_{n_+}$  in terms of only  $\Lambda$ -derivative,  $\beta$  and  $\alpha$ -terms. Indeed, if the computation of  $\beta_2$  is anything to go by, then it may very well be that such an expression can be further simplified. Recall how, at the two-loop level, we were able to remove the  $\beta$ -terms and also those  $\Lambda$ -derivative diagrams which were compelled (in dimensional regularisation) to go as  $\mathcal{O}(p^{2-2\epsilon})$ .

Irrespective of whether these final simplifications take place or not, being able to reduce  $\beta_{n_+}$  to  $\Lambda$ -derivative ( $\beta$ ) and  $\alpha$ -terms would have profound implications. First, at a stroke, almost all of the difficulty in extracting  $\beta$ -function coefficients within the MGI-ERG would be removed. (That said, the numerical extraction of  $\beta_2$  was hardly easy, as chapter 12 demonstrated; we will return to this point shortly.)

Perhaps more interesting is that such an expression for  $\beta_{n_+}$  would contain only Wilsonian effective action vertices and effective propagators. A very important consequence of this is that, in such an expression for  $\beta_{n_+}$ , there can be no diagrams in which a wine bites its own tail: this is trivially the case, since there are no wines! Now, claiming that we have solved the problem associated with wines biting their tails is specious, at this stage, since they have been excluded from our calculations, since the very beginning. However, the analysis of part-III makes it abundantly clear that, had we kept them, they would all have cancelled anyway.

This is a very deep statement. That the flow equation generates wine biting their tail diagrams means that it is not manifestly regulated. By excluding these terms, we cure this problem, but at the expense of a temporary loss of gauge invariance [51, 52]. Now we see this problem in a different light. Certainly, when it comes to perturbatively computing  $\beta$ -function coefficients, it turns out that the flow equation is effectively regulated (so long as the analysis of part III can indeed be completed, as intended), since one can demonstrate that all diagrams in which a wine bites its own tail cancel, amongst themselves.

In some sense, it seems that the real physics of the flow equation is better expressed in the compact expression of figure 10.25 than in the flow equation itself (at least for calculations of  $\beta$ -function coefficients). There are further

indications in this direction. When constructing the new flow equation, we commented that this flow equation is just one of an infinite number of manifestly gauge invariant flow equations that can distinguish between  $A^1$  and  $A^2$ , whilst respecting no- $\mathcal{A}^0$  symmetry. Each of these flow equations will have different, old-style diagrammatic rules. However, it now seems clear that these differences should not matter. We should be able to package all details into the new diagrammatic rules and since we do not expect such details to affect universal quantities, they should cancel out when we iterate the diagrammatic procedure. In other words, so long as we have a valid flow equation that can distinguish between  $A^1$  and  $A^2$ , we should always be able to generate figure 10.25.

Furthermore, if we continue to suppose that the  $\mathcal{O}(p^2)$  terms can be reduced to  $\Lambda$ -derivative,  $\alpha$  and  $\beta$ -terms, then it would seem that there is a diagrammatic prescription to implement the pre-regularisation. Recall that the pre-regularisation demands we throw away all surface terms. In our computation of  $\beta_2$ , the only place that these arose was as total momentum derivative terms, which have a unique diagrammatic form—see section 3.1.6. By adopting the prescription that we always throw away these diagrams, we can implement the pre-regularisation in an entirely diagrammatic fashion, without the need for explicitly using e.g. dimensional regularisation.<sup>2</sup>

Let us now return to the issue of the actual difficulty in extracting the numerical value of  $\beta_2$ . As discussed in section 13.8 the calculation actually has a very clear structure. The construction of subtractions is done in a systematic way and the final set of computable terms can be considerably simplified.

Given our experiences of refining the diagrammatic techniques of parts I and II in part III, this is highly suggestive. It is my belief that the entire procedure of constructing subtractions and re-expressing the  $\Lambda$ -derivative terms as the sum of computable terms can be radically simplified by working with partially decorated diagrams, rather than fully decorated diagrams.

If this is possible, then it opens up some very intriguing questions. Assuming that we can extend the analysis of part III to include  $\mathcal{O}(p^2)$  terms,

---

<sup>2</sup>The use of dimensional regularisation to implement the pre-regularisation is entirely independent of its use in extracting the numerical coefficient,  $\beta_2$ .

then this will demonstrate that arbitrary  $\beta_{n+}$  has no explicit dependence on the seed action and choice of covariantisation. If the process of constructing subtractions can be simplified in the way envisioned, then perhaps it is possible to also demonstrate that arbitrary  $\beta_{n+}$  has no implicit dependence on the seed action and choice of covariantisation. The end of this line of reasoning is to ask whether, within the MGI-ERG, it is possible to arrange for all  $\beta_{n+}$  to depend only on universal details.

One very encouraging indication in this direction is that the analysis of section 5.5 tells us that all running couplings, other than  $g$  and  $\alpha$ , can be tuned to zero. This removes an entire source of non-universality of  $\beta$ -function coefficients, to all orders in perturbation theory.

We note, though, that even if it is the case that  $\beta_{n+}$  can be arranged to depend only on universal details, within the MGI-ERG, we are not claiming that all  $\beta_n$  are universal. We would expect our values of  $\beta_{n>2}$  to disagree with those obtained in other schemes. However, our claim would be that, within the MGI-ERG scheme, there are an infinite number of sub-schemes which yield the same  $\beta_n$  (and also an infinite number that do not) and that this  $\beta_n$  can be arranged to depend only on universal details of the MGI-ERG.

If it proves to be possible to arrange such  $\beta_n$ , then this would represent some kind of ‘factorisation of universality’. In the computation of a physical observable, non-universal ingredients such as  $\beta$ -function coefficients have to combine with other non-universal objects, such that the final answer is universal. However, if the  $\beta_n$  can be arranged to depend only on universal details of the MGI-ERG, then the objects with which they must be combined would have to be universal in this sense, too.

### 14.3 Future Work

There are a number of very exciting avenues of research to pursue, as a result of the work in this thesis. Most obviously, there is an immediate need to complete the analysis of part III and thus hopefully demonstrate that an arbitrary  $\beta_{n+}$  can, indeed, be reduced to  $\Lambda$ -derivative,  $(\beta)$  and  $\alpha$ -terms.

If this can be achieved, then the next logical step is to perform a full in-

investigation of whether or not  $\beta_{>2}$  can be arranged to depend only on universal quantities. This is certainly an interesting question but it must be borne in mind that the real purpose of constructing the MGI-ERG is to do physics. Simply examining the properties of  $\beta$ -function coefficients in a scheme which currently has no mapping to existing schemes, in which calculations of amplitudes are done, is not a big enough step in this direction. One solution is to attempt to perturbatively match our scheme to (say)  $\overline{MS}$ .

However, we intend to be very much more ambitious than this. It is clear from this thesis that the MGI-ERG has far more than just novelty value: it is possible to harness the benefits of manifest gauge invariance whilst entirely removing the associated difficulties. Thus, an obvious project is to begin the examination of perturbative Yang-Mills amplitudes.

Nevertheless, we should remember that the possibility of these perturbative investigations came about entirely as a by-product of demonstrating the consistency of the formalism. The original aim, which should not be lost sight of, it to apply the formalism to the non-perturbative domain.

If it is the case that progress can be made in any of these directions, then it will be desirable to move from Yang-Mills to full QCD. We note, though, that the insertion of quarks is not trivial. The most obvious way of including physical quark fields,  $\psi$ , is to embed them, together with the unphysical bosonic spinor  $\varphi$ , in a field,  $\Psi$ , which transforms under the fundamental representation of  $SU(N|N)$

$$\Psi = \begin{pmatrix} \psi \\ \varphi \end{pmatrix}.$$

Now, the interaction of the field  $\Psi$  with the supergauge field  $\mathcal{A}$  is just

$$\sim \bar{\Psi} \gamma^\mu \mathcal{A}_\mu \Psi.$$

Immediately, we see that we have a problem since this term has a component involving  $\mathcal{A}^0$ . Indeed,  $\mathcal{A}^0$  now acts as a Lagrange multiplier enforcing the constraint

$$\bar{\varphi} \gamma_\mu \varphi + \bar{\psi} \gamma_\mu \psi = 0,$$

which seems to prevent the implementation of quarks in this manner. To make progress, one must perhaps look at embedding the quarks in fields which

transform under higher dimensional representations of  $SU(N|N)$ , with a view to constructing a supergauge invariant interaction term which is independent of  $\mathcal{A}^0$  [60].

## 14.4 Outlook

We have demonstrated the consistency of a formalism which allows continuum calculations to be done in Yang-Mills without fixing the gauge. The initial difficulties have been overcome and the benefits of manifest gauge invariance are being revealed. The stage is now set for application of this formalism to real physical problems, upon which I have utter faith that the MGI-ERG will prove itself to be an indispensable tool in gauge theory.

# Appendix A

## Ingredients of the Weak Coupling Flow Equations

### A.1 Two-Point, Tree Level Vertices

There follows a list of our choices for all independent (i.e. not related by no- $\mathcal{A}^0$  symmetry) seed action, two-point, tree level vertices.

$$\hat{S}_{0\mu\nu}^{11}(p) = \frac{\alpha + 1 + c_p(\alpha - 1)}{\alpha c_p} \square_{\mu\nu}(p), \quad (\text{A.1})$$

$$\hat{S}_{0\mu\nu}^{22}(p) = \frac{\alpha + 1 + c_p(1 - \alpha)}{\alpha c_p} \square_{\mu\nu}(p), \quad (\text{A.2})$$

$$\hat{S}_{0\mu\nu}^{B\bar{B}}(p) = \frac{\alpha + 1}{\alpha c_p} \square_{\mu\nu}(p) + \frac{4\Lambda^2}{\tilde{c}_p} \delta_{\mu\nu}, \quad (\text{A.3})$$

$$\hat{S}_0^{D\bar{B}}{}_{\mu}(p) = \frac{2\Lambda^2 p_{\mu}}{\tilde{c}_p}, \quad (\text{A.4})$$

$$\hat{S}_0^{D\bar{D}}(p) = \frac{\Lambda^2 p^2}{\tilde{c}_p}, \quad (\text{A.5})$$

$$\hat{S}_0^{C^1 C^1}(p) = \frac{\Lambda^2 p^2}{\tilde{c}_p} + 2\lambda\Lambda^4, \quad (\text{A.6})$$

$$\hat{S}_0^{C^2 C^2}(p) = \frac{\Lambda^2 p^2}{\tilde{c}_p} + 2\lambda\Lambda^4, \quad (\text{A.7})$$

$$\hat{S}_0^{C^1, C^1}(p) = 0, \quad (\text{A.8})$$

$$\hat{S}_0^{C^1, C^2}(p) = 0, \quad (\text{A.9})$$

$$\hat{S}_0^{C^2, C^2}(p) = 0. \quad (\text{A.10})$$

Equations A.8–A.10 allow us to set the corresponding Wilsonian effective

action vertices to zero. All other two-point, tree level Wilsonian effective action vertices are taken to be equal to the corresponding seed action vertices.

## A.2 The Zero-Point Kernels and Effective Propagators

Using the definitions

$$f_p = \frac{(1 + \alpha)\tilde{c}_p}{(1 + \alpha)x\tilde{c}_p + 4\alpha c_p}, \quad (\text{A.11})$$

$$g_p = \frac{2\alpha\tilde{c}_p}{(1 + \alpha)x\tilde{c}_p + 4\alpha c_p}, \quad (\text{A.12})$$

we give the zero-point kernels

$$\dot{\Delta}^{11}(p) = \frac{2}{\Lambda^2} \left[ \frac{\alpha c_p}{\alpha + 1 + c_p(\alpha - 1)} \right]', \quad (\text{A.13})$$

$$\dot{\Delta}^{22}(p) = \frac{2}{\Lambda^2} \left[ \frac{\alpha c_p}{\alpha + 1 + c_p(1 - \alpha)} \right]', \quad (\text{A.14})$$

$$\dot{\Delta}^{B\bar{B}}(p) = \frac{1}{\Lambda^2} [x\tilde{c}_p g_p]', \quad (\text{A.15})$$

$$\dot{\Delta}^{D\bar{D}}(p) = \frac{2}{\Lambda^4} \frac{1}{x} [x^2 \tilde{c}_p f_p]', \quad (\text{A.16})$$

$$\dot{\Delta}^{C^1 C^1}(p) = \frac{1}{\Lambda^4} \frac{1}{x} \left[ \frac{2x^2 \tilde{c}_p}{x + 2\lambda \tilde{c}_p} \right]', \quad (\text{A.17})$$

$$\dot{\Delta}^{C^2 C^2}(p) = \frac{1}{\Lambda^4} \frac{1}{x} \left[ \frac{2x^2 \tilde{c}_p}{x + 2\lambda \tilde{c}_p} \right]', \quad (\text{A.18})$$

and the effective propagators

$$\Delta^{11}(p) = \frac{1}{p^2} \frac{\alpha c_p}{\alpha + 1 + c_p(\alpha - 1)}, \quad (\text{A.19})$$

$$\Delta^{22}(p) = \frac{1}{p^2} \frac{\alpha c_p}{\alpha + 1 + c_p(1 - \alpha)}, \quad (\text{A.20})$$

$$\Delta^{B\bar{B}}(p) = \frac{1}{2\Lambda^2} \tilde{c}_p g_p, \quad (\text{A.21})$$

$$\Delta^{D\bar{D}}(p) = \frac{1}{\Lambda^4} \tilde{c}_p f_p, \quad (\text{A.22})$$

$$\Delta^{C^1 C^1}(p) = \frac{1}{\Lambda^4} \frac{\tilde{c}_p}{x + 2\lambda \tilde{c}_p}, \quad (\text{A.23})$$

$$\Delta^{C^2 C^2}(p) = \frac{1}{\Lambda^4} \frac{\tilde{c}_p}{x + 2\lambda \tilde{c}_p}, \quad (\text{A.24})$$

where we note that

$$xf_p + 2g_p = 1. \tag{A.25}$$

### A.3 The Gauge Remainders

The gauge remainders are defined via the equation

$$S_{0MS}^{XY}(p)\Delta_{SN}^{YY}(p) = \delta_{MN} - p'_M p_N,$$

where we sum over all realisations of the field  $Y$  and the components of the r.h.s. are identified in table A.1.

	$\delta_{MN}$	$p'_M$	$p_N$
$F$	$\delta_{MN}$	$(f_k p_\mu / \Lambda^2, g)$	$(p_\nu, 2)$
$A$	$\delta_{\mu\nu}$	$p_\mu / p^2$	$p_\nu$
$C$	$\mathbb{1}$	—	—

Table A.1: Summary of the gauge remainders in each sector

In both the  $A$  and  $F$ -sectors,

$$p_M p'_M = 1.$$

# Appendix B

## Diagrammatic Identities

**Diagrammatic Identity 1** Consider a two point, tree level (single supertrace) vertex, attached to an effective propagator which, only ever appearing as an internal line, attaches to an arbitrary structure. This is shown diagrammatically in figure 2.22, where the effective propagator is denoted by a long, solid line.

$$M \text{---} \textcircled{0} \text{---} \langle \equiv M \text{---} \langle - M \blacktriangleright \langle \equiv M \text{---} \langle - M \triangleright \langle$$

Figure B.1: The effective propagator relation.

The object  $\blacktriangleright$  decomposes into two constituents:

$$\frac{M \triangleright}{p \rightarrow} \equiv p'_M, \quad (\text{B.1})$$

$$\frac{\triangleright^N}{p \rightarrow} \equiv p_N. \quad (\text{B.2})$$

**Diagrammatic Identity 2** Using the definitions B.1 and B.2, together with the information of table A.1 and equation A.25 gives us the diagrammatic identity below.

$$\triangleright \triangleright = 1 \quad (\text{B.3})$$

The index at the apex of  $\triangleright$  is contracted into the index carried by  $\triangleright$ . Note that this relationship exists only in the  $A^{1,2}$  and  $F$ -sectors.

A number of corollaries follow from equation B.3 and the fact that  $p_N$  is independent of both  $\Lambda$  and  $\alpha$ , in all sectors.

### Corollaries

$$\begin{aligned} \left[ \triangleright \triangleright \right]^\bullet &= 0 \\ \Rightarrow \triangleright \triangleright^\bullet &= 0 \\ \frac{\partial}{\partial \alpha} \left[ \triangleright \triangleright \right] &= 0 \\ \Rightarrow \triangleright \frac{\partial}{\partial \alpha} \triangleright &\equiv \triangleright \triangleright^\circledast = 0 \end{aligned}$$

We have introduced  $\circledast$  to represent  $\partial/\partial\alpha$ .

**Diagrammatic Identity 3** Consider an effective propagator attached, at one end to the  $p'_M$  part of a gauge remainder. This can be redrawn as follow:

$$\longrightarrow \triangleright = \triangleleft \dashdot \triangleright ,$$

where the dash-dot line represents the pseudo effective propagators.

### Corollary

$$\longrightarrow \blacktriangleright = \triangleleft \dashdot \triangleright = \blacktriangleleft \longleftarrow$$

**Diagrammatic Identity 4** A sub-diagram comprising a two-point, tree level vertex, differentiated with respect to momentum and attached to an effective propagator can, using the effective propagator relation, be redrawn, in the following way:

$$\text{---} \textcircled{0} \text{---} \equiv \text{---} \textcircled{0} \text{---} \text{---} \textcircled{0} \text{---} \text{---} \textcircled{0} \text{---} .$$

The final diagram is interpreted as the derivative with respect to the momentum entering the encircled structure from the left. Had the arrow pointed the other way, then the derivative would be with respect to the momentum entering the structure from the right.

**Diagrammatic Identity 5** A sub-diagram comprising a two-point, tree level vertex, differentiated with respect to momentum and attached to two effective

propagators can, using diagrammatic identity 4 and the effective propagator relation, be redrawn in the following way:

$$\begin{array}{c} \text{---} \textcircled{0} \text{---} \end{array} \equiv - \begin{array}{c} \text{---} \textcircled{0} \end{array} + \frac{1}{2} \left[ \begin{array}{cc} \begin{array}{c} \text{---} \textcircled{0} \end{array} - \begin{array}{c} \text{---} \textcircled{0} \end{array} \\ \begin{array}{c} \text{---} \textcircled{0} \end{array} - \begin{array}{c} \text{---} \textcircled{0} \end{array} \end{array} \right].$$

We could re-express this in a less symmetric form by taking either of the two rows in the square brackets and removing the factor of half.

**Diagrammatic Identity 6** A sub-diagram comprising a two-point, tree level vertex, struck by  $\triangleright$  vanishes:

$$\begin{array}{c} \text{---} \textcircled{0} \end{array} \triangleright = 0.$$

**Corollaries**

$$\begin{array}{c} \begin{array}{c} \text{---} \textcircled{0} \end{array} \triangleright \equiv - \begin{array}{c} \text{---} \textcircled{0} \end{array} \triangleright \\ \begin{array}{c} \text{---} \textcircled{0} \end{array} \triangleright \equiv - \begin{array}{c} \text{---} \textcircled{0} \end{array} \triangleright = 0 \\ \begin{array}{c} \text{---} \textcircled{0} \end{array} \triangleright \equiv - \begin{array}{c} \text{---} \textcircled{0} \end{array} \triangleright = 0 \end{array}$$

Recall that  $\textcircled{\alpha}$  represents differentiation with respect to  $\alpha$ . We have used the independence of  $\triangleright$  on both  $\Lambda$  and  $\alpha$  (in all sectors).

**Diagrammatic Identity 7** A sub-diagram comprising a two-point, tree level vertex, differentiated with respect to momentum and attached to two effective propagators, one of which terminates with a  $\triangleright'$  can, using diagrammatic identities 3 and 4, be redrawn in the following form:

$$\begin{array}{c} \text{---} \textcircled{0} \end{array} \triangleright' \equiv - \begin{array}{c} \text{---} \textcircled{0} \end{array} \triangleright'.$$

**Diagrammatic Identity 8** A sub-diagram comprising a two-point, tree level vertex, attached to an un-decorated wine which terminates in a  $\triangleright'$  can be redrawn, using diagrammatic identities 3 and 2, the effective propagator relation and the tree level flow equation:

$$\begin{array}{c} \begin{array}{c} \text{---} \textcircled{0} \end{array} \triangleright' \equiv \left[ \begin{array}{c} \text{---} \textcircled{0} \end{array} \triangleright' \right] - \begin{array}{c} \text{---} \textcircled{0} \end{array} \triangleright' - \begin{array}{c} \text{---} \textcircled{0} \end{array} \triangleright' \\ \equiv \begin{array}{c} \text{---} \textcircled{0} \end{array} \triangleright' \end{array}$$

**Diagrammatic Identity 9** Consider the diagram shown on the LHS of figure B.2. We can re-draw this as shown on the RHS since, if the newly drawn  $\triangleright$  hits the external field, then the diagram vanishes.

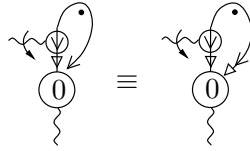


Figure B.2: The first step in re-drawing a diagram to yield a diagrammatic identity.

We now allow the original  $\triangleright$  to act. It must trap the remaining  $\triangleright$ . Taking the CC of the resultant diagram, we reflect it but pick up no net sign, since we have both one processed gauge remainder and one momentum derivative. Having done this, we then reverse the direction of the arrow on the derivative, which does yield a minus sign. This gives us the diagrammatic identity, shown in figure B.4.

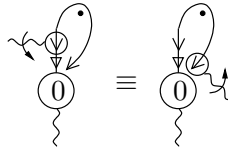


Figure B.3: A diagrammatic identity.

We can, however, generalise this diagrammatic identity by stripping off the two-point, tree level vertices. We are justified in doing this: the integral over loop momentum will, by Lorentz invariance, yield a Kronecker  $\delta$  for both diagrams of figure B.4. In other words, we need not worry that stripping off the two-point, tree level vertices is valid only up to some term which kills the vertex.



Figure B.4: Diagrammatic identity 9.

*Note that this identity holds if we replace the wire by an effective propagator.*

**Diagrammatic Identity 10** *Consider a vertex attached to an effective propagator, which ends in a hook. Suppose that a gauge remainder strikes this vertex. Focusing on the terms produced when the gauge remainder pushes forward / pulls back onto a socket, we suppose that a two-point, tree level vertex is generated. Applying the effective propagator relation, the gauge remainder dies, leaving us with the diagrammatic identity shown in figure B.5.*

$$\text{Diagram 1} - \text{Diagram 2} = 0$$

Figure B.5: Diagrammatic identity 10.

**Corollary** *The diagrammatic identity immediately implies that  $\text{Diagram 1}$ , alone, vanishes; this follows because we can re-express this sub-diagram as:*

$$1/2 \left[ \text{Diagram 1} - \text{Diagram 2} \right]$$

*(see section 3.1.2).*

**Diagrammatic Identity 11** *Consider a two-point, tree level vertex, attached to an effective propagator and then to a gauge remainder. The gauge remainder bites the remaining socket of the vertex in either sense. A second gauge remainder bites the first gauge remainder. These sub-diagrams can be redrawn as shown in figure B.6.*



Figure B.6: Diagrammatic identity 11.

**Diagrammatic Identity 12** Consider the diagrams of figure B.7. This equality holds, if we change nested gauge remainders from being struck on the left (right) to being struck on the right (left), in all independent ways.

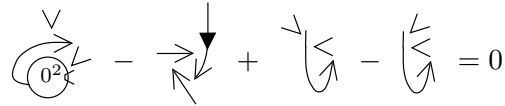


Figure B.7: Diagrammatic identity 12

**Assertion 1** If the diagrams of figure B.8 can be shown to sum to zero in the  $A$ -sector then we assert the following, without proof:

1. these diagrams will sum to zero in all sectors;
2. the sets of partner diagrams in which we exchange pushes forward for pulls back (and vice-versa) also sum to zero.

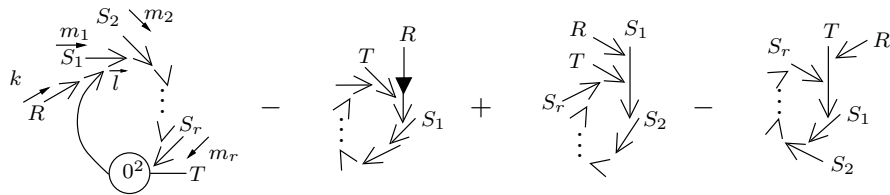


Figure B.8: Four diagrams for which it has been demonstrated that they sum to zero when all fields are in the  $A$ -sector.

**Diagrammatic Identity 13** The set of sub-diagrams of figure B.8 sum to zero. The complimentary sets of diagrams in which arbitrary numbers of pushes

forward (pulls back) are consistently changed to pulls back (pushes forward) also sum to zero.

**Diagrammatic Identity 14** *It is true in all sectors for which the gauge remainder is not null that*

$$\begin{array}{c} \nu \\ \curvearrowright \\ \textcircled{\alpha} \end{array} = \delta_{\alpha\nu}.$$

*It therefore follows that*

$$\begin{array}{c} \curvearrowright \\ \textcircled{\alpha} \\ \overleftarrow{k} \end{array} = \overbrace{\quad}^k.$$

**Diagrammatic Identity 15** *A sub-diagram comprising a two-point, tree level vertex, differentiated with respect to  $\alpha$  and attached to an effective propagator can, using the effective propagator relation, be redrawn, in the following form:*

$$\textcircled{\alpha} \textcircled{0} \equiv - \textcircled{\alpha} \textcircled{0} - \textcircled{\alpha} \triangleright.$$

**Diagrammatic Identity 16** *A sub-diagram comprising a two-point, tree level vertex, differentiated with respect to  $\alpha$  and attached to two effective propagators can, using diagrammatic identity 15 and the effective propagator relation, be redrawn in the following form:*

$$\textcircled{\alpha} \textcircled{0} \equiv - \textcircled{\alpha} + \frac{1}{2} \left[ \begin{array}{cc} \overleftarrow{\textcircled{\alpha}} & - & \overrightarrow{\textcircled{\alpha}} \\ \overrightarrow{\textcircled{\alpha}} & - & \overleftarrow{\textcircled{\alpha}} \end{array} \right].$$

*We could re-express this in a less symmetric form by taking either of the two rows in the square brackets and removing the factor of half.*

**Diagrammatic Identity 17** *A sub-diagram comprising a two-point, tree level vertex, differentiated with respect to  $\alpha$  and attached to an effective propagator which terminates in a  $\triangleright'$  vanishes:*

$$\overleftarrow{\textcircled{\alpha} \textcircled{0}} \equiv \overrightarrow{\textcircled{\alpha} \textcircled{0}} = 0,$$

*as follows from diagrammatic identities 3 and 6.*

**Diagrammatic Identity 18** *A sub-diagram comprising a two-point, tree level vertex attached to an effective propagator, differentiated with respect to  $\alpha$ , which*

terminates in a  $>$  can be re-drawn, using diagrammatic identity 17, the effective propagator relation diagrammatic identity 2:

$$\leftarrow \textcircled{0} \equiv - \textcircled{<}$$

# Appendix C

## Examples of Classical Flows

The first vertex whose flow we will need is a three-point, tree level vertex, decorated by three wildcard fields labelled  $R$ - $T$ . This is shown in figure C.1.

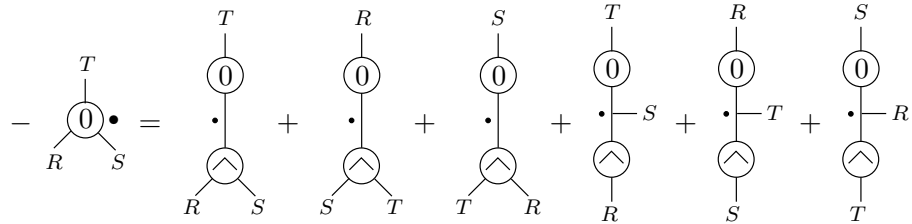


Figure C.1: The flow of a three-point, tree level vertex decorated by three wildcard fields.

We now specialise the previous example to give the flow of a three-point, tree level vertex decorated by  $A_\mu^1(p)$ ,  $A_\nu^1(-p)$  and a wildcard field, which we note carries zero momentum. This is shown in figure C.2 where we have suppressed all labels.

The third diagram vanishes. First, we note that the wine must be bosonic. Now, it cannot be in the  $C$ -sector, because  $AC$  vertices do not exist. If the wine is in the  $A$ -sector then, since the wildcard field carries zero momentum,

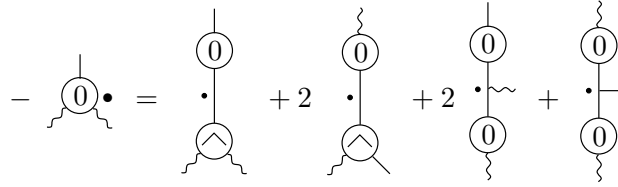


Figure C.2: Flow of a three-point, tree level vertex decorated by  $A_\mu^1(p)$ ,  $A_\nu^1(-p)$  and a dummy field. Lorentz indices, sub-sector labels and momentum arguments are suppressed.

this would require a two-point  $A$ -vertex carrying zero momentum, which is forbidden by gauge invariance.

The final diagram vanishes at  $\mathcal{O}(p^2)$ . The wine must be in the  $A$ -sector and so each of the vertices contributes at least  $\mathcal{O}(p^2)$ , as a consequence of gauge invariance.

Note that, if the wildcard field is in the  $C$ -sector, then the second diagram also vanishes at  $\mathcal{O}(p^2)$ . The top vertex contributes at least  $\mathcal{O}(p^2)$ . The bottom vertex must also contribute  $\mathcal{O}(p^2)$ , by gauge invariance, since  $AC$  vertices do not exist.

The last example is of the flow of a four-point, tree level vertex decorated by  $A_\mu^1(p)$ ,  $A_\nu^1(-p)$  and two dummy fields, as shown in figure C.3. Summing over the flavours of the dummy fields and noting that, in the current example, the dummy fields carry equal and opposite momenta, we can treat these fields as identical.

The penultimate diagram vanishes at  $\mathcal{O}(p^2)$ . The wine must be in the  $A$ -sector, but then the diagram possesses an  $\mathcal{O}(p^2)$  stub. However, the wine, which carries three Lorentz indices, cannot have an  $\mathcal{O}(p^0)$  contribution by Lorentz invariance. The final diagram, which possesses two  $\mathcal{O}(p^2)$  stubs, clearly vanishes at  $\mathcal{O}(p^2)$ .

The diagram shows an equation where a single vertex with a central dot and four external lines is equal to a sum of 16 terms. Each term consists of two vertices labeled '0' connected by a vertical line, with a central dot on this line. The external lines are distributed between the two vertices in various configurations. The terms are arranged in four rows of four, with coefficients 2, 4, 2, 4, and 4, 2, 4, 4 respectively.

Figure C.3: Flow of a four-point, tree level vertex decorated by  $A_{\mu}^1(p)$ ,  $A_{\nu}^1(-p)$  and two dummy fields. Lorentz indices and momentum arguments are suppressed.

## Appendix D

# Simplified Expression for $\beta_2$

There follows a reproduction of the simplified expression for  $-4\beta_2\Box_{\mu\nu}(p)$ .

$$\frac{1}{4} \left[ \begin{array}{l}
2 \text{ (diagram)} - 2 \text{ (diagram)} - 4 \text{ (diagram)} + 4 \text{ (diagram)} \\
- 2 \text{ (diagram)} - 2 \text{ (diagram)} + 2 \text{ (diagram)} + 2 \text{ (diagram)} \\
- \frac{1}{2} \text{ (diagram)} + \frac{2}{3} \text{ (diagram)} + 8 \left[ \text{diagram} \right]_{ES'} \\
+ \text{ (diagram)} - \text{ (diagram)} + 4 \left[ \text{diagram} \right]_{ES'} - \frac{1}{2} \text{ (diagram)} \\
+ \text{ (diagram)} - \text{ (diagram)} + 4 \left[ \text{diagram} \right]_{ES'}
\end{array} \right]$$

$$\left[ \begin{array}{l}
- \text{Diagram 1} + \text{Diagram 2} - 4 \left[ \text{Diagram 3} \right]_{ES'} + \text{Diagram 4} \\
+ 2 \text{Diagram 5} - 2 \text{Diagram 6} \\
+ 8 \left[ \text{Diagram 7} \right]_{ES'} - 2 \text{Diagram 8} \\
+ \text{Diagram 9} - \frac{2}{3} \text{Diagram 10} - \text{Diagram 11} + \frac{1}{2} \text{Diagram 12} \\
- \frac{2}{3} \text{Diagram 13} - 2 \text{Diagram 14} + 4 \text{Diagram 15} + 2 \text{Diagram 16} \\
+ \text{Diagram 17} - 2 \text{Diagram 18} + 16 \text{Diagram 19} - 8 \left[ \text{Diagram 20} \right]_{ES'} \\
+ 16 \text{Diagram 21} + 16 \text{Diagram 22} + 8 \text{Diagram 23}
\end{array} \right]$$

$$\left[ \begin{array}{c}
2 \left( \begin{array}{c} \text{Diagram 1} \\ \text{Diagram 2} \end{array} \right) - \left( \begin{array}{c} \text{Diagram 3} \\ \text{Diagram 4} \end{array} \right) \\
+ \left( \begin{array}{c} \text{Diagram 5} \\ \text{Diagram 6} \end{array} \right) - \left( \begin{array}{c} \text{Diagram 7} \\ \text{Diagram 8} \end{array} \right) + 2 \left( \begin{array}{c} \text{Diagram 9} \\ \text{Diagram 10} \end{array} \right) + 2 \left( \begin{array}{c} \text{Diagram 11} \\ \text{Diagram 12} \end{array} \right) \\
2 \left( \begin{array}{c} \text{Diagram 13} \\ \text{Diagram 14} \end{array} \right) - 2 \left( \begin{array}{c} \text{Diagram 15} \\ \text{Diagram 16} \end{array} \right) + 2 \left( \begin{array}{c} \text{Diagram 17} \\ \text{Diagram 18} \end{array} \right) + 2 \left( \begin{array}{c} \text{Diagram 19} \\ \text{Diagram 20} \end{array} \right) \\
+ 2 \left( \begin{array}{c} \text{Diagram 21} \\ \text{Diagram 22} \end{array} \right) + 2 \left( \begin{array}{c} \text{Diagram 23} \\ \text{Diagram 24} \end{array} \right) - 2 \left( \begin{array}{c} \text{Diagram 25} \\ \text{Diagram 26} \end{array} \right) + 2 \left( \begin{array}{c} \text{Diagram 27} \\ \text{Diagram 28} \end{array} \right) \\
- \left( \begin{array}{c} \text{Diagram 29} \\ \text{Diagram 30} \end{array} \right) - \left[ \begin{array}{c} \text{Diagram 31} \\ \text{Diagram 32} \end{array} \right]_{ES'} + \left[ \begin{array}{c} \text{Diagram 33} \\ \text{Diagram 34} \end{array} \right]_{ES'}
\end{array} \right]$$

$$\left[ \begin{array}{c}
\left[ \begin{array}{c}
\beta \\
\text{0} \\
\text{0} \\
\beta
\end{array} \right] + \left[ \begin{array}{c}
\beta \\
\text{0} \\
\beta
\end{array} \right] - 2 \left[ \begin{array}{c}
\beta \\
\text{0} \\
\beta
\end{array} \right] + 2 \left[ \begin{array}{c}
\beta \\
\text{0} \\
\beta
\end{array} \right] \\
\times \Delta_{\alpha\beta}^{11}(p) \left[ \begin{array}{c}
\alpha \\
\text{0} \\
\alpha \\
\alpha \\
\alpha
\end{array} \right] - \left[ \begin{array}{c}
\alpha \\
\text{0} \\
\alpha \\
\alpha \\
\alpha
\end{array} \right] + 4 \left[ \begin{array}{c}
\alpha \\
\text{0} \\
\alpha
\end{array} \right] - \left[ \begin{array}{c}
\alpha \\
\text{0} \\
\alpha
\end{array} \right] \\
+ \left[ \begin{array}{c}
\alpha \\
\text{0} \\
\alpha \\
\alpha \\
\alpha
\end{array} \right] + 4 \left[ \begin{array}{c}
\alpha \\
\text{0} \\
\alpha \\
\alpha \\
\alpha
\end{array} \right] + 4 \left[ \begin{array}{c}
\alpha \\
\text{0} \\
\alpha \\
\alpha \\
\alpha
\end{array} \right]
\end{array} \right] \bullet$$

$$-\frac{1}{2} \gamma^1 \frac{\partial}{\partial \alpha} \left[ \begin{array}{c}
\left[ \begin{array}{c}
\alpha \\
\text{0} \\
\alpha \\
\alpha \\
\alpha
\end{array} \right] - \left[ \begin{array}{c}
\alpha \\
\text{0} \\
\alpha \\
\alpha \\
\alpha
\end{array} \right] + 4 \left[ \begin{array}{c}
\alpha \\
\text{0} \\
\alpha
\end{array} \right] - \left[ \begin{array}{c}
\alpha \\
\text{0} \\
\alpha
\end{array} \right] \\
+ 8 \left[ \begin{array}{c}
\alpha \\
\text{0} \\
\alpha \\
\alpha \\
\alpha
\end{array} \right] + 4 \left[ \begin{array}{c}
\alpha \\
\text{0} \\
\alpha \\
\alpha \\
\alpha
\end{array} \right]
\end{array} \right]$$

# Bibliography

- [1] K. Wilson and J. Kogut, *Phys. Rep.* **12 C** (1974) 75.
- [2] F. J. Wegner and A. Houghton, *Phys. Rev.* **A 8** (1973) 401.
- [3] J. Polchinski, *Nucl. Phys.* **B 231** (1984) 269.
- [4] S. Arnone, Y. A. Kubyshin and T. R. Morris, J. F. Tighe, in *Proc. XVth Workshop on High Energy Physics and Quantum Field Theory*, eds. M. N. Dubinin and V. I. Savrin (Moscow University Press, 2001), p. 297, hep-th/0102011.
- [5] S. Arnone, Y. A. Kubyshin and T. R. Morris, J. F. Tighe, *Int. J. Mod. Phys.* **A 16** (2001) 1989.
- [6] S. Arnone, Y. A. Kubyshin and T. R. Morris, J. F. Tighe, *Int. J. Mod. Phys.* **A 17** (2002) 2283.
- [7] C. Wetterich, *Phys. Lett.* **B 301** (1993) 90.
- [8] M. Bonini *et al.*, *Nucl. Phys.* **B 409** (1993) 441.
- [9] M. Bonini, G. Marchesini and M. Simionato, *Nucl. Phys.* **B 483** (1997) 475.
- [10] T. Papenbrock and C. Wetterich, *Z. Phys.* **C 65** (1995) 519.
- [11] M. Pernici and M. Raciti, *Nucl. Phys.* **B 531** (1998) 560.
- [12] P. Kopietz, *Nucl. Phys.* **B 595** (2001) 493.
- [13] D. Zappala, *Phys. Rev.* **D 66** (2002) 105020.
- [14] A. Hasenfratz and P. Hasenfratz *Nucl. Phys.* **B 270** (1986) 687.

- [15] J.-I. Sumi, W. Soumma, K.-I. Aoki, H. Terao and K. Morikawa, hep-th/0002231.
- [16] C. Bagnuls and C. Bervillier, *Phys. Rept.* **348** (2001) 91.
- [17] J. Berges, N. Tetradis, C. Wetterich, *Phys. Rept.* **363** (2002) 233.
- [18] J. Polonyi, *Central Eur. J. Phys.* **1** (2004) 1.
- [19] T. R. Morris, *Int. J. Mod. Phys. A* **9** (1994) 2411.
- [20] T. R. Morris, *Prog. Theor. Phys. Suppl.* 131 (1998) 395.
- [21] T. R. Morris, *Nucl. Phys. B* **495** (1997) 477.
- [22] T. R. Morris, in *New Developments in Quantum Field Theory*, NATO ASI series 366, (Plenum Press, 1998), *Int. J. Mod. Phys. B* **12** (1998) 1343.
- [23] T. R. Morris and J. F. Tighe, *JHEP* 08 (1999) 7.
- [24] S. Arnone, A. Gatti and T. R. Morris *JHEP* 0205 (2002) 059.
- [25] S. Arnone, A. Gatti, T. R. Morris and O. J. Rosten, *Phys. Rev. D* **69** (2004) 065009.
- [26] M. Bonini, M. D'Attanasio and G. Marchesini, *Nucl. Phys. B* **418** (1994) 81.
- [27] M. Bonini, M. D'Attanasio and G. Marchesini, *Nucl. Phys. B* **421** (1994) 429.
- [28] M. Bonini, M. D'Attanasio and G. Marchesini, *Nucl. Phys. B* **437** (1995) 163.
- [29] M. Bonini and E. Tricarico, *Nucl. Phys. B* **606** (2001) 231.
- [30] C. Becchi, in *Elementary Particles, Field Theory and Statistical Mechanics* (Parma, 1993), hep-th/9607188.
- [31] K.-I. Aoki *et al.*, *Prog. Theor. Phys.* **97** (1997) 479.
- [32] K.-I. Aoki *et al.*, *Phys. Rev. D* **61** (2000) 045008.

- [33] K.-I. Kubota and H. Terao, *Prog. Theor. Phys.* **102** (1999) 1163.
- [34] M. Pernici *et al.*, *Nucl. Phys.* **B 520** (1998) 469.
- [35] M. Simionato, *Int. J. Mod. Phys.* **A 15** (2000) 2121; *Int. J. Mod. Phys.* **A 15** (2000) 2153.
- [36] M. Simionato *Int. J. Mod. Phys.* **A 15** (2000) 4811.
- [37] M. Simionato, *Int. J. Mod. Phys.* **A 16** (2001) 2125.
- [38] A. Panza and R. Soldati *Phys. Lett.* **B 493** (2000) 197.
- [39] M. Reuter and C. Wetterich, *Nucl. Phys.* **B 427** (1994) 291.
- [40] M. Reuter and C. Wetterich, *Nucl. Phys.* **B 417** (1994) 181.
- [41] F. Freire, D. F. Litim and J. M. Pawłowski, *Phys. Lett.* **B 495** (256) 2000.
- [42] D. F. Litim and J. M. Pawłowski, *Phys. Lett.* **B 546** (2002) 279.
- [43] U. Ellwanger, *Phys. Lett.* **B 335** (1994) 364.
- [44] M. D’Attanasio and T. R. Morris, *Phys. Lett.* **B 378** (1996) 213.
- [45] D. F. Litim and J. M. Pawłowski, *Phys. Lett.* **B 435** (1998) 181.
- [46] D. F. Litim and J. M. Pawłowski, hep-th/9901063.
- [47] J. M. Pawłowski, *Acta Phys. Slov.* **52** (2002) 475.
- [48] D. F. Litim and J. M. Pawłowski, *JHEP* 0209 (2002) 049.
- [49] V. Branchina, K. A. Meissner and G. Veneziano, *Phys. Lett.* **B 574** (2003) 319.
- [50] J. M. Pawłowski, hep-th/0310018.
- [51] T. R. Morris, in: *The Exact Renormalization Group*, Eds. Kraznitz et al. (World Sci, Singapore, 1999) p.1, hep-th/9810104.
- [52] T. R. Morris, *Nucl. Phys.* **B 573** (2000) 97.

- [53] T. R. Morris, *JHEP* 0012 (2000) 012.
- [54] T. R. Morris, *Int. J. Mod. Phys. A* **16** (2001) 1899.
- [55] A. Gatti, 'A Gauge Invariant Flow Equation', Ph.D. Thesis hep-th/0301201.
- [56] S. Arnone, A. Gatti and T. R. Morris, *Acta Phys. Slov.* **52** (2002) 621.
- [57] S. Arnone, A. Gatti and T. R. Morris, *Phys. Rev. D* **67** (2003) 085003.
- [58] O. J. Rosten, T. R. Morris and S. Arnone, The Gauge Invariant ERG, Proceedings of Quarks 2004, Pushkinskie Gory, Russia, 24-30 May 2004, <http://quarks.inr.ac.ru>, hep-th/0409042.
- [59] O. J. Rosten, A Manifestly Gauge Invariant and Universal Calculus in Yang-Mills Theory, in preparation.
- [60] Work in progress.
- [61] J.I. Latorre and T. R. Morris, *JHEP* 0011 (2000) 004.
- [62] J.I. Latorre and T. R. Morris, *Int. J. Mod. Phys. A* **16** (2001) 2071.
- [63] B. Bergerhoff, D. Litim, S. Lola and C. Wetterich, *Int. J. Mod. Phys. A* **11** (1996) 4273.
- [64] B. Bergerhoff, F. Freire, D. Litim, S. Lola and C. Wetterich, *Phys. Rev. B* **53** (1996) 5734.
- [65] K.-I. Aoki, K. Morikawa, J.-I. Sumi, H. Terao and M. Tomoyose, *Prog. Theor. Phys.* (1997) 479.
- [66] M. Reuter and C. Wetterich, *Phys. Rev. D* **56** (1997) 7893.
- [67] B. Bergerhoff and C. Wetterich, *Phys. Rev. D* **57** (1998) 1591.
- [68] H. Gies, *Phys. Rev. D* **66** (2002) 025006.
- [69] U. Ellwanger, M. Hirsch and A. Weber, *Z. Phys. C* **69** (1996) 687.
- [70] U. Ellwanger, M. Hirsch and A. Weber, *Eur. Phys. J. C* (1) 1998563.

- [71] J. M. Pawłowski, D. F. Litim, S. Nedelko and L. von Smekal, *Phys. Rev. Lett.* **93** (2004) 152002.
- [72] C. S. Fischer and H. Gies, *JHEP* 0410 (2004) 048.
- [73] U. Ellwanger, *Nucl. Phys.* **B 531** (1998) 593.
- [74] U. Ellwanger, *Nucl. Phys.* **B 560** (1999) 587.
- [75] U. Ellwanger and N. Wschebor, *Eur. Phys. J.* **C (28)** 2003415.
- [76] J. M. Pawłowski, *Phys. Rev.* **D 58** (1998) 045011.
- [77] H. Gies and C. Wetterich, *Phys. Rev.* **D 69** (2004) 025001.
- [78] U. Ellwanger, *Eur. Phys. J.* **C (7)** 1999673.
- [79] J. M. Pawłowski, D. F. Litim, S. Nedelko and L. von Smekal, *Phys. Rev. Lett.* **93** (2004) 152002.
- [80] K.-I. Aoki, K. Morikawa, J.-I. Sumi, H. Terao and M. Tomoyose, *Phys. Rev.* **D 61** (2000) 045008; K. I. Aoki, K. Morikawa, J.-I. Sumi, H. Terao and M. Tomoyose, *Prog. Theor. Phys.* **102** (1999) 1151.
- [81] S. Arnone, S. Chiantese and K. Yoshida, *Int. J. Mod. Phys.* **A 16** (2001) 1811.
- [82] S. Arnone, and K. Yoshida, *Int. J. Mod. Phys.* **B 18** (2004) 469.
- [83] U. Ellwanger, *Z. Phys.* **C 76** (1997) 721.
- [84] D. F. Litim, hep-ph/9811272.
- [85] M. D'Attanasio and M. Pietroni, *Nucl. Phys.* **B 498** (1997) 443.
- [86] M. Bonini and F. Vian, *Nucl. Phys.* **B 511** (1998) 479.
- [87] S. Falkenberg and B. Geyer, *Phys. Rev.* **D 58** (1998) 085004.
- [88] M. Bonini and F. Vian, *Nucl. Phys.* **B 532** (1998) 473.
- [89] M. Reuter, *Phys. Rev.* **D 57** (971) 1998.
- [90] O. Lauscher and M. Reuter, *Class. Quant. Grav.* **19** (2002) 483.

- [91] D. F. Litim, *Phys. Rev. Lett.* **92** (2004) 201301.
- [92] D. V. Shirkov, *Theor. Math. Phys.* **60** (1985) 778.
- [93] P. Hasenfratz and F. Niedermayer, *Nucl. Phys.* **B 414** (1994) 785.
- [94] G. A. Vilkovisky, in *Quantum Theory of Gravity*, ed. S. M. Christensen (Adam Hilger, 1984), 169-209; *Nucl. Phys.* **B 234** (1984) 125.
- [95] B. DeWitt, *The Effective Action in Quantum Field Theory and Quantum Statistics*, eds. I. A. Batalin. C. J. Isham and G. A. Vilkovisky (Adam Hilger: Bristol 1987).
- [96] A. A. Slavnov, *Theor. Math. Phys.* **33** (1977) 977; [Teor. Mat. Fiz. **33**, 210 (1977)]. L. D. Faddeev and A. A. Slavnov, *Gauge Fields, Introduction to Quantum Field Theory* 2nd ed. (Benjamin/Cummings, Reading, Massachusetts, 1980).
- [97] T. D. Bakeyev and A. A. Slavnov, *Mod. Phys. Lett.* **A 11** (1996) 1539.
- [98] M. Asorey and F. Falceto, *Phys. Rev.* **D 54** (1996) 5290.
- [99] I. Bars, in *Introduction to Supersymmetry in Particle and Nuclear Physics*, eds. Castanõs et al. (Plenum, New York, 1984) 107.
- [100] T. Appelquist and J. Carazzone, *Phys. Rev.* **D 11** (1975) 2856; K. Symanzik, *Comm. Math. Phys.* 34 (1973) 7. See also J. Collins, *Renormalization* (CUP, 1984).
- [101] See e.g. M. E. Peskin & D. V. Schroeder, *An Introduction to Quantum Field Theory* (Perseus Books Publishing, L.L.C., 1995).
- [102] See e.g. C. Itzykson and J. B. Zuber, *Quantum Field Theory* (McGraw-Hill, New York, 1980).
- [103] See e.g. S. Weinberg, *The Quantum Theory of Fields* (Cambridge University Press, Cambridge 1996), Vol. 2.
- [104] V. N. Gribov, *Nucl. Phys.* **B 139** (1978) 1.
- [105] J. Goldstone, *Nuovo Cim.* **19** (1961) 269.

- [106] B. J. Warr, *Ann. Phys.* **183** (1988) 1.
- [107] A. A. Slavnov, *Theor. Math. Phys.* **13** (1972) 1064; B. W. Lee and J. Zinn-Justin, *Phys. Rev.* **D 5** (1972) 3121.
- [108] T. van Ritburgen, J. A. M. Vermaseren and S. A. Larin, *Phys. Lett.* **B 400** (1997) 379.
- [109] M. Czakon, The Four-Loop QCD Beta-Function and Anomalous Dimensions, *Nucl. Phys.* **B 710** (2005) 485.